

# Leonhard, Control of Electrical Drives

---

**Springer**

*Berlin*

*Heidelberg*

*New York*

*Barcelona*

*Budapest*

*Hong Kong*

*London*

*Milan*

*Paris*

*Santa Clara*

*Singapur*

*Tokyo*

Werner Leonhard

# Control of Electrical Drives

2nd Completely Revised and Enlarged Edition

With 299 Figures



Springer

Prof. Dr.-Ing. Dr. h.c.  
Werner Leonhard

Technische Universität Braunschweig  
Institut für Regelungstechnik  
Hans Sommer Straße 66  
D-38106 Braunschweig

*Originally published in the series:  
Electry Energy Systems and Engineering Series*

ISBN-13: 978-3-642-97648-3      e-ISBN-13: 978-3-642-97646-9  
DOI: 10.1007/978-3-642-97646-9

Die Deutsche Bibliothek - CIP-Einheitsaufnahme  
Control of electrical drives / Werner Leonhard. - 2. ed. - Berlin; Heidelberg; New York; Barcelona;  
Budapest; Hongkong; London; Milan; Paris; Santa Clara; Singapur; Tokyo: Springer, 1996

This work is subject to copyright. All rights are reserved, whether the whole or part of the material is concerned, specifically the rights of translation, reprinting, re-use of illustrations, recitation, broadcasting, reproduction on microfilms or in other ways, and storage in data banks. Duplication of this publication or parts thereof is only permitted under the provisions of the German Copyright Law of September 9, 1965, in its current version, and a copyright fee must always be paid.

© Springer-Verlag Berlin Heidelberg 1996  
Softcover reprint of the hardcover 2nd edition 1996

The use of registered names, trademarks, etc. in this publication does not imply, even in the absence of a specific statement, that such names are exempt from the relevant protective laws and regulations and therefore free for general use.

Product liability: The publishers cannot guarantee that accuracy of any information about dosage and application contained in this book. In every individual case the user must check such information by consulting the relevant literature.

Production: PRODUserv Springer Produktions-Gesellschaft, Berlin  
Typesetting: Camera ready by author  
SPIN: 10089535      61/3020 - 5 4 3 2 1 0 - Gedruckt auf säurefreiem Papier

# Preface

Electrical drives play an important role as electromechanical energy converters in transportation, material handling and most production processes. The ease of controlling electrical drives is an important aspect for meeting the increasing demands by the user with respect to flexibility and precision, caused by technological progress in industry as well as the need for energy conservation.

At the same time, the control of electrical drives has provided strong incentives to control engineering in general, leading to the development of new control structures and their introduction to other areas of control. This is due to the stringent operating conditions and widely varying specifications — a drive may alternately require control of torque, acceleration, speed or position — and the fact that most electric drives have — in contrast to chemical or thermal processes — well defined structures and consistent dynamic characteristics.

During the last few years the field of controlled electrical drives has undergone rapid expansion due mainly to the advances of semiconductors in the form of power electronics as well as analogue and digital signal electronics, eventually culminating in microelectronics and microprocessors. The introduction of electronically switched solid-state power converters has renewed the search for AC motor drives, not subject to the limitations of the mechanical commutator of DC drives; this has created new and difficult control problems. On the other hand, the fast response of electronic power switching devices and their limited overload capacity have made the inclusion of protective control functions essential. The present phase of evolution is likely to continue for many more years; a new steady-state is not yet in sight.

This book, in its original form published 1974 in German, was an outcome of lectures the author held for a number of years at the Technical University Braunschweig. In its updated English version it characterises the present state of the art without laying claim to complete coverage of the field. Many interesting details had to be omitted, which is not necessarily a disadvantage since details are often bound for early obsolescence. In selecting and presenting the material, didactic view points have also been considered.

A prerequisite for the reader is a basic knowledge of power electronics, electrical machines and control engineering, as taught in most under-graduate electrical engineering courses; for additional facts, recourse is made to special literature. However, the text should be sufficiently self contained to be useful

also for non-experts wishing to extend or refresh their knowledge of controlled electrical drives.

These drives consist of several parts, the electrical machine, the power converter, the control equipment and the mechanical load, all of which are dealt with in varying depths. A brief resume of mechanics and of thermal effects in electrical machines is presented in Chaps. 1 – 4 which would be skipped by the more experienced reader. Chaps. 5 – 9 deal with DC drives which have for over a century been the standard solution when controlled drives were required. This part of the text also contains an introduction to line-commutated converters as used for the supply of DC machines. AC drives are introduced in Chap.10, beginning with a general dynamic model of the symmetrical AC motor, valid in both the steady-state and transient condition. This is followed in Chap.11 by an overview of static converters to be employed for AC drives. The control aspects are discussed in Chaps. 12 – 14 with emphasis on high dynamic performance drives, where microprocessors are proving invaluable in disentangling the multivariate interactions present in AC machines. Chapter 15 finally describes some of the problems connected with the industrial application of drives. This cannot by any means cover the wide field of special situations with which the designer is confronted in practice but some more frequent features of drive system applications are explained there. It will become sufficiently clear that the design of a controlled drive, in particular at larger power ratings, cannot stop at the motor shaft but often entails an analysis of the whole electro-mechanical system.

In view of the fact that this book is an adaptation and extension of an application-orientated text in another language, there are inevitably problems with regard to symbols, the drawing of circuit diagrams etc. After thorough consultations with competent advisors and the publisher, a compromise solution was adopted, using symbols recommended by IEE wherever possible, but retaining the authors usage where confusion would otherwise arise with his readers at home. A list of the symbols is compiled following the table of contents. The underlying principle employed is that time varying quantities are usually denoted by lower case latin letters, while capital letters are applied to parameters, average quantities, phasors etc; greek letters are used predominantly for angles, angular frequencies etc. A certain amount of overlap is unavoidable, since the number of available symbols is limited. Also the bibliography still exhibits a strong continental bias, even though an attempt has been made to balance it with titles in english language. The list is certainly by no means complete but it contains the information readily available to the author. Direct references in the text have been used sparingly. Hopefully the readers are willing to accept these shortcomings with the necessary patience and understanding.

The author wishes to express his sincere gratitude to two English colleagues, R. M. Davis of Nottingham University and S. R. Bowes of the University of Bristol who have given help and encouragement to start the work of updating and translating the original German text and who have spent considerable time and effort in reviewing and improving the initial rough translation; without their

assistance the work could not have been completed. Anyone who has undertaken the task of smoothing the translation of a foreign text can appreciate how tedious and time-consuming this can be. Thanks are also due to the editors of this Springer Series, Prof. J. G. Kassakian and Prof. D. H. Naunin, and the publisher for their cooperation and continued encouragement.

Braunschweig, October 1984

Werner Leonhard

## Preface to the 2nd edition

During the past 10 years the book on Control of Electrical Drives has found its way onto many desks in industry and universities all over the world, as the author has noticed on numerous occasions. After a reprinting in 1990 and 1992, where errors had been corrected and a few technical updates made, the book is now appearing in a second revised edition, again with the aim of offering to the readers perhaps not the latest little details but an updated general view at the field of controlled electrical drives, which are maintaining and extending their position as the most flexible source of controlled mechanical energy.

The bibliography has been considerably extended but in view of the continuous stream of high quality publications, particularly in the field of controlled AC drives, the list is still far from complete.

As those familiar with word processing will recognise, the text and figures are now produced as a data set on the computer. This would not have been possible without the expert help by Dipl.- Ing. Hendrik Klaassen, Dipl.- Math. Petra Heinrich, as well as Dr.-Ing. Rüdiger Reichow, Dipl.-Ing. Marcus Heller, Mrs. Jutta Stich and Mr. Stefan Brix, to whom the author wishes to express his sincere gratitude. The final layout remained the task of the publishers, whose patience and helpful cooperation is gratefully appreciated.

Braunschweig, May 1996

Werner Leonhard

# Table of Contents

1	Elementary Principles of Mechanics . . . . .	5
1.1	Newton's Law . . . . .	5
1.2	Moment of Inertia . . . . .	7
1.3	Effect of Gearing . . . . .	9
1.4	Power and Energy . . . . .	10
1.5	Experimental Determination of Inertia . . . . .	11
2	Dynamics of a Mechanical Drive . . . . .	15
2.1	Equations Describing the Motion of a Drive with Lumped Inertia . . . . .	15
2.2	Two Axes Drive in Polar Coordinates . . . . .	18
2.3	Steady State Characteristics of Different Types of Motors and Loads . . . . .	20
2.4	Stable and Unstable Operating Points . . . . .	23
3	Integration of the Simplified Equation of Motion . . . . .	27
3.1	Solution of the Linearised Equation . . . . .	27
3.1.1	Start of a Motor with Shunt-type Characteristic at No-load . . . . .	28
3.1.2	Starting the Motor with a Load Torque Proportional to Speed . . . . .	30
3.1.3	Loading Transient of the Motor Running at No-load Speed . . . . .	30
3.1.4	Starting of a DC Motor by Sequentially Shortcircuiting Starting Resistors . . . . .	32
3.2	Analytical Solution of Nonlinear Differential Equation . . . . .	35
3.3	Numerical and Graphical Integration . . . . .	36
4	Thermal Effects in Electrical Machines . . . . .	41
4.1	Power Losses and Temperature Restrictions . . . . .	41
4.2	Heating of a Homogeneous Body . . . . .	42
4.3	Different Modes of Operation . . . . .	45
4.3.1	Continuous Duty . . . . .	46
4.3.2	Short Time Intermittent Duty . . . . .	46
4.3.3	Periodic Intermittent Duty . . . . .	47

X Table of Contents

5	Separately Excited DC Machine . . . . .	49
5.1	Introduction . . . . .	49
5.2	Differential Equations and Block Diagram . . . . .	52
5.3	Steady State Characteristics with Armature and Field Control . . . . .	54
5.3.1	Armature Control . . . . .	55
5.3.2	Field Control . . . . .	56
5.3.3	Combined Armature and Field Control . . . . .	58
5.4	Dynamic Behaviour of DC Motor at Constant Flux . . . . .	61
6	DC Motor with Series Field Winding . . . . .	67
6.1	Block Diagram of a Series-wound Motor . . . . .	67
6.2	Steady State Characteristics . . . . .	70
7	Control of a Separately Excited DC Machine . . . . .	75
7.1	Introduction . . . . .	75
7.2	Cascade Control of DC Motor in the Armature Control Range . . . . .	77
7.3	Cascade Control of DC Motor in the Field-weakening Region . . . . .	87
7.4	Supplying a DC Motor from a Rotating Generator . . . . .	89
8	The Static Converter as Power Actuator for DC Drives . . . . .	95
8.1	Electronic Switching Devices . . . . .	95
8.2	Line-commutated Converter in Single-phase Bridge Connection . . . . .	99
8.3	Line-commutated Converter in Three-phase Bridge Connection . . . . .	115
8.4	Line-commutated Converters with Reduced Reactive Power . . . . .	125
8.5	Control Loop Containing an Electronic Power Converter . . . . .	127
9	Control of Converter-supplied DC Drives . . . . .	135
9.1	DC Drive with Line-commutated Converter . . . . .	135
9.2	DC Drives with Force-commutated Converters . . . . .	144
10	Symmetrical Three-Phase AC Machines . . . . .	155
10.1	Mathematical Model of a General AC Machine . . . . .	156
10.2	Induction Motor with Sinusoidal Symmetrical Voltages . . . . .	168
10.2.1	Stator Current, Current Locus . . . . .	168
10.2.2	Steady State Torque, Efficiency . . . . .	173
10.2.3	Comparison with Practical Motor Designs . . . . .	178
10.2.4	Starting of the Induction Motor . . . . .	178
10.3	Induction Motor with Impressed Voltages of Arbitrary Waveforms	181
10.4	Induction Motor with Unsymmetrical Line Voltages in steady State	192
10.4.1	Symmetrical Components . . . . .	192
10.4.2	Single-phase Induction Motor . . . . .	196
10.4.3	Single-phase Electric Brake for AC Crane-Drives . . . . .	198
10.4.4	Unsymmetrical Starting Circuit for Induction Motor . . . . .	200

11	Power Supplies for Adjustable Speed AC Drives . . . . .	205
11.1	PWM Voltage Source Transistor Inverter . . . . .	208
11.2	PWM Thyristor Converters with Constant Direct Voltage Supply	214
11.3	Thyristor Converters with Impressed Direct Current Supply . .	221
11.4	Converter Without DC Link (Cycloconverter) . . . . .	225
12	Control of Induction Motor Drives . . . . .	229
12.1	Control of Induction Motor Based on Steady State Machine Model	230
12.2	Rotor Flux Orientated Control of Current-fed Induction Motor .	240
12.2.1	Principle of Field Orientation . . . . .	240
12.2.2	Acquisition of Flux Signals . . . . .	247
12.2.3	Effects of Residual Lag of the Current Control Loops . .	249
12.2.4	Digital Signal Processing . . . . .	252
12.2.5	Experimental Results . . . . .	257
12.2.6	Effects of a Detuned Flux Model . . . . .	257
12.3	Rotor Flux Orientated Control of Voltage-fed Induction Motor .	262
12.4	Control of Induction Motor with a Current Source Inverter . .	266
12.5	Control of an Induction Motor Without a Mechanical Sensor .	273
12.5.1	Machine Model in Stator Flux Coordinates . . . . .	273
12.5.2	A possible Principle of “Encoderless Control” . . . . .	277
12.5.3	Simulation and Experimental Results . . . . .	280
12.6	Control of an Induction Motor Using a Combined Flux Model .	283
13	Induction Motor Drive with Restricted Speed Range . . . . .	287
13.1	Doubly-fed Induction Machine . . . . .	287
13.2	Wound Rotor Induction Motor with Slip-Power Recovery . . .	300
14	Variable Frequency Synchronous Motor Drives . . . . .	307
14.1	Control of Synchronous Motors with PM Excitation . . . . .	309
14.2	Control of Synchronous Motors with Supply by Cycloconverter .	318
14.3	Synchronous Motor with Load-commutated Inverter . . . . .	325
15	Some Applications of Controlled Drives . . . . .	335
15.1	Speed Controlled Drives . . . . .	336
15.2	Linear Position Control . . . . .	345
15.3	Linear Position Control with Moving Target Point . . . . .	354
15.4	Time-optimal Position Control with Fixed Target Point . . . .	360
15.5	Time-optimal Position Control with Moving Target Point . . .	365
	Bibliography . . . . .	373
	Index . . . . .	415

# Abbreviations and Symbols

## 1. Equations

All equations comprise physical variables, described by the product of a unit and a dimensionless number, which depends on the choice of the unit.

Some variables are nondimensional due to their nature or because of normalisation (p.u.).

## 2. Characterisation by Style of Writing

$i(t)$ , $u(t)$ , etc.	instantaneous values
$\bar{i}$ , $\bar{I}_d$ , $\bar{u}$ , $\bar{U}_d$ , etc.	average values
$I$ , $U$ , etc.	RMS-values
$\underline{I}$ , $\underline{U}$ , etc.	complex phasors for sinusoidal variables
$\underline{i}(t)$ , $\underline{u}(t)$ , etc.	complex time-variable vectors, used with multi-phase systems
$i^*(t)$ , $u^*(t)$ , $I^*$ , $U^*$ , etc.	conjugate complex vectors or phasors
${}^1\underline{i}(t)$ , ${}^1\underline{u}(t)$ , etc.	vectors in special coordinate systems
$I(s) = \underline{L}(i(t))$ etc.	Laplace transforms

## 3. Symbols

Abbreviation	Variable	Unit
$a(t)$	– current distribution – linear acceleration – nondimensional factor	A/m $\text{m/s}^2$
$A$	area	$\text{m}^2$
$b$	nondimensional field factor	
$B$	magnetic flux density	T
$C$	– electrical capacity – thermal storage capacity	F $\text{J/}^\circ\text{C} = \text{Ws/}^\circ\text{C}$
$D$	damping ratio	
$e(t)$ , $E$ , $\underline{E}$	induced voltage, e.m.f.	V

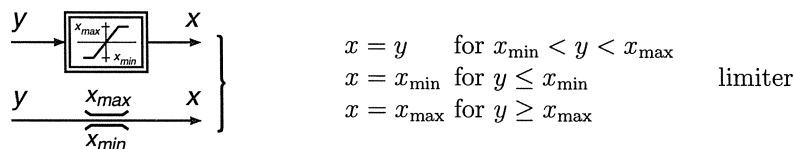
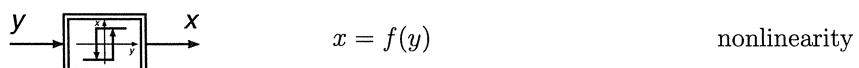
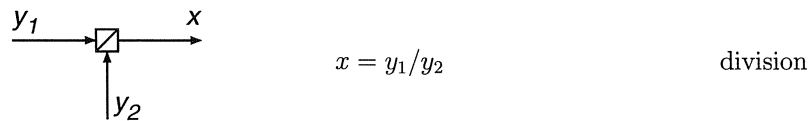
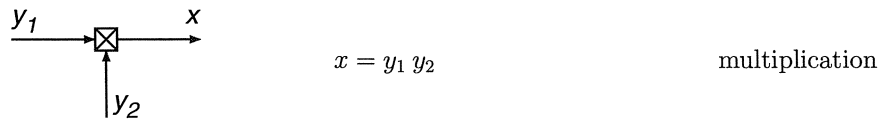
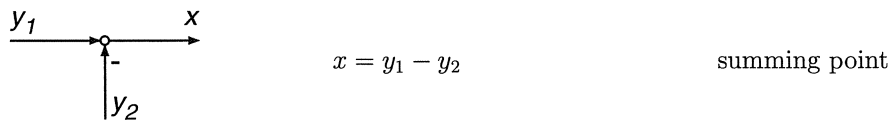
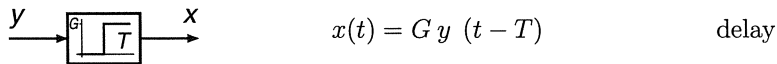
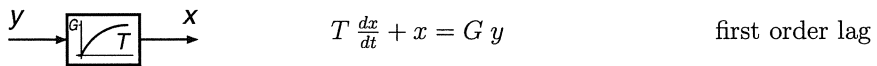
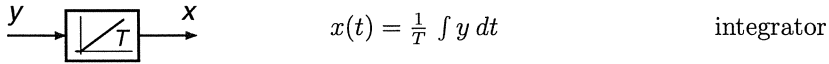
$f$	- frequency	Hz = 1/s
	- force	N
$F(s)$	transfer function	
$g$	gravitational constant	m/s <sup>2</sup>
$g(t)$	unit impulse response	
$G$	- weight	N
	- gain	
$h$	airgap	m
$i(t), I, \underline{I}$	current	A
$J$	inertia	kg m <sup>2</sup>
$k$	nondimensional factor	
$K$	torsional stiffness	Nm/rad
$l$	length	m
$L$	inductance	H
$m(t)$	torque	Nm
$M$	- mass	kg
	- mutual inductance	H
$n$	speed, rev/min	1/min
$N$	number of turns	
$p(t), P$	power	W
$Q$	reactive power	VA
$r$	radius	m
$R$	resistance	$\Omega$
$s = \sigma + j\omega$	Laplace variable	rad/s
$s, x$	distance	m
$S$	slip	
$t$	time	s
$T$	time constant	s
$u(t), U, \underline{U}$	voltage	V
$v(t)$	- velocity	m/s
	- unit ramp response	
$V$	volume	m <sup>3</sup>
$w(t)$	- unit step response	
	- energy	J = Ws
$x$	control variable	
$y$	actuating variable	
$z$	disturbance variable	
$z = e^{sT}$	discrete Laplace variable	
$Y$	admittance	$1/\Omega = S$
$Z$	impedance	$\Omega$
$\alpha$	- coefficient of heat transfer	W/m <sup>2</sup> °C
	- firing angle	
	- angular acceleration	
$\alpha, \beta, \delta, \zeta, \xi, \lambda, \mu, \varrho$ etc.	angular coordinates	rad
$\gamma = 2\pi/3$		

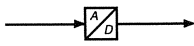
$\delta$	load angle	rad
$\Delta$	difference operator	
$\varepsilon$	angle of rotation	rad
$\kappa$	coupling factor	
$\eta$	efficiency	
$\vartheta$	temperature	°C
$\Theta$	absolute temperature	K
$\mu_0$	magnetomotive force, m.m.f.	A
$\nu$	coefficient of permeability	H/m
$\sigma$	integer number	
$\tau = \int \omega dt, \omega t$	leakage factor	
$\varphi$	normalised time, angle	rad
$\cos \varphi$	phase shift	rad
$\Phi$	power factor	
$\psi$	magnetic flux	Wb = Vs
$\omega$	flux linkage	Wb = Vs
	angular frequency	rad/s

#### 4. Indices

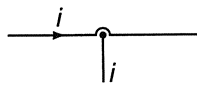
$i_a$	armature current
$i_e$	exciting current
$u_F$	field voltage
$i_S$	stator current
$i_R$	rotor current
$i_{Sd}, i_{Sq}$	direct and quadrature components of stator current
$i_{Rd}, i_{Rq}$	direct and quadrature components of rotor current
$i_m$	magnetising current
$i_{mR}$	magnetising current representing rotor flux
$i_{mS}$	magnetising current representing stator flux
$m_M$	motor torque
$m_L$	load torque
$m_p$	pull-out torque
$S_p$	pull-out slip

## 5. Graphical Symbols

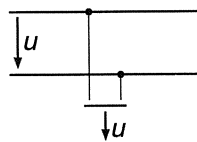




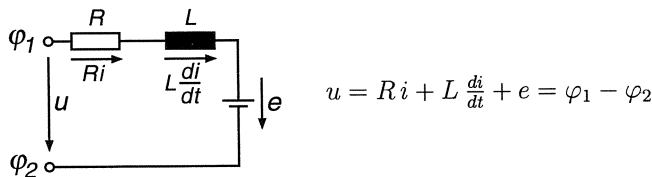
A/D- or D/A-  
converter



current sensor



voltage sensor



The voltage arrows indicating voltage sources ( $u, e$ ) or voltage drops ( $R i, L \frac{di}{dt}$ ) represent the differences of electrical potential, pointing from the higher to the lower assumed potential. Hence the voltages in any closed mesh have zero sum,  $\sum u = 0$ .

# Introduction

Energy is the basis of any technical and industrial development. As long as only human and animal labour is available, a main prerequisite for social progress and general welfare is lacking. The energy consumption per capita in a country is thus an indicator of its state of technical development, exhibiting differences of more than two orders of magnitude between highly industrialised and not yet developed countries.

In its primary form, energy is widely distributed (fossil and nuclear fuels, hydro and tidal energy, solar and wind energy, geothermal energy etc.), but it must be developed and made available at the point of consumption in suitable form, for example chemical, mechanical or thermal, and at an acceptable price. This creates problems of transporting the energy from the place of origin to the point of demand and of converting it into its final physical form. In many cases, these problems are best solved with an electrical intermediate stage, Fig. 0.1, because electricity can be

- generated from primary energy (chemical energy in fossil fuel, potential hydro energy, nuclear energy) in relatively efficient central generating stations,
- transported with low losses over long distances and distributed simply and at acceptable cost,
- converted into any final form at the point of destination.

This flexibility is unmatched by any other form of energy. Of particular importance is the mechanical form of energy which is needed in widely varying power ratings wherever physical activities take place, involving the transportation of goods and people or industrial production processes. For this final conversion at the point of utilisation, electro-mechanical devices in the form of electrical drives are well suited; it is estimated, that about half the electricity generated in an industrial country is eventually converted to mechanical energy. Most electrical motors are used in constant- speed drives that do not need to be controlled except for starting, stopping or protection, but there is a smaller portion, where torque and speed must be matched to the need of the mechanical load; this is the topic of this book. Due to the progress of automation and with a view to energy conservation, the need for control is likely to become more important in future.

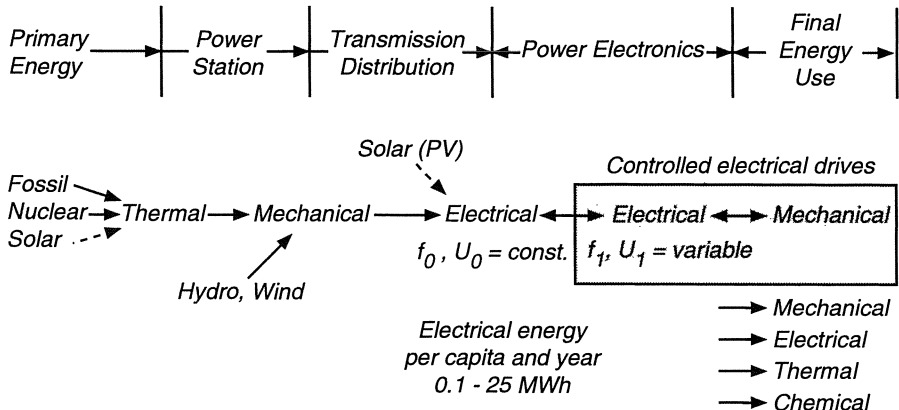
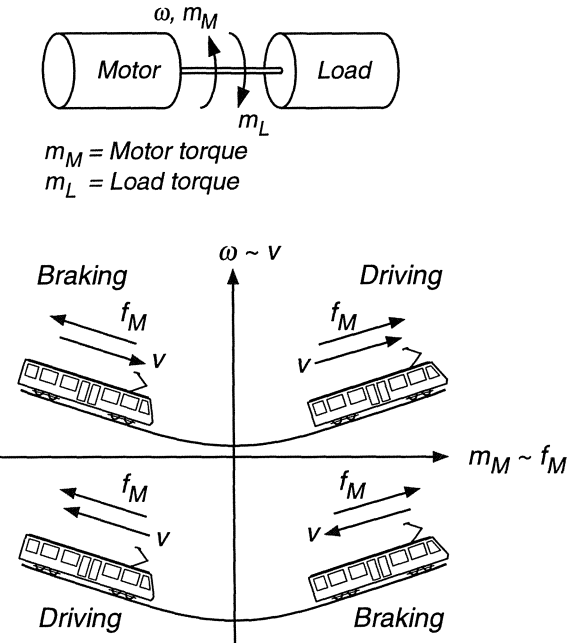


Fig. 0.1. From primary energy to final use, a chain of conversion processes

The predominance of electrical drives is caused by several aspects:

- Electric drives are available for any power, from  $10^{-6}$  W in electronic watches to  $> 10^8$  W for driving pumps in hydro storage plants.
- They cover a wide range of torque and speed,  $> 10^7$  Nm, for an ore mill motor,  $> 10^5$  1/min, for a centrifuge drive.
- Electric drives are adaptable to almost any operating conditions such as forced air ventilation or totally enclosed, submerged in liquids, exposed to explosive or radioactive environments. Since electric motors do not require hazardous fuels and do not emit exhaust fumes, electrical drives have no detrimental effect on their immediate environment. The noise level is low compared, for instance, with combustion engines.
- Electric drives are operable at a moment's notice and can be fully loaded immediately. There is no need to refuel, nor warm-up the motor. The service requirements are very modest, as compared with other drives.
- Electrical motors have low no-load losses and exhibit high efficiency; they normally have a considerable short-time overload capacity.
- Electrical drives are easily controllable. The steady state characteristics can be reshaped almost at will, so that railway traction motors do not require speed-changing gears. High dynamic performance is achieved by electronic control.
- Electrical drives can be designed to operate indefinitely in all four quadrants of the torque-speed-plane without requiring a special reversing gear (Fig. 0.2). During braking, i.e. when operating in quadrants 2 or 4, the

drive is normally regenerating, feeding power back to the line. A comparison with combustion engines or turbines makes this feature look particularly attractive.



**Fig. 0.2.** Operating modes of an electric drive

- The rotational symmetry of electrical machines and (with most motors) the smooth torque results in quiet operation with little vibrations. Since there are no elevated temperatures causing material fatigue, long operating life can be expected.
- Electrical motors are built in a variety of designs to make them compatible with the load; they may be foot- or flange-mounted, or the motor may have an outer rotor etc. Machine-tools which formerly had a single drive shaft and complicated mechanical internal gearing can now be driven by a multitude of individually controlled motors producing the mechanical power exactly where, when and in what form it is needed. This has removed constraints from machine tool designers.  
In special cases, such as machine-tools or the propulsion of tracked vehicles, linear electric drives are also available.

As would be expected, this long list of remarkable characteristics is to be supplemented by disadvantages of electric drives which limit or preclude their use:

- The dependance on a continuous power supply causes problems with vehicle propulsion. If a power rail or catenary is unavailable, an electric energy source must be carried on-board, which is usually bulky, heavy and expensive (storage battery, rotating generator with internal combustion engine or turbine, fuel- or solar cells). The lack of a suitable storage battery has so far prevented the wide-spread use of electric vehicles. The weight of a present day lead-acid battery is about 50 times that of a liquid fuel tank storing equal energy, even when taking the low efficiency of the combustion engine into account.
- Due to the magnetic saturation of iron and cooling problems, electric motors are likely to have a lower power-to-weight ratio than high pressure hydraulic drives that utilise normal instead of tangential forces. This is of importance with servo drives on-board vehicles, e.g. for positioning the control surfaces of aircraft.

# 1. Some Elementary Principles of Mechanics

Since electrical drives are linking mechanical and electrical engineering, let us recall some basic laws of mechanics.

## 1.1 Newtons Law

A mass  $M$  is assumed, moving on a straight horizontal track in the direction of the  $s$ -axis (Fig. 1.1 a). Let  $f_M(t)$  be the driving force of the motor in the direction of the velocity  $v$  and  $f_L(t)$  the load force opposing the motion, then Newtons law holds

$$f_M - f_L = \frac{d}{dt} (Mv) = M \frac{dv}{dt} + v \frac{dM}{dt}, \quad (1.1)$$

where  $Mv$  is the mechanical momentum.

Usually the forces are dependent on velocity  $v$  and position  $s$ , such as gravitational or frictional forces.

If the mass is constant,  $M = M_0 = \text{const.}$ , Eq. (1.1) is simplified

$$f_M - f_L = M_0 \frac{dv}{dt}; \quad (1.2)$$

with the definition of velocity  $v = ds/dt$ , this results in a second order differential equation for the displacement,

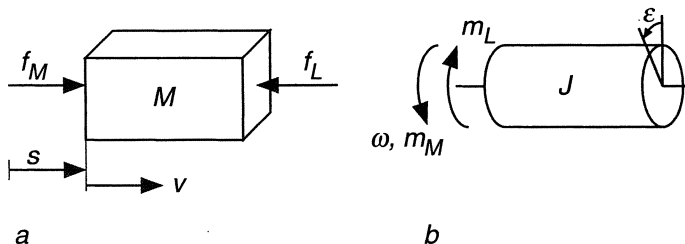


Fig. 1.1. Translational and rotational motion of lumped masses

$$f_M - f_L = M_0 \frac{d^2 s}{dt^2}, \quad (1.3)$$

where

$$a = \frac{dv}{dt} = \frac{d^2 s}{dt^2} \quad (1.4)$$

is the acceleration. If the motion is rotational, which is usually the case with electrical drives, there are analogous equations (Fig. 1.1 b),

$$m_M - m_L = \frac{d}{dt} (J\omega) = J \frac{d\omega}{dt} + \omega \frac{dJ}{dt}, \quad (1.5)$$

with  $m_M$  being the driving- and  $m_L$  the load torque.  $\omega = 2\pi n$  is the angular velocity, in the following called speed.  $J$  is the moment of inertia of the rotating mass about the axis of rotation,  $J\omega$  is the angular momentum. The term  $\omega(dJ/dt)$  is of significance with variable inertia drives such as centrifuges or reeling drives, where the geometry of the load depends on speed or time, or industrial robots with changing geometry. In most cases however, the inertia can be assumed to be constant,  $J = J_0 = \text{const.}$ ; hence

$$m_M - m_L = J_0 \frac{d\omega}{dt}. \quad (1.6)$$

With  $\varepsilon$  the angle of rotation and  $\omega = d\varepsilon / dt$  the angular velocity, we have

$$m_M - m_L = J_0 \frac{d^2 \varepsilon}{dt^2}, \quad (1.7)$$

where

$$\alpha = \frac{d\omega}{dt} = \frac{d^2 \varepsilon}{dt^2}, \quad (1.8)$$

is the angular acceleration.

It should be noted that  $m_M$  is the internal or electrical motor torque, not identical with the torque available at the motor shaft. The difference between internal torque and shaft torque is the torque required for accelerating the inertia of the motor itself and overcoming the internal friction torque of the motor.

Translational and rotational motions are often combined, for example in vehicle propulsion, elevator- or rolling mill-drives. Figure 1.2 shows a mechanical model, where a constant mass  $M$  is moved with a rope and pulley; when neglecting the mass of the pulley and with

$$m_M = r f_M, \quad m_L = r f_L \quad \text{and} \quad v = r \omega$$

we find with  $M = \text{const.}$

$$m_M - m_L = r \frac{d}{dt} (Mv) = M r^2 \frac{d\omega}{dt}. \quad (1.9)$$

$J_e = M r^2$  represents the equivalent moment of inertia of the linearly moving mass, referred to the axis of the pulley. Apparently the mass  $M$  can be thought of as being distributed along the circumference of the wheels.

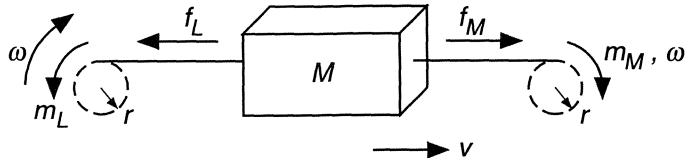


**Fig. 1.2.** Linking linear and rotational motion

## 1.2 Moment of Inertia

The moment of inertia, introduced in the preceding section, may be derived as follows:

A rigid body of arbitrary shape, having the mass  $M$ , rotates freely about a vertical axis orientated in the direction of gravity (Fig. 1.3). An element of the mass  $dM$  is accelerated in tangential direction by the force element  $df_a$ , which corresponds to an element  $dm_a$  of the accelerating torque

$$dm_a = r df_a = r dM \frac{dv}{dt} = r^2 dM \frac{d\omega}{dt} .$$

The total accelerating torque follows by integration

$$m_a = \int_0^{m_a} dm_a = \int_0^M r^2 \frac{d\omega}{dt} dM . \quad (1.10)$$

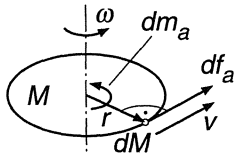


**Fig. 1.3.** Moment of inertia

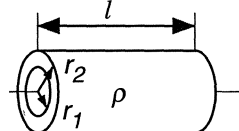


**Fig. 1.4.** Moment of inertia of concentric cylinder

Due to the assumed rigidity of the body, all its mass elements move with the same angular velocity; hence

$$m_a = \frac{d\omega}{dt} \int_0^M r^2 dM = J \frac{d\omega}{dt} . \quad (1.11)$$

The moment of inertia, referred to the axis of rotation,

$$J = \int_0^M r^2 dM \quad (1.12)$$

is a three dimensional integral. In many cases the rotating body possesses rotational symmetry; as an example, consider the hollow homogeneous cylinder with mass density  $\varrho$  (Fig. 1.4). As volume increment  $dV$  we define a thin concentric cylinder having the radius  $r$  and the thickness  $dr$ ; its mass is

$$dM = \varrho dV = \varrho 2\pi r l dr .$$

This reduces the volume integral to a simple integration along the radius

$$J = \int_0^M r^2 dM = \varrho 2\pi l \int_{r_1}^{r_2} r^3 dr = \frac{\pi}{2} \varrho l (r_2^4 - r_1^4) . \quad (1.13)$$

Hence the moment of inertia increases with the 4th power of the outer radius. Introducing the weight of the cylinder

$$G = \varrho g l \pi (r_2^2 - r_1^2) \quad (1.14)$$

results in

$$J = \frac{G}{g} \frac{r_2^2 + r_1^2}{2} = \frac{G}{g} r_i^2 , \quad (1.15)$$

where  $g$  is the gravitational acceleration. The quadratic mean of the radii

$$r_i = \sqrt{\frac{1}{2} (r_1^2 + r_2^2)} \quad (1.16)$$

is called the radius of gyration; it defines the radius of a thin concentric cylinder with length  $l$  and mass  $M$ , that has the same moment of inertia as the original cylinder.

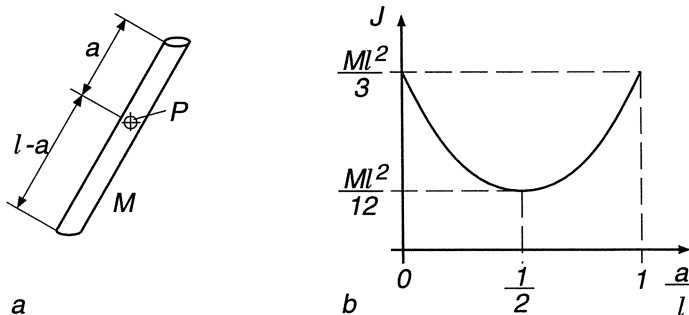


**Fig. 1.5.** Moment of inertia of a rod, pivoted out of centre

Another example is seen in Fig. 1.5 a, where a homogeneous thin rod of length  $l$  and mass  $M$  is pivoted around a point  $P$ , the distance of which from one end of the rod is  $a$ . With the mass element  $dM = (M/l) dr$  we find for the moment of inertia

$$\begin{aligned} J &= \int_0^M r^2 dM = \frac{M}{l} \left[ \int_0^a r^2 dr + \int_0^{l-a} r^2 dr \right] \\ &= \frac{M l^2}{12} \left[ 1 + 3 \left( 1 - 2 \frac{a}{l} \right)^2 \right]. \end{aligned} \quad (1.17)$$

The minimum inertia is obtained, when the rod is pivoted at the centre, Fig. 1.5 b.

### 1.3 Effect of Gearing

Many applications of electrical drives call for relatively slow motion and high torque, for instance in traction or when positioning robots. Since the tangential force per rotor surface, i.e. the specific torque of the motor, is limited by iron saturation and heat losses in the conductors, it is often preferable to employ gears, operating the motor at a higher speed and thus increasing its power density. This also affects the inertia of the coupled rotating masses.

In Fig. 1.6 an ideal gear is shown, where two wheels are engaged at the point  $P$  without friction, backlash or slip. From Newtons law it follows for the left hand wheel, assumed to be the driving wheel,

$$m_{M1} - r_1 f_1 = J_1 \frac{d\omega_1}{dt}, \quad (1.18)$$

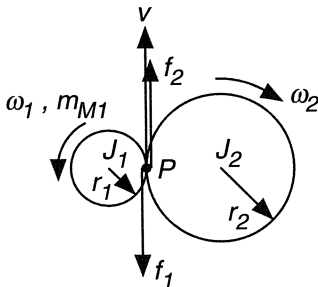


Fig. 1.6. Effect of gearing on inertia

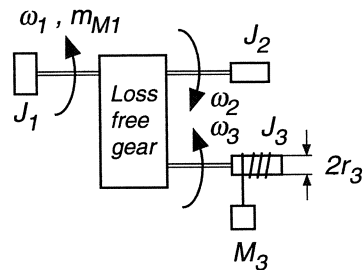


Fig. 1.7. Hoist drive with gear

where  $f_1$  is the circumferential contact force exerted by wheel 2. If there is no load torque applied we have, correspondingly, for wheel 2

$$r_2 f_2 = J_2 \frac{d\omega_2}{dt}. \quad (1.19)$$

$f_2$  is the force driving wheel 2.

Since the forces at the point of contact are in balance and the two wheels move synchronously,

$$f_1 = f_2, \quad r_1 \omega_1 = r_2 \omega_2, \quad (1.20)$$

elimination of  $f_1$ ,  $f_2$ ,  $\omega_2$  results in

$$\begin{aligned} m_{M1} &= J_1 \frac{d\omega_1}{dt} + \frac{r_1}{r_2} J_2 \frac{d\omega_2}{dt} = \left[ J_1 + \left( \frac{r_1}{r_2} \right)^2 J_2 \right] \frac{d\omega_1}{dt} \\ &= J_{1e} \frac{d\omega_1}{dt}. \end{aligned} \quad (1.21)$$

$J_{1e}$  is the moment of inertia effective at the axis of wheel 1; it contains a component reflected from wheel 2. In most cases it is easier to determine the speed ratio rather than the radii,

$$J_{1e} = J_1 + \left( \frac{\omega_2}{\omega_1} \right)^2 J_2; \quad (1.22)$$

this indicates that a rotating part, moving at higher speed, contributes more strongly to the total moment of inertia.

In Fig. 1.7 an example of a multiple gear for a hoist drive is seen.  $J_1$ ,  $J_2$ ,  $J_3$  are the moments of inertia of the different shafts. The total effective inertia referred to shaft 1 is

$$J_{1e} = J_1 + \left( \frac{\omega_2}{\omega_1} \right)^2 J_2 + \left( \frac{\omega_3}{\omega_1} \right)^2 [J_3 + M_3 r_3^2], \quad (1.23)$$

including the equivalent inertia of the mass  $M_3$  being moved in vertical direction. Applying Newtons law, taking the load of the hoist into account, results in

$$m_{M1} = J_{1e} \frac{d\omega_1}{dt} + \frac{\omega_3}{\omega_1} r_3 g M_3. \quad (1.24)$$

## 1.4 Power and Energy

The rotational motion of the mechanical arrangement shown in Fig. 1.8 is described by a first order differential equation for speed

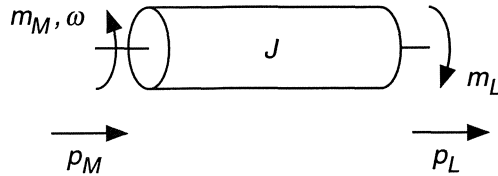
$$m_M = m_L + J \frac{d\omega}{dt}. \quad (1.25)$$

Multiplication by  $\omega$  yields the power balance

$$\omega m_M = \omega m_L + J \omega \frac{d\omega}{dt}, \quad (1.26)$$

where  $p_M = \omega m_M$  is the driving power,  $p_L = \omega m_L$  the load power and  $J \omega (d\omega/dt)$  the change of kinetic energy stored in the rotating masses.

By integrating Eq. (1.26) with the initial condition  $\omega(t=0)=0$  we find the energy input

**Fig. 1.8.** Power flow of drive

$$\begin{aligned}
 w_M(t) &= \int_0^t p_M d\tau = \int_0^t p_L d\tau + \int_0^t J \omega \frac{d\omega}{d\tau} d\tau \\
 &= \int_0^t p_L d\tau + J \int_0^\omega \Omega d\Omega \\
 &= w_L(t) + \frac{1}{2} J \omega^2.
 \end{aligned} \tag{1.27}$$

The last term represents the stored kinetic energy; the expression is analogous to

$$\frac{1}{2} M v^2, \quad \frac{1}{2} L i^2, \quad \frac{1}{2} C u^2.$$

of other energy storage devices. Since the energy content of a physical body cannot be changed instantaneously — this would require infinite power — the linear or rotational velocity of a body possessing mass must always be a continuous function of time. This is an important condition of continuity which will frequently be used.

Because of the definitions

$$v = \frac{ds}{dt} \quad \text{and} \quad \omega = \frac{d\varepsilon}{dt}$$

the positional quantities  $s$  and  $\varepsilon$  are also continuous functions of time, due to finite speed. This is also understandable from an energy point of view, since position may be associated with potential energy, as seen in Fig. 1.7, where the mass  $M_3$  is positioned vertically depending on the angle of rotation of the drive shaft.

## 1.5 Experimental Determination of Inertia

The moment of inertia of a complex inhomogeneous body, such as the rotor of an electrical machine, containing iron, copper and insulating material with complicated shapes can in practice only be determined by approximation. The problem is even more difficult with mechanical loads, the constructional details of which are usually unknown to the user. Sometimes the moment of inertia is not constant but changes periodically about a mean value, as in the case of a

piston compressor with crankshaft and connecting rods. Therefore experimental tests are preferable; a very simple one, called the run-out or coasting test, is described in the following. Its main advantage is that it can be conducted with the complete drive in place and operable, requiring no knowledge about details of the plant. The accuracy obtainable is adequate for most applications.

First the input power  $p_M(\omega)$  of the drive under steady state conditions is measured at different angular velocities  $\omega$  and with the load, not contributing to the inertia, being disconnected. From Eq. (1.26),

$$p_M = p_L + J\omega \frac{d\omega}{dt}, \quad (1.28)$$

the last term drops out due to constant speed, so that the input power  $p_M$  corresponds to the losses including the remaining load,  $p_M = p_L$ . This power is corrected by subtracting loss components which are only present during power input, such as armature copper losses in the motor. From this corrected power loss  $p'_L$  the steady-state effective load torque  $m'_L = p'_L/\omega$  is computed for different speeds; with graphical interpolation, this yields a curve  $m'_L(\omega)$  as shown in Fig. 1.9.

For the run-out test, the drive is now accelerated to some initial speed  $\omega_0$ , where the drive power is switched off, so that the plant is decelerated by the loss torque with the speed measured as a function of time,  $\omega(t)$ . Solving the equation of motion (1.25) for  $J$  results in

$$J \approx \frac{-m'_L(\omega)}{\frac{d\omega}{dt}(\omega)}, \quad m_M = 0. \quad (1.29)$$

Hence the inertia can be determined from the slope of the coasting curve, as shown in Fig. 1.9.

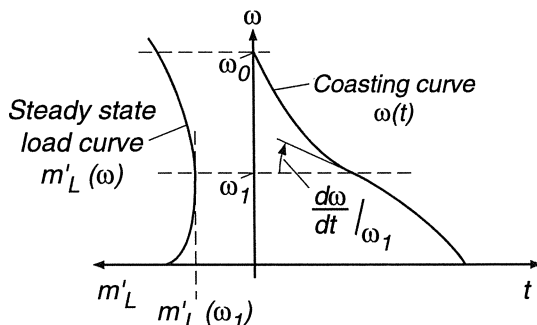


Fig. 1.9. Run-out test

Graphical constructions, particularly when a differentiation is involved, are only of moderate accuracy. Therefore the inertia should be computed at different

speeds in order to form an average. The accuracy requirements regarding inertia are modest; when designing a drive control system, an error of  $\pm 10\%$  is usually acceptable without any serious effect.

Two special cases lead to particularly simple interpretations:

- a) Assuming the corrected loss torque  $m'_L$  to be approximately constant in a limited speed interval,

$$m'_L \approx \text{const}, \quad \text{for} \quad \omega_1 < \omega < \omega_2,$$

then  $\omega(t)$  resembles a straight line; the inertia is determined from the slope of this line.

- b) If a section of the loss torque may be approximated by a straight line,

$$m'_L \approx a + b\omega, \quad \text{for} \quad \omega_1 < \omega < \omega_2.$$

a linear differential equation results,

$$J \frac{d\omega}{dt} + b\omega = -a.$$

The solution is, with  $\omega(t_2) = \omega_2$ ,

$$\omega(t) = -\frac{a}{b} + \left( \omega_2 + \frac{a}{b} \right) e^{-b(t-t_2)/J}, \quad t \geq t_2.$$

Plotting this curve on semi-logarithmic paper yields a straight line with the slope  $-b/J$ , from which an approximation of  $J$  is obtained.

## 2. Dynamics of a Mechanical Drive

### 2.1 Equations Describing the Motion of a Drive with Lumped Inertia

The equations derived in Chap. 1

$$J \frac{d\omega}{dt} = m_M(\omega, \varepsilon, y_M, t) - m_L(\omega, \varepsilon, y_L, t), \quad (2.1)$$

$$\frac{d\varepsilon}{dt} = \omega, \quad (2.2)$$

describe the dynamic behaviour of a mechanical drive with constant inertia in steady state condition and during transients. Stiff coupling between the different parts of the drive is assumed so that all partial masses may be lumped into one common inertia. The equations are written as state equations for the continuous state variables  $\omega, \varepsilon$  involving energy storage; only mechanical transients are considered. A more detailed description would have to take into account the electrical transients defined by additional state variables and differential equations. The same is true for the load torque  $m_L$  which depends on dynamic effects in the load, such as a machine tool or an elevator.

Also the control inputs  $y_M, y_L$  to the actuators on the motor and load side have to be included.

Figure 2.1 shows a block diagram, representing the interactions of the mechanical system in graphical form. The output variables of the two integrators are the continuous state variables, characterising the energy state of the system at any instant.

Linear transfer elements, such as integrators with fixed time constant, are depicted by blocks with single frames containing a figure of the step response. A block with double frame describes a nonlinear function; if it represents an instantaneous, i. e. static, nonlinearity, its characteristic function is indicated. The nonlinear blocks in Fig. 2.1 may contain additional dynamic states described by differential equations.

Dependence of the driving torque  $m_M$  on the angle of rotation is a characteristic feature of synchronous motors. However, the important quantity is not the angle of rotation  $\varepsilon$  itself but the difference angle  $\delta$  against the no-load angle  $\varepsilon_0$  which changes with time and is defined by the line voltages. Under steady state conditions this load angle  $\delta$  is constant.

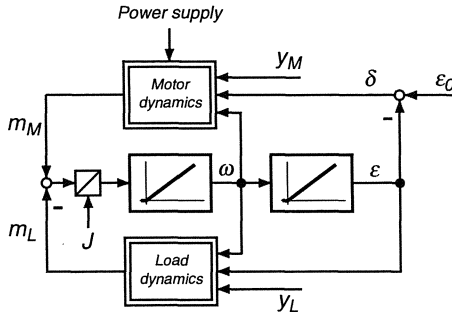


**Fig. 2.1.** Simplified block diagram of lumped inertia drive

In order to gain a better insight, let us first assume that the electrical transients within the motor and the internal load transients decay considerably faster than the mechanical transients of  $\omega$  and  $\varepsilon$ ; as a consequence, it follows that the motor and load torques  $m_M$ ,  $m_L$  are algebraic, i.e. instantaneous, functions of  $\omega$ ,  $\varepsilon$  and  $\delta$ . Hence, by neglecting the dynamics of motor and load, we arrive at a second order system that is completely described by the two state equations (2.1, 2.2).

So far we have assumed that all moving parts of the drive can be combined to form one effective inertia. However, for a more detailed analysis of dynamic effects it may be necessary to consider the distribution of the masses and the linkage between them. This leads to multi-mass-systems and in the limit to systems with continuously distributed masses, where transients of higher frequency and sometimes insufficient damping may be superimposed on the common motion.

The frequency of these free oscillations, describing the relative displacement of the separate masses against each other, increases with the stiffness of the connecting shafts; it is usually outside the frequency range of interest for control transients.

However, when the partial masses are connected by flexible linkages, such as with mine hoists, where drive and cage are connected by the long winding rope or in the case of paper mill drives with many gears, drive shafts and large rotating masses particularly in the drying section, a more detailed description becomes necessary. The free oscillations may then have frequencies of a few Hertz which are well within the range of a fast control loop.

In Fig. 2.2 an example is sketched, where the drive motor and the load having the moments of inertia  $J_1$ ,  $J_2$  are coupled by a flexible shaft with the torsional stiffness  $K$ . The ends of the shaft, the mass of which is neglected, have the angles of rotation  $\varepsilon_1$ ,  $\varepsilon_2$  and the angular velocities  $\omega_1$ ,  $\omega_2$ . Assuming a linear torsional law for the coupling torque  $m_c$ ,

$$m_c = K(\varepsilon_1 - \varepsilon_2), \quad (2.3)$$

and neglecting internal friction effects, the following state equations result

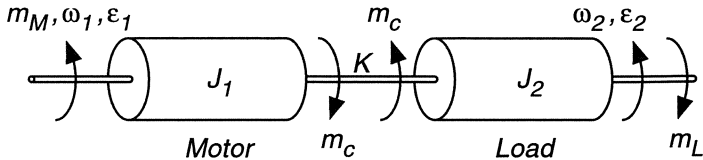


Fig. 2.2. Drive consisting of motor and load coupled by flexible shaft

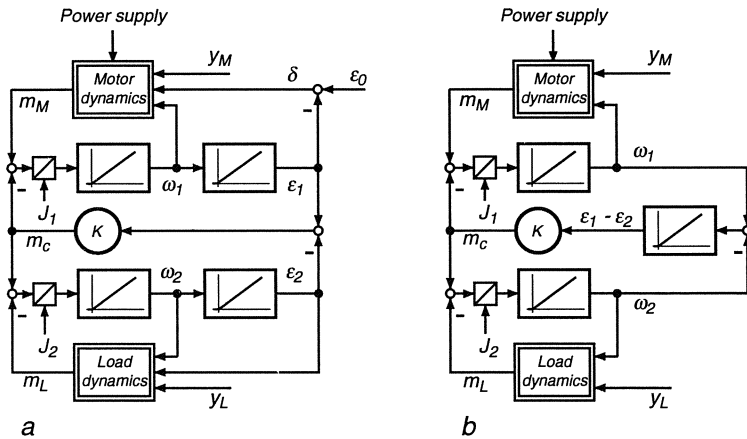


Fig. 2.3. Block diagram of twin-inertia drive with flexible shaft

$$J_1 \frac{d\omega_1}{dt} = m_M - m_c = m_M (\omega_1, \varepsilon_1, y_M) - K (\varepsilon_1 - \varepsilon_2), \quad (2.4)$$

$$J_2 \frac{d\omega_2}{dt} = m_c - m_L = K (\varepsilon_1 - \varepsilon_2) - m_L (\omega_2, \varepsilon_2, y_L), \quad (2.5)$$

$$\frac{d\varepsilon_1}{dt} = \omega_1, \quad (2.6)$$

$$\frac{d\varepsilon_2}{dt} = \omega_2. \quad (2.7)$$

A graphical representation is seen in Fig. 2.3 a. Here too, the torques \$m\_M\$, \$m\_L\$ are in reality defined by additional differential equations and state variables. If only the speeds are of interest, the block diagram in Fig. 2.3 b may be useful, which, containing three integrators, is described by a third order differential equation.

With increasing stiffness of the shaft, the quantities \$\varepsilon\_1\$, \$\varepsilon\_2\$ and \$\omega\_1\$, \$\omega\_2\$ become tighter coupled; in the limit the case of lumped inertia emerges, where \$\varepsilon\_1 = \varepsilon\_2\$, \$\omega\_2 = \omega\_1\$.

Obviously the subdivision of the inertia may be continued indefinitely; every time a new partial inertia is separated, two more state variables have to be considered, transforming Fig. 2.3 into a chainlike structure. A typical example,

where many partial masses must be taken into account for calculating stress and fatigue, is a turbine rotor.

## 2.2 Two Axes Drive in Polar Coordinates

On machine tools or robots there are normally several axes of motion, that must be independently driven or positioned. An example is seen in Fig. 2.4 a, where an arm, carrying a tool or workpiece, is rotated by an angle  $\varepsilon(t)$  around a horizontal axis. The radial distance  $r(t)$  from the axis to the center of the mass  $M_2$  represents a second degree of freedom, so that  $M_2$  can be positioned in polar coordinates in a plane perpendicular to the axis. The rotary and radial motions are assumed to be driven by servo motors, producing a controlled driving torque  $m_M$  and a driving force  $f_M$  through a rotary gear and a rotary to translational mechanical converter, for instance a lead screw. For simplicity, the masses are assumed to be concentrated in the joints, resulting in the inertias  $J_1, J_2$ . The coupling terms of the motion can be derived by expressing the acceleration of the mass  $M_2$  in complex form.

$$\frac{dr}{dt} = \frac{d}{dt} (r e^{j\varepsilon}) = (v + j r \omega) e^{j\varepsilon}, \quad (2.8)$$

$$\frac{d^2r}{dt^2} = \frac{d^2}{dt^2} (r e^{j\varepsilon}) = \left( \frac{dv}{dt} - \omega^2 r \right) e^{j\varepsilon} + j \left( 2\omega v + r \frac{d\omega}{dt} \right) e^{j\varepsilon}, \quad (2.9)$$

where  $\omega = d\varepsilon/dt$  and  $v = dr/dt$  are the rotational and radial velocities. After separating the terms of acceleration in tangential and radial direction and superimposing frictional and gravitational components, Newtons law is applied in both directions, resulting in the equations for the mechanical motion of the centre  $M_2$

$$\overbrace{(J_1 + J_2 + M_2 r^2)}^J \frac{d\omega}{dt} = m_M - \overbrace{2 M_2 r \omega v}^{\text{Coriolis}} - \overbrace{M_2 \dot{g} r \cos \varepsilon}^{\text{Gravitation}} - m_F - m_L, \quad (2.10)$$

$$\frac{d\varepsilon}{dt} = \omega, \quad (2.11)$$

$$M_2 \frac{dv}{dt} = f_M + \overbrace{M_2 r \omega^2}^{\text{Centrifugal}} - \overbrace{M_2 g \sin \varepsilon}^{\text{Gravitation}} - f_F - f_L, \quad (2.12)$$

$$\frac{dr}{dt} = v. \quad (2.13)$$

Clearly, the two motions are nonlinearly coupled though gravitational, Coriolis- and centrifugal effects; they are described by four nonlinear state equations.  $m_F, f_F$  and  $m_L, f_L$  are due to friction and external load forces with may exhibit their own complicated geometric or dynamic dependencies. If it is

important for the application to express the position of mass  $M_2$  in cartesian coordinates, this is achieved by a polar–cartesian conversion

$$x(t) = r \cos \varepsilon, \quad (2.14)$$

$$y(t) = r \sin \varepsilon. \quad (2.15)$$

The equations (2.10) – (2.13) are depicted in Fig. 2.4 b in the graphical form of a block diagram, containing four integrators for the state variables.

Despite the simple mechanics, there are complicated interactions, which increase with the rotary and radial velocities. The control of this mechanical structure is dealt with in a later chapter.

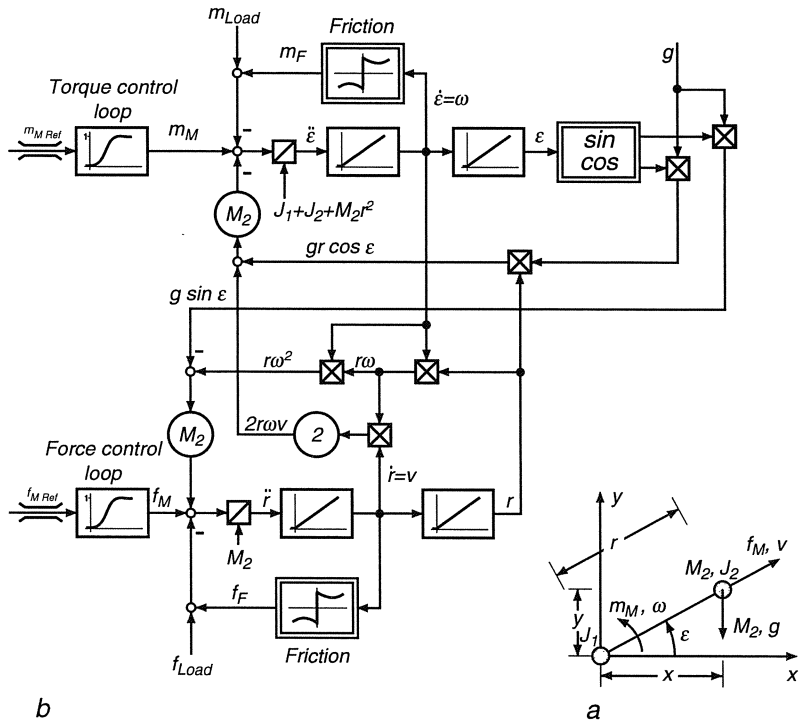


**Fig. 2.4.** Two axes drive in polar coordinates  
a) Mechanical plant b) Block diagram

Moving the arm in the direction of the axis of rotation, so that the mass  $M_2$  can be positioned in cylindrical coordinates, would introduce a third decoupled degree of freedom.

The dynamic interactions for a general motion, involving six degrees of freedom (three for the position, three for the orientation of the tool) are exceedingly complex, but they must be dealt with when controlling the motions of multi-axes robots with high dynamic performance.

## 2.3 Steady State Characteristics of Different Types of Motors and Loads

Consider first the steady state condition, when the torque and speed are constant and the angle changes linearly with time; this condition is reached when  $m_M - m_L = 0$ . With some motors, such as single phase induction motors, or loads, for example piston compressors or punches, the torque is a periodic function of the angle of rotation; in this case, the steady state condition is reached, when the mean values of both torques are equal,  $\bar{m}_M - \bar{m}_L = 0$ . The speed then contains periodic oscillations, which must be kept within limits by a sufficiently large inertia.

The steady state characteristics of a motor or load are often functions given in graphical form, connecting main variables, such as speed and torque; the provision is that auxiliary or control inputs, for example supply voltage, field current, firing angle, brush position or feed rate, are maintained constant. In Fig. 2.5 a, three typical characteristics of electric motors are shown. The "synchronous" characteristic is only valid for constant speed, since the variable is the load angle  $\delta$ , i. e. the displacement of the angular position of the shaft from its no-load position. When the maximum torque is exceeded, the motor falls out of step; asynchronous operation of larger motors is not allowed for extended periods of time because of the high currents and pulsating torque. The electrical transients usually cannot be neglected with synchronous motor drives.

The rigid speed of synchronous motors when supplied by a constant frequency source makes them suitable for few applications only, for example large slow-speed drives for reciprocating compressors or synchronous generators operating as motors in pumped storage hydropower stations; at the other extreme end of the power scale are synchronous electric clocks. The situation is different, when the synchronous motor is fed from a variable frequency inverter because then the speed of the drive can be varied freely. With the progress of power electronics, these drives are becoming more widely used (Chap. 14).

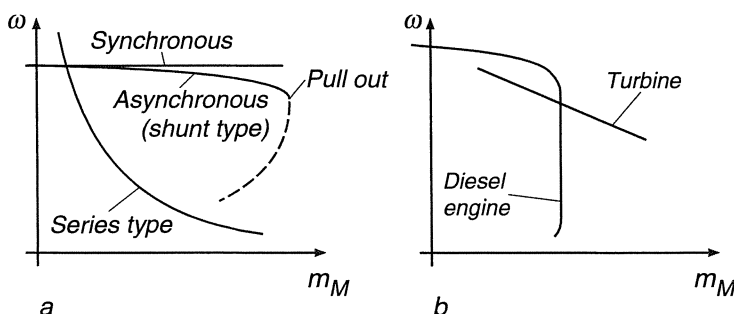


**Fig. 2.5.** Steady state torque–speed characteristics of  
a) electrical and b) mechanical drives

The "asynchronous" or "shunt-type" characteristic in Fig. 2.5 is slightly drooping; often there is also a pronounced maximum torque. The lower portion of the curve is forbidden in steady state due to the high losses. With three-phase asynchronous motors the rotor angle has no effect on the torque in steady state.

Motors with "series"-type characteristic show considerably larger speed drop under load; with DC or AC commutator motors, this is achieved by suitable connection of the field winding. The main area of applications at larger ratings is with traction drives because the curved characteristic resembling a hyperbola facilitates load sharing on multiple drives and permits nearly constant power operation over a wide speed range without gear changing; this is particularly suited to a Diesel-electric or turbo-electric drive, where the full power of the thermal engine must be used.

For comparison, some typical characteristics of a turbine and a Diesel engine at constant valve position or fuel per stroke, respectively, are seen in Fig. 2.5 b.

The curves in Fig. 2.5 a are "natural" characteristics which can be modified at will by different control inputs, e. g. through the power supply. With closed loop control a shunt motor could be given the behaviour of a synchronous or of a series type motor. As an example, typical steady state curves of a controlled DC drive are shown in Fig. 2.6; they consist of a constant speed branch (normal operation) which is joined at both ends by constant torque sections activated under overload condition through current limit. Figure 2.7 depicts the steady state curves of the motor for driving a coiler. If the electrical power reference is determined by the feed velocity  $v$  of the web or strip to be wound and includes the friction torque, the coiler operates with constant web force  $f$  independent of the radius  $r$  of the coil,  $p_L = vf + p_F$ .

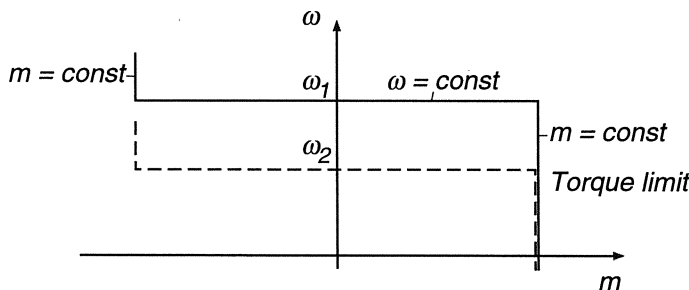


**Fig. 2.6.** Torque- speed curves of controlled motor with constant speed branch and torque limit

The steady state characteristics of mechanical loads are of even greater variety; however, they are often composed of simple elements. This is seen in Fig. 2.8 with the example of a hoist and a vehicle drive. The gravitational lift torque  $m_L$  is independent of speed (Fig. 2.8 c); in the first quadrant the load is raised, increasing its potential energy, hence the drive must operate in the motoring region. In the fourth quadrant, the power flow is reversed with the

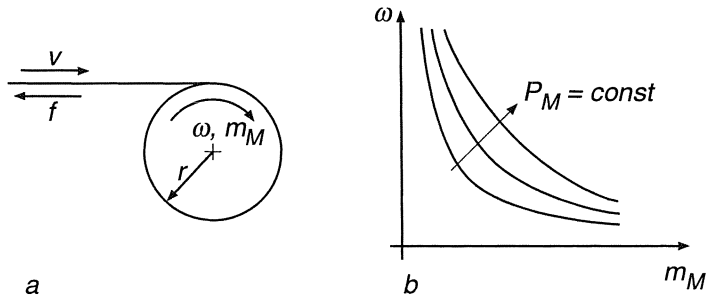


Fig. 2.7. Coiler drive

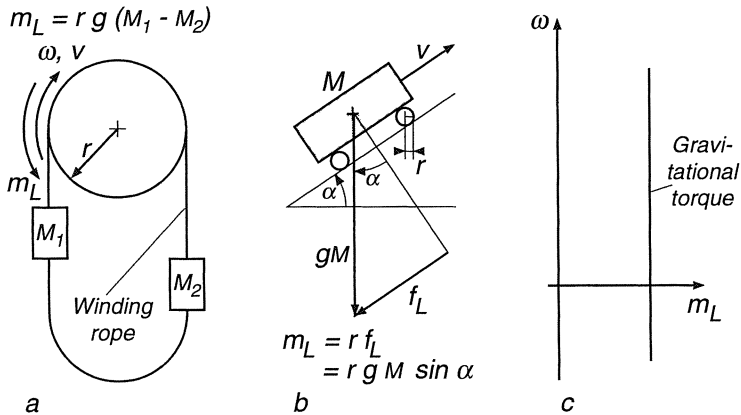


Fig. 2.8. Drives involving gravitational forces

load releasing some of its potential energy. Part of that power is flowing back to the line, the remainder is converted to heat losses. The lower half of the winding rope, seen in Fig. 2.8 a, serves to balance the torque caused by the weight of the rope; this effect would be substantial on a winder for a deep mine, tending to destabilise the drive.

All mechanical motion is accompanied by frictional forces between the surfaces where relative motion exists. There are several types of friction, some of which are described in Fig. 2.9. In bearings, gears, couplings and brakes we observe dry or Coulomb friction (a), which is nearly independent of speed; however one has to distinguish between sliding and sticking friction, the difference of which may be considerable, depending at the roughness of the surfaces. The forces when cutting or milling material also contain Coulomb type friction.

In well lubricated bearings there is a component of frictional torque which rises proportionally with speed; it is due to laminar flow of the lubricant and is

called viscous friction (b). At very low speed and without pressurised lubrication, Coulomb type friction again appears.

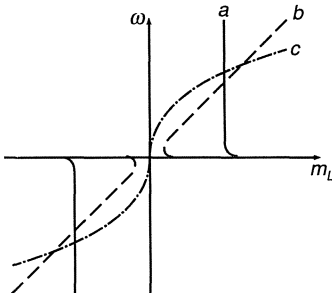


**Fig. 2.9.** Different types of frictional torque

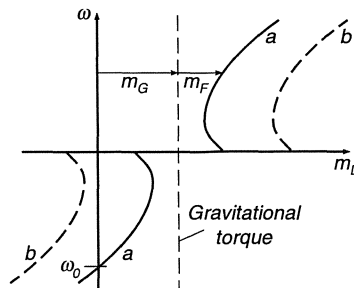


**Fig. 2.10.** Torque- speed curves of a hoist drive

With pumps and ventilators, where turbulent flow at high speed occurs, the torque rises with the square of speed; the drag force due to air flow around vehicles or the torque required by a centrifugal blower pushing cooling air through an electric motor also have this characteristic (c). In practical drives, with the motor as well as load, all these types of friction exist simultaneously, with one or the other component dominating. When driving a paper mill, printing presses or machine tools, Coulomb friction is usually the main constituent but with centrifugal pumps and compressors the torque following the square law is most important, representing the useful mechanical power. Note that frictional torques are always opposed to the direction of relative motion.

In Fig. 2.10 various torques, acting on a crane under load, are drawn;  $m_G$  is the constant gravitational torque caused by the load of the crane,  $m_F$  is the frictional torque, resulting in the total load torque curve (a). The speed  $\omega_0$  corresponds to the run-away speed with no external braking torque. When for safety reasons a self-locking transmission, such as a worm gear (b), is employed the crane must be powered even when lowering the load; this is due to the large sticking friction.

## 2.4 Stable and Unstable Operating Points

By ignoring the dependence of driving and load torques on the angle of rotation, the corresponding interaction seen in Fig. 2.1 vanishes and so does the effect of Eq. (2.2) on the static and transient behaviour of the drive. Equation (2.2) then becomes an indefinite integral having no effect on the drive. If we also neglect the electrical transients and the dynamics of the load, the remaining mechanical system is described by a first order, usually nonlinear, differential equation.

$$J \frac{d\omega}{dt} = m_M(\omega, t) - m_L(\omega, t) . \quad (2.16)$$

Because of the simplifications introduced, its validity is restricted to relatively slow changes of speed, when the transients in the electrical machine and the load can be neglected.

Apparently, a steady state condition with a constant rotational speed  $\omega_1$  is possible, if the characteristics are intersecting at that point,

$$m_M(\omega_1) - m_L(\omega_1) = 0.$$

In order to test whether this condition is stable, Eq. (2.16) can be linearised at the operating point  $\omega_1$ , assuming a small displacement  $\Delta\omega$ . With  $\omega = \omega_1 + \Delta\omega$ , we find the linearised equation

$$J \frac{d\Delta\omega}{dt} = \left. \frac{\partial m_M}{\partial \omega} \right|_{\omega_1} \Delta\omega - \left. \frac{\partial m_L}{\partial \omega} \right|_{\omega_1} \Delta\omega,$$

or, by rewriting it in normalised form

$$\frac{J}{k} \frac{d\Delta\omega}{dt} + \Delta\omega = 0, \quad \text{where} \quad k = \left. \frac{\partial}{\partial \omega} (m_L - m_M) \right|_{\omega_1}. \quad (2.17)$$

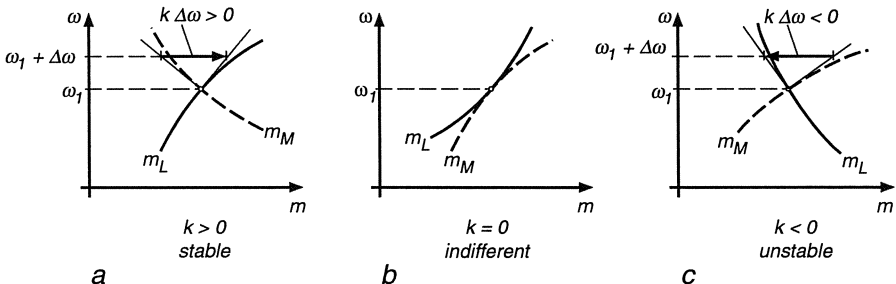


**Fig. 2.11.** Stable and unstable operating points

The assumed steady state is stable for  $k > 0$ ; in this case a small displacement  $\Delta\omega$ , that may have been caused by a temporary disturbance, is decaying along an exponential function with the time constant  $T_m = J/k$ .  $k$  can be interpreted as the slope of the retarding torque at the operating point, as is seen in Fig. 2.11.

For  $k < 0$  the operating point at  $\omega_1$  is unstable, i. e. an assumed deviation of speed increases with time. A new stable operating point may or may not be attained. The case  $k = 0$  corresponds to indeterminate stability; there is no definite operating point, with the speed fluctuating due to random torque variations. In Fig. 2.11 some sections of speed-torque curves are drawn for illustration.

Figure 2.12 depicts the steady state characteristic of an induction motor ( $m_M$ ) together with some load curves.  $L_1$  could be the characteristic of a ventilating fan; the intersection 1 is stable, roughly corresponding to rated load.

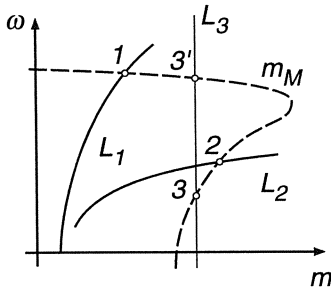


**Fig. 2.12.** Induction motor with different types of load

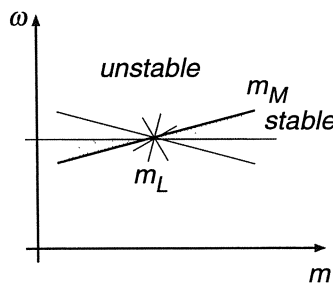


**Fig. 2.13.** Rising torque speed curve as cause of instability

With  $L_2$  there is also a stable operating point, but the motor would be heavily overloaded (Sect. 10.2). With the ideal lift characteristic  $L_3$ , there is an unstable (3) and a stable (3') operating point, but the motor would also be overloaded. In addition, the drive would fail to start since the load would pull the motor in the lowering direction when the brakes are released and there is insufficient frictional torque.

A particularly critical case is seen in Fig. 2.13. A slightly rising motor characteristic, which on a DC motor could be caused by armature reaction due to incorrect brush setting, leads to instability with most load curves except those intersecting in the shaded sector.

The stability test based on a linearised differential equation does not fully exclude instability if electrical transients or angle-dependent torques should have been included. The condition  $k > 0$  is only to be understood as a necessary condition, even though it is often a sufficient condition as well.

### 3. Integration of the Simplified Equation of Motion

With the assumptions introduced in the preceding section the motion of a single axis lumped inertia drive is described by a first order differential equation (Fig. 3.1)

$$J \frac{d\omega}{dt} = m_M(\omega, t) - m_L(\omega, t) = m_a(\omega, t), \quad (3.1)$$

which upon integration yields the mechanical transients. Several options are available for performing the integration.

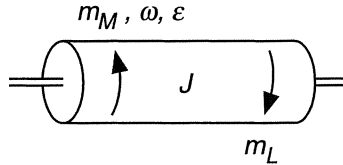


Fig. 3.1. Drive with concentrated inertia

#### 3.1 Solution of the Linearised Equation

The linearised homogeneous equation was (Eq. 2.17)

$$T_m \frac{d(\Delta\omega)}{dt} + \Delta\omega = 0, \quad T_m = \frac{J}{k} \quad (3.2)$$

with  $\Delta\omega$  being a small deviation from the steady state speed  $\omega_1$  and

$$k = \left. \frac{\partial}{\partial\omega} (m_L - m_M) \right|_{\omega_1} \quad (3.3)$$

a measure for the slope of the retarding torque at the operating point.  $T_m = J/k$  has the meaning of a mechanical time constant. The general solution is

$$\Delta\omega(t) = \Delta\omega(0) e^{-t/T_m}, \quad (3.4)$$

where  $\Delta\omega(0)$  is the initial deviation, that may be caused by switching from one motor characteristic to another resulting in a new steady state speed. Because of the stored kinetic energy, the speed is a continuous state variable (the only one because of the simplifications introduced).

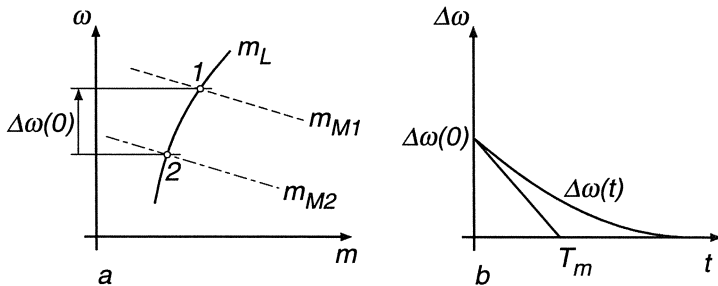


**Fig. 3.2.** Mechanical transient of linearised drive system

In Fig. 3.2 a it is assumed that the motor, initially in a steady state condition at point 1, is switched to another supply voltage so that a new characteristic for the driving torque  $m_{M2}$  is valid. This causes an initial deviation  $\Delta\omega(0)$  with respect to the new operating point 2. The deviation vanishes along an exponential function (Fig. 3.2 b), the time constant of which is determined by the inertia and the slope of the load- and the driving-torques. Let us now look at some simple examples.

### 3.1.1 Start of a Motor with Shunt-type Characteristic at No-load

A motor which initially is at rest is started at  $t = 0$ , Fig. 3.3. The torque-speed-curve of the motor is assumed to be linear between no-load speed  $\omega_0$  (neglecting friction load) and stalled torque  $m_0$ . With normal motors of medium size, the stalled torque may be 8 or 10 times rated torque; it is determined by extrapolating the drooping shunt type characteristic to standstill and hence represents only a reference quantity that cannot be measured in practice. In the present example we assume that a starting resistor has been inserted, reducing the stalled torque to perhaps twice rated torque and thus extending the validity of the linear characteristic to standstill. This, by the way, makes the simplifying assumptions more realistic since the electrical transients become faster while the mechanical transients are delayed.

Under ideal no-load conditions, we have  $m_L = 0$ ; also, due to the assumed linearity of the curves  $m_M(\omega)$ ,  $m_L(\omega)$  the deviation  $\Delta\omega$  is not restricted to small values.

The slope of the retarding torque is

$$k = \frac{\partial}{\partial\omega} (m_L - m_M) = \frac{m_0}{\omega_0} > 0;$$

hence the differential equation is stable, it has the form

$$T_m \frac{d(\Delta\omega)}{dt} + \Delta\omega = 0, \quad (3.5)$$

where

$$T_m = \frac{J\omega_0}{m_0}$$

is the mechanical time constant.

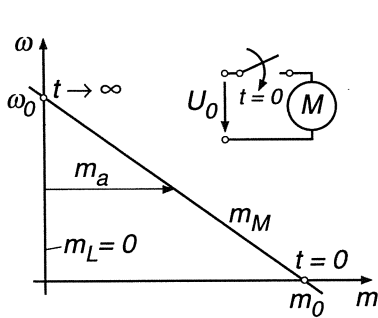


Fig. 3.3. Starting of motor at no-load

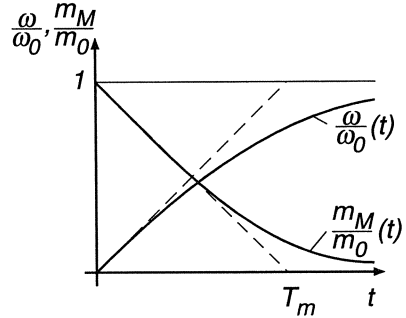


Fig. 3.4. Starting transient

The steady state operating point at the intersection of the two torque curves is  $\omega_1 = \omega_0$ ; due to the initial condition at standstill, we find  $\Delta\omega(0) = -\omega_0$ , which leads to the particular solution

$$\Delta\omega(t) = -\omega_0 e^{-t/T_m}$$

or with  $\omega = \omega_0 + \Delta\omega$

$$\omega(t) = \omega_0 (1 - e^{-t/T_m}). \quad (3.6)$$

From the torque-speed curve of the motor

$$\frac{\omega}{\omega_0} = 1 - \frac{m_M}{m_0} \quad (3.7)$$

the motor torque during the start-up is obtained,

$$m_M(t) = m_0 e^{-t/T_m}. \quad (3.8)$$

The starting transient is shown in Fig. 3.4.

The discontinuity of the motor torque is caused by the omission of the electrical transients. In reality the torque is also associated with energy states and, hence, is continuous.

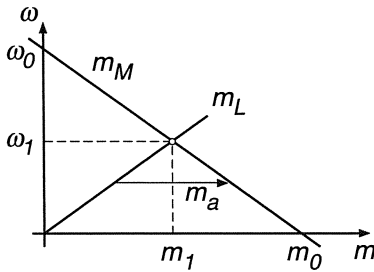


**Fig. 3.5.** Starting of motor with linearly rising load torque

### 3.1.2 Starting the Motor with a Load Torque Proportional to Speed

In Fig. 3.5 the curves of a drive with speed-proportional load torque are displayed. The steady state operating point is now at  $\omega_1 < \omega_0$ , hence  $\Delta\omega(0) = -\omega_1$ .

The slope of the retarding torque is

$$k_1 = \frac{\partial}{\partial \omega} (m_L - m_M) = \frac{m_0}{\omega_1} > 0 \quad (3.9)$$

which leads to a reduced mechanical time constant

$$T_{m1} = \frac{J \omega_1}{m_0} = \frac{\omega_1}{\omega_0} T_m. \quad (3.10)$$

The speed transient is

$$\omega(t) = \omega_1 (1 - e^{-t/T_{m1}}). \quad (3.11)$$

Elimination of speed from the motor characteristic Eq. (3.7) results in the driving torque

$$\begin{aligned} m_M(t) &= m_0 \left(1 - \frac{\omega}{\omega_0}\right) = m_0 \left[1 - \frac{\omega_1}{\omega_0} (1 - e^{-t/T_{m1}})\right] \\ &= m_1 + (m_0 - m_1) e^{-t/T_{m1}}. \end{aligned} \quad (3.12)$$

Both transients are plotted in Fig. 3.6, together with the no-load starting transient ( $m_L = 0$ ).

At  $t = 0$ , the slope of the speed curves is the same, because the accelerating torques are identical at  $\omega = 0$ .

### 3.1.3 Loading Transient of the Motor Running at No-load Speed

The motor is now supposed to be initially in a no-load condition at the speed  $\omega_0$  with the starting resistor short circuited, so that the speed droop is reduced

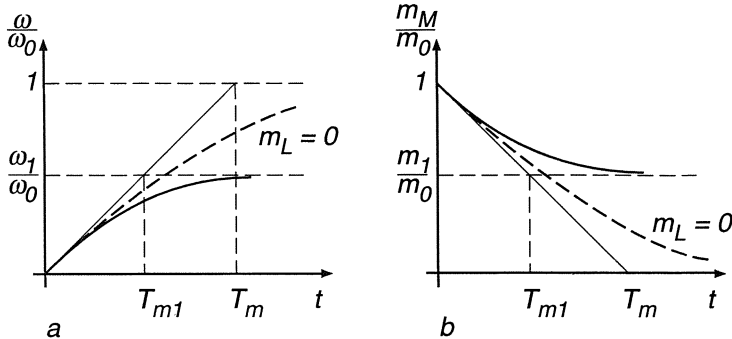


Fig. 3.6. Starting transient

and the extrapolated stalled torque assumes its large nominal value  $m_{0n}$ . The torque-speed-curve is then linear only in a narrow speed range around no-load speed.

At  $t = 0$  a constant torque load without inertia is applied to the motor shaft, possibly by a mechanical brake (Fig. 3.7), causing the motor to slow down to the steady state speed  $\omega_1$ ; hence the initial deviation is  $\Delta\omega(0) = \omega_0 - \omega_1$ .

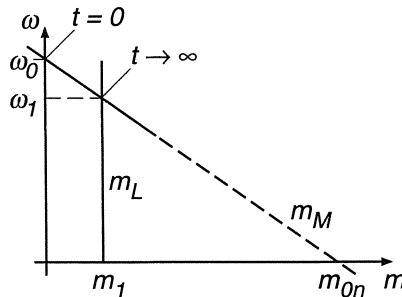


Fig. 3.7. Applying constant load torque to motor running at no-load

In view of the constant load torque, we find

$$k = \frac{\partial}{\partial\omega} (m_L - m_M) \Big|_{\omega_1} = \frac{m_{0n}}{\omega_0}, \quad T_m = \frac{J\omega_0}{m_{0n}} = T_{mn}. \quad (3.13)$$

Since  $m_{0n}$  corresponds to the extrapolated stalled torque with short circuited starting resistor,  $T_{mn}$  is also called short circuit mechanical time constant.

The solution of Eq. (3.5) is

$$\Delta\omega(t) = (\omega_0 - \omega_1) e^{-t/T_{mn}}$$

or

$$\omega(t) = \omega_1 + (\omega_0 - \omega_1) e^{-t/T_{mn}}. \quad (3.14)$$

The driving torque again follows from Eq. (3.7),

$$\begin{aligned} m_M(t) &= m_{0n} \left(1 - \frac{\omega}{\omega_0}\right) = m_{0n} \left(1 - \frac{\omega_1}{\omega_0}\right) (1 - e^{-t/T_{mn}}) \\ &= m_1 (1 - e^{-t/T_{mn}}). \end{aligned} \quad (3.15)$$

In Fig. 3.8 the transients are drawn for loading and unloading the motor. The driving torque apparently follows the applied load torque with a lag determined by  $T_{mn}$ . The reason for this is that during the deceleration phase some of the kinetic energy stored in the inertia is released and makes up for part of the load torque; conversely, the missing kinetic energy is restored when the drive is accelerated after disconnecting the load. The mechanical energy storage thus acts as a buffer between the load and the electrical supply feeding the motor. This effect may be accentuated by adding a flywheel to the drive, in order to protect the supply system from high load surges such as those caused by large rolling mill drives; conversely, a sensitive load, for example a computer, can be made immune against short time disturbances on the line side, when it is supplied by a rotating motor-generator set having a flywheel attached.

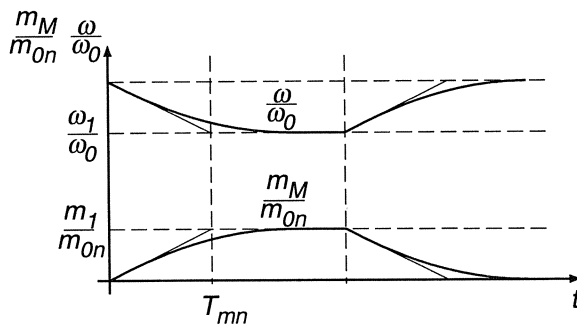


**Fig. 3.8.** Loading transient

### 3.1.4 Starting of a DC Motor by Sequentially Shortcircuiting Starting Resistors

With DC motors fed from a constant voltage bus the starting circuit shown in Fig. 3.9 may be used, where the contactors  $C_1, \dots, C_N$  are closed in succession. By suitable choice of the resistors, the droop of the resulting torque-speed characteristic is progressively reduced. In order to achieve fast starting without overloading the motor, the torque is specified to vary between the limits  $m_1$ ,

$m_2$  during the start, as is shown in Fig. 3.10. The armature current, being proportional to torque, then varies between the limits  $i_1, i_2$ . A similar starting procedure exists for AC induction motors having a wound rotor and starting resistors in the rotor circuit.

As the motor is accelerated, the torque  $m_M$  decreases until the lower limit  $m_1$  is reached; then the next section of the resistor is short circuited causing the torque to jump again to the upper limit  $m_2$ . This is repeated until all the starting resistors are switched out and the motor operates on its natural torque-speed curve. In the steady state the torque is determined by the load. The required number of sections of the starting resistor and their appropriate values can be calculated in closed form [34].

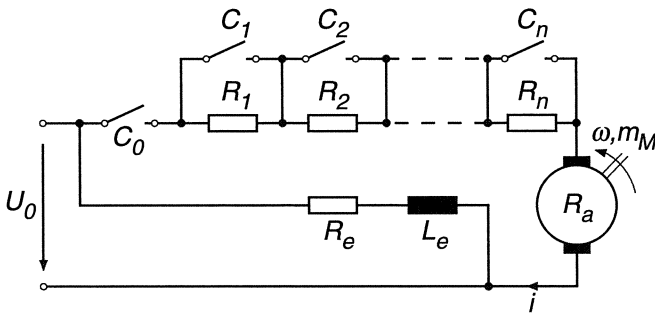


Fig. 3.9. Starting circuit for a DC motor

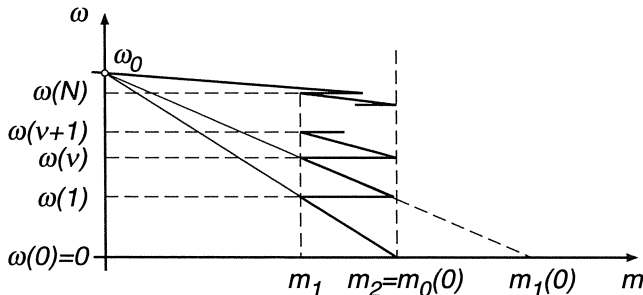


Fig. 3.10. Torque-speed curves for different values of starting resistor

By inspecting Fig. 3.10 we find the relation

$$\frac{m_2 - m_1}{m_2} = \frac{\omega(\nu + 1) - \omega(\nu)}{\omega_0 - \omega(\nu)}. \quad (3.16)$$

from which, with the abbreviation  $m_1/m_2 = a < 1$ , a recursive formula is obtained,

$$\omega(\nu + 1) = (1 - a)\omega_0 + a\omega(\nu) = \omega(1) + a\omega(\nu).$$

Assuming  $\omega(0) = 0$ , this leads to a geometric progression

$$\begin{aligned}\omega(2) &= (1 + a)\omega(1) \\ \omega(3) &= (1 + a + a^2)\omega(1) \\ &\vdots \\ \omega(\nu) &= (1 + a + \dots + a^{\nu-1})\omega(1)\end{aligned}$$

with the sum

$$\omega(\nu) = \frac{1 - a^\nu}{1 - a} \omega(1) = (1 - a^\nu) \omega_0. \quad (3.17)$$

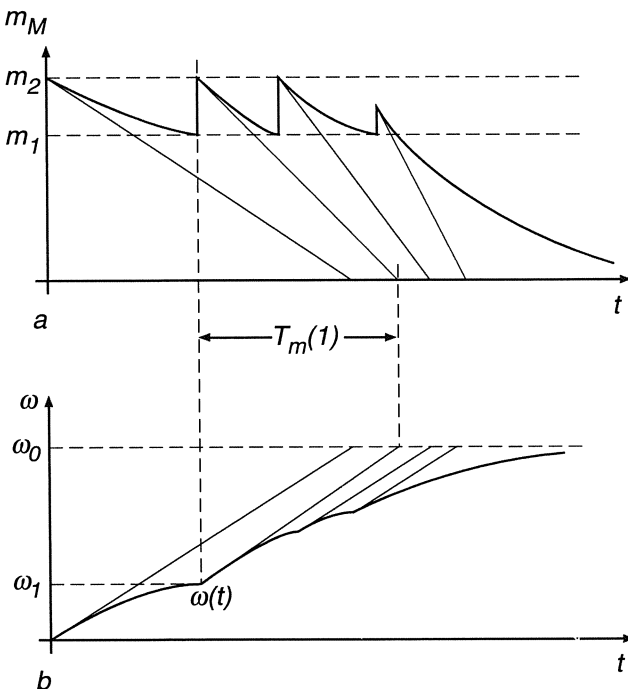


**Fig. 3.11.** Starting a motor by successively reducing the starting resistor

The last of the  $N$  switching instants is reached when the natural speed-torque curve yields a value of the torque which is less than the maximum,  $m_2$ ,

$$\omega(N) = (1 - a^N) \omega_0 \geq \left(1 - \frac{m_2}{m_{0n}}\right) \omega_0;$$

solving for  $N$ , this results in

$$N \geq \frac{\ln(m_{0n}/m_2)}{\ln(1/a)}, \quad N \text{ integer.} \quad (3.18)$$

From previous results it is known that, when assuming linear torque-speed curves, all variables are exponential functions of time, with the time constants depending on the angles of the curves at the point of intersection.

In Fig. 3.11 a starting transient without load is shown; in the interval  $\omega(\nu) \leq \omega \leq \omega(\nu + 1)$  the speed is

$$\omega(t) = \omega(\nu) + [\omega_0 - \omega(\nu)] [1 - e^{-(t-t_\nu)/T_m(\nu)}], \quad (3.19)$$

where  $t_\nu$  is the instant, when  $C_\nu$  closes.

The driving torque in the same interval follows also an exponential function

$$m_M(t) = m_2 e^{-(t-t_\nu)/T_m(\nu)}; \quad (3.20)$$

as soon as  $m_M(t)$  has dropped to  $m_1$ , the next contactor  $C_{\nu+1}$  is closed.

The mechanical time constant, valid in the interval, is

$$T_m(\nu) = \frac{J\omega_0}{m_0(\nu)} = \frac{J\omega_0}{m_2} a^\nu = T_{mn} \frac{m_{0n}}{m_2} a^\nu; \quad (3.21)$$

it decreases as the starting resistor is reduced.

### 3.2 Analytical Solution of Nonlinear Differential Equation

A direct solution of the equation

$$J \frac{d\omega}{dt} = m_M(\omega) - m_L(\omega)$$

by separation and integration,

$$t_2 - t_1 = J \int_{\omega_1}^{\omega_2} \frac{1}{m_M(\omega) - m_L(\omega)} d\omega \quad (3.22)$$

is rarely possible because there is either no analytical expression of the functions  $m_M(\omega)$  and  $m_L(\omega)$  or, if there is such a formula, the integral cannot be solved in general terms.

An exception is the no-load starting of an induction motor without stator resistance and skin effect in the rotor bars; the normalised steady state torque-speed function is

$$m_M = \frac{2m_p}{S/S_p + S_p/S},$$

with  $S = 1 - \omega/\omega_0$  being the slip and  $S_p$  the pull-out slip at which maximum torque  $m_p$  occurs. The function which will be derived in Chap. 10 is seen in Fig.

3.12 for  $S_p = 0.1$ . With no load ( $m_L = 0$ ) and the initial condition  $\omega(t_1 = 0) = 0$ ,  $S(0) = 1$  the integration yields

$$\begin{aligned} t_2 &= J \int_0^{\omega_2} \frac{d\omega}{m_M} = \frac{J \omega_0}{2 m_p} \int_{S_2}^0 \left( \frac{S}{S_p} + \frac{S_p}{S} \right) dS \\ &= \frac{J \omega_0}{2 m_p} \left[ \frac{1 - S_2^2}{S_p} - S_p \ln S_2 \right]. \end{aligned} \quad (3.23)$$

This function is plotted in Fig. 3.13. Since the speed approaches the synchronous speed  $\omega_0$  asymptotically, the definition of a starting time requires fixing a final slip  $S_2$ .

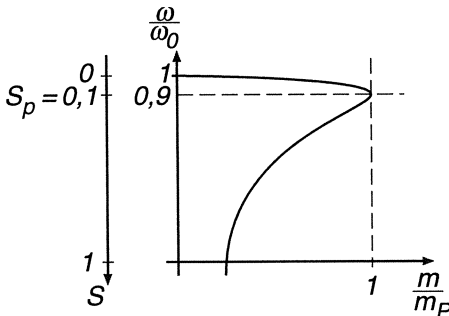


**Fig. 3.12.** Steady state torque–speed curve of induction motor

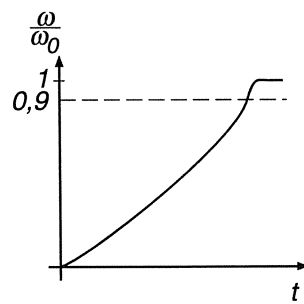


**Fig. 3.13.** Starting transient of induction motor

Computing the starting transient on the basis of the steady state torque–speed characteristic makes sense only if the starting is sufficiently slow in order to justify ignoring the electrical transients. This condition is met if the load contributes substantial additional inertia or if the start is delayed due to reduced voltage. Otherwise the start of a smaller motor would be completed within a few periods of the line voltages, long before the electrical transients have decayed; this will be discussed in Sect. 10.3.

### 3.3 Numerical and Graphical Integration

The most versatile method — with regard to accuracy and applicability — of integrating nonlinear differential equations is the stepwise integration with the digital computer.

It is known that by introducing state variables  $x_i(t)$ ,  $i = 1, 2, \dots, n$ , a differential equation of  $n^{th}$  order may be written as a system of  $n$  first order differential equations

$$\frac{dx_i}{dt} = \varphi_i(x_j, y_k, t), \quad i, j, k = 1, \dots, n, \quad (3.24)$$

where  $y_k(t)$  are the independent forcing functions and  $t$  the time as variable of integration. The  $\varphi_i$  may be arbitrary functions, given as analytical expressions, curves or even discrete samples. Once the state variables  $x_i(t)$  are known, the output variables  $z_i(t)$  can be calculated from algebraic expressions

$$z_i(t) = \Phi_i(x_j, y_k, t), \quad (3.25)$$

i.e. without further integration.

The simultaneous solution of the  $n$  state equations (3.24) is performed in steps of length  $\Delta t$

$$x_i((\nu + 1) \Delta t) = x_i(\nu \Delta t) + \int_{\nu \Delta t}^{(\nu + 1) \Delta t} \varphi_i(x_j, y_k, t) dt. \quad (3.26)$$

$x_i(\nu \Delta t) = x_i(\nu)$  are the results obtained in the preceding step,  $x_i(\nu + 1)$  is the new set of values at time  $(\nu + 1) \Delta t$ . Based on approximations provided by numerical mathematics and with sufficiently small step length we can write

$$x_i(\nu + 1) \approx x_i(\nu) + F[\varphi_i(\nu), \varphi_i(\nu - 1), \dots]. \quad (3.27)$$

where  $F$  is a linear combination of the functions  $\varphi_i$  at previous intervals. There exists a large number of integration formulae which differ in complexity, i.e. computing time, sensitivity to numerical instability and accuracy [19]. The ones best known are square-, trapezoidal- and Simpsons-rule, furthermore the Newton- and Runge-Kutta-algorithms. Because of its favourable properties the last mentioned algorithm is most widely used; it is usually available as a complete subroutine so that only the functions  $\varphi_i$  and the initial conditions  $x_i(0)$  need to be inserted as well as the integration interval  $\Delta t$  and the time  $t_2$  at which the integration is to be terminated. Often the integration interval  $\Delta t$  is chosen automatically, depending on the functions  $\varphi_i$  and the specified accuracy. We are not going to discuss details of numerical integration; there can be subtle problems interrelating step size, accuracy and numerical stability. Since a large number of steps may have to be computed sequentially, even minute systematic errors can accumulate under unfavourable conditions.

Obviously the two differential equations derived in Sect. 2.1 correspond to this general scheme, Eqs. (2.1, 2.2); when taking the angle of rotation into account, the order is  $n = 2$ , i. e. a very small system of differential equations results. The state variables are the rotational or linear speed and the angle of rotation or the linear distance. These variables represent storage effects and, hence, are continuous. If a more accurate description is desired, the electrical transients have to be included, thus increasing the number of differential equations and state variables; this is discussed in later sections.

When a timetable for the branch of a railway is computed, it is necessary to take into account the mass  $M$  of the trains, including the equivalent inertia of the wheel sets, the speed-dependent driving forces of the locomotives, distance-dependent conditions, such as grades, curves or speed restrictions, as well as

maximum values for deceleration. The task requires the simultaneous solution of the differential equations for velocity and distance

$$\begin{aligned}\frac{dv}{dt} &= \frac{1}{M} [f_M(v, t) - f_L(s, v, t)], \\ \frac{ds}{dt} &= v,\end{aligned}\tag{3.28}$$

where  $f_M$  is the internal driving force of the locomotive and  $f_L$  is the total load force, including frictional and braking forces as well as gravitational forces on grades. The task of finding an acceptable timetable is an optimisation problem of considerable complexity, since many restrictions and boundary conditions have to be taken into account. This includes the use of the same track by trains having different acceleration and velocity limits, such as intercity or heavy goods trains. The problem can only be solved by iteration, repeatedly integrating Eqs. (3.28) with different initial conditions. Today this is a typical problem for numerical integration with a digital computer. However, in the past it had to be solved manually by graphical means. Since it cannot be ruled out that, even today, this may have to be done occasionally, let us briefly consider the principle of graphical integration, using a simple example.

The Eq. (3.1)

$$J \frac{d\omega}{dt} = m_M(\omega) - m_L(\omega) = m_a(\omega)\tag{3.29}$$

where  $m_M(\omega)$  and  $m_L(\omega)$  are given as empirical curves (Fig. 3.14), is normalised with the help of arbitrary reference values  $\omega_1$ ,  $m_1$ ,

$$\frac{J \omega_1}{m_1} \frac{d}{dt} \left( \frac{\omega}{\omega_1} \right) = \frac{m_M}{m_1} - \frac{m_L}{m_1} = \frac{m_a}{m_1}.\tag{3.30}$$

$m_a/m_1$  corresponds to the normalised accelerating torque.

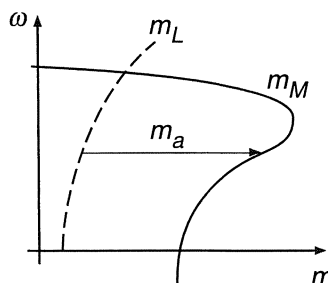


Fig. 3.14. Torque-speed curves of motor and load

With the abbreviations

$$\frac{J \omega_1}{m_1} = T_1, \quad \frac{t}{T_1} = \tau, \quad \frac{\omega}{\omega_1} = x, \quad \frac{m_a}{m_1} = y$$

a nondimensional equation results

$$\frac{dx}{d\tau} = y(x) . \quad (3.31)$$

Normalisation avoids the awkward choice of scale factors; the reference values  $\omega_1$ ,  $m_1$  are of no significance, even though it is recommendable to choose characteristic values such as rated speed and torque in order to work with handy numbers.

In Fig. 3.15 the normalised curve  $y(x)$ , derived from Fig. 3.14 is shown, with the normalised speed plotted against torque. The  $x$ -axis is subdivided into several intervals, not necessarily of equal length; it is in fact appropriate to reduce the lengths of the intervals in sections where  $y(x)$  is changing rapidly. In each interval  $y$  is approximated by a constant, visually representing the average of  $y(x)$  in that interval. Approximating  $y(x)$  by a staircase function has the consequence that  $dx/d\tau$  is assumed constant in each interval, so that  $x(\tau)$  assumes polygonal form.

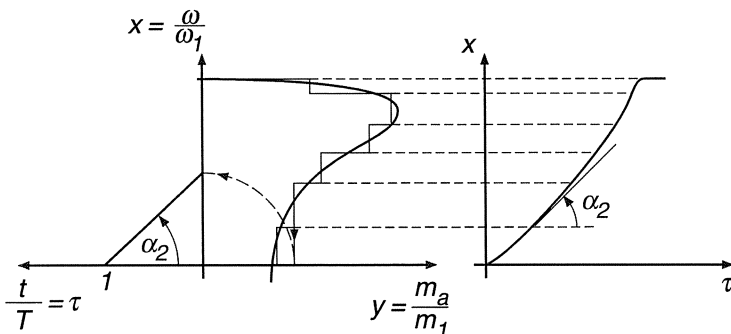


**Fig. 3.15.** Principle of graphical integration

By selecting the point  $\tau = 1$  at a suitable distance to the left of the origin, radii with the slope  $y(x)$  can be drawn which are then joined to form the polygonal curve approximating the exact solution  $x(\tau)$ . The graphical construction is indicated in Fig. 3.15.

The method described is related to the rectangular rule of integration, however with considerably improved accuracy because of the visual averaging process. Normally it does not pay to choose the  $x$ -intervals too small because then drafting inaccuracies may accumulate.

If, besides the speed, the angular rotation or the distance travelled is of interest, a second integration is required; the two graphical constructions must proceed in alternate steps if acceleration depends on distance, as is the case with the train due to grades or curves with speed restrictions and changing frictional forces.

## 4. Thermal Effects in Electrical Machines

### 4.1 Power Losses and Temperature Restrictions

So far our considerations have only dealt with mechanical phenomena and the pertinent steady-state and dynamic conditions, but suitable torque- speed curves and adequate power are not the only criteria for designing electrical drives.

Of equal importance are the thermal transients in the motor caused by the unavoidable power losses during the process of energy conversion and the ensuing heat flow from the points of origin to the cooling medium. The various materials used in an electrical machine naturally have different temperature limits; of particular importance are the insulating materials, which determine the temperature classes of the machine, for example

class A,	$\overline{\Delta\vartheta} < 60^\circ \text{ C}$ ,	cotton, synthetic, paper,
B,	$\overline{\Delta\vartheta} < 80^\circ \text{ C}$ ,	resin, shellac,
F,	$\overline{\Delta\vartheta} < 105^\circ \text{ C}$ ,	mica, epoxy,
H,	$\overline{\Delta\vartheta} < 125^\circ \text{ C}$ ,	glass fibre, silicone rubber.

$\overline{\Delta\vartheta}$  is the mean temperature rise above an assumed ambient temperature of  $\vartheta_0 = 40^\circ \text{C}$ . All temperatures are measured in degree Celsius (centigrades).

For a given frame size and type of cooling, the output power and the allowable power losses are higher for the elevated temperature insulation classes; at the same time the cost of the machine increases.

The main causes of power losses in an electrical machine are:

- a) *Conductor heat loss (copper losses)* in the windings, cables, brushes, slip-rings and commutator. If there is alternating current, the effective resistance of the conductor may be noticeably increased by eddy currents (skin effect); this is accentuated with large conductors surrounded by magnetic material and may have to be counteracted by the use of stranded conductors.
- b) *Iron heat losses* in stationary or moving magnetic material exposed to changing magnetic fields. The losses consist of eddy current- and hysteresis-losses; being of separate nature, they are determined by different properties of the material and follow different laws with regard to amplitude and frequency of the magnetic field.

c) *Friction losses*, including bearing-, brush- and ventilation losses.

The various types of losses depend in complicated fashion on the operational state of the machine. The main factors of influence are speed and load torque, as well as voltages and currents with their RMS-values and waveforms.

In order to induce heat flow from the points of origin to the cooling surfaces, a temperature gradient arises inside the machine determining the direction and intensity of the heat flow. The temperatures are usually highest in the windings because the loss density in the conductors being covered by insulating material is high; also the windings are partly embedded in slots and thus are not directly exposed to the cooling air. The hot-spot temperature with class B insulation could be, for example,

$$\begin{aligned}\vartheta_{max} &= \overline{\Delta\vartheta} + (\Delta\vartheta_{max} - \overline{\Delta\vartheta}) + \vartheta_0 \\ &= 80^\circ\text{C} + 10^\circ\text{C} + 40^\circ\text{C} = 130^\circ\text{C}.\end{aligned}$$

When operating the machine at elevated ambient temperatures, e.g. in the tropics, the power rating may have to be reduced.

An accurate prediction of the heat flow and the temperature distribution in an electrical machine is exceedingly difficult; this is due to the complex geometrical shapes, the use of heterogeneous and anisotropic materials (laminated iron, insulation), furthermore the complicated laws of heat production with respect to space and time, as well as the different cooling conditions. Also, the heat conductivity of the various materials does not differ by orders of magnitude, as is the case with electrical or magnetic fields. As a result, the temperature distribution can only be computed in restricted areas and with considerable simplifications.

The user of electrical drives has normally little influence on the temperature distribution within the machine. He must be confident that the designer has chosen sufficiently large conductors and cooling channels, in order not to exceed temperature limits under specified operating conditions. With this assumption it is usually adequate to drastically simplify the thermal model of the "motor" by regarding it as a homogeneous body exhibiting thermal storage, whose internal transients are unknown and of no interest. Naturally, such a crude model cannot offer any detailed information on specific internal thermal conditions.

## 4.2 Heating of a Homogeneous Body

The simplified thermal model is characterised by the following assumptions (Fig. 4.1):

A homogeneous body with the surface  $A$ , the thermal capacity  $C$ , measured in  $\text{Ws}/^\circ\text{C}$ , and the mean surface temperature  $\vartheta$  is heated by the input power  $p_1$ , at the same time emitting heat power  $p_2$  by convection. The ambient temperature is  $\vartheta_0$ , the coefficient of heat transfer  $\alpha$ . The component of radiated

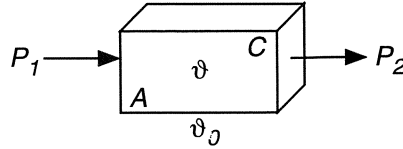


**Fig. 4.1.** Homogeneous body with thermal storage capacity

heat is assumed to be negligible due to the relatively low operating temperatures (it rises with the fourth power of absolute temperature) and due to back radiation, for example at the cooling fins. Hence the equation, describing the power balance is

$$C \frac{d\vartheta}{dt} = p_1 - p_2 . \quad (4.1)$$

The heat transfer by convection is a linear function of the temperature difference

$$p_2 = \alpha A (\vartheta - \vartheta_0) ; \quad (4.2)$$

with  $\vartheta - \vartheta_0 = \Delta\vartheta$  this results in

$$C \frac{d(\Delta\vartheta)}{dt} + \alpha A \Delta\vartheta = p_1 \quad (4.3)$$

or

$$T_\vartheta \frac{d\Delta\vartheta}{dt} + \Delta\vartheta = \frac{p_1}{\alpha A} , \quad (4.4)$$

a linear first order differential equation;  $T_\vartheta = C/\alpha A$  is the thermal time constant.

With  $p_1 = p_{10} = \text{const.}$  and  $\Delta\vartheta(0) = 0$  the solution is

$$\Delta\vartheta(t) = \Delta\vartheta(\infty) (1 - e^{-t/T_\vartheta}) , \quad (4.5)$$

where

$$\Delta\vartheta(\infty) = p_{10}/\alpha A \quad (4.6)$$

is the steady state end temperature, at which the heat transfer by convection equals the input power.

In Fig. 4.2 a thermal transient is seen. The shaded area between  $p_1/\alpha A$  and  $\Delta\vartheta(t)$  corresponds to the energy stored as heat. Hence, the storage effect tends to delay the temperature changes, causing the temperature to be a continuous function of time.

The approximation incurred with this simple model is mainly due to the assumption of evenly distributed heat sources in the homogeneous body and the neglect of an internal heat flow; hence, transportation delays are not contained in the simplified model.

A rough estimate of a typical thermal lag may be derived from the data sheet of an enclosed 100 kW standard induction motor cooled by an external fan (TEFC):

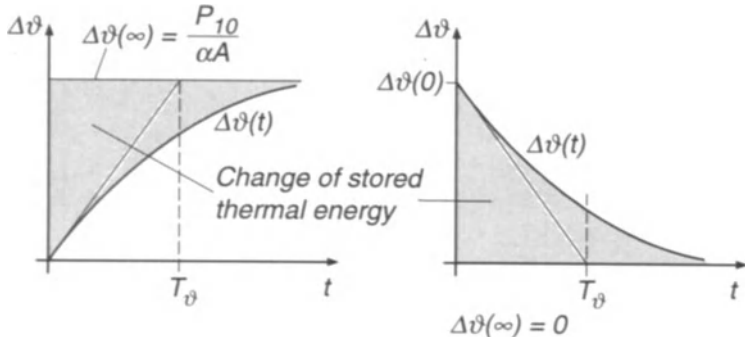


Fig. 4.2. Thermal transients

$p_r = 100 \text{ kW}$ , rated power

$M = 800 \text{ kg}$ , mass

$\eta = 0.92$ , rated efficiency

$\Delta\vartheta(\infty) = 50^\circ\text{C}$  is the steady-state temperature rise due to the losses  $p_1$  at rated power

$$p_1 = p_r \left( \frac{1}{\eta} - 1 \right) ;$$

the convective heat conductivity is

$$\alpha A = \frac{p_1}{\Delta\vartheta(\infty)} .$$

Assuming that the motor consists of solid iron having the specific heat  $c_{Fe}$ , the heat capacity is

$$C = c_{Fe} M .$$

This yields the thermal time constant

$$T_\vartheta = \frac{C}{\alpha A} = \frac{c_{Fe} M \Delta\vartheta(\infty)}{\frac{1-\eta}{\eta} p_r} = \frac{0.48 \text{ kW s/kg}^\circ\text{C} \cdot 800 \text{ kg} \cdot 50^\circ\text{C}}{9 \text{ kW}} \approx 34 \text{ min.}$$

Typically, thermal transients are much slower than electrical or mechanical effects. Of course, there are exceptions such as disk motors, where the armature winding is printed directly on an insulating disk and possesses very little thermal storage capacity. The following time scales are usually valid with electrical machines:

electromagnetic	mechanical	thermal transients
0.1 – 100 ms	10 ms – 10 s	10 – 60 min

Travelling wave phenomena in windings are not considered; they are faster yet by several orders of magnitude. The large difference of more than a factor of 100 between the time scales of mechanical and thermal transients usually permits a separate treatment which results in considerable simplification.

The heat transfer by convection from a ventilated surface depends strongly on the velocity of the cooling air; the usual range of the transfer coefficient is

$$\alpha = 50 \text{ to } 500 \text{ W/m}^2\text{C} ;$$

at  $\Delta\vartheta = 50^\circ\text{C}$  this results in a power flow by convection of

$$\frac{p_{2c}}{A} = 2.5 \text{ to } 25 \text{ kW/m}^2 ;$$

the dependence of the heat transfer on the velocity of the cooling air has the consequence that self-cooled motors exhibit at standstill a cooling time constant that is much longer than the thermal time constant of the motor when running. Larger motors operating at variable speed and load are usually provided with separate forced cooling, causing the motor speed to have little effect on the cooling conditions.

In order to show that the heat transfer by radiation can normally be neglected, a rough estimate of the power flow by radiation is given for comparison.

A "black body" emits to the environment power by radiation according to Boltzmanns law,

$$\frac{p_R}{A} = \sigma T^4 ,$$

where

$$\sigma = 5.710^{-8} \text{ W/K}^4 \text{ m}^2$$

is the coefficient of radiation and  $T$  the absolute temperature. With  $\vartheta = 70^\circ\text{C}$ , i.e.  $T = 343 \text{ K}$ , the power flow due to radiation is

$$\frac{p_R}{A} = 0.77 \text{ kW/m}^2 .$$

This relatively small amount is further reduced by inverse radiation. Also, the radiation coefficient of a motor surface is much lower than that of a "black body".

### 4.3 Different Modes of Operation

In contrast to internal combustion engines, most electrical drives possess considerable overload-capacity, the limit of which is determined by the power losses rising with the load. Since the temperature follows the power loss with a substantial lag, a temporary overload is admissible without exceeding the temperature limits, provided that the motor is initially below the rated temperature. This effect may be utilised when selecting a drive for a particular application. Let us look at some modes of operation frequently occurring in practice.

### 4.3.1 Continuous Duty

This mode of operation exists if the load torque is constant during an extended period of time, corresponding to a multiple of the thermal time constant, so that the temperature reaches its steady-state value (Fig. 4.2). This is the normal continuous duty, e.g. with paper mill drives or boiler feed pumps. The motor must be so rated, that its nominal output power equals or exceeds the continuous load. With traction drives, other definitions are also in use, such as a one-hour- or five-minutes-rating of the drive motors.

### 4.3.2 Short Time Intermittent Duty

In this case the time of operation is considerably less than the thermal time constant and the motor is allowed to cool off before a new load cycle begins. This duty applies for example to some crane drives or small motors in household appliances. Under these conditions the motor can be overloaded until the temperature at the hottest point reaches the permissible limit; however, the internal temperature rise is particularly large with high overload. The simplified thermal model provides only a rough estimate under these conditions.

In Fig. 4.3 the temperature transient is drawn, following a short time power loss  $p_{1s}$  which may be considerably in excess of the nominal power loss  $p_{1r}$ . The temperature rises rapidly towards an extrapolated steady-state value  $\Delta\vartheta_\infty$ ; when  $\Delta\vartheta_1$  is reached, the motor is disconnected, giving it the opportunity to cool. In the example it is assumed that the motor is self-cooled causing the thermal time constant at standstill to have an increased value.

The maximum temperature  $\Delta\vartheta_1$ , at the time of disconnection is

$$\Delta\vartheta_1 = \Delta\vartheta_\infty [1 - e^{-t_1/T_\vartheta}] \leq \Delta\vartheta_{max}, \quad (4.7)$$

where

$$\Delta\vartheta_\infty = \Delta\vartheta_{max} \frac{p_{1s}}{p_{1r}} \quad (4.8)$$

is the extrapolated end temperature during overload. Hence

$$\frac{p_{1s}}{p_{1r}} \leq \frac{1}{1 - e^{-t_1/T_\vartheta}} \approx \frac{T_\vartheta}{t_1}, \quad t_1 \ll T_\vartheta, \quad (4.9)$$

is the maximum relative power loss during the time  $t_1$ .

Increasing the output power while simultaneously reducing the time  $t_1$  of operation is of course only feasible within the available torque range; this is illustrated in Fig. 4.4. At the left, a typical curve relating torque to power loss is drawn, while the other curve depicts Eq. (4.9). This indicates that the power loss rises much faster than the torque (assuming constant speed).

The shaded contour corresponds to the admissible short time overload range. With motors exhibiting a pull-out effect there is an absolute torque limit, whereas the losses continue to rise up to the stalled condition; on commutator machines, the commutator is usually the weakest link.

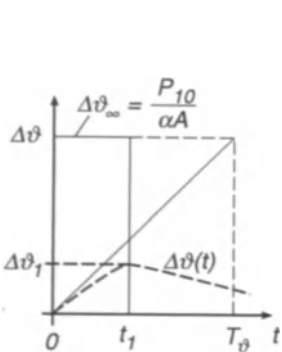


**Fig. 4.3.** Thermal transient during short time duty

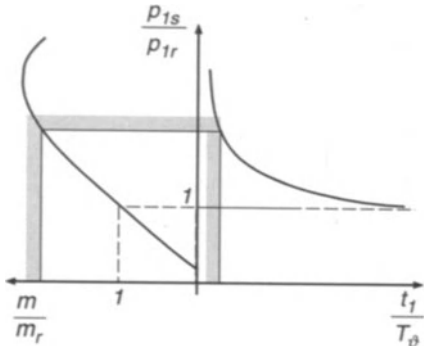


**Fig. 4.4.** Short time overload limits

In order to obtain high torque pulses which exceed even the short time overload capacity described by Fig. 4.4, a mechanical energy storage device, for instance a flywheel, may be used; of course, the inertia must be accelerated to sufficient speed before the load can be applied. This is the usual solution with highly pulsating loads such as punching presses.

#### 4.3.3 Periodic Intermittent Duty

With some types of load, for example elevators, automatic machine tools, mine hoists or rolling mill drives typical load cycles exist which are repeated periodically. A very simple case is seen in Fig. 4.5, where the power loss  $p_{1i}$  follows a rectangular periodic pattern.

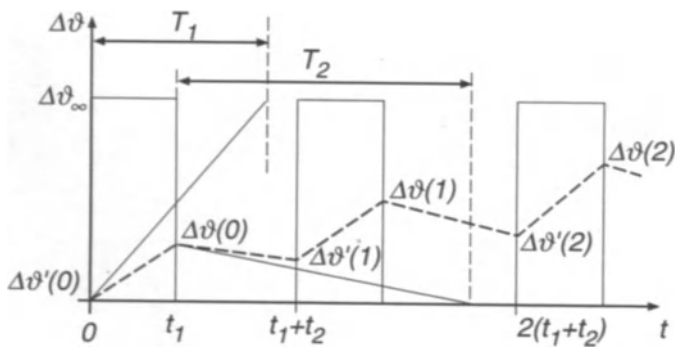


**Fig. 4.5.** Thermal transients for intermittent duty

This results in temperature fluctuations, the mean of which rises until a steady state condition is reached. With the thermal time constants  $T_1$ ,  $T_2$  valid during on- and off-times  $t_1$ ,  $t_2$ , the following relations hold:

$$\begin{aligned}\Delta\vartheta'(\nu + 1) &= \Delta\vartheta(\nu) e^{-t_2/T_2}, \\ \Delta\vartheta(\nu + 1) &= \Delta\vartheta'(\nu + 1) e^{-t_1/T_1} + \Delta\vartheta_\infty [1 - e^{-t_1/T_1}].\end{aligned}\quad (4.10)$$

Eliminating  $\Delta\vartheta'(\nu + 1)$  yields

$$\Delta\vartheta(\nu + 1) = \Delta\vartheta(0) + a \Delta\vartheta(\nu), \quad (4.11)$$

where

$$\begin{aligned}\Delta\vartheta(0) &= [1 - e^{-t_1/T_1}] \Delta\vartheta_\infty, \\ a &= e^{-(t_1/T_1+t_2/T_2)} < 1.\end{aligned}\quad (4.12)$$

Equation (4.11) represents a linear recursion between two successive peak values of the temperature. The solution is a geometrical progression

$$\begin{aligned}\Delta\vartheta(\nu) &= \frac{1 - a^{\nu+1}}{1 - a} \Delta\vartheta(0) = \\ &= \frac{1 - e^{-t_1/T_1}}{1 - e^{-(t_1/T_1+t_2/T_2)}} [1 - e^{-(\nu+1)(t_1/T_1+t_2/T_2)}] \Delta\vartheta_\infty.\end{aligned}\quad (4.13)$$

Because of  $t = t_1 + \nu(t_1 + t_2)$  the peak values lie on an exponential function having a time constant

$$T_\vartheta \approx \frac{t_1 + t_2}{t_1/T_1 + t_2/T_2}, \quad \text{where } T_1 < T_\vartheta < T_2. \quad (4.14)$$

The steady state temperature follows from Eq. (4.13)

$$\Delta\vartheta(\infty) = \frac{1 - e^{-t_1/T_1}}{1 - e^{-(t_1/T_1+t_2/T_2)}} \Delta\vartheta_\infty. \quad (4.15)$$

With forced ventilation, a special case exists, resulting in

$$T_1 = T_2 = T_\vartheta.$$

## 5. Separately Excited DC Machine

### 5.1 Introduction

Direct current (DC) motors have been dominating the field of adjustable speed drives for over a century; they are still the most common choice if a controlled electrical drive operating over a wide speed range is specified. This is due to their excellent operational properties and control characteristics; the only essential disadvantage is the mechanical commutator which restricts the power and speed of the motor, increases the inertia and the axial length and requires periodic maintenance. With alternating current (AC) motors, fed by variable frequency static power converters, the commutator is eliminated, however at the cost of increased complexity. This is one of the reasons why controlled AC drives could not immediately supplant DC drives, once the semiconductor-technology had sufficiently advanced.

The principle of a DC machine operating in steady state is assumed to be known [3, 59], but let us recall some basic facts.

In Fig. 5.1a a schematic cross-section through a two-pole DC machine is shown, containing the fixed stator  $S$  and the cylindrical rotor, called armature  $A$ . While rotor and pole shoes are always laminated in order to reduce the iron losses caused by the varying magnetic field, the rest of the stator is laminated only in larger machines, when the motor is required to operate with rapidly varying torque and speed or when a static power converter with highly distorted voltages and currents is employed as the power supply. The main poles  $MP$  are fitted with the field windings, carrying the field current  $i_e$  which drives the main flux  $\Phi_e$  through stator and rotor. A closed armature winding is placed in the axial slots of the rotor and connected to the commutator bars; it is supplied through the brushes and the commutator with the armature current  $i_a$ . This creates a distributed ampereturns (m.m.f.) wave, fixed in space and orientated in the direction of the quadrature axis, orthogonal to the main field axis, so that maximum torque for a given armature current is produced.

In view of the large airgap in the quadrature direction the resulting armature flux  $\Phi_a$  is much smaller than the main flux  $\Phi_e$ . It can be reduced even further by placing compensating windings  $CW$  in axial slots on the pole shoes and connecting them in series with the armature. Their opposing ampereturns all but cancel the quadrature field excited by the armature and removes the undesired armature reaction, which otherwise tends to distort the even distribution of the

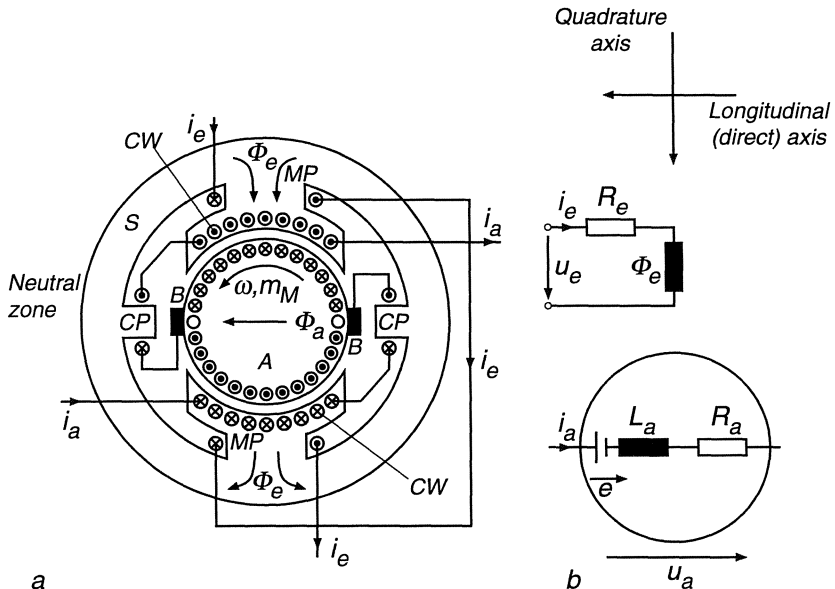


Fig. 5.1. Cross-section (a) and schematic circuit (b) of a DC machine

main field under the poles along the circumference of the rotor. Compensating windings are common only on larger machines or converter-fed motors for heavy duty applications such as traction or steel-mill drives. Compensated DC machines can withstand higher overloads than uncompensated ones; also the armature current may rise much faster and higher current harmonics are acceptable without detrimental effects on commutation, i.e. sparking of brushes. This is of particular importance if the machine is supplied by a static converter.

The commutating poles  $CP$ , placed between the main poles and also carrying the armature current, have the task of locally modifying the field in the neutral zone, in order to achieve rapid and sparkfree commutation. This is done by inducing a suitable voltage in the armature coil temporarily shorted by the brushes.

The principle of commutation is illustrated in Fig. 5.2, where the closed armature winding of a two-pole DC motor is schematically drawn, showing the brush positions at two consecutive instants of time. Clearly, when the feeding points of the winding are shifted by the relative motion of the brushes to the next commutator bars, the commutating coil is temporarily short circuited, while the current is inverted. Since each coil, being embedded in slots surrounded by iron, exhibits some inductance, the commutation is a continuous process which takes a finite time; this limits the speed at which the motor can operate without excessively sparking brushes.

The electric torque  $m_M$  is exerted at the rotor surface; more precisely, by magnetic forces acting on the sides of the slots. It is proportional to the product

of main flux and armature current. The voltages in the armature circuit consist of an induced voltage (e.m.f.) proportional to main flux and speed, in addition to resistive and inductive voltage drops in the armature-, commutating- and compensating windings as well as the armature connections and brushes. The main flux is thus of prime importance for operating and controlling the DC machine; greatest flexibility exists, when the field current is supplied by an independent source so that it can be varied at will.

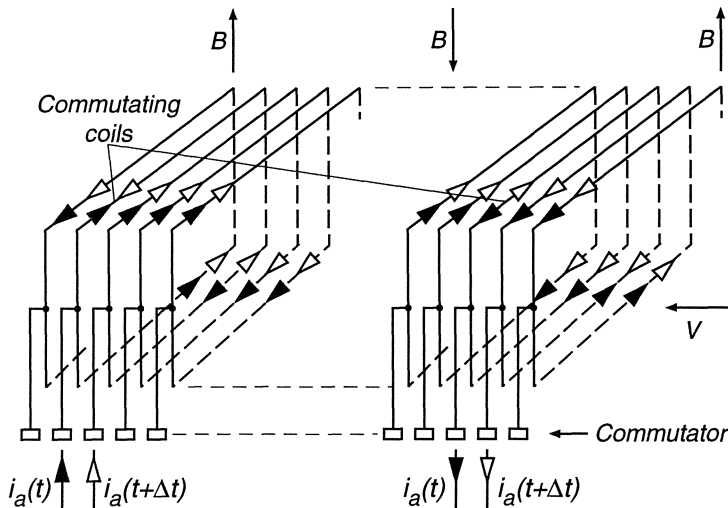


Fig. 5.2. Commutation of current in an armature coil

In Fig. 5.1 b a simplified scheme of a separately excited DC machine is shown, where the resulting magnetic fluxes are concentrated into lumped inductances which are orientated parallel and orthogonal to the main field axis. The total armature voltage  $u_a$  thus consists of the voltage  $e$ , induced by rotation, the voltage of self induction  $L_a \frac{di_a}{dt}$  and the ohmic drop  $R_a i_a$ , where  $L_a$ ,  $R_a$  are the resultant parameters in the armature circuit. With larger machines,  $R_a i_a \ll u_a$  is valid at normal speed and load. Also, the power required for excitation, i.e. the losses in the field winding, amounts to only a few percent of the power converted in the armature.

With motors having permanent magnet excitation the power losses in the field winding and the need for a separate field power supply are avoided at the cost of operational flexibility. Servomotors for machine tool feed drives are usually of the permanent magnet type.

The DC machine as a dynamic system, including the interactions of the electromagnetic and the mechanical effects, is dealt with in the next section.

## 5.2 Differential Equations and Block Diagram

The equivalent circuit of the separately excited DC machine can be represented in schematic form by Fig. 5.3 containing concentrated components and showing no longer a geometrical resemblance to the actual system.

The pertinent differential equations are

$$R_a i_a + L_a \frac{di_a}{dt} + e = u_a \quad \text{armature circuit}^1$$

$$e = c_1 \Phi_e \omega \quad \text{induced voltage (e.m.f.)}$$

$$J \frac{d\omega}{dt} = m_M - m_L \quad \text{Newton's law, assuming lumped inertia}$$

$$m_M = c_2 \Phi_e i_a \quad \text{electric torque}$$

$$R_e i_e + N_e \frac{d\Phi_e}{dt} = u_e \quad \text{field circuit}$$

$$\Phi_e = f(i_e) \quad \text{static magnetising curve (omitting hysteresis)}$$

$$\frac{d\omega}{dt} = \omega \quad \text{angular velocity.}$$

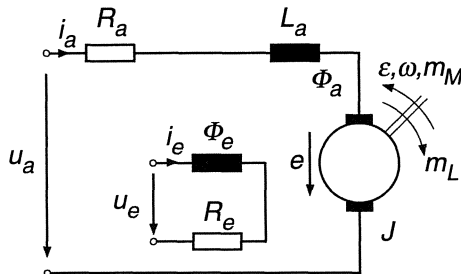


Fig. 5.3. Equivalent circuit of DC machine

Eliminating  $\Phi_e$  from the second and fourth equation results in

$$e i_a = \frac{c_1}{c_2} m_M \omega ,$$

where  $e i_a$  is the instantaneous electrical power converted in the armature to the mechanical power  $m_M \omega$ . Both must be identical, hence  $c_1 = c_2 = c$ .

Normalisation by the rated values

$\omega_0$  nominal no-load speed (base speed)

$\Phi_{e0}$  nominal flux

$u_{a0} = e_0 = c \Phi_{e0} \omega_0$  nominal armature voltage

$i_{a0} = \frac{u_{a0}}{R_a}$  extrapolated stalled armature current at nominal voltage (8–10 times rated current)

$m_0 = c \Phi_{e0} i_{a0}$  extrapolated stalled rotor torque

$u_{e0} = R_e i_{e0}$  nominal field voltage

<sup>1</sup>The voltage arrows in Fig. 5.1 b and all later figures are drawn according to the continental usage, being in direct correspondence with the pertinent mesh equation

results in the following non-dimensional state equations

$$T_a \frac{d}{dt} \left( \frac{i_1}{i_{a0}} \right) = \frac{u_a}{u_{a0}} - \frac{i_a}{i_{a0}} - \frac{\omega}{\omega_0} \frac{\Phi_e}{\Phi_{e0}}, \quad T_a = \frac{L_a}{R_a}; \quad (5.1)$$

$$T_{e0} \frac{d}{dt} \left( \frac{\Phi_e}{\Phi_{e0}} \right) = \frac{u_e}{u_{e0}} - f_e \left( \frac{\Phi_e}{\Phi_{e0}} \right), \quad T_{e0} = \frac{N_e \Phi_{e0}}{u_{e0}}; \quad (5.2)$$

$$T_{mn} \frac{d}{dt} \left( \frac{\omega}{\omega_0} \right) = \frac{i_a}{i_{a0}} \frac{\Phi_e}{\Phi_{e0}} - \frac{m_L}{m_0}, \quad T_{mn} = \frac{J \omega_0}{m_0}; \quad (5.3)$$

$$T_\varepsilon \frac{d}{dt} \left( \frac{\varepsilon}{\varepsilon_0} \right) = \frac{\omega}{\omega_0}, \quad T_\varepsilon = \frac{\varepsilon_0}{\omega_0}. \quad (5.4)$$

$i_e/i_{e0} = f_e(\Phi_e/\Phi_{e0})$  is the inverse normalised magnetisation curve,  $\varepsilon_0$  is an arbitrary reference angle.

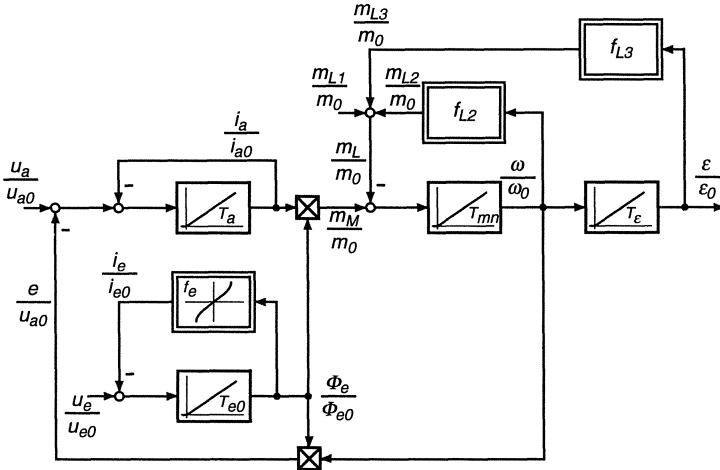


Fig. 5.4. Block diagram of the separately excited DC machine

The voltages  $u_a, u_e$  are assumed to be independently controllable,  $m_L$  is the applied load torque. The output variables of the four integrators correspond to the four storage quantities, subject to continuous change only. Due to the larger airgap in the quadrature axis and the possible presence of a compensating winding  $T_a \ll T_{e0}$  holds. Magnetic saturation in the quadrature direction is usually negligible.

The dynamic system, described by Eqs. (5.1 – 5.4), is represented as a block diagram in Fig. 5.4, where it is assumed that the load torque consists of an independent component  $m_{L1}$  acting as a disturbance and two components as nonlinear functions of speed and position respectively,

$$\frac{m_L}{m_0} = \frac{m_{L1}}{m_0} + f_{L2} \left( \frac{\omega}{\omega_0} \right) + f_{L3} \left( \frac{\varepsilon}{\varepsilon_0} \right). \quad (5.5)$$

If the load torque shows no such dependence, the corresponding functions are zero.

The block diagram contains linear integrators with their respective time constants and nonlinear algebraic functional blocks.

### 5.3 Steady State Characteristics with Armature and Field Control

The steady state condition, valid with constant input quantities  $u_a$ ,  $u_e$ ,  $m_L$  is obtained by setting the derivatives in Eqs. (5.1 – 5.3) equal to zero,

$$\frac{u_a}{u_{a0}} - \frac{i_a}{i_{a0}} - \frac{\omega}{\omega_0} \frac{\Phi_e}{\Phi_{e0}} = 0 , \quad (5.6)$$

$$\frac{u_e}{u_{e0}} - f_e \left( \frac{\Phi_e}{\Phi_{e0}} \right) = 0 , \quad (5.7)$$

$$\frac{i_a}{i_{a0}} \frac{\Phi_e}{\Phi_{e0}} - \frac{m_L}{m_0} = 0 . \quad (5.8)$$

The angle of rotation  $\varepsilon$  changes linearly with time; it is of no consequence for the time being. For the following discussion the normalised flux

$$b = \frac{\Phi_e}{\Phi_{e0}} \leq 1 ,$$

which is limited by saturation of the iron core, is assumed as an independent control input, instead of  $u_e/u_{e0}$ . This results in

$$\frac{\omega}{\omega_0} = \frac{1}{b} \frac{u_a}{u_{a0}} - \frac{1}{b^2} \frac{m_L}{m_0} , \quad (5.9)$$

$$\frac{i_a}{i_{a0}} = \frac{1}{b} \frac{m_L}{m_0} . \quad (5.10)$$

Here the steady state behaviour of the controlled motor,

$$\frac{\omega}{\omega_0} = f_1 \left( \frac{u_a}{u_{a0}}, \frac{m_L}{m_0} \right) ,$$

$$\frac{i_a}{i_{a0}} = f_2 \left( \frac{m_L}{m_0} \right)$$

is characterised by linear functions, connecting speed, torque and armature current.

Depending on whether  $u_a$  or  $\Phi_e$ , i.e.  $u_e$ , serves as control input, the term armature- or field control applies.

### 5.3.1 Armature Control

Assuming  $b = \Phi_e/\Phi_{e0} = 1$ , the nonlinear effect of the two multiplications in Fig. 5.4 vanishes and a particularly simple set of linear control curves results,

$$\frac{\omega}{\omega_0} = \frac{u_a}{u_{a0}} - \frac{m_L}{m_0}, \quad (5.11)$$

$$\frac{i_a}{i_{a0}} = \frac{m_L}{m_0}; \quad (5.12)$$

they are drawn in Fig. 5.5 as straight lines. The torque-speed curves are valid in all four quadrants permitting continuous control and reversal of torque and speed.

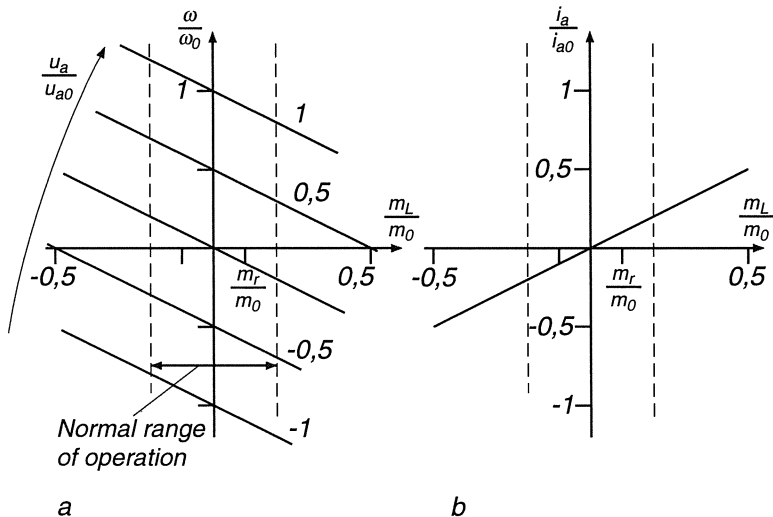


**Fig. 5.5.** Steady state curves of DC motor with armature control,  $\Phi_e = \Phi_{e0}$

Since the armature voltage  $u_a$  is referred to its rated value  $u_{a0}$ , only the range  $-1 \leq u_a/u_{a0} \leq 1$  is of interest. Excessive voltage would cause sparking of the brushes and possibly commutation failure by formation of an arc short-circuiting the brushes (flashover).

The armature current is proportional to the torque, independent of voltage and speed. Armature current and torque are normalised with their extrapolated values at standstill. Therefore the normal operating region is contained in a narrow band,

$$-0.2 \leq \frac{m_L}{m_0} = \frac{i_a}{i_{a0}} \leq 0.2,$$

even when allowing a temporary overload of about twice rated torque. Outside this range, the curves are likely to be distorted by armature reaction and there

may be commutation problems, particularly when no compensating winding is present.

### 5.3.2 Field Control

The second option for controlling the motor is by changing the main flux  $\Phi_e$ . Due to saturation  $\Phi_e$  cannot be increased much beyond  $\Phi_{e0}$  - otherwise the motor designer would not have fully utilised the potential of the motor - hence it is only feasible to weaken the field,

$$-1 \leq b = \Phi_e/\Phi_{e0} \leq 1 .$$

If the armature power supply permits operation in all four quadrants of the  $u_a$ ,  $i_a$ -plane, it is sufficient to restrict field control to positive values,  $b_{min} < b \leq 1$ .

The purpose of field weakening is to raise the speed at light load, as seen from Eq. (5.9), accepting the disadvantage of increasing the armature current for a given torque, Eq. (5.10). Therefore it is normally not appropriate to employ field weakening unless the possibilities of armature control have already been fully exploited.

Inserting  $u_a/u_{a0} = \pm 1$  into Eq. (5.9) yields a new set of steady state curves with the normalised field factor  $b$  as control parameter; the characteristics are again straight lines, however with increased slope (Fig. 5.6). The speed-torque curves intersect with the axes at

$$\text{no-load: } m_L = 0, \quad \frac{\omega_{NL}}{\omega_0} = \frac{1}{b},$$

$$\text{standstill: } \omega = 0, \quad \frac{m_{st}}{m_0} = b.$$

With reduced flux, the no-load speed rises, while the (extrapolated) stalled torque is reduced. Hence the slope of the curve is varying with  $1/b^2$ ; this inherently "soft" load behaviour is undesirable with drives to be controlled for constant speed.

As is seen in Fig. 5.6 b, the armature current and the armature losses increase when the motor is operated at a given torque with reduced field; therefore, as already mentioned, field weakening makes only sense if the desired operating point in the torque-speed plane cannot be reached by armature voltage control at full field or if the armature voltage is fixed. At less than maximum armature voltage, operation at reduced field is uncommon, except in special circumstances discussed later. Neither is field weakening a solution for the start-up of motors since at standstill the armature current is not affected by the main flux.

Figure 5.6 a indicates also that a reduction of the field does not necessarily lead to higher speed; because of the steeper torque-speed curves the result of field-weakening may even be reduced speed at higher armature current which is of course most undesirable. The maximum speed at a given torque is obtained by differentiating Eq. (5.9), assuming  $u_a = u_{a0}$ ,

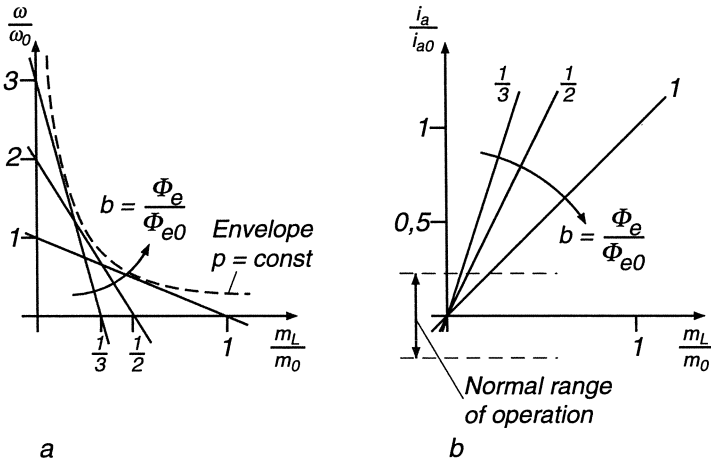


Fig. 5.6. Steady-state curves of DC motor in field control range,  $u_a = u_{a0}$

$$\left. \frac{d \frac{\omega}{\omega_0}}{db} \right|_{m_L=\text{const}} = -\frac{1}{b^2} + \frac{2}{b^3} \frac{m_L}{m_0} = 0,$$

which results in a practical lower limit for the field

$$b_{\min} = 2 \frac{m_L}{m_0}, \quad (5.13)$$

where the undesirable speed reduction begins. Note that  $m_0$  is the extrapolated stalled torque for rated armature voltage and field. Inserting Eq.(5.13) into Eq. (5.9) and assuming  $u_a = u_{a0}$  yields a hyperbolic function

$$\frac{\omega}{\omega_0} = \frac{1}{4} \frac{m_0}{m_L} \quad (5.14)$$

which represents an envelope for the family of torque-speed-curves with parameter  $b$ . Maximum power is obtained at the point, where the straight line is tangent to the hyperbola. In order to avoid the situation mentioned before, the motor should never be operated at the right hand side of the tangent point.

DC machines without compensating windings show a pronounced armature reaction in the field weakening range because the field distribution in the airgap is no longer stabilised by saturation. Therefore the validity of the torque-speed-curves is restricted to small values of the normalised armature current; higher currents have a detrimental effect on commutation and may result in sparking of the brushes. This calls for a reduction of the maximum armature current at reduced field and hence a power derating.

In spite of these drawbacks, field weakening is a valuable means for increasing the speed in the low torque region; typical applications are spindle drives on machine tools, in order to allow cutting at full power, even with a small

diameter workpiece or tool. Other examples are reversing rolling mills for rods or rails, where the first few passes call for high torque in order to squeeze the short and wide slabs whereas in the later passes, when the material is thin and long, low torque but high rolling speed are required in order to save time. A similar situation exists with coilers where high speed and low torque are needed when the diameter of the coil is small, while the reverse is true with a large coil diameter.

After eliminating with  $u_a/u_{a0} = 1$  the field factor  $b$  from Eqs. (5.9, 5.10) an expression for the mechanical power is derived

$$\frac{\omega}{\omega_0} \frac{m_L}{m_0} = \frac{i_a}{i_{a0}} \left( 1 - \frac{i_a}{i_{a0}} \right) \quad (5.15)$$

which only depends on the normalised armature current. Hence, with limited armature current, the motor can be operated at variable speed with a given maximum power, indicating that field weakening has a similar effect as a variable gear for stepping up the speed of the load. For the reasons already mentioned and because of the mechanical stresses, the maximum speed achieved by field weakening is seldom higher than two or three times base speed depending on the design and the size of the machine. However, there are exceptions, where a much higher speed ratio may be necessary.

The similarity of a speed increase by field control and by a variable gear is corroborated by their effects on the mechanical time constant. At rated field,  $\Phi_e = \Phi_{e0}$ , the nominal time constant is  $T_{mn} = J\omega_0/m_{0n}$ , where  $\omega_0$  is the base (no load) speed and  $m_0$  the extrapolated stalled torque at rated armature voltage and field. With reduced field, the no load speed is raised to  $b^{-1}\omega_0$ , while the stalled torque is lowered to  $b m_0$ . Hence the mechanical time constant is a quadratic function of the field factor,

$$T_m (b \leq 1) = \frac{J\omega_0}{m_{0n}} b^{-2} = T_{mn} b^{-2} .$$

A similar effect is observed if the load is coupled to the motor through a step-up gear having the speed ratio  $b^{-1}$ ; as explained in Sect. 1.3, this would increase the effective inertia of the load, as seen from the motor side, by  $b^{-2}$ .

### 5.3.3 Combined Armature and Field Control

From the preceding paragraph it is seen that armature and field-control of DC motors each have their merits but that their normal applications exclude each other. Below base speed  $\omega_0$  the main flux is best kept at nominal value  $\Phi_{e0}$  while the speed is varied through the armature voltage  $u_a$ . This is called the base speed- or armature control range. When the rated armature voltage  $\pm u_{a0}$  is reached, a further speed increase is only possible by lowering the main flux, thus creating separate field-control regions which extend the base speed range in each direction of rotation. This is depicted in the diagram Fig. 5.7.

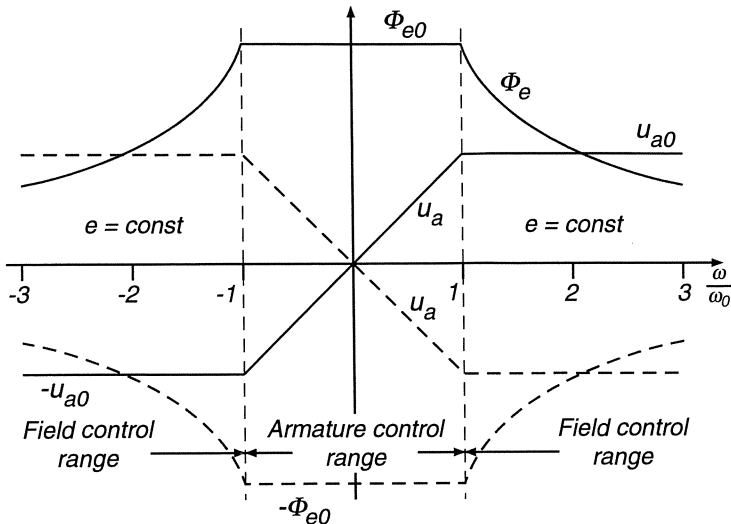


Fig. 5.7. Control ranges of DC motor in steady state

It is seen that a reversal of the no-load speed requires reversed armature voltage. In principle it would also be possible to reverse the motor speed with the same polarity of the armature voltage by reversing the field (dashed curves); at the same time the torque would be reversed so that the motor operates in the third quadrant. However, this method of "field reversal" which was frequently used in the past is rarely employed today since it calls for the de-excitation and subsequent re-excitation of the motor; this requires time in view of the large magnetic energy stored in the field circuit. If high forcing voltage is applied to the field winding in order to accelerate the flux reversal, considerable voltages are also induced in the armature winding endangering the commutator. Also, the armature current must be blocked during the time of flux reversal causing an interruption of the torque. With larger motors, this transition time with zero torque may be up to 1s which is not acceptable for a fast reversing drive. It is for these reasons that drives which are expected to operate with both directions of torque and speed ("four quadrant drive", capable of operation in all quadrants of the torque-speed plane) are today usually equipped with an armature power supply providing both polarities of voltage and current (a "four quadrant DC power supply", capable of operation in all quadrants of the voltage-current plane); this has the advantage that the polarity of the main flux can remain unchanged.

When several motors are fed from a common armature bus voltage, a slight adjustment of the fields is sometimes the simplest solution for closely matching the speeds of the motors to the requirements of the load; this may be the case with paper mill- drives where a continuous web of material is passing sequentially through the working stations with their separate drive motors. In

this case, some individual field weakening, such as  $\Phi_e > 0.8\Phi_{e0}$ , may be applied simultaneously with armature voltage control.

At low power, the combined armature-field control shown in Fig. 5.7 can be realised by a circuit containing resistors. With larger machines this is not feasible in view of the high losses, so that separate power supplies are provided for feeding the armature and the field windings. Field weakening may be performed automatically by an auxiliary control loop which, by adjusting the field supply voltage, limits the induced armature voltage according to

$$\frac{e}{u_{a0}} = \frac{\omega}{\omega_0} \frac{\Phi_e}{\Phi_{e0}} \leq 1. \quad (5.16)$$

This causes the desired variation of the flux in the field weakening range (see also Sect. 7.3)

The operating regions with armature and field control in the torque- speed plane are displayed in Fig. 5.8. The curves  $i_a = \text{const.}$  are represented by parallel straight lines in the armature control regime; in the field weakening region, the torque at a given armature current is reduced, because of  $m_M \approx \Phi_e i_a$ . For the same reason, the curves for  $u_a = \text{const.}$  become steeper when the flux is reduced. In the upper right hand corner a typical commutation limit is indicated caused by a lower maximum armature current when the field is weakened.

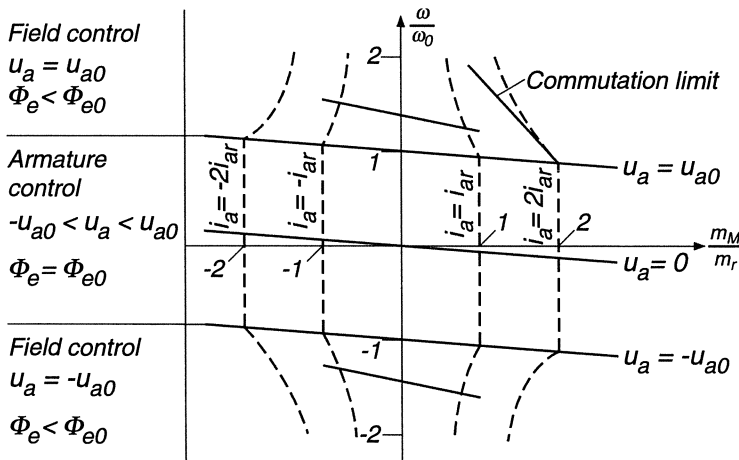


**Fig. 5.8.** Operating regions of separately excited DC motor in torque-speed plane

The figure clearly shows that the DC motor represents a linear control plant only in the armature control region; beyond base speed, there are considerable non-linearities even in steady state condition.

Simultaneous field- and armature-control is sometimes proposed as a means of reducing motor losses through diminished copper losses in the field windings and iron losses in the armature; of course, this is only applicable at very light

load when the increased conduction losses in the armature are not masking this effect.

Also, this may cause an objectionable delay in building up motor torque, should an unexpected load surge occur, because the flux would first have to be raised to full value. Hence, this practice can only be a marginal option in few applications, such as battery supplied electric car drives, where energy conservation is of overriding importance and where sudden load surges do not occur.

## 5.4 Dynamic Behaviour of DC Motor at Constant Flux

In order to have a clearer view of the transient behaviour of a DC machine the block diagram in Fig. 5.4 is simplified by assuming the armature voltage to be an impressed and independently variable input quantity, the load torque  $m_L$  as an independent disturbance and the flux  $\Phi_e$  a suitably chosen parameter. This results in Fig. 5.9; the angle of rotation is again left out of the consideration for the time being, as it does not affect the operation of the motor.

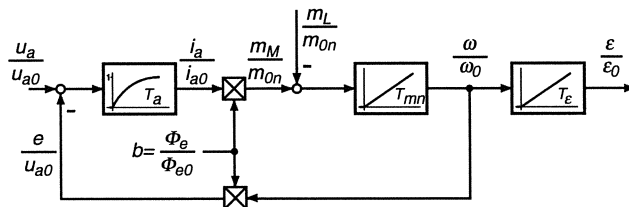


Fig. 5.9. Linear block diagram of DC motor

Assuming the main flux  $\Phi_e$  to be a constant parameter, a linear system results which may be described by transfer functions; with the Laplace-transform

$$L(x(t)) = \int_0^\infty x(t) e^{-st} dt = X(s), \quad s = \sigma + j\omega,$$

of the nondimensional variables

$$L\left(\frac{u_a}{u_{ao}}\right) = U_a(s), \quad L\left(\frac{\omega}{\omega_0}\right) = \Omega(s), \quad L\left(\frac{i_a}{i_{ao}}\right) = I_a(s), \quad \text{etc.}$$

and the normalised field parameter

$$\frac{\Phi_e}{\Phi_{eo}} = b \leq 1$$

the following equations are obtained

$$\Omega(s) = F_1(s) U_a(s) + F_2(s) M_L(s) = \frac{b U_a(s) - (T_a s + 1) M_L(s)}{T_{mn} s (T_a s + 1) + b^2}, \quad (5.17)$$

$$I_a(s) = F_3(s) U_a(s) + F_1(s) M_L(s) = \frac{T_{mn} s U_a(s) + b M_L(s)}{T_{mn} s (T_a s + 1) + b^2}. \quad (5.18)$$

$U_a(s)$  is the independent input or actuating variable,  $M_L(s)$  is a disturbance, also assumed to be impressed.  $\Omega(s)$  and  $I_a(s)$  stand for output variables, which appear in the frequency domain as linear combinations of the input variables  $U_a(s)$  and  $M_L(s)$ .

All partial transfer functions of the multivariable plant have the same denominator,

$$N(s) = T_{mn} s (T_a s + 1) + b^2 = T_{mn} T_a (s - s_1)(s - s_2), \quad (5.19)$$

which is identical with the characteristic polynomial of the pertinent linear differential equation. The zeros of  $N(s)$  are the eigenvalues of the system,

$$s_{1,2} = \frac{1}{2 T_a} \left[ -1 \pm \sqrt{1 - (2b)^2 T_a / T_{mn}} \right]; \quad (5.20)$$

the natural frequency is

$$\omega_e = \sqrt{s_1 s_2} = \frac{b}{\sqrt{T_a T_{mn}}}, \quad (5.21)$$

the damping ratio

$$D = \frac{-\text{Re}(s_1)}{|s_1|} = \frac{1}{2b} \sqrt{\frac{T_{mn}}{T_a}}. \quad (5.22)$$

Field weakening ( $b < 1$ ) causes the motor to respond more sluggishly to control or disturbance inputs as is manifested by a lower natural frequency and increased damping ratio. Figure 5.10 shows the root locus, i.e. the locus of the eigenvalues in the complex plane, for different values of the parameter  $b$ . Real eigenvalues, corresponding to asymptotic transients ( $D > 1$ ) exist for

$$T_{mn} > (2b)^2 T_a.$$

In Fig. 5.10 it is assumed that the motor exhibits below base speed ( $b = 1$ ) a damped oscillatory response. This may in practice be the case if the inertia of the drive is deliberately kept small as with servo drives or rolling-mill reversing drives. In most cases, the eigenvalues of a drive are real because of the added inertia of the load.

In Fig. 5.11 the step responses of the motor speed and the armature current are depicted when the motor, initially at standstill, is started without load ( $m_L = 0$ ) at  $t = 0$  by applying armature voltage  $u_a = 0.1 u_{a0}$ . After attaining its steady state condition, load is applied at  $t_1$  in the form of constant torque,  $m_L = 0.02 m_{0n}$ , corresponding approximately to 0.2 of rated torque.

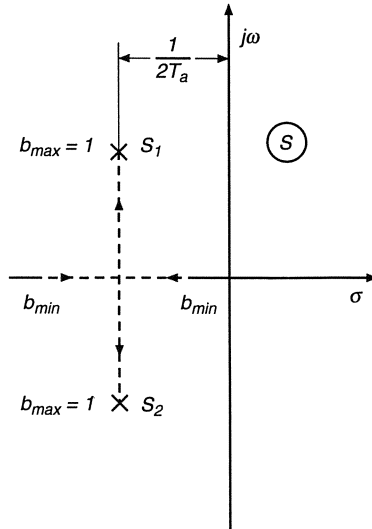


**Fig. 5.10.** Root locus of DC motor for different field factor  $b \leq 1$

The transients in Fig. 5.11 have been computed for three different values of  $b$ , which result in the damping ratios  $D = 1/\sqrt{2}, 1, \sqrt{2}$ . It is seen that field weakening makes the motor much more sensitive to load; at higher torque the speed under load would even drop below the value at full flux ( $b = 1$ ), as indicated in Fig. 5.6 a.

However, the initial slope of the speed at  $t_1$  is the same in all cases being solely dependent on the nominal mechanical time constant  $T_{mn}$ ,

$$\left. \frac{d}{dt} \left( \frac{\omega}{\omega_0} \right) \right|_{t_1} = -\frac{m_L}{m_0} \frac{1}{T_{mn}} \neq f(b).$$

This is immediately understood from inspection of Fig. 5.9, as the current  $i_a$  is delayed by the armature inductance  $L_a$ .

The steady-state value of the armature current for no-load condition (neglecting friction and windage) is zero; this is apparent from the factor  $s$  in the numerator of the transfer function  $F_3$ , Eq.(5.18), which indicates a differentiating effect.

If the load torque contains a component rising with speed (Fig. 5.12 a)

$$\frac{m_L}{m_0} = \frac{m_{L1}}{m_0} + k_L \frac{\omega}{\omega_0}, \quad (5.23)$$

block diagram 5.12 b results; the integrator now possesses proportional negative feedback, thus assuming the properties of a lag element. The partial transfer function  $F_3$  connecting armature voltage and current is then

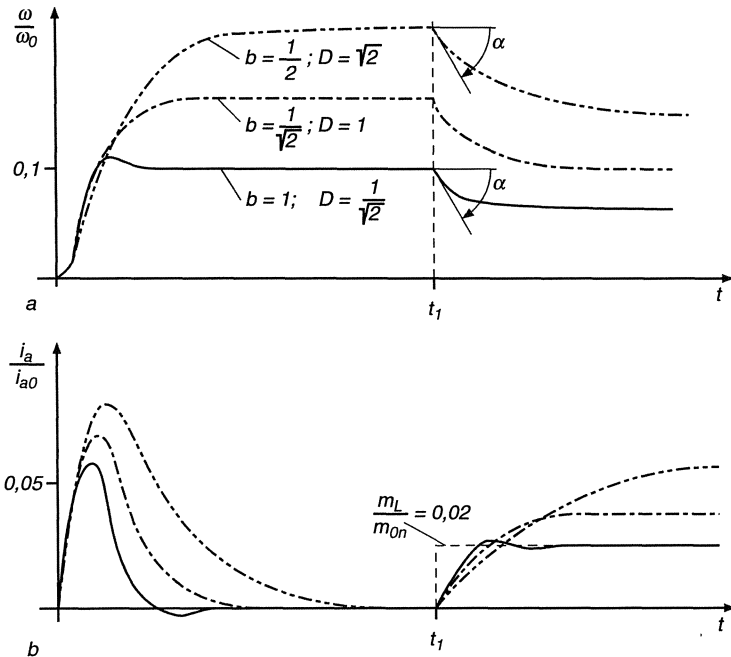


**Fig. 5.11.** Starting and load transients of DC motor for different field factor  $b \leq 1$

$$\frac{I_a}{U_a}(s) = \frac{T_{mn}s + k_L}{T_{mn}T_a s^2 + (T_{mn} + k_L T_a)s + b^2 + k_L}, \quad (5.24)$$

with  $k_L > -b^2$  and  $k_L > -T_{mn}/T_a$  being required for stability. The damping ratio  $D_1$  may be referred to the damping ratio  $D$  at no load

$$D_1 = D \frac{1 + \frac{1}{(2D)^2} \frac{k_L}{b^2}}{\sqrt{1 + \frac{k_L}{b^2}}}. \quad (5.25)$$

The differentiating effect in Eq. (5.18) disappears in the presence of load torque.

Some drives are subject to disturbances by periodic components in the supply voltage or the load torque causing continuous oscillations of armature current and speed about their steady state values. The transfer function permits a simple computation. When a torque consists of a constant and a sinusoidally varying component

$$\frac{m_L}{m_0} = \frac{m_{L1}}{m_0} + \frac{\widehat{\Delta m_L}}{m_0} \cos \omega_m t,$$

each variable of the linear drive will in steady state contain a periodic component of the same frequency that may be computed by linear superposition.

With the complex expression

$$\frac{\Delta m_L}{m_0} \cos \omega_m t = \frac{\widehat{\Delta m_L}}{2m_0} [e^{j\omega_m t} + e^{-j\omega_m t}]$$

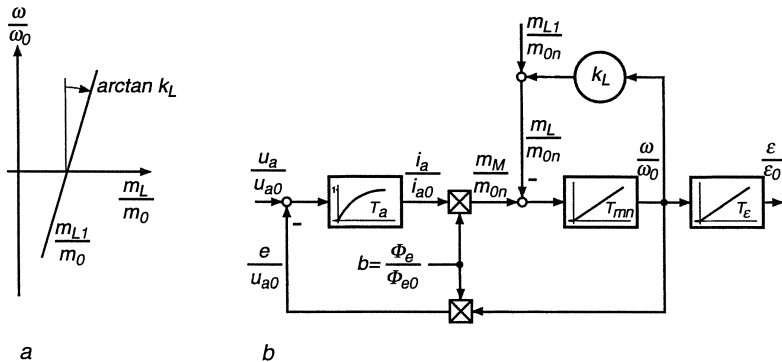


Fig. 5.12. DC motor with speed- dependent load

we find from Eq. (5.18) the peak value of the alternating current component ( $k_L = 0$ )

$$\widehat{\Delta i_a} = \left| \frac{b}{T_{mn} T_a (j \omega_m)^2 + T_{mn} j \omega_m + b^2} \right| \frac{\widehat{\Delta m_L}}{m_0} . \quad (5.26)$$

Similarly the phase of the oscillatory current may be determined. If the frequency of a periodic disturbance lies in the neighbourhood of the eigenvalues of a poorly damped drive, a resonant condition could exist causing large amplitudes of the oscillatory current and speed deviations.

The dynamic behaviour of separately excited DC motors will be further discussed in later sections in connection with control problems.

## 6. DC Motor with Series Field Winding

This motor differs from the one previously discussed only by the design and the connection of the field winding which, according to Fig. 6.1, now carries part or all of the armature current.  $R_{a1}$  is the armature resistance, possibly increased by an external resistor,  $R_p$  is an adjustable shunt resistor for field weakening.

Because of their operating characteristics, series wound motors of larger rating are restricted to traction drives. In urban transportation, such as trolley buses or subways, motors up to about 200 kW are used but for main line locomotives motors up to about 1000 kW are common. In principle, series wound motors can be fed with either direct or alternating current; naturally the constructional design would be quite different; for example, a laminated stator and special provisions with regard to commutation are required for the AC motor. When AC traction was developed at the begin of the century, the current induced by transformer action in the armature coil temporarily shorted by the brushes during commutation, Fig. 5.2, caused problems, which were then solved by choosing a lower supply frequency; this is the reason for the  $16\frac{2}{3}$  Hz power supply in use until today on central European railways. Since compact and rugged power electronic components have become available, main line locomotives with AC supply are often equipped with rectifier-fed DC motors. In future, all these schemes are likely to be supplanted by AC motors fed from variable frequency inverters.

Small high-speed AC series motors, so called universal motors, have a wide field of application in household appliances and power tools.

The typical operating characteristics of a series wound motor could also be realised with a suitably controlled separately excited motor; this is preferable in view of the added flexibility, for example when a traction motor is supposed to serve as a regenerative brake.

### 6.1 Block Diagram of a Series-wound Motor

The equations describing the dynamics of the series wound motor are similar to those derived in Chap. 5. We assume that the field and the armature windings are orthogonal to each other and hence magnetically decoupled. Due to the large airgap in the armature axis, the magnetic circuit is assumed to be linear in quadrature direction.

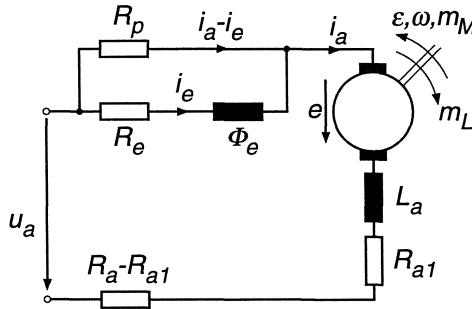


Fig. 6.1. DC motor with series field winding

$$L_a \frac{di_a}{dt} = u_a - R_a i_a - R_p (i_a - i_e) - e, \quad (6.1)$$

$$N_e \frac{d\Phi_e}{dt} = -R_e i_e + R_p (i_a - i_e), \quad (6.2)$$

$$e = c \Phi_e \omega, \quad (6.3)$$

$$m_M = c \Phi_e i_a, \quad (6.4)$$

$$J \frac{d\omega}{dt} = m_M - m_L. \quad (6.5)$$

A nominal operating point (index 1) is defined at rated armature voltage  $u_{a1}$ , without field weakening ( $R_p \rightarrow \infty$ ) and with no external armature resistor ( $R_a = R_{a1}$ ). At this reference point, the following steady state equations hold:

$$\begin{aligned} e_1 &= c \Phi_{e1} \omega_1 = \eta_1 u_{a1} \\ i_{a1} &= i_{e1} = (1 - \eta_1) \frac{u_{a1}}{R_{a1} + R_e}, \\ m_1 &= c \Phi_{e1} i_{a1}. \end{aligned}$$

$\eta_1 = e_1/u_{a1}$  is the electrical efficiency at the nominal operating point (not accounting for iron- and friction losses). These quantities are used for normalising the Eqs. (6.1 – 6.5).

$$\frac{i_e}{i_{a1}} = f_e \left( \frac{\Phi_e}{\Phi_{e1}} \right) \quad (6.6)$$

is the magnetisation curve in the longitudinal axis of the machine.

As a result, three dimension-less first order state equations for the three energy storage variables  $i_a$ ,  $\Phi_e$ ,  $\omega$ , are obtained:

$$\begin{aligned} T_{a1} \frac{d}{dt} \left( \frac{i_a}{i_{a1}} \right) &= \frac{1}{1 - \eta_1} \left( \frac{u_a}{u_{a1}} - \eta_1 \frac{\Phi_e}{\Phi_{e1}} \frac{\omega}{\omega_1} \right) - \frac{R_a}{R_{a1} + R_e} \frac{i_a}{i_{a1}} \\ &\quad - \frac{R_p}{R_{a1} + R_e} \frac{i_a - i_e}{i_{a1}}, \quad T_{a1} = \frac{L_a}{R_{a1} + R_e}, \\ T_{e1} \frac{d}{dt} \left( \frac{\Phi_e}{\Phi_{e1}} \right) &= -\frac{R_e}{R_{a1} + R_e} \frac{i_e}{i_{a1}} + \frac{R_p}{R_{a1} + R_e} \frac{i_a - i_e}{i_{a1}}, \end{aligned} \quad (6.7)$$

$$T_{e1} = \frac{N_e \Phi_{e1}}{(R_{a1} + R_e) i_{a1}}, \quad (6.8)$$

$$T_{m1} \frac{d}{dt} \left( \frac{\omega}{\omega_1} \right) = \frac{\Phi_e}{\Phi_{e1}} \frac{i_a}{i_{a1}} - \frac{m_L}{m_1}, \quad T_{m1} = \frac{J \omega_1}{m_1}. \quad (6.9)$$

A graphical representation of these normalised equations is seen in Fig. 6.2; the continuous state variables appear at the outputs of integrators. The effect of the parallel resistor  $R_p$  in coupling the two magnetic circuits is clearly recognisable.

Without field weakening, i.e.  $R_p \rightarrow \infty$ ,  $i_e = i_a$  follows; armature and field winding then form part of a common electrical circuit, hence

$$\frac{d}{dt} (N_e \Phi_e + L_a i_a) = u_a - e - (R_a + R_e) i_a. \quad (6.10)$$

Normalisation, as before, yields

$$T_{e1} \frac{d}{dt} \left( \frac{\Phi_e}{\Phi_{e1}} + \frac{L_a i_{a1}}{N_e \Phi_{e1}} \frac{i_a}{i_{a1}} \right) = \frac{1}{1 - \eta_1} \left( \frac{u_a}{u_{a1}} - \eta_1 \frac{\Phi_e}{\Phi_{e1}} \frac{\omega}{\omega_1} \right) - \frac{R_a + R_e}{R_{a1} + R_e} \frac{i_a}{i_{a1}}.$$

Because of the larger airgap in the quadrature axis,

$$q = \frac{L_a i_{a1}}{N_e \Phi_{e1}} = \frac{\Psi_{a1}}{\Psi_{e1}} \ll 1.$$

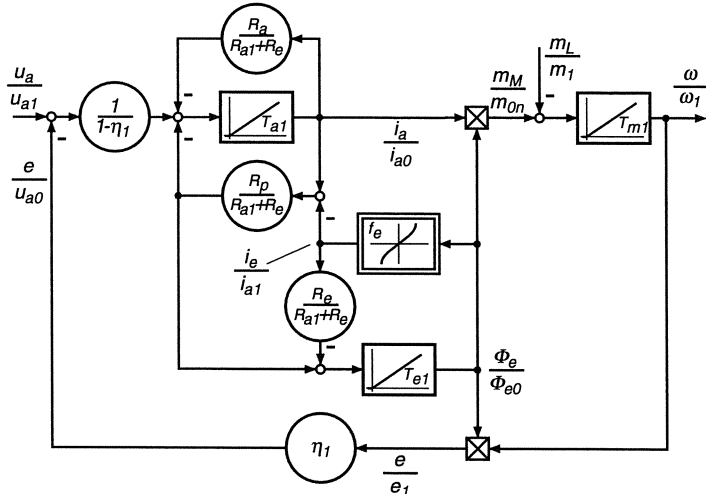


**Fig. 6.2.** Block diagram of series wound DC motor

With Eq. (6.6), noting  $i_e = i_a$ , Eq. (6.10) is transformed into

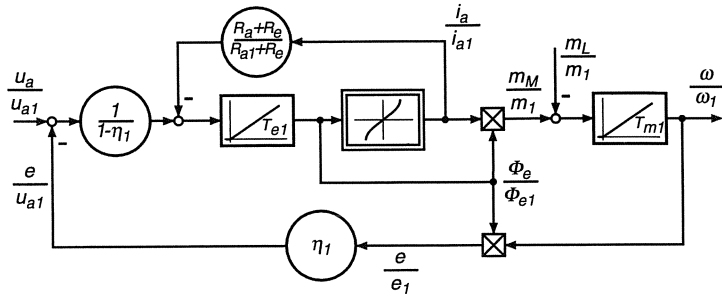


**Fig. 6.3.** Block diagram of series wound DC motor without field weakening

$$T_{e1} \frac{d}{dt} \left[ \frac{\Phi_e}{\Phi_{e1}} + q f_e \left( \frac{\Phi_e}{\Phi_{e1}} \right) \right] = \frac{1}{1 - \eta_1} \left( \frac{u_a}{u_{a1}} - \eta_1 \frac{\Phi_e}{\Phi_{e1}} \frac{\omega}{\omega_1} \right) - \frac{R_a + R_e}{R_{a1} + R_e} \frac{i_a}{i_{a1}}. \quad (6.11)$$

The associated block diagram is drawn in Fig. 6.3 for  $q \ll 1$ .

A characteristic feature of the series wound motor is the dependence of the flux on the armature current, which causes the flux to vary with the load. Since most of the armature voltage is balanced by the induced voltage,  $u_a \approx e = c\Phi_e \omega$ , high speed is to be expected at light load; this is reflected by the steady state curves discussed next. In order to gain a better insight, saturation of the iron is neglected. In Figs. 6.2 and 6.3 this is achieved when replacing the nonlinear functional block (Eq. 6.6) by

$$\frac{i_e}{i_{a1}} = f \left( \frac{\Phi_e}{\Phi_{e1}} \right) = \frac{\Phi_e}{\Phi_{e1}}. \quad (6.12)$$

At high current, when saturation cannot be neglected, the motor characteristics approach those of a separately excited motor, having constant main flux.

## 6.2 Steady State Characteristics

The steady state behaviour of the motor is again found by putting the right hand sides of Eqs. (6.7 – 6.9) equal zero; with Eq. (6.12), a linear magnetic circuit is assumed in the longitudinal direction of the machine. Elimination of  $i_e/i_{a1}$ , from Eqs. (6.7, 6.8) results in

$$\frac{u_a}{u_{a1}} = \left[ \eta_1 b \frac{\omega}{\omega_1} + (1 - \eta_1) r \right] \frac{i_a}{i_{a1}}, \quad (6.13)$$

where

$$b = \frac{i_e}{i_a} = \frac{R_p}{R_e + R_p} \quad (6.14)$$

is a factor characterising field weakening and

$$r = \frac{R_a + b R_e}{R_{a1} + R_e} = \frac{R_a + \frac{R_e R_p}{R_e + R_p}}{R_{a1} + R_e} \quad (6.15)$$

is the ratio of the effective armature circuit resistance to the nominal resistance without parallel and series resistors. Eq. (6.13) indicates that the armature circuit of an unsaturated series wound motor appears like a resistive circuit, whose effective resistance depends on speed; this is of course due to the induced armature voltage  $e$  which is proportional to armature current and speed. Likewise we find from Eqs. (6.5, 6.9) with  $m_M = m_L$

$$\frac{i_a}{i_{a1}} = \sqrt{\frac{1}{b} \frac{m_L}{m_1}}. \quad (6.16)$$

Eliminating  $i_a/i_{a1}$  from Eqs. (6.13, 6.16) finally yields the torque- speed curves of the unsaturated series wound motor

$$\frac{\omega}{\omega_1} = \frac{\frac{u_a}{u_{a1}}}{\eta_1 \sqrt{b \frac{m_L}{m_1}}} - \frac{1 - \eta_1}{\eta_1} \frac{r}{b}, \quad (6.17)$$

where the normalised armature voltage  $u_a/u_{a1}$  may be continuously variable whereas field weakening ( $b$ ) and armature resistance ( $r$ ) are regarded as being subject to discontinuous control actions; the load torque  $m_L/m_1$  again represents a disturbance.

A set of these curves is shown in Fig. 6.4, calculated for  $\eta_1 = 0.9$ . As expected, the torque-speed curves are very steep at light load. This is desirable for vehicle drives, because the motor can be operated over a wide speed range; sharing the load is no problem on multi-motor drives. The similarity of the curves to the dashed hyperbola pertaining to constant power – which is the ideal characteristic of a vehicle drive without changing gears – is striking. The speed rise at no-load could of course be a source of danger in other than traction applications.

The armature current-torque curves, also depicted in Fig. 6.4, show a similar increase under field weakening as was observed with the separately excited motor. In view of the higher copper losses in the armature and the more critical commutation at reduced field, the amount of field weakening must be restricted here too.

On street-cars, trolley buses and subways, where normally a constant direct voltage is used for supply, as well as with battery operated vehicles, switched armature circuit resistors may be employed for control. In recent years electronic choppers have been introduced which permit continuous variation of the mean armature voltage. At higher speed the field may be weakened by parallel resistors. In addition, if several drive motors are present, they can be connected in series or parallel thus providing a simple way of changing the voltage in a few steps. With city trains or main line locomotives having an AC catenary the armature voltage can be varied continuously (by power electronic devices)

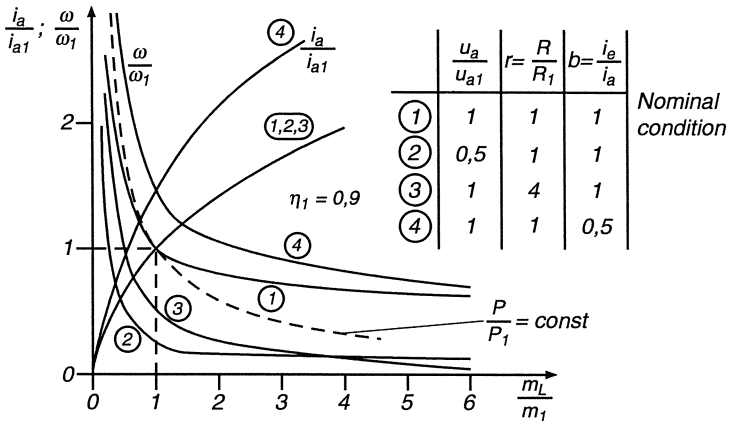


Fig. 6.4. Steady state characteristics of series wound DC motor

or in fine steps (by transformer tap changer). Rectification may or may not be included.

In order to reverse the torque, which is proportional to  $\Phi_e i_a$ , a reversal of the field winding is required; the machine can so be operated in the motoring, i.e. the first and third, quadrants of the torque-speed plane. When operating in the second and fourth, i.e. the generating quadrants, an unstable condition exists which is manifested by a horizontal asymptote of the torque- speed curve, Eq. (6.17), at a critical speed

$$\frac{\omega_c}{\omega_1} = -\frac{1-\eta_1}{\eta_1} \frac{r}{b} < 0 . \quad (6.18)$$

This constitutes a state of self-excitation, where the effective armature resistance, contained in the brackets in Eq. (6.13) becomes zero. This means that the armature, being driven, for example, in the fourth quadrant by an active load torque, is supplying the losses of the armature circuit. This results in a steep increase of the braking torque produced by the machine. The critical speed  $\omega_c$  is a function of the total armature circuit resistance and field weakening but independent of the applied armature voltage.

The effect of self-excitation is seen in Fig. 6.5 showing a calculated transient with an unsaturated machine. At first, the motor is accelerated at no load with a small value of the armature voltage  $u_a$  until time  $t_1$ , when a constant load torque  $m_L$  is applied which decelerates and eventually reverses the motor.

When the critical speed  $\omega_c < 0$  is reached, self-excitation in the form of a nonlinear transient sets in with speed oscillations and high peak torques which in practice could endanger the motor shaft. Since this effect does not depend on the supply voltage  $u_a$ , it can be utilised as a supply-independent electric brake in vehicles; this is described in Fig. 6.6.

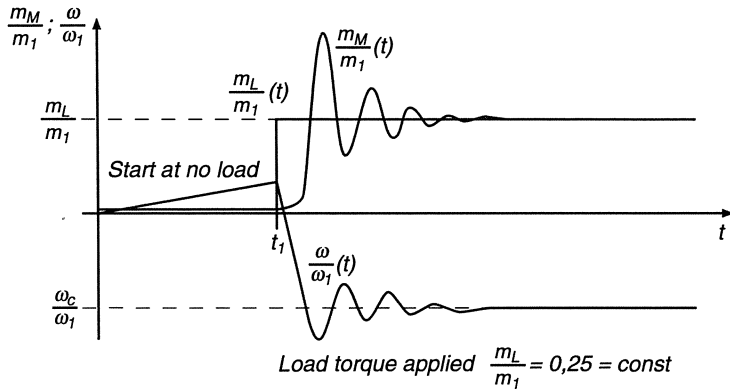


**Fig. 6.5.** Transient of self-excitation of a series wound motor

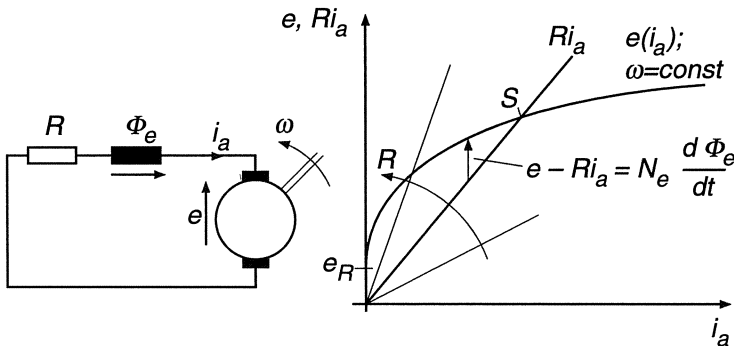


**Fig. 6.6.** Short circuit electric brake with series wound DC motor.

a) Circuit; b) Characteristics

It is assumed that the field winding has been reversed and the circuit is closed through a braking resistor. The motor is running with  $\omega > 0$ , so that braking requires operation in the second quadrant of the torque- speed plane; it is controlled by the effective armature circuit resistance, Eq. (6.15). A detailed analysis of the braking transient requires the inclusion of iron saturation, but the principle may be deduced qualitatively from the curves in Fig. 6.6 b.  $e(i_a)$  is the induced armature voltage at a given overcritical speed,  $R i_a$  is the voltage across the total braking resistor including the resistance  $R_{al}$  of the armature itself. In the initial phase, the current is caused by the remanence voltage  $e_R$ , without external voltage being applied. The rate of rise and the eventual stable operating point  $S$  are determined by the differential equation

$$N_e \frac{d\Phi_e}{dt} = e(i_a) - R i_a ,$$

again neglecting the self-inductance of the armature compared with that of the field winding. In the steady-state condition the machine then operates as a generator, converting mechanical power to heat in the predominantly external braking resistor  $R$ .

On main line locomotives, the drive motors are often reconnected as separately excited generators during braking operation, in order to have more direct control. The auxiliary field power may be taken from a battery, if supply-independent braking is specified.

An example of controlling a DC series motor is discussed in Sect. 9.2.

## 7. Control of a Separately Excited DC Machine

### 7.1 Introduction

In Chap. 5 the steady state and dynamic behaviour of a separately excited DC machine with adjustable armature and field voltage has been explained; this discussion is now extended by considering the machine as part of a feedback control system. The reason for this is that in practice the choice of a DC drive is normally motivated by the possibility of operating over a wide speed range with low losses and matching the behaviour of the motor to the needs of the load. In order to achieve the desired operating characteristics in the presence of

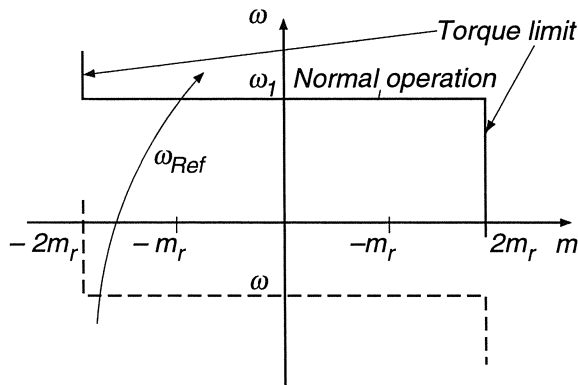


**Fig. 7.1.** Steady-state torque-speed curves of an adjustable speed drive with torque limit

supply- and load-disturbances, feedback control is usually necessary. Another reason why DC drives are normally contained in feedback loops is that the armature of a larger motor represents a very small impedance which – when supplied with rated voltage – would result in an excessive current of up to 10 times rated value. Under normal operating conditions this is prevented by the induced armature voltage  $e$ , which cancels most of the applied voltage  $u_a$  so that only the difference determines the armature current  $i_a$ . It is these two quantities which are performing the actual electromechanical energy conversion.

In transient operation, for example while accelerating or braking, there is always the danger of excessive current due to the rapidly changing armature voltage or speed; the same is true with a steady state overload on the motor. It is therefore important to provide some kind of fast current or torque limit in order to protect the motor, the power supply and the load; this is best realised by feedback control. In this way an effective safeguard against electrical or mechanical stresses is established. At the same time an unequivocal criterion is gained for distinguishing tolerable temporary overcurrents from currents due to a functional fault which call for immediate clearance by a breaker or by fuses.

In most cases the user of a controlled drive wants to be able to select a reference speed  $\omega_{Ref}$  which the motor should maintain as long as it is not overloaded. When overload occurs, the motor should produce maximum torque in the prescribed direction; twice rated torque is often specified as a short time limit. This results in steady state characteristics of the type shown in Fig. 7.1.

For many applications, such as elevators, these specifications are insufficient because there are operating conditions when the acceleration or the angular position must be controlled according to prescribed references. Also on machine tools or robots, the feed drives in the different axes must accurately follow prescribed angular commands as functions of time, in order to move the tool or workpiece along a desired spatial trajectory.

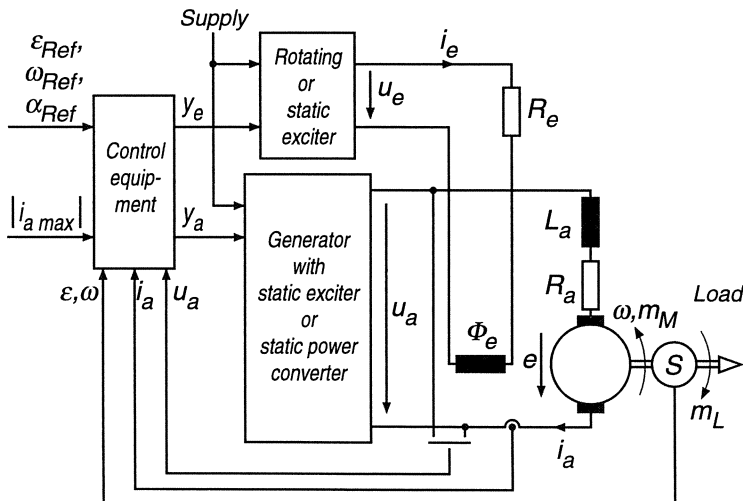


Fig. 7.2. General schematic of DC drive control

All these requirements can be fulfilled with the general scheme shown in Fig. 7.2 where the armature and field of the motor are fed from separate controllable power supplies. Rotating generators have been the common choice in the past, forming the well known Ward Leonard scheme, but, after brief interludes by magnetic amplifiers and mercury arc converters, power electronic converters

employing solid state semiconductor switching elements (various types of thyristors or power transistors) are now the standard solution. The steady state power required for the field winding is only a few percent of that for the armature.

With a "four quadrant" armature supply allowing both polarities of voltage and current, the power flow to the motor can be reversed, with the machine operating in all four quadrants of the torque-speed plane. This is the case if a rotating DC generator driven by a line-fed AC motor serves as a power supply; the same can be achieved with switched converters. With magnetic amplifiers, containing only diodes, regeneration was not possible. Of course, there is always the option of electrical braking by placing resistors in the armature circuit.

Figure 7.2 contains a block "control equipment" which is controlled by references signals  $\varepsilon_{Ref}$ ,  $\omega_{Ref}$ ,  $\alpha_{Ref}$ ,  $|i_{a\ max}|$  as well as feedback signals  $\varepsilon$ ,  $\omega$ ,  $\alpha$ ,  $i_a$ , as needed for specific control tasks. The speed signal is normally obtained from a small permanent magnet tachometer generator, delivering a speed-proportional voltage from which a signal proportional to acceleration can also be derived. When higher accuracy is specified, a digital solution may be preferred where the speed signal is taken from a magnetic or optical sensor generating pulses for each angular increment. The frequency of the pulse train is proportional to speed, while the sum of the individual pulses is a measure of angular position change; the sign of the rotation is determined from the sequence of pulses generated by a dual track sensor with the two signals being  $90^\circ$  out of phase (Chap. 15.2).

The controllers transform these input signals into the actuating variables  $y_a$ ,  $y_e$  which serve as control inputs for the two adjustable power supplies.

In the following paragraphs some proven control procedures for DC drives will be discussed, making no specific reference to the type of power supply used since this topic is dealt with separately in later sections.

## 7.2 Cascade Control of DC Motor in the Armature Control Range

Let us first look at the case when the motor operates below base speed,  $-\omega_0 \leq \omega \leq \omega_0$ . As explained in Chap. 5, the main flux is kept at nominal value  $\Phi_{e0}$  in order to have the lowest possible armature current for a given torque and to guard against unexpected load surges.

In Fig. 7.3 the schematic diagram of the armature circuit is drawn;  $e_a$  is the internal voltage source of the power supply. This synthetic voltage which is controlled by  $y_a$  differs from the armature voltage  $u_a$  due to the internal impedance  $R_i$ ,  $L_i$  of the supply circuit; the impedance must be taken into account when normalising the motor parameters,

$$i_{a0} = \frac{e_{a0}}{R_a + R_i}, \quad T_a = \frac{L_a + L_i}{R_a + R_i}.$$

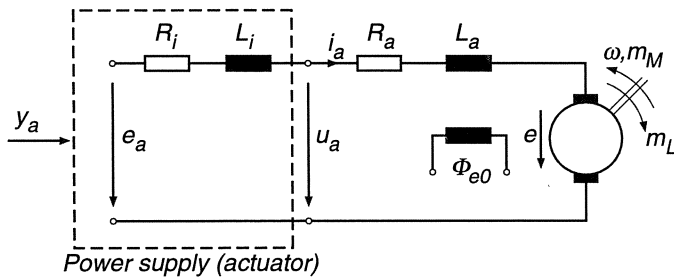


**Fig. 7.3.** DC motor with armature power supply

With the results of Sect. 5.3,  $b = 1$ , the block diagram of the motor assumes the form shown in Fig. 7.4 a, where the controllable voltage source  $e_a$  is represented by a first order lag element having the voltage gain  $G_{as}$  and the time constant  $T_{as}$ , which strongly depends on the type of power supply. When a rotating generator is used,  $T_{as}$  corresponds to its field time constant and may be between 0.1 and 1.0 s, whereas the corresponding value would be 1 to 5 ms, if the residual delay of a line-commutated converter is to be modelled. Naturally this difference greatly affects the dynamics of the control system; this must be taken into account, when designing the controllers. Fig. 7.4 b is an equivalent structure, redrawn for better access to the armature current.

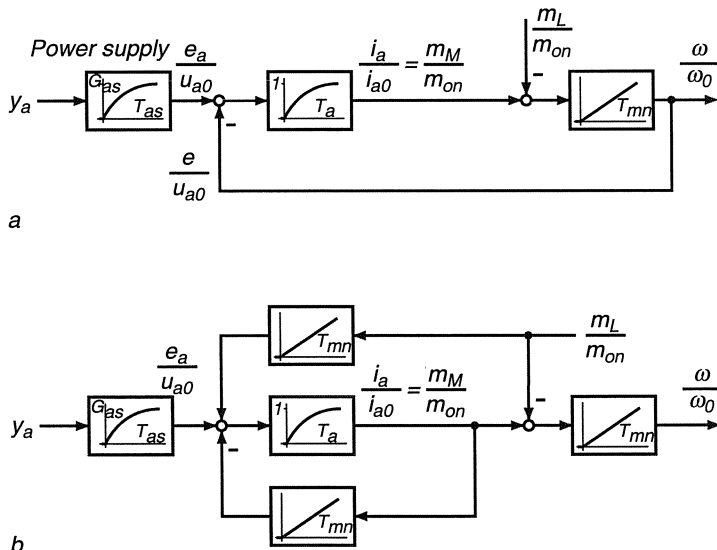


**Fig. 7.4.** Block diagrams of DC motor with armature power supply,  $\Phi_e = \Phi_{e0}$

The armature time constant  $T_a$  usually has values between 10 ms and 100 ms; it is determined by the impedance of the complete armature circuit including possibly a smoothing choke which may be needed for reducing the current ripple caused by switching converters; with small servo motors having an iron-free rotor the armature time constant could be less than 1 ms. The mechanical time constant  $T_{mn}$  comprises the total inertia of the drive (assuming rigid coupling); therefore it covers a wide range from a few milliseconds (servo motors and reversing rolling mill drives) to several seconds (paper mill drives and mine hoists).

There seems to be general agreement that the most effective control scheme for drives is a cascaded or nested structure with a fast inner control loop, limiting torque or, on a DC motor, armature current, to which an outer speed control loop is superimposed [K19, L65, S70]. This multi-loop system proves very flexible; for example, in order to have position control, it can be extended by a position loop superimposed on the existing speed control loop. Also, if acceleration is of importance, a corresponding inner control loop may be added.

The idea of cascade control is exemplified by Fig. 7.5, where a lumped inertia drive is equipped with most of the control loops mentioned; it is seen that the sequence: torque-acceleration-speed-position is a natural one as it conforms to the structure of the plant. The torque (or armature current) loop, forming the innermost control function may be regarded as approximately creating an impressed current source for the armature. The current controller primarily has to deal with the dynamics of the power supply and the armature, cancelling the effect of the induced armature voltage; thus it provides the fastest available control action. By limiting the reference  $m_{M\ Ref}$  (or  $i_{a\ Ref}$ ), the inner control loop also assumes a protective function. An acceleration control loop which is not shown in Fig. 7.5 could be desirable with high dynamic performance drives, such as servo or elevator drives; its main purpose would be to counteract the effects of load torque  $m_L$ , as well as changes of inertia, by generating – within the admissible range – a suitable current reference  $i_{a\ Ref}$ . The hierarchical structure is then continued with a speed controller which controls the closed inner loop in conjunction with the subsequent integrator; the same idea is once more extended when going to a position control loop where the position controller generates a suitable speed reference.

Of course, this multiloop structure can only function under the assumption that the bandwidth of the control increases towards the inner loops with the current loop being the fastest and the position loop the slowest; clearly, the position controller can only perform well if the speed loop is quickly executing the commands it is given, etc. Following this reasoning, the design of the controllers proceeds in the direction from the lower to the higher control levels, at every stage approximating by a simple model whatever has been achieved before. Obviously, the design of the control system is greatly simplified by such an iterative procedure, where only a part of the complete plant is dealt with at a time. The fact that each feedback variable can be limited by limiting the pertinent reference is a major advantage of cascade control; also, field work is

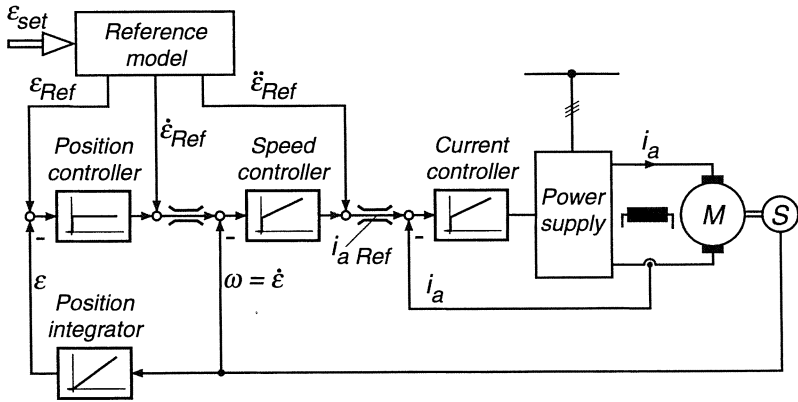


**Fig. 7.5.** Cascade control structure of drive including position-, speed-, and current control with feed-forward

considerably simplified, since the control loops can be put into operation and tested one after another.

It can be argued that a control system containing several inner loops is likely to respond slower to changes of the reference than an equivalent single loop control (provided that it can be stabilised). Therefore, when highest dynamic performance is important, e.g. with position controlled servo drives, the inner loops should be activated in parallel by feed-forward reference signals derived from a reference generator, as indicated in Fig. 7.5; thus, all disadvantages with regard to dynamic response are avoided. Cascade control involving torque, speed, position etc. may be considered as a special form of state variable control, making use of all the available, physically important quantities.

It should be mentioned that cascade control represents a very powerful control technique that is not restricted to drives; in fact there is hardly any control system put into operation today that does not contain inner loops. Of course, this principle, known for some time, could be widely applied only once the cost of control amplifiers was dramatically reduced by transistor operational amplifiers and electronic integrated circuitry.

When comparing the structure of the plant in Fig. 7.5 with the block diagram of a DC machine in Fig. 7.4 a it is seen that the machine-internal feedback by the induced voltage is not immediately compatible with cascade control because it represents a deviation from the nested loop structure of the plant. However, by redrawing Fig. 7.4 a in the form of Fig. 7.4 b, a non-interacting structure is obtained; the fact that the load torque is now entering the plant in two places is no problem since  $m_L$  is assumed to be an independent disturbance. The variables not specified in Fig. 7.4 b have no immediate physical significance.

The part of the plant that lies between  $e_a/u_{a0}$  and  $i_a/i_{a0}$  may be described by the transfer function

$$\frac{I_a}{E_a}(s) = \frac{T_{mn} s}{T_{mn} T_a s^2 + T_{mn} s + 1} \quad (7.1)$$

corresponding to  $F_3(s)$  in Eq. (5.18) for  $b = 1$ . The differentiating effect vanishes with speed dependent load, as was seen from Eq. (5.24).

The design of the current controller is explained with the help of Fig. 7.6 assuming no inherent damping by the load. The feedback signal derived from the current transducer is passed through a low-pass filter in order to reduce possible ripple; a filter time constant of 2 to 5 ms is usually sufficient.

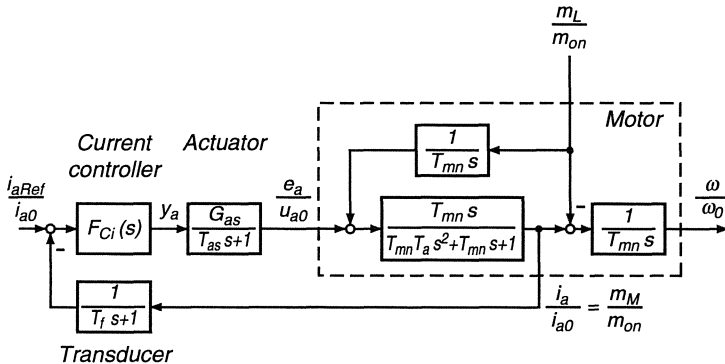


**Fig. 7.6.** Design of the current controller,  $\Phi_e = \Phi_{e0}$

If a power electronic converter is employed as armature supply, a proportional-integral controller (PI) is adequate as will be discussed later; for a rotating generator having a much larger time lag, the current controller may be extended by a lead-lag term (PDT) to form a PID-controller. When realising the controller function by an analog operational amplifier, the difference is a minor addition to the RC-feedback network of the amplifier. A typical example of an analogue PID-controller is shown in Fig. 7.7.

With these assumptions the open loop transfer function of the current control becomes

$$F_{0L,i}(s) = G_{Ci} \underbrace{\frac{T_1 s + 1}{T_1 s}}_{\text{PID-controller, } T_2 \ll T_2} \underbrace{\frac{T_2 s + 1}{T'_2 s + 1}}_{\text{PDT}} \underbrace{\frac{G_{as}}{T_{as} s + 1}}_{\text{supply}} \underbrace{\frac{T_{mn} s}{T_{mn} T_a s^2 + T_{mn} s + 1}}_{\text{armature}} \underbrace{\frac{1}{T_f s + 1}}_{\text{filter}}. \quad (7.2)$$

Because of the factor  $s$  in the numerator of the armature transfer function, a proportional loop results,  $\lim_{s \rightarrow 0} F_{0L}(s) = F_{0L}(0)$  finite, even though the controller itself comprises an integral term; as a result the closed loop will exhibit a steady state error. The reason is of course the e.m.f.-feedback which remains effective also in the transformed block diagram of Fig. 7.4 b. Clearly, when supplying constant current to the armature of a DC motor at no load, the motor speed,

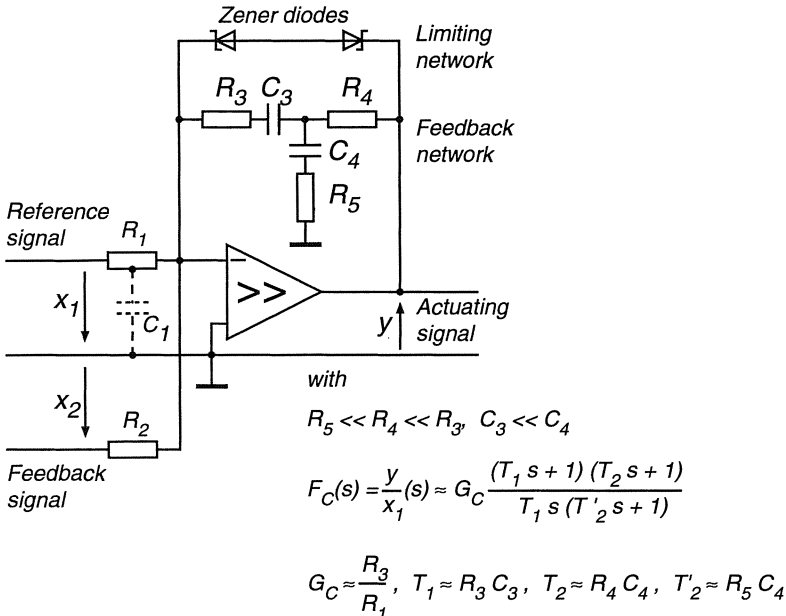


**Fig. 7.7.** Circuit of analogue PID-controller employing an operational amplifier

the induced voltage and the applied voltage increase linearly with time; with other words, generation of a ramp function with a controller containing a single integration calls for a constant control error.

For the practical application it is normally of no consequence whether the current controller admits a steady state control error during acceleration, because current control represents an inner (auxiliary) function, being part of the superimposed speed loop. The main purpose of the current controller is to linearise the plant and prevent overloading the motor; at constant speed, this is accomplished by a controller with a single integration.

It would in principle be possible to use a current controller performing double integration, e.g. a dual PI-controller having the transfer function

$$F'_{C,i}(s) = G_{C,i} \frac{T_1 s + 1}{T_1 s} \frac{T_2 s + 1}{T_2 s}, \quad (7.3)$$

in order to avoid a steady state control error during acceleration. However this is not normally done in view of the reduced margin of stability. If maintaining a prescribed acceleration is a necessary condition, as may be the case with machine tool- or elevator-drives, it would be easier to include a separate acceleration control loop as will be shown in Fig. 15.9.

The choice of parameters for the current controller according to Eq. (7.2) follows the usual lines for the design of cascade control systems [K20, 35]. In the case of a Ward Leonard scheme containing a rotating generator and with

aperiodic damping of the drive ( $T_{mn} > 4 T_a$ ) the lead time constants  $T_1$ ,  $T_2$  of the PID-controller could be tuned to  $T_a$  and one of the emerging lag time constants of the drive, while the rest can be dealt with by approximation on the basis of the principle of “equivalent lag”, e.g. [35].

The closed current control loop is now inserted into the speed loop forming the next higher level of control, as is shown in Fig. 7.8. Provided the current loop is well damped, it is acceptable to replace its closed loop transfer function by a proportional lag element having the gain  $G_{CL,i}$  and the time constant  $T_{CL,i}$ . Since this equivalent lag, being a first order approximation at low frequency of a much more complicated transfer function, cannot be simplified by lead time constants, a PI-controller for speed is the appropriate choice. Hence the transfer function of the open speed loop is approximated by

$$F_{0L,\omega}(s) \approx G_{0\omega} \underbrace{\frac{T_{c,\omega}s + 1}{T_{c,\omega}s}}_{\text{PI-speed controller}} \underbrace{\frac{G_{CL,i}}{T_{CL,i}s + 1}}_{\text{Current control loop (approx.)}} \frac{1}{T_{mn}s}. \quad (7.4)$$

The parameters  $G_{c,\omega}$ ,  $T_{c,\omega}$  may be chosen in accordance with the “symmetrical optimum” [K18, L29, 35], which is a standard design procedure for transfer functions containing a double integration when the controller is included.

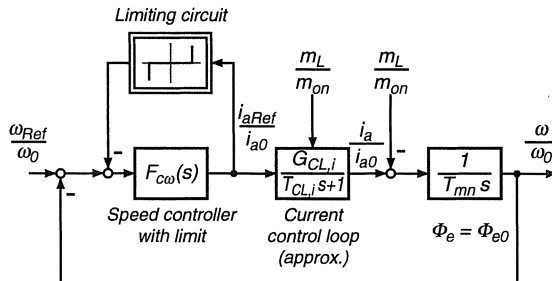


**Fig. 7.8.** Speed control loop including approximate representation of current control loop

The main idea is to choose the cross-over frequency at the geometric mean of the two corner frequencies, in order to obtain maximum phase margin  $\psi_d$  which in turn will result in optimum damping of the speed loop. The name stems from the Bode-diagram that shows symmetry with respect to the cross-over frequency (Fig. 7.9).

By normalising

$$T_{c,\omega} = a^2 T_{CL,i}, \quad a > 1, \quad (7.5)$$

the cross-over frequency is

$$\omega_{cross} = \frac{1}{\sqrt{T_{c,\omega} T_{CL,i}}} = \frac{1}{a T_{CL,i}}. \quad (7.6)$$

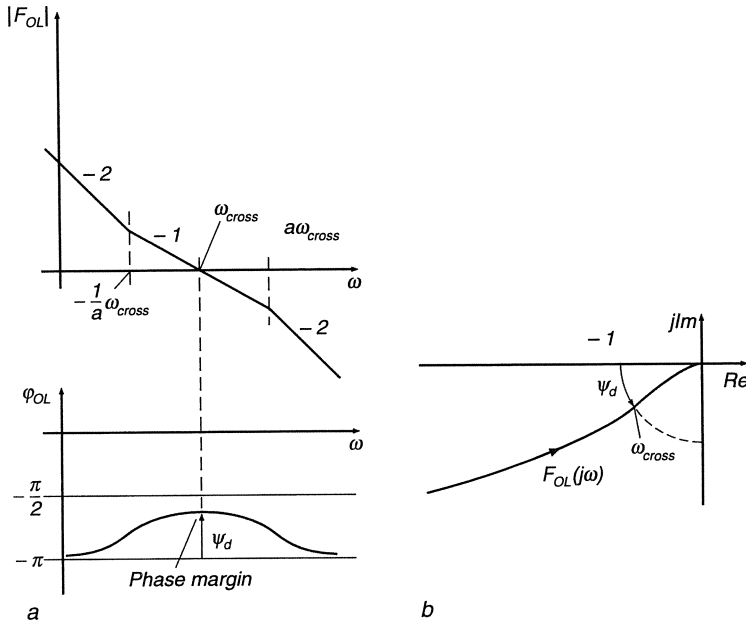


**Fig. 7.9.** Bode-diagram (a) and frequency response locus (b) according to “symmetrical optimum”

From the cross-over condition

$$|F_{0L,\omega}(j\omega_{cross})| = 1 , \quad (7.7)$$

we find with Eq.(7.5, 7.6)

$$G_{c,\omega} = \frac{1}{a G_{CL,i}} \frac{T_{mn}}{T_{CL,i}} . \quad (7.8)$$

The poles of the resulting transfer function of the closed speed control loop, i.e. the eigenvalues of the speed control loop, can be calculated explicitly. They are, assuming a conjugate complex pair,

$$s_1 = -\omega_{cross}, \quad s_{2,3} = \omega_{cross} \left[ -\frac{a-1}{2} \pm j \sqrt{1 - \left( \frac{a-1}{2} \right)^2} \right] . \quad (7.9)$$

Hence

$$D = \frac{a-1}{2} \quad (7.10)$$

is the damping ratio of the oscillatory part of the response. Assuming a slightly underdamped response,  $D = 1/\sqrt{2}$ , we have  $a = 1 + \sqrt{2} \approx 2.41$ . When aperiodic transients are specified,  $D = 1$ , leading to  $a = 3$ , a triple pole at  $s = -\omega_{cross}$  results.

Due to the double integrating term in the open loop transfer function, the closed speed loop exhibits zero control area or, synonymously, zero velocity error [35, 82]. This means that the step response is characterised by considerable overshoot even though the transients are well damped. In order to eliminate this effect which is caused by the lead term of the PI-controller, a corresponding lag term

$$\frac{1}{T_{c,\omega} s + 1}$$

may be inserted into the reference channel of the speed controller. In practice this can be done by connecting a suitable capacitor  $c_1$  between a center tap of the input resistor and ground, as is indicated in Fig. 7.7.

The speed controller shown in Fig. 7.8 contains a nonlinear feedback block which limits the current reference to the range  $-i_{a\max} \leq i_{Ref} \leq i_{a\max}$ . This serves as effective protection for the power supply and the drive, producing the desired steady state torque-speed characteristics (Fig. 7.10); of course, a short overshoot of the current, for example following a load disturbance, cannot be ruled out by clamping the current reference. If the electronic controller is realised with the help of an operational amplifier, the clamping can be achieved by placing Zener-diodes in the feedback branch (Fig. 7.7).

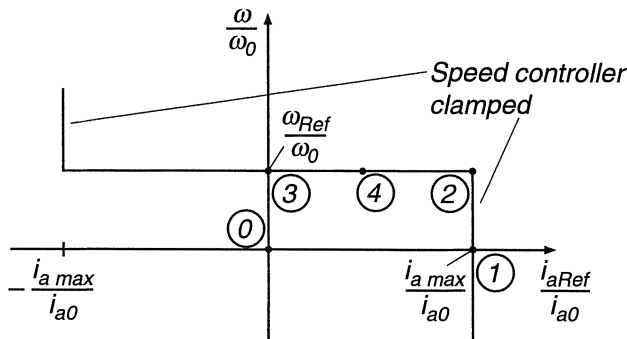


**Fig. 7.10.** Steady-state torque- speed characteristics of speed control loop with torque limit

Limiting the current reference removes in principle all restrictions on the rate of change of the speed reference, which is important if the drive is manually controlled. Whenever the speed controller, e.g. due to a rapidly changing command, reaches clamped condition, the speed loop is disconnected while the current control loop remains operative. As soon as the speed has caught up with the command, the speed controller reverts to linear operation and resumes control. However, with larger motors under manual control, a rate-of-change limiter is often inserted in the reference channel of the speed controller in order to ensure that the current limit, which may correspond to twice rated current, is not reached unnecessarily. A block diagram of this device, together with typical

transients, is seen in Fig. 7.11; it restricts the occurrence of current limit to load surges, for instance when a reversing rolling mill is jammed because of a wrong screw-down setting calling for an excessive reduction of the billet thickness.

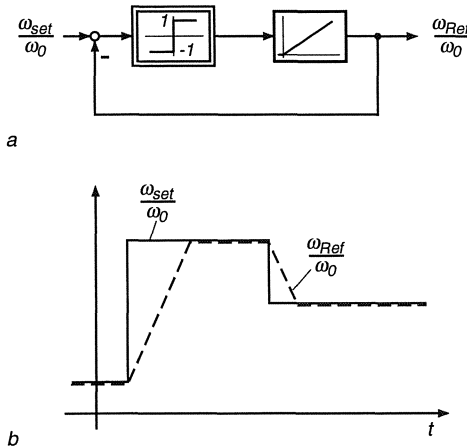


Fig. 7.11. Rate-of-change limiter

Computed transients of a DC drive with current-speed-cascade control are seen in Fig. 7.12. The parameters assumed correspond to those of a thyristor-fed drive with a six-pulse-converter (Chap. 8). The controllers have been designed as outlined in the preceding paragraph. If a rotating motor-generator were used instead of the electronic converter, the response would naturally be much slower, particularly in the current loop.

At first, a starting transient is displayed, caused by a step of the speed reference from zero to  $0.3 \omega_0$ . The effect of current limit during the acceleration phase as well as the dynamic control error are clearly seen. This transient corresponds roughly to the transition of the operating point in Fig. 7.10 from 0 via 1, 2 to 3. At time  $t = 1$  s the drive, having attained the no-load point (3), is loaded with rated torque. This causes a slight transient speed drop but the drive remains in the linear control regime; eventually the steady state operating point 4 is reached.

From Fig. 7.12 it is seen that the source voltage  $e_a$  rises with the induced voltage, which is proportional to speed; in addition there is the resistive and inductive voltage drop in the armature circuit.

The cascade control structure described has proven its usefulness over the years by innumerable applications; as mentioned before, the two levels of control may be extended in both directions, for example by adding acceleration or position control. Since cascade control is by no means restricted to DC drives, we will come across more examples where this exceedingly flexible principle of control can be used to great advantage, see also Chap. 15.

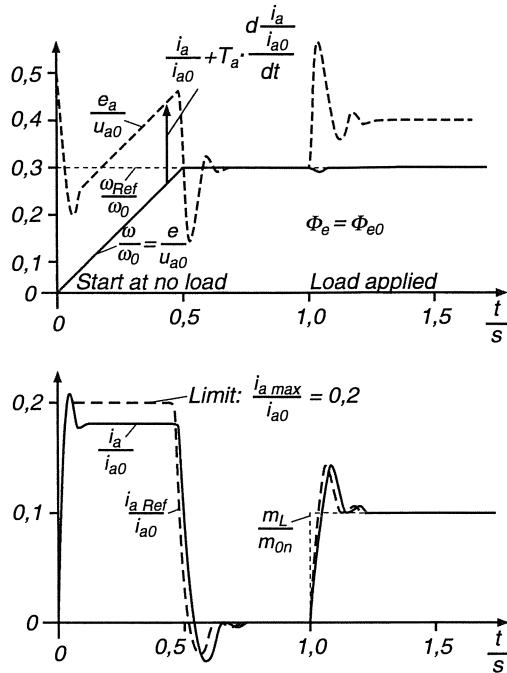


Fig. 7.12. Computed transients of DC motor with speed-current cascade control

### 7.3 Cascade Control of DC Motor in the Field-weakening Region

In Sect. 5.3 it was shown that by reducing the main field, a DC motor can be operated above base speed. For good utilisation it is important that the motor should be supplied either with maximum field- and reduced armature voltage or with maximum armature voltage and reduced field voltage; as mentioned before there may be some overlap for convenience of control.

Since the motor may alternately operate in either one of these regions it is appropriate to choose a control strategy which fulfills both requirements and permits a continuous and automatic transition from one operating regime to the other.

A control scheme that has proved useful in practice, is shown in Fig. 7.13 in simplified form [G18, V5]. It contains the current-speed cascade control acting through the armature voltage, as discussed before; in addition, there is an auxiliary control loop with the field voltage as actuating variable, which has the purpose of limiting the induced armature voltage as the speed rises beyond base speed. The adjustable voltage source supplying the field winding is usually realised by a thyristor converter, which is represented in Fig. 7.13 by a lag element. The nonlinear model of the magnetic circuit corresponds to Fig. 5.4.

A feedback signal for the induced voltage can be reconstructed from the measured armature voltage and current according to the voltage equation

$$e = u_a - R_a i_a - L_a \frac{di_a}{dt}; \quad (7.11)$$

an analogue computing circuit, not shown in Fig. 7.13, may be used for this purpose. This signal – after rectification on reversing drives – is compared with a constant reference  $|e_{max}| \approx 0.9u_{a0}$ ; the *e*-controller then attempts to remove the difference by adjusting the field voltage. Since, however, the reference voltage is beyond reach as long as the motor operates below base speed, the controller containing an integral term will be saturated and the field power supply produces maximum field voltage which is the aim in the armature control range. When the speed is rising, the induced voltage  $|e|$  may approach the reference value  $|e_{max}|$ ; as balance is reached the *e*-controller begins to lower the field voltage in order to limit the induced voltage, thus automatically weakening the field as desired. Of course, the initiative for a change in field voltage must always come from the armature because this is the direct channel of the speed controller, working through the armature current loop.

The arrangement drawn in Fig. 7.13 represents a complex and highly nonlinear control system, confounding all general design methods; considerable simplification results if one succeeds in speeding up the *e*-control loop, active in the field weakening range only, so that *e* may be approximated in that operating region by a constant impressed voltage. Such an approximation is not entirely unrealistic if the field power is supplied from a converter having a sufficiently large ceiling voltage (only one polarity of the field current is required). If the stator and the field poles are laminated, the “plant” may be represented by a simple lag element, having a speed-dependent gain, and the fast dynamics of the actuator; no serious stability problems are to be expected even at high controller gain. Neither is the nonlinearity of the magnetic circuit of great concern since the *e*-controller operates predominantly at reduced flux where saturation is not pronounced. For these reasons a PI-controller is quite adequate; its lead time may be tuned to the field time constant of the motor while the residual delays are taken care of by the remaining I-term of the controller.

Assuming fast *e*-control in the field weakening range, the simplified equivalent block diagram in Fig. 7.14 results. There the effect of the *e*-control loop is approximated by a constant voltage acting like an external disturbance; the flux approximately becomes a nonlinear algebraic function of speed,

$$\frac{\Phi_e}{\Phi_{e0}} \approx \left| \frac{\omega}{\omega_0} \right|^{-1} \quad \text{for} \quad \left| \frac{\omega}{\omega_0} \right| > 1$$

affecting the mechanical time constant. In principle, this undesirable change of parameter could be compensated by dividing the speed error at the input of the speed controller by  $\Phi_e/\Phi_{e0}$ , as indicated in Fig. 7.14; however, in most cases this is omitted and practical results prove that the correction is usually not necessary. Some consideration must of course be given that the speed controller

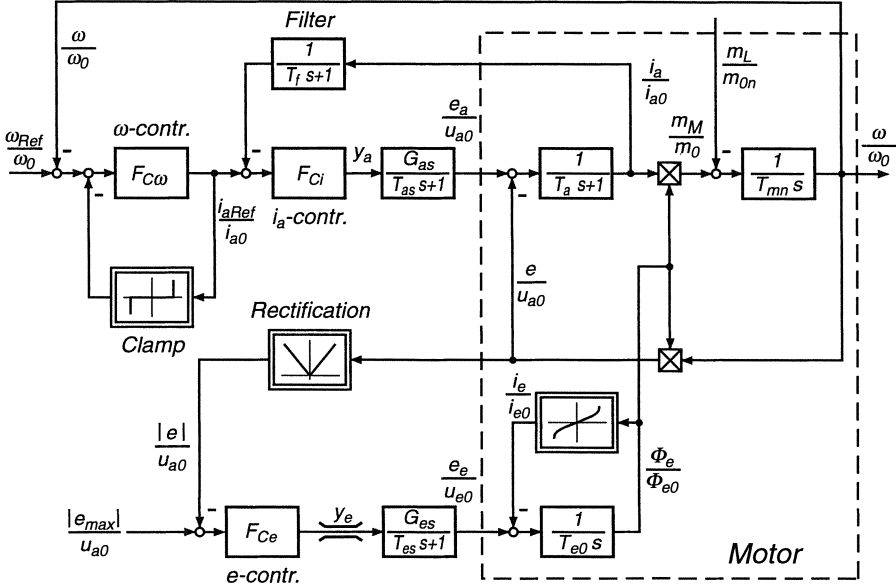


Fig. 7.13. Control of DC motor in the armature and field weakening regions

yields acceptable results in the armature as well as the field control regime. As an example, Fig. 7.15 shows a simulated no-load reversing transient between  $\pm 1.5\omega_0$  that was computed on the basis of the system shown in Fig. 7.13. The effect of the  $e$ -control loop is clearly recognisable from the  $\Phi_e$ - and the  $e$ -traces.

It has been mentioned that the use of a fast  $e$ -control loop with high forcing voltage across the field winding calls for a laminated motor frame. With large motors it may be necessary to employ a more accurate model of the field circuit for the design of the  $e$ -control loop, taking eddy currents in the iron into account [G18]. Also the high voltages induced by transformer action in the armature winding affecting the commutator must be considered. In order to eliminate the effects of winding temperature and supply voltage fluctuations on the main flux in the base speed region, an inner field current control loop is often included which maintains a prescribed maximum field current in the armature control range in spite of field resistance changes and helps to speed up flux control.

## 7.4 Supplying a DC Motor from a Rotating Generator

In the preceding sections was mentioned that any adjustable voltage source could serve as power supply for the armature of the DC motor. The classical scheme of DC motor control developed by Ward Leonard [L18, L19, Y2, Y3], employs for this purpose a rotating DC generator, the armature voltage of which is controlled through the field. Combined with up-to-date control, drives of this

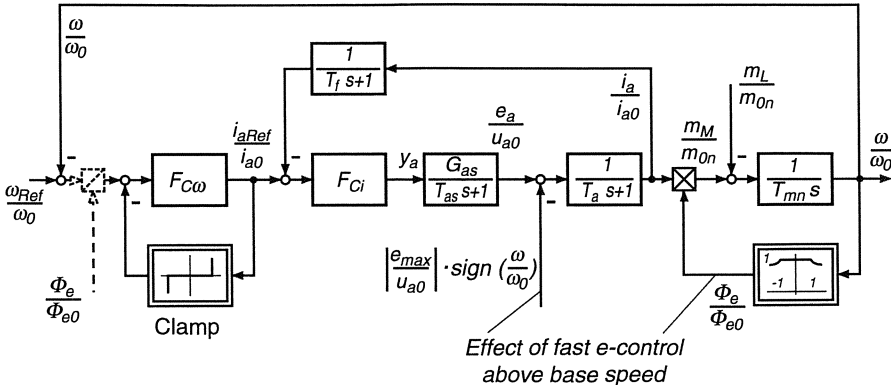


**Fig. 7.14.** Simplified representation of speed control loop in field weakening range

type are still in use today. The basic circuit is seen in Fig. 7.16; the separately excited DC motor (2) driving the load, for instance a rolling mill or an elevator, is fed from a separately excited DC generator, running at approximately constant speed. While a rolling mill or a gear-less elevator drive would normally operate at very low speed, for example between  $\pm 100$  1/min, resulting in high torque and a relatively large frame size, the generator being of similar power rating as the motor can run at any conveniently higher speed  $\omega_1$ , with the aim of reducing its size and cost. Instead of a DC generator, an AC generator with rectifier could be used for supplying the DC-link; of course, this would rule out regeneration.

The prime mover of the rotating converter is most frequently an AC induction motor (1) with cage or wound rotor (Chap. 10), requiring no continuous control. The power flow of the drive is reversible with the controlled motor being able to operate in all quadrants of the speed-torque plane. In case of a ship- or vehicle-propulsion scheme a turbine or a Diesel engine could be substituted as prime mover (1) (Turbo- or Diesel-electric drive), but there the drive motor (2) would most likely be a series type motor. Resistive braking could be employed instead of regeneration which is of course not possible with a unidirectional prime mover.

With large rolling mill- or mine hoist-drives the total drive is often split up into several machines; for instance, on a large reversing mill, two twin motors may drive the upper and lower rolls without direct mechanical connection apart from the frictional forces through the material being rolled. All machines constituting the rotating converter, such as AC motors, DC generators and, possibly, secondary machines are normally coupled to form a long drive shaft, sometimes 50 m long, which is located in a hall adjacent to the controlled drive and the load.

An advantage of the rotating motor-generator-set is the storage of kinetic energy in the masses rotating with  $\omega_1$ , which may be accentuated by connecting

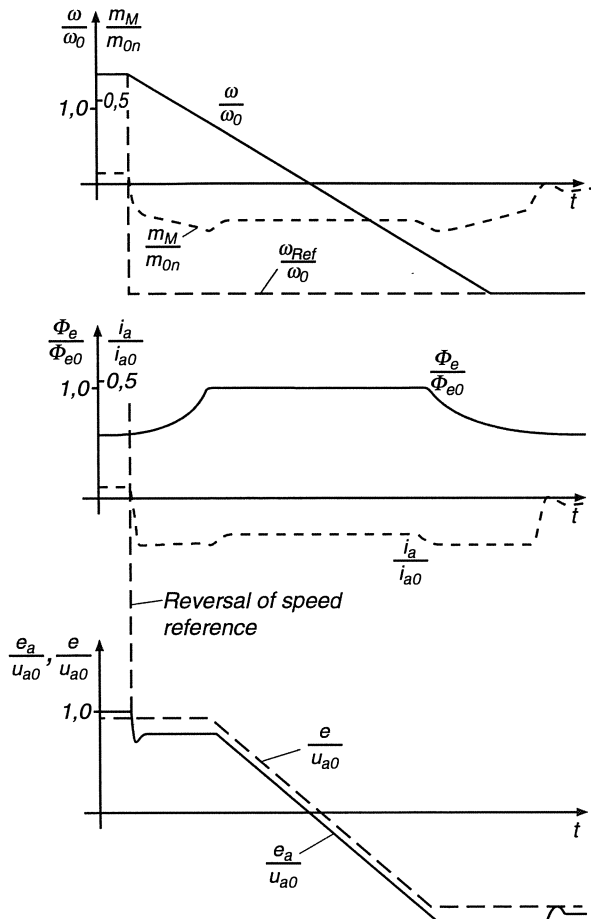
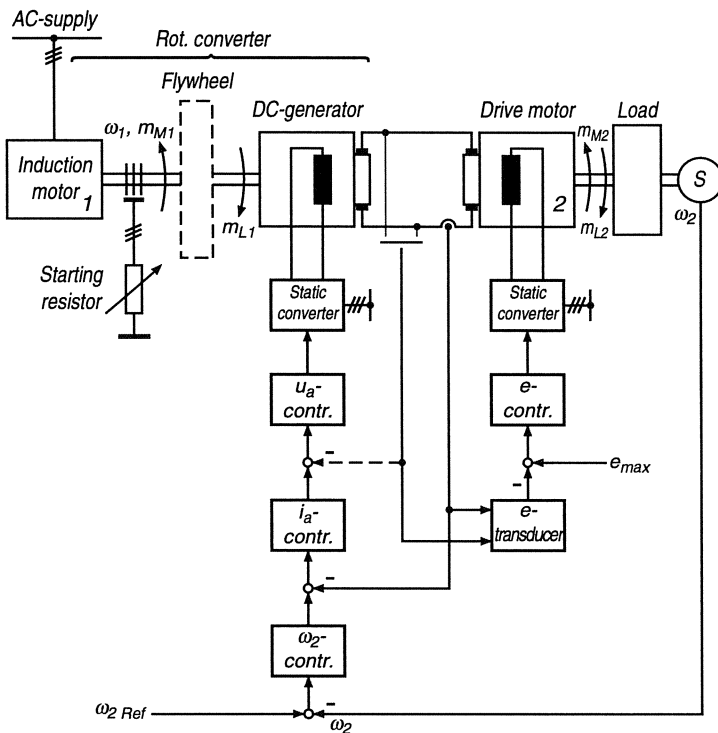


Fig. 7.15. Computed reversing transient of speed control system in Fig. 7.13

flywheels to this shaft and increasing the slip of the wound rotor driving motor (1). (A converter of this type is then called an Ilgner-set.) For large drives (MW) special schemes have been developed in order to recuperate slip power in the rotor circuit (Sect. 13.2). The kinetic energy of the rotating masses provides a convenient means of dynamically decoupling the AC supply from the load; there may be different motives for this, depending on the application. With reversing rolling mills there has always been the desire to smooth the load fluctuations of 20 MW or more lasting a few seconds; this point of view has been of particular interest with weak supply systems but its importance tends to recede as the supplies have become stronger and more closely interconnected. Conversely, a rotating converter can serve for protection of sensitive loads, such as paper mill drives, against short-time line disturbances. Similar arguments are valid when



**Fig. 7.16.** Control scheme of Ward Leonard-drive

uninterruptible power for important loads is required, for example computers, elevators or operating rooms in hospitals; with an intermediate motor-generator-set supplying these loads, there is more time for switching to an alternative voltage source.

A disadvantage of the Ward-Leonard-drive is of course that, apart from the adjustable speed drive, two additional machines of about the same power rating are necessary. Even though they may be smaller in size because of higher speed, large machines will still require a machine hall with heavy foundations and continuous service of bearings and commutators. It is for these reasons that static power converters, particularly of the modern semiconductor type have supplanted rotating motor-generator-sets in new installations.

If the field of a rotating generator is fed from a rotating exciter, both responding relatively slowly, it is – exercising some care – quite possible to control the drive motor manually and without any automatic equipment. However, due to the danger of overcurrent the machine cannot be fully utilised; feedback control with its much faster response then offers considerable advantages making it possible to take various side conditions into account. With feedback control the drive assumes well defined operating characteristics and may be inserted

into automatic production processes. By exciting the generator and the drive motor through static converters with high ceiling voltage (2 to 3 times steady state voltage) the speed of response of the drive may be sufficiently improved for enabling the drive to meet most dynamic specifications. This, of course, renders the use of feedback control mandatory.

The control structure shown in Fig. 7.16 is essentially in line with that in Fig. 7.13. The only difference is the possible introduction of an inner control loop for the armature voltage  $u_a$  of the generator [S64]. Since the pertinent portion of the control plant comprises only the field time constant of the generator and the residual delay of the electronic field power supply, the response of this control loop can be made quite fast. Its advantages are the linearisation of the inner part of the plant, the reduction of the effective armature impedance of the generator and the possibility of precisely limiting the armature voltage. This is important with large machines where the permissible limits of commutation must be fully utilised without running the risk of excessively sparking brushes. For the superimposed current controller the closed voltage control loop looks like a linear actuator with constant gain and considerably reduced lag.

## 8. The Static Converter as Power Actuator for DC Drives

### 8.1 Electronic Switching Devices

A characteristic feature of the rotating converter discussed in Sect. 7.4 is the consecutive power conversion from electrical (constant AC line voltage) to mechanical (speed of motor-generator) and back to electrical form (variable direct voltage) from which it is eventually transformed into controlled mechanical power in the drive motor. These conversions constitute the advantages of the control scheme (separate electrical circuits, decoupling by rotating masses) as well as its drawbacks (cost of machines, foundations, power losses, servicing, limited speed of response).

This naturally gave rise to early ideas for eliminating the intermediate mechanical stage by supplying the DC drive motor directly from the AC supply through static electronic devices. That such possibilities exist in the form of static switching converters has been known for a long time [43, A12, W22]. In fact, switching devices are the only available means for high power converters because any other circuit components would result in prohibitive power losses.

The basic element of a power converter is an electronic switch having the properties of a controllable rectifier; the idealised steady state characteristics of a thyristor are seen in Fig. 8.1. With reverse voltage ( $u < 0$ ), there is negligible leakage current, whereas in forward direction ( $u, i > 0$ ) two possible states exist: the device may either be conducting or blocking. The first state is associated with a low conducting resistance, typically  $10^{-3}\Omega$ , while in blocking condition the device exhibits a very high blocking resistance, for example  $10^5\Omega$ . Hence the thyristor valve may be approximately described by a mechanical switch in series with an uncontrolled rectifier (diode). The only main difference between a thyristor and a diode is the existence of the forward blocking state.

In the past the function of controlled electronic switches has been realised with various devices utilising different physical effects; most of these early solutions are obsolete today. Since electron tubes with heated cathodes could not supply enough current to drive motors and were plagued with high voltage drop resulting in poor efficiency, they were soon superseded by gas-filled tubes with heated cathode, called thyratrons; however, power rating, life time and reliability were also rather limited so that they were only useful for small drives. High power in the MW-range, such as needed for rolling mills or mine hoists, could

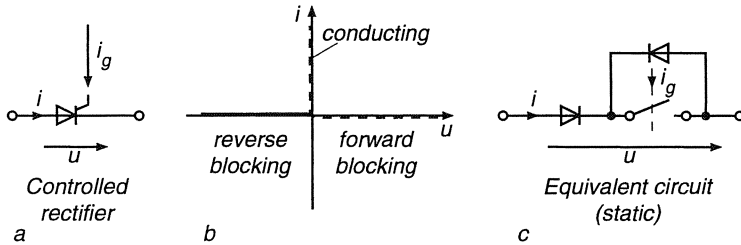


Fig. 8.1. Controlled rectifier

only be supplied by mercury arc valves having a liquid mercury cathode. These electronic valves were developed to high perfection by the 1950's but the liquid Hg-cathode limited their use in vehicles and remained a disadvantage, as well as the large size and the relatively high voltage drop across the electric arc connecting cathode and anode (20–25 V). Outside a narrow operating temperature range, controlled mercury-arc valves showed a tendency to occasional spontaneous arc-backs, i.e. conduction in reverse direction resulting in short circuits and high over-currents. This required close temperature control by heating or cooling the steel vessels. Also, mercury-arc converters needed relatively long intervals for deionisation which made them unsuitable for operation at higher frequency.

These difficulties are now completely overcome with semiconductor switches in the form of thyristors which have been available at steadily increasing power and with improved performance since about 1960. They have replaced the former mercury-arc valves even at the largest power ratings such as required for high voltage DC transmission.

The physics of a thyristor are extensively dealt with in the literature [14, 21], a simple description may suffice here. In Fig. 8.2 a a small disc of highly purified monocrystalline silicon having four electrons in the valence band is shown, which is doped by material of valence three and five such that three  $p - n$  junctions are created, separating the layers of  $p$ - and  $n$ -conducting material.

The inner layers are relatively weakly doped while the outer ones, forming the anode and cathode terminals, contain more doping material; the inner  $p_2$  layer is also connected to a gating electrode supplied by a low impedance control circuit. The following steady state operating conditions exist:

- With negative voltage between anode and cathode,  $u < 0$ , the diode junction  $p_1 - n_1$  is reversely biased; this corresponds to the reverse blocking state seen in Fig. 8.1 b.
- If positive voltage is applied ( $u > 0$ ) but without gate current ( $u_g < 0$ ), the diode  $n_1 - p_2$  has reverse bias which constitutes the state of forward blocking. Again, only negligible current flows in the load circuit.

- With positive voltage,  $u > 0$ , and with a sufficiently large gate current,  $i_g > 0$ , the junction  $n_1 - p_2$  becomes conducting, with the load current  $i$  saturating the region  $n_1$  from both sides with charge carriers. Thus the thyristor assumes very low resistance in forward direction. When  $i$  has exceeded a certain latching threshold  $i_L$ , the conducting state persists even after the gate current is removed.

Only by reducing the load current  $i$  below a lower holding threshold  $i_H$  can the thyristor again revert to blocking state; hence it represents a switch that can be closed by a low power control signal, whereas opening it requires the load current to become very small or zero.

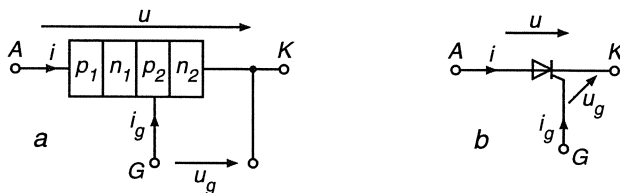


Fig. 8.2. Thyristor model

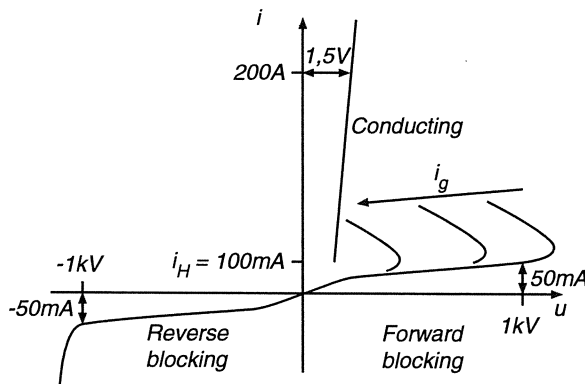


Fig. 8.3. Static characteristics of thyristor

Simplified characteristics of a typical power thyristor are shown in Fig. 8.3; the scales of the curves are different in order to bring out the details. While the leakage current in both directions could be below 100 mA, the load current in conducting state may be several thousand A. The voltage drop of the conducting thyristor is about 1.5 V and the maximum voltage in blocking state can be more than 8 kV.

When the maximum reverse voltage is exceeded, the leakage current rises rapidly, as with semiconductor diodes, leading to break-down and thermal destruction of the thyristor. In the forward direction ( $u > 0$ ) the effects are more

complex. When the voltage reaches a breakdown level, which can be reduced by the gate current, the thyristor switches spontaneously to the conducting state. However, turn-on by increased forward blocking voltage is not a suitable mode of control for a power thyristor because the firing instant is not sufficiently well defined and there may be local overheating of the semiconductor element. Instead, the switching to the On-state should always be effected by a low power pulse of gate current having a short rise time; this has the additional advantage that the thyristor fires at a precisely defined instant independent of the individual thyristor parameters.

Due to the small dimensions of the active semiconductor wafer and its low thermal capacity, the safe use of thyristors calls for meeting a number of restrictions; apart from limits on temperature, voltage and current there are maximum values for the rate of rise of the current ( $di/dt$ ) while switching on, as well as the voltage rate ( $du/dt$ ) during and after turn-off. This requires the inclusion of protective circuitry such as a series inductance and a parallel capacitor (snubber). Considering also the switching surges that are unavoidable in power supply systems, it is necessary to maintain a proper safety margin of the operating voltages against the specified peak values. For example, a 1.2 kV thyristor may be specified in a converter connected to the 400 V line where the maximum operating voltage is only 565 V. However, when all the recommendations by the supplier are observed, the thyristor has proved to be a reliable and very robust switching element which can stand high short time over-load current, such as a 10 fold surge for one cycle. Persistent overload must be prevented by a fast acting closed loop control and in the limit by fuselinks.

An important design parameter of thyristors, particularly when applied in forced commutated converters, is the recovery time  $t_r$ . It indicates the time that must elapse from the instant when the load current has reached zero, until the thyristor has attained full blocking capability in forward direction ( $u > 0$ ). The purpose of this interval is to give the residual charge carriers accumulated in region  $n_1$  during the conduction period time to decay through diffusion and recombination; depending on the type of thyristor, reverse voltage and junction temperature, the recovery time ranges from a few  $\mu s$  for a high frequency thyristor to several hundred  $\mu s$  for a high power thyristor designed for low voltage drop.

A typical transient of the voltage  $u(t)$  and the current  $i(t)$  of a thyristor during turn-off is depicted in Fig. 8.4 a. As the load current  $i$  reaches zero, the thyristor remains conducting for a short period with reverse current, thus clearing the charge-carriers from the junction. After this charge has disappeared, current flow decays rapidly causing high reverse blocking voltage due to the circuit inductance; this voltage peak must be limited by a protective parallel capacitor shown in Fig. 8.4 b; in the subsequent interval the reverse voltage is determined by the external load circuit. When the recovery time  $t_r$  has elapsed, the voltage can again become positive without there being the danger of breakdown and unwanted forward conduction. The recovery time is considerably reduced if reversed voltage  $u < 0$  exists after current zero. The resistor in the snubbing

circuit (Fig. 8.4 b) is required for limiting the discharge current of the capacitor at turn-on; frequently the resistor has a diode in parallel in order to make the capacitor more effective at limiting  $du/dt$  in forward direction.

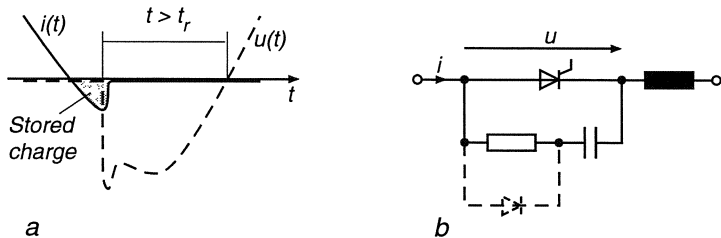


Fig. 8.4. Turn-off transient of thyristor

There are thyristors available, which - while still possessing all the characteristics of normal thyristors - may also be switched off by a control signal. These "gate turn off" thyristors (GTO) are preferably used with AC drives, they are discussed in Chap. 11.

## 8.2 Line-commutated Converter in Single-phase Bridge Connection

Thyristors, which are available in a variety of voltage and current ratings, are combined to form converter circuits; they represent highly efficient electronic power supplies for a wide power range.

Of particular importance for the supply of DC motors are the so called line-commutated converter circuits fed from a single- or three-phase AC supply of constant voltage and frequency. They are suitable for supplying adjustable direct voltage and current to the armature and field winding of the motor.

The single-phase circuits discussed first are, apart from railway traction drives, of interest only for low power applications up to a few kW. The circuit shown in Fig. 8.5 a contains four thyristors, which are made conducting ("fired", a relict of plasma discharge valves) in diagonal pairs during every alternate half cycle of the line voltage  $u_A$ . Provided there is a continuous direct current  $i_D$ , the function of the circuit may be described by a mechanical commutating switch, which connects the DC circuit with alternate polarity to the line voltage

$$u_A = \hat{u}_A \sin \tau, \quad \omega t = \tau. \quad (8.1)$$

If we assume for the time being that the direct current is smooth,  $i_D = I_D$ , being maintained by a fictitious current source, and that the impedance of the AC circuit is negligible, with  $u_A$  coming from an ideal voltage source, the voltage  $u_D(\tau)$  between the DC terminals consists of periodic sections of the AC voltage or its inverse; this is seen in Fig. 8.6 for different firing angles  $\alpha$ , which

determine the instant at which the diagonal pairs of thyristors are alternately made conducting.

The firing angle represents the switching delay with respect to a “natural” firing instant which would be valid for a circuit consisting of diodes; for the thyristors 1,1' the “natural” firing instants are  $\tau = 0, 2\pi, \dots$  when the voltage  $u_A(\tau)$  and — with thyristors 2,2' conducting — the voltages  $u_{T1}(\tau), u_{T1'}(\tau)$  become positive. The maximum firing delay is  $\alpha_{max} = \pi$ ; for  $\alpha > \pi$ , the thyristors 1,1' cannot be made conducting since they are reversely biased. This is also seen from the curve of the voltage across the thyristor,  $u_{T1}(\tau)$ , drawn in Fig. 8.6 c for different firing angles  $\alpha$ . Later the range of the control angle will have to be further narrowed.

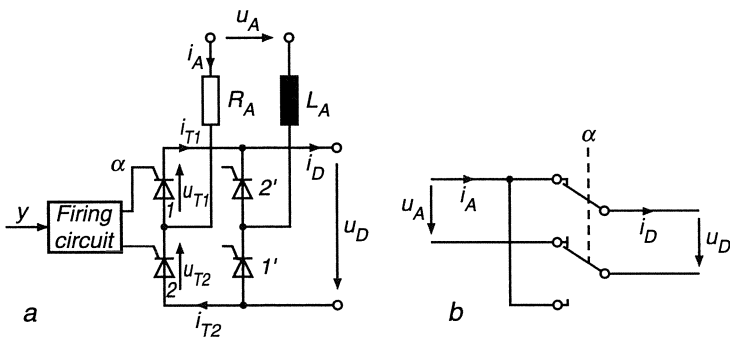


**Fig. 8.5.** Single phase line-commutated converter (a) with equivalent circuit (b)

The trace of the thyristor current  $i_{T1}(\tau)$ , also seen in Fig. 8.6 c, clearly indicates the switching action of the thyristors; at least one of the quantities  $u_{T1}(\tau), i_{T1}(\tau)$  is zero at any time. In steady state condition with  $\alpha = \text{const.}$  the voltages and currents in thyristors 2,2' pertaining to the opposite diagonal pair are identical, being shifted by a half period.

Finally, in Fig. 8.6 d the input current  $i_A(\tau)$  for the three different values of the firing angle  $\alpha$  is drawn. As a consequence of the periodic commutation between the two pairs of switches the impressed continuous current  $I_D$  appears at the line side of the converter as a square wave alternating current  $i_A(\tau)$ , whose phase lag  $\varphi$  with respect to the line voltage  $u_A(\tau)$  is prescribed by the firing delay,  $\varphi = \alpha$ . The active power (mean of the instantaneous power) at the line side is — assuming sinusoidal line voltage — determined by the fundamental component  $i_{A1}(\tau)$  of the line current

$$P_{AC} = U_A I_{A1} \cos \varphi = \frac{2\sqrt{2}}{\pi} U_A I_D \cos \alpha , \quad (8.2)$$

where  $U_A, I_{A1}$  are RMS-values of the line voltage and the fundamental current component. For  $0 < \alpha < \frac{\pi}{2}$ , the power flows from the AC- to the DC- side, while for  $\frac{\pi}{2} < \alpha < \alpha_{max}$  the power flow is reversed.

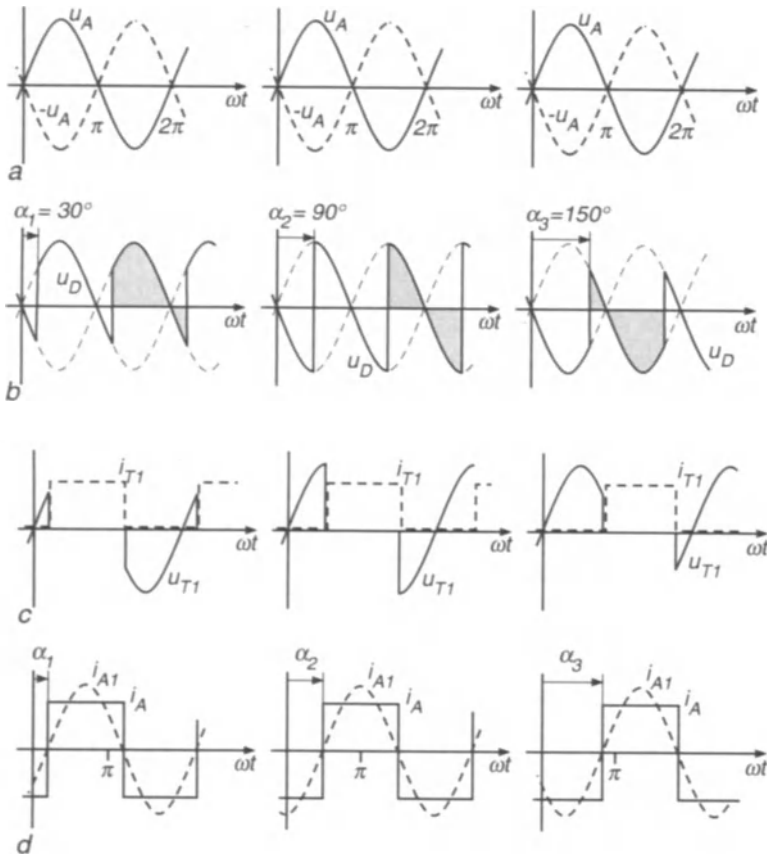


**Fig. 8.6.** Voltages and currents of an ideal single phase converter

The first mode corresponds to controlled rectifier-, the other to inverter operation. In Fig. 8.7 a phasor diagram is shown containing the phasors of the line voltage  $U_A$  and of the fundamental component of the line current,  $I_{A1}$ . Clearly, a controlled converter appears as an inductive load at the line side, drawing lagging reactive current; this is due to the control principle allowing only delayed firing. Firing advance is not possible with line commutated converters because the firing pulses would be applied to valves having reverse bias voltage which prevents them from becoming conductive; advance firing is only possible with force commutated converters, where an interval with forward blocking voltage  $u_T > 0$  is created for  $\alpha < 0$ , during which the thyristor can be fired. Forced commutation calls for additional components and thyristors with short recovery time which involves increased cost and complexity; this will be discussed later.

The possibility of reversing the power flow by electronic control is of importance if the converter is to supply a DC drive motor since it permits regener-

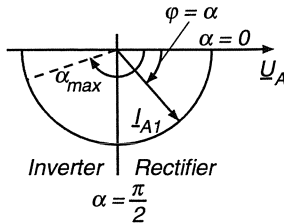


Fig. 8.7. Phasor diagram at AC side of single phase converter

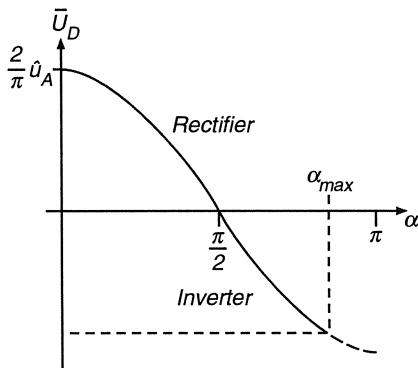


Fig. 8.8. Control curve of phase controlled converter

ation. It is pointed out, however, that firing control affects not only the active but also the reactive power flow at the line side. At  $\alpha = \frac{\pi}{2}$  the reactive power assumes a maximum value (for  $I_D = \text{const.}$ ) while the active power is zero. This would be the case if the motor is producing torque at standstill.

Identical results are obtained if we examine the DC side of the converter, where the mean voltage is

$$\bar{U}_D = \frac{1}{\pi} \int_{\alpha}^{\alpha+\pi} \hat{U}_A \sin \tau d\tau = \frac{2}{\pi} \hat{U}_A \cos \alpha = \frac{2\sqrt{2}}{\pi} U_A \cos \alpha = U_{D0} \cos \alpha . \quad (8.3)$$

This is described by the control characteristic  $\bar{U}_D(\alpha)$  seen in Fig. 8.8; for reasons discussed later the curve is only valid in the interval  $0 < \alpha < \alpha_{max}$ , with  $\alpha_{max} \approx 150^\circ$ . Because of  $i_D = I_D = \text{const.}$ , the mean of the output power is

$$P_{DC} = \bar{U}_D I_D = \frac{2\sqrt{2}}{\pi} U_A I_D \cos \alpha , \quad (8.4)$$

which confirms Eq. (8.2). This is so because the idealised switching converter consumes no power; it functions by shifting the  $180^\circ$ -blocks of the direct current with respect to the line voltage. The transferred mean power changes sign in

accordance with the direct voltage as the firing angle  $\alpha$  exceeds  $\frac{\pi}{2}$ . Since the current cannot change sign because of the unidirectional thyristors, the line commutated converter circuit in Fig. 8.5 represents a controlled power supply operable in the two quadrants of the  $I_D$ ,  $\bar{u}_D$ -plane, as seen in Fig. 8.9. The control is performed by electronically delaying the firing pulses to the thyristors.

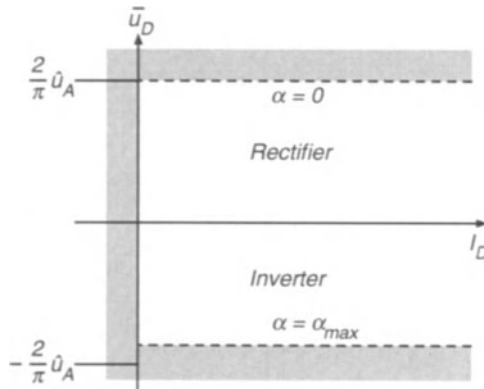


**Fig. 8.9.** Two quadrant operation of line commutated converter

Clearly, a switched converter causes interactions with the line, involving lagging reactive power as well as current harmonics. Because of the supply- and the transformer leakage impedances this causes voltage fluctuations and harmonic distortion which must be taken into consideration as the rating of the converter increases. While the harmonics problem may be relieved by going to multi-phase circuits, the reactive power is a characteristic feature of all line commutated converters with delayed firing control; it is independent of the number of phases and can only be counteracted by reactive compensation. At high power both effects may require correction by harmonic filters having a leading input power factor at line frequency.

Controlling a converter by electronic phase shift of firing pulses requires little control power and involves only very short delay. This is seen in Fig. 8.10 showing the output voltage  $u_D(\tau)$  with the firing angle being switched between  $\alpha = 30^\circ$  and  $\alpha = 150^\circ$ .

Since only one diagonal pair of thyristors can be fired in each half period, there is a maximum delay of 10 ms with a 50 Hz supply until the converter output responds to a command calling for a change in firing angle. Hence a static converter represents an actuator of high dynamic performance combining

- high power gain
- large output power and low losses
- very fast response.

These features may yet be enhanced by employing multi-phase circuits, as will be shown in the next section.

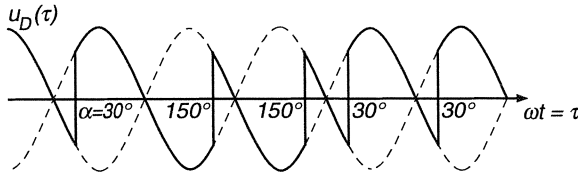


**Fig. 8.10.** Output voltage of single phase converter with changing firing angle

One drawback, though of little practical importance, is the fact that the steady-state and the dynamic behaviour of the converter is highly nonlinear, corresponding to a nonlinear sampled data system with one firing transient in each half period. From Fig. 8.10 it is apparent that, following a changing firing command, the result may not become effective immediately because there are variable waiting intervals. This is particularly pronounced when the firing angle is increased for inverter operation because it is necessary to allow for the relatively “slow” reversal of the line voltage. When going to rectifier operation, i.e. reducing the firing angle, the converter may respond instantaneously. An accurate analysis of dynamic converter operation is quite complex; for small perturbations linearised difference equations can be derived but large signal dynamics are governed by non-linear difference equations for which there is no analytical solution [F8, L30, P32]. Fortunately the converter is usually followed by an inductive load having low-pass transfer characteristics, such as the armature circuit of a DC machine; therefore the converter dynamics may be approximated by very simple models when designing the inner current control loop. The low-pass properties of the load are also desirable in order to smooth the current at the output of the converter.

Another aspect where high power converters may occasionally cause problems is a direct consequence of its advantages mentioned before; the power supplied to the load must instantaneously come from the AC line side. There is no smoothing or decoupling effect from internal stored energy because an ideal converter contains only loss-free switches. As was mentioned before, the importance of these effects has receded as the capacity of the interconnected supply systems has increased.

The control of the converter is normally performed by the output signal of an electronic controller influencing the phase of the firing pulses through a firing control device. Its basic function is explained with the help of Fig. 8.11. The output signal  $y_1(t)$  of the innermost controller, usually a current controller, is compared with a saw-tooth-shaped periodic ramp function  $y_T$  which is synchronised by the zero intersections of the line voltage  $u_A$ . Whenever the difference becomes positive for the first time in each half period, the diagonal pair of thyristors (Fig. 8.5) having forward bias voltage is fired. The selection is done by alternately activating one of two monostable trigger circuits  $MT_1$ ,  $MT_2$ . One of the trigger circuits produces a short pulse which, after amplification, is passed through a small isolating transformer to the gates of the thyristors to

be fired; in high voltage applications, such as high voltage DC-transmission or static reactive power compensators, optical fibres may be used for transmitting the firing pulses.

It is seen that the comparison of the control signal  $y_1$  with the saw-tooth function represents a sampling method, at the same time providing a voltage-to-phase conversion.

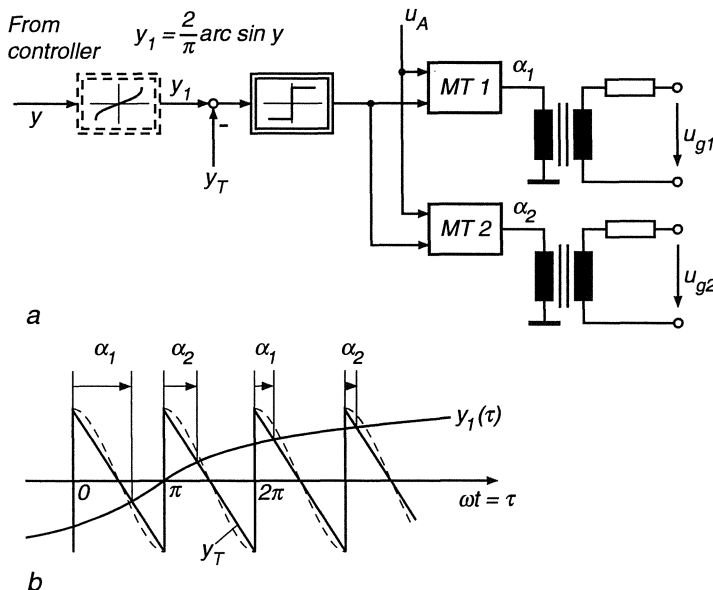


**Fig. 8.11.** Principle of an electronic firing control circuit.  
a) Block diagram; b) Mode of operation

The basic principle shown in Fig. 8.11 can be modified in various ways. If, instead of a saw-tooth function, sections of cos-functions are employed, as is indicated by dashed lines in Fig. 8.11 b, the control curve  $\bar{u}_D(y_1)$  seen in Fig. 8.8 becomes a straight line, i.e. the converter assumes constant voltage gain  $d\bar{u}_D/dy_1$ . The same effect is achieved, at least in steady state, by inserting an arcsin-function generator  $y_1 = \arcsin y$  in the input channel of the firing circuit; this is indicated in Fig. 8.11 a. Control devices for converters are now available in a variety of integrated circuits.

In order to gain a better insight into the principle of converter operation, some simplifications that are not fully realised in practice have been introduced; one is the assumption of a smooth current  $I_D$ , the other of an impressed voltage  $u_A$  neglecting the line impedance. These points will now be discussed in a little more detail. When a resistor  $R_D$  is connected to the output of the converter in Fig. 8.5,  $u_D = R_D i_D$  holds in the DC branch, with the current having the same waveform as the voltage. Hence the conducting valves will be blocked when

the driving voltage  $u_A$  becomes negative; this is so because  $i_D$  cannot change sign and the passive DC circuit cannot – even instantaneously – feed power back to the line. Thus the current will exhibit the pulsating shape seen in Fig. 8.12; during the zero current intervals the voltage across the series connected non-conducting valves is divided according to their blocking resistances.

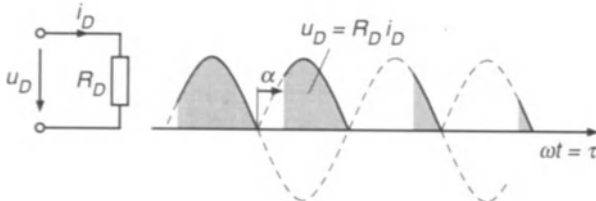


Fig. 8.12. Single phase converter with resistive load

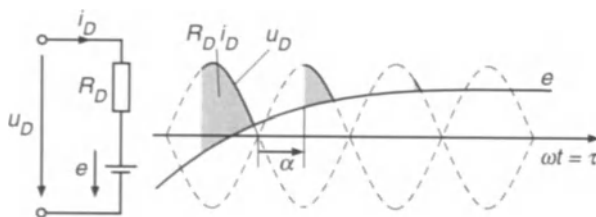


Fig. 8.13. Single phase converter with back voltage and resistive load

The discontinuity of the load current is accentuated if an impressed back voltage  $e(\tau) > 0$  is connected in series with the resistor  $R_D$ . Now a thyristor pair can only begin to conduct if the line voltage exceeds the back voltage,  $|u_A| > e$ , because otherwise the thyristors would be reversely biased; the current ceases to flow as soon as this condition is violated; Fig. 8.13 shows the effect.

A further complication arises, if the DC circuit contains an inductance  $L_D$  in addition to the resistor  $R_D$  and the back voltage  $e$ , which is the case of a converter feeding the armature of a DC motor. Now the current  $i_D$  may become continuous even for  $\alpha > 0$  because the armature inductance with its stored energy can maintain the current  $i_D$  during part of the interval where  $|u_A| < e$ . This is drawn in Fig. 8.14 for different values of the firing angle  $\alpha$  and assuming  $e = E = \text{const.}$  The internal impedance of the line voltage source is still neglected.

Let us assume an initial zero current state,  $i_D = di_D/dt = 0$  and consequently  $u_D = E$ . At time  $\omega t = \tau = \alpha_1$ , with the condition  $\hat{u}_A \sin \alpha_1 > E$ , the thyristors 1,1' are fired so that the current  $i_D$  begins to rise with finite slope and quickly exceeds the latching value  $i_L$ . In view of the conducting thyristors 1, 1',  $u_D(\tau) = u_A(\tau)$  holds, and the following differential equation is valid

$$\omega L_D \frac{di_D}{d\tau} + R_D i_D = \hat{u}_A \sin \tau - E, \quad \alpha_1 \leq \tau \leq \beta_1. \quad (8.5)$$

The solution, satisfying the initial condition  $i_D(\alpha_1) = 0$ , and with the abbreviations

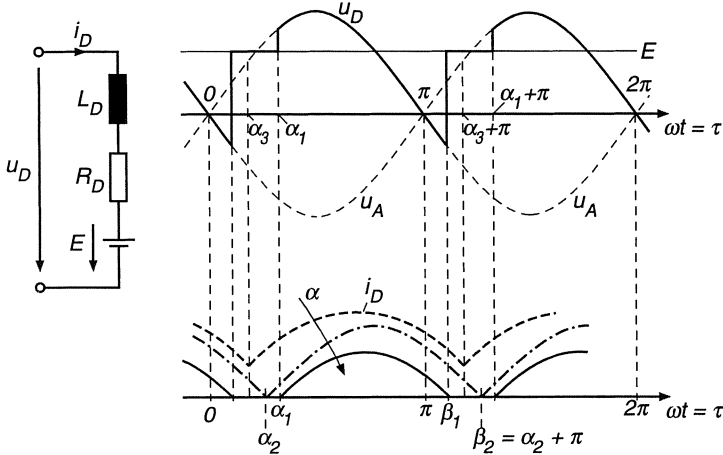


**Fig. 8.14.** Discontinuous and continuous current

viation  $L_D/R_D = T_D$  is

$$\begin{aligned} i_D(\tau) &= \frac{\hat{u}_A}{R_D} \frac{1}{\sqrt{1 + (\omega T_D)^2}} \\ &\times [\sin(\tau - \arctan \omega T_D) - e^{-(\tau-\alpha_1)/\omega T_D} \sin(\alpha_1 - \arctan \omega T_D)] \\ &- \frac{E}{R_D} [1 - e^{-(\tau-\alpha_1)/\omega T_D}]. \end{aligned} \quad (8.6)$$

At  $\beta_1 < \alpha_1 + \pi$  the current  $i_D$  becomes zero,  $i_D(\beta_1) = 0$ , see Fig. 8.14, at which time the thyristors return to blocked condition; the current remains zero until  $\tau = \alpha_1 + \pi$ , when the thyristors 2, 2' are fired and the same transient is repeated.

Thus in steady-state the direct current is discontinuous, consisting of separate pulses. The mean of the current is a function of all parameters,

$$\bar{i}_D = \frac{1}{\pi} \int_{\alpha_1}^{\beta_1} i_D(\tau) d\tau = F[\alpha, \hat{u}_A, \omega T_D, R_D, E]. \quad (8.7)$$

When evaluating Eq. (8.7) the impedance ( $R_D, L_D$ ) must be augmented by a small line-side impedance as is shown later.

A similar expression holds for the mean voltage

$$\bar{u}_D = \frac{1}{\pi} \int_{\alpha_1}^{\alpha_1+\pi} u_D(\tau) d\tau. \quad (8.8)$$

This integral may be simplified with the help of Eq. (8.5) considering the periodic boundary condition

$$i_D(\alpha_1) = i_D(\alpha_1 + \pi) = 0 ; \quad (8.9)$$

thus it assumes the form

$$\bar{u}_D = E + R_D \bar{i}_D , \quad (8.10)$$

where  $\bar{i}_D$  is given by Eq. (8.7).

This load characteristic  $\bar{u}_D(\bar{i}_D)$  for  $\alpha = \text{const.}$  and different values of the back voltage  $E$  is highly nonlinear as long as the current is discontinuous; this is due to the variable period of conduction,  $\beta_1 - \alpha_1 < \pi$ ; it is seen in Fig. 8.16.

When gradually reducing the firing angle,  $\alpha < \alpha_1$ , with the same initial conditions as before, the amplitude and the duration of the current pulses increase until a limiting case occurs,  $\alpha = \alpha_2$ , where one pair of thyristors is fired at the moment the other pair ceases conducting. The current then only touches zero once every half period.

If the firing angle is still further reduced,  $\alpha < \alpha_2$ , the current will not have reached zero by the time the other thyristors are fired. This then constitutes the region of continuous conduction, where the current is no longer discontinuous.

The bordering case to continuous conduction may be determined with the periodic boundary condition

$$i_D(\alpha_2) = i_D(\alpha_2 + \pi) = 0 ; \quad (8.11)$$

from Eq. (8.6),

$$\frac{\hat{u}_A}{\sqrt{1 + (\omega T_D)^2}} (1 + e^{-\pi/\omega T_D}) \sin(\alpha_2 - \arctan \omega T_D) + E (1 - e^{-\pi/\omega T_D}) = 0 . \quad (8.12)$$

Solving for  $\alpha_2$ , the condition for continuous conduction can be written as

$$\alpha < \alpha_2 = \arctan \omega T_D - \arcsin \left[ \frac{E \sqrt{1 + (\omega T_D)^2}}{\hat{u}_A} \tanh \left( \frac{\pi}{2 \omega T_D} \right) \right] . \quad (8.13)$$

For each value of the back voltage  $E$  a firing angle  $\alpha_2$  exists, at which the range of continuous conduction begins. With  $\omega T_D \gg 1$ , i.e. assuming a perfectly smooth current, Eq. (8.13) yields the obvious result

$$\bar{u}_D = \frac{2}{\pi} \hat{u}_A \cos \alpha \geq E , \quad (8.14)$$

indicating that the mean output voltage  $\bar{u}_D$  must exceed the back voltage in order that continuous load current can flow.

All the preceding equations are valid for  $E \gtrless 0$ , that is, for rectifier as well as inverter operation.

As was mentioned before, continuous current flow occurs if the firing angle is reduced beyond the bordering case,  $\alpha_3 < \alpha_2$ ; reducing the back voltage  $E$

or increasing the lag term  $\omega T_D$  would have a similar effect. With the current flowing continuously, Eq. (8.5) is valid during the full half period following the firing of the thyristors 1, 1',  $\alpha_3 \leq \tau \leq \alpha_3 + \pi$ ; in steady state the periodic boundary condition is

$$i_D(\alpha_3) = i_D(\alpha_3 + \pi) > 0 ; \quad (8.15)$$

Hence the solution of Eq. (8.5) may be written as

$$\begin{aligned} i_D(\tau) = & \frac{\hat{u}_A}{R_D} \frac{1}{\sqrt{1 + (\omega T_D)^2}} \\ & \times \left[ \sin(\tau - \arctan \omega T_D) - e^{-(\tau-\alpha_3)/\omega T_D} \sin(\alpha_3 - \arctan \omega T_D) \right] \\ & - \frac{E}{R_D} [1 - e^{-(\tau-\alpha_3)/\omega T_D}] + i_D(\alpha_3) e^{-(\tau-\alpha_3)/\omega T_D}, \end{aligned} \quad (8.16)$$

where the initial value  $i_D(\alpha_3)$  in steady-state is obtained with the help of Eq. (8.15).

If the mean value of the current is mainly of interest as is the case with drives, a much simpler solution exists for continuous current in steady-state. By integrating Eq. (8.5) over a half period and inserting the condition (8.15) for periodicity, we find

$$\overline{i_D}(\alpha_3) = \frac{1}{\pi} \int_{\alpha_3}^{\alpha_3+\pi} \frac{1}{R_D} (\hat{u}_A \sin \tau - E) d\tau = \frac{1}{R_D} (\overline{u_D}(\alpha_3) - E), \quad (8.17)$$

where the average voltage  $\overline{u_D}$  is given by Eq. (8.3). Thus the converter acts as a linear controllable voltage source only if the current in the load branch is continuous.

The mean current  $\overline{i_D}(\alpha_2)$ , at which discontinuous operation sets in, Eq. (8.13), is an important design parameter for the possible selection of a smoothing choke, resulting in an adequate value of the normalised time constant  $\omega T_D$ . As is shown in Fig. 8.16 this current also depends on the back voltage  $E$ , its peak occurs around  $E \approx 0$ , where the AC component contained in  $u_D(\tau)$  assumes a maximum. With large drives the specification may call for the maximum discontinuous current to be less than 10% of rated current,  $\overline{i_D}(\alpha_2) < 0.1 I_{Dr}$ , in order to limit the ripple current which produces additional losses in the armature and may impair commutation. However, with medium and smaller drives the smoothing choke is frequently omitted for reasons of cost, so that only the armature inductance is left for filtering the current. This may result in discontinuous current of half rated value, affecting not only the losses but also the design of the current controller, as will be explained in Sect. 8.5.

Another important effect neglected so far is the finite commutation interval caused by the impedance in the AC circuit, which consists mainly of the leakage inductance and winding resistance of the transformer; also, line inductances may be inserted for protective reasons to limit the rate of change of currents (including fault currents) through the thyristors. At medium and larger power

rating, the line impedance is predominantly inductive,  $R_A \approx 0.1\omega L_A$ , which for approximate calculations justifies neglecting the resistive component.

The line-side inductance  $L_A$ , even though it is small when compared with the inductance  $L_D$  in the load circuit, causes the line current to become a state variable subject to continuous change only; hence  $i_A(\tau)$  and the currents in the thyristor branches can no longer exhibit the discontinuities seen in Fig. 8.6. Instead, the rise and decay of the thyristor currents and, correspondingly, the reversal of the alternating current  $i_A(\tau)$  now assume the form of continuous commutating transients requiring a finite time, called the commutation interval  $\tau_c$  or overlap; naturally, this effect only arises with continuous load current.

For example it may be assumed that the thyristors 2,2' of the circuit in Fig. 8.15 a are initially conducting and that at  $\tau = \alpha$ , i.e. with positive line voltage  $u_A$ , the thyristors 1,1' are fired. Since the currents  $i_D$  and  $i_A$  are continuous on account of  $L_D$  and  $L_A$ , the thyristors 2,2' remain also conducting at first, so that the four thyristors represent temporarily a short circuit connection,  $u_D = u_B = 0$ , decoupling the line current from the load circuit. Hence, from Kirchhoff's laws, it follows with  $\omega t = \tau$ ,

$$i_{T1} + i_{T2} = i_D , \quad (8.18a)$$

$$i_{T1} - i_{T2} = i_A , \quad (8.18b)$$

$$\omega L_A \frac{di_A}{d\tau} + R_A i_A = u_A , \quad (8.18c)$$

$$\omega L_D \frac{di_D}{d\tau} + R_D i_D = -E . \quad (8.18d)$$

The initial conditions are

$$\begin{aligned} i_{T1}(\alpha) &= 0 , \\ i_{T2}(\alpha) &= -i_A(\alpha) = i_D(\alpha) . \end{aligned}$$

Because of the much smaller inductance  $L_A$ , the line current changes rapidly whereas the load current may be assumed to be approximately constant during the commutation interval,  $i_D(\tau) \approx i_D(\alpha)$ . Hence, with the abbreviation  $T_A = L_A/R_A$  we find for  $\alpha \leq \tau \leq \alpha + \tau_c$

$$i_A(\tau) \approx \hat{i}_A \sin(\tau - \arctan \omega T_A) - [i_D(\alpha) + \hat{i}_A \sin(\alpha - \arctan \omega T_A)] e^{-(\tau-\alpha)/\omega T_A} \quad (8.19)$$

where

$$\hat{i}_A = \frac{\hat{u}_A}{\sqrt{R_A^2 + (\omega L_A)^2}}$$

is the peak value of the (steady state) short circuit current at the line terminals. From Eqs. (8.18) the thyristor currents are obtained,

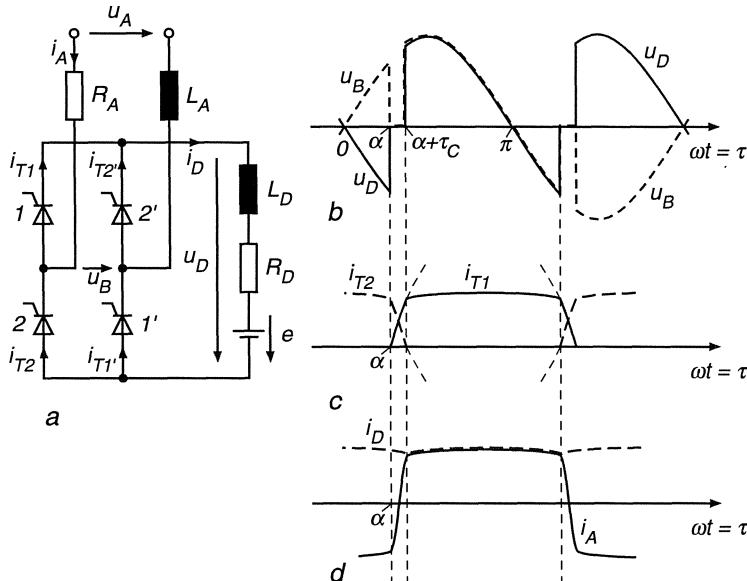


**Fig. 8.15.** Commutation of a single phase converter

$$\begin{aligned} i_{T1}(\tau) &\approx \frac{1}{2} [i_D(\alpha) + i_A(\tau)] , \\ i_{T2}(\tau) &\approx \frac{1}{2} [i_D(\alpha) - i_A(\tau)] . \end{aligned} \quad (8.20)$$

These results apply only as long as the four thyristors are conducting. The commutation terminates at time  $\alpha + \tau_c$ , when

$$i_{T2}(\alpha + \tau_c) = 0 ; \quad (8.21)$$

after this instant, Eq. (8.5) is again valid.

The various voltages and currents, when including the line impedance, are seen in Figs. 8.15, assuming continuous current  $i_D$ . All the currents are now continuous functions of time; in contrast, the voltages  $u_D(\tau)$  and  $u_B(\tau)$  exhibit characteristic discontinuities during commutation, when all thyristors are conducting.

As a consequence of the finite commutation interval, the line current experiences a further shift in time resulting in an additional component of reactive power due to commutation; this increases the reactive power caused by the delayed firing control as discussed before (Fig. 8.7).

Another effect of the line impedance is a loss in output voltage due to the temporary short circuit,

$$u_D(\tau) = 0, \quad \alpha \leq \tau \leq \alpha + \tau_c ; \quad (8.22)$$

it causes a drop of the mean voltage by

$$\overline{\Delta u_D} \approx \frac{1}{\pi} \int_{\alpha}^{\alpha+\tau_c} u_A d\tau , \quad (8.23)$$

which may be estimated from the current change in the AC circuit. With the simplification mentioned before,

$$R_A \ll \omega L_A ,$$

we find from Eq. (8.20)

$$\overline{\Delta u_D} \approx \frac{1}{\pi} \int_{\alpha}^{\alpha+\tau_c} u_A d\tau \approx \frac{1}{\pi} \omega L_A i_A(\tau) \Big|_{\alpha}^{\alpha+\tau_c} = \frac{1}{\pi} \omega L_A [i_A(\alpha+\tau_c) - i_A(\alpha)] . \quad (8.24)$$

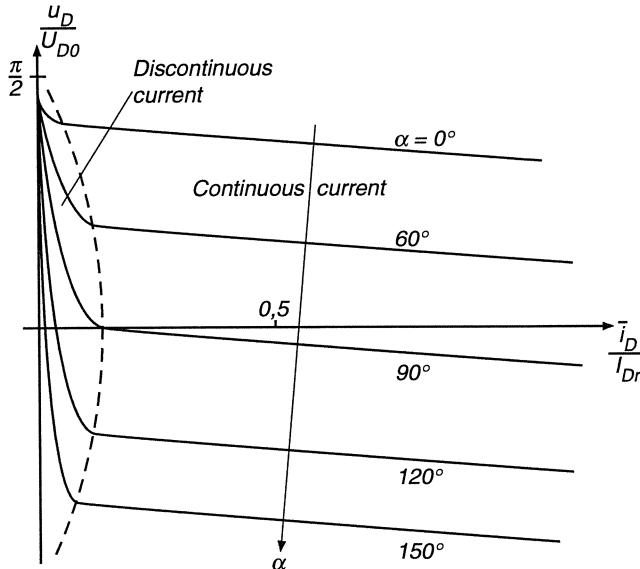


**Fig. 8.16.** Characteristics of single phase converter with inductive load

Hence the voltage-time-area lost during commutation is related to the flux change in the line inductance.

If a sufficiently large smoothing inductance  $L_D$  is employed, such that the ripple current contained in  $i_D(\tau)$  may be neglected,  $i_A(\alpha + \tau_c) \approx -i_A(\alpha) \approx \overline{i_D}$ ; Eq. (8.24) then yields a voltage drop proportional to load current

$$\overline{\Delta u_D} \approx \frac{2}{\pi} \omega L_A \overline{i_D} ; \quad (8.25)$$

this indicates that the line commutated converter acts like a controlled voltage source having an apparent internal resistance proportional to the reactance of the AC line; of course, this drop of the terminal voltage does not involve real power losses, as it is caused by commutation at the AC side of the converter. As a consequence, the load curves of the converter  $\overline{u_D(i_D)}$  for  $\alpha = \text{const.}$  are inclined in the continuous current region (Fig. 8.16), even though all ohmic resistances apart from that in the load branch have been neglected. In contrast to the intermittent current range where the curves are strongly nonlinear, the characteristics in the continuous current region are linear exhibiting only a slight droop. By normalising Eq. (8.25) with the no-load voltage  $U_{D0}$  and rated current  $I_{Dr}$ , we find

$$\frac{\overline{\Delta u_D}}{U_{D0}} \approx \frac{\omega L_A I_{Dr}}{\sqrt{2} U_A} \frac{\overline{i_D}}{I_{Dr}} = k \frac{\overline{i_D}}{I_{Dr}} . \quad (8.26)$$

The normalised impedance factor  $k$  is mainly determined by the leakage reactance of the line transformer; a common value is  $k \approx 0.05$  to  $0.10$ .

The commutation interval  $\tau_c$ , which usually lasts only a few degrees, depends also on the firing angle  $\alpha$ ; this is seen from a rough estimate of the integral in Eq. (8.24)

$$\overline{\Delta u_D} \approx \frac{1}{\pi} \int_{\alpha}^{\alpha+\tau_c} \hat{u}_A \sin \tau d\tau \approx \frac{\sqrt{2}}{\pi} \tau_c U_A \sin \alpha , \quad (8.27)$$

which shows that for constant load current the overlap is minimal at  $\alpha = \frac{\pi}{2}$ , when the AC voltage has its peak amplitude. A more accurate result is obtained by evaluating the integral, Eq. (8.23),

$$\tau_c \approx \arccos \left[ \cos \alpha - \frac{\sqrt{2} \omega L_A}{U_A} \frac{\overline{i_D}}{I_{Dr}} \right] - \alpha . \quad (8.28)$$

The knowledge of the overlap is of particular importance if the converter operates as inverter, i.e. with large firing delay  $\alpha$ , because then it must be assured that the commutation is completed and in addition the outgoing thyristors have recovered and are ready to block forward voltage when the line voltage changes sign; otherwise an unintentional refiring will occur. Since the back voltage is negative during inverter operation,  $E < 0$ , this would connect in series two voltages ( $E, u_A$ ) having (for a half period) the same sign; the result would be a short circuit condition with a fast current rise which is only limited by the smoothing inductance. This malfunction is called a commutation failure.

In Fig. 8.17 the disturbance is described in more detail. The inverter is assumed to operate initially at the safe firing angle  $\alpha_1 = 150^\circ$ , when an additional firing delay  $\Delta\alpha$  for the thyristors 1,1' is introduced. Due to the low voltage  $u_A(\tau)$  in this interval the commutation proceeds quite slowly as it takes time to accumulate the necessary voltage-time-area. The commutating transient is eventually completed at  $\alpha + \tau_c$ , when the current through thyristors 2,2' has become zero. There is still some negative blocking voltage  $u_{T2} < 0$  across the outgoing thyristors but it is small and the time until the voltage  $u_A$  changes sign

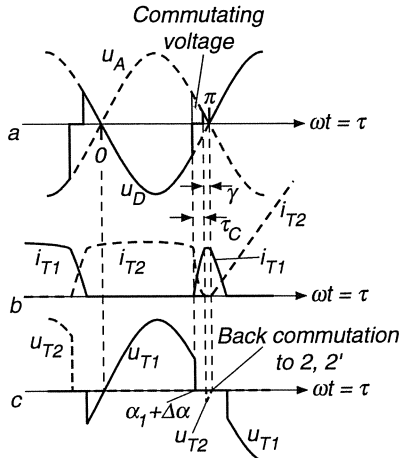


Fig. 8.17. Commutation failure due to late firing of thyristors 1,1'

may be too short for the thyristors 2,2' to regain their forward blocking capacity. In other words, the time equivalent of the extinction angle  $\gamma = \pi - (\alpha + \tau_c)$  no longer exceeds the recovery time which is increased by the low reversed bias voltage across the outgoing thyristors.

The consequence would be a spontaneous refiring of thyristors 2,2' and back-commutation to these valves. This leads to the series connection of  $u_A < 0$  and  $E < 0$  through thyristors 2,2' and a subsequent steep rise of the current. The next regular commutation of the inverter is possible one period after the attempted firing of thyristors 1,1', where the controller must now assure a sufficiently advanced timing of the firing pulses in order to successfully complete the commutation despite the increased current. Otherwise a circuit breaker would have to clear the fault.

It is seen that the danger of a commutation failure increases with the magnitude of the current and the line-side reactance, since both effects prolong the commutation interval  $\tau_c$ . In order to utilise fully the voltage of the inverter, a sufficient magnitude of the extinction angle  $\gamma$  may be assured by a separate control loop. However, in view of the additional complexity and the remaining uncertainty in case of a sudden voltage dip of the AC line voltage (which would unexpectedly increase the overlap), extinction angle control is seldom used except with very high power installations, such as HVDC, where operation of the inverter at the maximum firing angle is important for power factor considerations and the cost of the control system is less significant [71, F17]. The usual practice with drives is to limit the firing angle to "safe" values, e.g.  $\alpha < \alpha_{max} = 150^\circ$ , and to prevent excessive currents by a fast acting control loop.

### 8.3 Line-commutated Converter in Three-phase Bridge Connection

The single phase circuit discussed in the preceding paragraph is normally used for low power applications only, with the exception of traction drives having a single phase supply. Beyond a few kW there are strong incentives for three-phase converter circuits which require two more thyristors but have a number of important advantages:

- The three- phase line is symmetrically loaded in steady state.
- The line currents have a lower harmonic content; as a consequence there is less distortion of the line voltages than with a single phase circuit.
- The same is true for the direct voltage  $u_D(\tau)$  which contains ripple components of higher frequencies and lower amplitudes, thereby permitting a reduction of the filter components and causing lower losses in the load.
- The dynamic performance of three-phase converters is superior because valves are fired at shorter intervals; the reduced delay for control signals permits more rapid control.

Figure 8.18 depicts a bridge connection which is the three-phase circuit most commonly used with thyristors or power transistors. In contrast to the single-phase bridge circuit (Fig. 8.5) where the thyristors had to be fired in pairs, the commutations alternate between the upper and lower row of thyristors, so that in steady state six regularly spaced firing transients occur during each period. Hence the three-phase bridge is a “six pulse” circuit while the single phase bridge with two firing instants per period belongs to the class of “two pulse” circuits.

With Hg-arc valves, having a much higher voltage drop, center tap circuits without series connection of valves had been in widespread use; they were the natural choice with multi-anode valves having a common Hg-cathode. However, since the introduction of thyristors as individual devices with small physical dimensions and low voltage drop these points of view have become less important.

The AC voltages in Fig. 8.18 represent the line-to-neutral voltages of a balanced three-phase system. The thyristors 1, 3, 5 connect the AC line-terminals in cyclic sequence to the upper DC bus  $S_1$ , the valves 2, 4, 6 to the lower bus  $S_2$ . In normal steady-state operation and with continuous direct current, each thyristor in the upper and lower row carries the current for  $120^\circ$ ; also, the two thyristors connected to one AC line-terminal do not normally conduct at the same time, as this constitutes a short circuit of the DC-terminals. Figures 8.19 and 8.20 show various voltages and currents in steady-state conditions with the firing angles  $\alpha_1 = 45^\circ$  and  $\alpha_2 = 135^\circ$ , belonging to rectifier- and inverter-operation respectively. The line inductances  $L_A$  are neglected for the time being so that no overlap between subsequent thyristors takes place; the constant direct

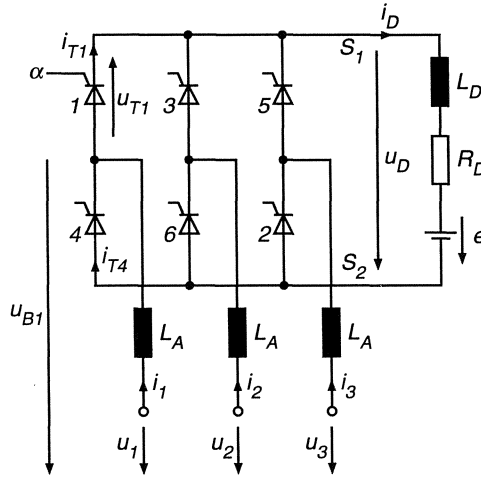


**Fig. 8.18.** Three-phase line commutated converter

current  $i_D = I_D$  is assumed to be generated by a current source. The conducting thyristors are indicated in each  $120^\circ$  interval, always comprising one of the upper and one of the lower row; the firing alternates between these two groups. Hence the output voltage  $u_D(\tau)$  consists of  $60^\circ$  sections of sequential line-to-line voltages, for example  $u_{12} = u_1 - u_2$ . As long as thyristor 1 is conducting, thyristor 3 sees a negative bias voltage for  $u_2 - u_1 < 0$ ; hence thyristor 3 can only be fired, after  $u_2 - u_1$  has become positive.

This “natural” firing instant ( $\tau = \pi/6$  for thyristor 1) serves as a reference for the firing angle  $\alpha$ , which can again vary from  $\alpha = 0$  (maximum output voltage, rectifier) to  $\alpha = \alpha_{max}$  (minimum output voltage, inverter). An appropriate safety margin  $\pi - \alpha_{max}$  is again required, which must exceed the maximum overlap plus recovery time in order to prevent commutation failures.

With the assumed simplifications and the definitions for the line-to-neutral voltages

$$\begin{aligned} u_1(\tau) &= \sqrt{2} U_A \sin \tau, & u_2(\tau) &= \sqrt{2} U_A \sin \left( \tau - \frac{2\pi}{3} \right), \\ u_3(\tau) &= \sqrt{2} U_A \sin \left( \tau - \frac{4\pi}{3} \right), \end{aligned}$$

the mean of the output voltage is

$$\begin{aligned} \bar{u}_D &= \frac{3}{\pi} \int_{\frac{\pi}{6}+\alpha}^{\frac{\pi}{2}+\alpha} (u_1 - u_2) d\tau = \frac{3\sqrt{6}}{\pi} U_A \int_{\frac{\pi}{6}+\alpha}^{\frac{\pi}{2}+\alpha} \sin(\tau + \frac{\pi}{6}) d\tau \\ &= \frac{3\sqrt{6}}{\pi} U_A \cos \left( \tau + \frac{\pi}{6} \right) \Big|_{\frac{\pi}{6}+\alpha}^{\frac{\pi}{2}+\alpha} = \frac{3\sqrt{6}}{\pi} U_A \cos \alpha = U_{D0} \cos \alpha. \quad (8.29) \end{aligned}$$

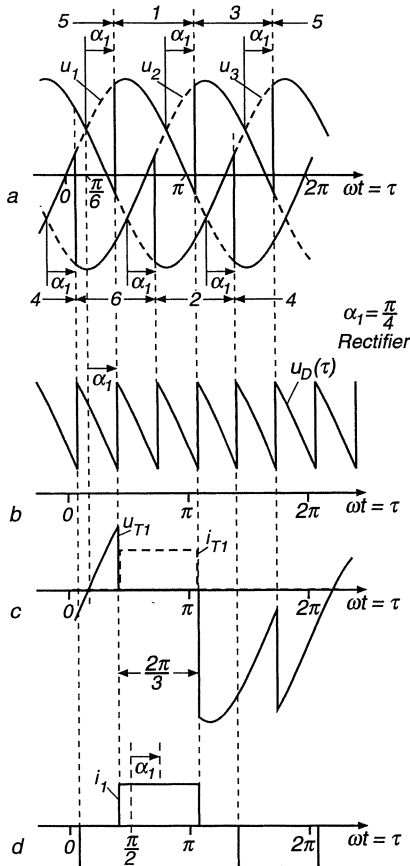
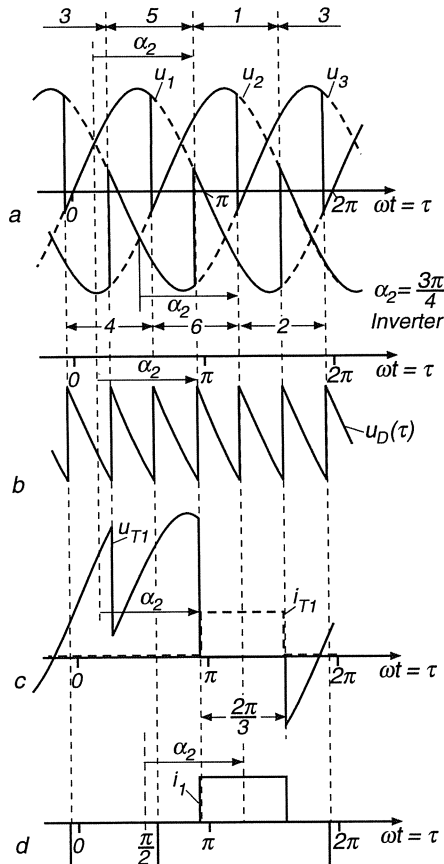


Fig. 8.19. Voltages and currents of a 6-pulse converter at  $\alpha_1 = 45^\circ$

Here too, the control curve follows a cos-function. When the converter is connected to the 230/400 V three-phase line, the maximum mean output voltage is  $U_{D0} = 540$  V.

The output voltage  $u_D(\tau)$  shown in Figs. 8.19 and 8.20 contains in steady-state harmonics, the frequencies of which are multiples of  $6f_0$ , i.e. 300 Hz for a 50 Hz line.

Voltage and current of a thyristor are plotted in Fig. 8.19 c for rectifier- and in Fig. 8.20 c for inverter-operation. Reverse bias voltage ( $u_{T1} < 0$ ) dominates in the first, forward blocking voltage ( $u_{T1} > 0$ ) in the second case. This indicates that rectifier operation is insensitive to overload, while at the inverter limit the danger of commutation failure always lurks in the background, because negative voltage is required across the outgoing thyristor for a sufficient time in order to let it resume its forward blocking capability.



**Fig. 8.20.** Voltages and currents of a 6-pulse converter at  $\alpha_2 = 135^\circ$

In Figs. 8.19 d and 8.20 d the current  $i_1$  in one of the AC terminals is drawn, the fundamental component of which is again lagging the pertinent line-to-neutral voltage  $u_1$  by the firing angle  $\alpha$  (neglecting overlap).

A comparison with Fig. 8.6 d shows that the harmonics content of the line currents is reduced; whereas all odd harmonics of line frequency  $f_0$  were present in the single-phase circuit, the odd harmonics of frequency  $3f_0$  disappear in the three-phase circuit. Hence the lowest order harmonics of the line currents, assuming perfect symmetry of the line voltages and the firing sequence, are the 5th and the 7th.

So far, it had again been assumed that the commutation between the conducting thyristors occurs instantaneously; in reality, it requires finite time because of the presence of leakage inductances in the supply lines and the thyristor branches. As mentioned before, line inductances are often introduced deliberately in order to limit the rise of the current during commutation; if no trans-

former for supplying the converter is used, this is mandatory. Again the line impedance is assumed to be purely inductive,  $R_A \ll \omega L_A$ .

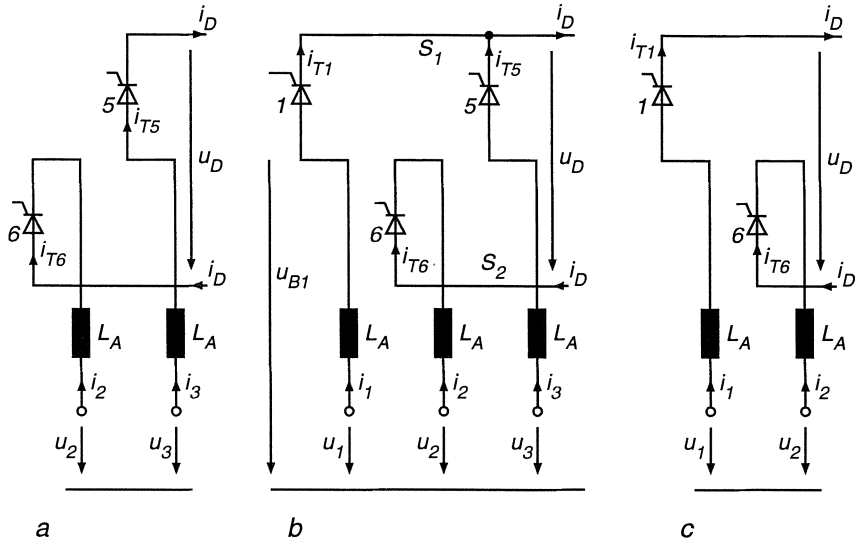


**Fig. 8.21.** Commutation of three-phase converter, circuit diagram

The commutation described in Fig. 8.21 proceeds in three stages: Initially the thyristors 5 and 6 may carry the constant current  $i_D = I_D$  (Fig. 8.21 a); at time  $\tau = \frac{\pi}{6} + \alpha$  thyristor 1 is fired leading to the situation in Fig. 8.21 b, where two AC terminals are connected through thyristors 1, 5; due to the small inductances  $L_A$  a short circuit current builds up transferring the current  $I_D$  from thyristor 5 to thyristor 1. As soon as  $i_{T5}$  has become zero, thyristor 5 blocks and the circuit finds itself in the position shown in Fig. 8.21 c. The overlap during which three valves are simultaneously conducting extends normally over a few degrees only; however there may be exceptions if the line inductances are unusually large.

The commutation according to Fig. 8.21 b is described by the following equations, valid for  $\frac{\pi}{6} + \alpha \leq \tau \leq \frac{\pi}{6} + \alpha + \tau_c$ ,

$$i_{T1} + i_{T5} = i_{T6} \approx I_D , \quad (8.30a)$$

$$\omega L_A \frac{d}{d\tau} (i_{T1} - i_{T5}) \approx u_1 - u_3 . \quad (8.30b)$$

Elimination of  $i_{T5}$  results in

$$2 \omega L_A \frac{di_{T1}}{d\tau} \approx u_1 - u_3 = \sqrt{6} U_A \sin(\tau - \pi/6) ; \quad (8.31)$$

with the initial condition  $i_{T1}(\frac{\pi}{6} + \alpha) = 0$  we find

$$i_{T1}(\tau) \approx \frac{\sqrt{6} U_A}{2 \omega L_A} \left[ \cos \alpha - \cos \left( \tau - \frac{\pi}{6} \right) \right], \quad (8.31a)$$

and

$$i_{T5}(\tau) \approx I_D - i_{T1}(\tau). \quad (8.31b)$$

When  $i_{T5}$  has attained zero,

$$i_{T5} \left( \frac{\pi}{6} + \alpha + \tau_c \right) = 0, \quad (8.32)$$

the commutating transient is completed and Eqs. (8.30 a, b) are no longer valid.

Figure 8.22 shows a sequence of commutations as obtained by a digital simulation of the converter circuit [E4, M11]; for the sake of clarity the commutation intervals have been enlarged. In view of the equal inductances in each line terminal, the potential of the upper bus  $S_1$  corresponds to the mean of the two line-to-neutral voltages affected by the short circuit condition. Hence, the output voltage during overlap is

$$u_D(\tau) \approx \frac{1}{2} (u_1 + u_3) - u_2, \quad (8.33)$$

which causes a loss in output voltage according to the shaded area in Fig. 8.22. Its mean value is

$$\overline{\Delta u_D} = \frac{3}{\pi} \int_{\frac{\pi}{6} + \alpha}^{\frac{\pi}{6} + \alpha + \tau_c} \frac{1}{2} (u_1 - u_3) d\tau. \quad (8.34)$$

On the other hand, integrating Eq. (8.31) between the limits  $0 \leq i_{T1} \leq I_D$  results in

$$\int_{\frac{\pi}{6} + \alpha}^{\frac{\pi}{6} + \alpha + \tau_c} \frac{1}{2} (u_1 - u_3) d\tau = \omega L_A I_D \quad (8.35)$$

so that the voltage drop due to commutation becomes again a linear function of the load current,

$$\overline{\Delta u_D} = \frac{3}{\pi} \omega L_A I_D; \quad (8.36)$$

a fictitious ohmic resistor in series with the controllable voltage source  $\overline{u_D}(\alpha)$  would have a similar effect. The load characteristics of the three-phase converter shown in Fig. 8.23 have a corresponding droop in the continuous current range.

As was explained in the case of the single-phase converter, a load circuit consisting of a finite inductive impedance in series with a back voltage  $E$  can lead to discontinuous current flow, causing the curves  $\overline{u_D}(i_D, \alpha)$  to become highly nonlinear; this is seen at the left of Fig. 8.23. With an appropriate choice of the smoothing inductance  $L_D$  the range of discontinuous current can be restricted to light load so that it is not noticeable in normal operation; the requirement for the filter time constant  $T_D$  to achieve continuous current is considerably relieved with a three-phase converter.

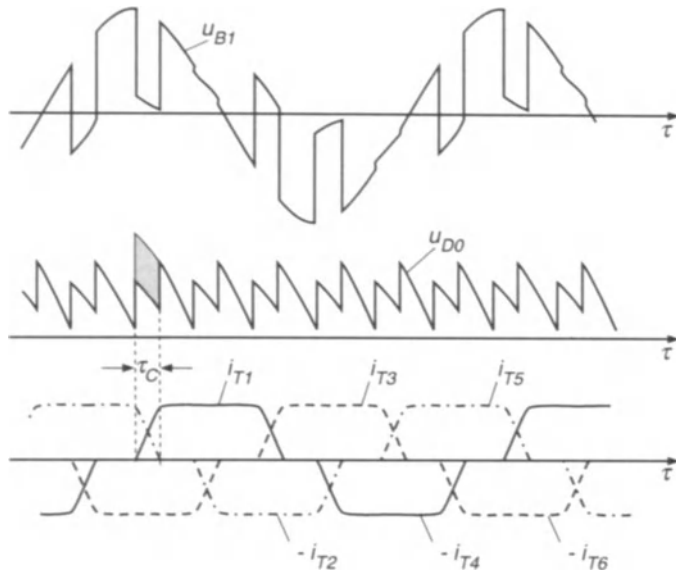


Fig. 8.22. Commutation transients of three-phase converter

If, however, the smoothing reactor is reduced further or completely omitted for cost reasons, discontinuous current flow can occur under load as well. In view of the altered motor dynamics this may require special provisions when designing the control, as will be explained in Sect. 8.5.

The temporary short circuits of the AC terminals during commutation have of course an immediate effect on the waveform of the AC voltages, possibly influencing neighbouring equipment. One of the terminal voltages  $u_{B1}$  with respect to neutral (Fig. 8.18) is plotted in Fig. 8.22. In a weak supply system having a large internal impedance, the danger of feedback to the converter through the synchronising signals exists which may cause instability [A8]. Apart from the obvious, but not always feasible, solution of filtering the synchronising signals, there are various “supply-independant” firing schemes with internal oscillators that permit stable operation even with highly distorted line voltages [H45, M11]. Integrated circuits (chips) are also available for controlling three- phase converters.

The dynamic behaviour of the six pulse converter is similar to that of the 2- pulse converter with the exception that now the steady-state firing intervals are  $\pi/3$ , instead of  $\pi$ , thus permitting much faster access to the output voltage  $u_D(\tau)$ . The waiting interval is now between 0 and  $1/6f_o$  corresponding to 3.3 ms for a 50 Hz-supply.

The firing control of a three-phase converter is simply an extension of the firing scheme for single phase converters (Fig. 8.11), employing several time-displaced saw-tooth functions in order to sample the output signal of the con-

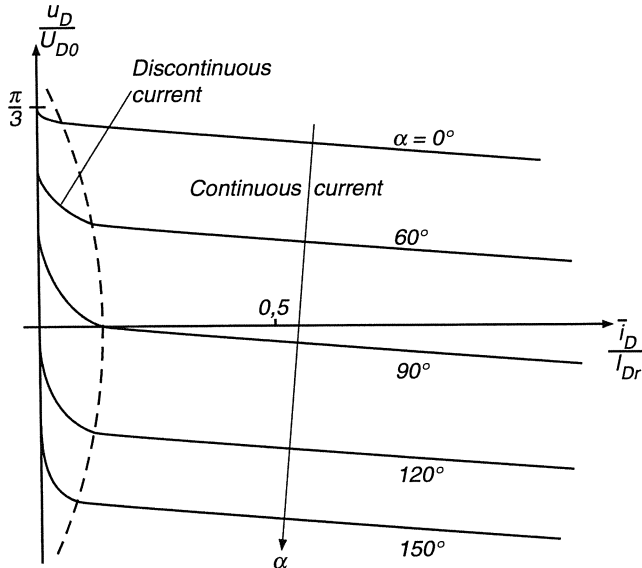


Fig. 8.23. Load curves of a 6-pulse converter

troller. For example, Fig. 8.24 displays the voltage transient  $u_D(\tau)$ , neglecting commutation, which follows a step change of the firing angle from rectifier- to inverter operation and back. When the firing is retarded, the current carrying thyristors simply remain conducting until the line voltage has changed its sign, while in opposite direction an immediate response is possible. It may even occur, as seen in Fig. 8.24, that some thyristors may be skipped because a multiple commutation occurs with several – in principle all – thyristors temporarily conducting, with the ones at the highest and lowest potential eventually prevailing.

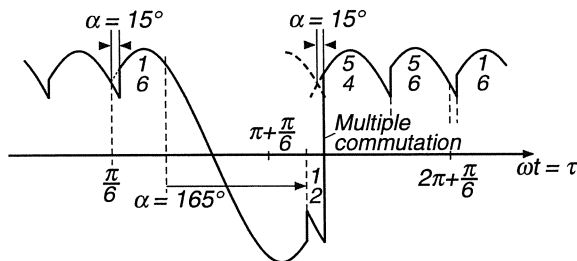
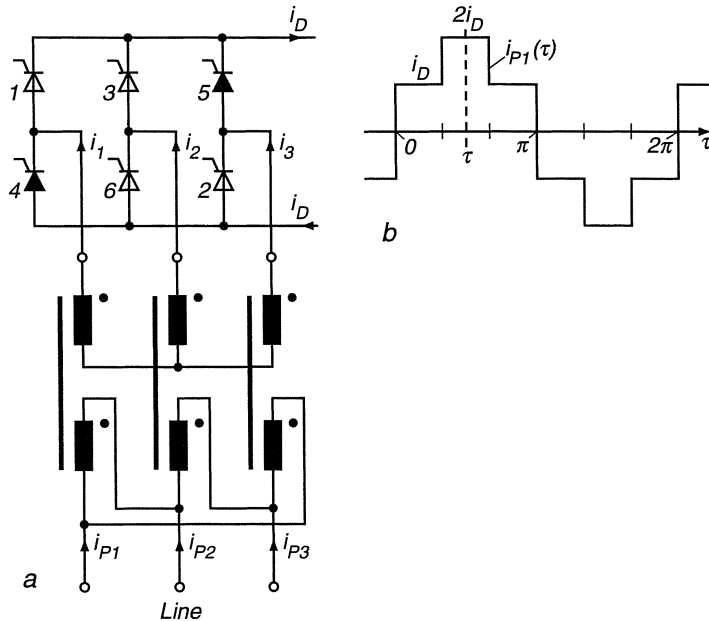


Fig. 8.24. Control transients of a 6-pulse converter

A feature of the three-phase bridge connection is that two thyristors have to be fired simultaneously for start-up and in discontinuous current mode, one in each row; otherwise the current could not begin to flow. This is achieved either



**Fig. 8.25.** Three-phase converter supplied by  $\text{Y}/\Delta$ -connected transformer.

(a) Circuit; (b) Waveform of primary current

by employing wide pulses ( $\Delta\tau > \pi/3$ ) so that they overlap or by generating for each thyristor two short firing pulses,  $\pi/3$  apart. Normally the second pulse would find a thyristor that is already conducting and be of no consequence. If the first solution is preferred, the firing pulse may be chopped into narrow impulses in order to reduce the voltage-time-area and hence the size of the pulse transformers.

The input current of the converter, drawn in Figs. 8.19 d and 8.20 d without taking commutation into account, is the same as the current that would flow in the primary winding of a  $\text{Y}/\text{Y}$ -connected transformer supplying the converter. However, the waveform of the primary current would change if one of the transformer windings were  $\Delta$ -connected; this is explained in Fig. 8.25. Assume that the constant load current  $I_D$  is initially flowing through the thyristors 4 and 5, closing its path through the  $\text{Y}$ -connected secondary windings of the transformer. When neglecting the magnetising current and assuming – for sake of simplicity – equal numbers of turns, the following equations then hold for the primary currents

$$\begin{aligned} i_{p1} &= i_3 - i_1 = 2i_D, \\ i_{p2} &= i_1 - i_2 = -i_D, \\ i_{p3} &= i_2 - i_3 = -i_D. \end{aligned} \quad (8.37)$$

Permutation of the six possible states yields the primary current waveform

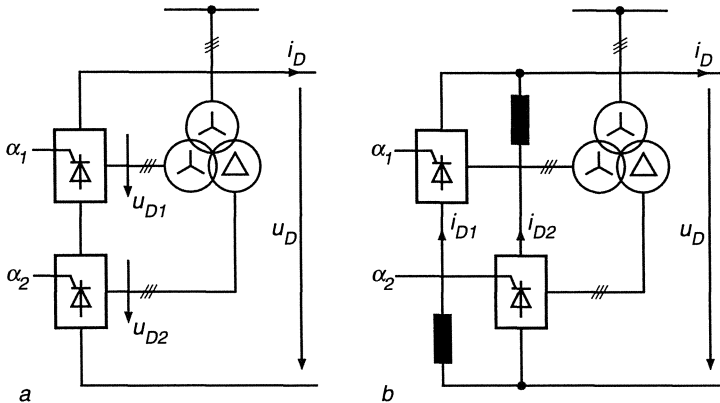


**Fig. 8.26.** 12-pulse-converter consisting of two 6-pulse converters in series- and parallel connection

$i_{p1}(\tau)$  shown in Fig. 8.25 b which also contains the 5th and the 7th as the lowest order harmonics. With the appropriate choice of the number of turns the  $\text{Y}$ - and the  $\Delta$ -connected windings could be interchanged without altering the current waveforms.

Frequently in the past, though less commonly now, the output voltage obtainable with a converter having one thyristor per branch was insufficient so that thyristors had to be connected in series. In this case additional advantages may be gained if — instead of series-connecting individual thyristors — complete three-phase circuits are connected in series, as seen in Fig. 8.26 a. Rather than taking precautions for equal voltage sharing between series connected blocking thyristors we now rely on the output voltages of the transformer to produce the correct voltages. Also, if a  $\text{Y}/\Delta$ -connection with its inherent  $30^\circ$  phase shift is chosen for the secondaries there is an added benefit in the reduction of harmonics on the load-side, where only multiples of  $12 f_0$  occur, as well as at the line-side, where the harmonics are those of a 12-pulse converter, with the 11<sup>th</sup> and the 13<sup>th</sup> being the lowest harmonics. There is also a further improvement in dynamic response. Another similar circuit is seen in Fig. 8.26 b where two six-pulse converters supplied from a  $\text{Y}/\Delta$ -connected transformer are connected in parallel, employing two separate chokes or an interphase transformer for summation of the currents.

This brief introduction into the fundamentals of line-commutated converters seems sufficient for dealing with most drive problems. A more detailed analysis such as harmonics, circuitry or protective measures is given in the specialised literature [47]. It should have become clear that multiphase static power converters are electrical actuators of superb dynamic performance providing an excellent tool for controlling large output power (MW) with low power control signals (mW) in very short time (ms). This combination is unmatched by any other type of power actuator. On the other hand it should be noted that due to

the switching action static power converters are inherently nonlinear. Since they have no internal energy storage the output power is instantaneously transferred into the AC supply system causing harmonics and reactive power; hence strong grids are required to support the operation of large power converters.

## 8.4 Line-commutated Converters with Reduced Reactive Power

In the preceding paragraphs it was shown that line commutated converters draw reactive power from the line; this is inherent in the principle of control by delayed firing which results in lagging current at the AC side of the converter. Since the phase shift of the fundamental component of the line current is directly related to the firing angle  $\alpha$ , the situation is particularly severe at  $\alpha \approx \frac{\pi}{2}$ , where the line current is, apart from the losses, purely reactive. This condition is unavoidable, if the converter is supplying the armature of a DC motor because when the motor starts from standstill, with the induced voltage being initially zero, the converter must be controlled close to  $\alpha = \frac{\pi}{2}$ . Therefore a large motor, for example a mine hoist drive starting with twice rated current causes a huge surge of reactive power on the supply side; there is no easy cure because capacitors cannot be switched in and out as the speed changes and the cost of rotating or static reactive power compensators could be too high.

The situation is tolerable with strong power supply systems but may be unacceptable on traction drives, where the reactive current in combination with the large inductance of the power supply including the catenary would cause heavy voltage fluctuations, in addition to the harmonic distortion. Mainly for the benefit of traction drives special circuits and control techniques have been developed with the aim of limiting the reactive power at reduced output voltage. Some of these circuits contain diodes as well as thyristors.

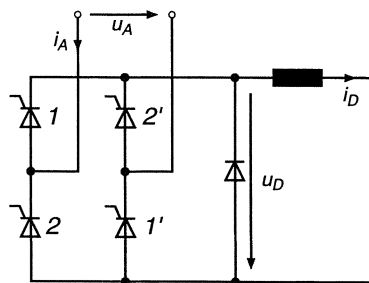


**Fig. 8.27.** Single-phase converter with a shunting diode

A simple though uneconomical solution is the use of a diode parallel to the load, as shown in Fig. 8.27 for a single-phase bridge circuit. The diode has the effect of cutting off the negative edges of the output voltage, essentially acting

as bypass during the intervals when  $u_D$  would otherwise be negative. Thus the trailing end of the line current (during interval  $\pi < \tau < \pi + \alpha$  in Fig. 8.6 d) does not flow through the converter and the line as it is short circuited through the diode. The result is an offset of the fundamental component of the line current in leading direction and a correspondent improvement of the power factor. This has, of course, the effect that the circuit can no longer act as inverter; the conditions

$$i_D(\tau) \geq 0, \quad u_D(\tau) \geq 0$$

restrict the operation to a single quadrant in the  $\bar{u}_D$ ,  $\bar{i}_D$ -plane. With traction drives employing series wound motors this would not be objectionable.

A simpler circuit with similar properties is shown in Fig. 8.28 a, which belongs to a class of half-controlled converter circuits containing diodes in place of some of the thyristors. Here too, the line current cannot flow against the line voltage and thus cause a temporary power flow from the DC to the AC side, since the opposite diode would conduct and act as bypass. Figure 8.28 b shows a simplified diagram of the voltages and currents, neglecting the commutation intervals. Again the trailing end of the line current is cut-off, thereby advancing the fundamental component and improving the power factor. Clearly, this circuit could be easily extended to form a half-controlled three-phase bridge connection.

Another technique for improving the power factor at the input of the converter is outlined in Fig. 8.29, showing a “boost and buck”-scheme of a three-phase rectifier containing only diodes, and a three phase thyristor converter; by employing a transformer with  $Y/\Delta$  secondary windings the harmonics situation may be improved as well. This connection makes use of the fact that a converter operating at  $\alpha = 0$  or  $\alpha = \alpha_{max}$  has a tolerable power factor while operation at  $\alpha \approx \frac{\pi}{2}$  should be avoided, if ever possible. The total mean output voltage, assuming continuous current, covers the range

$$U_{D10} + U_{D20} \cos \alpha_{max} \leq \bar{u}_D \leq U_{D10} + U_{D20}. \quad (8.38)$$

By selecting the voltages according to the condition

$$U_{D10} + U_{D20} \cos \alpha_{max} = 0,$$

the complete first quadrant of the  $\bar{u}_D$ ,  $\bar{i}_D$ -plane is within reach. That this circuit has a better reactive power balance than a single converter circuit follows from the fact that for minimum and maximum voltage, i.e.  $\bar{u}_D \approx 0$  and  $\bar{u}_D = \bar{u}_{Dmax}$ , both sections operate with good power factor. It is only in the centre,  $\bar{u}_D \approx U_{D10}$ , where the controlled converter, accounting for about half the total power, is fired at  $\alpha \approx \frac{\pi}{2}$ . At full output voltage,  $\alpha = 0$ , the circuit corresponds to Fig. 8.26 a, causing approximately 12-pulse line interactions.

The principle of boost-and-buck operation may be generalised by subdividing the full voltage range  $\pm U_0$  and assigning the bands of  $\pm U_0/n$  to  $n$  series-connected thyristor converters which are supplied from separate transformer secondaries. The control is then arranged on a sequential basis such that only one section is phase-controlled with  $0 < \alpha < \alpha_{max}$ , while all  $n - 1$  other sections

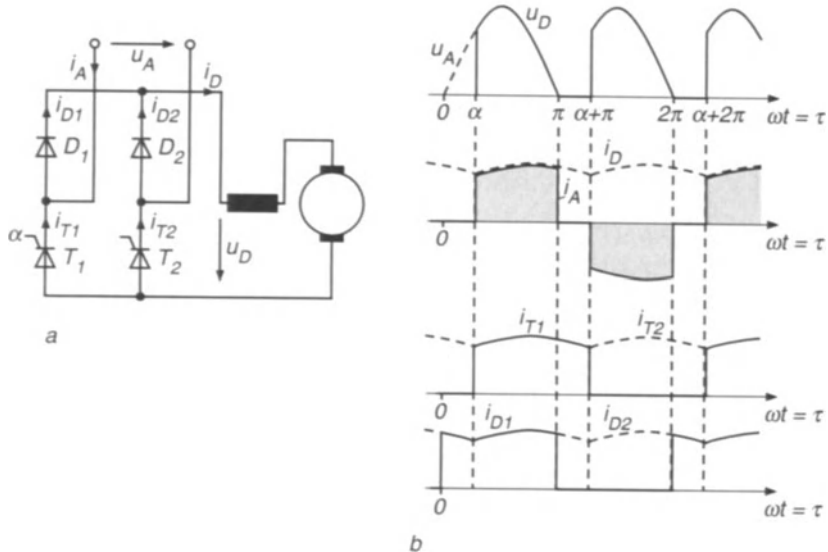


**Fig. 8.28.** Half-controlled single-phase converter.

(a) Circuit diagram; (b) Waveforms of voltages and currents

are operating either with  $\alpha = 0$  or with  $\alpha = \alpha_{max}$ . Sequential phase control is of particular interest if the converter needs to be subdivided anyway for reasons of the high voltage required. This technique has found application for rail traction drives [K54].

## 8.5 Control Loop Containing an Electronic Power Converter

Line commutated converters are ideal actuators for electrical drives; a main feature, apart from their simplicity, proven reliability and practically unlimited output power is their excellent dynamic performance. Also, electronic controllers can be directly connected to the firing circuit which consists of integrated circuitry and logic devices operating at signal level.

When a control loop containing a converter is to be designed, the question arises, how the dynamic behaviour of the converter should be approximated by a mathematical model. The difficulties stem from the fact that the firing of a thyristor is a discrete process - the firing angle is not a continuous function of time - and that the steady-state and dynamic behaviour of the converter is highly nonlinear. Pulse- and phase-modulated systems of this or similar kind have been frequently dealt with in the literature but no coherent theory exists which is simple enough for general application [G25, L3, P32, S21].

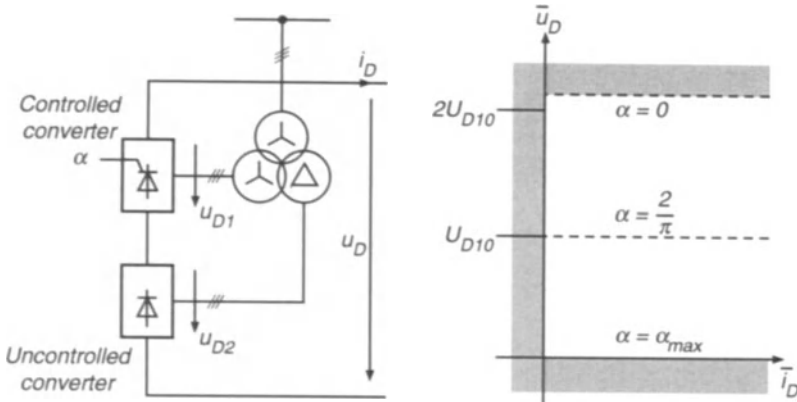


**Fig. 8.29.** Boost- and -buck connection of controlled and uncontrolled converter

A detailed analysis of dynamic processes in line commutated converters is rather complex; the transients are described by nonlinear difference equations which defy an analytical solution. Linearisation of the equations is of course possible but the validity is then restricted to the vicinity of the chosen operating point. However, as a first order approximation it is found that the converter dynamics can be entirely neglected as long as the control plant, fed by the converter, has a low-pass characteristic, the controller contains an integrating term and the control loop is to be well damped [F9, L31]; these conditions are usually met in drive applications. Close to the stability limit this simplification is of course no longer valid; here it is necessary to revert to the accurate model equations.

Another simple model that has served well in practice is based on the observation that a variable waiting period elapses until a small change of the input signal  $y_1$  to the firing circuits (Fig. 8.11) shows an effect by the first shift of a firing pulse. As the waiting period depends on the instant at which the input signal is changed, varying between zero and  $20/6 \text{ ms} = 3.3 \text{ ms}$  for a six-pulse converter operating on the 50 Hz supply, a mean equivalent delay time  $T_T = 1.67 \text{ ms}$  is postulated [49]. This heuristic model produces useful results, as long as well damped transients of the closed loop are the objective but again, as the stability limit is approached, considerable deviations from the predictions must be expected.

The most effective method of neutralising the nonlinear and discontinuous behaviour of the converter is to enclose it in a tight feedback control loop which then imposes the characteristics of a nearly linear actuator, such as unity gain. There is also a need for protecting the converter (containing thyristors, diodes or power transistors), the motor and the load through a fast acting current limit. Both objectives are achieved, if this innermost control is a current control loop formed around the converter, where the current reference  $i_{D\text{Ref}}$  is electronically limited.

This is outlined in Fig. 8.30, showing a converter with inductive impedance and a back voltage  $e$  in the load circuit. With the help of a current controller the output current is tracking the current reference  $i_{DRef}$ , independent of the back voltage which acts as a disturbance. In order to correspond to the conditions valid for a DC drive, where the load circuit is represented by the armature, possibly in series with a smoothing inductor, the parameters could be such that the voltage drop  $\Delta u_D$  at rated current is only a few percent of nominal voltage and that for  $\alpha = 0$ ,  $e = 0$  about eight or ten times rated current would flow, assuming continuous load current. A function-generator, as indicated in dashed lines, could be included in order to linearise the control characteristic of the converter (Fig. 8.8), but it makes little difference as long as the flat ends of the converter characteristic are considered only as a voltage margin, not to be used in normal steady state operation. For the subsequent simulation, a firing circuit with an internally synchronised oscillator was modelled.

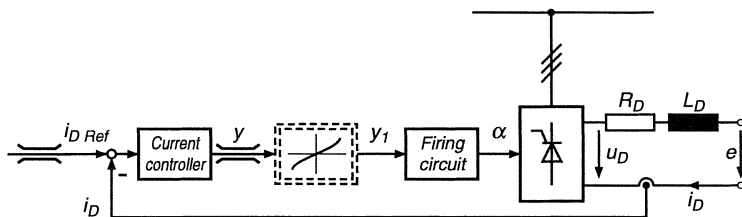


Fig. 8.30. Converter with current control

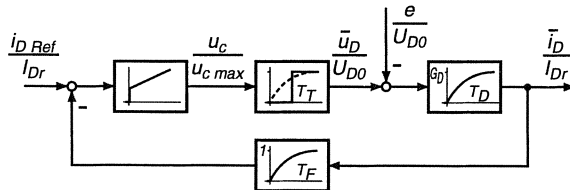


Fig. 8.31. Simplified block diagram of current control loop

The circuit in Fig. 8.30 is now transformed into the linearised block diagram depicted in Fig. 8.31, where the converter with its control circuit is approximated by an equivalent mean delay, which for a 6-pulse converter and 50 Hz-supply is  $T_T \approx 1.7$  ms. For smoothing the feedback signal,  $T_F = 2$  ms may be assumed with a six pulse converter. This value depends also on whether the current sensor is installed on the AC or DC side of the converter. Sensing the line current is simpler because current transformers with an output rectifier offer inexpensive isolation, whereas a DC sensor in the load circuit, while being faster and more accurate, is likely to be more costly. The use of low level control signals, typically 10 V, which are electrically isolated from line potential is a

necessary condition for safety. When designing the controller, the delay of the converter and the filter time constant, which are both small in comparison with the time constant  $T_D$ , are lumped together to form an equivalent lag  $T_e \approx 4$  ms.

A possible design of the current control loop was discussed in Sect. 7.2. Instead of the PID-controller that would be desirable with slowly responding rotating generator, a PI-controller is quite adequate here. In fact, a PID-controller, whose step response begins with an impulse, may cause inconsistent results in conjunction with the discrete firing circuit so that the additional lead term is not recommended.

Hence the open loop transfer function of the current control scheme is

$$F_{0L}(s) \approx G_{c,i} \frac{T_i s + 1}{T_i s} \frac{1}{T_e s + 1} \frac{G_D}{T_D s + 1}, \quad (8.39)$$

where  $G_{c,i}$  is the gain and  $T_i$  the integrating time constant of the current controller. A typical time constant of the load circuit is  $T_D = 30$  ms. Because of  $T_e \ll T_D$  the transfer function may be simplified in the region of the cross-over frequency, which determines the band width of the closed loop,

$$F_{0L}(s) \approx G_{c,i} G_D \frac{1}{T_i T_D s^2} \frac{T_i s + 1}{T_e s + 1}. \quad (8.40)$$

This is in line with the “symmetrical optimum” mentioned in Sect. 7.2. The best choice of parameters is [K18, 35]

$$T_i = a^2 T_e, \quad G_{0L} = G_{c,i} G_D = \frac{1}{a} \frac{T_D}{T_e}, \quad (8.41)$$

where  $a = 1 + 2D$  follows from the desired damping ratio  $D$  of the complex pair of eigenvalues;  $D = \frac{1}{2}$  or  $D = 1/\sqrt{2}$  is frequently chosen.

The design of the current controller leads to the closed loop transients shown in Fig. 8.32. The curves were obtained by accurately simulating the operation of the three-phase bridge circuit, including the leakage inductances of the transformer and the thyristor branches. The effects of the commutation are seen on both AC and DC voltages  $u_{B1}(\tau)$ ,  $u_D(\tau)$ . The transients include step changes of the reference signal as well as large synthetic load disturbances caused by inverting the back voltage  $e$ .

Despite the severe simplifications made in designing the current controller, the transients decay rapidly and are well damped. The equivalent lag of the closed loop for small changes of the reference is  $T_{eCL} \approx 10$  ms, which is in line with the model computations for the symmetrical optimum. As the current loop represents the innermost control loop of a nested structure, it provides a good starting point for the higher level control system.

When studying the details of Fig. 8.32 more closely, differences become apparent at time  $t_1$ ,  $t_2$ , following the inversion of the back voltage  $e$ . The reason is that at  $t_1$  the voltage was reversed immediately after a thyristor had been fired, while at  $t_2$  the reversal took place slightly before a firing pulse was due. At  $t_1$ , a waiting interval was unavoidable whereas the converter could respond

immediately at  $t_2$ . The difference in overshoot of the current is a consequence of the discontinuous and nonlinear nature of the converter. The control is only partially successful in compensating this effect, because the disturbance is acting directly on the plant.

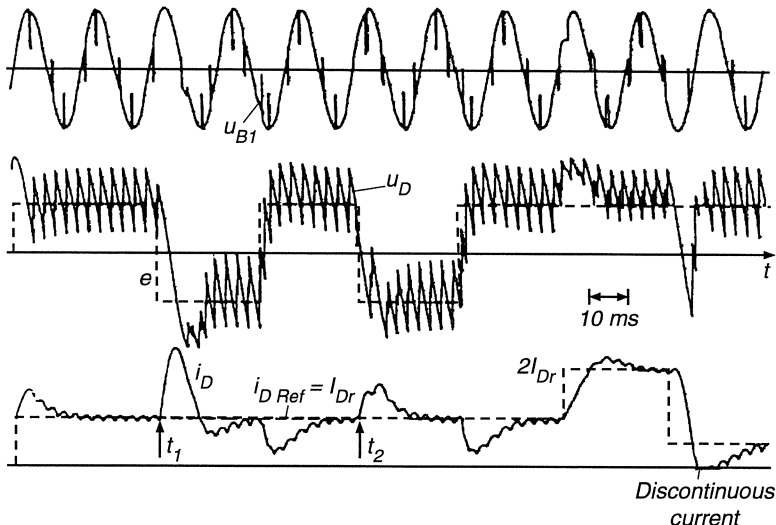


**Fig. 8.32.** Computed transients of current control loop

In this figure the transients are better damped than would be expected on the basis of the assumed parameters ( $a = 2$ ,  $D = 1/2$ ). The reason for this is most likely the fact that the assumed mean delay represents a somewhat pessimistic approximation of the dynamic response of the converter; another reason is the simplification

$$\frac{1}{T_D s + 1} \approx \frac{1}{T_D s},$$

when applying the rules for the symmetrical optimum.

The operating conditions assumed for Fig. 8.32 were so selected that continuous current prevailed except for one brief interval, where the load current became discontinuous. As mentioned before, the current is in general not always continuous; for example, if the smoothing reactor is omitted, the region of discontinuous current may cover a large portion of the operating range.

If a current control loop, the controller of which has been designed on the basis of continuous current, is operated in the region of discontinuous current, the transients become very sluggish and the quality of control deteriorates. The reason for this is that the gain of the converter is greatly reduced when the current becomes discontinuous; in addition, the load circuit is no longer characterised by the relatively large lag time constant  $T_D$ , as the current begins at

zero in every firing interval, i.e. every 3.3 ms with a 6-pulse converter. Therefore the PI-controller, Eq. (8.39), is poorly tuned to the controlled plant.

If consistency of the dynamic response is important, which is the case e.g. with servo drives on machine tools, the current controller should be readjusted during discontinuous current operation, i.e. use of an adaptive current controller becomes desirable [B68, S31].

The fact that the voltage gain of the converter is reduced with discontinuous current is qualitatively explained with the help of Fig. 8.33 for a 2-pulse converter.

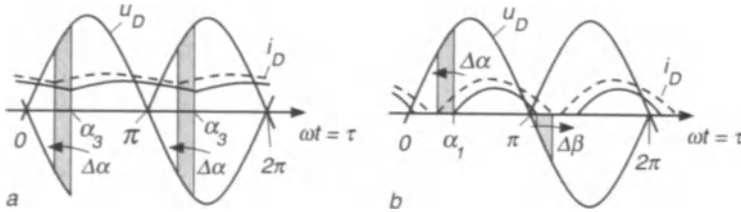


**Fig. 8.33.** Voltage gain of converter for continuous and discontinuous current

If with continuous current ( $\alpha = \alpha_3$ ) the firing angle is reduced by a small amount  $\Delta\alpha$ , the interval where the voltage  $u_D(\tau)$  is positive,  $\alpha < \tau < \pi$ , is increased, while the time, when the voltage is negative ( $\pi < \tau < \pi + \alpha$ ), is reduced. With discontinuous current ( $\alpha = \alpha_1$ ) the situation is different; the interval, where  $u_D(\tau) > 0$ , is still increasing when  $\alpha$  is reduced by  $\Delta\alpha$ , but so is the time, where  $u_D(\tau) < 0$ . Hence, the voltage gain  $d\bar{u}_D/d\alpha$  is now much smaller than in the case of continuous current.

The block diagram of the current control loop for discontinuous current corresponds to that shown in Fig. 8.31 but the normalised voltage gain of the converter is now considerably lower; also, the lag element with time constant  $T_D$  is now replaced by a lag having a time constant approximately equal to the firing interval  $T_D \approx 3.3$  ms, which is about 1/10 of the former value. Clearly this calls for a different design of the controller; for example, an integral controller with the transfer function

$$F'_{c,i}(s) = \frac{1}{T'_i s} \quad \text{with} \quad T'_i = G'_D (T_e + T'_D) ,$$

characterised by a small time constant  $T'_i$ , i.e. high gain, could now be expected to produce fast and well damped closed loop transients.

In order to adapt the controller to the new situation, the condition of intermittent current must be detected which requires a few additional electronic circuits but presents no major difficulty.

The realisation of an adaptive current controller is particularly attractive if the control is performed by a microprocessor because then the controller parameters can be adapted by changes in the program, i.e. by software. In Fig.

8.34 an oscillogram of a current transient with a 6-pulse converter is shown, where the entire control, including the firing, was performed by a microprocessor [M3, M4]. In both regions, with continuous as well as discontinuous current, very satisfactory transients are obtained. In addition to the adaptive current control, the initial condition of the integral channel of the controller was also preset on the basis of current reference and reconstructed back voltage in order to prevent a large first current overshoot which would be objectionable on servo drives. This flexibility is an important feature of digital control by microprocessor.

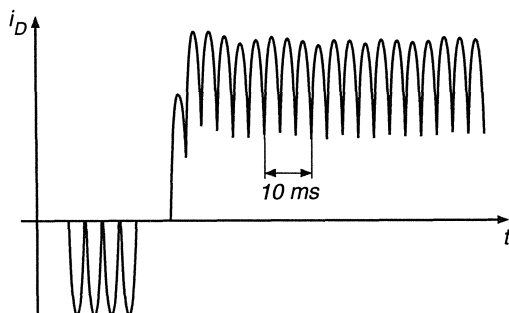


Fig. 8.34. Step response of current control loop with adaptive current controller

## 9. Control of Converter-supplied DC Drives

Static converters are ideal electronic actuators for DC drives because of their virtually unlimited output power and excellent controllability. The speed of response is usually adequate to handle the electromechanical transients occurring in drives. Line-commutated converters or, as they are also called, converters with natural commutation, are the most frequent choice for industrial applications, where a three-phase supply is available; this is due to the simplicity of the circuits requiring a minimum number of active and passive components.

For vehicle drives, where no AC catenary or independent AC supply is available or where the reactive current and the harmonics caused by a line-commutated converter would be unacceptable, it may be necessary to employ forced commutated converters having a more complex circuitry and involving higher losses; a special situation exists also with small DC servo drives, where the response of a line commutated converter may be insufficient to cope with the stringent dynamic demands and where a chopper converter supplied by a DC link and operated with a higher switching frequency is necessary.

### 9.1 DC Drive with Line-commutated Converter

When connecting a line commutated converter, for example the three-phase bridge circuit in Fig. 8.18, to the armature of a DC machine (Fig. 7.2), it should be kept in mind that the converter can only operate in two quadrants of the  $\bar{u}_D$ ,  $\bar{i}_D$ -plane as seen in Fig. 8.23. Because of  $\bar{u}_D = \bar{u}_a$ ,  $\bar{i}_D = \bar{i}_a$  it follows from Eqs. (5.6, 5.8) that, assuming constant sign of the flux  $\Phi_e$ , the machine can run in both directions, but the torque is unidirectional. Therefore the current-speed cascade control scheme shown in Fig. 9.1 is capable of operating in two quadrants of the torque- speed plane, hence it is called a two-quadrant drive, Fig. 9.2.

Since the converter cannot produce negative output current, there is no point in admitting a command signal calling for negative current; with an integrating current controller this would only cause unnecessary waiting intervals after the current reference becomes positive again (“controller wind-up”). Thus, the output signal of the speed controller should be limited at the lower as well as the upper end,  $0 \leq i_{a\text{ Ref}} \leq i_{a\text{ max}}$ .

Braking of the drive in the 2<sup>nd</sup> quadrant by regeneration is not immediately feasible; of course, there is always the possibility of non-regenerative braking with the help of external resistors.

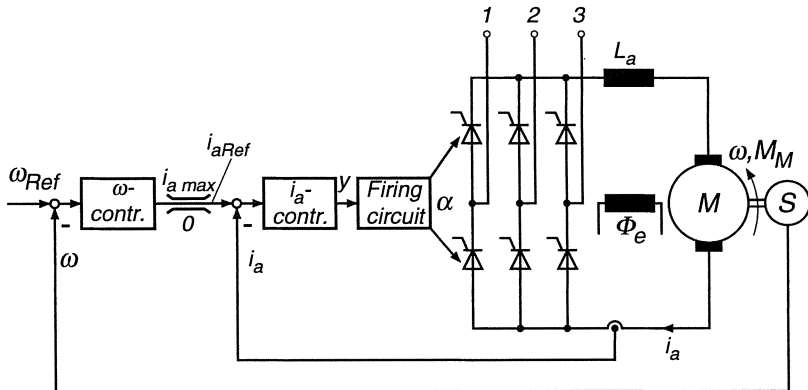


**Fig. 9.1.** Cascade control scheme of DC motor with two-quadrant converter

A two-quadrant drive of this type is suitable for unidirectional loads, the torque of which contains a large component of friction, such as paper- or printing machines, calenders, also for pumps or blowers; in principle, it would also be applicable to hoists without self-locking gears, but reverse torque is usually needed because of counter weights or for helping to accelerate in the lowering direction. With the driving torque being proportional to the product of armature current  $i_a$  and flux  $\Phi_e$  there are two options for achieving reverse torque, i.e. four-quadrant operation: reversing the armature current or the main flux. Both methods are in use, though with markedly different preference.

The principle of armature reversal is realised in Fig. 9.3 with the help of a reversing contactor. In order to avoid inductive voltage surges in the armature circuit and to reduce the size of the contactor it is necessary to perform the switching at zero armature current. Hence, a switching command must only be given when the conditions

$$i_{a\text{Ref}} = 0, \quad i_a = 0 \quad (9.1)$$

are simultaneously fulfilled. The first signal indicates that the superimposed speed controller calls for a reversal of torque while the second confirms that the current controller has reduced the armature current to zero, possibly after the converter has been operating temporarily as an inverter. Since there may be some uncertainty with the second condition in the face of intermittent current, it is important to wait a short interval with the converter blocked, before the switching command is actually issued; resuming the firing must be inhibited until the mechanical switching is completed. Special hydraulically operated contactors with small contact gap have been developed in the past; still, a full

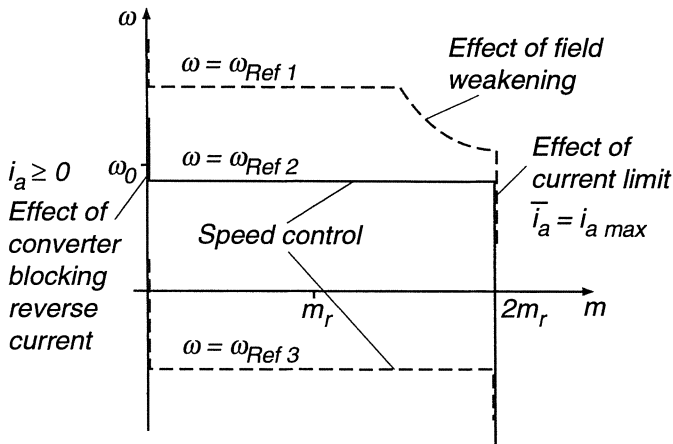


Fig. 9.2. Operating range of a two-quadrant drive

torque reversal including the reduction of the current to zero, evaluation of the conditions in Eq. (9.1), switching and current build-up may take 100 ms which excludes this mechanical solution from high performance drives.

It is noted that the duty of the reversing contactor could also be assigned to four reversing thyristors, two of which are continuously made conducting while the others are blocked. When zero current is reached, the opposite pair of thyristors can be fired in order to reverse the polarity of the armature current.

If the current transducer senses the load current at the converter side of the contactor (as shown in Fig. 9.3) or with current transformers at the AC side, the current control loop is unaffected by the switching operation. However, the sign in the speed control loop is reversed due to the fact that a given output current of the converter now produces reverse torque. In order to offset this effect, one more inversion is needed when the armature circuit is reversed; this is also indicated in Fig. 9.3.

A second possibility for reversing the torque of a DC motor is to reverse the flux  $\Phi_e$  while maintaining the direction of the armature current unchanged. This can be done by reversing the field through contactors or a bidirectional converter (of considerably reduced power than for the armature). However, because of the large amount of energy stored in the magnetic field circuit the flux reversal requires much more time than inverting the armature; even when applying 3 or 5 times rated field voltage, the reversing transient may take up to a second, during which time the armature current must be kept at zero; hence, a noticeable zero-torque interval occurs, which is very detrimental to the response of the control. A motor subjected to this duty must be fully laminated; the voltage induced by transformer action in the armature is also to be considered. It is for these reasons that field reversing is seldom used today.

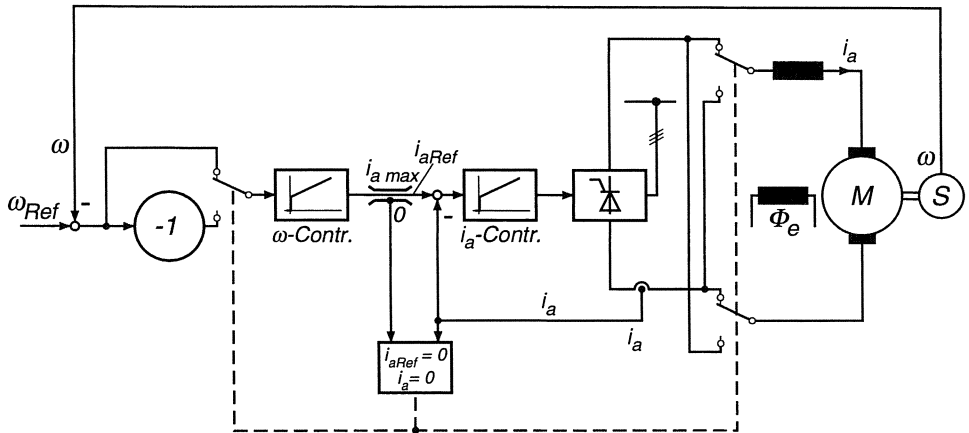


Fig. 9.3. Four quadrant operation of a DC drive by armature reversal

There is now a general preference for fully electronic reversal of the armature current with the help of bidirectional or dual converters. The cost of these schemes has been reduced as a result of advanced semiconductors and manufacturing techniques. The most common circuit of this type is shown in Fig. 9.4; it consists of two 6-pulse bridge-converteres connected in opposition. Clearly, in order to exclude short circuits between line terminals, only one of the converters,  $C_1$  or  $C_2$ , can be allowed to conduct at any one time; this, by the way, has the advantage that only one thyristor of each pair produces conduction- and switching- losses so that the pair can be mounted on the same heat sink. However, having opposite polarity, they must be electrically insulated from each other. At lower power ratings, complete thyristor modules are available, having the necessary interconnections built-in.

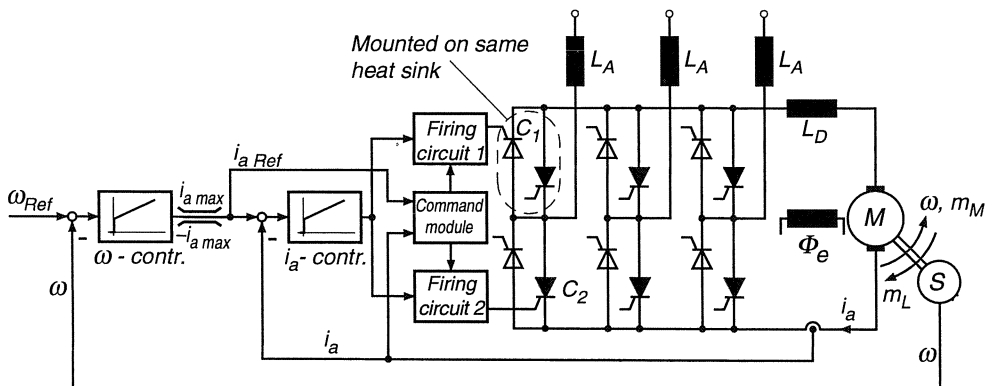


Fig. 9.4. DC drive employing a three-phase dual converter without circulating current

The current controller supplies an input signal to both firing circuits but only one is allowed to produce pulses for firing the thyristors; the selection of the active converter is performed by a command module on the basis of the polarity of the current reference  $i_{a\text{Ref}}$  and the feedback signal  $i_a$ . As in the case of the armature reversal, the speed controller determines the need for a torque reversal, for instance  $i_{a\text{Ref}} < 0$ ; the current controller responds by lowering the armature voltage  $\bar{u}_D = \bar{u}_a$  with the consequence that the armature current eventually reaches zero,  $i_a = 0$ . As soon as this condition exists, the firing pulses for the conducting converter  $C_1$  are inhibited by the control module, while those of the incoming converter  $C_2$  are activated. Hence the switching conditions are

$$\begin{aligned} [i_{a\text{Ref}} > 0 \wedge i_a = 0] &\rightarrow C_1 \text{ on}, & C_2 \text{ off}, \\ [i_{a\text{Ref}} < 0 \wedge i_a = 0] &\rightarrow C_1 \text{ off}, & C_2 \text{ on}. \end{aligned} \quad (9.2)$$

Additional features must be incorporated in order to enhance the safety of operation and to improve the control transients. For example, a waiting interval of 2 to 5 ms may be included before firing pulses are issued to the incoming converter, in order to be certain that the current in the outgoing converter is really zero. Activating the firing pulses of the incoming converter before all opposing thyristors are safely blocked would cause a line-side short circuit current that cannot be suppressed by control but must be cleared by fuse links or by a breaker.

On the other hand, inhibiting the firing pulses of a converter while it is still conducting, prevents its commutation and, in inverter mode, causes a commutation failure leading to a short circuit condition as was explained in Fig. 8.17. Therefore, the decision to switch from one converter to the other is of considerable consequence; in particular, the state  $i_a \equiv 0$  must be ascertained safely and with a high resolution. For instance, a converter having a rated current of 1000 A may contain two arms where at the critical time a residual current of 100 mA is flowing. If now the opposite converter is turned on, a short circuit is still likely. Sometimes two current sensors are employed on large drives, one having a linear characteristic over the full current range, to be used for feedback control, while the other serves as a zero-current detector for the command module; its characteristic would have to be linear in the low current region only. It is noted that the currents through the snubbing circuits may also affect the current measurements, which tends to increase the noise of the signal. Clearly, great emphasis must be given to the reliability of the sensors and control components if this circuit is to operate safely under practical conditions. Indeed, this has initially been a problem which has delayed the general use of this exceedingly simple converter circuit.

Today, reversible converters with antiparallel thyristors are produced in large numbers in the form of very compact units covering a wide power range from a few kW to about 10 MW. For the higher ratings modular designs with air- or water-cooled heat sinks are available.

Besides the control scheme shown in Fig. 9.4 there are a number of variations; for example, only one firing circuit might be used with the output pulses being switched from one converter to the other. Also, the drive is usually extended to include field weakening as discussed in Sect. 7.3. The field winding would then be supplied from a separate unidirectional converter of smaller size.

There are other ways to further improve the performance of the control. The adaptive current controller has already been mentioned in Sect. 8.5; also, the current controller may be given a suitable initial condition, in order to optimise the current transient after the zero current interval, when the incoming converter is activated. The best initial condition depends on the existing current reference and the magnitude of the back voltage which is known from the firing angle existing before the switching operation. Sophisticated techniques of this type are particularly attractive if the control is realised by microprocessor, because they are then implemented by software, without increasing the complexity of the control circuitry [M4, S17]. The reversing transient, shown in Fig. 8.34 was executed with a microprocessor being programmed as an adaptive current controller for continuous and discontinuous current; the variable initial condition was precalculated before firing pulses were sent to the incoming converter. The brief current pause, seen in Fig. 8.34, is typical for this type of reversing scheme; when comparing this time to the long zero-current interval required for the armature reversal by contactor, the advantages of the fully electronic solution are obvious.

Another feature, which is easily implemented with microprocessor control is the compensation of the variable gain in the speed loop which occurs in the field weakening range; this was mentioned in Sect. 7.3. Further sophistication may be added by predictive digital control, all but eliminating any control transients [L24].

The zero current interval, required for safely switching the armature current from one converter in Fig. 9.4 to the other, is very short but there are applications, such as some rolling mill drives, where even 5 ms may not be tolerable and where a completely continuous transition of armature current and torque is specified. This is achieved with another dual converter circuit, shown in Fig. 9.5 a, where both two-quadrant converters are conducting simultaneously. This calls for separate transformer secondaries as well as decoupling reactors because of the instantaneous voltage differences which exist between the two converters  $C_1$ ,  $C_2$ . As seen from Fig. 9.5 a the armature current can assume either sign,

$$i_a = i_1 - i_2 \gtrless 0 , \quad (9.3)$$

depending on which of the currents prevails. The smaller of the currents represents a circulating current which flows through the converters but bypasses the load branch,

$$\min(i_1, i_2) = i_c ; \quad (9.4)$$

it should be kept as small as possible in order to reduce the associated active and reactive power losses. On the other hand, the circulating current should be

continuous so that there are no unnecessary waiting intervals delaying possible control action.

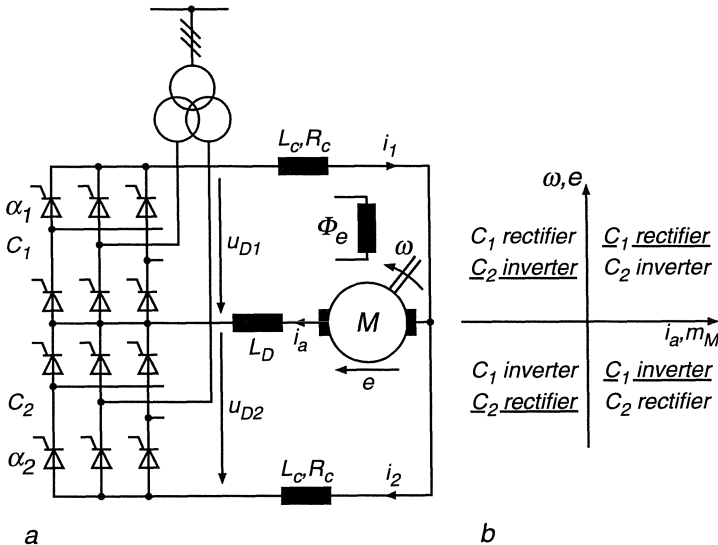


Fig. 9.5. Reversible converter with circulating current supplying DC machine

The operating states of the two converters are indicated in the four quadrants of the torque- speed- plane in Fig. 9.5 b; for  $m_M > 0$ , the armature- and circulating currents flow through  $C_1$  whereas the auxiliary converter  $C_2$  carries only the circulating current. The inverse is true for  $m_M < 0$ . In order to keep the circulating current at a sufficiently low level, such as 10% of rated current, the mean voltage of the auxiliary converter must closely track the mean voltage of the main converter which is determined by the armature of the motor. If this condition is maintained all the time, both converters are active and ready to accept the motor current in a continuous transient, without any waiting interval. This two-variable control must be effected with the help of the two firing circuits.

The auxiliary converter must be controlled to satisfy the condition

$$\bar{u}_{D1} + \bar{u}_{D2} = R_c(\bar{i}_1 + \bar{i}_2) \approx 0 , \quad (9.5)$$

i.e. the sum of the mean voltages should be approximately zero; however, this is not true for the instantaneous voltages  $u_{D1}(\tau)$ ,  $u_{D2}(\tau)$ , because one of the converters operates as rectifier, the other as inverter. The two voltages and their sum are plotted in Fig. 9.6 for three different conditions, neglecting commutation and internal voltage drops. Clearly at  $\alpha_1 = \alpha_2 = \frac{\pi}{2}$  the sum of the instantaneous voltages assumes very large values even though the sum of the mean values is zero. In order to prevent these large alternating voltages from causing excessive currents, the circulating current reactors  $L_C$  seen in Fig. 9.5 a

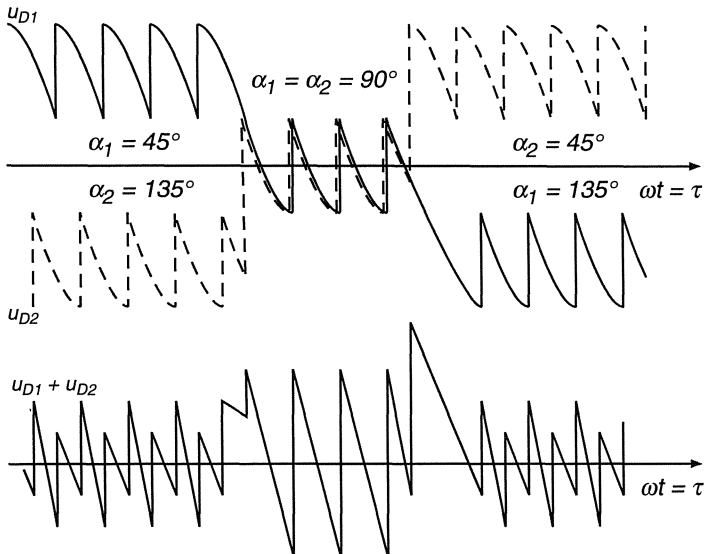


**Fig. 9.6.** Voltages in reversible converter with circulating current

are required. Since there is always one which carries the small continuous circulating current, these reactors need not be entirely linear; in fact, by allowing the one carrying the armature current to saturate, their physical size is reduced. For smoothing the armature current  $i_a$ , a separate filter reactor  $L_D$  may be included.

In order to obtain the desired current distribution for the respective main- and auxiliary-converter, given a certain load current  $i_a$ , one might first think of an open loop control scheme, where both firing angles are controlled jointly according to  $\alpha_2 \approx \pi - \alpha_1$ , which approximately fulfills condition (9.5). However, the result would be far from satisfactory since the characteristics  $\alpha(y)$  of the two firing circuits are likely to be somewhat different; also the current-dependent voltage drops would have to be taken into account. Thus the circulating current would either be too large causing unnecessary losses in the transformer, converters and reactors, or it would become discontinuous, preventing fast response, should the need for a reversal of armature current arise. The closed loop control scheme shown in Fig. 9.7 a promises a very simple and effective solution to this problem; it is proven in numerous applications over many years [K19].

The idea behind this scheme is as follows: Based on the current reference  $i_{a\text{Ref}}$  prescribed by the speed controller, separate current references  $i_{1\text{Ref}}, i_{2\text{Ref}}$  are derived for each of the converters. This is done by an electronic function generator, the characteristics of which are shown in Fig. 9.7 b; they are so chosen that the conditions

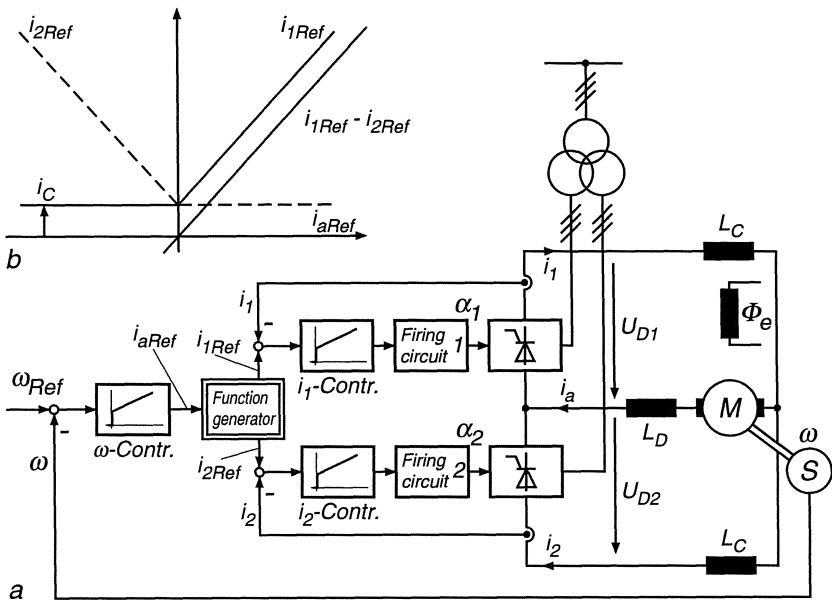


Fig. 9.7. Control of reversible converter with controlled circulating current

$$i_{1\text{Ref}} - i_{2\text{Ref}} = i_{a\text{Ref}}, \quad (9.6)$$

$$\min(i_{1\text{Ref}}, i_{2\text{Ref}}) = i_{c\text{Ref}} = \text{const}$$

are fulfilled, with the circulating current reference assuring continuous current flow. Thus the task of controlling armature current and circulating current is assigned to two separate current control loops as described in Sect. 8.5. The circuit shown in Fig. 9.7 a can also be extended to include field weakening beyond base speed.

With this control method the drive can operate in all quadrants of the torque-speed plane permitting smooth transitions between the quadrants. However, this is achieved with considerable additional cost and complexity (transformer, reactors). Some savings may be possible, for example with continuous rolling mills, where the converter for reverse torque is only used for occasional braking and can be designed for a lower current rating; more substantial economies are made by turning to the reversible converter without circulating current that was discussed before. This circuit permits use of full rectifier voltage ( $\alpha = 0$ ), whereas with the circuit in Fig. 9.5, the rectifier voltage must be limited to the maximum value that can be supported by the inverter operating at maximum firing angle ( $\alpha_{\max}$ ). With today's state of control the loss in dynamic performance caused by the discontinuity at current reversal is very slight, rendering the circuit in Fig. 9.4 the best compromise for most applications.

## 9.2 DC Drives with Force-commutated Converters

The converter circuits dealt with so far have in common that they are fed from single or three-phase alternating voltages; this is a prerequisite for phase control employing natural commutation. As soon as a valve, having forward bias voltage, is fired, one of the supply voltages assumes the task of commutating the load current from the previously conducting to the newly fired valve.

In a number of potential applications AC supply voltages are not available, so that this simple method of commutation is not feasible. Because a conducting thyristor cannot be turned off by electronic control, special provisions in the power circuit are then required in order to ensure that the thyristor to be fired has forward bias voltage and that the outgoing thyristor becomes nonconducting and is briefly exposed to reverse voltage as a condition for blocking. A multitude of circuits exists which perform this "forced commutation".

In recent years thyristors have been developed that can also be switched off by suitable control signals while conducting (Gate-Turn-Off thyristors, GTO); this is a major improvement, even though the current gain for turn-off is very low, requiring a short high pulse of inverse control current. These devices have in the last 10 years been developed to the point, where they can replace normal thyristors with several kV and kA capacity in high power applications, such as traction drives.

The most common switching device at lower power permitting electronic turn-off is, of course, the bipolar transistor. Since it can only conduct, when it is activated by a base current, it may be switched on and off at will, as long as the switching losses are not too high and the transistor is protected against over-voltages caused, for example, by an inductive load. Even though bipolar transistors are now available for voltages exceeding 1.2 kV and currents of several hundred A, so that experimental drives for battery vehicles (100 kW) and traction drives (500 kW) have been built, their main field of applications is in the lower to medium power range, up to about 50 kW, such as needed for servo motors for feed- and spindle-drives on machine tools. The main advantage of transistors, as compared with line-commutated converters, is that it is possible to choose a higher switching frequency, thus improving the dynamic response of the drive.

Another area where promising developments are under way are field effect transistors (MOSFET) for low power applications. These transistors are characterised by very short switching time and, consequently, high switching frequency, beyond the audible range; being inherently voltage controlled, they require practically no steady state gate current, similar to vacuum tubes. However, caused by the relatively large gate capacity there is a substantial charging current which must be supplied by the control device for switching; also, the on-state resistance is larger than with bipolar transistors.

A more recent important development are insulated gate bipolar transistors (IGBT), combining the high current carrying capacity of bipolar transistors with the simple control of field effect transistors as well as high switching speed.

There are predictions that IGBT's are the most promising switching devices for future higher power applications. Converters with a rating of several hundred kW are already in service. A further possibility, but still at an early stage of development, are MOSFET-controlled thyristors (MCT); their potential cannot be assessed as yet.

Clearly, the work on new and improved high power electronic switching devices is continuing at a rapid pace and a state of consolidation is not in sight. This strongly affects the development of circuitry and control methods for converter equipment. In this section it is shown with the example of a single quadrant DC-chopper, how the new devices can result in better dynamic performance, simplifications and, possibly, a cost reduction for the converter drive.

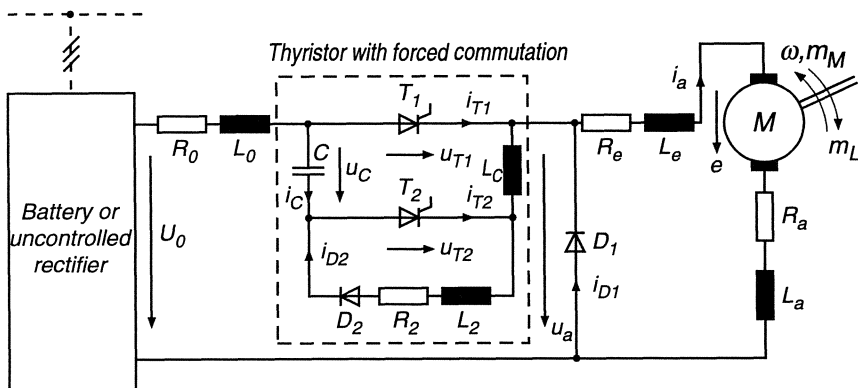


**Fig. 9.8.** DC/DC converter supplying series wound motor

A typical thyristor converter circuit employing forced commutation is depicted in its basic form in Fig. 9.8. Its purpose is to transform a constant direct voltage  $U_0$  into a lower adjustable voltage  $\bar{u}_a < U_0$ , in order to control the speed of a DC motor. This problem arises frequently with vehicles supplied through a DC rail or catenary or from a storage battery. Fig. 9.8 refers to this case, assuming a series connected drive motor.

A similar situation exists with vehicles having AC supply from a catenary, where a line commutated single phase converter would not be applicable in view of the high AC impedance causing excessive fluctuations of the voltage and distortions of the waveform. The following options for a DC drive could then be considered:

- Line commutated converter with reduced reactive power, for example a half controlled bridge circuit as discussed in Sect. 8.4,
- Transformer with tap-changer supplying adjustable voltage to an uncontrolled rectifier,

- c) Uncontrolled rectifier with subsequent DC/DC converter as shown in Fig. 9.8.

The DC/DC converter operates as a chopper, which, by means of an electronic switch, connects the inductive load with the parallel shunting diode  $D_1$  periodically to the constant supply voltage. By varying the duty cycle, the mean voltage  $\bar{u}_a$  is changed. The switching frequency is chosen sufficiently high ( $> 100$  Hz) so that a relatively smooth continuous current  $i_a$  flows in the load circuit. The converter shown in Fig. 9.8 is of the single quadrant variety, which is adequate for a series motor; with additional components it could be extended for two- or four-quadrant operation as well. The circuit should only be considered as an example; there are many different versions having similar properties.

The operation of the DC/DC converter in Fig. 9.8 will be explained in steady-state where all variables are periodic functions with period  $T$ . The curves in Fig. 9.9 have been obtained by a detailed simulation of the circuit on a digital computer.

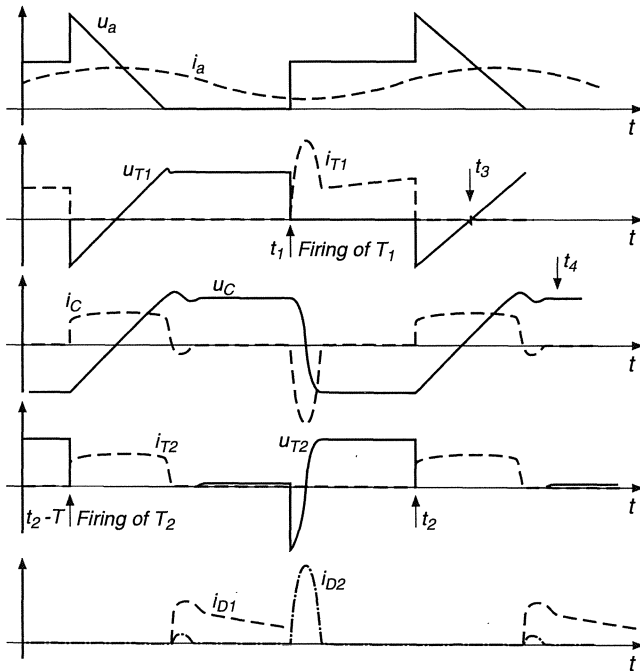


Fig. 9.9. Simulation results for DC/DC converter

The main thyristor  $T_1$  is periodically fired at time  $t_1 + \nu T$ ,  $\nu = 0, 1, \dots$  connecting the supply voltage  $U_0$  to the inductive load circuit,  $u_a(t) = U_0$ , at the same time blocking the shunting diode  $D_1$  which had carried the continuous load current  $i_a$ . This causes the positively charged capacitor,  $u_c(t_1) > 0$ , to be

discharged through the resonant commutation circuit consisting of  $L_c$ ,  $L_2$ ,  $R_2$ ,  $D_2$ ; after the first half wave this transient is interrupted by  $D_2$  as the current is about to change its sign, leaving the capacitor with negative voltage,  $u_c(t) < 0$ . This voltage now serves as forward bias voltage for the commutation auxiliary thyristor  $T_2$  while the main thyristor  $T_1$  is conducting; as  $T_1$  cannot be turned off by a control signal, it must be blocked by temporarily cutting off the current  $i_{T1}$  and applying a negative bias voltage to the thyristor. This is achieved by firing the auxiliary thyristor  $T_2$  at time  $t_2$ , thus connecting the negatively charged capacitor across  $T_1$  and temporarily increasing the output voltage  $u_a$ . The load current  $i_a$  transfers quickly into the auxiliary thyristor, at the same time recharging the capacitor at a rate proportional to the load current

$$\frac{du_c}{dt} = \frac{1}{C} i_c = \frac{1}{C} i_a . \quad (9.7)$$

The bias voltage across thyristor  $T_1$  eventually becomes positive at time  $t_3$ , when  $u_c$  passes through zero; in the interval  $t_3 - t_2$  the recovery of  $T_1$  must have been completed. The recharging of the capacitor continues until  $u_c = U_0$ , when the free wheeling diode takes over the load current and  $T_2$  reverts to blocking condition. The electronic switch then remains in this state, with both thyristors blocked and  $u_c > 0$ , until the next switching cycle begins. In Fig. 9.9 the commutation interval has been enlarged for better visibility.

Clearly it is critical for the functioning of the circuit that the alternating voltage of the commutating capacitor is of sufficient magnitude in order to ensure an adequate hold-off interval  $t_3 - t_2$  when the main thyristor is reversely biased. If this time becomes too short because the charge on the capacitor was insufficient or there is excessive load current,  $T_1$  will refire and a short circuit condition develops which can only be cleared by a fuse link or a breaker. In this respect a commutation failure of this circuit is more serious than with a line commutated converter where the situation could be resolved by advancing the next firing instant. This danger of losing control over the converter exists with all thyristor circuits employing forced commutation; it can only be avoided through careful design of the circuit and by having a fast current control which prevents excessive load current before it approaches the commutation limit.

Another detail is seen in Fig. 9.9 at time  $t_4$  where the capacitor, having been charged beyond  $U_0$  due to the effect of the source inductance  $L_0$ , returns some of its charge to the battery through diode  $D_2$ ; since it is desirable to have the capacitor well charged for added commutation capability, this loss of charge could be avoided by using instead of  $D_2$  another thyristor that is fired together with  $T_1$ .

The switching sequence is repeated at a frequency  $f$  between 50 Hz and perhaps 1 kHz, depending on the type and power rating of the thyristors. The control effect is achieved by pulse-width modulation; for example, if thyristor  $T_1$  is fired at the frequency  $f$  with a fixed phase, the On-Off ratio is altered by advancing or retarding the firing instant  $t_2$  of thyristor  $T_2$ . When neglecting the commutating transients the voltage can be approximated by a periodical

square wave having constant amplitude  $U_0$  and variable pulse-width  $t_2 - t_1$ , so that the mean output voltage may be continuously changed,

$$0.1 < \frac{\overline{u_a}}{U_0} = \frac{t_2 - t_1}{T} < 0.9 ; \quad (9.8)$$

this avoids the large power losses that would occur with a series resistor. Of course, all components in the converter circuit involve some losses which have to be examined very carefully at the design stage; still, the over-all efficiency of a typical DC/DC converter may be better than 95%. The limits  $(t_2 - t_1) \rightarrow 0$  and  $(t_2 - t_1) \rightarrow T$  cannot be reached by continuous pulse-width control because some time is needed for the commutating transients.

From this simplified description it is apparent that the analysis and, consequently, the design of a converter with forced commutation is much more complex than that of a line commutated converter. The voltages and currents, for example those directly affecting the thyristors, can only be determined by tedious hand calculations in the successive intervals, by measurement on a laboratory unit or by simulating the complete circuit on a digital computer. Very efficient programs have been developed for this purpose which require only a topological description of the circuit; from this information the differential equations are automatically generated. With given initial conditions, the numerical integration proceeds until either a control input occurs (e.g. firing of a thyristor) or one of the components reaches a discontinuity, such as a diode blocking, at which time new equations are defined (or new parameters entered into the former equations) in order to continue the integration, starting from the boundary conditions reached before [E4]. In complex converter circuits there may be a multitude of intervals, corresponding to different switching states of the circuit, before the operation repeats itself. Computations of this type are very time consuming because the integration must be performed in very small time steps as dictated by the rapid transients, for example in the commutating branches; nevertheless, digital simulation is an indispensable tool at the design stage. Naturally, after the converter design is completed, much simpler models can be used for designing the control system. An extensive specialised literature exists on DC/DC converters describing numerous details, particularly with regard to commutation circuits [2, 45, 48].

The DC/DC converter, like the line-commutated converter, is a power amplifier with fast response having limited overload capacity; hence it calls for effective protection which is best provided by closed loop control. With vehicle drives which are often coupled to a large load inertia this is of particular importance because acceleration normally takes place at a prescribed current limit. Therefore cascade control having an inner current loop is well suited also to DC/DC converters.

As was shown in Sect. 8.5, very simple dynamic models are quite adequate for the design of the control system, provided the innermost loop contains – besides the switching converter – a simple control plant with low-pass characteristics. When neglecting the commutation transients and assuming continuous

load current  $i_a$ , the converter in Fig. 9.8 looks from the load side like an impressed voltage source, changing between  $U_0$  and zero with variable duty cycle. Hence the circuit can be represented by a mechanical switch as seen in Fig. 9.10a that may be operated by an On-Off-controller having a narrow hysteresis loop of width  $2\Delta$ . With the real converter, the controller would issue firing pulses to the main- and the auxiliary thyristor.

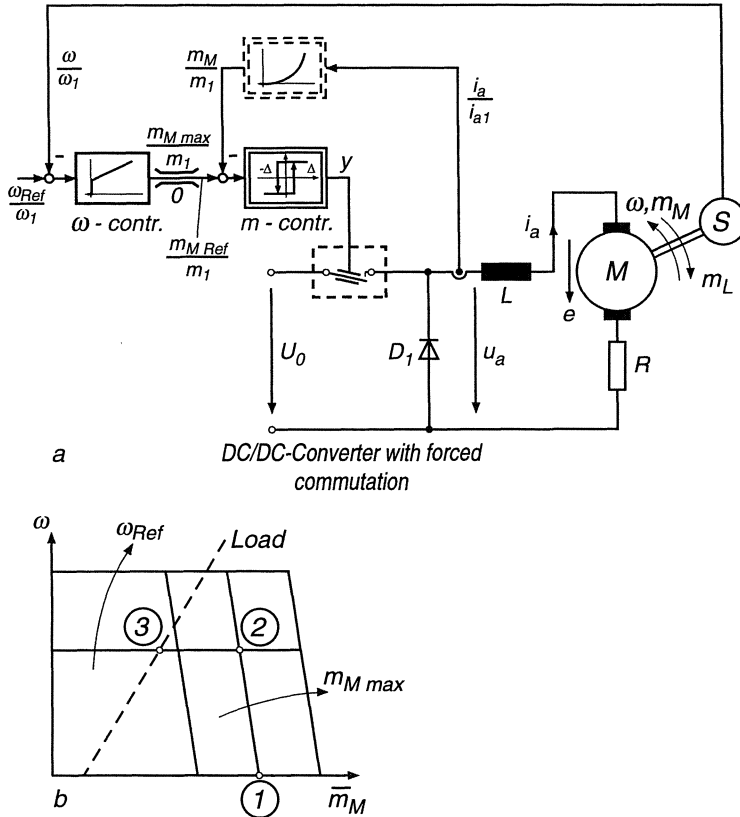


**Fig. 9.10.** a) Simplified control scheme of drive with DC/DC converter,  
b) steady-state characteristics

The block diagram of a series wound motor (Fig. 6.3) is quite nonlinear, but with an On-Off-controller for the inner current control loop no problems are encountered. The system results in a quasi-linear inner closed loop with approximately unity gain. In the superimposed speed control loop the mechanical integration is added (neglecting friction), however with variable gain, because the torque of a series motor is determined by  $\Phi_e i_a \approx i_a^2$ . The result would be different speed transients depending on the operating point of the motor. In order to avoid this effect, it may be advantageous to add a nonlinear function generator producing a torque signal,

$$\frac{m_M}{m_1} = f \left( \frac{i_a}{i_{a1}} \right), \quad i_a \geq 0, \quad (9.9)$$

and to form an inner torque control loop instead. No particular accuracy of the function generator is required. The result is seen in the block diagram Fig. 9.10a, where all nonlinearities are now contained in the inner loop. The pulse-width modulated waveform is generated by the closed torque control loop without the need for an external clock; the frequency can be adjusted by the choice of the hysteresis loop width. Again, with a simple On-Off-controller, the switching frequency of the converter is not constant but exhibits a maximum in the centre of the control range [35]; this causes no harm as long as the minimum frequency is sufficiently high. However, when a constant switching frequency is specified in order to avoid interference with signalling circuits laid along the railway tracks, a constant frequency pulse-width modulator of the type seen in Fig. 8.11 would be preferable. If the vehicle contains several independently fed drive motors, the firing of the converters is synchronised out of phase in order to increase the ripple frequency of the current in the supply line.

The function generator (Eq. 9.9) in the feedback branch of the inner loop has the effect that, as the speed controller is clamped, the torque rather than the current will be limited. However, as the function is monotonic for  $i_a > 0$ , the effect is similar. It leads to the steady-state motor characteristics depicted in Fig. 9.10 b. Because of the PI-speed controller, constant speed is maintained up to the maximum torque, while the branches for torque limit are slightly inclined as a result of the on-off-control scheme. Both references  $\omega_{Ref}$ ,  $m_{Mmax}$  are represented by electronic signals allowing convenient matching of the drive to changing needs of the load. Thus the steady state velocity of the vehicle could be prescribed as well as the maximum torque. A rate-of-change (acceleration) limiter as seen in Fig. 7.11 could also be included.

Figure 9.11 shows a simulated starting transient with speed-dependent load torque; the operating point in Fig. 9.10 b moves from 1 via 2 to 3. The inertia of the drive was chosen very small in order to clarify the details of the switching operation; with an actual traction drive, the acceleration phase may last many seconds while the switching takes place at several hundred Hz. When selecting the parameters of the controllers, simple design methods are applicable, for example as discussed in [35].

As was mentioned in Sect. 8.5, the DC/DC converter with torque controller could be analyzed as a nonlinear sampled data control system, but there are considerable mathematical complications which, in view of the good accuracy of simpler approximations, are normally not worth solving.

When examining again the chopper circuit in Fig. 9.8, it is obvious that all the complexities of the commutation circuit and the associated transients are caused by the need to extinguish the current in the main thyristor  $T_1$  so that it can revert to blocking state, supporting forward voltage. With a switching device that can be turned off by a control signal, for instance a GTO, Bipolar transistor or IGBT, the complete circuit in dashed lines can be replaced by a simple switch and possibly a snubber circuit. This not only reduces complexity, power losses

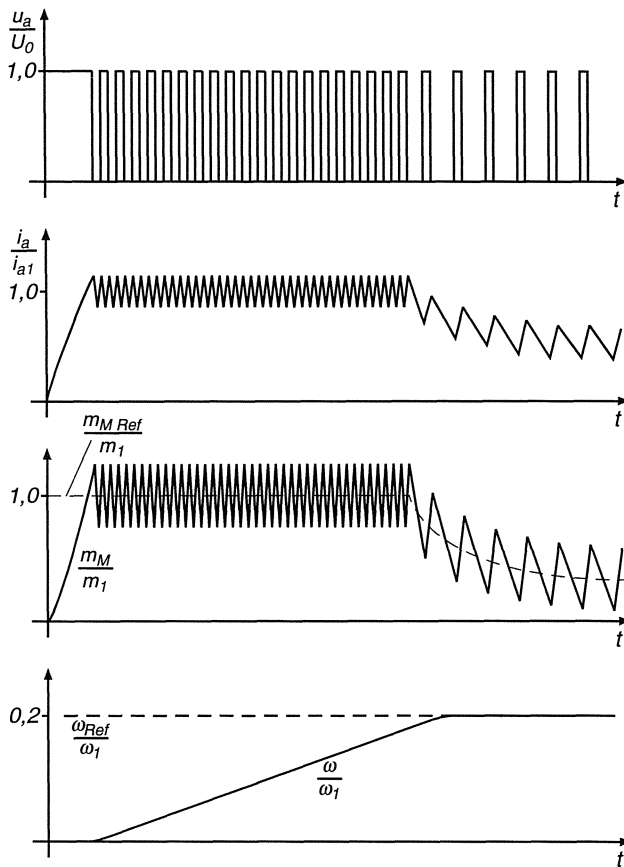


**Fig. 9.11.** Simulated starting transient of drive with DC/DC converter

and cost, it would also make the chopper less sensitive to overload; in addition, the switching frequency might be increased, thus relieving the filtering problems and improving the control response.

Position controlled low power servo drives (usually  $< 10$  kW) for machine tools and robots have to meet very demanding specifications with regard to dynamic performance in order to successfully compete with hydraulic actuators. This calls for specially designed motors having a high ratio of torque to inertia and a large short- time overload capability. Two types of DC motors have emerged for this duty showing a comparable torque to inertia ratio:

- Motors having long rotors with small diameter, usually employing permanent magnet excitation, but otherwise of conventional drum design,
- Motors with iron-free disc rotor having an axial magnetic field also produced by permanent magnets. The armature winding is printed directly

on a disc of fibre-reinforced resin; in contrast to the “slim” motors they are short compared to their diameter. The armature inductance and the inertia are very small, but so is their thermal time constant resulting in limited overload capability. Motors of this type are only produced for low power, as required for positioning of machine tools or robots, Fig. 14.1.

Servo motors do not normally operate at constant speed; the intermittent duty includes rapid acceleration and deceleration in both directions, in addition to overcoming large frictional torques. These characteristics call for a four-quadrant drive having a power supply which is, at least temporarily, capable of absorbing braking energy. However, in view of the intermittent operation and the small size of the motors, regeneration is usually not worthwhile unless a battery of limited capacity serves as a power source.

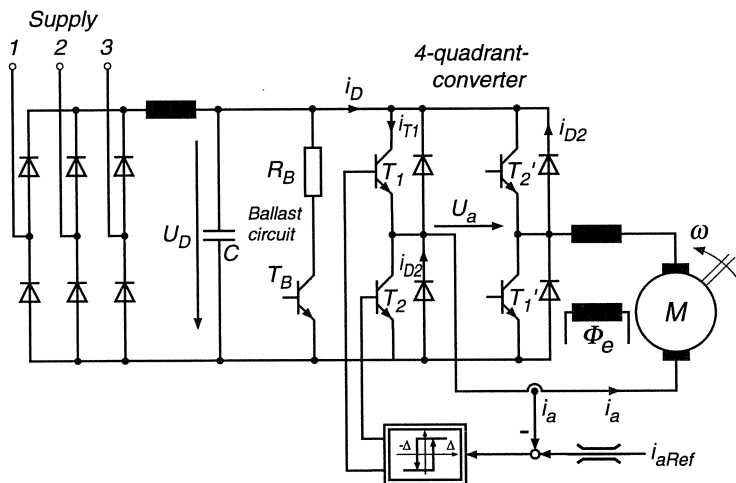


Fig. 9.12. Switched transistor converter

For drives of this type, switched transistor converters supplied by a constant direct voltage are often used. If, instead of a battery, an AC line voltage feeds the converter through an uncontrolled rectifier, the braking energy must be absorbed by a switched braking resistor or, if regeneration is specified, by an additional line-side inverter. Transistor converters have the important advantage that they can be switched at higher frequency ( $> 5$  kHz), thus eliminating all dynamic restrictions associated with line-commutated converters. With field effect transistors or IGBT's, the frequency can even be increased beyond the audible threshold ( $> 16$  kHz) so that the converter is not emitting objectionable acoustic noise.

The simplified circuit of a typical switched transistor converter with constant direct supply voltage is shown in Fig. 9.12. The four transistors in the bridge circuit are pulse-width modulated in diagonal pairs with the stringent condition, that there must be no overlap of the conducting intervals in order to

avoid short circuiting the DC bus, thus endangering the transistors. The antiparallel diodes provide paths for the load current independent of the switching state of the transistors; this is necessary because at the high switching frequency the current through the inductive load is nearly always continuous. The antiparallel diodes can, depending on the type of switch, be integrated into the semiconductor or may be part of a module, containing most or all of the converter components.

The circuit in Fig. 9.12 is considerably simplified; leakage inductances and deliberately introduced capacitive and inductive components (snubbers) aimed at reducing the switching losses in the transistors are omitted. Idealised waveforms of some currents are seen in Fig. 9.13. The current  $i_D$  in the supply bus contains a strong alternating component which is supplied by the smoothing capacitor  $C$ . However, should there be a surge of reverse current  $i_D < 0$ , for example as a consequence of rapid deceleration of the drive, the continuous voltage  $u_D$  could increase beyond the maximum voltage of the transistors; this is prevented by pulse-width modulated switching of the transistor  $T_B$ , dissipating the excess energy in the ballast resistor  $R_B$ .

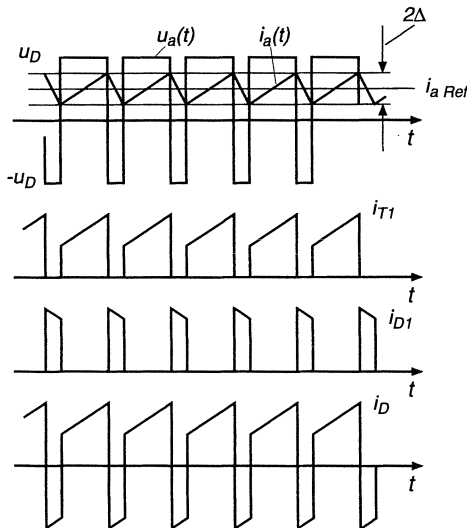


**Fig. 9.13.** Current wave forms of transistor converter in steady state

The control of the converter can be arranged as before; an inner current loop controlling the converter via a pulse-width modulator is essential for safe operation. In Fig. 9.12 the current controller is again of the simple on-off type, but this is only an illustrative example as discussed before. Current limit is achieved by limiting the current reference produced by the superimposed speed controller. The next higher level of control could be a position control loop as shown in Fig. 15.9, where the response is further improved by feed-forward signals from a reference generator.

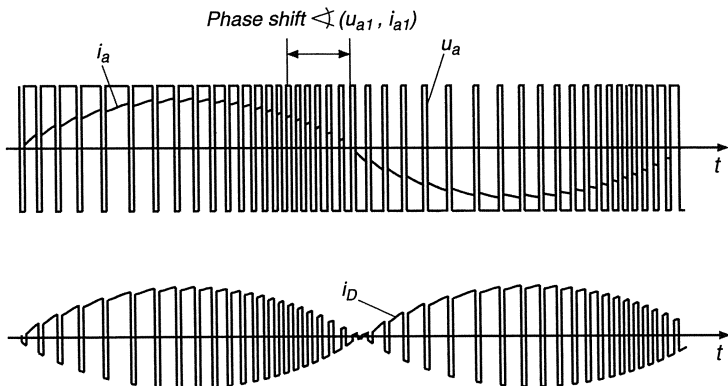


**Fig. 9.14.** Alternating current control by pulse-width modulated transistor converter

The typical response time of the current loop, employing a switched transistor converter in combination with a DC disc motor, is 1 or 2 ms. For many applications this justifies the assumption that the current control loop acts as controllable current source having instantaneous response.

From Fig. 9.12 it is seen that the converter circuit can produce not only an adjustable direct current but also alternating current, provided its frequency is sufficiently below the switching frequency of the converter. This is shown in Fig. 9.14, again assuming a simplified circuit with On- Off current control; we will deal with some of these circuits again when discussing AC drives.

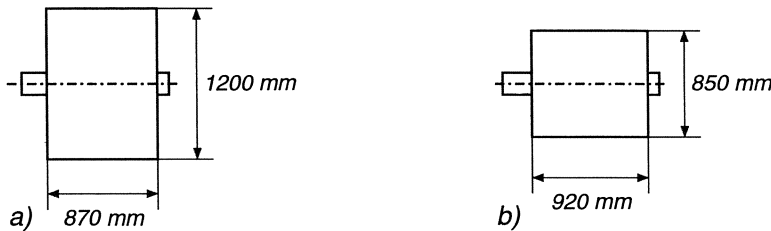
## 10. Symmetrical Three-Phase AC Machines

The asynchronous or induction motor is the most widely used electrical drive motor; its invention at the end of the last century has given a strong impetus for the transition from DC to AC in the field of generation, transmission and distribution of electrical energy. Its main advantage is the elimination of all sliding contacts, resulting in an exceedingly simple and rugged construction. Induction machines are built in a variety of designs with ratings from a few watts to many megawatts.

Unfortunately, the speed of line-fed induction motors cannot be continuously varied without additional equipment or without incurring heavy power losses. Even though the problems of efficiently controlling the speed of induction motors have been investigated for decades, all solutions realisable until a few years ago were unsatisfactory with regard to complexity, efficiency, dynamic performance or cost. It is only due to the progress of semiconductor technology in the last 20 years that suitable static frequency converters can now be built at acceptable cost, making the induction machine the most promising adjustable speed drive for many applications.

The substitution of the commutator, acting as a mechanical converter, by a power electronic, solid state converter reduces the AC machine solely to the task of electromechanical energy conversion, resulting in much higher power density per volume or mass. This is exemplified by two main line traction motors, the outlines of which are shown in Fig. 10.1, together with some characteristic data. The motor at left is a proven design, operated for many years in Intercity locomotives; it is a single phase series wound commutator motor as mentioned in Chap. 6, voltage controlled by transformer tap changer. At the right is a modern AC induction motor, fed and controlled by a GTO voltage source inverter. Clearly, the new motor is superior in every respect; it is also suitable for high dynamic performance torque control, thus allowing full utilisation of the adhesive frictional forces. As a result, a locomotive containing four of the new motors can produce a similar traction force as the former much heavier locomotive with six single phase motors, the torque of which is pulsating at double the supply frequency.

The theory of the induction motor under dynamic conditions is somewhat involved because of the rotating magnetic fields, the spatial relationships of which depend on speed and load; it will be treated here only in simplified form. On the other hand, the equivalent circuits, derived for steady state operation



AC commutator motor		AC induction motor
1230 kW, 7730 Nm at 1520 min <sup>-1</sup>	Cont. Rating	1428 kW, 9155 Nm at 1490 min <sup>-1</sup>
8530 Nm 1600 min <sup>-1</sup>	Torque (5 min)	11600 Nm
3550 kg	Max. Speed	4200 min <sup>-1</sup>
120 kg cm <sup>2</sup>	Mass	2660 kg
	Inertia	22 kg cm <sup>2</sup>

**Fig. 10.1.** Comparison of traction motors (Siemens).

- a) Single phase series wound AC commutator motor,
- b) Three phase AC induction motor

with sinusoidal voltages and currents, are inadequate when dealing with transients or when the motor is supplied from a switching converter. The steady state condition will be treated as a special case of the general dynamic case.

The mathematical model to be used is tailored to the needs of controlled drives. It incorporates most of the qualitative features of an actual motor but would not, of course, be accurate enough for the purpose of designing the machine.

## 10.1 Mathematical Model of a General AC Machine

It is assumed that the stator  $S$  of the machine is represented by a hollow iron cylinder with circular cross section, containing a concentric rotor  $R$  so that a narrow airgap of constant radial length  $h$  exists between the smooth cylindrical surfaces to which symmetrical three-phase windings of negligible depth are assumed to be attached; their spatial ampereturns distributions may be thought of as being produced by suitably placed thin strands of conductors or conductive sheets. Both neutrals of the star-connected windings are isolated, the terminals of the rotor winding are either connected to slippings or short circuited internally.  $N_S$ ,  $N_R$  are the numbers of full pitch turns in each phase winding. The permeability of the fully laminated stator and rotor iron is as-

sumed to be infinite; saturation, iron losses, end-windings and slot-effects are ignored.

The following discussion applies to two-pole motors; with multi-pole machines the synchronous speed is reduced correspondingly. This effect is exploited with pole-changing windings, however at some loss in utilisation of the motor.

The variables are defined in Fig. 10.2 a.  $\alpha$  is the angular coordinate in the stator with reference to the axis of stator winding 1 which is indicated by its central turn. The centres of the identical windings 2 and 3 are positioned at  $\alpha = \gamma = 120^\circ$  and  $\alpha = 2\gamma = 240^\circ$  respectively. Corresponding definitions hold for the rotor windings, where  $\beta$  is the angular coordinate, again with reference to the centre of winding 1.  $\varepsilon(t)$  is the angle of rotation of the rotor, measured in the stator frame of coordinates,  $\omega(t) = d\varepsilon/dt$  is the instantaneous angular velocity of the rotor.

The magnetic field in the airgap of the machine has radial direction because of the smooth parallel stator and rotor surfaces and the postulated infinite permeability of the iron. Since end-effects are neglected, we are dealing with a two dimensional magnetic field problem.

The three stator currents  $i_{S1}(t), i_{S2}(t), i_{S3}(t)$  may exhibit any waveforms; for reasons of symmetry all currents are retained throughout the calculations, even though one of the currents is redundant because, due to the isolated neutral,

$$i_{S1}(t) + i_{S2}(t) + i_{S3}(t) = 0 \quad (10.1)$$

is valid at any instant, i.e. the currents are balanced.

With these simplifications and definitions, the radial ampereturns wave of the stator windings consists of three spatially sinusoidal, stationary terms, which are modulated by the currents

$$\Theta_S(\alpha, t) = N_S [i_{S1}(t) \vartheta(\alpha) + i_{S2}(t) \vartheta(\alpha - \gamma) + i_{S3}(t) \vartheta(\alpha - 2\gamma)] , \gamma = \frac{2\pi}{3} . \quad (10.2)$$

According to Fig. 10.2,  $\Theta_S(\alpha, t)$  corresponds to the stator ampereturns enclosed by a radial magnetic field line crossing the motor at angle  $\alpha$ ; because of the assumed high permeability of the iron these ampere turns appear as magnetomotive forces at the two airgap crossings. The spatial function  $-1 \leq \vartheta(\alpha) \leq 1$  in Fig. 10.2 c characterises the ampereturns distribution of one phase of the stator winding, it could be written as a Fourier series. When the windings are fed with alternating currents, each term in Eq. (10.2) oscillates as a standing wave, fixed in space; their superposition results in a travelling wave  $\Theta_S(\alpha, t)$ , as seen in Fig. 10.2 d. The spatial harmonics may be diminished by reduced pitch and by skew of the windings, resulting in  $\vartheta(\alpha) = \cos \alpha$ . By introducing complex notation,

$$\cos \alpha = \frac{1}{2} (e^{j\alpha} + e^{-j\alpha}), \quad \text{etc.}$$

and rearranging, Eq. (10.2) then becomes

$$\Theta_S(\alpha, t) = \frac{1}{2} N_S [i_S(t) e^{-j\alpha} + i_S^*(t) e^{j\alpha}] , \text{ real} , \quad (10.3)$$

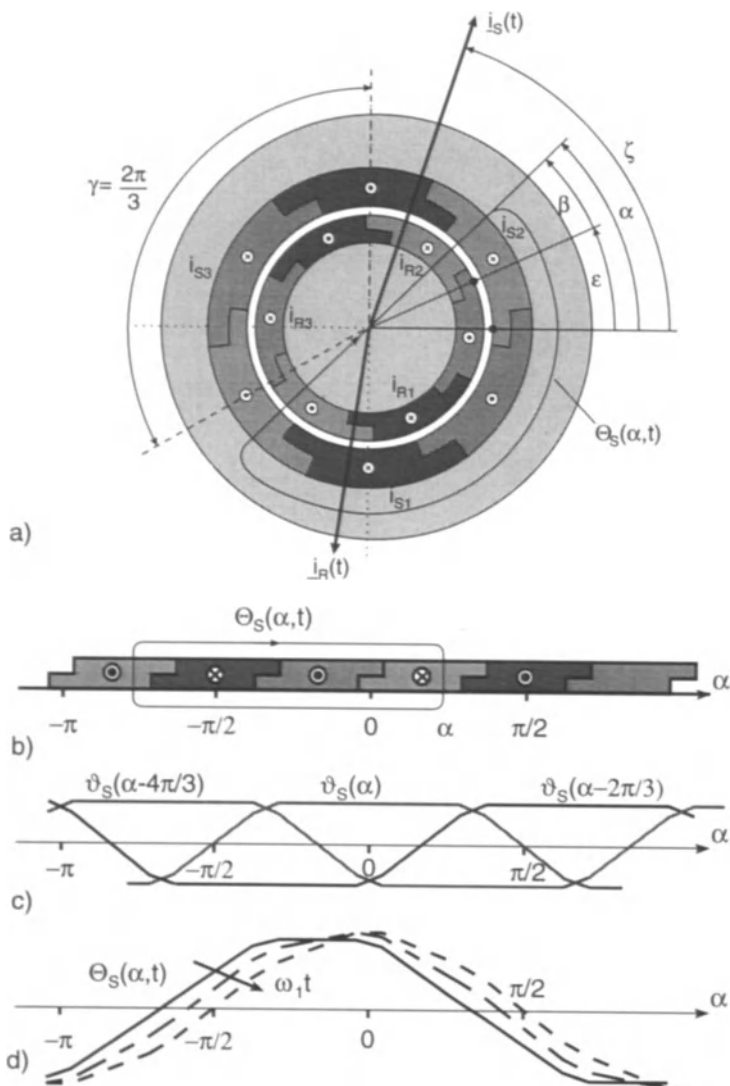


**Fig. 10.2.** Symmetrical AC machine

- a) Cross section with two-layer airgap windings,
- b) Unwrapped stator windings,
- c) Ampereturns or magnetomotive force  $\vartheta_S(\alpha, t)$  of stator windings,
- d) Travelling ampereturns wave caused by three-phase currents

where

$$\underline{i}_S(t) = i_{S1}(t) + i_{S2}(t)e^{j\gamma} + i_{S3}(t)e^{j2\gamma} \quad (10.4a)$$

is a time-dependent current vector in the complex plane and

$$\underline{i}_S^*(t) = i_{S1}(t) + i_{S2}(t)e^{-j\gamma} + i_{S3}(t)e^{-j2\gamma} \quad (10.4b)$$

is the corresponding conjugate complex vector. The ampereturns  $\Theta_S(\alpha, t)$  are of course real, being a measurable physical quantity depending on  $\alpha$  and  $t$ .

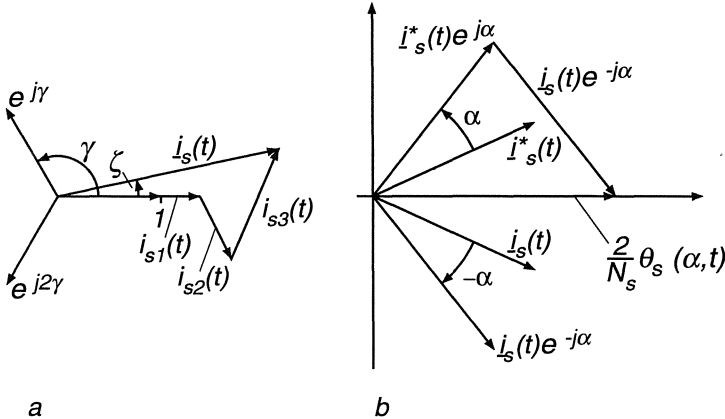


**Fig. 10.3.** Complex current vector

The construction of the current vector  $i_S(t)$  is shown in Fig. 10.3 for assumed values of  $i_{S1} > 0$ ,  $i_{S2}$ ,  $i_{S3} < 0$ . Magnitude and angle each vary with time according to

$$i_S(t) = i_S(t) e^{j\zeta(t)} . \quad (10.5)$$

The current vector determines the instantaneous magnitude and angular position of the peak of the sinusoidally distributed ampereturns wave produced by the three spatially displaced stator windings. By combining Eqs.(10.3, 10.5) the ampereturns may be expressed as a travelling wave, the peak of which follows the angle  $\zeta(t)$  of the current vector,

$$\Theta_S(\alpha, t) = N_S i_S(t) \cos(\zeta(t) - \alpha) . \quad (10.6)$$

If the stator currents are sinusoidal and form a symmetrical three phase system, the ampereturns wave moves with constant magnitude and velocity  $\omega_1 = d\zeta/dt$  in the airgap of the motor.

Since the complex vectors defined in Eqs. (10.4 – 10.6) describe the spatial distribution of a magnetic field in a plane perpendicular to the motor axis, they are also called space-vectors or space-phasors [28, N7, S61]. However, they are not to be confused with the constant complex phasors for describing steady state sinusoidal alternating quantities.

The same reasoning as before holds for the ampereturns wave produced by the moving three-phase rotor windings,

$$\Theta_R(\beta, t) = N_R [i_{R1}(t) \cos \beta + i_{R2}(t) \cos(\beta - \gamma) + i_{R3}(t) \cos(\beta - 2\gamma)] . \quad (10.7)$$

When defining a rotor current vector,

$$i_R(t) = i_{R1}(t) + i_{R2}(t) e^{j\gamma} + i_{R3}(t) e^{j2\gamma} = i_R(t) e^{j\xi(t)} , \quad (10.8a)$$

$$i_R^*(t) = i_{R1}(t) + i_{R2}(t) e^{-j\gamma} + i_{R3}(t) e^{-j2\gamma} = i_R(t) e^{-j\xi(t)} , \quad (10.8b)$$

the ampereturns-wave, excited by the rotor currents and moving with the rotor, assumes the form

$$\Theta_R(\beta, t) = \frac{1}{2} N_R [i_R(t) e^{-j\beta} + i_R^*(t) e^{j\beta}] , \text{ real} ; \quad (10.9)$$

its effect on the stator is obtained by substituting

$$\beta = \alpha - \varepsilon , \quad (10.10)$$

$$\Theta_R(\alpha, \varepsilon, t) = \frac{1}{2} N_R [i_R(t) e^{-j(\alpha-\varepsilon)} + i_R^*(t) e^{j(\alpha-\varepsilon)}] . \quad (10.11)$$

The resultant wave is a superposition of the stator- and rotor-ampere turns

$$\Theta(\alpha, \varepsilon, t) = \Theta_S(\alpha, t) + \Theta_R(\alpha, \varepsilon, t) . \quad (10.12)$$

Since the permeability of the iron was assumed infinite, the magnetomotive force becomes effective at the two airgap crossings, causing a local flux density at the stator side of the airgap,

$$B_S(\alpha, \varepsilon, t) = \frac{1}{2h} \mu_0 [\Theta_S(\alpha, t) + \kappa \Theta_R(\alpha, \varepsilon, t)] , \quad (10.13)$$

where  $\kappa < 1$  is a global coupling factor, taking magnetic leakage into account;  $\mu_0$  is the permeability constant. A detailed modelling of leakage effects is not possible with the simplifications made.

When calculating flux linkages, the spatial distribution of the conductors must be considered as indicated in Fig. 10.4 for the example of one stator winding. By assuming a quasi-continuous distribution of turns with an “incremental density”  $\frac{1}{2} N_S \cos \lambda$ , the postulated sinusoidal distribution results; at the same time the total number of turns becomes  $N_S$ , as proved by integration in the interval  $-\frac{\pi}{2} < \lambda < \frac{\pi}{2}$ . Thus the flux linkage in stator winding 1 is obtained by a double integration,

$$\psi_{S1}(t) = \frac{1}{2} N_S \int_{\lambda=-\frac{\pi}{2}}^{\frac{\pi}{2}} \cos \lambda \left[ \int_{\alpha=\lambda-\frac{\pi}{2}}^{\lambda+\frac{\pi}{2}} l r B_S(\alpha, \varepsilon, t) d\alpha \right] d\lambda , \quad (10.14)$$

where  $l$  is the effective axial length and  $r$  the radius of the rotor. The integration over  $\alpha$  is a consequence of the non-uniform field in the airgap while the integration over  $\lambda$  is required by the nonuniform distribution of the winding.

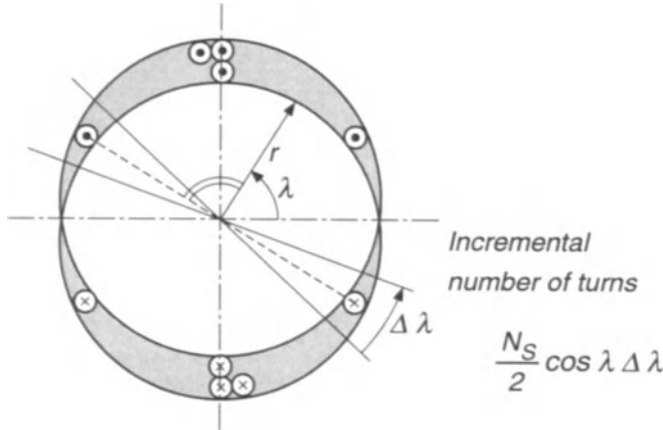


**Fig. 10.4.** Distributed winding

Inserting Eqs. (10.3, 10.11, 10.13) results in

$$\begin{aligned}\psi_{S1}(t) &= \frac{N_S^2 l r}{16 h} \mu_0 \int_{-\frac{\pi}{2}}^{\frac{\pi}{2}} [e^{j\lambda} + e^{-j\lambda}] \int_{\lambda - \frac{\pi}{2}}^{\lambda + \frac{\pi}{2}} [i_S(t) e^{-j\alpha} + i_S^*(t) e^{j\alpha}] d\alpha d\lambda \\ &+ \kappa \frac{N_S N_R l r}{16 h} \mu_0 \int_{-\frac{\pi}{2}}^{\frac{\pi}{2}} [e^{j\lambda} + e^{-j\lambda}] \int_{\lambda - \frac{\pi}{2}}^{\lambda + \frac{\pi}{2}} [i_R(t) e^{-j(\alpha-\varepsilon)} + i_R^*(t) e^{j(\alpha-\varepsilon)}] d\alpha d\lambda.\end{aligned}\quad (10.15)$$

The evaluation of the integral is greatly simplified by the complex notation due to the periodicity of the integrand. With the abbreviations for self and mutual inductances

$$\frac{N_S^2 l r}{8 h} \pi \mu_0 = \frac{1}{3} L_S, \quad (10.16a)$$

$$\kappa \frac{N_S N_R l r}{8 h} \pi \mu_0 = \frac{1}{3} M, \quad (10.16b)$$

a simple result is obtained

$$\psi_{S1}(t) = \frac{1}{3} L_S [i_S(t) + i_S^*(t)] + \frac{1}{3} M [i_R(t) e^{j\varepsilon} + i_R^*(t) e^{-j\varepsilon}]. \quad (10.17a)$$

The flux linkage in the stator winding 1 is a physical integral quantity and must, of course, be real. The flux in the other stator windings is computed likewise, with the exception that the integration over  $\lambda$ , reflecting the position of the windings, is shifted to  $\gamma \pm \frac{\pi}{2}$  and  $2\gamma \pm \frac{\pi}{2}$  respectively. This results in

$$\psi_{S2}(t) = \frac{1}{3} L_S [i_S(t) e^{-j\gamma} + i_S^*(t) e^{j\gamma}]$$

$$+ \frac{1}{3} M [\underline{i}_R(t) e^{j(\varepsilon-\gamma)} + \underline{i}_R^*(t) e^{-j(\varepsilon-\gamma)}] , \quad (10.17b)$$

$$\begin{aligned} \psi_{S3}(t) = & \frac{1}{3} L_S [\underline{i}_S(t) e^{-j2\gamma} + \underline{i}_S^*(t) e^{j2\gamma}] \\ & + \frac{1}{3} M [\underline{i}_R(t) e^{j(\varepsilon-2\gamma)} + \underline{i}_R^*(t) e^{-j(\varepsilon-2\gamma)}] . \end{aligned} \quad (10.17c)$$

The symmetry of these equations gives rise to the definition of a complex vector of flux linkages

$$\underline{\psi}_S(t) = \psi_{S1}(t) + \psi_{S2}(t) e^{j\gamma} + \psi_{S3}(t) e^{j2\gamma} , \quad (10.18)$$

allowing Eqs. (10.17 a – c) to be combined,

$$\underline{\psi}_S(t) = L_S \underline{i}_S(t) + M \underline{i}_R(t) e^{j\varepsilon(t)} . \quad (10.19)$$

This flux vector describes the magnitude and angular position of the peak of the sinusoidal flux distribution in the airgap of the machine. The exponential term attached to  $\underline{i}_R(t)$  indicates that the rotor current vector must be turned by the angle of mechanical rotation before its effect can be superimposed upon that of the stator current vector  $\underline{i}_S(t)$ .

The flux linkage of the moving rotor windings is computed in exactly the same way. Conversion of the stator current vector into rotor coordinates by means of Eq. (10.10) yields

$$\Theta_S(\beta, \varepsilon, t) = \frac{1}{2} N_S [\underline{i}_S(t) e^{-j(\beta+\varepsilon)} + \underline{i}_S^*(t) e^{j(\beta+\varepsilon)}] , \quad (10.20)$$

which, together with the rotor current, generates a flux density on the rotor surface, corresponding to Eq. (10.13)

$$B_R(\beta, \varepsilon, t) = \frac{1}{2h} \mu_0 [\Theta_R(\beta, t) + \kappa \Theta_S(\beta, \varepsilon, t)] . \quad (10.21)$$

The same global coupling factor  $\kappa$  has been assumed in order to take unavoidable leakage effects into account.

Integration around the circumference of the rotor, again presupposing a finely distributed rotor winding, leads to an expression for the flux linkage in rotor winding 1,

$$\psi_{R1}(t) = \frac{1}{3} L_R [\underline{i}_R(t) + \underline{i}_R^*(t)] + \frac{1}{3} M [\underline{i}_S(t) e^{-j\varepsilon} + \underline{i}_S^*(t) e^{j\varepsilon}] , \quad (10.22a)$$

which has a similar form as Eq. (10.17 a). However, as this flux is defined in rotor coordinates, the stator current vector is now turned backwards relative to the position of the rotor.

$$\frac{N_R^2 l r}{8h} \pi \mu_0 = \frac{1}{3} L_R \quad (10.16c)$$

defines the self inductance of a rotor winding.

Likewise the flux linkages of the other rotor windings are obtained,

$$\begin{aligned}\psi_{R2}(t) &= \frac{1}{3} L_R [i_R(t) e^{-j\gamma} + i_R^*(t) e^{j\gamma}] \\ &\quad + \frac{1}{3} M [i_S(t) e^{-j(\varepsilon+\gamma)} + i_S^*(t) e^{j(\varepsilon+\gamma)}] ,\end{aligned}\quad (10.22b)$$

$$\begin{aligned}\psi_{R3}(t) &= \frac{1}{3} L_R [i_R(t) e^{-j2\gamma} + i_R^*(t) e^{j2\gamma}] \\ &\quad + \frac{1}{3} M [i_S(t) e^{-j(\varepsilon+2\gamma)} + i_S^*(t) e^{j(\varepsilon+2\gamma)}] .\end{aligned}\quad (10.22c)$$

These expressions are again simplified by forming a complex vector for the rotor flux

$$\begin{aligned}\underline{\psi}_R(t) &= \psi_{R1}(t) + \psi_{R2}(t) e^{j\gamma} + \psi_{R3}(t) e^{j2\gamma} \\ &= L_R \underline{i}_R(t) + M \underline{i}_S(t) e^{-j\varepsilon} .\end{aligned}\quad (10.23)$$

The magnetic linkages described by Eqs. (10.17, 10.22) are now used to derive the voltage equations for the stator and rotor circuits, depicted in Fig. 10.5.

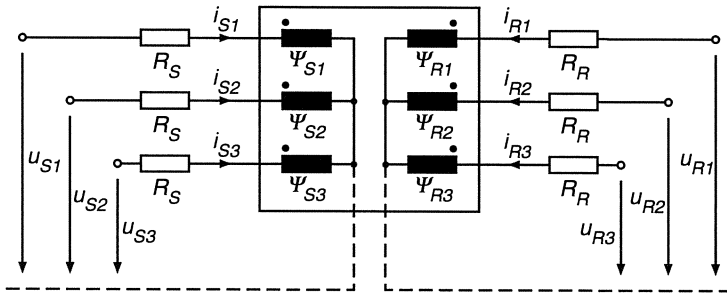


Fig. 10.5. Magnetic linkages and voltages

The line-to-neutral voltages in the stator circuit are

$$\begin{aligned}R_S i_{S1} + \frac{d\underline{\psi}_{S1}}{dt} &= u_{S1}(t) , \\ R_S i_{S2} + \frac{d\underline{\psi}_{S2}}{dt} &= u_{S2}(t) , \\ R_S i_{S3} + \frac{d\underline{\psi}_{S3}}{dt} &= u_{S3}(t) ,\end{aligned}\quad (10.24)$$

where  $R_S$  is the stator resistance per phase and  $u_{S1}$ ,  $u_{S2}$ ,  $u_{S3}$  are voltages of arbitrary waveforms. These equations may again be combined by introducing complex vectors. By formal definition of a voltage vector

$$\underline{u}_S(t) = u_{S1}(t) + u_{S2}(t) e^{j\gamma} + u_{S3}(t) e^{j2\gamma} \quad (10.25)$$

and with Eqs. (10.4, 10.19), this results in

$$R_S \underline{i}_S + \frac{d\underline{\psi}_S}{dt} = R_S \underline{i}_S + L_S \frac{di_S}{dt} + M \frac{d}{dt} (i_R e^{j\varepsilon}) = \underline{u}_S(t) . \quad (10.26)$$

Employing the rules of differentiation, this equation assumes the form

$$R_S \underline{i}_S + L_S \frac{d\underline{i}_S}{dt} + M \frac{d\underline{i}_R}{dt} e^{j\epsilon} + j\omega M \underline{i}_R e^{j\epsilon} = \underline{u}_S(t), \quad (10.27)$$

where  $\omega = d\epsilon/dt$  is the angular velocity of the rotor. The two terms containing the rotor current may be interpreted as voltages due to mutual induction and rotation, respectively.

By inserting Eqs. (10.17 a – c) into Eq. (10.24) and considering Eq. (10.1) which is due to the isolated neutral, it is found that the line-to-neutral voltages of the symmetrical machine are also balanced at any instant,

$$u_{S1}(t) + u_{S2}(t) + u_{S3}(t) \equiv 0. \quad (10.28)$$

On most motors the neutral point of the stator winding is not accessible, so that only the terminal voltages  $u_{S12} = u_{S1} - u_{S2}$  etc. are available for external use, while the line- to neutral voltages are dependent quantities. This corresponds to the actual situation, where the motor may in fact be delta – connected.

The same arguments are valid for the rotor winding, where the currents are also balanced, due to the assumed fictitious neutral point

$$i_{R1}(t) + i_{R2}(t) + i_{R3}(t) \equiv 0; \quad (10.29)$$

the dotted connections to the neutrals in Fig. 10.5 are redundant in reality. Hence the voltage equations are

$$\begin{aligned} R_R i_{R1} + \frac{d\psi_{R1}}{dt} &= u_{R1}(t), \\ R_R i_{R2} + \frac{d\psi_{R2}}{dt} &= u_{R2}(t), \\ R_R i_{R3} + \frac{d\psi_{R3}}{dt} &= u_{R3}(t). \end{aligned} \quad (10.30)$$

With the help of Eqs. (10.8, 10.23) they are again combined to a vectorial equation,

$$R_R \underline{i}_R + \frac{d\underline{\psi}_R}{dt} = R_R \underline{i}_R + L_R \frac{di_R}{dt} + M \frac{d}{dt} (\underline{i}_S e^{-j\epsilon}) = \underline{u}_R(t), \quad (10.31)$$

where all variables are defined in rotor coordinates. The vector of the rotor voltages,

$$\underline{u}_R(t) = u_{R1}(t) + u_{R2}(t) e^{j\gamma} + u_{R3}(t) e^{j2\gamma} \quad (10.32)$$

may be impressed by an external voltage source. In case of a cage rotor, the voltages are zero and the rotor circuit is internally short circuited.

The vector differential equations (10.26) and (10.31) describing the electromagnetic interactions of the symmetrical AC motor in steady state and transient condition are now to be supplemented by equations for the electrical torque and the mechanical transients. With a real motor the tangential forces are acting on

the sides of the slots, where the magnetic field enters the iron. Since there are no slots in our simplified model with airgap windings, the torque is computed with the help of the tangential Lorentz- forces exerted on the axial current carrying conductors orthogonally crossed by the radial magnetic field.

The component of the flux density on the rotor surface which is due to the stator currents follows from Eq. (10.21)

$$B_{RS}(\beta, \varepsilon, t) = \kappa \frac{N_S \mu_0}{4 h} \left[ i_S(t) e^{-j(\beta+\varepsilon)} + i_S^*(t) e^{j(\beta+\varepsilon)} \right]. \quad (10.33)$$

The magnetic field produced by the rotor currents themselves does not generate any net tangential forces with the rotor currents since with the uniform airgap, there is no reluctance torque; this could be shown by carrying out the calculations with  $B_R$  instead of  $B_{RS}$ .

The current distribution  $a_R(\beta, t)$  along the circumference of the rotor is also, with the assumptions made, sinusoidal. According to Fig. 10.6, it is defined as the spatial derivative of the rotor ampereturns,

$$a_R(\beta, t) = \frac{1}{2} \frac{\partial \Theta_R(\beta, t)}{\partial(r \beta)} = -j \frac{N_R}{4 r} \left[ i_R e^{-j\beta} - i_R^* e^{j\beta} \right]. \quad (10.34)$$

The tangential force  $df$  acting on an axial strip of width  $r d\beta$  of the rotor surface is the product of flux density and rotor current distribution

$$df = -B_{RS}(\beta, \varepsilon, t) a_R(\beta, t) l r d\beta,$$

which by integration yields the electric torque in the direction of rotation,

$$m_M(t) = r \int_F df = -r^2 l \int_0^{2\pi} B_{RS}(\beta, \varepsilon, t) a_R(\beta, t) d\beta. \quad (10.35)$$

Inserting Eqs. (10.33, 10.34) results in

$$m_M(t) = -\frac{M}{6 \pi j} \int_0^{2\pi} \left[ i_S e^{-j(\beta+\varepsilon)} + i_S^* e^{j(\beta+\varepsilon)} \right] \left[ i_R e^{-j\beta} - i_R^* e^{j\beta} \right] d\beta,$$

where  $M$  is the coefficient of mutual inductivity defined in Eq. (10.16 b). When integrating over the full circumference of the rotor, the exponential terms containing  $\beta$  cancel. Hence we find

$$m_M(t) = \frac{M}{3 \pi} \int_0^{2\pi} \frac{i_S i_R^* e^{-j\varepsilon} - i_S^* i_R e^{j\varepsilon}}{2 j} d\beta = \frac{2}{3} M \operatorname{Im} \left[ i_S(t) (i_R e^{j\varepsilon})^* \right]; \quad (10.36)$$

the imaginary part of the bracket is equivalent to a vector-product, being proportional to the product of the two current vectors and the sine of the angular displacement  $\chi$ , as seen in Fig. 10.6 b.

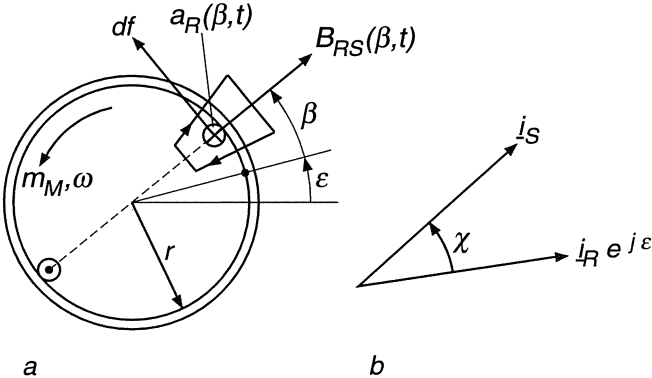


**Fig. 10.6.** Rotor current distribution and torque

By assuming that the stator and rotor windings have an equal number of turns,  $N'_R = N_S$ , and introducing the usual leakage factors,

$$L_S = (1 + \sigma_S) L_0, \quad L_R = (1 + \sigma_R) L_0, \quad M = L_0 \quad (10.37)$$

the complete mathematical model of the symmetrical doubly fed AC machine with the lumped inertia  $J$  then assumes the following form, with  $m_L$  being the net load torque at the coupling of the motor,

$$R_S \dot{i}_S + L_S \frac{di_S}{dt} + L_0 \frac{d}{dt} (\underline{i}_R e^{j\epsilon}) = \underline{u}_S(t), \quad (10.38)$$

$$R_R \dot{i}_R + L_R \frac{di_R}{dt} + L_0 \frac{d}{dt} (\underline{i}_S e^{-j\epsilon}) = \underline{u}_R(t), \quad (10.39)$$

$$J \frac{d\omega}{dt} = m_M(t) - m_L(t) = \frac{2}{3} L_0 \operatorname{Im} [\underline{i}_S (\underline{i}_R e^{j\epsilon})^*] - m_L(\epsilon, \omega, t), \quad (10.40)$$

$$\frac{d\epsilon}{dt} = \omega. \quad (10.41)$$

Since the first two equations can be split into real and imaginary parts, this represents a set of 6 scalar nonlinear differential equations. They are valid for any waveforms of voltages, currents and at varying load torque and speed.

The physical currents, for example in the stator windings, are easily derived from the vectorial representation. With Eq. (10.1), the current vector, defined in Eq. (10.4 a), becomes

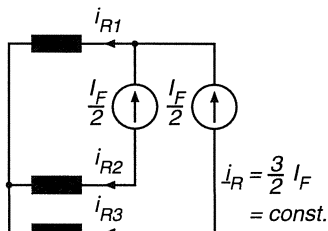
$$\underline{i}_S(t) = \frac{3}{2} i_{S1}(t) + j \frac{\sqrt{3}}{2} [i_{S2}(t) - i_{S3}(t)];$$

hence we find

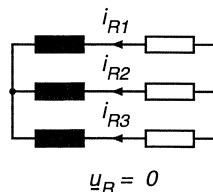
$$i_{S1}(t) = \frac{2}{3} \operatorname{Re} [\underline{i}_S(t)], \quad (10.42a)$$

and correspondingly,

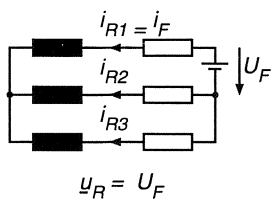
**Table 10.1.** Mathematical models for the rotors of different types of AC machines used in controlled electrical drives



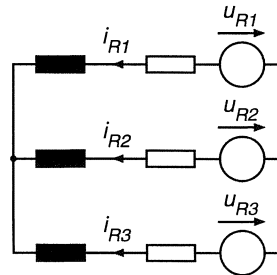
a) Synchronous machines with high energy permanent magnets on the rotor surface



b) Induction machine with cage or wound rotor



c) Synchronous machine with combined field- and damper-windings



d) Doubly-fed machine with impressed rotor voltages

$$i_{S2}(t) = \frac{2}{3} \operatorname{Re} [i_S e^{-j\gamma}] , \text{ etc.} \quad (10.42b)$$

Likewise the currents in the rotor winding are obtained; of course, in case of a squirrel cage rotor, the notion of phase currents loses its physical meaning, even though the simplified theory remains applicable.

The Eqs. (10.38 – 10.41) are the starting point for all subsequent discussions of transient and steady state phenomena. They describe the electromechanical interactions of a symmetrical AC machine and can be adapted to various constraints, imposed by the type of machine used, as long as the basic assumptions on which the model was based, are upheld. This mainly refers to radial symmetry and constant airgap, excluding saliency of the stator or rotor.

Table 10.1 contains four types of AC machines used in controlled drives that may be represented by the model equations. The details of the constraints are discussed in later chapters.

- a) Synchronous machines with high energy permanent magnets on the rotor surface
- b) Induction machine with cage or wound rotor
- c) Synchronous machine with combined field- and damper windings

- d) Doubly-fed machine with impressed rotor voltages

The model equations contain, of course, the special case of steady state operation, when the AC motor is fed with sinusoidal impressed voltages by a symmetrical three-phase supply and is loaded with constant torque. In order to form a link to this commonly used presentation and to gain a better understanding of the model equations, this case will be treated first. With  $\underline{u}_R = 0$ , a cage motor or a wound rotor results, where external symmetrical rotor resistors may have been added.

## 10.2 Operation of an Induction Motor with Sinusoidal Symmetrical Three-phase Supply Voltages

### 10.2.1 Stator Current, Current Locus

A symmetrical three-phase system of sinusoidal voltages having the angular frequency  $\omega_1$  may be defined as follows, using complex notation,

$$\begin{aligned} u_{S1}(t) &= \sqrt{2} U_S \cos(\omega_1 t + \tau_1) = \operatorname{Re} [\sqrt{2} U_S e^{j\tau_1} e^{j\omega_1 t}] \\ &= \frac{\sqrt{2}}{2} [\underline{U}_S e^{j\omega_1 t} + \underline{U}_S^* e^{-j\omega_1 t}] , \end{aligned} \quad (10.43a)$$

where  $\underline{U}_S = U_S e^{j\tau_1}$  is the voltage phasor; correspondingly,

$$\begin{aligned} u_{S2}(t) &= u_{S1} \left( t - \frac{\gamma}{\omega_1} \right) \\ &= \frac{\sqrt{2}}{2} [\underline{U}_S e^{j(\omega_1 t - \gamma)} + \underline{U}_S^* e^{-j(\omega_1 t - \gamma)}] , \quad \gamma = \frac{2\pi}{3} \end{aligned} \quad (10.43b)$$

$$\begin{aligned} u_{S3}(t) &= u_{S1} \left( t - \frac{2\gamma}{\omega_1} \right) \\ &= \frac{\sqrt{2}}{2} [\underline{U}_S e^{j(\omega_1 t - 2\gamma)} + \underline{U}_S^* e^{-j(\omega_1 t - 2\gamma)}] . \end{aligned} \quad (10.43c)$$

The voltage phasor  $\underline{U}_S$  is a complex constant, having a magnitude equal to the RMS line-to-neutral voltage and an arbitrary phase angle  $\tau_1$  which may be set at will because it is defined by the chosen instant for time zero.

When the complex voltage vector according to Eq. (10.25) is formed, a very simple result is obtained,

$$\underline{u}_S(t) = u_{S1} + u_{S2} e^{j\gamma} + u_{S3} e^{j2\gamma} = \frac{3\sqrt{2}}{2} \underline{U}_S e^{j\omega_1 t} ; \quad (10.44)$$

the conjugate complex part drops out, leaving a vector with constant magnitude and constant angular velocity. Hence the vector describes a circular path around the origin.

The stator and rotor currents too form symmetrical three-phase systems in steady state. With

$$i_{S1}(t) = \frac{\sqrt{2}}{2} [I_S e^{j\omega_1 t} + I_S^* e^{-j\omega_1 t}] , \quad \text{etc.}$$

we find

$$\underline{i}_S(t) = \frac{3\sqrt{2}}{2} I_S e^{j\omega_1 t} , \quad (10.45)$$

where the current phasor  $\underline{I}_S$  is still to be determined. A similar definition exists for the rotor currents oscillating with slip frequency  $\omega_2 = \omega_1 - \omega$

$$i_{R1}(t) = \frac{\sqrt{2}}{2} [I_R e^{j(\omega_1 - \omega)t} + I_R^* e^{-j(\omega_1 - \omega)t}] , \quad \text{etc.}$$

which results in

$$\underline{i}_R(t) = \frac{3\sqrt{2}}{2} I_R e^{j(\omega_1 - \omega)t} . \quad (10.46)$$

The rotor current in stator coordinates is, with  $\varepsilon = \omega t$  because of constant speed,

$$\underline{i}_R(t) e^{j\varepsilon(t)} = \frac{3\sqrt{2}}{2} I_R e^{j\omega_1 t} . \quad (10.47)$$

Hence the rotor current wave, moving with slip frequency across the rotor surface, rotates in synchronism with the stator current wave; this is a precondition for constant electrical torque. By introducing these expressions into Eqs. (10.38, 10.39) and omitting the redundant terms, the differential equations are converted to algebraic equations for the phasors

$$\begin{aligned} (R_S + j\omega_1 \sigma_S L_0) \underline{I}_S + j\omega_1 L_0 (\underline{I}_S + \underline{I}_R) &= \underline{U}_S \\ (R_R + j\omega_2 \sigma_R L_0) \underline{I}_R + j\omega_2 L_0 (\underline{I}_S + \underline{I}_R) &= 0 . \end{aligned} \quad (10.48)$$

Normalising the second equation by the slip

$$S = \frac{\omega_2}{\omega_1} = \frac{\omega_1 - \omega}{\omega_1} \quad (10.49)$$

results in

$$\left( \frac{R_R}{S} + j\omega_1 \sigma_R L_0 \right) \underline{I}_R + j\omega_1 L_0 (\underline{I}_S + \underline{I}_R) = 0 . \quad (10.50)$$

Equations (10.48, 10.50) lead immediately to the familiar single phase equivalent circuit seen in Fig. 10.7 a; its validity is restricted, however, to steady state, assuming sinusoidal symmetrical currents and constant load torque.

By inspecting the equivalent circuit in Fig. 10.7a, the stator impedance per phase is derived. It may be written in the form

$$Z_S = R_S + j\omega_1 L_S \frac{1 + j \frac{S\omega_1 \sigma R_R}{R_R}}{1 + j \frac{S\omega_1 L_R}{R_R}} , \quad (10.51)$$

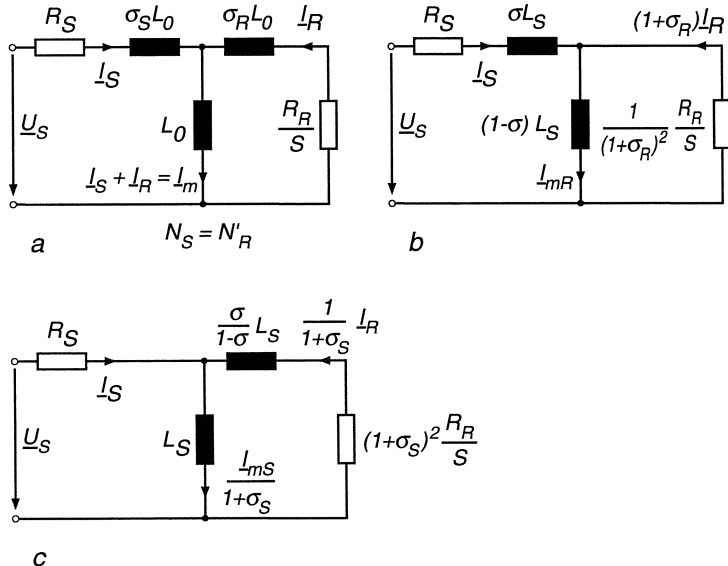


Fig. 10.7. Single phase equivalent circuits of induction motor in steady state.

- with leakage inductances on stator and rotor side,
- with leakage inductance on stator side,
- with leakage inductance on rotor side

where

$$\sigma = 1 - \frac{1}{(1 + \sigma_S)(1 + \sigma_R)} \quad (10.52)$$

is the total leakage factor of the motor, which bears an important influence on the characteristics of the machine; it is chosen by suitable design parameters such as the shape of the slots and the length of the airgap. Normal values of  $\sigma$  range between 0.05 for low leakage machines to about 0.20.

The expression in Eq. (10.51) gives rise to the definition of yet another parameter

$$S_p = \frac{R_R}{\omega_1 \sigma L_R} = \frac{1}{\omega_1 \sigma T_R}, \quad T_R = \frac{L_R}{R_R}, \quad (10.53)$$

which is called pull-out slip because the motor with zero stator resistance produces maximum torque at  $S = S_p$ , as will be shown later. The pull-out slip of normal medium size motors is  $S_p < 0.25$ .

The steady state equivalent circuit in Fig. 10.7a contains three inductances which, because of  $L_m = L_S + L_R$ , do not represent independent energy storages. Hence the circuit diagram can be redrawn with only two inductances. One possibility is shown in Fig. 10.7 b, where all the leakage is concentrated on the stator side. There is a different fictitious rotor resistance leading to different currents in the right hand side branches of the circuit but the stator impedances

are identical. The new synthetic magnetising current  $I_{mR}$  represents the rotor flux, as will be shown in a later chapter. A third equivalent circuit is seen in Fig. 10.7 c, where all the leakage is referred to the rotor side and where  $I_{ms}$  represents the stator flux. This arrangement may also be used for designing controls.

The stator current is now computed with the added simplification  $R_S = 0$  which is of little significance with larger machines operating at line frequency. Thus the normalised expression for the stator current phasor becomes

$$\underline{I}_S = \frac{\underline{U}_S}{j \omega_1 L_S} \frac{1 + j \frac{1}{\sigma} \frac{S}{S_p}}{1 + j \frac{S}{S_p}}, \quad (10.54)$$

which is a linear complex function mapping the real  $S/S_p$ -axis onto the  $\underline{I}_S$ -plane. According to the rules of conformal mapping, the result is a circular locus, the circle diagram, also called Ossanna's or Heyland's circle. This is confirmed by the following transformation

$$\begin{aligned} \underline{I}_S &= \underline{I}_{S0} \left[ \frac{1 + \sigma}{2\sigma} - \frac{1 - \sigma}{2\sigma} \frac{1 - j \frac{S}{S_p}}{1 + j \frac{S}{S_p}} \right] \\ &= \underline{I}_{S0} \left[ \frac{1 + \sigma}{2\sigma} - \frac{1 - \sigma}{2\sigma} e^{-j 2 \arctan S/S_p} \right], \end{aligned} \quad (10.55)$$

where

$$\underline{I}_{S0} = \frac{\underline{U}_S}{j \omega_1 L_S} \quad (10.56)$$

is the ideal no load current valid for  $S = 0$ , i.e. when the rotor moves synchronously with the revolving stator field. When no speed difference exists, no rotor current will be induced and there is no torque; hence the no-load current is a purely reactive magnetising current. This is confirmed by the equivalent circuits in Fig. 10.7 for  $S = 0$ .

The complex locus  $\underline{I}_S(S/S_p)$  is depicted in Fig. 10.8 with the voltage phasor assumed imaginary,  $\underline{U}_S = j \underline{U}_S$ , in order to place the circle in the customary position. The curve covers the full range  $-\infty < S/S_p < \infty$ ; for  $S > 0$  the motor runs below synchronism, drawing active power, while for  $S < 0$  it operates as a generator supplying active power to the line. Reactive power for magnetisation is always necessary; this is a characteristic of induction machines having no internal voltage source which is present in synchronous machines. At  $S = 0$  the current assumes its minimum value representing (for  $R_S = 0$ ) the no-load magnetising current as mentioned before.

Minimum phase shift  $\varphi = \arg(\underline{U}_S, \underline{I}_S)$ , i.e. maximum power factor is reached when the current phasor forms a tangent to the circle. The optimal power factor then follows from the geometrical relations of Fig. 10.8,

$$\cos \varphi_r = \frac{1 - \sigma}{1 + \sigma}; \quad (10.57)$$

this is usually defined as the nominal or rated operating point. The pertinent value of  $S_r/S_p$  is obtained by deriving the phase angle from Eq. (10.54),

$$\varphi = \frac{\pi}{2} - \arctan \frac{1}{\sigma} \frac{S}{S_p} + \arctan \frac{S}{S_p} . \quad (10.58)$$

The minimal value is found by differentiation,  $\frac{d\varphi}{d(S/S_p)} = 0$ ; the result is

$$\frac{S_r}{S_p} = \sqrt{\sigma} . \quad (10.59)$$

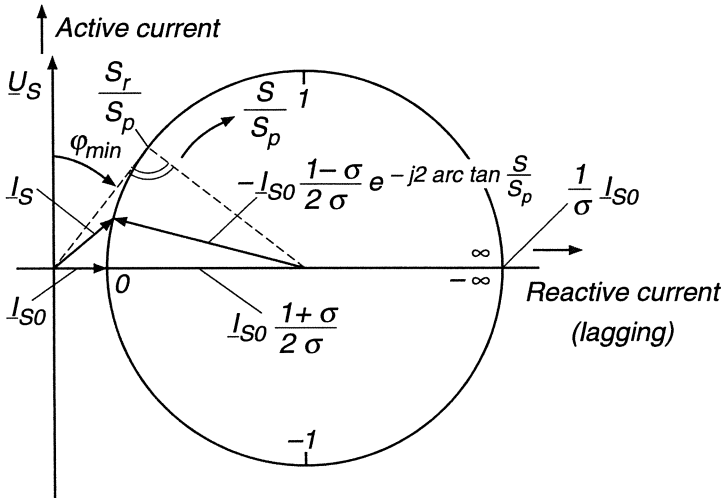


**Fig. 10.8.** Locus of stator current with stator resistance neglected, circle diagram for an induction motor

Hence, not only the geometry of the current locus, but also the maximum power factor, the pull-out slip and the normalised slip at rated operating point are all determined by the leakage factor  $\sigma$ . The magnitude of the normalised stator current,

$$\frac{I_S}{I_{S0}} = \frac{\sqrt{1 + \left(\frac{1}{\sigma} \frac{S}{S_p}\right)^2}}{\sqrt{1 + \left(\frac{S}{S_p}\right)^2}} \quad (10.60)$$

is an even function of slip, as seen in Fig. 10.9 a. The normal operating region comprises only the central portion of the curve. At larger values of slip, for example, when starting the motor at  $S = 1$ , the current rises sharply so that the simplifications employed become rather dubious. This is particularly true for the iron saturation that is not negligible at high currents.

The stator current at rated slip,  $S_r/S_p = \sqrt{\sigma}$ , is

$$\frac{I_{Sr}}{I_{S0}} = \frac{1}{\sqrt{\sigma}} , \quad (10.61)$$

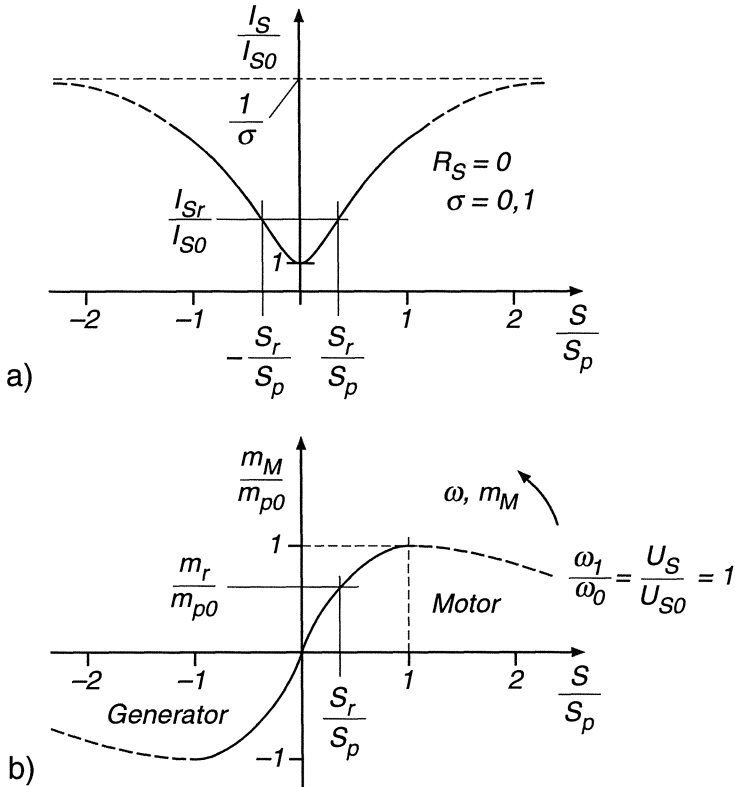


Fig. 10.9. Stator current and torque as a function of slip ( $R_S = 0$ )

while the asymptotic value of the current is

$$\lim_{S \rightarrow \infty} \frac{I_S}{I_{S0}} = \frac{1}{\sigma}. \quad (10.62)$$

This underlines the importance of the leakage factor  $\sigma$  as a design parameter.

The maximum and minimum values of the active current and active power, assuming  $U_S = \text{const.}$ , are reached at  $S = \pm S_p$ , i.e. in the vertices of the circle. In the next section it will be shown that these are also the points where the torque assumes its peak values.

### 10.2.2 Steady State Torque, Efficiency

An expression for the steady state torque is obtained by inserting the vectors for sinusoidal symmetrical currents, Eqs. (10.45, 10.47), into the general formula for the torque, Eq. (10.36),

$$m_M = 3 L_0 \operatorname{Im} (\underline{I}_S \underline{I}_R^*), \quad (10.63)$$

yielding a constant value, as expected. From Fig. 10.7 a the following relation between stator- and rotor-current is derived,

$$\underline{I}_R = \frac{-j \omega_1 L_0}{R_R/S + j \omega_1 L_R} \underline{I}_S , \quad (10.64)$$

which leads to

$$m_M = 3 L_0 I_S^2 \operatorname{Im} \left[ \frac{j \omega_1 L_0}{R_R/S - j \omega_1 L_R} \right] .$$

With the help of Eq. (10.60) this can be rearranged to

$$m_M = \frac{3}{2} \frac{1-\sigma}{\sigma} \frac{U_S^2}{\omega_1^2 L_S} \frac{2}{S/S_p + S_p/S} = m_p \frac{2}{S/S_p + S_p/S} , \quad (10.65)$$

where  $m_p$  represents the peak torque, available at the pull-out slip  $S = \pm S_p$ . The function of torque vs. normalised slip is plotted in Fig. 10.9 b.

When the induction motor is part of a variable speed drive, the stator voltage  $U_S$  and frequency  $\omega_1$  may differ from their rated values  $U_{S0}$ ,  $\omega_0$  indicated on the nameplate; hence the following extension of Eq. (10.65) applies

$$m_M = m_{p0} \left( \frac{U_S/\omega_1}{U_{S0}/\omega_0} \right)^2 \frac{2}{S/S_p + S_p/S} , \quad (10.66)$$

where

$$m_{p0} = \frac{3}{2} \frac{1-\sigma}{\sigma} \frac{U_{S0}^2}{\omega_0^2 L_S} \quad (10.67)$$

is the maximum torque (for  $R_S = 0$ ) at rated voltage and frequency. This indicates that the torque rises with the square of the flux; the reason for this is of course that the rotor current, being caused by magnetic induction, is also a linear function of flux.

The torque vs. slip curve seen in Fig. 10.9 b may be qualitatively described as follows:

When the rotor speed deviates from the angular velocity  $\omega_1$  of the stator field, currents are induced in the rotor winding producing a torque with the tendency of reducing the speed difference. Below synchronism ( $S > 0$ ) the torque acts in the direction of the rotating field, i.e. the machine operates between standstill and synchronous speed as motor; above synchronous speed, the torque is opposed to the direction of rotation, hence the machine acts as generator, feeding electrical power to the line. Thus steady state supersynchronous speed can only occur if the machine is mechanically driven. Because of the reactive power problem, induction generators are rarely used except in small unattended hydro or wind power stations, but temporary regeneration is a normal feature of controlled AC drives.

The occurrence of a peak torque can be explained by a simplified model of the rotor circuit as shown in Fig. 10.10. The rotor may be represented by a  $R-L$ -circuit that is supplied from a voltage source, the amplitude  $U_2$  of which is proportional to frequency  $\omega_2$ . The current phasor

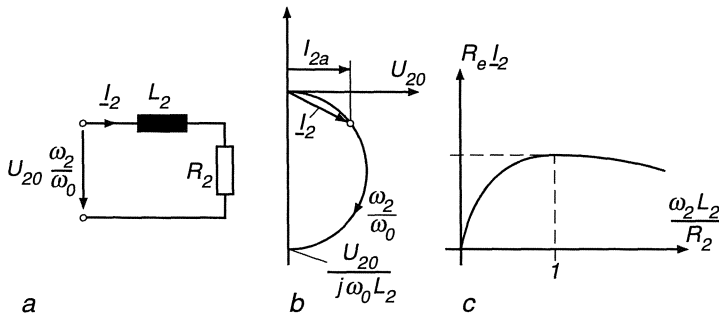


**Fig. 10.10.** Simplified model of rotor circuit.

- a) Circuit;
- b) Locus of current phasor;
- c) Real current component

$$I_2 = \frac{U_{20} \frac{\omega_2}{\omega_0}}{R_2 + j \omega_2 L_2} = \frac{U_{20}}{j \omega_0 L_2} \frac{1}{1 - j \frac{R_2}{\omega_2 L_2}}$$

as a function of frequency  $\omega_2$  is described by the semicircle shown in Fig. 10.10 b. While the magnitude  $I_2$  rises asymptotically with  $\omega_2$ , the active component

$$\text{Re } I_2 = \frac{U_{20}}{\omega_0 L_2} \frac{1}{\frac{R_2}{\omega_2 L_2} + \frac{\omega_2 L_2}{R_2}}$$

passes through a peak value; the curve, which is plotted in Fig. 10.10 c, is of a similar shape as the torque characteristic depicted in Fig. 10.9 b.

This similarity points to the reason for the decreasing torque of the induction motor at higher slip frequency. Due to the rotor leakage, the rotor current is increasingly lagging, causing the rotor current wave to be shifted and eventually become orthogonal to the stator flux wave. Hence the torque is reduced whereas the stator and rotor currents continue to increase asymptotically.

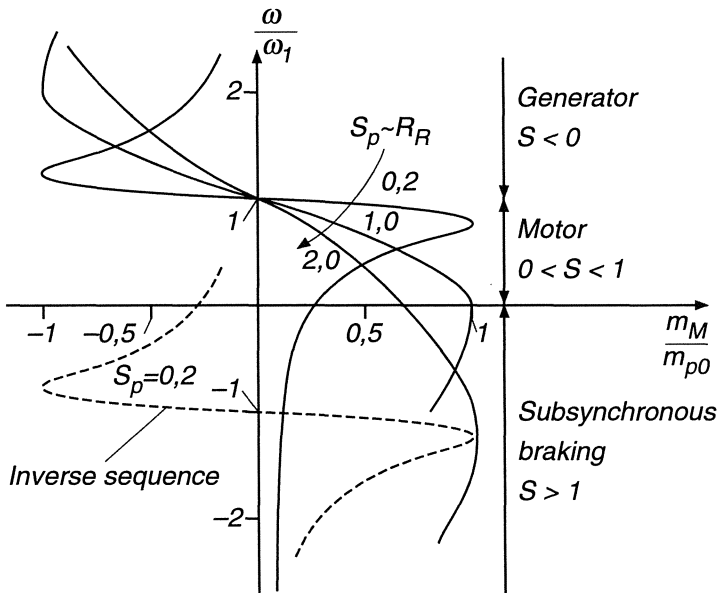
In view of the stability of the drive and the rising losses, steady state operation of the motor makes only sense below pull-out slip.

When declaring the point, where the power factor is optimal, as the rated operating point,  $S_r/S_p = \sqrt{\sigma}$ , the ratio of the peak to rated torque is

$$\frac{m_{p0}}{m_r} = \frac{1 + \sigma}{2\sqrt{\sigma}}, \quad (10.68)$$

which is a measure for the overload capacity of the motor. The torque, Eq. (10.65), shows that the rotor resistance has no effect on the maximum torque but only influences the pull-out slip. A wound rotor motor with external resistors in the rotor circuit then offers a possibility of modifying the speed torque characteristics by changing the pull-out slip  $S_p$  through the rotor resistance. The resulting family of curves is depicted in Fig. 10.11 in the accustomed orientation. In combination with the dashed curves for inverse rotation of the

field by interchanging two stator terminals a fairly complete coverage of the four quadrants of the speed-torque plane is achieved, albeit the shape of some curves is unfavourable due to the steep or even negative slope. Lowering the stator voltages, for instance through a step transformer, reduces the peak torque by the square of the voltage reduction, thus compressing the curves further in horizontal direction.



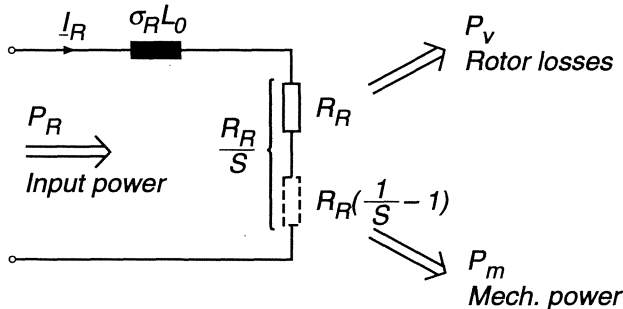
$$\frac{\omega_1}{\omega_0} = \frac{U_S}{U_{S0}}, R_S = 0$$

Fig. 10.11. Torque-speed curves of a wound rotor induction motor

The main objection against continuous speed control by rotor resistors or by reducing the stator voltages is the decrease in efficiency. Only for short time duty, for instance when starting the motor or with crane hoist applications, are these losses tolerable; simple control schemes of this type are in widespread use.

The efficiency of the simplified symmetrically fed induction machine in steady state operation may be assessed as follows: Because of the neglected iron and stator copper losses the active power  $P_S$  supplied to the stator windings is passed on to the rotor, where it is transformed into mechanical power and heat losses. In the steady state equivalent circuit (Fig. 10.7 a) all this power is dissipated in the synthetic resistance  $R_R/S$ ,

$$P_R = 3 I_R^2 \frac{R_R}{S} .$$



**Fig. 10.12.** Power balance in the rotor

In reality the resistance in each rotor phase is only  $R_R$ , hence the difference in power must correspond to mechanical power that cannot be modelled directly by a static circuit (Fig. 10.12),

$$P_m = 3 I_R^2 R_R \left[ \frac{1}{S} - 1 \right] = 3 I_R^2 R_R \frac{1 - S}{S} .$$

This provides an estimate for the efficiency in the motoring region,  $0 < S < 1$ ,

$$\eta_m = \frac{P_m}{P_R} = 1 - S = \frac{\omega}{\omega_1} < 1 , \quad (10.69)$$

as well as for operation as a generator,  $S < 0$ ,

$$\eta_g = \frac{P_R}{P_m} = \frac{1}{1 - S} = \frac{\omega_1}{\omega} < 1 . \quad (10.70)$$

This means that the efficiency even of an idealised motor is lowered in proportion to speed, independent of whether the reduction in speed is caused by additional rotor resistors or by reduced stator voltage. A similar situation exists in the generation region, where the losses rise also with the magnitude of the slip. With a real motor, having primary copper losses as well as iron and friction losses, the efficiency will drop below this upper limit.

This offers the explanation that the induction motor functions like a mechanical clutch, where the product of the speed difference and torque represents an unavoidable power loss.

With high slip control schemes for short duty drives the main problem is the dissipation of the rotor heat loss. In this respect a wound rotor motor with external rotor resistors is preferable, however at the cost of moving contacts. The definition of efficiency in the braking region at reverse speed,  $S > 1$ , does not make sense, because electrical as well as mechanical power is supplied to the rotor and converted to heat.

These considerations give ample evidence that an efficient adjustable speed AC drive can only be realised when either the slip power is recovered by some means or the stator frequency  $\omega_1$  is changed to track the mechanical speed, thus restricting the rotor frequency to small values.

### 10.2.3 Comparison with Practical Motor Designs

The simplified theory of a symmetrical induction motor in steady state contains the total leakage factor  $\sigma$  as the most influential parameter of the machine. As was mentioned before,  $\sigma$  depends on the shape of the slots and increases with the airgap.

The scale of the circular current locus is determined by the ideal no-load current  $I_{S0}$  which also depends to a large extent on the airgap. For mechanical reasons, the airgap is larger with multipole- than two pole-machines of equal power.

The scale of the normalised slip-torque curve, finally, is fixed by the pull-out slip  $S_p$  and the peak torque  $m_p$ ; in the interest of good efficiency in steady state,  $S_p$  should be as small as possible. The peak torque is also affected by the leakage factor.

In Table 10.2 some of the characteristic parameters obtained with the simplified model are compared to those of standard motors, which have been taken from manufacturers lists for medium size ( $> 100$  kW) 50 Hz motors, for a two pole- and an eight pole-machine. The comparison indicates a fairly close agreement, at least from the standpoint of the user.

**Table 10.2.** Comparison of model with actual motor parameters

	Model for $\sigma = 0.05$	Real $n_0 = 3000$ 1/min	Model for $\sigma = 0.1$	Real $n_0 = 750$ 1/min
$\frac{S_r}{S_p}$	$\sqrt{\sigma} = 0.22$	0.20	0.32	0.30
$\frac{I_{S0}}{I_{Sr}}$	$\sqrt{\sigma} = 0.22$	0.30	0.32	0.40
$\cos \varphi_r$	$\frac{1 - \sigma}{1 + \sigma} = 0.90$	0.90	0.82	0.84
$\frac{m_{p0}}{m_r}$	$\frac{1 + \sigma}{2\sqrt{\sigma}} = 2.35$	2.30	1.82	2.0

### 10.2.4 Starting of the Induction Motor

When selecting suitable values for efficiency, power factor and overload capacity at the rated operating point, the starting performance of the motor is unsatisfactory; this is apparent from Fig. 10.13, where characteristic variables of a motor with a leakage factor  $\sigma = 0.05$  are plotted against normalised slip. The conditions for acceptable performance at the rated operating point are:

- a) The rated normalised slip should be about  $S_r/S_p \approx \sqrt{\sigma}$  in order to achieve a good power factor and adequate overload capacity.

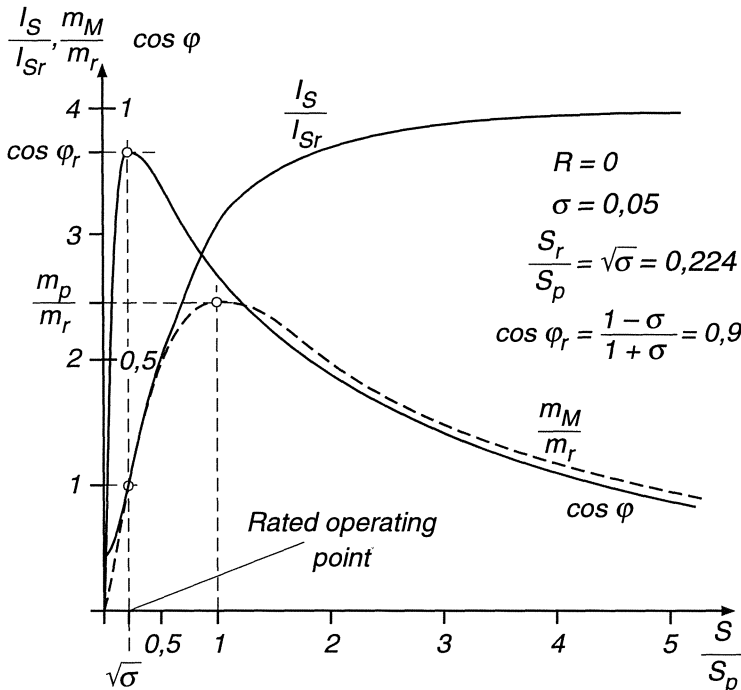


**Fig. 10.13.** Characteristic curves of induction motor with constant rotor resistance

- b) The need for good efficiency  $\eta_r < 1 - S_r$  calls for a minimal value of rated and, hence, pull-out slip. With motors above 100 kW, a rated slip  $S_r \approx 0.02$  is realisable; the pull-out slip would then be about  $S_p \approx 0.10$ .

This means that an induction motor with a short circuited, constant resistance rotor would have to start from standstill ( $S = 1$ ) at  $S/S_p \approx 10$  which corresponds to an operating point at the far right of the circular diagram, Fig. 10.8. The starting performance at  $S = 1$ , characterised by

$$\frac{I_S}{I_{Sr}} \approx \frac{1}{\sqrt{\sigma}} \approx 4.5, \quad \cos \varphi \approx 0.095, \quad \frac{m}{m_r} \approx 0.47,$$

would be very poor, since low torque is combined with a large predominantly reactive current. When the motor is fed from a grid with relatively high internal impedance, there would be an appreciable voltage drop, reducing the current linearly but the torque with the square of the voltage. This may even lead to a situation where the motor does not start under load; the protective devices would then have to disconnect it from the line in order to prevent damage due to overheating. The conditions are particularly severe in small grids such as on board ship, where the generators are not orders of magnitude larger than the largest motors; this also calls for fast voltage control of the generators. Two options are available in order to improve the starting performance:

- a) Use of a motor with wound instead of a cage rotor which permits the rotor resistance and, hence, the pull-out slip  $S_p$  to be temporarily increased at will, creating optimal conditions for starting as well as rated speed. The rotor resistance may be shorted in steps by contactors controlled in a fixed time sequence or depending on stator current or speed. The larger part of the power losses during start occurs in the starting resistor, i.e. outside the motor, so that there are no additional cooling problems. When the operating speed has been reached, the slip-rings can be shorted internally with a special mechanism while the brushes are lifted in order to avoid the unnecessary friction and wear. A motor with  $\sigma = 0.05$ , starting with  $S_p = 1.0$  would show the following starting performance at  $S = 1$

$$\frac{I_S}{I_{Sr}} \approx 3.2, \quad \cos \varphi \approx 0.66, \quad \frac{m}{m_r} \approx 2.35,$$

signifying a decisive improvement over the case with a short circuited rotor winding. With larger motors the starting resistor may have the form of a tank of water with enhanced conductivity into which the electrodes connected to the sliprings are progressively submerged.

- b) A more elegant method requiring no moving contacts is the utilisation of eddy currents in the rotor bars leading to a concentration of the current in the outer portions of the conductors at higher rotor frequency (skin effect), thus increasing the effective rotor resistance at higher slip. As a consequence, the starting torque is improved with an accompanying reduction of current, while in normal operation at low slip the desirable features of the motor with short circuited rotor are maintained.

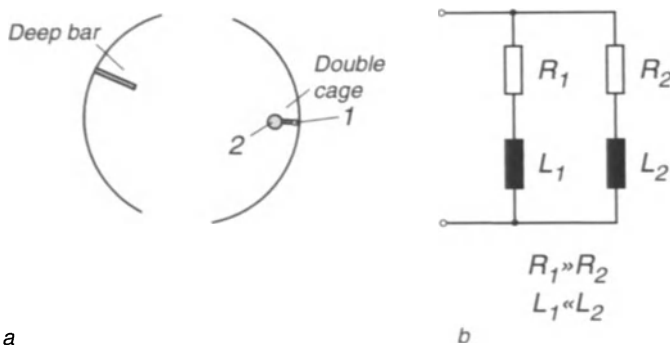


**Fig. 10.14.** Cross section of eddy current rotors and equivalent circuit

There are various designs which tend to emphasise the effect of eddy currents in the rotor bars. One solution employing two cage windings is shown in Fig. 10.14 a. The starting cage (1), being of higher resistivity, is placed in open slots immediately below the rotor surface and exhibits low magnetic leakage; as a

consequence this winding produces a high pull-out slip  $S_{p1}$ . Because of the low leakage this winding dominates at high rotor frequency, i.e. at low speed.

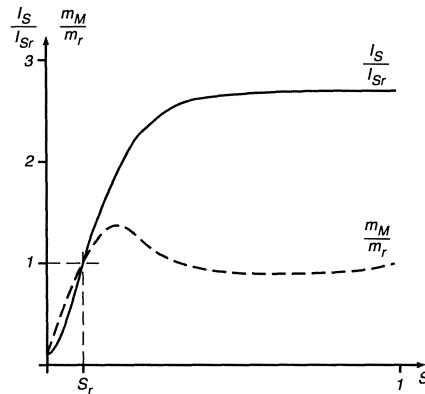


**Fig. 10.15.** Characteristic curves of induction motor with eddy current rotor

The operational rotor winding (2), in contrast, is characterised by a larger cross section of the conductors, possibly employing material of lower resistivity; the leakage reactance is increased because the bars are now embedded in the rotor iron. Clearly, this winding becomes mainly effective at low slip frequency. Figure 10.14 b shows the equivalent circuit with the two rotor windings connected in parallel.

Because of  $R_1 \gg R_2$ ,  $L_1 \ll L_2$  the two windings are complementary. The current locus of the machine is, of course, no longer a circle. In Fig. 10.15 some typical curves of an induction motor with double cage rotor are depicted; a comparison with Fig. 10.13 gives indications of the improvements achieved. Another design of a rotor winding with strong eddy-current effect is a cage with narrow bars extending deep into the rotor iron; this is also shown in Fig. 10.14 a.

When line-starting larger motors it is sometimes necessary to reduce the inrush current by lowering the stator voltages or by using only part of the stator winding, thus increasing the leakage factor. In both cases the starting torque is further reduced which restricts this method to starts with light load. The simplest possibility for reducing the voltage during the start is, of course, a  $\text{Y}/\Delta$ -reconnection of the stator windings. It entails a reduction of voltage and current by  $1/\sqrt{3}$  and of input power and torque by  $1/3$ .

### 10.3 Induction Motor with Impressed Voltages of Arbitrary Waveforms

After this discussion of the steady state with sinusoidal symmetrical three phase voltages let us now return to the more general model of the symmetrical induction motor for dynamic conditions, where torque and speed are varying.

We assume that the stator is supplied by impressed voltages having, in principle, variable frequency and arbitrary waveform, as long as Eq. (10.28) is fulfilled. In fact, due to the isolated neutral point of the motor, even a violation of this condition would be of no consequence; it would simply mean that the neutral of the windings assumes a different potential as the neutral of the supply voltages  $u_{S1}$ ,  $u_{S2}$ ,  $u_{S3}$ . Also, the results may be generalised to a supply having constant and equal internal impedances in each phase; they could simply be included in the stator impedances ( $R_S$ ,  $\sigma_S L_0$ ) of the motor.

Should the motor be fed with sinusoidal symmetrical three-phase voltages of constant frequency and loaded with constant torque, the transients will eventually decay and the steady state condition discussed in Sect. 10.2 will emerge, where all quantities in the stator are periodic functions with the angular frequency  $\omega_1$ . A better insight into the dynamic behaviour of the machine is obtained by choosing a moving system of coordinates, where these steady state oscillations disappear.

A suitable choice of coordinate system, independent of the waveform of the voltages, is that defined by the vector of stator voltages, Eq. (10.25),

$$\underline{u}_S(t) = u_{S1}(t) + u_{S2}(t) e^{j\gamma} + u_{S3}(t) e^{j2\gamma} = u_S(t) e^{j\lambda(t)} ; \quad (10.71)$$

its instantaneous angular velocity

$$\omega_1(t) = \frac{d\lambda}{dt} \quad (10.72)$$

corresponds to the angular frequency of the stator voltages. Should the motor be supplied with sinusoidal symmetrical three phase voltages of constant frequency and amplitude, Eq. (10.44) again becomes valid

$$\underline{u}_S(t) = \frac{3\sqrt{2}}{2} U_S e^{j(\omega_1 t + \tau_1)} , \quad (10.73)$$

resulting in

$$u_S(t) = \frac{3\sqrt{2}}{2} U_S , \quad \lambda(t) = \omega_1 t + \tau_1 , \quad (10.74)$$

where  $U_S$  is the RMS line-to-neutral voltage.

All electrical variables are now defined in this coordinate system; i.e. they are transformed as they appear to a fictitious moving observer positioned at angle  $\lambda(t)$ ; by making use of Eqs. (10.5, 10.8) we define

$$\underline{i}_S(t) e^{-j\lambda} = i_S(t) e^{j(\zeta - \lambda)} = {}^1\underline{i}_S(t) \quad (10.75)$$

and

$$\underline{i}_R(t) e^{j\epsilon} e^{-j\lambda} = i_R(t) e^{j(\xi + \epsilon - \lambda)} = {}^1\underline{i}_R(t) \quad (10.76)$$

as the current vectors in moving coordinates. With sinusoidal symmetrical three phase stator voltages of fixed frequency and constant load torque, these quantities are constant in steady state. When multiplying Eq. (10.38) by  $e^{-j\lambda}$  we find

$$R_S \underline{i}_S e^{-j\lambda} + L_S \frac{d\underline{i}_S}{dt} e^{-j\lambda} + L_0 \frac{d}{dt} (\underline{i}_R e^{j\varepsilon}) e^{-j\lambda} = \underline{u}_S e^{-j\lambda}, \quad (10.77)$$

which may be transformed by substitution.

Developing the expression

$$\frac{d^1 \underline{i}_S}{dt} = \frac{d}{dt} (\underline{i}_S e^{-j\lambda}) = \frac{d\underline{i}_S}{dt} e^{-j\lambda} - j \frac{d\lambda}{dt} \underline{i}_S e^{-j\lambda},$$

results in

$$\frac{d\underline{i}_S}{dt} e^{-j\lambda} = \frac{d^1 \underline{i}_S}{dt} + j \omega_1 {}^1 \underline{i}_S \quad (10.78)$$

and correspondingly

$$\frac{d(\underline{i}_R e^{j\varepsilon})}{dt} e^{-j\lambda} = \frac{d^1 \underline{i}_R}{dt} + j \omega_1 {}^1 \underline{i}_R. \quad (10.79)$$

By inserting Eqs. (10.78, 10.79) into Eq. (10.77), the stator voltage equation in the moving reference frame results,

$$R_S {}^1 \underline{i}_S + \frac{d}{dt} (L_S {}^1 \underline{i}_S + L_0 {}^1 \underline{i}_R) + j \omega_1 (L_S {}^1 \underline{i}_S + L_0 {}^1 \underline{i}_R) = \underline{u}_S(t). \quad (10.80)$$

The rotor voltage equation (10.39) is transformed accordingly, with  $\underline{u}_R(t) \equiv 0$ ,

$$R_R {}^1 \underline{i}_R + \frac{d}{dt} (L_R {}^1 \underline{i}_R + L_0 {}^1 \underline{i}_S) + j (\omega_1 - \omega) (L_R {}^1 \underline{i}_R + L_0 {}^1 \underline{i}_S) = 0. \quad (10.81)$$

These equations may be simplified by substituting the flux vectors, defined in Eqs. (10.19, 10.23) which are also transformed into moving coordinates,

$${}^1 \underline{\psi}_S = \underline{\psi}_S e^{-j\lambda} = L_S {}^1 \underline{i}_S + L_0 {}^1 \underline{i}_R, \quad (10.82)$$

$${}^1 \underline{\psi}_R = \underline{\psi}_R e^{j(\varepsilon-\lambda)} = L_R {}^1 \underline{i}_R + L_0 {}^1 \underline{i}_S. \quad (10.83)$$

Hence the current vectors are

$${}^1 \underline{i}_S = \frac{1}{\sigma L_S} \left( {}^1 \underline{\psi}_S - \frac{1}{1 + \sigma_R} {}^1 \underline{\psi}_R \right), \quad (10.84)$$

$${}^1 \underline{i}_R = \frac{1}{\sigma L_R} \left( {}^1 \underline{\psi}_R - \frac{1}{1 + \sigma_S} {}^1 \underline{\psi}_S \right). \quad (10.85)$$

Inserting Eqs. (10.82 – 10.85) into Eqs. (10.80, 10.81) results in

$$T'_S \frac{d^1 \underline{\psi}_S}{dt} + [1 + j \omega_1 T'_S] {}^1 \underline{\psi}_S - \frac{1}{1 + \sigma_R} {}^1 \underline{\psi}_R = T'_S \underline{u}_S(t), \quad (10.86)$$

$$T'_R \frac{d^1 \underline{\psi}_R}{dt} + [1 + j (\omega_1 - \omega) T'_R] {}^1 \underline{\psi}_R - \frac{1}{1 + \sigma_S} {}^1 \underline{\psi}_S = 0, \quad (10.87)$$

where

$$T'_S = \frac{\sigma L_S}{R_S}, \quad T'_R = \frac{\sigma L_R}{R_R} \quad (10.88)$$

are transient time constants.

The expression for the electrical torque, derived in Sect. 10.1, can be written in the form

$$m_M(t) = \frac{2}{3} L_0 \operatorname{Im} \left[ \underline{i}_S (\underline{i}_R e^{j\omega t})^* \right] = \frac{2}{3} L_0 \operatorname{Im} \left[ {}^1\underline{i}_S ({}^1\underline{i}_R)^* \right],$$

because the inverse transformations with  $e^{j\lambda}$  are cancelling. Hence, using Eqs. (10.84, 10.85) we have

$$m_M(t) = \frac{2}{3} \frac{L_0}{\sigma^2 L_S L_R} \operatorname{Im} \left[ \left( {}^1\underline{\psi}_S - \frac{1}{1 + \sigma_R} {}^1\underline{\psi}_R \right) \left( {}^1\underline{\psi}_R - \frac{1}{1 + \sigma_S} {}^1\underline{\psi}_S \right)^* \right].$$

Considering that only the mixed terms of the product contribute to the imaginary part, this reduces to

$$\begin{aligned} m_M(t) &= \frac{2}{3} \frac{L_0}{\sigma^2 L_S L_R} \operatorname{Im} \left[ {}^1\underline{\psi}_S {}^1\underline{\psi}_R^* + \frac{1}{(1 + \sigma_S)(1 + \sigma_R)} {}^1\underline{\psi}_R {}^1\underline{\psi}_S^* \right] \\ &= \frac{2}{3} \frac{1 - \sigma}{\sigma} \frac{1}{L_0} \operatorname{Im} \left[ {}^1\underline{\psi}_S {}^1\underline{\psi}_R^* \right], \end{aligned} \quad (10.89)$$

which can be inserted in Eqs. (10.40, 10.41) for the mechanical motion.

In order to arrive at dimensionless real equations, the transformed flux vectors are now normalised and split in real and imaginary parts, representing the components that are parallel ( $x$ ) and orthogonal ( $y$ ) to the voltage vector. The flux linkages in steady state operation with rated sinusoidal voltages, nominal frequency, as indicated on the nameplate, and neglected stator resistance serve as flux references,

$${}^1\underline{\psi}_S(t) = \frac{3\sqrt{2}}{2} \frac{U_{S0}}{\omega_0} [x_S(t) + j y_S(t)], \quad (10.90)$$

$${}^1\underline{\psi}_R(t) = \frac{3\sqrt{2}}{2} \frac{U_{S0}}{\omega_0} [x_R(t) + j y_R(t)]. \quad (10.91)$$

The magnitude of the voltage vector in Eq. (10.74) is also referred to the magnitude at nominal operating conditions,

$$u_S(t) = \frac{3\sqrt{2}}{2} U_{S0} \frac{U_S(t)}{U_{S0}}. \quad (10.92)$$

It is noted, however, that no restrictions with regard to waveform or frequency of the stator voltages have been imposed so far.

With these definitions the voltage equations (10.86, 10.87) and the expression for the torque (10.89) assume the following form

$$\begin{aligned} T'_S \frac{d}{dt} (x_S + j y_S) + [1 + j \omega_1 T'_S] (x_S + j y_S) \\ - \frac{1}{1 + \sigma_R} (x_R + j y_R) = \omega_0 T'_S \frac{U_S}{U_{S0}}, \end{aligned} \quad (10.93)$$

$$\begin{aligned} T'_R \frac{d}{dt} (x_R + j y_R) + [1 + j (\omega_1 - \omega) T'_R] (x_R + j y_R) \\ - \frac{1}{1 + \sigma_S} (x_S + j y_S) = 0, \end{aligned} \quad (10.94)$$

$$m_M = 2 (1 + \sigma_S) m_{p0} (y_S x_R - x_S y_R), \quad (10.95)$$

where  $m_{p0}$  is the nominal peak torque for  $R_S = 0$ , as defined in Eq. (10.67). With the following abbreviations for

$$\text{Pull-out slip at nominal frequency and } R_S = 0 \quad S_{pR} = \frac{R_R}{\omega_0 \sigma L_R} = \frac{1}{\omega_0 T'_R}, \quad (10.96)$$

$$\text{Pull-out slip of rotor-fed motor, nominal frequency and } R_R = 0 \quad S_{pS} = \frac{R_S}{\omega_0 \sigma L_S} = \frac{1}{\omega_0 T'_S}, \quad (10.97)$$

$$\text{Mechanical time constant} \quad T_m = \frac{J \omega_0}{m_{p0}}, \quad (10.98)$$

and the instantaneous normalised frequencies

$$\text{stator frequency} \quad \frac{\omega_1}{\omega_0},$$

$$\text{mechanical rotational frequency (speed)} \quad \frac{\omega}{\omega_0},$$

$$\text{rotor frequency} \quad \frac{\omega_2}{\omega_0} = \frac{\omega_1 - \omega}{\omega_0}, \quad (10.99)$$

six real differential equations emerge for the direct and quadrature flux components as well as motor speed and position.

$$T'_S \frac{dx_S}{dt} = -x_S + \frac{1}{S_{pS}} \frac{\omega_1}{\omega_0} y_S + \frac{1}{1 + \sigma_R} x_R + \frac{1}{S_{pS}} \frac{U_S(t)}{U_{S0}} \quad (10.100a)$$

$$T'_S \frac{dy_S}{dt} = -\frac{1}{S_{pS}} \frac{\omega_1}{\omega_0} x_S - y_S + \frac{1}{1 + \sigma_R} y_R, \quad (10.100b)$$

$$T'_R \frac{dx_R}{dt} = \frac{1}{1 + \sigma_S} x_S - x_R + \frac{1}{S_{pR}} \frac{\omega_2}{\omega_0} y_R, \quad (10.100c)$$

$$T'_R \frac{dy_R}{dt} = \frac{1}{1 + \sigma_S} y_S - \frac{1}{S_{pR}} \frac{\omega_2}{\omega_0} x_R - y_R, \quad (10.100d)$$

$$T_m \frac{d(\frac{\omega}{\omega_0})}{dt} = 2 (1 + \sigma_S) (y_S x_R - x_S y_R) - \frac{m_L}{m_{p0}} (\omega, \varepsilon, t), \quad (10.100e)$$

$$\frac{\varepsilon_0}{\omega_0} \frac{d(\frac{\varepsilon}{\varepsilon_0})}{dt} = \frac{\omega}{\omega_0}. \quad (10.100f)$$

$\varepsilon_0$  is an arbitrary angle of reference.

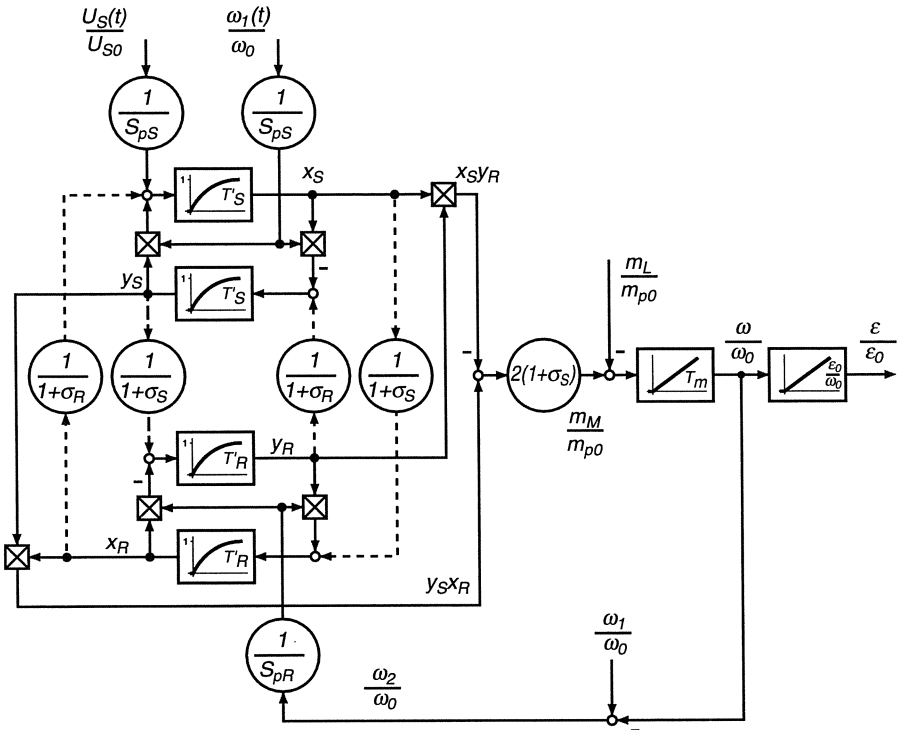


**Fig. 10.16.** Block diagram of symmetrical induction motor fed by impressed voltages of arbitrary wave form

These equations may be represented in graphical form by the block diagram in Fig. 10.16, where the integrators with feedback are redrawn to form unity gain lag elements. Due to the rotational symmetry of the machine the angles  $\varepsilon(t)$ ,  $\lambda(t)$  do not enter the right hand side of the model equations (10.100 a – f) with the exception of load torque  $m_L$  that may depend on the mechanical angle.

The block diagram describes the dynamic behaviour of the symmetrical motor, fed by impressed stator voltages independent of waveform; the magnitude  $u_S(t)$  of the voltage vector is given by Eq. (10.92), its instantaneous angular frequency  $\omega_1(t)$  by Eq. (10.72). As special case with  $U_S = \text{const.}$ ,  $\omega_1 = d\lambda/dt = \text{const.}$ , the transient condition of the motor operating on the symmetrical three phase supply results, where  $U_S$  is the RMS value of the line-to-neutral voltages.

Because of the transformation into the voltage based coordinate system moving with stator frequency, the steady state values of the flux components and speed, assuming constant load torque, are constant. The steady state values are derived by setting the derivatives in Eqs. (10.100 a – e) equal to zero; the

resulting system of algebraic equations is equivalent to the results obtained in Sect. 10.2.

Of course, under dynamic conditions the flux components are no longer constant because there may be transient flux waves which are linked to the stator or rotor windings and, hence, move with the angular velocity  $\omega_1$  or  $\omega_2 = \omega_1 - \omega$  relative to the coordinate system, where they appear as AC components of appropriate frequencies; as a result there are torque and speed variations.

When inspecting the general structure of Fig. 10.16 it is recognised that it can be reduced to the form shown in Fig. 10.17 which reminds one of a DC machine (Fig. 5.9). The generation of the electric torque  $m_M$  is now much more involved, which is due to the fact that the currents in the rotor winding are magnetically induced rather than impressed through a galvanic contact; also, the angle between the stator- and rotor-ampereturn waves depends on the operating condition, whereas it is essentially fixed by the field- and armature-axes in the case of the DC machine. The presence of AC quantities also tends to blur the view, even though this has been alleviated by the coordinate transformation.

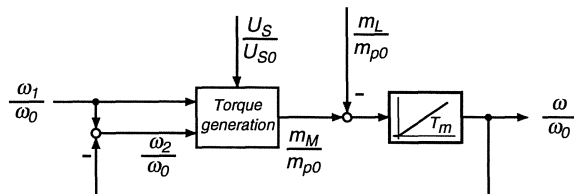


**Fig. 10.17.** Simplified block diagram of symmetrical induction motor

While no analytical solution of the nonlinear differential equations exists, some of the interactions contained in Fig. 10.16 can be qualitatively explained. For example, two feedback loops are recognisable, one belonging to the stator and the other to the rotor, that contain multiplications by  $\omega_1/\omega_0$  and  $\omega_2/\omega_0$  respectively. When neglecting for a moment the cross couplings drawn in dotted lines, a homogeneous second order equation may be gained describing the flux components, for instance in the stator; by eliminating  $y_S$  we find

$$T'_S \frac{d^2 x_S}{dt^2} + 2 T'_S \frac{dx_S}{dt} + \left[ 1 + \frac{1}{S_{pS}^2} \left( \frac{\omega_1}{\omega_0} \right)^2 \right] x_S = 0 , \quad (10.101)$$

with the eigenvalues

$$s_{1,2} = \omega_0 \left( -S_{pS} \pm j \frac{\omega_1}{\omega_0} \right) ; \quad (10.102)$$

hence the pertinent transient is a damped oscillation with the angular frequency  $\omega_1$ , belonging to a flux wave that is linked to the stator winding and thus remains fixed in space. The damping is achieved by the dynamic short circuit through the voltage source at the stator terminals.

Likewise the lower feedback circuit is found to be described by a differential equation with the eigenvalues

$$s_{3,4} = \omega_0 \left( -S_{pR} \pm j \frac{\omega_2}{\omega_0} \right) . \quad (10.103)$$

The associated physical effect is a flux wave linked to the rotor winding which moves with slip frequency relative to the coordinate axis.

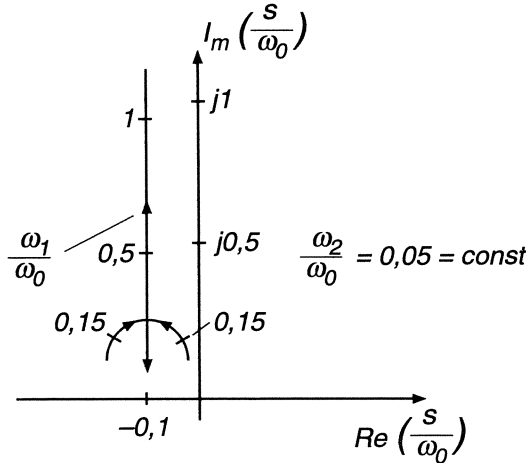


**Fig. 10.18.** Root locus of induction machine for  $\omega_2 = 0.05 = \text{const.}$  at different stator frequencies and speeds

Considering now the special case  $\omega_1 = \omega_2 = 0$ , when the mechanically locked motor is fed with direct voltage, and taking the dotted cross-couplings into account, two new non-interacting feedback loops are formed, where each embraces stator and rotor. The differential equations for transients in the  $x$ -axis may be combined to

$$T'_S T'_R \frac{d^2 x_S}{dt^2} + (T'_S + T'_R) \frac{dx_S}{dt} + \sigma x_S = 0 . \quad (10.104)$$

Both eigenvalues are negative real, belonging to aperiodic transients; a corresponding equation is valid for the quadrature axis of the machine. Clearly these equations correspond to those of two-winding transformers, describing the decoupled magnetic interactions in the two axes of the machine; under the assumed test conditions and in view of the voltage-based coordinate system, the flux in the quadrature axis must be zero,  $y_S = y_R = 0$ , hence there is no torque. This is in agreement with the practical experience of a symmetrical induction motor with DC excitation at standstill.

When analysing the block diagram in Fig. 10.16 more closely, i.e. for  $\omega_1, \omega_2 \neq 0$ , the mutual interactions of the two damped oscillators, coupled directly and through the speed, must be taken into account. This leads to a complicated resonant system of 6th order, the response of which is difficult to assess. However, assuming  $\omega_1 = \text{const.}$  and  $\omega_2 \approx \text{const.}$ , i.e. large inertia, there

are considerable simplifications because the multiplications with  $\omega_1$ ,  $\omega_2$  are reduced to constant factors; assuming complete symmetry between stator and rotor,

$$S_{pS} = S_{pR} = S_p, \quad \sigma_S = \sigma_R = \sigma_0, \quad T'_S = T'_R = T_0,$$

the characteristic equation pertaining to Eqs. (10.100 a – d) becomes

$$\left[ (T_0 s + 1)^2 - (1 - \sigma) + \frac{1}{S_p^2} \left( \frac{\omega_1}{\omega_0} \right)^2 \right] \left[ (T_0 s + 1)^2 - (1 - \sigma) + \frac{1}{S_p^2} \left( \frac{\omega_2}{\omega_0} \right)^2 \right] + \frac{1 - \sigma}{S_p^2} \frac{(\omega_1 + \omega_2)^2}{\omega_0^2} = 0. \quad (10.105)$$

The solutions of this equation, i.e. the eigenvalues of the system, have been computed numerically for different values of stator frequency  $\omega_1$ , assuming the following parameters

$$S_p = 0.10, \quad \sigma = 0.08, \quad \frac{\omega_2}{\omega_0} = 0.05 = \text{const.}$$

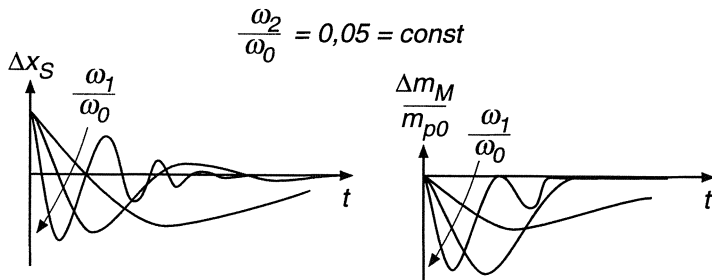


**Fig. 10.19.** Flux and torque transients for  $\omega_2 = 0.05 = \text{const.}$  at different stator frequencies and speeds

The result is plotted in Fig. 10.18 in the form of a root locus in the complex  $s$ -plane, omitting the conjugate branch of the locus. The shape of the curve indicates that there is little interaction between the two oscillators in Fig. 10.16 for  $\omega_1 \gg \omega_2$ , approximately leading to the “decoupled” eigenvalues mentioned before; on the other hand, the interactions are strong at low values of the stator frequency,  $\omega_1 \approx \omega_2$ , resulting in slowly decaying transients. Figure 10.19 depicts the decay of a flux component at different stator frequencies but assuming the same initial conditions; the transient torque is also displayed; there is a remarkable effect of stator frequency and speed on the dynamic behaviour of the nonlinear plant. Therefore the induction machine, when operated in a wide speed range, represents a very difficult control plant, which calls for special control procedures; some will be discussed in Chap. 12.

As a qualitative test for the validity of the mathematical model of the induction machine, which was derived with considerable simplifications, a line start

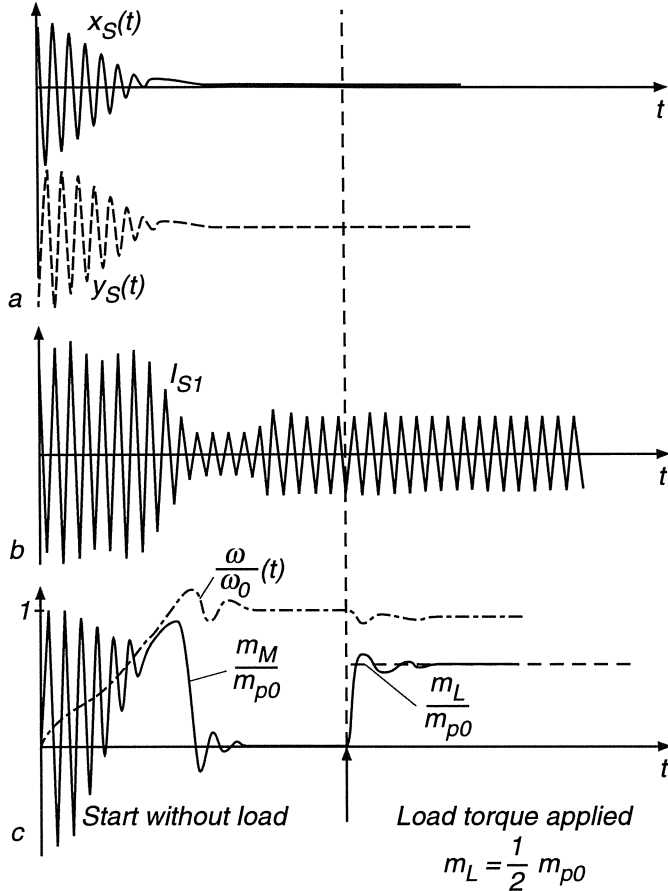


**Fig. 10.20.** Starting transient of induction motor with low value of inertia (computed results)

at nominal voltage and frequency has been computed by numerical integration of Eqs. (10.100 a – e); the load torque is initially zero but, after steady state speed has been reached, half the peak torque is applied as load. The results are plotted in Fig. 10.20, assuming a low value of inertia so that the start is completed in a few periods of line voltage; the other parameters were the same as before.

Besides the flux components in direct and quadrature direction, the stator currents are of main interest. The associated vector is produced by inverse transformation with the help of Eqs. (10.84, 10.85)

$$i_S(t) = {}^1i_S e^{j\omega_1 t} = \frac{1}{\sigma L_S} \left[ {}^1\psi_S(t) - \frac{1}{1 + \sigma_R} {}^1\psi_R \right] e^{j\omega_1 t}$$

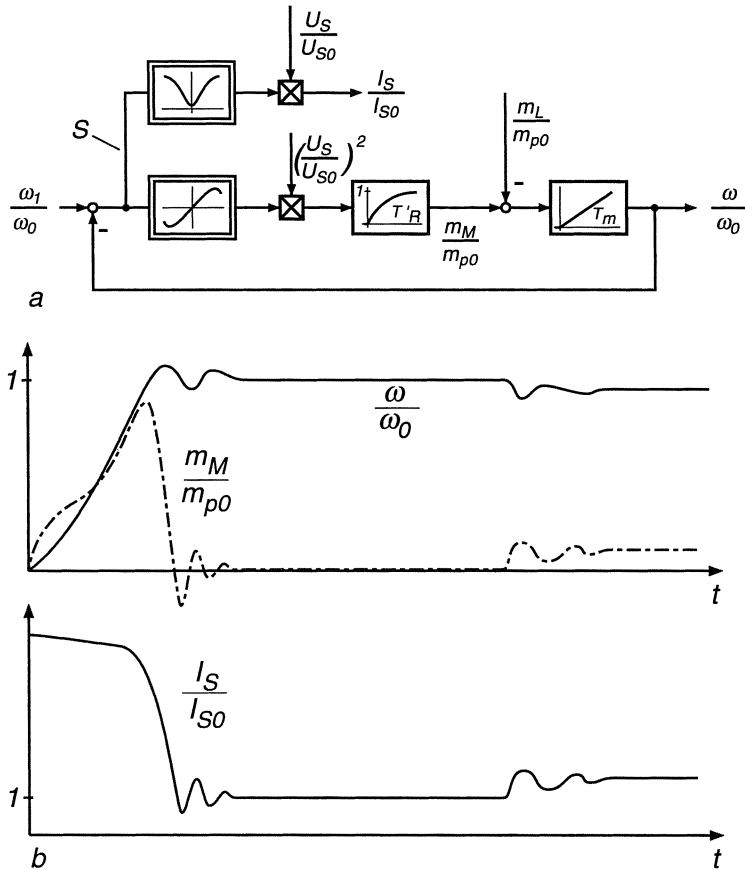


**Fig. 10.21.** (a) Simplified block diagram of induction machine,  
(b) calculated transients

$$= \frac{3\sqrt{2}}{2} \frac{U_{S0}}{\omega_0 \sigma L_S} \left[ \left( x_S - \frac{1}{1 + \sigma_R} x_R \right) + j \left( y_S - \frac{1}{1 + \sigma_R} y_R \right) \right] e^{j\omega_1 t}. \quad (10.106)$$

With Eq. (10.42 a) it follows

$$\begin{aligned} i_{S1}(t) &= \frac{2}{3} \operatorname{Re}[i_S(t)] \\ &= \sqrt{2} \frac{U_{S0}}{\omega_0 \sigma L_S} \left[ \left( x_S - \frac{1}{1 + \sigma_R} x_R \right) \cos \omega_1 t - \left( y_S - \frac{1}{1 + \sigma_R} y_R \right) \sin \omega_1 t \right]. \end{aligned} \quad (10.107)$$

This current is also plotted in Fig. 10.20; it shows the characteristic high inrush value which, as the motor approaches synchronism, settles down to the small sinusoidal no-load current until the load torque is applied; the currents in the other stator phases are similar.

There are strong alternating components of torque which also affect the speed, even though, because of the inertia, with reduced amplitude. If the inertia is predominantly concentrated on the load side, the shaft and the mechanical coupling may be severely stressed during the start. The speed, as a function of time, follows a similar curve as obtained in Sect. 3.2 when the electrical transients were totally ignored (Fig. 3.13); this explains also the absence of the overshoot in speed which is present in Fig. 10.20.

As an intermediate step between the quasi-steady-state model and the complete model of the induction motor, the heuristic block diagram in Fig. 10.21 a is sometimes helpful. It differs from the purely mechanical model by the inclusion of a lag  $T'_R$ , following the steady-state torque-slip-function. For small values of slip, where the torque function is linear, this clearly resembles the block diagram of a DC machine. A comparison of the starting transient computed with this model shows good qualitative agreement with the transients obtained by integrating the Eqs. (10.100 a – e). Of course, the oscillations superimposed on speed and torque cannot be present but the mean values are well modelled.

## 10.4 Induction Motor with Unsymmetrical Line Voltages in steady State

### 10.4.1 Symmetrical Components

For intermittent duty drives, such as cranes or hoists, where simplicity of hardware is more important than high efficiency, induction motors with unsymmetrical voltage supply may be used. By way of example, a phasor diagram of sinusoidal but unsymmetrical line-to-neutral voltages is shown in Fig. 10.22 a. Due to the isolated neutral of the symmetrical stator winding, the sum of the instantaneous phase voltages is still zero, Eq. (10.28); hence the phasor diagram forms a closed triangle,

$$\underline{U}_{S1} + \underline{U}_{S2} + \underline{U}_{S3} = 0. \quad (10.108)$$

The same holds of course, if the stator windings are  $\Delta$ -connected.

It is known, that an unsymmetrical three phase system may be decomposed into “symmetrical components” defined by

$$\begin{aligned} \underline{U}_{S1} &= \underline{U}_{S+} + \underline{U}_{S-} + \underline{U}_0, \\ \underline{U}_{S2} &= e^{-j\gamma} \underline{U}_{S+} + e^{j\gamma} \underline{U}_{S-} + \underline{U}_0, \quad \gamma = \frac{2\pi}{3}, \\ \underline{U}_{S3} &= e^{j\gamma} \underline{U}_{S+} + e^{-j\gamma} \underline{U}_{S-} + \underline{U}_0, \end{aligned} \quad (10.109)$$

where  $\underline{U}_{S+}$  is the positive-,  $\underline{U}_{S-}$  the negative- and  $\underline{U}_0$  the zero-sequence voltage component per phase. The symmetrical components  $\underline{U}_{S+}$ ,  $\underline{U}_{S-}$  form two symmetrical three-phase systems of opposite phase-sequence. Solving Eq. (10.109) yields

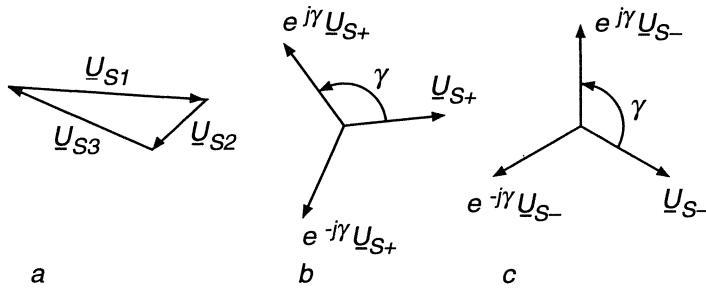


**Fig. 10.22.** Decomposition of unsymmetrical balanced three phase system into symmetrical components

$$\begin{aligned}\underline{U}_{S+} &= \frac{1}{3} [\underline{U}_{S1} + e^{j\gamma} \underline{U}_{S2} + e^{-j\gamma} \underline{U}_{S3}] , \\ \underline{U}_{S-} &= \frac{1}{3} [\underline{U}_{S1} + e^{-j\gamma} \underline{U}_{S2} + e^{j\gamma} \underline{U}_{S3}] , \\ \underline{U}_{S0} &= \frac{1}{3} [\underline{U}_{S1} + \underline{U}_{S2} + \underline{U}_{S3}] = 0 .\end{aligned}\quad (10.110)$$

Since the voltages between the motor terminals and the isolated neutral are not directly available (the motor may be  $\Delta$ -connected), it is appropriate to introduce the line-to-line voltages instead. By expanding Eq. (10.110 a) we find

$$\begin{aligned}\underline{U}_{S+} &= \frac{1}{3} [\underbrace{\underline{U}_{S1} - \underline{U}_{S2}}_{\underline{U}_{12}} - e^{-j\gamma} (\underbrace{\underline{U}_{S2} - \underline{U}_{S3}}_{\underline{U}_{23}}) + \underline{U}_{S2} (1 + e^{j\gamma} + e^{-j\gamma})] \\ &= \frac{1}{3} [\underline{U}_{12} - e^{-j\gamma} \underline{U}_{23}]\end{aligned}\quad (10.111a)$$

and similarly

$$\underline{U}_{S-} = \frac{1}{3} [\underline{U}_{12} - e^{j\gamma} \underline{U}_{23}] . \quad (10.111b)$$

Two of the line-to-line voltages are sufficient to determine the positive and negative sequence components, because

$$\underline{U}_{12} + \underline{U}_{23} + \underline{U}_{31} = 0$$

is valid by definition. Generally the use of line-to-line voltages does not exclude the appearance of an arbitrary zero sequence component, but as seen before, it vanishes with a symmetrical load. If the motor is fed from a line possessing noticeable internal impedance, the symmetrical components of the terminal voltages depend also upon the load, i.e. the operating state of the motor.

Should the voltages  $\underline{U}_{12}$ ,  $\underline{U}_{23}$ ,  $\underline{U}_{31}$  form a symmetrical three-phase system,

$$\underline{U}_{23} = e^{-j\gamma} \underline{U}_{12} ,$$

the result is, of course,

$$\underline{U}_{S+} = \frac{1}{\sqrt{3}} e^{-j\pi/6} \underline{U}_{12} = \underline{U}_{S1} , \quad \underline{U}_{S-} = 0 .$$

The case of a symmetrical induction motor fed by unsymmetrical supply voltages is fully contained in the theory developed in Sect. 10.1 but the subsequent discussion of some examples will be restricted to steady-state.

When forming the time-varying voltage vector according to Eqs. (10.43, 10.44) and with the definition (10.109), we find

$$\underline{u}_S(t) = \frac{3\sqrt{2}}{2} [U_{S+} e^{j\omega_1 t} + U_{S-}^* e^{-j\omega_1 t}], \quad (10.112)$$

a result, that can be interpreted as the superposition of two constant vectors rotating with equal angular velocity in opposite direction; hence the pointer of the vector  $\underline{u}_S(t)$  follows a periodic elliptical path, as shown in Fig. 10.23.

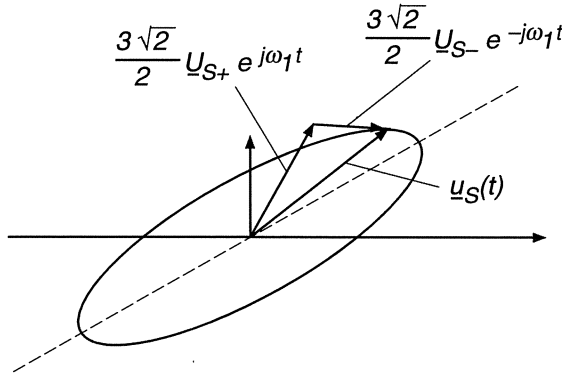


**Fig. 10.23.** Voltage vector of unsymmetrical balanced supply

In steady state, assuming constant speed, similar definitions hold for the vector of the stator currents,

$$\underline{i}_S(t) = \frac{3\sqrt{2}}{2} [I_{S+} e^{j\omega_1 t} + I_{S-}^* e^{-j\omega_1 t}], \quad (10.113)$$

where  $I_{S+}$ ,  $I_{S-}$  are the symmetrical components of the stator currents which are defined in accordance with Eq. (10.109). Likewise the rotor current vector in stator coordinates may be written as

$$\underline{i}_R(t) e^{j\varepsilon} = \frac{3\sqrt{2}}{2} [I_{R+} e^{j\omega_1 t} + I_{R-}^* e^{-j\omega_1 t}], \quad (10.114)$$

while the rotor current vector in rotor coordinates is, with  $d\varepsilon/dt = \omega = \text{const.}$ ,

$$\underline{i}_R(t) = \frac{3\sqrt{2}}{2} [I_{R+} e^{j(\omega_1 - \omega)t} + I_{R-}^* e^{-j(\omega_1 + \omega)t}]. \quad (10.115)$$

The speed  $\omega$  is counted in the direction of the positive sequence field. Hence the frequency of the positive and negative sequence rotor currents is  $\omega_1 - \omega$  and  $\omega_1 + \omega$  respectively.

The physical interpretation of Eqs. (10.113, 10.114) is that of two separate ampereturns waves rotating with  $\pm\omega_1$  in opposite directions and causing corresponding flux density waves in the airgap which in turn induce the voltage components of Eq. (10.112). As long as iron saturation is ignored and the speed may be assumed constant due to a sufficiently large inertia, there is no interaction between the two symmetrical three-phase systems so that linear relations exist between voltage and current components,

$$\underline{I}_{S+} = Y_{S+} \underline{U}_{S+}, \quad \underline{I}_{S-} = Y_{S-} \underline{U}_{S-}, \quad (10.116)$$

where  $Y_{S+}$ ,  $Y_{S-}$  are the positive and negative sequence stator admittances per phase. Because of the effective values of slip for positive and negative sequence components, respectively,

$$\frac{\omega_1 - \omega}{\omega_1} = S \quad \text{and} \quad \frac{\omega_1 + \omega}{\omega_1} = 2 - S, \quad (10.117)$$

the admittances, derived from Eq. (10.54) with  $R_S = 0$ , are

$$\begin{aligned} Y_{S+} &= \frac{1}{j\omega_1 L_S} \frac{1 + j\frac{1}{\sigma} \frac{S}{S_p}}{1 + j\frac{S}{S_p}}, \\ Y_{S-} &= \frac{1}{j\omega_1 L_S} \frac{1 + j\frac{1}{\sigma} \frac{2-S}{S_p}}{1 + j\frac{2-S}{S_p}}. \end{aligned} \quad (10.118)$$

When substituting Eqs. (10.113, 10.114) into the torque equation (10.36), four terms arise, two of which are alternating torque components having the frequency  $2\omega_1$ ; contributions to the mean torque come only from interactions between stator and rotor currents of the same sequence; hence the mean torque, counted in positive sequence direction, is

$$\overline{m_M} = 3L_0 \operatorname{Im} [\underline{I}_{S+} \underline{I}_{R+}^* + \underline{I}_{S-}^* \underline{I}_{R-}] = m_{M+} + m_{M-}. \quad (10.119)$$

These two components of the mean torque may be derived by the same reasoning as shown in Sect. 10.2, because each is produced by a symmetrical three-phase voltage system.

In accordance with Eq. (10.66) we find

$$\begin{aligned} \frac{\overline{m_M}}{m_{p0}} &= \frac{m_{M+}}{m_{p0}} + \frac{m_{M-}}{m_{p0}} \\ &= \frac{2}{\frac{S}{S_p} + \frac{S_p}{S}} \left[ \frac{U_{S+}}{U_{S0}} \frac{\omega_0}{\omega_1} \right]^2 - \frac{2}{\frac{2-S}{S_p} + \frac{S_p}{2-S}} \left[ \frac{U_{S-}}{U_{S0}} \frac{\omega_0}{\omega_1} \right]^2, \end{aligned} \quad (10.120)$$

where  $m_{p0}$  is again the peak torque, Eq. (10.67), at nominal voltage and  $S_p$  the pull-out slip for  $R_S = 0$ , Eq. (10.53).

Equation (10.120) may be interpreted as the net torque produced by two identical motors coupled to the same shaft which are supplied by symmetrical

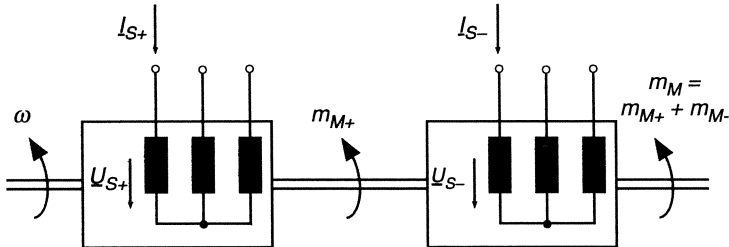


**Fig. 10.24.** Induction motor with unsymmetrical supply voltages, equivalent scheme

three-phase voltage systems  $U_{S+}$ ,  $U_{S-}$  of equal frequency but opposite phase sequence, i.e. with two stator terminals of the second motor interchanged (Fig. 10.24).

Equation (10.120) clearly demonstrates the basic disadvantage of all control schemes employing asymmetrical supply; while the torque is reduced, the power losses are increased by the negative sequence voltage and current components.

By changing the rotor resistance ( $S_p$ ) and with different circuit connections, resulting in speed-dependent positive and negative sequence voltages, a large variety of torque-speed-characteristics can be obtained. This is discussed with the help of three examples.

#### 10.4.2 Single-phase Induction Motor

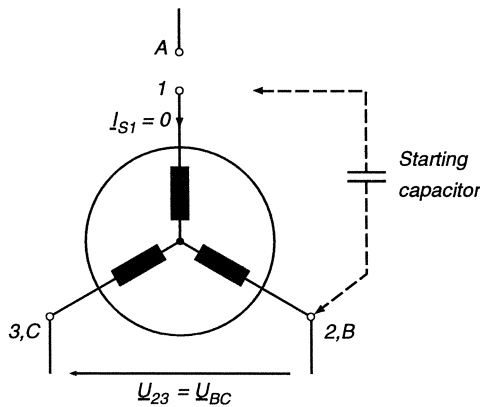


**Fig. 10.25.** Symmetrical induction motor with single phase supply

By disconnecting one stator terminal of a symmetrical induction motor, the single phase circuit in Fig. 10.25 results,  $A$ ,  $B$ ,  $C$  are the terminals of the symmetrical line voltages. The constraint imposed by the open circuit is

$$\underline{I}_{S1} = Y_{S+} \underline{U}_{S+} + Y_{S-} \underline{U}_{S-} = 0 ; \quad (10.121)$$

another condition is derived from Eqs. (10.111),

$$\underline{U}_{S+} - \underline{U}_{S-} = \frac{1}{3} (e^{j\gamma} - e^{-j\gamma}) \underline{U}_{23} = j \frac{1}{\sqrt{3}} \underline{U}_{23} = \underline{U}_{AM} , \quad (10.122)$$

where  $\underline{U}_{AM}$  is the line-to-neutral voltage of the disconnected line-phase. When combining the two equations, we find

$$\begin{aligned} \underline{U}_{S+} &= \frac{Y_{S-}}{Y_{S+} + Y_{S-}} \underline{U}_{AM} = \frac{Z_{S+}}{Z_{S+} + Z_{S-}} \underline{U}_{AM} , \\ \underline{U}_{S-} &= -\frac{Y_{S+}}{Y_{S+} + Y_{S-}} \underline{U}_{AM} = -\frac{Z_{S-}}{Z_{S+} + Z_{S-}} \underline{U}_{AM} , \end{aligned} \quad (10.123)$$

with  $Z_S = 1/Y_S$  being the impedance of a stator phase in symmetrical three-phase operation. The same voltage magnitudes would result if the stator windings of the two coupled motors in Fig. 10.24 were connected in series to the symmetrical three-phase voltages. According to Fig. 10.26 the positive and negative sequence admittances can be taken from the normalised circular diagram (Fig. 10.8), where  $\underline{I}_S/\underline{I}_{S0} = Y_S/Y_{S0}$  was plotted for  $R_S = 0$  as a function of slip. This indicates that a large difference exists between  $Y_{S+} = Y_S(S)$  and  $Y_{S-} = Y_S(2-S)$  for small values of pull-out slip, i.e. for a motor with a cage rotor.

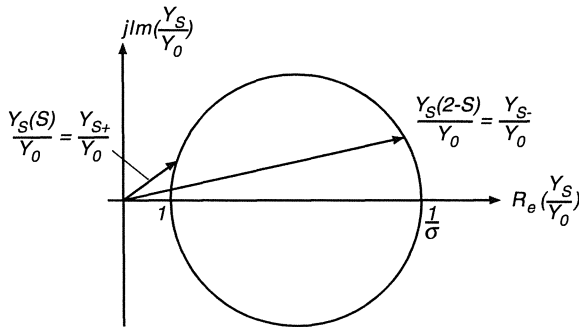


**Fig. 10.26.** Circular diagram showing positive and negative sequence admittance

If the motor operates near the positive synchronous speed ( $S \approx 0$ ),  $|Y_{S+}| \ll |Y_{S-}|$  holds, resulting in  $\underline{U}_{S+} \approx \underline{U}_{AM}$ ,  $\underline{U}_{S-} \approx 0$ . This means that the negative sequence field is almost completely suppressed by the rotor winding due to the large relative speed  $2-S \approx 2$ . Hence the motor operates with nearly symmetrical voltages despite the fact that one terminal is not connected. In the vicinity of the negative synchronous speed the conditions are inverted.

The steady-state torque of the single phase motor is obtained by substituting Eqs. (10.123) into Eq. (10.120)

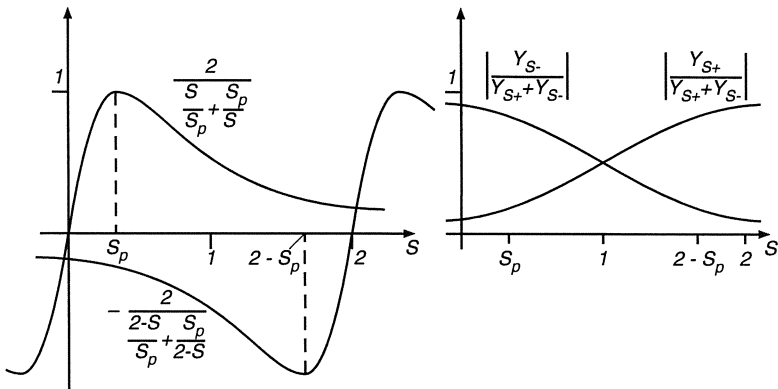


**Fig. 10.27.** Symmetrical components of single-phase motor

$$\frac{\bar{m}_M}{\bar{m}_{p0}} = \left[ \frac{2}{\frac{S}{S_p} + \frac{S_p}{S}} \left| \frac{Y_{S-}}{Y_{S+} + Y_{S-}} \right|^2 - \frac{2}{\frac{2-S}{S_p} + \frac{S_p}{2-S}} \left| \frac{Y_{S+}}{Y_{S+} + Y_{S-}} \right|^2 \right] \left[ \frac{U_{AM}}{U_{S0}} \frac{\omega_0}{\omega_1} \right]^2. \quad (10.124)$$

Since the torque rises with the square of the voltage, the negative sequence torque is even further reduced than the voltage. Some of the functions contained in Eq. (10.124) are sketched in Fig. 10.27; by combining these curves the speed-torque characteristic of the single-phase motor is obtained, drawn in the usual orientation, Fig. 10.28. The curve is symmetrical with respect to the origin because at  $S = 1$ ,  $Y_{S+} = Y_{S-}$  holds and the opposing torque components cancel. Hence the motor develops no net torque at standstill and cannot start without external assistance. If a small motor at standstill is turned manually in either direction, the corresponding sequence prevails and the motor continues to accelerate at light load up to the operating speed.

In order to make the motor self-starting, either some asymmetry has to be built into it, as is done with shaded-pole motors, or a starting capacitor must be connected to the third or an auxiliary winding, as is shown in Fig. 10.25; in both cases the direction of rotation is fixed. The value of the starting torque depends on the design of the auxiliary winding and the capacitor.

Besides the starting problems, the drawbacks of single-phase operation lie in the residual pulsating torque as well as reduced utilisation and efficiency of the motor which are always below that of a symmetrically fed motor. It is for these reasons that single-phase induction motors are only used at low power ratings, for example in household appliances.

#### 10.4.3 Single-phase Electric Brake for AC Crane-Drives

A simple intermittent-duty AC crane-drive required to operate as electric brake in the lowering direction may have the asymmetrical circuit connection shown

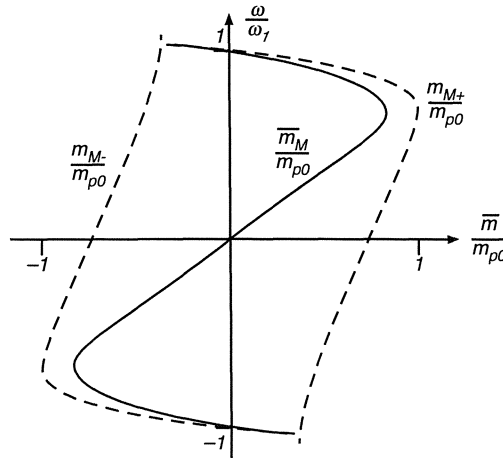


**Fig. 10.28.** Torque-speed characteristic of single-phase motor

in Fig. 10.29, where two stator terminals of a symmetrical wound rotor motor with large rotor resistor are short-circuited while single-phase voltage is applied between the short-circuit connection and the remaining stator terminal [G21]. This is one of several possible connections having similar properties. The analysis of the circuit is easy with the help of symmetrical components.

Introducing the constraints of the circuit

$$\underline{U}_{12} = \underline{U}_{AB}, \quad \underline{U}_{23} = 0$$

into Eqs. (10.111) results in

$$U_{S+} = U_{S-} = \frac{1}{3} U_{AB} = \frac{1}{\sqrt{3}} U_{AM}, \quad (10.125)$$

indicating that the symmetrical voltage components are of equal magnitude, independent of speed. Hence, the two machines in the equivalent circuit (Fig. 10.24) would have to be supplied by constant and equal three-phase voltages with two terminals of one motor interchanged; this renders the superposition of the two opposing torques particularly simple.

The torque curves are depicted in Fig. 10.30 assuming  $S_p = 2.0$  caused by a large external rotor resistor. Due to the reduced voltages the peak torques are only  $\frac{1}{3}$  of the nominal peak torque, hence the motor is again only partially utilised. Since the resulting torque-speed curves lie in quadrants 2 and 4 the drive can only operate as an electric brake, regeneration is not possible with this scheme.

An advantage of this connection, when used as a lowering brake in crane applications, is the fact that the resulting torque-speed curve (a) passes through the origin; unintentional speed reversal (raising) at light load does not occur as

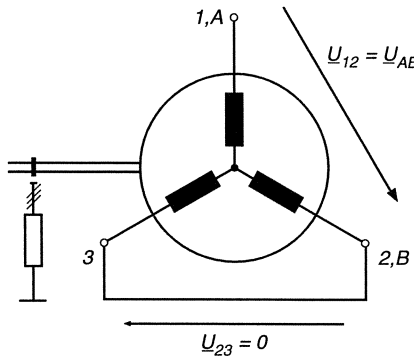


**Fig. 10.29.** AC motor in asymmetrical connection for electric braking duty

would be possible with symmetrical supply and the rotor resistance increased still further.

Similar braking characteristics are obtained with a smaller rotor resistance by feeding the stator winding with direct current (b). The motor then operates like an eddy-current brake.

Finally, Fig. 10.30 also contains the torque-speed curve with symmetrical voltages but inverted sequence and short-circuited rotor resistance (c). This operation allows regeneration, however at higher than synchronous speed in lowering direction. It could be used as the “Full speed, Lowering” set-point of a contactor-controlled AC crane drive.

#### 10.4.4 Unsymmetrical Starting Circuit for Induction Motor

Smooth acceleration during start-up is important in some applications, such as textile machines, where there is a danger of breaking fibre threads; an asymmetrical circuit like the one shown in Fig. 10.31 can provide a simple solution for this problem. An external impedance  $Z_1$  is inserted between a line phase and one of the stator terminals of a symmetrical cage- or wound-rotor induction motor. The circuit depicted in Fig. 10.31 is one of several similar connections. Assuming the impedance  $Z_1$  to be constant, all voltages and currents remain sinusoidal in steady state; with the symmetrical components introduced in Sect. 10.4.1 the following mesh-equations hold:

$$Z_1 I_{S1} + \underline{U}_{12} = \underline{U}_{AB} = (1 - e^{-j\gamma}) \underline{U}_{AM}, \quad (10.126)$$

$$\underline{U}_{23} = \underline{U}_{BC} = (e^{-j\gamma} - e^{j\gamma}) \underline{U}_{AM}. \quad (10.127)$$

The stator current can be expressed by symmetrical components, Eq. (10.121),

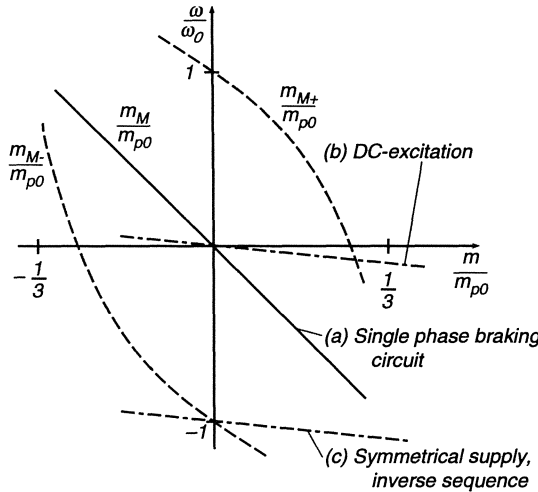


**Fig. 10.30.** Torque-speed curves of AC motor in asymmetrical connection

$$Z_1 \underline{I}_{S1} = Z_1 [Y_{S+} \underline{U}_{S+} + Y_{S-} \underline{U}_{S-}] ;$$

likewise the line-to-line voltages Eqs. (10.109) are

$$\begin{aligned}\underline{U}_{12} &= \underline{U}_{S1} - \underline{U}_{S2} = (1 - e^{-j\gamma}) \underline{U}_{S+} + (1 - e^{j\gamma}) \underline{U}_{S-}, \\ \underline{U}_{23} &= \underline{U}_{S2} - \underline{U}_{S3} = (e^{-j\gamma} - e^{j\gamma}) \underline{U}_{S+} + (e^{j\gamma} - e^{-j\gamma}) \underline{U}_{S-};\end{aligned}$$

substituting these equations into Eqs. (10.126, 10.127) and solving for  $\underline{U}_{S+}$ ,  $\underline{U}_{S-}$  results in

$$\underline{U}_{S+} = \frac{3 + Z_1 Y_{S-}}{3 + Z_1 (Y_{S+} + Y_{S-})} \underline{U}_{AM} , \quad (10.128)$$

$$\underline{U}_{S-} = \frac{-Z_1 Y_{S+}}{3 + Z_1 (Y_{S+} + Y_{S-})} \underline{U}_{AM} , \quad (10.129)$$

which contains the limiting cases of the symmetrically fed motor ( $Z_1 = 0$ ) and the single phase induction motor ( $Z_1 \rightarrow \infty$ ) discussed in the previous paragraph. In general, the positive and negative sequence voltages are complicated functions of the motor admittances which in turn depend on speed and pull-out slip.

The voltage across the series impedance

$$Z_1 \underline{I}_{S1} = Z_1 [Y_{S+} \underline{U}_{S+} + Y_{S-} \underline{U}_{S-}] = -3 \underline{U}_{S-} \quad (10.130)$$

is a measure of the asymmetry of the stator voltages. With these results the phasor diagram of the motor can be drawn for any chosen operating point.

The torque-speed curves may be computed from Eq. (10.120); their shape depends on the impedance  $Z_1$  and the motor parameters, but they lie inside

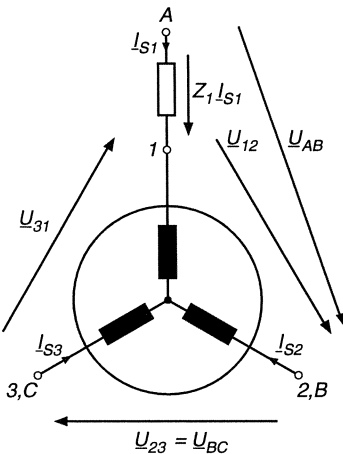


Fig. 10.31. Asymmetrical starting circuit

the area which is bounded by the curves for  $Z_1 = 0$  and  $Z_1 \rightarrow \infty$ . This is qualitatively indicated in Fig. 10.32 for a low-power induction motor having fairly large pull-out slip and assuming a resistive impedance,  $Z_1 = R_1$ . Of course, this and all similar arrangements are associated with additional losses in the external components as well as the motor itself and are only suitable for short duty operation.

The function of the circuit shown in Fig. 10.31 is further illustrated by discussing the phasor diagram of the stator voltages in locked rotor condition. At  $S = 1$  we have  $Y_{S+} = Y_{S-} = Y_S(1)$ . Hence it follows from Eqs. (10.130) with  $Z_1 = R_1$

$$R_1 I_{S1} = \frac{3 R_1 Y_S(1)}{3 + 2 R_1 Y_S(1)} U_{AM}, \quad 0 \leq R_1 < \infty; \quad (10.131)$$

as a limiting case ( $R_1 \rightarrow \infty$ ) this comprises again the single phase motor

$$\lim_{R_1 \rightarrow \infty} (R_1 I_{S1}) = \frac{3}{2} U_{AM},$$

with the phasor diagram of the stator voltages at  $S = 1$  degenerating into a straight line (Fig. 10.33). Equation (10.131) represents a linear function which maps the real  $R_1$ -axis into a circular arc in the complex plane, extending from  $R_1 = 0$  to  $R_1 \rightarrow \infty$ . When the rotor is running,  $0 < S < 1$ , the phasor diagram is reshaped with the tendency of reducing the voltage  $R_1 I_{S1}$ , thus achieving improved symmetry. This corresponds to the situation found with the single-phase motor.

The shaded area  $AR$  of the triangle (Fig. 10.33), formed by the terminal voltages  $U_{12}$ ,  $U_{23}$ ,  $U_{31}$  at standstill ( $S = 1$ ), can be expressed as

$$AR = \frac{1}{2} \operatorname{Im} [U_{23} U_{21}^*], \quad (10.132)$$

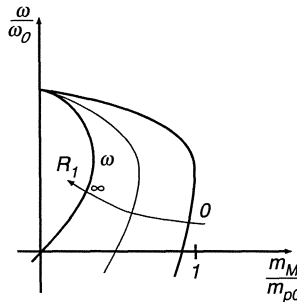


**Fig. 10.32.** Torque–speed curves of unsymmetrical starting circuit for large pull-out slip

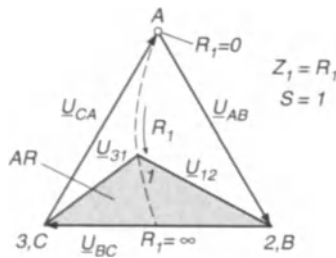


Fig. 10.33. Phasor diagram of asymmetrical circuit at standstill

which by inserting Eqs. (10.111) may be written as

$$AR = k [U_{S+}^2 - U_{S-}^2] . \quad (10.133)$$

Comparison with Eq. (10.120) shows that  $AR$  is a measure of the torque at standstill [25]; it vanishes for  $R_1 \rightarrow \infty$  and assumes its maximum value at  $R_1 = 0$ , i.e. with symmetrical supply.

The circuit shown in Fig. 10.31 can be extended by additional variable impedances to allow continuous speed control, even four-quadrant operation. This has been realised in the past with saturable reactors, the impedance of which could be varied by direct current in specially connected control windings. Because of the high losses these drives were restricted to short duty operation; also the control was rather slow due to the sluggish response of the large reactors, making this type of equipment obsolete today [L25]. A similar control effect, however with greatly reduced size and cost of the components as well as much more rapid response can be achieved by inserting antiparallel thyristors into the stator supply leads of the motor; this causes considerable nonlinear distortion of the motor voltages, resulting in yet increased losses but it may be acceptable in short duty applications.

## 11. Power Supplies for Adjustable Speed AC Drives

An important result of the preceding chapter is that the application of AC motors in continuous duty adjustable speed drives calls for static inverters of adequate power, generating three-phase voltages of variable amplitude and frequency. This is necessary in order to maintain at all speeds a low rotor frequency, which is a precondition for acceptable overall efficiency of the drive. Inverters of this type are available today employing thyristors, including gate turn-off thyristors (GTO), or switched power transistors, but the complexity and cost of the converter equipment and control still exceeds that of line commutated converters of similar rating. While part of the increased cost for the inverter can be recovered by the savings on the AC motor which is considerably less expensive than a DC machine of comparable rating, the overall cost of the AC drive may still be somewhat higher than that of a standard DC drive. Of course, AC drives exhibit a number of important advantages, most conspicuous in the case of an induction motor with cage rotor, that will influence the decision in their favour:

- Power rating and speed of an AC motor is not limited by a mechanical commutator,
- Drive is applicable in explosive and contaminated environment,
- Reduced axial length, volume and weight of an AC motor, as was seen in Fig. 10.1,
- Rugged design, reduced maintenance and service requirements.

The last features are of particular interest with traction and servo drives.

Of course, there are applications at high power and speed, where DC drives cannot be built and only AC drives can provide a solution. Since the cost problems will diminish as the technology matures, it is likely that DC drives will eventually be completely superseded by the more advanced AC drives.

The basic lay-out of an adjustable speed AC drive is shown in Fig. 11.1; it consists of an AC motor, a static converter, which generates a variable voltage, variable frequency AC system and the associated control equipment. The increased complexity of the converter is caused by the fact that inverters with

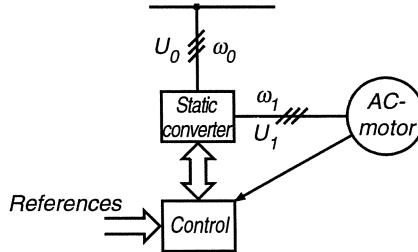


**Fig. 11.1.** General scheme of AC motor control

forced commutation may require additional components and a more complicated mode of operation. Similar arguments apply also to the structure of the inner torque control loop which is much more complex than for a DC-motor. The reason is that an AC-motor with its simple mechanical design represents an involved nonlinear multivariable control plant. The motor must be fed with alternating currents of variable amplitude, frequency and phase; in addition, the rotor currents cannot be measured with ordinary cage motors. This is in contrast to a DC-machine, which has a very simple decoupled control structure but a more complex mechanical design. The mechanical part of the control scheme dealing with speed and position is, of course, the same for DC- and AC-drives.

A characteristic feature of controlled AC- drives is that — once the machine and the commutator have been mechanically separated as shown in Fig. 11.2 — there are many different ways of combining AC-machines and power converters.

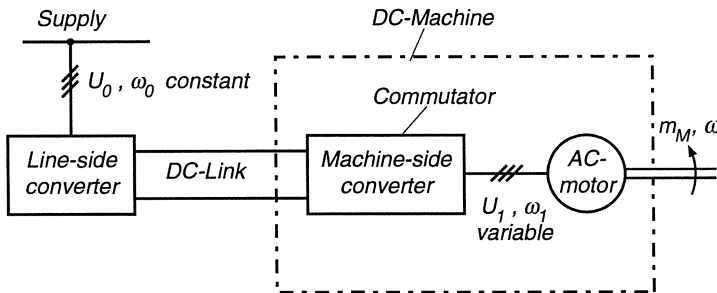


**Fig. 11.2.** Controlled AC-drive with DC-link converter

Table 11.1 presents an overview of controlled AC-drives, showing five basic forms of power electronic converters for changing from the fixed line- to variable motor-frequency. Four of the circuits contain a DC-link for decoupling the two sides of the converter, whereas the cyclo-converter performs this operation in a single conversion stage. All of the converters are adaptable to four quadrant operation, they could also be used with adjustable speed generators. In the vertical column of Table 11.1 five basic types of AC-machines are listed that

may be used for controlled drives; with the exception of the reluctance motor, they can all be treated with the mathematical model derived in Sect. 10.1.

Table 11.1. Synopsis of controlled AC-drive configurations

Converters	DC link converters			Cycloconverters
	Voltage-source converters	Current-source converters	Force-commutated thyristor inverters (GTO)	Naturally-commutated thyristor inverters (with line commutation)
Machines	Transistor inverters (IGBT)	Thyristor inverters (GTO)		
	Low power (10 kW), very good dynamic performance (servo drives)	Medium power (1 MW), high power density		
Reluctance motor		Low to medium power (100 kW)		
Squirrel-cage induction motor	Low to medium power (500 kW), high speed, very good dynamic performance (spindle and servo drives)	Medium to high power (2 MW), good dynamic performance (Traction drives)	Medium to high power (4 MW), high speed	High power (7.5 MW), low speed, very good dynamic performance
Doubly fed slip-ring induction motor		Shaft generators on ships (2 MW)		High power (100 MW), limited speed control range
Synchronous motor with field and damper windings				High power (5 MW), low speed, good dynamic performance

In principle, most of the 25 possible converter-machine combinations could be realised but only those, where comments are entered, are presently employed in practice; since each exhibits particular advantages, it is unlikely that the field will eventually narrow to one or two major circuits as has been the case with DC-drives. In fact, new combinations may be added as new switching devices and converter circuits appear on the scene. An example of the ongoing development are resonant-link converters, presently restricted to low power ap-

plications such as switched mode power supplies; cyclo converters with forced commutation (matrix converters) are also a possible future option. Only a few typical converter schemes that show promise to stay will be discussed in this chapter.

### 11.1 PWM Voltage Source Transistor Inverter Operating at High Switching Frequency

A four quadrant DC/DC converter was shown in Fig. 9.12 which, by adding two more arms, can be extended as seen in Fig. 11.3 to form a three-phase inverter for the supply of AC-motors in the lower and medium power range, from small high dynamic performance servo drives with speed and position control ( $< 10$  kW) to most auxiliary drives in industry, ranging up to several hundred kW. The inverter is suitable for supplying induction as well as synchronous motors.

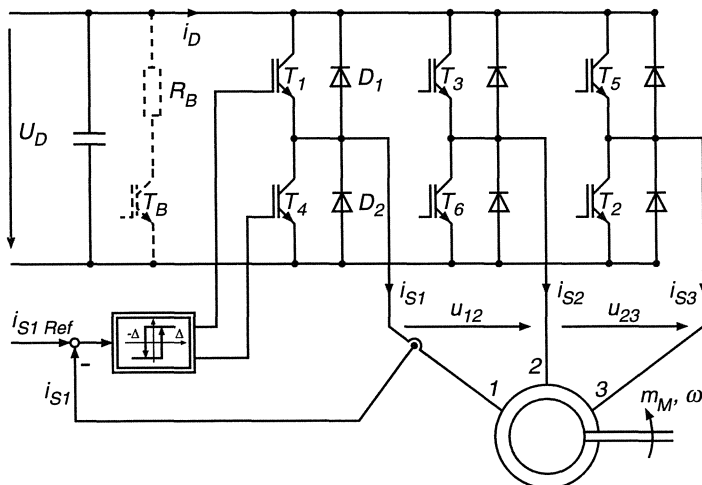


**Fig. 11.3.** Switched IGBT- inverter for three-phase AC motor (simplified circuit)

When the motor, fed from a voltage source inverter, is regenerating, the mean link current  $I_D$  is reversed, calling for a two quadrant power supply. As long as the power level is low or when regeneration occurs only occasionally, for instance during dynamic braking of a servo drive, the reverse power is usually dissipated in a ballast resistor, as indicated in Fig. 11.3 in dashed lines. The pulse-width modulated ballast circuit begins to discharge the link capacitor as soon as the link voltage rises above a preset value. Of course, any other source of direct voltage could also serve for feeding the inverter, for example a battery on an electrically driven vehicle.

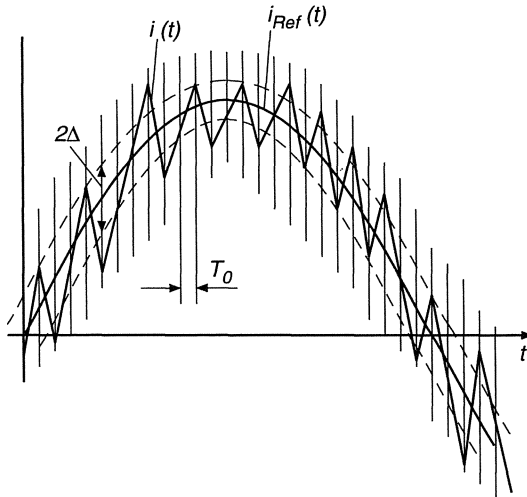
With bipolar transistors, the switching frequency is limited to a few kHz, but with low power Insulated Gate Bipolar Transistors (IGBT), as shown in

Fig. 11.3, or Field Effect Transistors (MOSFET), having a switching time in the order of a microsecond, the mean switching frequency may be above 16 kHz, i.e. beyond the audible range, so that no objectionable acoustic noise is produced by magnetic components. This has the additional advantage that the inverter then exhibits a large bandwidth for control. If the link voltage  $U_D$  is of sufficient magnitude, fast current control loops can be designed which keep the stator currents close to the alternating reference values. This effectively results in near ideal current sources for the stator windings of the motor, thus eliminating the effects of the stator voltage equation (10.38) on the dynamics of the drive; as a consequence, considerable simplification of the control is achieved because the stator voltage interactions are now dealt with by the current controllers. These could either employ pulse-width modulators operating at constant frequency or simple On-Off comparators having a narrow hysteresis band, as indicated in Fig. 11.3. The resulting current waveform with a single-phase load and On-Off-control was shown in Fig. 9.14; it has the advantage of fast response but exhibits variable switching frequency that may be undesirable in view of interference problems.

When extending the principle to three-phase loads, as in Fig. 11.3, the tolerance band is helpful to avoid interactions between the controllers because, in view of the isolated neutral of the machine winding, one of the controllers is redundant and is only retained for symmetry. The line-to-line voltages at the motor terminals have three level waveforms, assuming the values  $U_D$ , 0,  $-U_D$ .

In order to produce a preferred switching frequency, a triangular clock signal may be added at the summing point of the current controllers [S25]. Another possibility is the synchronization of the controllers, i.e. allowing a switching operation to occur only at equidistant sampling instants  $t = \nu T_0$  defined by a fixed clock frequency  $f_0 = 1/T_0$  [B37]. While Fig. 9.14 was derived with a simple free running On-Off controller, the effect of synchronization is sketched in Fig. 11.4, again for a single-phase converter with inductive load; the amplitude of the ripple superimposed on the load current is now increased, because the switching operations are delayed until the next sampling instants, thus creating waiting intervals ranging between zero and  $T_0$ . If synchronised On-Off controllers are employed, the hysteresis band  $\Delta$  can be omitted because there is now a minimum time interval  $T_0$  between subsequent switching operations.

When a very low ripple content of the currents is specified, as may be the case with machine tool feed drives, the use of a pulse-width modulator in combination with a linear current controller is preferable to On-Off current control. This is demonstrated in Fig. 11.5 where measured current waveforms obtained with the same three-phase transistor inverter are compared. Fig. 11.5 a depicts the current produced by a synchronised controller having a sampling period  $T_0 = 22\mu s$  whereas the curves in Fig. 11.5 b show the result of linear current control with a pulse-width modulator operating at 5 kHz. The audible noise is of course more pronounced with PWM control unless a higher clock frequency is chosen, but the current waveform is much more acceptable.



**Fig. 11.4.** Current waveform produced by a single-phase transistor inverter with inductive load impedance and synchronised On-Off controller

Pulse-width modulators are now available in a variety of integrated circuits, which greatly simplifies the design of PWM inverters. There is also the possibility of software-based modulation using fast signal processors offering unlimited flexibility by combining PWM with sophisticated, such as predictive or time-optimal current control; this is of interest with high power converters switching at a lower frequency [H51, H55].

The assumption of virtual current sources for the stator windings is, of course, only valid as long as the ceiling voltage of the inverter is not reached. This is demonstrated in Fig. 11.6 for a free running On-Off controller when the frequency of the current reference is gradually increased. Due to the inductive load impedance, the necessary fundamental component of the voltage rises with frequency according to  $\hat{u}_1 = \hat{i}_1 \sqrt{R^2 + (\omega_1 L)^2}$ . It is seen that, beginning with Fig. 11.6 b, there are signs of saturation as indicated by prolonged intervals where no switching occurs, caused by insufficient supply voltage. Clearly, this results in a rising control error between the sinusoidal current reference and the piecewise exponential feedback signal and must be taken into account when designing a drive control system.

A very effective method of pulse-width-modulation that is particularly suited for fast switching inverters is called vectorial PWM because it represents an attempt at reproducing in a given time interval  $\nu T_0 < t \leq (\nu + 1) T_0$  a voltage vector  $\underline{u}_{S\text{ Ref}}(t)$  demanded by the current controllers [P15]. For this it is important to remember that the inverter circuit must be so operated that none of the legs is short-circuiting the link voltage  $U_D$  and that each motor terminal assumes a potential defined by the control. (Note that the shunting diodes paralleling the conductive transistors still permit the motor currents to

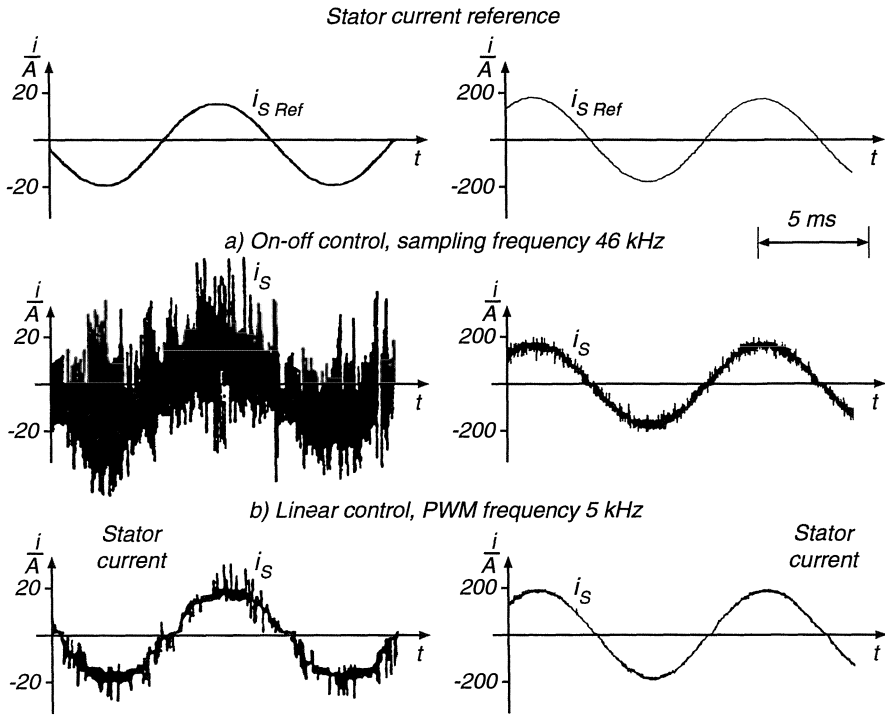


**Fig. 11.5.** Comparison of current waveforms with different types of controllers;  
 a) Current waveform with synchronised On-Off control,  $T_0 = 22\mu s$   
 b) Current waveform with linear current controller and PWM,  
 operating at 5 kHz

flow in either direction). Hence one transistor in each leg must be blocked while the other is conductive, except for the short protective intervals, where both transistors are blocked and the motor current is flowing through one of the shunting diodes. When indicating the switching state of each leg by a binary variable 0 or 1, depending on the upper or lower transistor being conductive, the switching state of the inverter may be described by a three bit word characterising 8 permissible states; it includes the states 000 and 111, where all output terminals are connected to the upper or lower bus of the link circuit, essentially short-circuiting the motor terminals.

When writing the voltage vector  $\underline{u}_S(t)$  in terms of line-to-line voltages

$$\underline{u}_S(t) = u_{S1} + u_{S2} e^{j\gamma} + u_{S3} e^{j2\gamma} = u_{12} + u_{32} e^{-j\gamma} \quad (11.1)$$

where each of the line-to-line voltages can assume the values  $U_D$ , 0 and  $-U_D$ , six distinct voltage vectors and two zero vectors result, as seen in Fig. 11.7. Clearly, when going from one corner of the hexagon to the next, only one leg of the inverter needs to change its state.

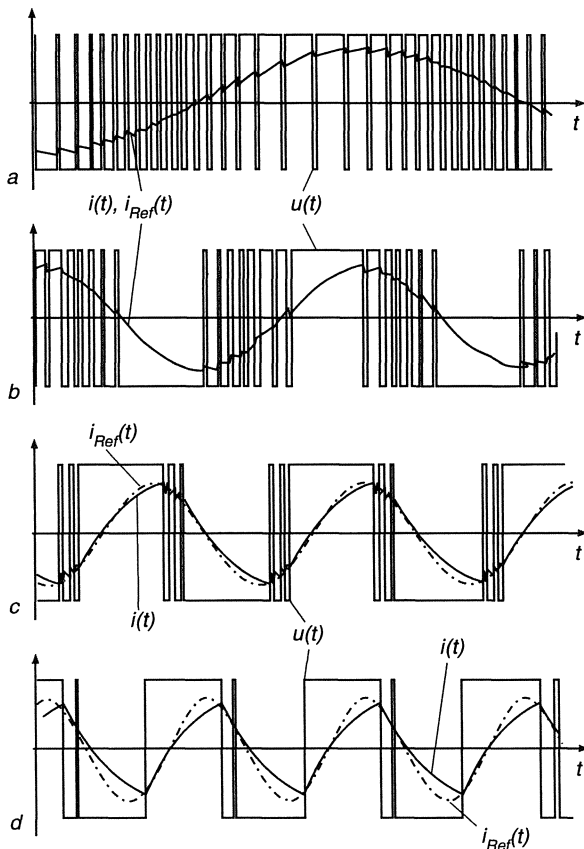


**Fig. 11.6.** Saturation effects of single-phase switched transistor inverter with On-Off current control supplying a passive R-L load impedance

We now assume that the inverter is switched at a basic clock frequency  $f_0 = 1/T_0$ , which may either be fixed or synchronised to the variable fundamental stator frequency, and that the current controllers have determined a command value  $\underline{u}_{S\text{Ref}}$  for the next interval  $T_0$  which may be inside the first sector, as shown in Fig. 11.7.

Since this commanded voltage vector is not normally coinciding with one of the available 8 voltage vectors, it is to be approximated by a switching sequence comprising the adjacent vectors  $\underline{u}_1 = \underline{u}_S(011) = U_D$  and  $\underline{u}_2 = \underline{u}_S(001) = U_D e^{j\pi/3}$  and filling up the rest of the interval with zero-vectors. The sub-intervals  $t_1$  and  $t_2$  for the two adjacent vectors are to be computed from the following equivalence

$$\underline{u}_{S\text{Ref}} = (\underline{u}_{Sa} + j \underline{u}_{Sb})_{\text{Ref}} = \underline{u}_1 \frac{t_1}{T_0} + \underline{u}_2 \frac{t_2}{T_0} = U_D \left( \frac{t_1}{T_0} + e^{j\pi/3} \frac{t_2}{T_0} \right); \quad (11.2)$$

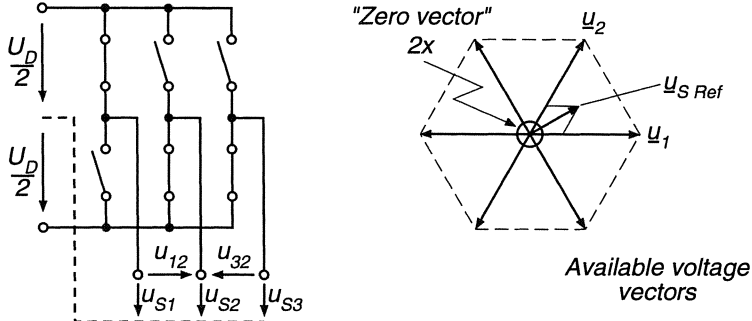


**Fig. 11.7.** Voltage vectors created by the switching states of the inverter in Fig. 11.3

in addition  $t_1 + t_2 + 2t_0 = T_0$  holds, where  $t_0$  is the zero vector interval. Solving for  $t_1$ ,  $t_2$  results in

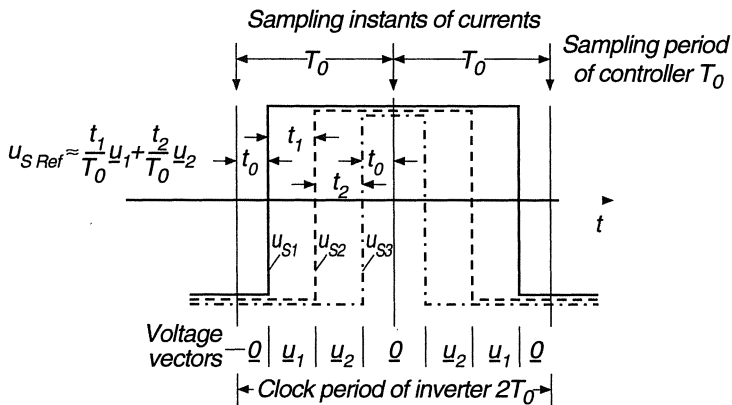


**Fig. 11.8.** Vectorial PWM with symmetrical switching sequence

$$\begin{aligned}\frac{t_1}{T_0} &= \frac{u_{Sa\text{Ref}}}{U_D} - \frac{1}{\sqrt{3}} \frac{u_{Sb\text{Ref}}}{U_D} \quad \text{and} \\ \frac{t_2}{T_0} &= \frac{2}{\sqrt{3}} \frac{u_{Sb\text{Ref}}}{U_D} \\ \frac{2t_0}{T_0} &= 1 - \frac{u_{Sa\text{Ref}}}{U_D} - \frac{1}{\sqrt{3}} \frac{u_{Sb\text{Ref}}}{U_D} \geq 0.\end{aligned}\tag{11.3}$$

When a zero vector is omitted,  $t_0 = 0$ , the resulting equivalent voltage vector ends on the straight line connecting the two adjacent switching vectors according to

$$u_{S\text{ Ref}} = (u_1 - u_2) \frac{t_1}{T_0} + u_2. \tag{11.4}$$

The limits for  $t_1 = 0$  and  $t_1 = T_0$  confirm this result. Hence, with the inclusion of  $t_0$ , any desired voltage vector inside the hexagon defined by the six switching vectors may be realised. Of course, the adjoining switching vectors must be chosen according to the sectorial position of  $\underline{u}_S \text{Ref}(t)$ . If the switching frequency  $f_0$  is high enough, fluctuations of the link voltage may be taken into account by replacing  $U_D$  in the modulating equations by a recent measurement of  $u_D(t)$ .

The switching sequence pertaining to the example in Fig. 11.7 is plotted in Fig. 11.8, depicting the potentials of the motor terminals. In order to remove the ambiguity with respect to which of the two adjoining switching states should be applied first, it is advantageous to repeat the same switching cycle with reverse sequence so that a symmetrical interval of length  $2T_0$  is created. Sampling the motor currents in the center of the short circuit intervals  $t_0$  reduces the sampling noise, as will be discussed later.

Of course, Eq. (11.2) describes an idealised situation, where the protective intervals and the inherent delays of the switching devices are neglected. For the actual design of modulators, these effects must be taken into account, particularly the differences between turn- On and turn- Off times, which can cause considerable distortion of the inverter characteristics at low output voltage and frequency. Hardware- as well as software- solutions have been proposed for this problem [K30, S67, W9].

## 11.2 Pulse-width modulated Thyristor Converters with Constant Direct Voltage Supply (Voltage Source Converters)

The use of transistors (MOSFET, Bipolar, IGBT) is presently restricted to lower and medium power applications, up to several hundred kW. With thyristors and GTO's the power of semiconductor converters extends far into the MW-region. A power circuit, resembling the transistor inverter in Fig. 11.3 is the voltage source thyristor inverter shown in Fig. 11.9. Because of the constant link voltage and the low AC impedance of the DC link it is also called a voltage source inverter. In view of the higher power rating and the fact that the motor may have to operate for longer periods of time in the generating region, the line-side converter is usually extended for regeneration, feeding power back to the line by reverse direct current in the DC link.

When employing gate turn off (GTO) thyristors, which are now available in kV, kA- ratings, the inverter circuit corresponds directly to the one in Fig. 11.3, with the transistors replaced by GTO's. On the other hand, with normal thyristors that cannot be blocked by gate signals, additional components are needed for the forced commutation of the machine-side inverter; this is so because the stator windings of an induction motor do not contain current- independent voltage sources as in the case of a line-connected transformer or a synchronous machine. Hence, natural commutation of the machine-side inverter feeding an induction motor is not feasible. This is understood when remember-

ing that a converter with delayed firing calls for lagging reactive power which a normal induction machine is unable to supply.

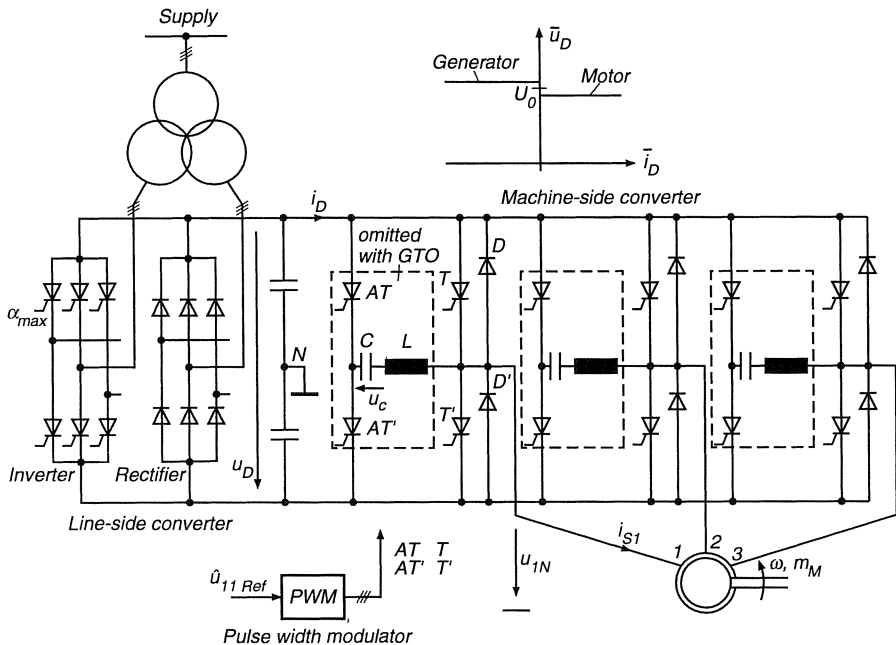


**Fig. 11.9.** Thyristor converter with constant DC-link voltage (Mc Murray circuit)

The converter depicted in Fig. 11.9 is an example of a variety of different circuits; it is considerably simplified, showing only the main components. Instead of a pair of transistors as in Fig. 11.3, each phase contains a force-commutated thyristor switch, comprising two main thyristors  $T$ ,  $T'$ , with antiparallel diodes  $D$ ,  $D'$ , two auxiliary thyristors  $AT$ ,  $AT'$ , a commutation capacitor  $C$  and an air cored inductor  $L$ . Briefly, a commutating process takes place as follows: Assume that the main thyristor  $T$  initially carries the load current  $i_{S1}$  and that the commutating capacitor  $C$  is positively charged,  $u_c > 0$ ; then firing of the auxiliary thyristor  $AT$  causes  $T$  to be blocked so that the load current flows temporarily through  $AT$  and  $C$  thus recharging the capacitor. At the same time a resonant circuit is formed consisting of  $AT$ ,  $C$ ,  $L$  and the diode  $D$ ; when about a half period of the oscillation is concluded and the charging current tends to reverse its sign,  $AT$  and  $D$  are blocked, which leaves the capacitor with opposite voltage, ready for the next commutating transient when  $T'$  has to be extinguished. The load current is now flowing through  $D'$ . If the current pulse through the resonant circuit is of sufficient magnitude as compared to the load current, the commutation is almost independent of the load so that the voltage  $u_{1N}$  can be approximated by a square wave  $\pm U_D/2$  with short but continuous commutating transients.

The load current  $i_{S1}$ , being continuous due to the motor leakage reactance, can in principle flow in either direction, even though all four thyristors may be blocked temporarily, because there is always a path open through one of the diodes  $D$ ,  $D'$ . During regeneration, the conducting periods of the diodes are increasing, eventually causing the mean of the link current,  $\bar{i}_D$ , to change sign which indicates reversed power flow.

It is realised that the initial transient, when  $i_{S1}$  is commutated from  $T$  to  $AT$ , is of course also continuous because small inductances, some not shown in Fig. 11.9, limit the rate of change of the thyristor currents. Likewise there are parallel  $RC$  snubbing circuits connected to each thyristor in order to limit the rate of change of the voltages. A detailed analysis of converter circuits, taking all these effects into account, is best performed by digital simulation; this is particularly true for transient operation, when the initial conditions, for instance the charge on the capacitor when  $AT$  is fired, are changing. As with all inverter circuits, the function of the circuit is eventually endangered when the required recovery time of the thyristors cannot be maintained, for example due to excessive load current or insufficient initial charge on the commutating capacitor. Hence the accurate analysis of the commutating transients is of major concern to the circuit designer. Special types of thyristors with short recovery time ( $< 20\mu s$ ) are usually specified for pulse-width modulated inverters, which limits the power rating to some MW. Also, the occurrence of unacceptable load currents must be prevented by fast control action.

The firing instants for the main- and auxiliary thyristors are determined by voltage and/or current controllers. In view of the limited switching frequency, which is usually below 1 kHz for thyristor inverters of higher power rating, the load currents can no longer be considered close to sinusoidal as was possible with transistor inverters operating at a higher switching frequency. Hence PWM-thyristor inverters of the type shown in Fig. 11.9 are naturally suited to act as voltage sources, presenting to the load pulse-width modulated rectangular voltages, the fundamental components of which are prescribed by voltage command signals. Because of the large superimposed harmonics, caused by the chosen switching strategy, closed loop control of the fundamental currents at variable frequency is not normally practical; it was different with transistor inverters, where the switching frequency is higher and the currents are sufficiently filtered by the load impedances. Therefore, open loop voltage control through a pulse-width modulator is the standard solution, while the current loops are normally closed on the next higher level of drive control, as will be shown in Chap. 12.

The pulse-width modulators may again be of a variety of designs. One frequently used scheme with inverters of higher power (Fig. 11.10) employs a triangular sampling signal [J5, M32, S25], the frequency  $f_0$  of which is a multiple  $n$  of the stator fundamental frequency  $f_1$  in order to avoid beat effects;  $n$  is reduced in stages as the stator frequency and voltage rise in order to limit the switching frequency and to fully utilise the voltage capability of the inverter. A drawback of this otherwise simple scheme is the appearance of large harmonics at the

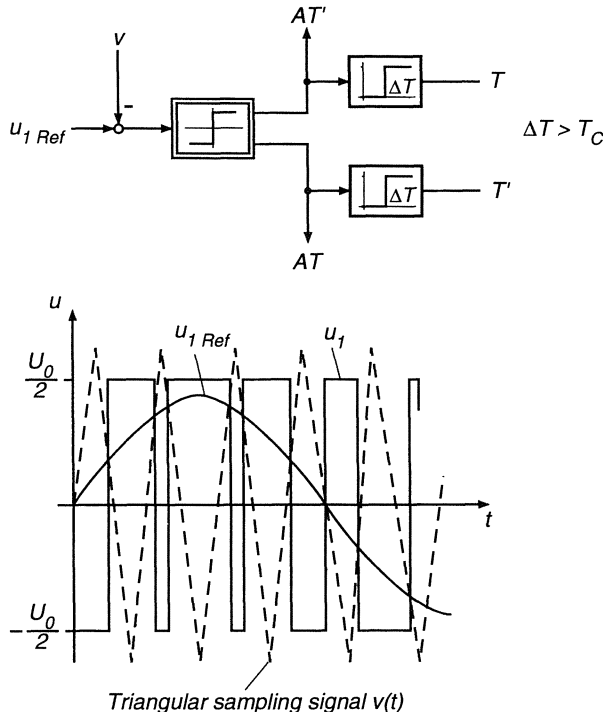


**Fig. 11.10.** Pulse-width modulator with a triangular sampling signal

frequencies  $f_0 \pm 2f_1$ . The load currents are smoothed by the leakage inductance of the motor which should not be chosen too small with this type of inverter. All triplen harmonics are eliminated from the currents in steady state due to the isolated neutral of the stator winding. There are still noticeable additional losses as well as sometimes objectionable noise emanating from the converter and the motor. A typical current waveform with a PWM-inverter and this type of "synchronous modulation" is shown in Fig. 11.12 b.

This unsatisfactory situation has given rise to the development of a multitude of advanced modulation schemes such as digital pattern generators where binary switching sequences for different amplitudes of the fundamental voltage are kept in a microelectronic memory to be called up in real time for small increments of angle  $\tau = f \omega_1 dt$ . This is depicted in Fig. 11.11 [B62, D7, P5, P28, T28]. The patterns are precalculated off-line with the objective of reducing voltage- and current-harmonics or power losses, torque pulsations or noise under steady state conditions. Clearly, the more often per period the voltage is reversed, the more side conditions can be satisfied, given a prescribed fundamental voltage component.

The restrictions of the inverter with regard to the minimum time between two subsequent switching operations must of course be observed in order to allow

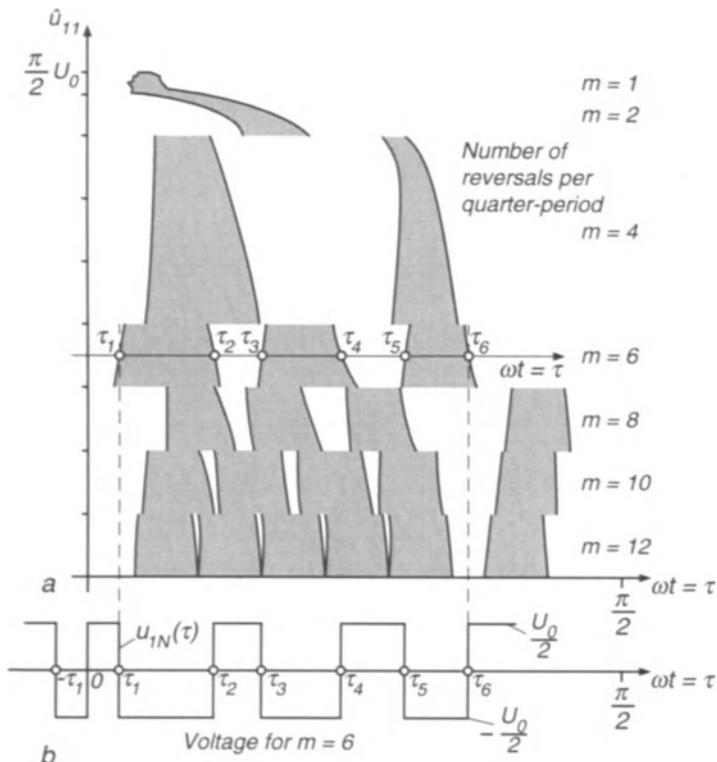


**Fig. 11.11.** Optimised pulse-width modulation with precalculated switching patterns

the commutation to be completed. Also, the losses in the inverter caused by each commutation should be considered, which means that there is an upper limit for the switching frequency. At the maximum fundamental frequency, which corresponds to full output voltage of the inverter when feeding an AC motor, the optimal waveform is a square wave with one reversal per half period; this is included in the switching pattern shown in Fig. 11.11.

When realising a suitable modulator it is of course desirable to keep the required volume of memory small; this can be achieved by storing only one quarter cycle  $0 \leq \tau \leq \frac{\pi}{2}$  of the binary pattern for one phase and obtaining the remaining information by transposing and inverting this pattern table. On the other hand, considerable angular resolution is needed in order to satisfy the various conditions with adequate accuracy. Assuming for example a resolution in amplitude of the fundamental voltage of  $2^7 = 128$  levels and an angular resolution of  $2^{10} = 1024$  steps per quadrant, this results in a memory of 16 kByte which could easily be accommodated by one microelectronic chip of read only memory (ROM).

At the very low end of the frequency range some other means of modulation must be employed because even 4000 steps of angular resolution per period will eventually prove to be insufficient.

In order to avoid continued fluctuations of the voltage amplitude, which would disturb the switching sequences and render the notion of "harmonics" meaningless, the superimposed control should contain a hysteresis band in the amplitude channel; fine and rapid speed control would still be possible through the frequency input of the modulator but the voltage would be changed more slowly and temporarily in somewhat coarser steps. Some results of the current waveforms and spectra obtained with different modulators are shown in Fig. 11.12. The curves were recorded on a 22 kw drive supplied by a voltage source thyristor inverter [P30].

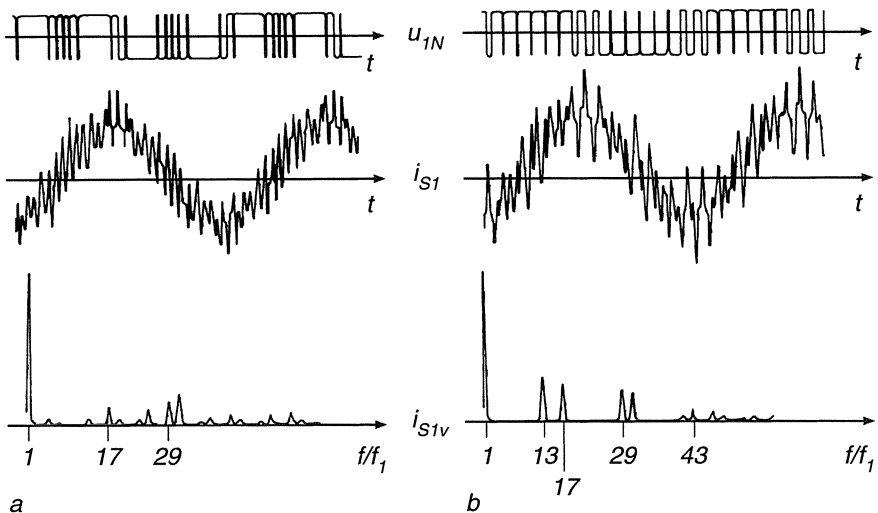


**Fig. 11.12.** Current waveforms and spectra achieved with different methods of pulse-width modulation. **a)** Optimised switching pattern; **b)** Subharmonic modulation with triangular sampling signal

A particular feature of the pulse-width modulator with optimised switching pattern is the fact that the pattern can easily be changed for different applications, placing higher emphasis for instance on losses, torque pulsations or noise.

With the rapid advances of micro-electronics even on-line optimisation of the individual switching instants has been shown to be feasible which opens the way to optimal modulation under dynamic conditions, so that even on-line current control could become practical with high power inverters [H48, H51]. The load-independent commutation, resulting in low impedance motor voltages makes the PWM inverter an excellent choice for drives with high dynamic performance at power ratings where transistor inverters are unavailable; an example are

high power traction drives with GTO-inverters which require good dynamic performance in order to prevent wheel slippage during starting and braking.

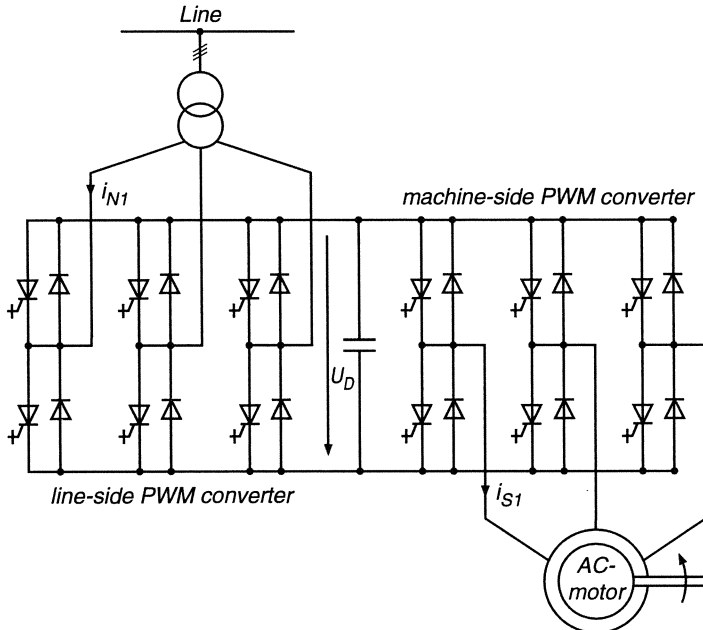


**Fig. 11.13.** Symmetrical voltage source converter with forced commutation at machine- and line-side

With increased use of controlled drives the problem of line-side interference by power electronic converters is becoming an important issue for the utilities. A line-commutated converter supplying the DC-link is particularly notorious because it not only produces distorted line currents with low orders of harmonics but draws also substantial reactive currents of line frequency. The first mentioned effect can be alleviated by increasing the pulse number of the converter but the other requires capacitive compensation or, combining both aspects, filters with capacitive fundamental input currents.

Another possibility that is likely to be of strong future interest, is to extend the forced commutation also to the line-side converter. An example is seen in Fig. 11.13 where a PWM voltage source converter with GTO-thyristors at both ends is shown in simplified form. The line-side PWM converter could be controlled such that the line currents  $i_N$  are not only approaching sinusoidal waveform but that their fundamental components are also in phase with the line voltages, thus eliminating reactive currents. Converters of this type are already common on large AC-traction drives, where the line impedance caused by the single phase catenary is quite large so that voltage fluctuations and distortions would be particularly severe.

### 11.3 Thyristor Converters with Impressed Direct Current Supply (Current Source Converters)

The converter circuit shown in Fig. 11.14 comprises once again a line-side and a machine-side converter connected through a DC-link; the two converters operating at different frequencies are now decoupled by a smoothing reactor  $L_D$  which, in combination with a current control loop, serves to maintain a direct link current  $i_D$  as prescribed by the current reference. Thus the machine-side converter is effectively supplied from a current source [F2, K41, P18].

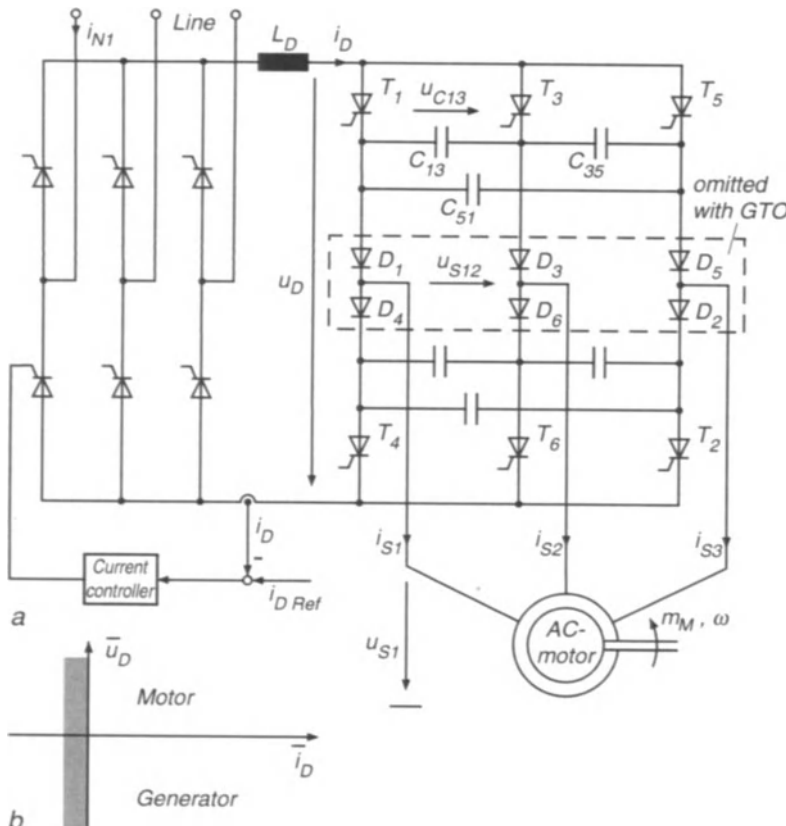


**Fig. 11.14.** Thyristor converter with direct current link.  
a) Circuit; b) Operating regions of DC link

The simplifications made possible with this circuit are twofold:

- The unidirectional link current  $i_D$  allows the use of a two-quadrant line converter, where reverse power flow is achieved by inverting the mean of the link voltage  $u_D$  through delayed firing.

- The link reactor permits the voltage  $u_D$  to be temporarily raised or lowered during commutation of the machine-side converter, thus avoiding the auxiliary thyristors; commutation is now performed with capacitors and decoupling diodes.

Altogether there are 12 thyristors, the same number as would be needed for a reversible DC-drive; also, the thyristor for the machine-side converter need not be of the more expensive fast recovery type necessary for voltage source inverters.

It is noted that, instead of the line-side converter, the DC-link could also be supplied from another force commutated converter such as a chopper with current control; this is of interest with urban traction drives fed by constant direct voltage.

The mode of operation of the machine-side converter in Fig. 11.14 differs considerably from that of the voltage source converter (Fig. 11.9). While the motor current supplied from a PWM voltage source inverter was at least crudely sinusoidal, it has now a three step square waveform, assuming the values  $-i_D$ , 0,  $i_D$  as seen in Fig. 11.15; the corners are rounded-off due to finite commutating time. The vector of the stator current follows the pattern of a six pointed star; this is shown in Fig. 11.15 b which was recorded during a speed reversal of a 22 kW drive. The commutating transients are more involved now because the motor impedance is part of the commutation circuit which means that the commutating time depends on the loading of the motor and increases at light load.

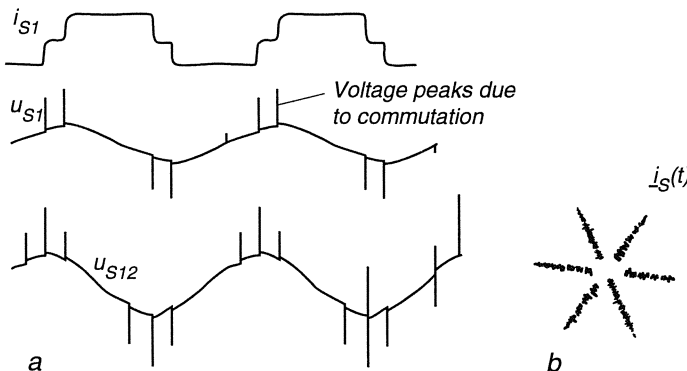


**Fig. 11.15.** Current and voltage waveforms of a current source inverter. **a)** Wave forms; **b)** Stator current vector

The commutating transient may be briefly described as follows: With no commutation in progress, two thyristors, for example  $T_1$  and  $T_2$  carry the direct current  $i_D$  and the capacitor  $C_{13}$  is positively charged as a result of the preceding commutation. If thyristor  $T_3$  is now fired,  $T_1$  is extinguished in a rapid transient and  $T_3$  assumes the direct current; this is the starting condition of the

commutating transient proper. While the current  $i_{S1}$  is now reduced towards zero,  $i_{S2}$  is rising towards  $i_D$ ; during this interval phase 1 of the motor is fed through  $C_{13}$  as well as through the series-connected capacitors  $C_{35}$ ,  $C_{51}$ . Eventually diode  $D_1$  is blocked and the commutation is completed with  $T_2$  and  $T_3$  conducting. Clearly the motor transient impedance between terminal 1 and 2 is part of the commutation circuit, as mentioned before. The diodes are required for decoupling in order to prevent the capacitors from losing their charge necessary for the next commutation. The commutating interval can be reduced by choosing a motor with low leakage reactance.

Commutation intervals are manifested by voltage spikes superimposed on the otherwise sinusoidal terminal voltages of the motor; this is an obvious consequence of the changing stator current. Outside commutation, with

$$\frac{di_{S\nu}}{dt} = 0, \quad \nu = 1, 2, 3 \quad (11.5)$$

the terminal voltage of the motor is practically sinusoidal since the magnetising current is filtered by the main time constant of the motor.

Depending on the phase of the voltage surge due to commutation as related to the sinusoidal voltage component it can be recognised whether the machine is operative as motor or in the generating region (Fig. 11.15a). While motoring or regenerating operation is reflected by the sign of the mean voltage  $\bar{u}_D$ , the direction of rotation is solely determined by the firing sequence of the machine-side converter. The firing signals may for instance be derived from the state of a ring counter having 6 states, which is stepped forward or backwards as commanded by the speed controller.

With a suitable control structure, this converter is also useful for high dynamic performance drives, operating in four quadrants over a wide speed range. Apart from its simplicity and, because of the link reactor, the ease of protection in case of commutation failure, it has the advantage of little audible noise due to the absence of 'high frequency' modulation. However, there are considerable additional losses caused by the large harmonic content of the currents. Also the torque pulsations due to the interactions of the stepped stator currents and the sinusoidal flux wave can be objectionable at low speed below, say 100 1/min. In order to alleviate this condition, the machine-side converter may be commutated back and forth by pulse-width modulating the ring counter, i. e. superimposing an alternating component on the slow progression of the state of the counter. Of course, due to the relatively slow commutation at light load, the switching frequency is bound to be much lower than with a voltage source PWM inverter [W8]. It is for this reason that this converter is not very well suited for drives requiring continuous position control such as machine tool feed drives.

Apart from this special restriction, the current-source converter may be controlled nearly as rapidly as a voltage source inverter, because the firing instants of the machine-side inverter can be quickly shifted; changing the magnitude of the link current involves some delay due to the large smoothing reactor but with adequate ceiling voltage the equivalent lag can be reduced to about 10 ms with a 50 Hz supply, as was discussed in Sect. 8.5.

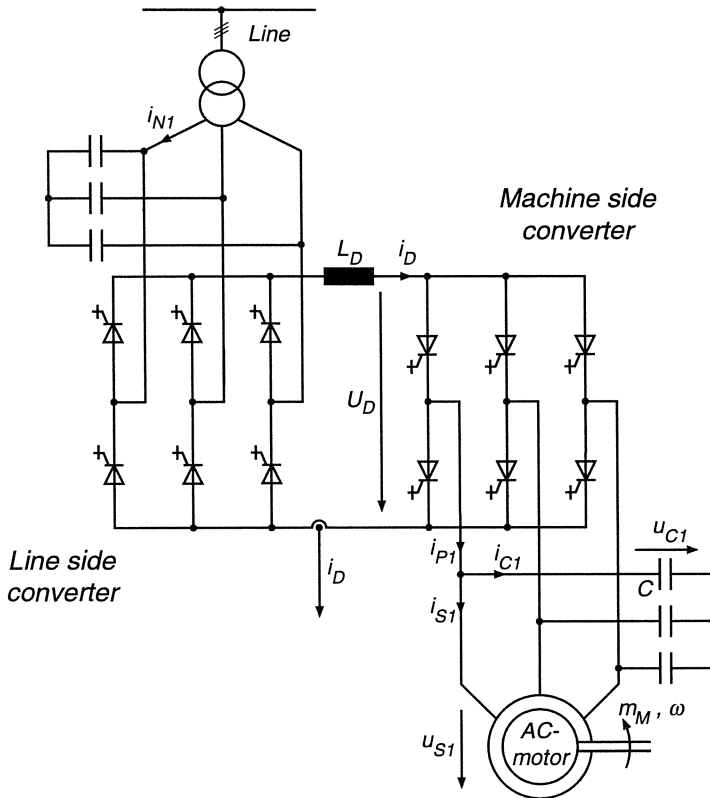


**Fig. 11.16.** Symmetrical current source converter with GTO-thyristors

As mentioned before, the current vector defined in Eq. (10.4 a) assumes with this converter a rather unique shape; because of  $i_{S\nu} = \pm i_D$  and with one of the motor currents (except for commutation intervals) being zero, the vector describes a regular six-pointed star with the radius  $\sqrt{3}i_D$ ,

$$i_S(t) = i_{S1} + i_{S2} e^{j\gamma} + i_{S3} e^{j2\gamma} = \sqrt{3} i_D e^{j(\nu\gamma/2 + \pi/6)} \quad (11.6)$$

Some measured traces are shown in Sect. 12.4.

When assessing the relative merits of the different inverter schemes, it is of course necessary to compare not only the number of components but also their rating and how this is reflected in the total cost.

The circuitry of the current source converter is again considerably simplified when GTO-thyristors are employed; this is indicated in Fig. 11.14 and shown more clearly in Fig. 11.16 for a symmetrical converter, where the load- and the line- currents are pulse width modulated and may approach sinusoidal waveforms.

The motor voltages and currents are now continuously filtered by capacitors; the converter is pulse-width modulated with the link current  $i_D$  being

switched between the output terminals connected to the motor-capacitor combination. Another possibility is to introduce zero current vectors, bypassing the load through a short circuited leg of the converter, which corresponds to the zero voltage vector with a voltage source inverter; thus, this converter creates new possibilities for high dynamic performance drives. However, in view of the increased complexity of the plant, caused by the capacitors, sophisticated control algorithms and a powerful microcomputer are needed; in particular, the question of L-C resonances requires detailed study [A15, N15, N16, N17].

## 11.4 Converter Without DC Link (Cycloconverter)

The types of converters discussed so far had in common that line-side and machine-side converters operated at different frequencies and were decoupled by a DC-link containing energy storage devices in the form of low-pass filter components. This twofold conversion provides a degree of independence in controlling the converter ends, but at the same time causes additional power losses. The double conversion may be avoided with direct AC/AC-converters which perform the conversion from constant frequency, constant voltage to variable frequency, variable voltage in one stage and without resorting to intermediate energy storage [47, 54].

The reversible line-commutated AC/DC converter without circulating current shown in Fig. 9.4 is capable of operating in all 4 quadrants of the  $\bar{u}_a - \bar{i}_a$ -plane supplying an inductive load (in order to assure continuous current flow). Hence, by providing it with closed loop current control and applying a low frequency current reference, the converter will act as a low frequency current source. Clearly, 4-quadrant capability is necessary when supplying a motor because, when a sinusoidal current  $i_a$  is fed to a  $R-L$ -load impedance, the operating point in the voltage-current-plane describes an elliptical path around the origin, passing through all quadrants. In order to avoid undesirable interactions between the three current controllers (one of which is redundant because of the zero sum of the currents), they may be chosen as  $P$ -instead of  $PI$ -controllers thus allowing some flexibility.

By supplying each phase of the motor winding from a reversible converter, a low frequency AC drive system is formed, as seen in Fig. 11.17. Again, the neutral of the stator winding remains isolated in order to exclude zero sequence, such as triplen harmonic, currents. The main feature of this circuit is that only standard line-commutated thyristor-converters are required which have been in use for many years with DC drives and HVDC systems up to the highest power ratings. Also, the cost of the thyristors is reasonable since no particular specifications with regard to turn-off time are needed with line-commutated converters.

On the other hand, the large number of thyristors seems at first sight staggering; for a six-pulse converter with three-phase output a minimum of 36 thyristors is required as well as a transformer with three complete three-phase sec-

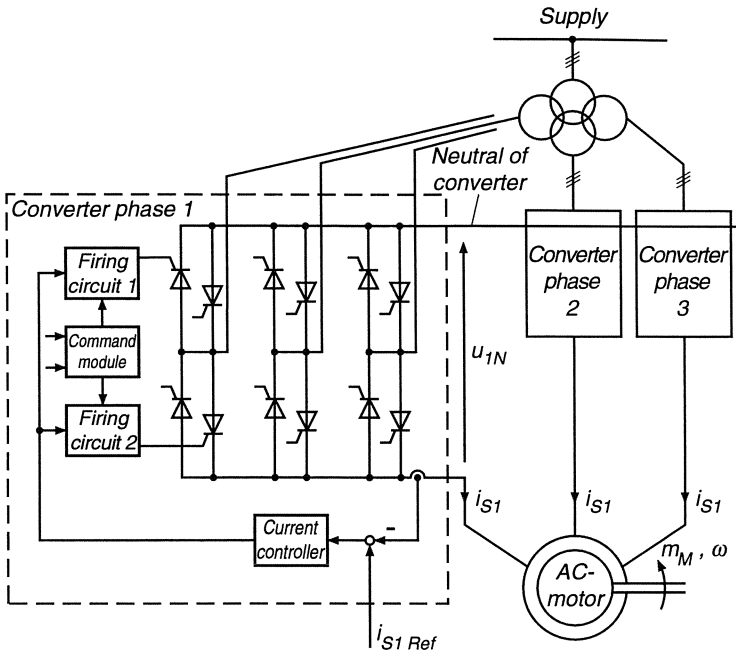


Fig. 11.17. Six-pulse cycloconverter for a three-phase motor load

ondary windings. This indicates that cycloconverters are mainly of interest for large drives, where parallel thyristor branches would be necessary in other converter circuits. An important restriction is the limitation of output frequency which is caused by the discrete nature of the control process and the presence of a carrier frequency, since the output voltages are assembled from sections of the line voltages. As the output frequency rises, the output voltages and hence the output currents are tracking the sinusoidal references with increasing errors and consequent distortion. The frequency range

$$0 \leq f_1 \leq f_{1\max} \approx \frac{p f_0}{15} \quad (11.7)$$

is usually considered as the useful range of operation, where  $f_0$  is the line frequency and  $p$  is the pulse number. With a 50 Hz grid and a three-phase bridge circuit ( $p = 6$ ) this results in  $f_{1\max} \approx 20$  Hz. At this frequency, a period of the output voltage would on the average consist of 15 sections of line voltages. Of course, if a three-phase line of higher frequency is available, the range of output frequency is extended accordingly; this may be the case on vehicles or ships, when a diesel- or turbine-driven generator provides on-board power for variable frequency AC drives. Also, a somewhat wider frequency range may be achieved by cycloconverters with circulating current, as discussed in Sect. 9.1 [H21].

When reversing the sequence of the current references, the sequence of the three-phase output system is inverted. It is of interest to note that the nature

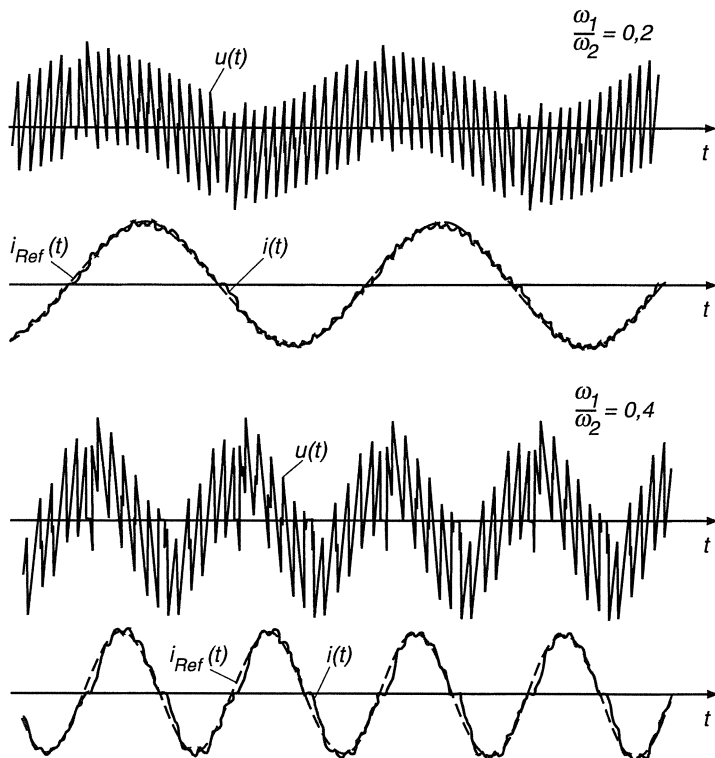


**Fig. 11.18.** Waveforms of six-pulse cycloconverter supplying a single phase-load at different output frequencies (simulation)

of the load supplied by the cycloconverter is unimportant as long as there is a sufficiently large inductive impedance in order to assure continuous current flow. In particular, there is no difference whether the load is active or passive, i.e. whether the machine operates as motor or generator because operation in all four quadrants is possible.

When considering the effects of a cycloconverter on the line-side currents it is helpful to remember that a symmetrical three-phase system of sinusoidal voltages and currents results in constant net power. Since the cycloconverter contains only switches but no storage devices (apart from the unavoidable leakage inductances, snubber circuits, etc.), the total three-phase input power corresponds to the output power. Hence it is mainly the effects of harmonics that have to be considered. In addition there will be reactive power at the line side which is inherent in the control of line-commutated converters by delayed firing.

In Fig. 11.18 the results of a computer simulation are shown, where a reversible six-pulse converter with current control, operating on the 50 Hz grid, supplies a predominantly inductive single-phase impedance with current of 10

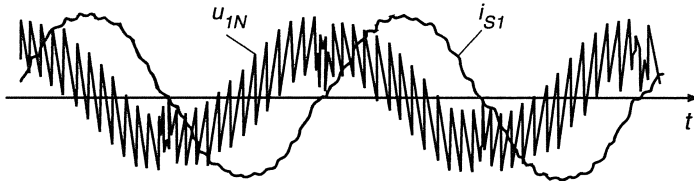


**Fig. 11.19.** Measured output current and voltage of a six-pulse cycloconverter with three-phase inductive load at 10 Hz

Hz and 20 Hz. At these frequencies there is still a reasonable agreement between reference current and feedback signal, even though some phase shift becomes apparent in the 20 Hz-trace, which might be corrected by a lead-term in the reference channel. The 2 ms-zero current interval, which is desirable for safe operation is clearly seen. With a three-phase output and symmetrical load, all triplen harmonics would be removed from the load current. Due to the inductive load the voltage rises with increasing frequency. This will eventually lead to additional distortion of the voltages and currents caused by the ceiling voltage of the converters. For very large drives, synchronous motors are often preferred over induction motors since there the reactive power does not have to be supplied through the converter and because of the larger airgap which is desirable for mechanical reasons. Cycloconverters are very suitable for this duty, provided the stator frequency is sufficiently low, which is often the case with large low speed motors such as required for rolling mill and mine hoist drives; synchronous drives will also be discussed in Chap. 13.

Finally in Fig. 11.19 oscillograms of the measured output current and line-to-neutral voltage of a cycloconverter are shown; the converter is supplied from the 50 Hz three-phase line and feeds a symmetrical three-phase inductive load at 10 Hz.

## 12. Control of Induction Motor Drives

When comparing the dynamic model of a separately excited DC machine, Eqs. (5.1-5.4), Fig. 5.4, with that of an AC induction machine, Eqs. (10.38- 10.41), Fig. 10.16, it is obvious that the latter represents a much more complex control plant. This is caused by the fact that the main flux and the armature current distribution of a DC machine are fixed in space and can be directly and independently controlled while with an AC machine these quantities are strongly interacting and move with respect to the stator as well as the rotor; they are determined by the instantaneous values of the stator currents, two of which represent independent control variables. An additional complication stems from the fact that the rotor currents cannot be measured with ordinary cage rotors. Hence the AC motor is a highly interacting nonlinear multi-variable control plant that kept control engineers puzzling for a long time.

The differences in control dynamics of a DC and an AC motor are best explained by the simplified mechanical models shown in Fig. 12.1. In Fig. 12.1 a, corresponding to a DC motor with a mechanical load, a disk is driven by the tangential force  $f_T$  acting on a pin  $P$  which can be moved in a radial slot by a radial force  $f_R$  acting against a spring. Caused by velocity-dependent friction, the radial motion of the pin is assumed to be relatively slow.

Between this mechanical arrangement and the electric model of a DC machine the following analogy holds:

$$\begin{aligned} f_T &\cong \text{armature current}, & R f_T &\cong \text{electrical torque}, \\ R &\cong \text{main flux}, & R \omega &\cong \text{induced voltage (e.m.f.)}, \\ f_R &\cong \text{field voltage}, & R \omega f_T &\cong \text{electrical power}. \end{aligned}$$

Controlling torque, speed and angular position of the disk is straight-forward if  $f_T$  and  $f_R$  can be separately chosen; the analogy applies to operation below base speed as well as in the field-weakening range with the limitation being either saturation (length of the slot) or maximum induced voltage (circumferential velocity of pin).

A similar arrangement applies to the AC motor (Fig. 12.1b); however, the pin is now driven by three connecting rods that apply forces  $f_1$ ,  $f_2$ ,  $f_3$  in three fixed directions spaced by  $120^\circ$ . In order to produce a smooth circular motion while at the same time keeping the pin at a given radius, a well coordinated set of alternating forces is required for producing constant radial and tangential resultant forces. With the analogy that the orientation of the pin ( $R$ ,  $\varrho$ )

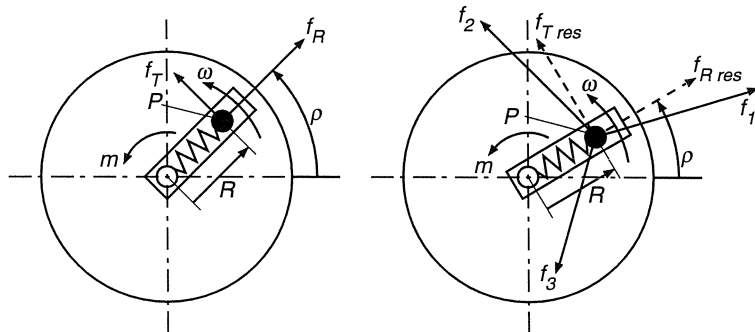


**Fig. 12.1.** Mechanical model of (a) DC and (b) AC motor

corresponds to the position of the fundamental flux wave and the forces to the stator currents, it is easy to see why an AC motor is so much more difficult to control than a DC motor.

This is one reason why it has taken a long time before generally accepted solutions for controlling AC motors have emerged, as had been the case with DC motors; instead, a large number of contending proposals existed, most of which were only useful for special cases or particular applications. However, since the beginning of the 70's, new methods adapted to vectorial machine models have been proposed that have the potential of forming the basis for a unified theory of controlling AC machines. In the following chapters, some of these methods will be discussed.

## 12.1 Control of Induction Motor Based on Steady State Machine Model

For many mechanical loads, such as pumps or fans, there is no need for high dynamic performance, as long as the speed can be varied with good efficiency over the desired speed range; this permits the use of steady state machine models for the design of the drive control. Two of the many schemes that have been proposed for this purpose and are in frequent use, will be discussed first. They are based on the assumption that the induction motor is supplied by a PWM-voltage source inverter, producing symmetrical three-phase voltages and currents of a fundamental frequency related to the desired speed.

In view of the simple and very effective control schemes for DC motors it was appropriate to search for similar methods that might be applicable to the control of AC motors. A salient feature with DC motor control was to maintain constant flux below base speed in order to fully utilise the given motor size with regard to torque, which was then controlled through the armature current; a similar approach may be followed here.

When for the moment neglecting the stator resistance and assuming symmetrical sinusoidal stator voltages  $U_1$  of frequency  $\omega_1$ , the electric torque of the induction motor is given by Eq.(10. 66) where the normalised slip derived from Eqs.(10. 49, 10. 53) is

$$\frac{S}{S_p} = \frac{(\omega_1 - \omega) \sigma L_R}{R_R} = \omega_2 \sigma T_R . \quad (12.1)$$

By varying the stator voltages in proportion with frequency,

$$\frac{U_1}{U_{S0}} = \frac{\omega_1}{\omega_0} , \quad (12.2)$$

the stator flux is kept constant, hence the steady state torque is

$$m_M = m_{p0} \frac{2}{\frac{S}{S_p} + \frac{S_p}{S}} = 2 m_{p0} \frac{\omega_2 \sigma T_R}{1 + (\omega_2 \sigma T_R)^2} . \quad (12.3)$$

The torque-speed curves are clearly obtained by shifting this reference curve along the frequency axis according to  $\omega = \omega_1 - \omega_2$ , while maintaining its shape; this is seen in Fig. 12.2.

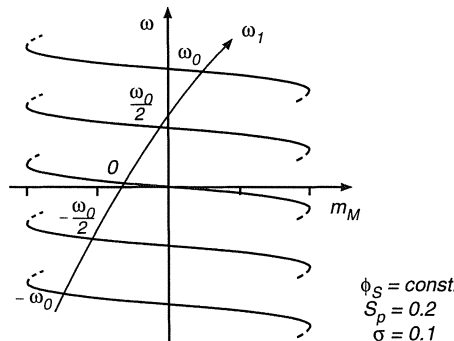


**Fig. 12.2.** Steady state torque-speed curves at different stator frequencies, assuming constant stator flux and neglecting stator resistance

If only the centre portion of the curves having negative slope is used, i. e. by limiting the rotor frequency to values below pull-out slip, the curves exhibit a marked resemblance to the steady state torque- speed curves of a DC- machine at constant flux (Fig. 5.5a); hence, the rotor frequency may be regarded as representing torque, serving as a substitute for the armature current [J12, B24].

As long as the voltage drop across the stator resistor can be neglected, Eq. (12.2) is adequate for maintaining constant stator flux; however, large errors would occur at low speed, where the resistive voltage component will eventually exceed the induced voltage; hence, a correction of the stator voltage according to Fig. 12.3a is required,

$$U_S = \left| j \frac{\omega_1}{\omega_0} U_{S0} + R_S I_S \right| , \quad (12.4)$$

if the operating range is to extend to low speed. With Eq. (10.54) this results in

$$U_S = \left| \frac{\omega_1}{\omega_0} + \frac{R_S}{j \omega_0 L_S} \frac{1 + j \omega_2 T_R}{1 + j \omega_2 \sigma T_R} \right| U_{S0} . \quad (12.5)$$

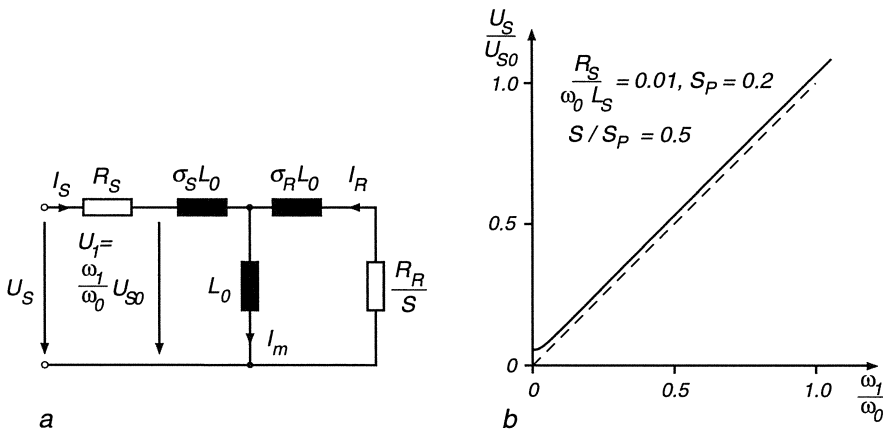


**Fig. 12.3.** Induction motor at variable stator frequency;  
a) equivalent circuit, b) stator voltage as a function of stator frequency for constant stator flux at  $S = S_p/2$ .

The curve depicted in Fig. 12.3b is calculated for  $R_S/\omega_0 L_S = 0.01$ ,  $S = 0.1$ . Deviations from Eq. (12.2) are noticeable mainly at low frequency. At  $\omega_1 = 0$ , the necessary voltage is due only to the stator resistance, which also depends on the winding temperature.

In Fig. 12.4 it is seen how this function can be incorporated into a simple speed control scheme of an induction motor. The speed controller is producing a reference for the rotor frequency which is taken to represent torque; it must be limited to the range where the torque - speed relationship is approximately linear, in order to avoid pull-out. By adding the signal for measured speed, a reference for the stator frequency  $\omega_1$  is obtained. Naturally, such a simple control scheme is only suitable for speed adjustment in steady state, not for high performance drives.

Open loop compensating control schemes like the one described are sensitive to side effects such as temperature changes that are not accounted for. An improvement would be to convert from impressed voltages to currents in order to eliminate the effects of stator resistance and the primary leakage reactance; this would also simplify the dynamics of the drive by removing Eq. (10.38) from the model equations. In addition, the assumption of a sinusoidal supply is much more realistic with stator currents than with voltages when a switched

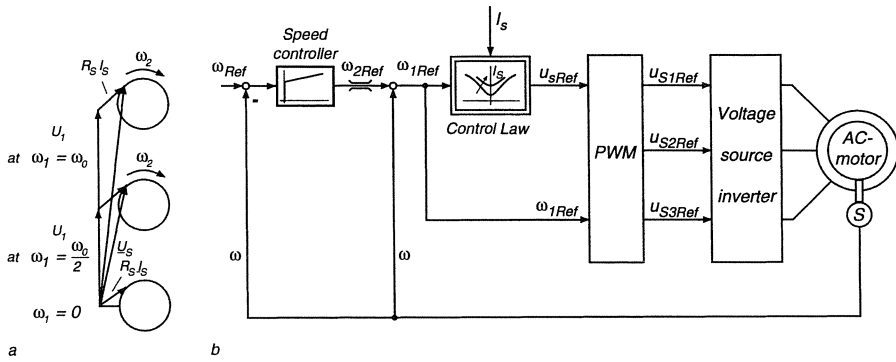


**Fig. 12.4.** Speed control of an induction motor with impressed stator voltages and open loop flux control, based on a steady state model of the machine

power converter is employed. As explained in Chap. 11, either a PWM voltage source inverter or a cycloconverter with current control could be used, covering a wide range of power ratings.

When supplying the motor with impressed sinusoidal currents, it is advantageous to aim for constant air-gap flux or rotor flux, because this eliminates not only the effects of stator resistance but also of leakage inductance; in the equivalent circuit in Fig. 10.7 b, this corresponds to the condition of maintaining a constant rotor-based magnetising current  $I_{mR}$  or rotor flux, independent of speed and load. The pertinent stator currents are obtained from the equivalent circuit, resulting in

$$I_S = \left[ 1 + \frac{j \omega_1 (1 - \sigma) L_S S (1 + \sigma_R)^2}{R_R} \right] I_{mR} = (1 + j \omega_2 T_R) I_{mR}. \quad (12.6)$$

Hence in order to maintain a given rotor flux, the magnitude (RMS-value) of the stator currents must follow a function which depends on the rotor frequency  $\omega_2$  and contains only rotor parameters,

$$I_S = \sqrt{1 + (\omega_2 T_R)^2} I_{mR}. \quad (12.7)$$

This is achieved with the help of another function generator which produces a reference according to Eq. (12.7) for the amplitude of the stator currents. The function is plotted in Fig. 12.5 for two values of the rotor time constant; it is symmetrical to  $\omega_2 = 0$ , i.e. for operation below and above synchronous speed. Of course, the fact that the function depends on the rotor time constant constitutes also a source of inaccuracy since the rotor resistance may vary considerably with temperature and the inductance with the degree of saturation. Even though this might be alleviated by making the function generator dependent on temperature, the realisation would be difficult in practice because a measurement of rotor temperature is not easy with the motor in operation.

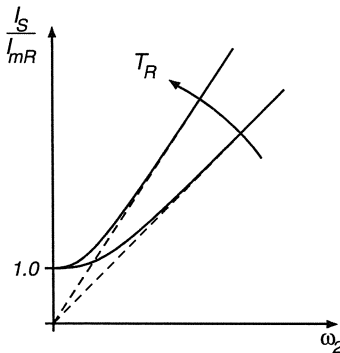


**Fig. 12.5.** Amplitude of stator currents required for constant rotor flux

With the definition of the rotor- based magnetising current in Fig. 10. 7 b

$$I_{mR} = I_S + (1 + \sigma_R) I_R \quad (12.8)$$

the steady state torque according to Eq. (10.63) may be written in the form

$$m_M = 3 L_0 \operatorname{Im}[I_S I_R^*] = 3 (1 - \sigma) L_S \operatorname{Im}[I_S I_{mR}^*]. \quad (12.9)$$

Assuming a correctly tuned function generator, the magnetising current will be maintained at rated value, corresponding to the ideal no-load current, hence

$$I_{mR} I_{mR}^* = I_{S0}^2, \quad (12.10)$$

which, inserting in Eq. (12.9) yields

$$m_M = 3 (1 - \sigma) L_S I_{S0}^2 \operatorname{Im}[I_S / I_{mR}]. \quad (12.11)$$

From this follows with Eq. (12.6)

$$m_M = 3 (1 - \sigma) L_S I_{S0}^2 \omega_2 T_R. \quad (12.12)$$

This confirms the earlier observation that the torque- speed curves may be shifted along the speed axis without changing their shape, Fig. (12.2). Since it is now the rotor flux instead of the stator flux that is maintained at constant value, the effect of stator leakage is eliminated resulting in a reduced slope of the curves.

The next task in the design of the AC motor control consists in converting the current amplitude reference  $I_{S\text{Ref}}$  produced by the function generator to a system of three-phase variable frequency AC signals to be used as current references for the power converter and motor. This is a modulation process for which various realisations exist; two possibilities will be discussed here, one analogue and the other digital.

The block diagram of an amplitude-controlled, variable frequency two-phase oscillator is shown in Fig. 12.6a which is suitable for providing the required AC reference signals [H19]; similar structures were contained in Fig. 10.16. The input signals  $y_1, y_2$  and the output signals  $x_1, x_2$  are connected by the following nonlinear differential equations

$$\begin{aligned} T_0 \frac{dx_1}{dt} &= -y_1 x_2 + y_2 x_1, \\ T_0 \frac{dx_2}{dt} &= y_1 x_1 + y_2 x_2. \end{aligned} \quad (12.13)$$

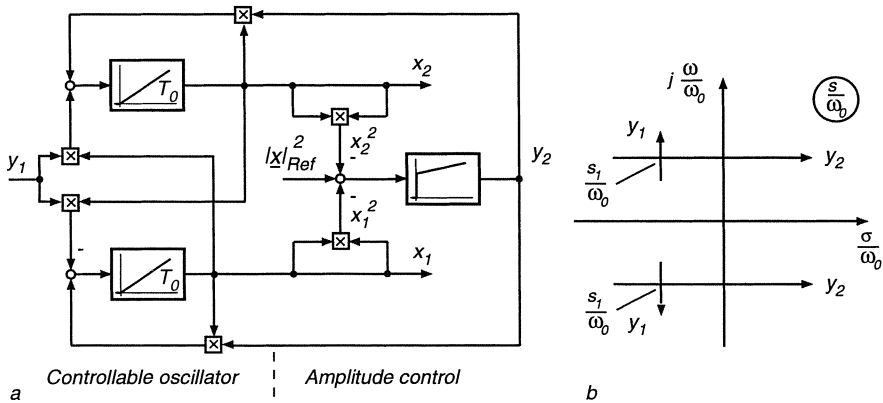


**Fig. 12.6.** Variable frequency, variable amplitude two-phase oscillator.  
a) Block diagram, b) Eigenvalues in  $s$ -plane

Elimination of  $x_2$  results in a second order equation

$$T_0^2 \frac{d^2 x_1}{dt^2} - 2 y_2 T_0 \frac{dx_1}{dt} + (y_1^2 + y_2^2) x_1 = -T_0 \frac{dy_1}{dt} x_2 + T_0 \frac{dy_2}{dt} x_1. \quad (12.14)$$

Assuming  $y_1, y_2 = \text{const.}$ , a linear homogeneous differential equation is obtained, the characteristic equation of which is

$$T_0 s^2 - 2 y_2 T_0 s + y_1^2 + y_2^2 = 0. \quad (12.15)$$

With  $\omega_0 = 1/T_0$  the two complex roots are

$$\frac{s_{1,2}}{\omega_0} = y_2 \pm j y_1; \quad (12.16)$$

hence real and imaginary parts are subject to decoupled adjustment by  $y_1, y_2$ , as seen in Fig. 12.6b.

$y_1 = \text{const.} \neq 0$  and  $y_2 \equiv 0$  give rise to an undamped oscillation of frequency  $\omega_1 = y_1 \omega_0$ ; changing the sign of  $y_1$  results in an inversion of the phase

sequence. Correspondingly, the amplitude of the oscillation decays for  $y_2 < 0$  and rises for  $y_2 > 0$ . Since a constant amplitude  $|\underline{x}| = \sqrt{x_1^2 + x_2^2}$  is desired in steady state, this calls for an amplitude control loop as is indicated in Fig. 12.6a, where  $y_2$  serves as actuating input. Even though the control loop is nonlinear, its stability is uncritical so that a PI-controller proves adequate; when entering the square of the amplitude reference,  $|\underline{x}|_{Ref}^2$ , the root function can be omitted.

Some computed transients of the controlled oscillator are plotted in Fig. 12.7, showing time functions  $x_1(t)$ ,  $x_2(t)$  as well as the path of the state vector  $\underline{x}(t) = x_1(t) + jx_2(t)$  in the state plane. The curves indicate that the oscillator responds rapidly and in a well damped transient to changes of  $y_1$  and  $|\underline{x}|_{Ref}^2$ . Following a step change of  $y_1$ , there are no transients at all as the oscillator simply continues from the existing initial conditions with the new frequency. The state vector  $\underline{x}(t)$  is a continuous function that is well suited for use as current reference, as it enables the current control loops to track the references with small dynamic errors.

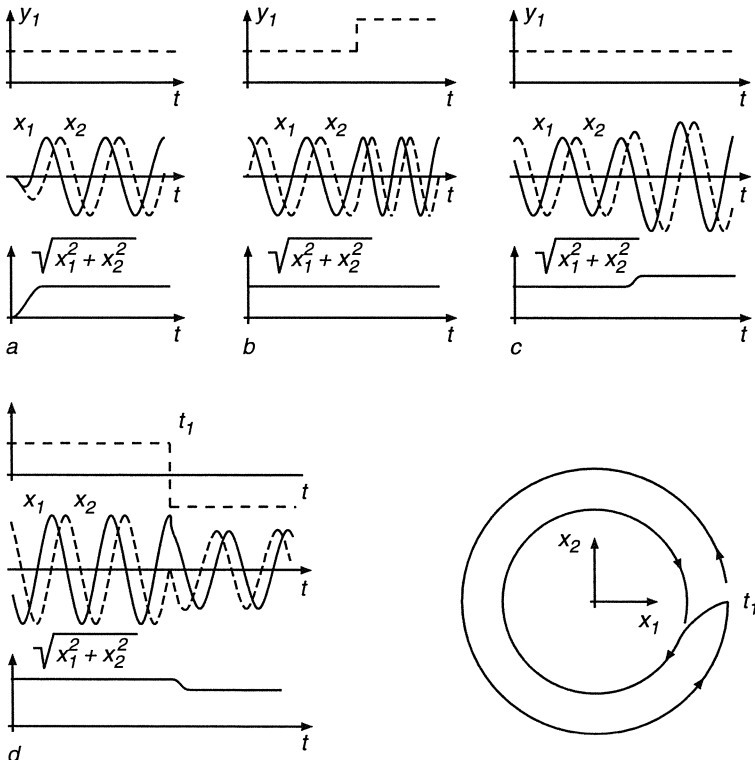


**Fig. 12.7.** Transients of controlled two-phase oscillator

The two-phase orthogonal signals  $x_1, x_2$  are now combined to form an equivalent three-phase system  $w_1, w_2, w_3$  to be used as current references

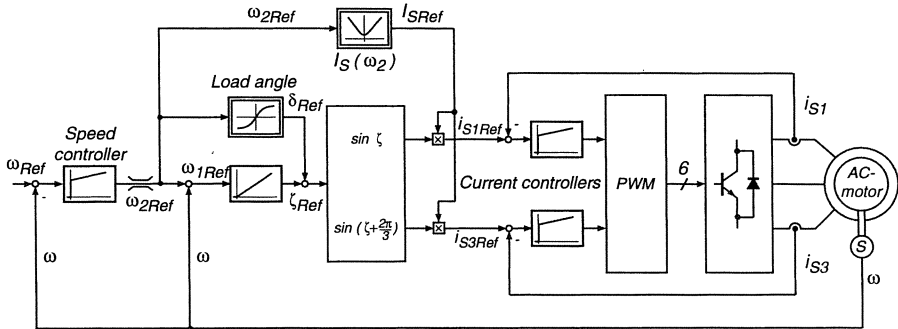


**Fig. 12.8.** Speed control scheme with impressed stator currents and open loop control of rotor flux

$$\underline{x}(t) = x_1(t) + j x_2(t) = \frac{2}{3} [w_1(t) + e^{j\gamma} w_2(t) + e^{-j\gamma} w_3(t)], \quad \gamma = \frac{2\pi}{3}. \quad (12.17)$$

In order to render the transformation unique and exclude a zero sequence component,

$$w_1(t) + w_2(t) + w_3(t) = 0 \quad (12.18)$$

is added as a side condition. A linear combination of  $x_1$ ,  $x_2$  results in a set of symmetrical three-phase reference signals for the stator currents,

$$\begin{aligned} w_1(t) &= x_1(t) = \frac{i_{S1\ Ref}}{I_{S0}}, \\ w_2(t) &= -\frac{1}{2}x_1(t) + \frac{\sqrt{3}}{2}x_2(t) = \frac{i_{S2\ Ref}}{I_{S0}}, \\ w_3(t) &= -\frac{1}{2}x_1(t) - \frac{\sqrt{3}}{2}x_2(t) = \frac{i_{S3\ Ref}}{I_{S0}}. \end{aligned} \quad (12.19)$$

A block diagram of the complete speed control system is drawn in Fig. 12.8, where the reference signals for the stator currents are supplied by the oscillator; the amplitude is derived from the function- generator which in turn is controlled by the desired rotor frequency  $\omega_2 = \omega_1 - \omega$ . By making the output of the function generator dependent on stator frequency, field weakening can also be implemented with this scheme.

The other actuating input of the controlled oscillator,  $y_1 = \omega_1 T_0$ , determining the frequency of the stator currents is obtained by combining the measured speed signal  $\omega$  with the rotor frequency reference  $\omega_{2Ref}$  as produced by the speed controller. In order to restrict the operation of the motor to the “linear” range, the rotor frequency reference must be again limited as shown in Fig. 12.8. Thus the stator frequency is determined on the basis of the measured speed and the required torque. For larger motors having low pull-out slip ( $S_p < 0.1$ ), the signal for the stator frequency is derived as the sum of two greatly differing quantities,  $\omega_1 = \omega + \omega_{2Ref} \approx \omega$ , which makes the realisation of an accurate

torque limit difficult. In order to improve this situation, the  $\omega_1$ -signal may be formed digitally. In fact, with the micro-electronic components available today the complete control scheme can be realised on a digital basis. This is of particular interest with the field orientated control described in the next chapter; only a digital equivalent of the controllable oscillator is shown here.

Part of the digital control scheme is seen in Fig. 12.9, where sections of the trigonometric functions are stored in the form of a function table in a memory chip, the address of which is the angle  $\zeta = \int \omega_1 dt$  in suitable increments. The two variables  $\cos \zeta$ ,  $\sin \zeta$  moving on a unit circle are then multiplied by the output of the function generator for the magnitude of the stator currents, before the signals are split into three phases. The dynamic response may be greatly improved by a feed forward signal based on the load angle  $\delta$ . By choosing

$$\delta = \arctan \omega_2 T_R$$

according to Eq. (12.6), the angular position of the stator ampereturns-wave is correctly advanced under load, while the flux wave remains at its former position. This simple example shows how digital techniques can be employed to great advantage.

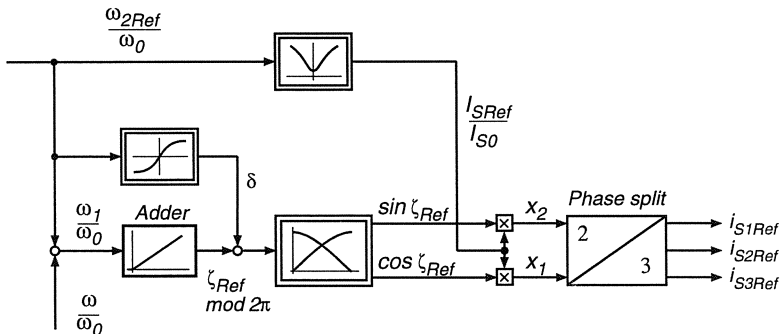


**Fig. 12.9.** Digital signal processing for obtaining variable frequency, variable amplitude current references

The control scheme shown in Fig. 12.8 was simulated on a digital computer with Eqs. (10.38 - 10.41) representing the motor, while the control loops for the stator currents were simplified by unity gain, first order lag elements [T13]. The results are plotted in Fig. 12.10 showing a starting transient with subsequent loading (Fig. 12.10a) and a speed reversal (Fig. 12.10b) commanded by inverting the speed reference. Due to the rotor frequency limit, the speed varies approximately linearly with time. It is interesting to note that the magnetising current is fairly well maintained during the transients, despite the fact that the design of the control scheme is based on a steady state model of the motor.

A digitally controlled experimental drive using a 5 kW induction motor supplied by a voltage source transistor inverter with fast current control was

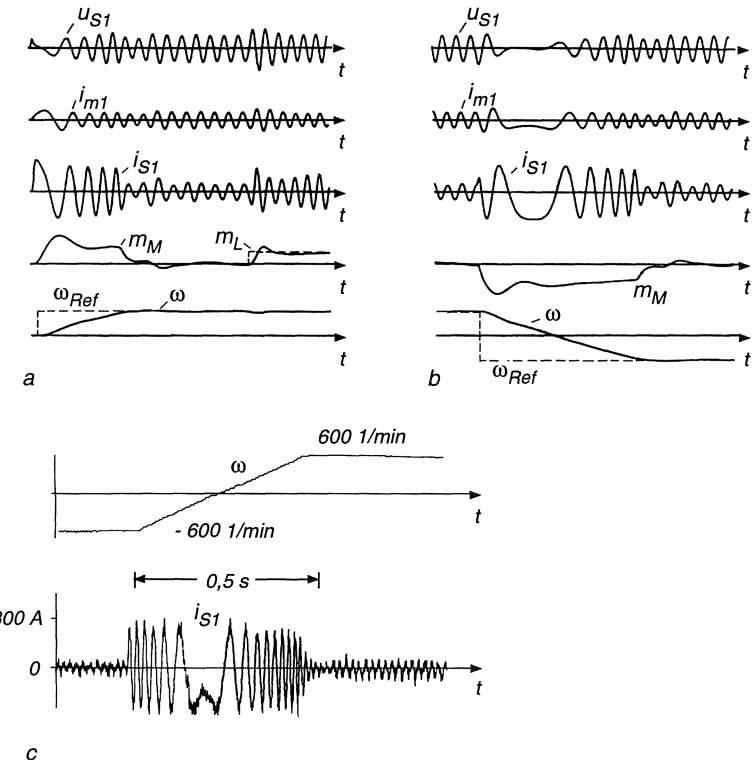


**Fig. 12.10.** Transients of induction motor drives

- a, b) Simulated results for starting, loading and speed reversal with control scheme in Fig. 12.8..
- c) Measured transient of experimental drive with digital speed control according to Fig. 12. 9

built and tested [H17]. Fig 12.10c depicts a speed transient with a high inertia load. Clearly, as the stator frequency is tracking the speed, the motor cannot be "pulled out of step" but, if overloaded, operates temporarily at the torque limit.

Even though acceptable results can be obtained with a well tuned control that is based on a steady state model of the machine, these restrictions are undesirable with high dynamic performance drives; they are avoided with the control strategies described in the following sections.

## 12.2 Rotor Flux Orientated Control of Current-fed Induction Motor

### 12.2.1 Principle of Field Orientation

The heuristic control scheme described in the preceding section is, in spite of the acceptable results obtained, not best suited for high dynamic performance drives. Because of the open loop flux control it would be difficult or impossible to operate the motor with full torque at low speed or even standstill; this, for example, excludes its application as a servo-drive. In order to remove these restrictions it is necessary to return to the dynamic model equations of the induction motor, based on instantaneous currents and voltages, as derived in Sect. 10.1. Of particular interest must be the interaction of stator and rotor currents resulting in flux and torque. Assuming initially the stator currents to be impressed by the action of fast current control loops yields again considerable simplifications since the stator voltage equation (10.38) becomes a concern of the current controllers and can be omitted from the model equations of the drive. Also, the restrictions of steady state are now avoided which is a precondition for achieving rapid transients. The power supply could be a transistor inverter with high switching frequency and adequate ceiling voltages or a cycloconverter, resulting in very fast response of the stator currents.

The expression for the electric torque (10.36)

$$m_M = \frac{2}{3} L_0 \operatorname{Im} [\underline{i}_S (\underline{i}_R e^{j\varphi})^*] \quad (12.20)$$

was obtained by describing the interaction between the rotor currents and the flux wave resulting from stator currents. Since the rotor currents cannot be measured with cage motors, it is appropriate to replace  $\underline{i}_R e^{j\varphi}$  by an equivalent quantity that could be measured with stator based sensing equipment. A good choice, as will be shown later, is the rotor flux or the equivalent magnetising current vector, defined in stator coordinates,

$$\underline{\psi}_R(t) e^{j\varphi} = L_0 \underline{i}_{mR}(t) = L_0 i_{mR}(t) e^{j\varphi(t)} = L_0 [\underline{i}_S(t) + (1 + \sigma_R) \underline{i}_R e^{j\varphi}] . \quad (12.21)$$

Eliminating the rotor current from Eq. (12.20) results in

$$m_M(t) = \frac{2}{3} \frac{L_0}{1 + \sigma_R} \operatorname{Im} [\underline{i}_S (\underline{i}_{mR} - \underline{i}_S)^*] ,$$

which is simplified to

$$m_M(t) = \frac{2}{3} (1 - \sigma) L_S \operatorname{Im} [\underline{i}_S \underline{i}_{mR}^*] . \quad (12.22)$$

Inserting the magnetising current vector according to Eq. (12.21) yields

$$m_M(t) = \frac{2}{3} (1 - \sigma) L_S i_{mR} \operatorname{Im} [\underline{i}_S e^{-j\varphi}] , \quad (12.23)$$

where

$$\underline{i}_S e^{-j\varrho} = i_S e^{j\delta} = i_{Sd} + j i_{Sq} \quad (12.24)$$

represents the stator current vector as seen from a moving frame of reference which is defined by the rotor flux or the magnetising current vector  $\underline{i}_{mR}$ . The angular relationships of the current vectors are depicted in Fig. 12.11; the stator current vector in field coordinates is seen to consist of two orthogonal components,

$$\begin{aligned} i_{Sd} &= \operatorname{Re} [\underline{i}_S e^{-j\varrho}] = i_S \cos \delta \\ i_{Sq} &= \operatorname{Im} [\underline{i}_S e^{-j\varrho}] = i_S \sin \delta \end{aligned} \quad (12.25)$$

one in the direction of the magnetising current vector and the other perpendicular to it. In steady state condition  $i_{Sd}$  and  $i_{Sq}$  are constant apart from converter induced ripple, i.e. the stator current vector  $\underline{i}_S$  and the magnetising current vector  $\underline{i}_{mR}$  rotate in synchronism. The steady state current trajectories entered in Fig. 12.11 for better clarity were derived from actual measurements with the drive shown in Fig. 12.28.

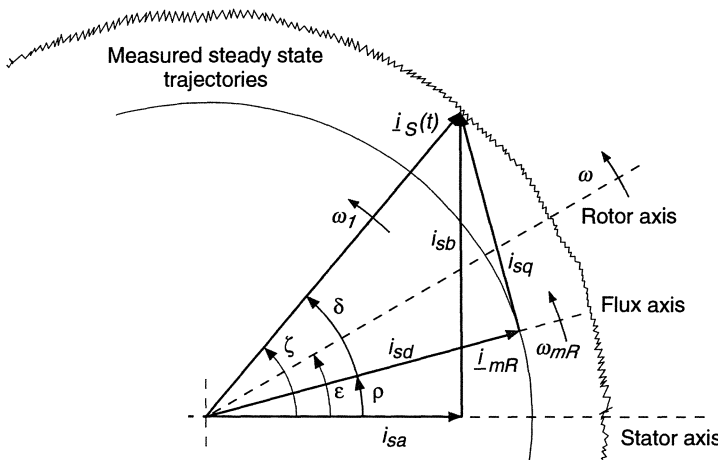


Fig. 12.11. Angular relationships of current vectors in steady state

Introducing the quadrature current component into Eq. (12.23) leads to a simple expression

$$m_M(t) = k i_{mR} i_{Sq}, \quad k = \frac{2}{3} (1 - \sigma) L_S, \quad (12.26)$$

which gives a clue, why the transformation of the stator current vector into field coordinates, also called field orientation, is the key to rapid control of AC machines. This principle has been proposed by Blaschke [B26, B27, B28, B29, B30, B31], extending earlier work [H19].

Clearly Eq. (12.26) reminds us of the expression for the electric torque of a DC machine, Eq. (5.3), where  $i_{mR}$  corresponds to the main flux  $\Phi_e$  and  $i_{Sg}$  to the armature current  $i_a$ . As seen in Fig. 12.11, the magnetising current  $i_{mR}$  is controlled by the direct component  $i_{Sd}$  of the stator current vector, which may be compared to the field voltage of the DC machine because, as will be seen, there is also considerable magnetic lag between  $i_{Sd}$  and  $i_{mR}$ . Hence,  $i_{Sd}$ ,  $i_{Sg}$  are the two independent input quantities controlling the torque of the motor;  $\delta$  represents a load angle that vanishes at no load.

The  $d - q$ -axes established by  $i_{mR}$  differ from those commonly used with synchronous machines where the transformation is based on the rotor position  $\varepsilon$ ; here the frame of reference is the rotor flux vector which moves across the stator at stator frequency and across the rotor with slip frequency.

In order to obtain the complete model of the AC motor in field coordinates,  $i_{mR}$  is now used for elimination of the rotor current from the rotor voltage equation (10.39),

$$R_R \underline{i}_R + L_0 \frac{d}{dt} \underbrace{[(1 + \sigma_R) \underline{i}_R + \underline{i}_S e^{-j\varepsilon}]}_{\underline{i}_{mR} e^{-j\varepsilon}} = 0 ,$$

which results in

$$T_R \frac{di_{mR}}{dt} + (1 - j\omega T_R) \underline{i}_{mR} = \underline{i}_S , \quad (12.27)$$

where  $d\varepsilon/dt = \omega$ .

The definitions (10.5) and (12.21) yield also the instantaneous angular velocities of the magnetising and stator current vectors

$$\begin{aligned} \frac{d\varrho}{dt} &= \omega_{mR}(t) , \\ \frac{d\zeta}{dt} &= \omega_1(t) = \omega_{mR} + \frac{d\delta}{dt} . \end{aligned} \quad (12.28)$$

Multiplying Eq. (12.27) by  $e^{-j\varrho}$  and expanding the left hand expression results in

$$T_R \frac{di_{mR}}{dt} + j\omega_{mR} T_R i_{mR} + (1 - j\omega T_R) i_{mR} = \underline{i}_S e^{-j\varrho} ,$$

which may be split into real and imaginary parts,

$$T_R \frac{di_{mR}}{dt} + i_{mR} = i_{Sd} , \quad (12.29)$$

$$\frac{d\varrho}{dt} = \omega + \frac{i_{Sg}}{T_R i_{mR}} = \omega + \omega_2 . \quad (12.30)$$

The Eqs. (12.26, 12.29, 12.30), together with the mechanical equations (10.40, 10.41) constitute a model of the induction motor in field coordinates, as described by the block diagram in Fig. 12.12. The two field-orientated input currents are produced by transforming the stator currents into a coordinate system

defined by the flux angle  $\varphi$ . This is performed in two steps, first converting the three stator currents to an orthogonal two-phase AC system,

$$i_S(t) = i_{S1} + i_{S2} e^{j\gamma} + i_{S3} e^{j2\gamma} = i_{Sa} + j i_{Sb}. \quad (12.31)$$

With the condition for balanced three phase currents,  $i_{S1} + i_{S2} + i_{S3} = 0$ , this results in

$$\begin{aligned} i_{Sa}(t) &= \frac{3}{2} i_{S1}(t), \\ i_{Sb}(t) &= \frac{\sqrt{3}}{2} [i_{S2}(t) - i_{S3}(t)]. \end{aligned} \quad (12.32)$$

These AC currents are then, by transformation into field coordinates, converted to DC quantities in steady state

$$i_S(t) e^{-j\varphi} = (i_{Sa} + j i_{Sb}) (\cos \varphi - j \sin \varphi) = i_{Sd} + j i_{Sq}; \quad (12.33)$$

hence we have

$$\begin{aligned} i_{Sd}(t) &= i_{Sa} \cos \varphi + i_{Sb} \sin \varphi, \\ i_{Sq}(t) &= i_{Sb} \cos \varphi - i_{Sa} \sin \varphi. \end{aligned} \quad (12.34)$$

The flux angle  $\varphi$  is obtained by integration of Eq. (12.30), i.e. it is an internal variable. The coordinate transformation essentially constitutes a demodulation.

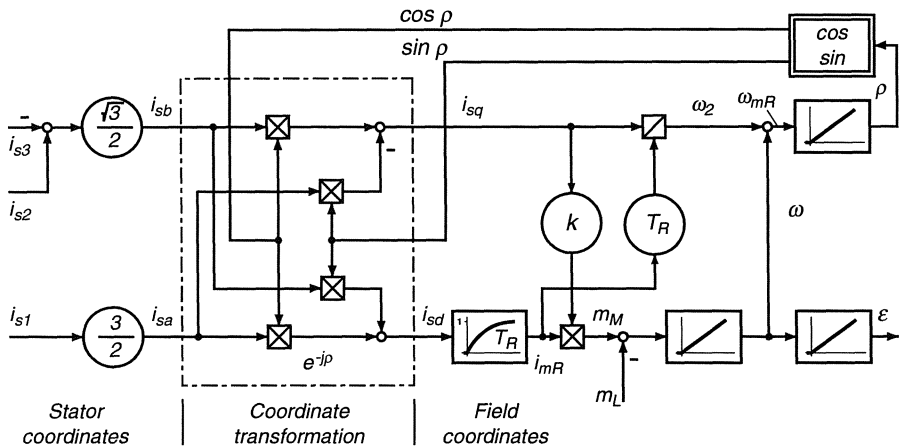


**Fig. 12.12.** Block diagram of induction motor in field coordinates, assuming impressed stator currents

Once the transformation has been completed, the dynamic-structure of the AC motor is quite straight-forward, not unlike that of a DC machine. In particular there is a large lag time constant  $T_R$  comparable to the field lag of a DC machine. Therefore the magnitude of the rotor flux or the equivalent magnetising current vector,  $i_{mR}$ , is not suitable for fast control action influencing

torque; this task should be assigned to the quadrature current  $i_{Sq}$ . The leakage time constant in the quadrature axis, which would be the equivalent of the DC armature time constant, is not effective in view of the assumed impressed stator currents.

For achieving high dynamic performance control of the AC drive, the same strategy as with the DC machine is appropriate: The magnetising current  $i_{mR}$  should be maintained at maximum level, limited below base speed by saturation of the iron core and above base speed by the ceiling voltage of the inverter, while the torque should be controlled through the quadrature current. When highest efficiency of a drive is of utmost importance, as in battery supplied vehicles, the flux level could be reduced when operating the motor for extended periods at part load, in effect balancing reduced iron losses against increased conduction losses in the motor and inverter. This was mentioned in Sect. 5.3.3 on combined armature and field control of DC motors. Of course, there is an increased delay when the flux level needs to be raised in case of sudden torque demand.

In order to alleviate the complexities of the AC control plant, it can now be attempted to cancel the coordinate transformation by an inverse transformation at the control side of the inverter; this idea, which is part of the principle of control in field coordinates as suggested by Blaschke, is illustrated in simplified form in Fig. 12.13.

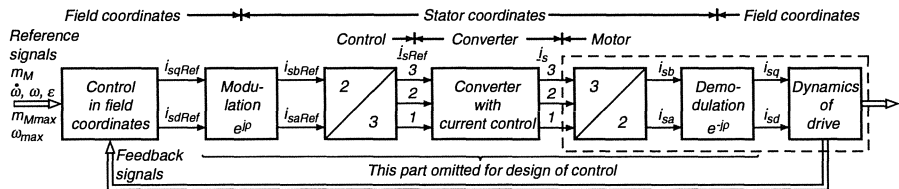


Fig. 12.13. Principle of control in field coordinates

Clearly, when inserting a modulation based on the real flux angle ( $e^{j\varphi}$ ) and a 2 to 3 phase split at the reference-, i.e. the low power- side of the current controlled inverter, the machine internal processes of phase reduction and demodulation are cancelled for the design of the control; a condition is of course that the effective lag of the inverter can be neglected and the current control loops have constant gain, i.e. the controlled inverter acts as a perfect current source.

If this condition holds, the design of the remaining control system becomes very similar to that of a DC motor control scheme; this is shown in Fig. 12.14 for a position control configuration. The three current references for the controlled inverter are obtained from the two- phase current references  $(i_{Sa}, i_{Sb})_{Ref}$  with the help of Eq. (12.31),

$$\begin{aligned} i_{S1\ Ref} &= \frac{2}{3} i_{Sa\ Ref} \\ i_{S2\ Ref} &= -\frac{1}{3} i_{Sa\ Ref} + \frac{1}{\sqrt{3}} i_{Sb\ Ref} , \end{aligned} \quad (12.35)$$

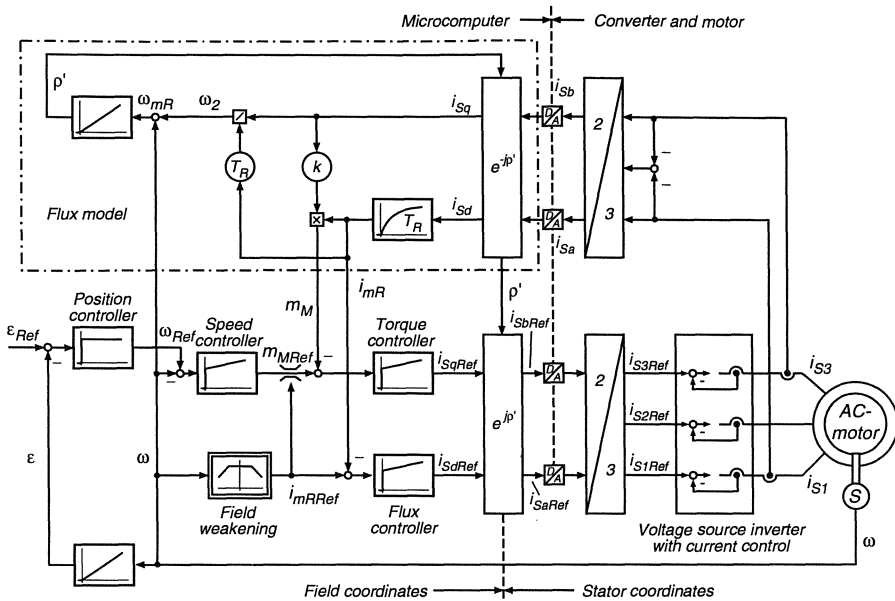


Fig. 12.14. Speed/position control in field coordinates of AC motor

$$i_{S3 \text{ Ref}} = -\frac{1}{3} i_{Sa \text{ Ref}} - \frac{1}{\sqrt{3}} i_{Sb \text{ Ref}}.$$

Preceding this phase splitting operation is the modulation of the signals  $(i_{Sd}, i_{Sq})_{\text{Ref}}$ , calling for four multiplications with trigonometric functions of the unbounded flux angle,

$$(i_{Sa} + j i_{Sb})_{\text{Ref}} = (i_{Sd} + j i_{Sq})_{\text{Ref}} e^{j\varphi'} = i_{Sd \text{ Ref}} \cos \varphi' - i_{Sq \text{ Ref}} \sin \varphi' \\ + j [i_{Sq \text{ Ref}} \cos \varphi' + i_{Sd \text{ Ref}} \sin \varphi']. \quad (12.36)$$

In order to achieve cancellation of the machine-internal demodulation, the available flux signal  $\varphi'$  should be in close agreement with the actual position  $\varphi$  of the fundamental flux wave; this aspect of flux acquisition still has to be discussed.

Proceeding in Fig. 12.14 further to the left, it is seen that the remaining control structure is the same as that of a DC machine. Instead of the armature current controller, a torque controller, whose synthetic feedback signal is derived on the basis of Eq. (12.26) from flux and stator currents, generates the quadrature axis current reference. Speed and position control loops may be superimposed. With a digital realisation, the position controller may be a simple proportional (P)-controller, as is discussed in Sec. 15.2. It would also be possible to omit the torque controller and generate  $i_{Sq \text{ Ref}}$  directly with the speed controller.

In the direct axis there is a flux controller, the reference signal of which is reduced above base speed in order to achieve field weakening; the flux reference signal also serves to reduce the torque limit at high speed.

When recalling the mechanical model in Fig. 12.1b, the strategy of field orientation is as follows: When the speed controller determines that a certain value of torque is required in order to maintain the commanded speed, a reference for the necessary tangential and radial forces is computed which is then, by coordinate transformation, converted to reference quantities for the forces  $f_1$ ,  $f_2$ ,  $f_3$ . The transformation must be based on the instantaneous position of the pin; hence the need for flux acquisition in a field orientated control scheme.

Clearly, the principle of control in field coordinates looks like a very effective way of decoupling the complex multivariable control structure of the induction machine. Its main advantages are:

- Direct access to flux and torque permitting controlled field weakening and torque limit.
- Provided the angle  $\varphi'$  used for modulation is sufficiently accurate, the motor is self controlled and cannot be pulled out of step; this corresponds to the function of the commutator on a DC-machine. When overloaded, the motor is stalled with maximum torque.
- In contrast to the schemes discussed in Sect. 12.1 the decoupling is effective in dynamic as well as steady state conditions.
- In steady state the drive controllers process DC quantities which makes the control less sensitive to unavoidable phase shifts.

The speed control system contained in Fig. 12.14 has been simulated on a digital computer, using the same set of parameters as for Fig. 12.10a, b [T13]. The current control loops were again approximated by unity gain first order lag elements. When comparing the starting, loading and reversing transients in Fig. 12.15 with those of Fig. 12.10, the superior performance of the field orientated control scheme is obvious. The flux is maintained constant and the electrical torque shows a rapid rise, limited only by the lag of the inverter; when the speed controller is clamped, the torque is precisely fixed at its maximum value.

Of course, these are only simulated results which have been computed with a highly idealised system; when realising a field orientated control scheme in practice, some serious obstacles first have to be overcome:

- Acquisition of frequency independent flux signals, representing amplitude and position of the fundamental flux wave.
- Effects of residual lag of the current controlled converter.
- Implementation of the complex signal processing shown in Fig. 12.14.
- Effects of a detuned flux model.

These problems will now be discussed separately.

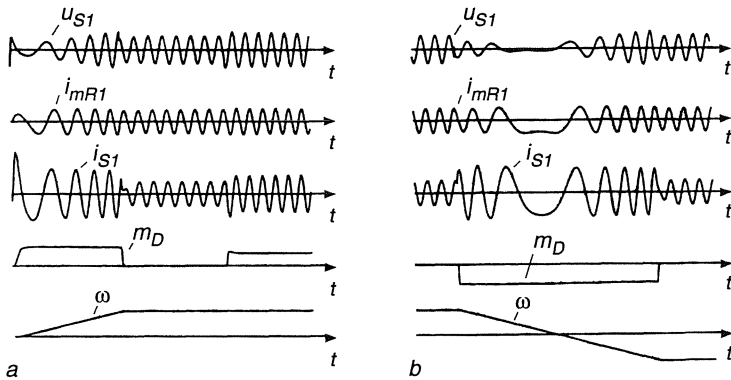


**Fig. 12.15.** Computed transients of AC motor controlled in field coordinates

### 12.2.2 Acquisition of Flux Signals

Clearly, having up-to-date information on the magnitude and phase of the fundamental flux wave is of paramount importance since this is the basis of coordinate transformation, leading to decoupled control of the currents [B30, L6].

For obtaining frequency-independent one could attempt to measure the flux density in the airgap of the machine directly by placing suitably spaced magneto-galvanic or magneto-resistive devices such as Hall-sensors on the face of stator teeth; by interpolating the local samples of flux density, an estimate of the magnitude and position of the airgap flux wave could be obtained. Then by adding a voltage component proportional to the stator current vector, a signal representing the rotor flux  $\psi_R e^{j\epsilon}$  or the magnetising current  $i_{mR}$  would result, Eq. (12.21). However, apart from the fact that the tiny Hall sensors are mechanically fragile elements which would not stand up very well under the severe vibrations and thermal stress, there are large harmonics caused by the rotor slots, the frequency of which changes with speed. This calls for adjustable filters that would be difficult to design, particularly when zero phase shift is specified. Also, the a torque signal computed from this information is likely to be unreliable since torque is an integral surface-related quantity which is difficult to estimate on the basis of a few local field measurements. Another disadvantage of this scheme is that the motor would have to be fitted with these sensors, so that it would no longer be a standard motor which could easily be exchanged for another motor taken from stock.

In order to avoid active semiconductor elements in the motor and at the same time suppress the undesirable slot harmonics, sensing coils having a width equal to full pole pitch could be installed in the stator, for example enclosed in the wedges covering the stator slots; this would geometrically filter the disturbance by the rotor slots and produce signals proportional to flux change which, after integration, would be a measure of the main flux. Again by using sev-

eral sensing coils, displaced around the circumference of the stator, and adding voltages proportional to stator currents, signals representing rotor flux could be obtained [G1, G2].

This scheme was found to work well in the laboratory down to very low frequency ( $> 0.5$  Hz), where the drift of the integrators eventually became too large; this limitation precludes the application of this scheme to drives requiring position control. Again, a specially prepared motor would have to be used.

The last mentioned disadvantage is avoided by measuring terminal voltages, i.e. using the stator windings as sensing coils. This, however, may complicate the situation even further because of the resistive voltage drop, that dominates at low frequency and must be compensated prior to integration; as the stator resistance changes with temperature this measuring scheme can become quite involved. Tests without temperature compensation have indicated a practical lower frequency limit of about 3 Hz with a 50 Hz motor. The situation may be improved when performing the integration in field coordinates, as discussed in Sect. 12.5.

Another quite different approach is based on the model equations of the motor. The equation representing rotor voltages, Eq.(12.27), a first order vectorial differential equation, may be used for computing  $\underline{i}_{mR}(t)$  in stator coordinates on-line. The measured stator currents  $\underline{i}_S$  and speed  $\omega$  could serve as input functions, with the motor being described by a single parameter, the rotor time constant  $T_R$ .

By again introducing orthogonal two phase current components

$$\underline{i}_S(t) = i_S(t) e^{j\zeta(t)} = i_{Sa}(t) + j i_{Sb}(t), \quad (12.37)$$

$$\underline{i}_{mR}(t) = i_{mR}(t) e^{j\varrho(t)} = i_{mRa}(t) + j i_{mRb}(t), \quad (12.38)$$

the block diagram of Fig. 12.16 a results which illustrates in graphical form the interactions of Eq. (12.27). The structure is similar to the controllable oscillator shown in Fig. 12.6 for  $y_1 = \omega T_R$ ,  $y_2 = -1$ .

A more direct method of computing the magnitude and position of the fundamental flux wave is to immediately convert the flux model into field coordinates, as described by Eqs. (12.29, 12.30) [S37, S40]. Again, stator currents and speed serve as input signals while the transformed stator currents  $i_{Sd}$ ,  $i_{Sq}$  and the magnetising current  $i_{mR}$  are now directly available as output signals for controlling flux and torque. The flux model in field coordinates (Fig. 12.16b) is preferable because of its greater simplicity and potential accuracy; also the output signals are constant in steady state. Of course the influence of the rotor time constant  $T_R$  is still present; this parameter may have to be updated during operation. Fig. 12.16 b corresponds directly to the model of the motor shown in Fig. 12.12 and is included as a "flux model" in Fig. 12.14.

The use of a dynamic flux model such as shown in Fig. 12.16 b offers several advantages:

- Flux signals are not based on local measurements and are not affected by slot harmonics and stator resistances.

- Use of standard motor without additional sensors is possible.
- Flux sensing is operative down to zero frequency, because no open ended integration is needed which would be subject to drift.
- The model immediately generates the variables needed for feedback control.

However, there are stringent accuracy requirements, for example with respect to the modulo  $2\pi$  integration of  $\rho$ ; this can best be solved by digital computation in a microprocessor as will be shown later. The dependence of the rotor model on the time constant  $T_R$  still constitutes a source of error because an incorrect orientation  $\rho'$  of the flux wave leads to undesirable coupling between the  $d$ - and  $q$ -axes and could endanger the control in field coordinates, eventually resulting in instability.

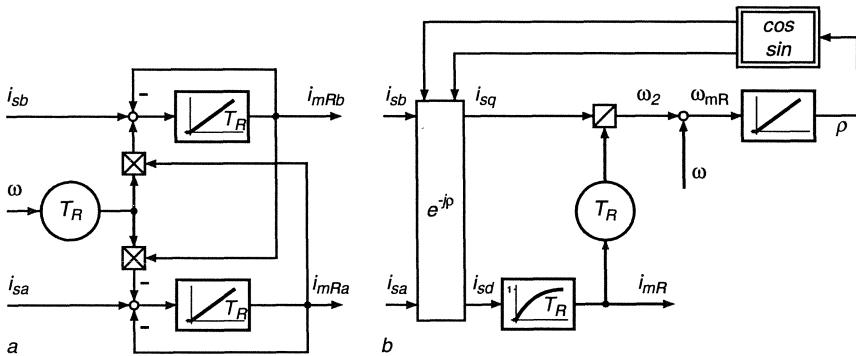


**Fig. 12.16.** Flux model for obtaining magnetising current vector  
 (a) in stator coordinates and (b) in field coordinates

Another possibility for obtaining a flux signal is the evaluation of the stator voltage equation, Eq. 10.38, when sensing the terminal voltages and currents. However, after eliminating the unaccessible rotor currents, Eq. 12.45 results which contains the rotor flux in derivative form so that an open ended integration would be necessary; again, this is likely to produce unreliable results at low speed due to changes of the stator resistance and integrator drift. This option is not pursued here, it will be further discussed in Sect. 12.5.

### 12.2.3 Effects of Residual Lag of the Current Control Loops

When explaining the principle of control in field coordinates, Fig. 12.13, it has been assumed that the stator windings are supplied from perfect current sources, i.e. that the lag of the current control loops can be neglected. This calls for a cycloconverter or a voltage source inverter with high frequency pulse-width modulation, allowing rapid access to the currents through the reference signals,

as well as adequate ceiling voltage throughout the operating range. Clearly the second condition is in conflict with an economical design of the converter because it would preclude a full utilisation of the available voltage at high speed. On the other hand, if the lag of the current controlled converter is not negligible, the decoupling by the inverse model becomes inaccurate and undesirable coupling terms arise which will eventually render the field orientated control inoperative. In order to avoid this effect, two options are available:

- Inclusion of a lead- lag network with the transfer function

$$F(s) = \frac{T_1 s + 1}{T_2 s + 1}, \quad T_2 < T_1, \quad (12.39)$$

in the reference channel of the stator current control loops.

- Addition of decoupling terms in field coordinates, i.e. prior to the transformation into stator coordinates.

For the following it is assumed that the first approach has been taken but that its potential is exhausted, leaving a residual lag  $T_e$  that cannot be reduced any further; hence the second option must be pursued.

The situation is depicted in Fig. 12.17 showing the two opposite transformations supposed to cancel and the unavoidable lag effects placed in between.

With the vectorial notation for the currents in stator- and field coordinates

$$\begin{aligned} \underline{i}_S(t) &= i_S(t) e^{j\varphi} = i_{Sa}(t) + j i_{Sb}(t) \\ {}^F\underline{i}_S(t) &= \underline{i}_S e^{-j\vartheta} = i_{Sd}(t) + j i_{Sq}(t) \end{aligned} \quad (12.40)$$

and, correspondingly, for the reference signals,

$$\underline{i}_{S\text{Ref}} = {}^F \underline{i}'_{S\text{Ref}} e^{j\vartheta}, \quad (12.41)$$

the lag effect of the inverter may be described by

$$T_e \frac{di_S}{dt} + \underline{i}_S = \underline{i}_{S\text{Ref}}. \quad (12.42)$$

With the assumption that the lag time constant  $T_e$  has been reduced to a relatively small value, the undesirable coupling is mainly due to phase shift rather than amplitude. In steady state condition, with  $i_S = \text{const.}$ ,  $\omega_{mR} = \omega_1$  and inserting Eqs. (12.40, 12.41), Eq. (12.42) yields

$${}^F \underline{i}_S = \frac{1}{1 + j \omega_1 T_e} {}^F \underline{i}'_{S\text{Ref}}; \quad (12.43)$$

when specifying a decoupled transmission,

$${}^F \underline{i}_S \stackrel{!}{=} {}^F \underline{i}_{S\text{Ref}},$$

the result is

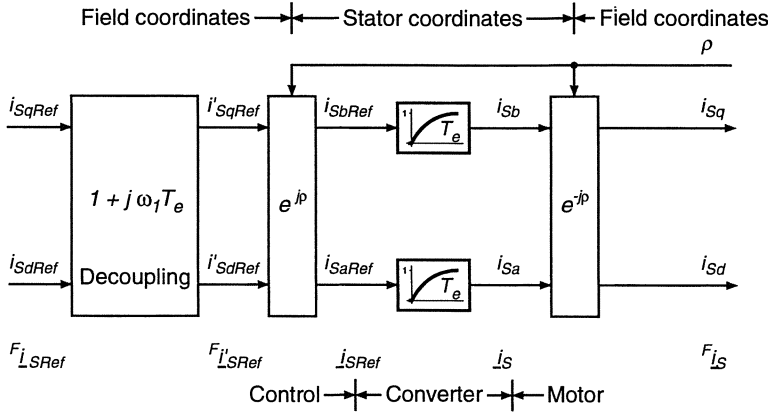


**Fig. 12.17.** Removal of undesired coupling effects caused by the residual lag of current control loops

$$F i'_{S Ref} = (1 + j \omega_1 T_e) F i_{S Ref} .$$

This means that corrective terms should be applied to the output signals of the controllers. Written in orthogonal components, this calls for

$$\begin{aligned} i'_{Sd Ref} &= i_{Sd Ref} - \omega_1 T_e i_{Sq Ref} , \\ i'_{Sq Ref} &= i_{Sq Ref} + \omega_1 T_e i_{Sd Ref} . \end{aligned} \quad (12.44)$$

The practical realisation of this additive correction is quite easy since DC signals are involved in steady state. For simplification, the speed signal  $\omega$  could be used instead of  $\omega_1$  with low slip motors. In view of the limited ceiling voltage of the inverter, the residual lag  $T_e$  of the current control loops is likely to increase with the stator frequency but if the control is implemented in a microcomputer, this effect can be offset by varying the decoupling parameter  $T_e$  as the speed changes.

The rating of the inverter is determined by the specified values of stator voltages, currents and frequency. After eliminating the rotor current from Eqs. (10.38, 12.21), the stator voltage reads

$$u_S(t) = R_S i_S + \sigma L_S \frac{di_S}{dt} + (1 - \sigma) L_S \frac{di_{mR}}{dt} , \quad (12.45)$$

where the derivatives may be obtained from Eq. (12.28). In steady state condition, i.e. with constant speed and sinusoidal currents,

$$\omega_{mR} = \omega_1 , \quad i_S = \text{const} , \quad i_{mR} = \text{const}$$

hence

$$u_S(t) = (R_S + j \omega_1 \sigma L_S) i_S + j \omega_1 (1 - \sigma) L_S i_{mR} . \quad (12.46)$$

This confirms that the fundamental component of the stator voltage rises with frequency (Fig. 12.4). When the available voltage range is nearly exhausted at the frequency  $\omega_{10}$  – some margin must be left for control – a further increase of the speed is only possible by reducing the magnetising current, i.e. by field weakening. This can be achieved with

- an open loop scheme employing a speed dependent reference  $i_{mRRef}(\omega)$  as shown in Fig. 12.14 or
- an auxiliary control loop which limits the magnitude of the stator voltage by reducing the flux reference  $i_{mRRef}$ ; a similar scheme has earlier been described for DC machines (Fig. 7.13).

When the field is reduced, the ceiling voltage of the inverter should normally be fully utilised, resulting in gradual cessation of pulse-width modulation so that each leg of the inverter eventually produces square wave output voltages (Fig. 11.6). The stator currents would then be no longer sinusoidal but the field orientated control still remains functioning as the computation of the flux and the magnetising current is based on the measured stator currents. Because of the limited voltage and stator currents, the maximum torque is, of course, reduced in the field weakening range (Eq. 10.66).

#### 12.2.4 Digital Signal Processing

The signal processing required for the field-orientated control of AC motors (Fig. 12.14) as well as the flux acquisition using a dynamic model (Fig. 12.16) is of considerable complexity; in particular, the various multipliers and function generators needed for the coordinate transformation are difficult to adjust accurately when realised with analogue components. On the other hand, on-line digital control was economically impractical as long as it had to be performed by large and costly process computers. These obstacles have delayed widespread application of the sophisticated control schemes needed for AC drives.

However, this situation has changed dramatically since digital processors have now shrunk to minute size thanks to the progress of microelectronics. The reduction in volume and cost and the advances in processing power have in the meanwhile reached a point where all the signal processing required for a high dynamic performance AC drive can be executed by a single microprocessor which, together with the associated peripheral components, finds room on a postcard sized printed circuit board. The main advantage of digital control with microprocessors is that the same standard hardware can be used for many different applications because the function of the processor is determined by a flexible and individually designed program, i.e. by software; once the program has been developed and verified it can be duplicated at negligible cost and transferred to a read-only memory chip connected to the processor.

A precondition for the digitalisation of signal processing is, of course, an adequate resolution of the signals with respect to amplitude and time, i.e. sufficient

word length and computing speed. The current 16 bit-processors are quite suited from these points of view; a 16-bit representation of variables corresponds to an internal resolution of one part in more than 65,000; if 10- or 12-bit analogue-to-digital converters are employed for converting the analogue signals from the plant, such as stator currents or motor speed, the effects of quantisation are usually unnoticeable; however, there are still exceptions, when higher internal resolution, such as 32 bit, proves to be necessary with some variables. A reduced word length, such as 10 bit, is usually adequate for the *D/A*-converters, i.e. at the output of the microprocessor because the *D/A*-converter is part of the plant and thus under the surveillance of the digital controller, whereas errors in the *A/D*-converter produce false signals.

The choice of the required resolution in time is more complex as it depends not only on the type of drive but also on the particular function within the drive control. Clearly, when sampling and processing non-sinusoidal currents having a fundamental frequency of 100 Hz, a higher sampling frequency is necessary than for the digital realisation of speed or position control, where the rate of change is restricted by the inertia of the drive. As long as computational speed of the processors was a major consideration which is no longer the case with todays microprocessors, an advantage could be gained by employing different sampling periods for the different tasks. For example, for an experimental 1.5 kW induction motor servo drive having a PWM-transistor power supply and an 8086 control unit, the following sampling periods proved commensurable with fast control transients [S37].

- a) Sampling period of 1 ms for

- A/D*-conversion of stator currents
- Updating of flux model
- Conversion to field-coordinates
- Current and torque control
- Conversion of *d/q*-currents to stator coordinates
- Output of current references

- b) Sampling period of 5 ms for

- Flux control including field weakening
- Speed control
- Position control

1 ms-sampling of the stator currents is adequate up to a stator frequency of about 100 Hz, when the currents are sampled and processed ten times per period; at this frequency the flux vector is computed at 36° intervals which can make the use of a simple extrapolation scheme desirable. At still higher stator frequency, faster sampling of the variables is required. For high dynamic performance servo drives, a sampling period of  $200\mu s$ , corresponding to a 5 kHz sampling frequency is often specified; this can be achieved with signal processors [S38, S39]. Another possibility are application specific integrated circuit

(ASIC's), where all the control software is incorporated as custom-hardware on special chips [K27, K28, K29, K30, T10].

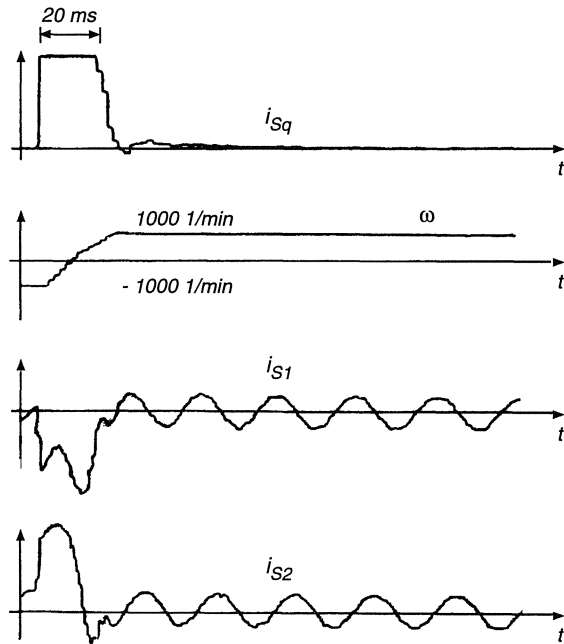


**Fig. 12.18.** No-load speed reversal of 1.5 kW induction motor with transistor inverter and microprocessor control

With a high resolution incremental speed/position sensor producing 8000 increments per revolution the speed signal has a frequency of 200 kHz at the rated speed of 1500 1/min for a 4-pole, 50 Hz motor. Hence a 5 ms sampling period of the speed controller results in a speed measurement of 1000 counts at rated speed and correspondingly less at lower speed. Since this is usually inadequate with regard to resolution and accuracy, a quasi-analogue sensing scheme providing finer resolution at low speed could be employed [S41]; another option is to convert the sensing scheme from frequency- to time-measurements which allows better resolution at low speed; this is discussed in Sect. 15. 2.

The incremental position sensor mentioned before can serve for sensing angular position as well as speed; when the forward/reverse pulses are accumulated in a reversible counter, which is initially set by a reference pulse, the angular position of the shaft may be detected at the sampling instants by the microprocessor. Forming the difference between two subsequent samples provides a measure of the average speed in the last interval. Naturally, an encoder, delivering at any instant the absolute angular position of the shaft would be preferable

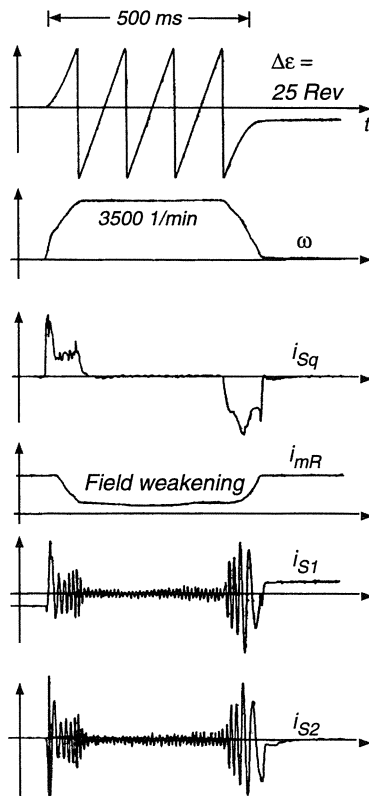


**Fig. 12.19.** Step-response of position control loop of 1.5 kW induction motor drive with microprocessor control

for speed and position sensing as it removes the ambiguity with regard to initial position, but this advantage has to be balanced against considerably increased cost and complexity.

The design of linear sampled data control systems is part of the general control theory that has been exhaustively covered in the literature; there is no lack of proven design methods, e.g.[40]. A look at Figs. 12.13 and 12.14 reveals that even though the control plant is highly nonlinear, a considerable degree of decoupling and linearisation is achieved through the method of field orientation. In addition, the principle of cascade control, identical to that applied to DC drives, serves for consolidation by allowing a step-by-step design of the control structure. All that has been said about the design of controlled DC drives, including the combination of feed-forward and feed-back control as seen in Fig. 7.5, remains applicable here, because the difference between a DC and an AC drive is, apart from changed parameters, confined to the block "Torque

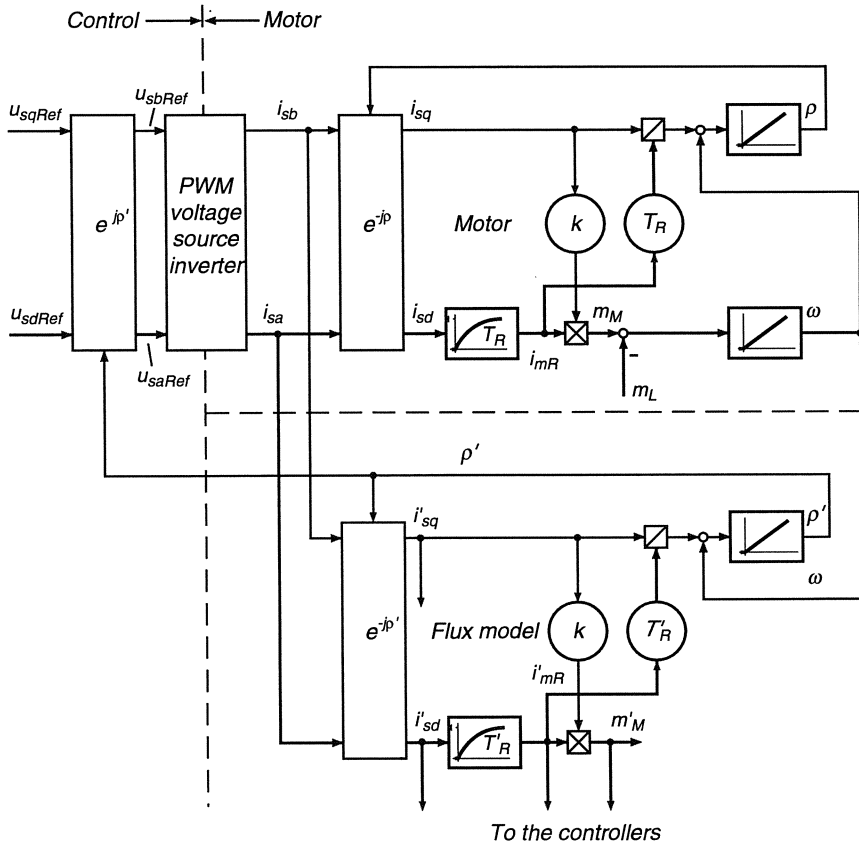


**Fig. 12.20.** Flux model acting as an open loop observer for the motor flux and the field orientated currents

control loop". Further simplification is due to the fact that relatively high sampling frequencies can be chosen with a suitable microprocessor; as a result, the control functions in the outer loops are practically continuous so that the added complexity of sampled data design procedures is avoided.

As an example, the difference equation of a PID-controller relating the sampled control error  $e(\nu)$  to the actuating signal  $y(\nu)$  may be written in straight parallel form

$$y(\nu) = G \left[ e(\nu) + \frac{T}{T_i} \sum_{-\infty}^{\nu} e(\mu) + \frac{T_d}{T} [e(\nu) - e(\nu - 1)] \right] \quad (12.47)$$

where  $T$  is the sampling interval,  $G$  the controller gain and  $T_i, T_d$  the time constants of the integrating and derivative channels respectively. The equation is to be solved in real time by the microcomputer. The integrating term would normally be computed recursively in the form

$$y_i(\nu) = \sum_{-\infty}^{\nu} e(\mu) = y_i(\nu - 1) + e(\nu). \quad (12.48)$$

It is important that all the variables are bounded in order to prevent numerical overflow with integer arithmetic, or undesirable signal overshoot if floating point arithmetic is employed.

The discrete transfer function of this controller is, letting  $z = e^{Ts}$ ,

$$F(z) = \frac{Y(z)}{E(z)} = G \left[ 1 + \frac{T}{T_i} \frac{z}{z-1} + \frac{T_d}{T} \frac{z-1}{z} \right]. \quad (12.49)$$

### 12.2.5 Experimental Results

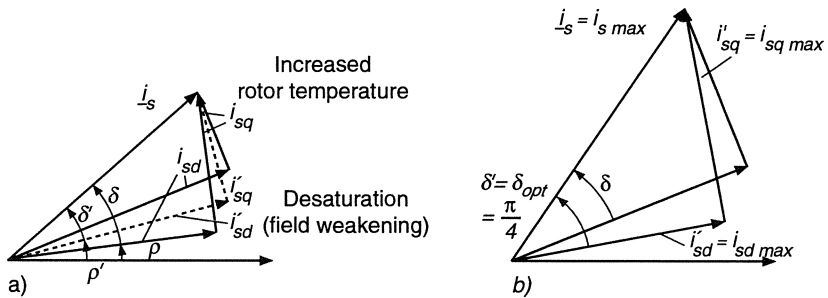
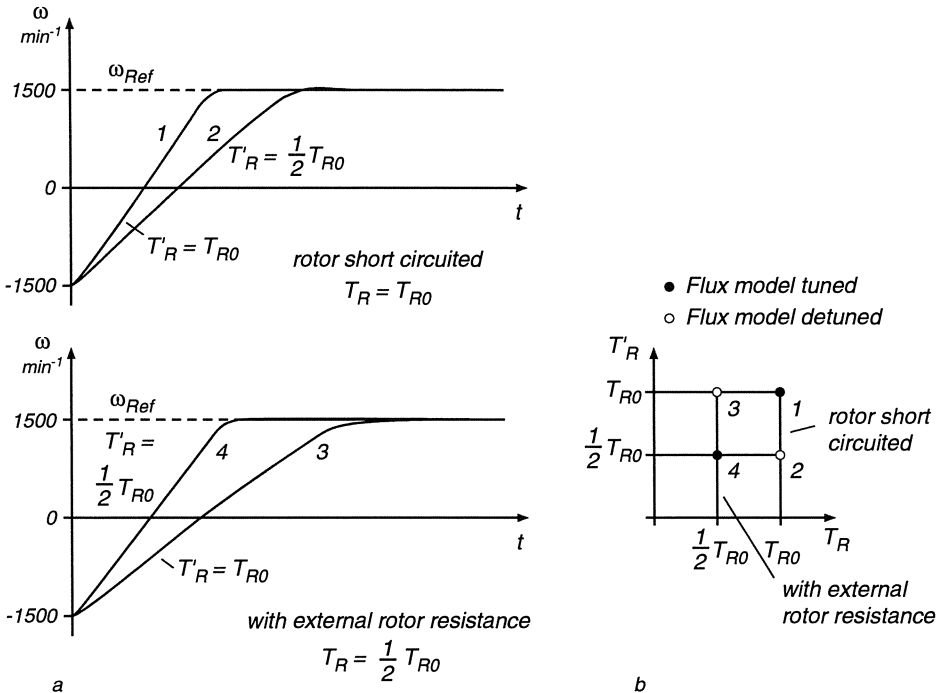


Fig. 12.21. Vector diagram of detuned flux model

Figures 12.18 and 12.19 show speed and position control transients of a 1.5 kW induction motor with a switched transistor power supply and microprocessor control; the motor was not loaded during the tests. The 8086-based control algorithm comprised altogether 8 k bytes of read-only-memory [S40]. The response of the drive is exemplified by the fact that after a fraction of one revolution the motor reaches field weakening speed. The smooth and rapid transients, resembling the simulated results in Fig. 12.15, indicate that field orientation is indeed a powerful concept of controlling AC drives with high dynamic performance.

### 12.2.6 Effects of a Detuned Flux Model

The parameter  $T_R$  can be expected to change slowly due to changes of rotor temperature, but instantaneously when operating into the field weakening range, when the motor core becomes desaturated. The interaction is described by Fig. 12.20, where it is seen that the flux model of Fig. 12.16 b, controlled by the measured stator currents and speed, functions as an open loop observer in parallel to the motor dynamics. It produces estimates of the flux angle  $\rho'$  and



**Fig. 12.22.** Reversing transients of 22 kW wound rotor motor with correctly set and detuned flux model. **a)** Reversing transients at limited currents; **b)** operating points in  $T_R, T'_R$ -plane.

the field orientated current components  $i'_{Sd}$ ,  $i'_{Sq}$  and  $i'_{mR}$  to be used as feedback variables for the control.

The vector diagram in Fig.12.21 indicates the deviation of the load angle  $\delta' = \arctan \omega_2 T'_R$  produced by a flux model, that may have been tuned to the motor at nominal temperature and flux level, and the actual load angle of the motor  $\delta = \arctan \omega_2 T_R$ . The deviation is

$$\Delta\delta = \delta' - \delta = \arctan \frac{\omega_2(T'_R - T_R)}{1 + \omega_2^2 T'_R T_R}, \quad (12.50)$$

$\Delta\delta > 0$  for  $T_R < T'_R$  caused by overheated motor

$\Delta\delta < 0$  for  $T_R > T'_R$  caused by cold or desaturated motor

The maximum deviation may cover a range of  $0.75T_{R0} < T_R < 1.5T_{R0}$  with a converter-fed motor where full line voltage starts do not occur, assuming a setting of the flux model according to nominal conditions at rated load of the motor.

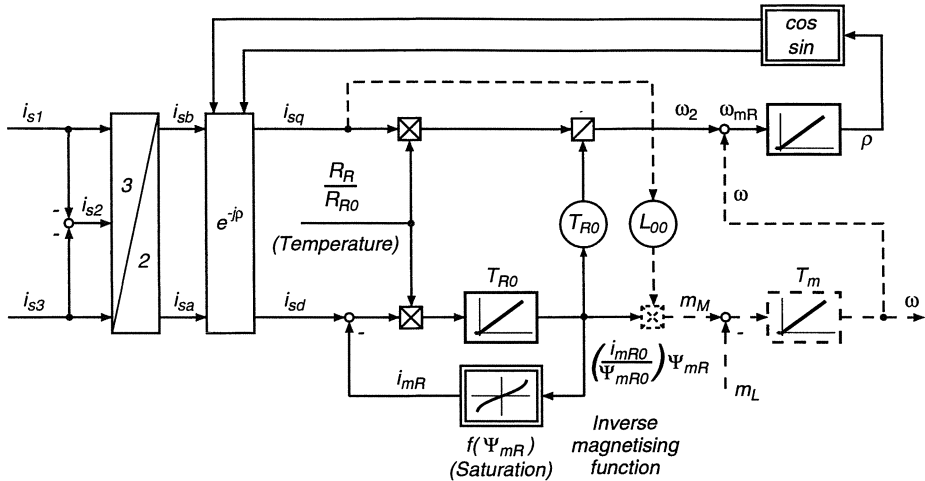


**Fig. 12.23.** Nonlinear flux model, containing a nonlinear function for saturation effects and a control input for on-line tuning the rotor resistance

The effect of a detuned flux model is unnoticeable when the motor is only partially loaded, because the speed controller would generate the quadrature current reference  $i'_{SqRef}$  needed for producing the torque, even though the flux may be somewhat increased or reduced. When the motor is fully loaded, however, so that  $i'_{SqRef}$  becomes limited, there is an actual loss of torque, i.e. the motor cannot be fully loaded. This is demonstrated in Fig.12.22, where a 22 kW wound rotor motor was controlled through a speed reversal with tuned and detuned flux model. The tests were performed with two values of rotor resistance and corresponding rotor time constants  $T_R$ , [H23, L40]. When the flux model is correctly set (1,4 in Fig.12.22 a,b), full torque is produced, whatever the rotor resistance; with detuned flux model (2,3 in Fig.12.22 a,b), the torque is reduced, resulting in a lower value of acceleration.

Of course, with an increased rotor resistance the motor operates at higher rotor frequency and lower efficiency for producing the same torque, as was shown in Fig.10.11.

The flux model in Fig.12.16 b may be further refined by adding a nonlinear function representing saturation [S40] and an additional input for a temperature-dependent rotor resistance, as shown in Fig.12.23 [H24]. The saturation curve could be identified for a given motor in the factory or prior to commissioning in the field, whereas the slow variations of the rotor resistance can be tuned on-line, based on temperature measurements or some identification procedure. An experimental result is seen in Fig.12.24, where the same motor used before is accelerated at current limit through a wide speed range with a linear flux model according to Fig.12.16 b and with the nonlinear model of Fig.12.23; the variation of the magnetising current  $i_{mR}$  is also shown in both

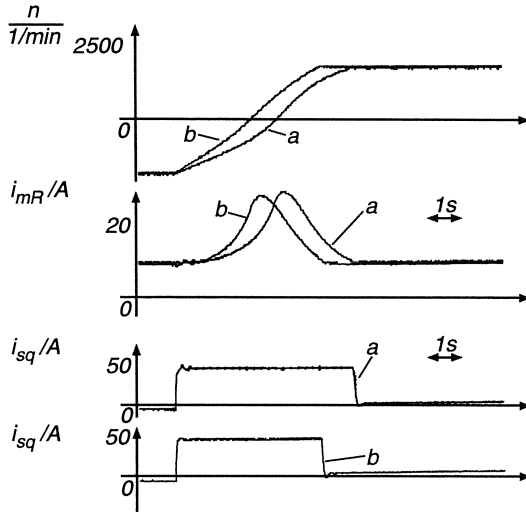


**Fig. 12.24.** Reversing transients of 22 kW motor through the field weakening speed range, (a) without and (b) with a saturation-dependent flux model

cases. Clearly, taking the magnetic nonlinearity into account results in a better tracking of the flux and again increases the maximum torque at the given current level.

A variety of schemes has been suggested for identifying the varying motor parameter  $T_R$ , most of which call for additional measurements by making use of the stator voltage equation e.g. [G7]. An identification method without the need of a voltage measurement [G5, G6] is based on the observation that the output signals  $i'_{SdRef}$ ,  $i'_{SqRef}$  of the controllers in Fig. 12.25 allow decoupled control of the plant in the  $d$ -,  $q$ -axes only if the angle  $\varrho'$  used for the modulation is in agreement with the actual position  $\varrho$  of the flux wave. Hence a low level characteristic test disturbance injected into the presumed  $i'_{SdRef}$  channel must be uncorrelated with the noise in the real  $i_{Sq}$ -channel, expressed for example by the speed error at the input of the speed controller. If there is noticeable correlation it can serve as an indication that the supposed  $d'$ -axis is not orthogonal with the actual  $q$ -axis and, neglecting other sources of error, the parameter  $T'_R$  in the flux model needs to be corrected in order to track the plant. The correlation process is manageable when it can be performed in the microprocessor used for controlling the drive. For example, by employing a pseudo-random binary sequence (PRBS) as a test disturbance, the generation of the signal, its correlation with the speed error and the adjustment of the parameter in the flux model are straight-forward, requiring very little additional computing time. The sign of the cross correlation function points to the direction in which  $T'_R$  should be adjusted. The sampling time of the PRBS should be chosen sufficiently small in order to allow the field lag to attenuate the signal, i.e. to avoid an immedi-

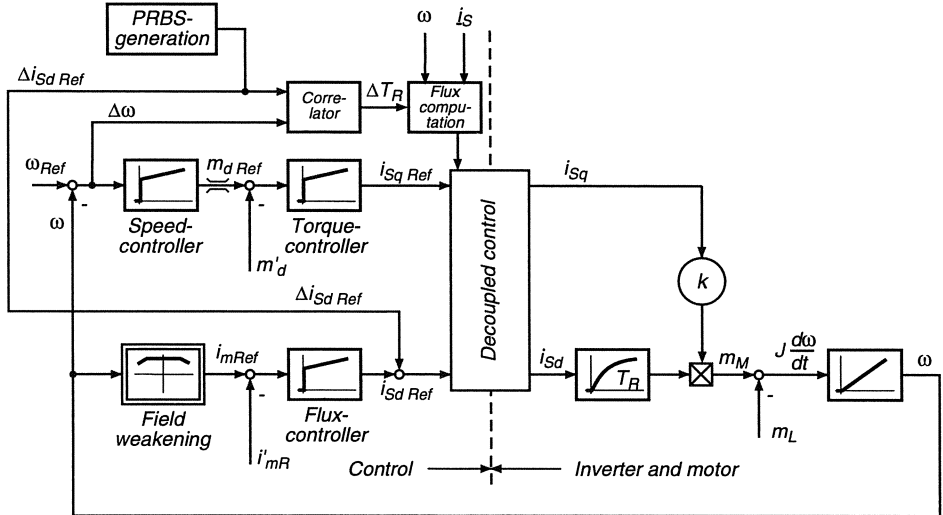


Fig. 12.25.  $T_R$ - Identification through correlation

ate effect on the torque through variation of  $i_{mR}$ . On the other hand, building up a meaningful correlation function requires averaging time for suppressing irrelevant noise components.

Another  $R_R$ - adaptation method that is somewhat easier to implement was described in [H23, H24, S38]; it is based on a comparison of voltage signals obtained by measurements and derived from the flux model. Eq.(12.45) may be written in the form

$$e_S(t) = (1 - \sigma) L_S \frac{di_{mR}}{dt} = u_S(t) - R_S i_S - \sigma L_S \frac{di_S}{dt}, \quad (12.51)$$

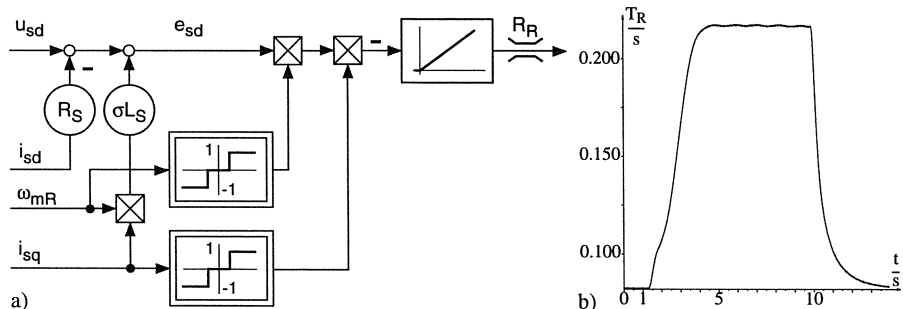


Fig. 12.26.  $R_R$ - self-tuning employing terminal voltages. a) Self-tuning scheme; b) experimental results with 22kW wound rotor motor.

where  $e_S(t)$  is the "voltage behind the transient stator impedance". Assuming  $R_S$  to be known, for instance from a temperature sensor in the stator winding, and  $\sigma L_S$  to be relatively unaffected by saturation,  $e_S(t)$  may be derived from a measurement of terminal voltages and currents. When converting this equation to field coordinates defined by the rotor flux model in Fig. 12.20 or 12.23, we find for the direct component

$$e_{Sd} = (1 - \sigma) L_S \frac{di_{mR}}{dt} = u_{Sd} - R_S i_{Sd} - \sigma L_S \frac{di_{Sd}}{dt} + \omega_{mR} \sigma L_S i_{Sq}, \quad (12.52)$$

which reduces in steady state to

$$e_{Sd} \approx u_{Sd} - R_S i_{Sd} + \omega_{mR} \sigma L_S i_{Sq} \Rightarrow 0. \quad (12.53)$$

As the angle of transformation  $\rho'$  being derived from an initially detuned model, may be incorrect, this condition is not automatically satisfied but may be used for self-tuning the model according to

$$T_{adapt} \frac{d(T'_R/T_{Ro})}{dt} = \frac{e_{Sd}}{U_{So}}. \quad (12.54)$$

This scheme is shown in Fig. 12.26 a; in order to obtain convergence, the signs of  $\omega_{mR}$  and  $i_{Sq}$  have to be correctly chosen. Also, there are lower practical limits of speed and load, for which the adaptation yields reliable results. When the rotor current is close to zero at low load, a correct setting of  $T'_R$  is not important, provided the parameter is quickly adjusted when load is applied. A test result is seen in Fig. 12.26 b taken on a 22 kW wound rotor motor, with external rotor resistors being switched in and out. The lag of a few seconds would normally be acceptable for correcting a temperature induced variation of the rotor resistance.

### 12.3 Rotor Flux Orientated Control of Voltage-fed Induction Motor

The field orientated control scheme in Sect. 12.2 was introduced with the simplifying assumption of current sources in the stator circuits; this was achieved by fast control loops for the stator currents, making use of MOSFET- or IGBT-inverters with ample ceiling voltage and short access time caused by high switching frequency. Of course, these conditions cannot be met at maximum speed, where square voltage waveforms are desired in order to fully utilise the inverter; hence the concept of impressing currents becomes impractical in the field weakening speed range.

Another area of application, where the approach with current sources and, in steady state condition, nearly sinusoidal stator currents has to be abandoned is that of pulse-width modulated voltage-source inverters for higher power drives employing thyristors and GTO-thyristors. The switching frequency of such inverters is usually below 1 kHz, as compared to 10 kHz for IGBT- or 20 kHz for MOSFET-inverters. As a consequence, the harmonics of the stator currents

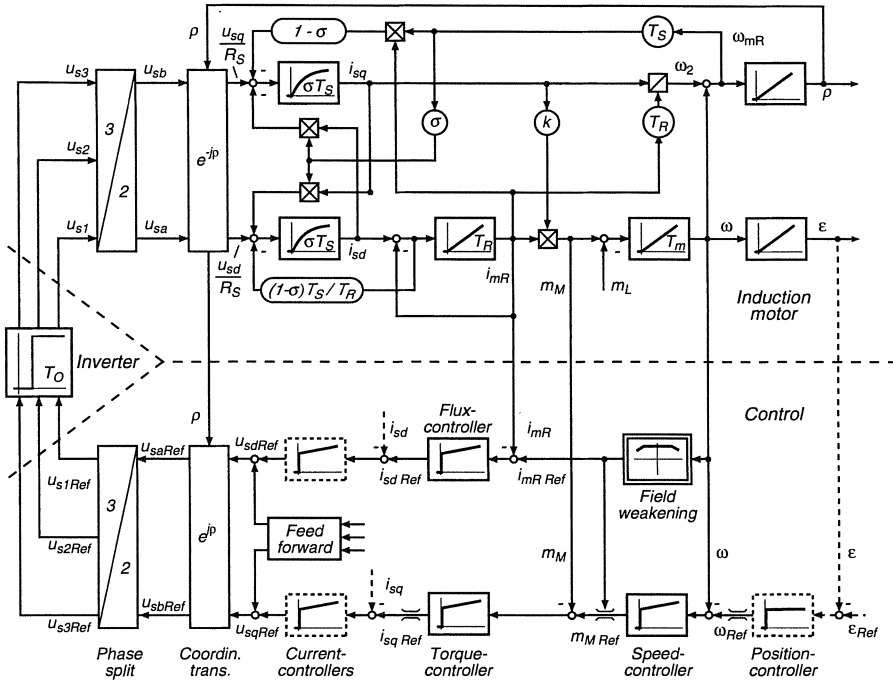


**Fig. 12.27.** Block diagram of induction motor control in field coordinates, assuming voltage source inverter (- - - optional)

may be of appreciable magnitude and the assumption of nearly “instantaneous” current control becomes questionable.

As a result, the stator voltage equation (10.38) now has to be taken into account as well; by inserting the magnetising current vector, Eq. (12.21), which represents the rotor flux and converting the voltage vector to field coordinates as in Eq. (12.24),

$$\underline{u}_S(t) e^{-j\varrho} = u_{Sd} + j u_{Sq}, \quad (12.55)$$

the stator voltage equation (10.38) is transformed into field coordinates,

$$\sigma T_S \frac{di_{Sd}}{dt} + i_{Sd} = \frac{u_{Sd}}{R_S} - (1 - \sigma) T_S \frac{di_{mR}}{dt} + \sigma T_S \omega_{mR} i_{Sq}, \quad (12.56)$$

$$\sigma T_S \frac{di_{Sq}}{dt} + i_{Sq} = \frac{u_{Sq}}{R_S} - (1 - \sigma) T_S \omega_{mR} i_{mR} - \sigma T_S \omega_{mR} i_{Sd}. \quad (12.57)$$

These equations describe the interactions between the field-orientated stator voltages and currents; together with Eqs. (12.26, 12.29, 12.30) and the equations for the mechanical part of the plant (10.40, 10.41) they form the mathematical model of the voltage-fed induction motor in field coordinates. This model is contained in graphical form in the upper part of Fig. 12.27. The additional right-hand side terms in Eqs. (12.56, 12.57) constitute undesirable coupling terms

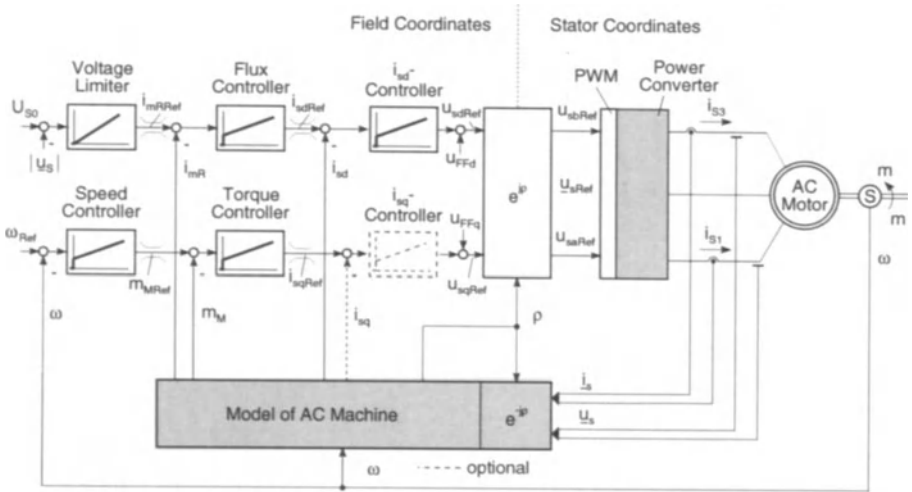


**Fig. 12.28.** Microcomputer control of induction motor with a voltage source PWM–inverter

which could be compensated by suitable feed forward signals at the output side of the current controllers [G3, G4].

The principle of field orientated control, applied to this scheme, is as follows: when representing the control dynamics of the voltage source inverter by a small delay that is related to the clock frequency of the modulator, the transformations within the plant are again cancelled by inverse operations performed on the reference side. Of particular importance is of course the transformation from the field-orientated into the fixed stator coordinate system

$$u_{S\text{ Ref}} = (u_{sd} + j u_{sq})_{\text{Ref}} e^{j\varphi'}, \quad (12.58)$$

where  $\varphi'$  is again the angle of the fundamental flux wave as determined by a flux acquisition scheme, for instance the flux model shown in Fig. 12.16 b. The main difference between the control schemes in Fig. 12.14 and Fig. 12.27 is that the current control is now performed in field coordinates, where the controllers are processing DC signals in steady state, thus avoiding the problem of phase shift of AC current loops. Also, the digital part of the control may now include the pulse-width-modulator and can be extended up to the generation of the switching signals for the inverter.

The remaining part of the control system is similar to the one shown in Fig. 12.14. The control structure in Fig. 12.27 is somewhat redundant since the task of  $i_{sd}$ - and  $i_{sq}$ -control could be assumed by the flux and torque controllers. Field weakening is achieved with a function generator defining a speed-dependent reference for the magnetising current; limiting the stator voltages with a superimposed voltage control loop would be equally possible.

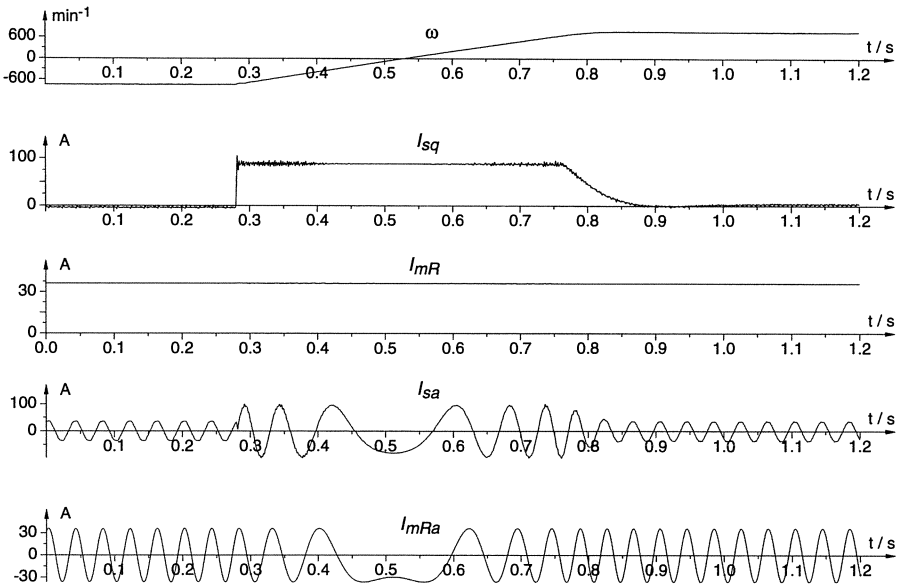


**Fig. 12.29.** Reversing transient of 22 kW induction motor drive with voltage source inverter and microcomputer control at no load

A 22 kW induction motor fed by a voltage source transistor inverter with vectorial PWM and controlled by a signal processor programmed in C language has been designed and tested in the laboratory. The block diagram of the somewhat modified control structure is seen in Fig. 12.28 [K39].

In contrast to the scheme in Fig. 12.27, field-weakening is here performed by a limiting controller for the magnitude of the stator voltages, corresponding to the solution shown in Fig. 7.13 for a DC motor. The inverter was a 30 kVA experimental unit with a clock frequency of 1.37 kHz; the sampling frequency for the inner loops is twice the clock frequency and an integer fraction thereof for the outer control loops.

A reversing transient of the speed controlled drive is depicted in Fig. 12.29, with the inertia of the drive increased by a DC dynamometer. The transient confirms the expectations by showing nearly perfect decoupling of the  $d - q$ -axes; this is manifested by the constant magnetising current and the rapid rise to maximum value of the quadrature current representing torque. While the stator currents exhibit large transient terms, the magnetising current remains practically sinusoidal; this is due to the large lag  $T_R$ , acting as a low pass filter.

The rise time of the torque is less than 2 ms which is the limit given by the control dynamics of the PWM-inverter; this rapid response is superior to that of a high-performance DC drive with 6-pulse line-fed converter at 50 Hz. The pertinent loci of the stator- and the magnetising current vectors  $i_S(t)$ ,  $i_{mR}(t)$  are seen in Fig. 12.30. Again, the magnetising current vector reverses on a near

perfect circular path, while the stator current vector is temporarily boosted in order to produce the desired torque.

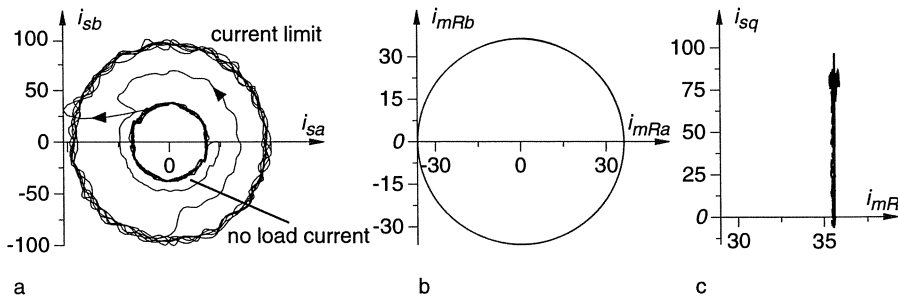


**Fig. 12.30.** Stator current and magnetising current vectors of PWM-inverter drive during the speed reversal shown in Fig. 12.29 **a,b)** Currents in stator coordinates, **c)** in field coordinates.

## 12.4 Field Orientated Control of Induction Motor with a Current Source Inverter

The current source thyristor converter described in Sect. 11.3 is of interest for many AC drive problems because of the simplicity of the power circuit. As indicated in Fig. 11.14 the control function is naturally performed in polar coordinates, where the magnitude of the stator current vector, being in noncommutation state directly proportional to the link current, is controlled through the line side converter, while the angle  $\zeta(t)$  of the stator current vector,

$$\underline{i}_S(t) = i_S(t) e^{j\zeta(t)} = \sqrt{3} i_D(t) e^{j\zeta(t)}, \quad (12.59)$$

is determined by the switching state of the machine side converter. Due to the link reactor and the reactances of the motor,  $i_S(t)$  and  $\zeta(t)$  are both continuous functions. Outside the commutation intervals  $\zeta(t)$  is identical with the switching state  $\xi(t)$  of the machine side converter, where  $\xi(t)$  advances in forward or reverse direction in increments of  $60^\circ$ . Control of  $\xi(t) \bmod 2\pi$  may be accomplished by switching a hardware ring counter with six states.

To this basic control structure which is motivated by the power converter circuit, the principle of field orientation can also be applied; one possible solution is drawn in Fig. 12.31. In the upper right hand corner it contains the model of the induction motor in field coordinates assuming impressed stator currents. The direct and quadrature current components  $i_{Sa}$ ,  $i_{Sq}$  are obtained from  $i_S$  and  $\delta = \zeta - \varrho$  by a polar to rectangular conversion ( $P/R$ ). The inverse operation ( $R/P$ ) is seen at the output of the flux and torque controllers. The transformation into stator coordinates is achieved by simply adding to the load angle reference

$\delta_{Ref}$  the angle  $\varrho$  mod  $2\pi$  of the flux wave as obtained by some method of flux acquisition. The output signals of the drive control are the reference values for the magnitude and angle of the stator current vector,  $i_{SRef}$  and  $\zeta_{Ref}$  respectively. The former is supplied to the control loop for the direct link current which is represented in Fig. 12.31 in simplified form.  $T_D$  is the filter time constant of the DC link circuit,  $U_S$  the effective supply voltage of the machine side converter which acts as a disturbance to the current control loop;  $U_S$  depends on speed, flux and stator current of the motor.

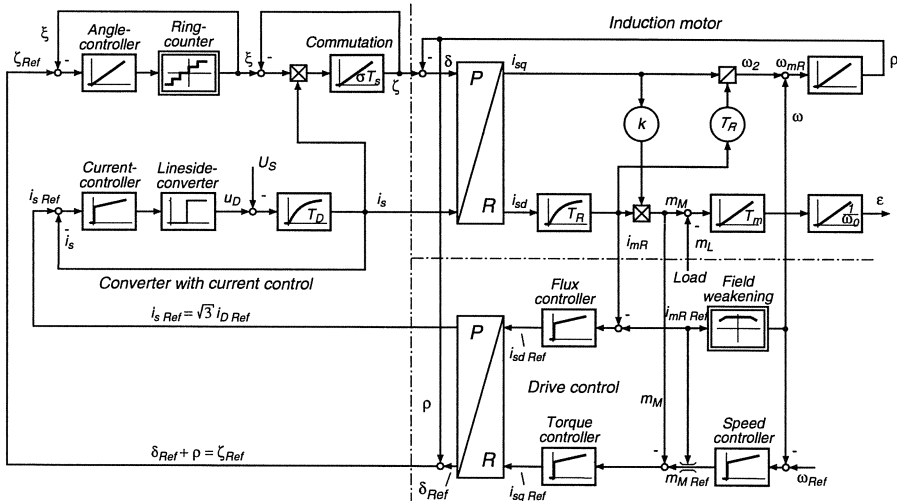


Fig. 12.31. Control scheme of induction motor supplied by current source inverter

A problem arises in the second channel where a finely discretised reference angle  $\zeta_{Ref}$  is to be tracked by a feedback signal having only six discrete angular states. An approximate solution is to employ pulse-width modulation, i.e. switching the ring counter back and forth between two adjacent states [W8]; this can be achieved with the help of an angle control loop. For this purpose the state  $\xi$  of the ring counter which is readily available in digital form can be used as feedback signal. The current angle  $\zeta$  follows the position of the ring counter with a commutation lag that is related to the leakage reactance of the motor; the time required for commutation depends on the link current because at reduced current it takes longer to recharge the capacitors. This is qualitatively modelled in Fig. 12.31 by a current dependent gain factor. The reversible switching of the ring counter takes place only at low speed, it gradually ceases as the stator frequency rises; the angle controller then reverts to unidirectional switching.

The pulse-width modulation achieved by the angle control loop has the added benefit of reducing the effect of torque pulsations at low speed which are caused by the interactions of the stepped stator ampereturns-wave and the continuously moving flux wave. However, as was mentioned before, the frequency of

the pulse-width modulation is much lower than in the case of a voltage source inverter, where the commutation is practically independent of the motor reactances. Hence the current source inverter is not best suited for continuous position control, where extended operation at very low speed or even standstill with controlled torque may be required. The situation is different with discontinuously operated drives having position control such as needed for boring machines or screw-down drives on reversing rolling mills; in these applications the positioning drive is made inoperative and the brakes are set, once the desired angular position has been reached.

The speed control scheme of an experimental 22 kW drive, employing a commercial current source inverter and an 8086 single board computer is seen in Fig. 12.32 [G5, G6]. The main portion of the block diagram is similar to the one shown in Fig. 12.28; differences are evident in the output section, where an analogue reference for the link current and a pulse sequence for controlling the ring counter are now generated; another addition is the feed-forward signal to the angle control loop in order to reduce its velocity error. It is noted that the converter is controlled on the lower level by a hardware sequencer which maintains minimum separation of the firing pulses in order to assure complete commutation; these protective functions are not shown in the diagram. At an advanced stage of development they can also be realised by software or special integrated hardware.

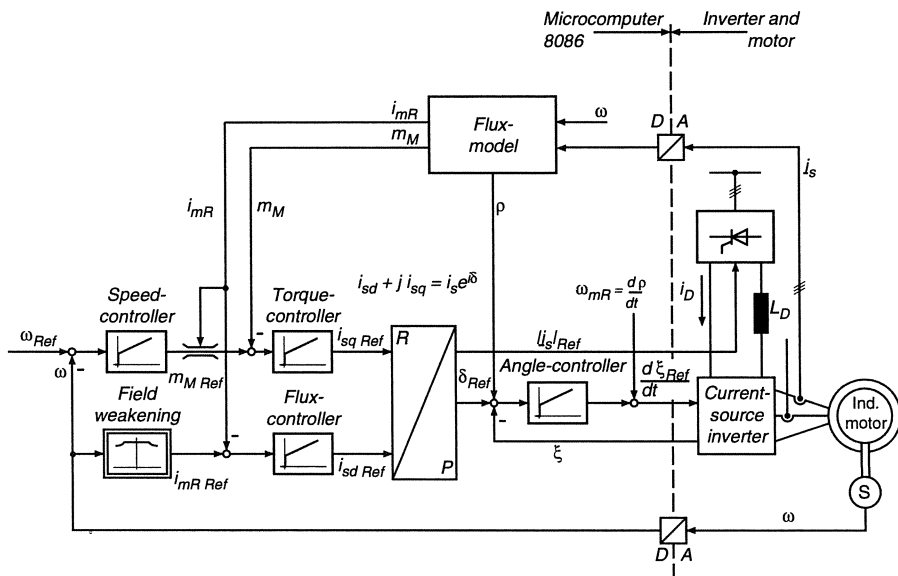


**Fig. 12.32.** Microcomputer control of induction motor with current source inverter

A reversing transient of the 22 kW drive at half rated speed is recorded in Fig. 12.33 which again shows the good decoupling of the  $d - q$ -axes achieved

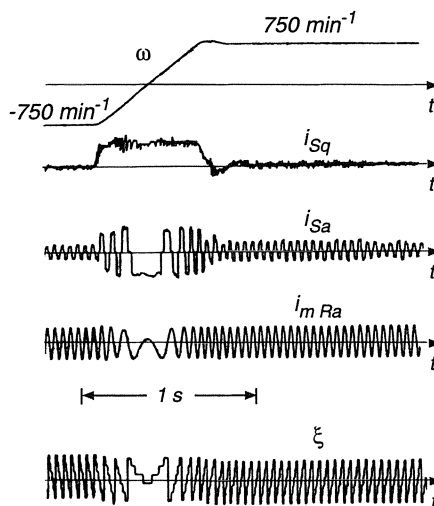


**Fig. 12.33.** Reversing transient at half rated speed of a 22 kW current source inverter drive

by field orientated control. The rise time of the torque is about 10 ms, the magnitude of the flux is maintained nearly constant. As seen in the lower traces the magnetising current is practically sinusoidal while the stator currents have a highly distorted waveform. The motor was again connected to a DC dynamometer at no load.

The behaviour of the drive at low speed is demonstrated by the transient in Fig. 12.34 where a slow speed ramp causes the pulse-width modulation to take effect around zero speed. This is clearly seen from the trace of the switching state  $\xi(t)$  of the ring counter; as soon as the speed leaves the narrow band around standstill, the modulation ceases and the angle controller continues with a unidirectional switching sequence.

Characteristic loci of the current vectors are seen in Fig. 12.35 during a speed reversal at very low speed. Initially the stator current vector is stepping around the six-pointed star; when, a reversal of the speed is commanded, the magnitude increases sharply and the direction of the rotation is inverted. After a few steps the speed reversal is completed and the magnitude of the current vector is reduced to its former no-load value.

The locus of the magnetising current vector is again nearly unaffected by the switching operation, even though the radius of the locus is not quite as perfectly constant as in the case of the voltage source inverter drive (Fig. 12.30), indicating a somewhat reduced dynamic quality of control; this is of course due to the lower switching frequency of the current source inverter.

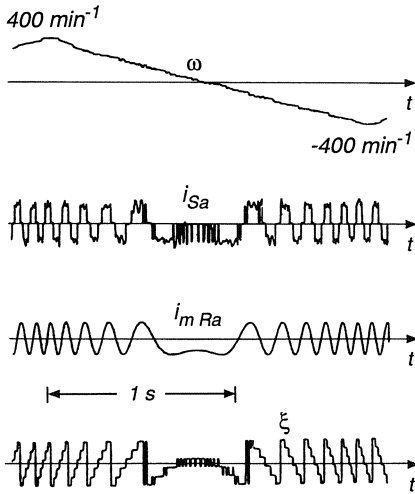


**Fig. 12.34.** Slow speed reversal of current source inverter drive

In general it can be stated that both types of thyristor fed induction motor drives show similar behaviour in steady state operation and for large amplitude transients. Differences do exist, however, at very low speed, where the current source inverter causes a slightly cogging motion while the voltage source PWM inverter produces a perfectly smooth operation even at standstill. A noteworthy feature of the current source inverter is that it performs with very little audible noise which is in contrast to some voltage source PWM inverters unless higher switching frequency or special modulation techniques are employed.

Further progress is achieved with the circuit in Fig. 11.16, where a current source PWM-inverter with GTO-thyristors is supplying an ACmotor having filter capacitors across its terminals [A14, A15, N15, N16, N17, N19]. With a suitable choice of the capacitors and the switching frequency this results in greatly improved waveforms of the motor voltages and currents than is possible with either voltage source or current source inverters discussed so far. As a consequence, the additional copper- and iron- losses in the motor are reduced; there are also lower voltage stresses on the insulation of the windings .

Since the inverter is now feeding a low impedance load, the commutation again becomes independent of the motor, as with a voltage source inverter, and can operate at a comparable switching frequency, producing smoother motor torque. Instead of zero voltage intervals there is now the possibility of employing zero current intervals where the link current bypasses the motor, thus creating additional degrees of freedom for designing PWM strategies. At the same time, the advantages of regeneration by inverting the link voltage instead of the current and the ease of protection, with the link reactor limiting the rise of the current in case of malfunction of the inverter, are the same as in the

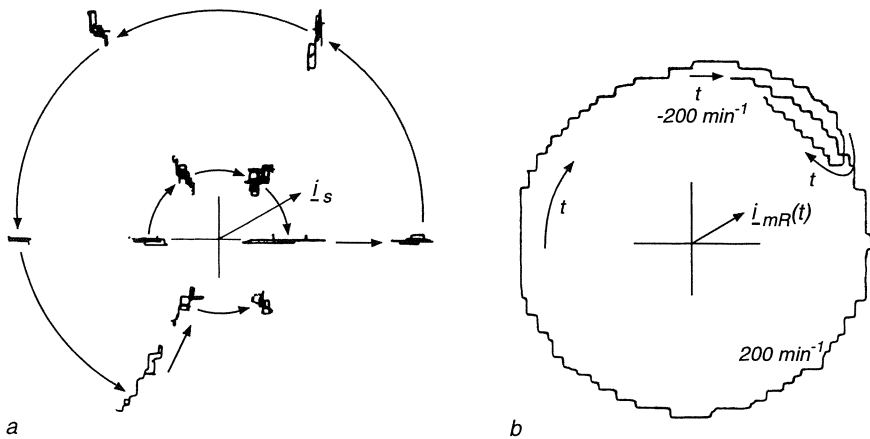


**Fig. 12.35.** Stator and magnetising current vectors of current source inverter drive during a speed reversal at 200 1/min

original current source inverter circuit in Fig. 11.14. The circuit can also be combined with a symmetrical PWM line side converter as was shown in Fig. 11.13 for the case of a voltage link. Since the diodes are no longer needed, a very simple circuit with only 12 GTO-thyristor branches results; reversing the power flow requires the link voltage  $U_D$  to change sign.

Naturally, because of the additional energy storages, the circuit in Fig. 11.16 presents more formidable control problems in the form of resonances between the motor reactances and the capacitors. This is made evident by the extended mathematical model of the drive.

The stator voltage differential equation (10.38) which, after substituting the rotor current  $i_R e^{j\varphi}$  with the rotor based magnetising current  $i_{mR}$ , became, (Eq.12.51),

$$\sigma T_S \frac{di_S}{dt} + i_S = \frac{u_S}{R_S} - (1 - \sigma) T_S \frac{di_{mR}}{dt} = \frac{u_S}{R_S} - \frac{e_S}{R_S}; \quad (12.60)$$

the voltage  $e_S$  was interpreted as the main field voltage “behind the transient impedance” of the motor,

$$e_S(t) = (1 - \sigma) L_S \frac{di_{mR}}{dt} = (1 - \sigma) L_S \left[ \frac{di_{mR}}{dt} + j \omega_{mR} i_{mR} \right] e^{j\varphi}. \quad (12.61)$$

This is now supplemented by the stator current equation

$$C \frac{du_S}{dt} = i_P - i_S, \quad (12.62)$$

where  $i_P$  is the current vector supplied by the GTO-inverter,

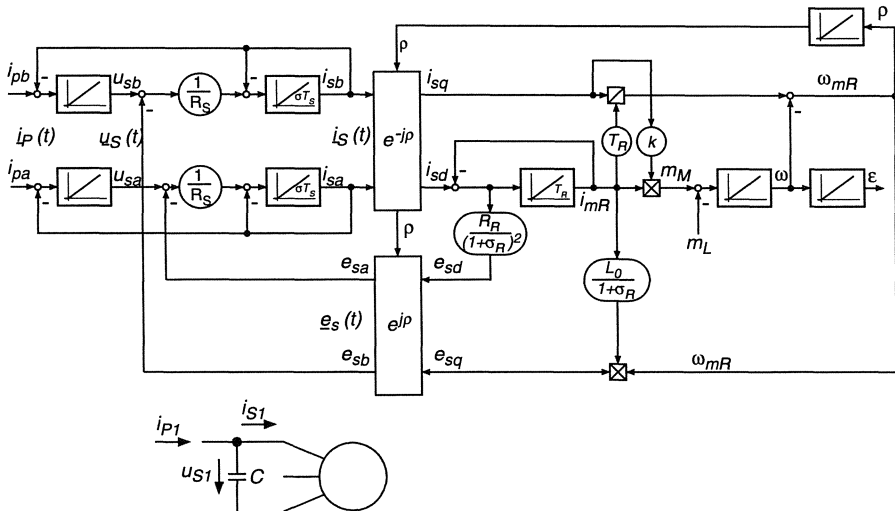


**Fig. 12.36.** Block diagram of current source PWM inverter with GTO–thyristors and capacitive filter

$$i_P = \sqrt{3} i_D(t) e^{j\xi(t)}, \quad (12.63)$$

and  $\underline{i}_S = i_S(t) e^{j\xi(t)}$  is the vector of the stator currents. As with a voltage source inverter (Fig. 11.7) the angle  $\xi(t)$  of the inverter current can assume six discrete equidistant values; in addition there are zero vectors  $\underline{i}_P = 0$  caused by short circuits of the inverter, when the current bypasses the load.

The block diagram in Fig.12.36 describes the extended dynamic system, using a hybrid representation of the motor, where the stator side quantities are left in stator coordinates, while the remaining motor dynamics are in field coordinates. The block diagram of the GTO–inverter, in accordance with its mode of operation, could also be drawn in polar form.

As mentioned before, the control of this type of drive is more complex, it requires a high performance signal processor in order to achieve a stable and well damped response. Some steady state and dynamic results, that have been obtained with a 55 kW motor using a model based predictive control strategy [A14, A15], are seen in Fig. 12.37 and 12.38. Clearly, this could be a very promising approach to future AC motor drives, combining smooth waveforms of voltages and currents with excellent dynamic performance. These advantages are also beneficial for the design of the motor, because the electrical stresses of the winding insulation are reduced when the steeply rising voltages caused by the "hard-switching" inverter are avoided and the motor is relieved from the task of serving as a filter choke.

For higher power ratings such as compressor-, mine hoist- or rolling mill drives, cycloconverters employing natural commutation are the natural choice as long as their frequency limit is not exceeded. Their control structure is similar

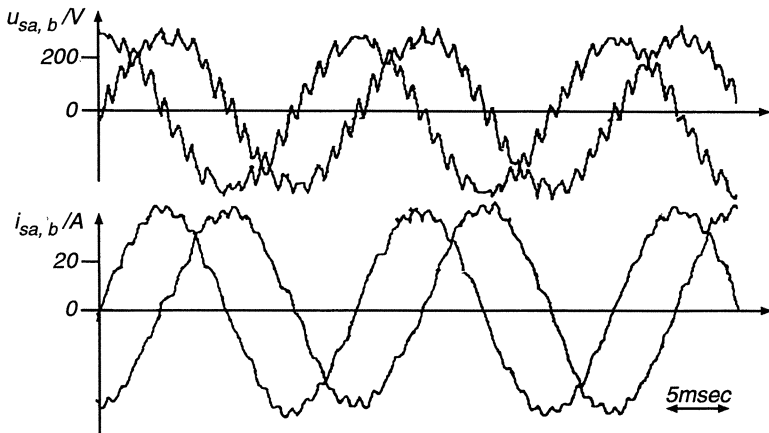


**Fig. 12.37.** Waveforms of terminal voltages and currents of a 55 kW, 50 Hz motor with current source GTO inverter operating at a stator frequency of 50 Hz. Reactive power of the capacitive filter is 24 kVA, switching frequency of inverter 500 Hz.

to the one described in Sect. 12.2 where control loops for the stator currents provide nearly impressed and close to sinusoidal currents.

If the range of stator frequency rules out the use of a cycloconverter, a synchronous motor with a load commutated current source inverter could be used; this is discussed in Sect. 14.3.

## 12.5 Stator Flux Orientated Control of an Induction Motor Without a Mechanical Sensor

### 12.5.1 Machine Model in Stator Flux Coordinates

After the basic problems of controlling induction motors with high dynamic performance had been solved by applying the principle of field orientation, where information on the magnitude and orientation of the flux wave is derived from a “flux model”, i.e. a mathematical model to be computed in real time on a microcomputer, the attention of researchers has turned towards simplification as well as refinement of these quite sophisticated control methods. One point where further progress is desirable is the omission of the mechanical speed/position sensor needed with many of these control schemes; for instance, the rotor flux model introduced in Fig. 12.16 calls for a measurement of speed, even in cases where the specification of a moderate accuracy would not make a speed sensor mandatory. Electrical measurements are usually acceptable since the sensors can be placed anywhere, preferably inside the inverter cabinet, but a mechan-

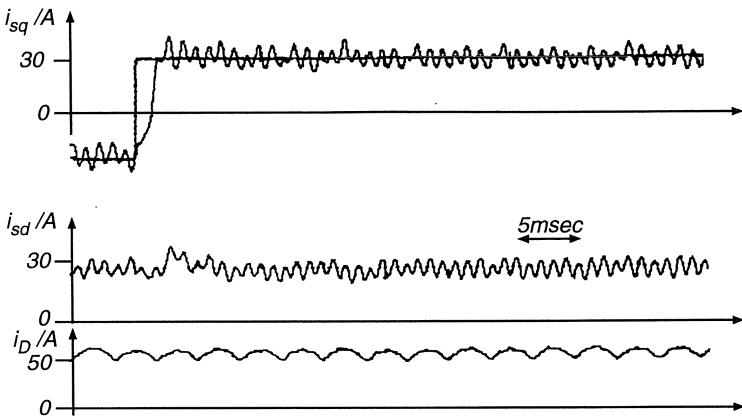


**Fig. 12.38.** Step response of torque control loop with the 55 kW current source GTO inverter drive used for Fig. 12.37

ical sensor is often undesirable because of space restrictions or the added cost and complexity; such arguments have particular weight with smaller motors. Of course, a certain loss of accuracy and dynamic response will be unavoidable when the speed sensor is omitted, making such schemes not immediately applicable to highest performance, for instance as required by machine tool feed drives.

One reason, why the omission of a mechanical sensor has become such a prominent topic, is surely the fact that the powerful microcomputers which are now available at reasonable cost for the control can be applied to estimating and controlling unmeasurable internal quantities; hence it makes sense to employ their potential also for producing an estimate of speed. Had microcomputers been widely used for controlling DC machines, the same demands would have been raised there.

The various proposals for the design of controlled AC drives without a mechanical sensor have in common that only terminal quantities, i.e. stator voltages and currents are measured from which the information on flux and speed of the motor must be derived, given a nominal knowledge of the important motor parameters. An ideal estimation algorithm should produce the necessary signals on the flux wave as well as mechanical speed and, in addition, provide information on changing motor parameters, so that the flux- and speed- models can remain tuned to the motor. Of course, it is unlikely that all these expectations can be fulfilled simultaneously, still it is a goal worth pursuing and, when applying powerful numerical procedures, there may be effective ways for solving some of these problems, e.g. [H35, H53, O6, O10, T4].

The three tasks mentioned may be classified as “Observation” and “Identification”

- Acquisition of flux wave,
- Reconstruction of speed,
- Estimation of machine and load parameters;

they are posing different demands with regard to response time as well as accuracy. The estimation can only be based on the available mathematical model of the motor, a set of six nonlinear real-valued differential equations with uncertain parameters, Eqs.(10.38 - 10.41). Since flux acquisition is the most time-critical, being a basis for the control, it is reasonable to select a coordinate frame of reference that can be directly employed for the subsequent control; the choice is either a stator flux- or a rotor flux-based coordinate system. Both have their advantages and disadvantages as discussed, for example in Sect. 12.2 and 13.1. Since rotor currents cannot be measured with cage motors and all measurements have to be stator based, a stator flux coordinate system related to the equivalent circuit in Fig. 10.7c could be chosen for a change.

With the definition of a stator flux vector

$$\underline{\psi}_S(t) = L_0 \underline{i}_{mS}, \quad (12.64)$$

where

$$\underline{i}_{mS} = i_{mS}(t) e^{j\mu(t)} = (1 + \sigma_S) \underline{i}_S + \underline{i}_R e^{j\epsilon} \quad (12.65)$$

represents a stator based magnetising current, the unaccessible rotor current may be eliminated from Eqs.(10.38, 10.39), resulting in two equations for  $\underline{i}_{mS}$  and  $\underline{i}_S$ ,

$$L_0 \frac{d\underline{i}_{mS}}{dt} = \underline{u}_S - R_S \underline{i}_S \quad (12.66)$$

and

$$\sigma L_S \frac{di_S}{dt} + L_S (1/T_R - j\omega\sigma) i_S = L_0 \frac{d\underline{i}_{mS}}{dt} + L_0 (1/T_R - j\omega) i_{mS}. \quad (12.67)$$

The “voltages behind the stator resistances” are integrated in Eq.(12.66) resulting in  $i_{mS}$  and  $\mu$ . This is the moving frame of reference defining “stator flux coordinates”; the stator current vector in field coordinates is then

$$i_S e^{-j\mu} = i_{Sd} + j i_{Sq}. \quad (12.68)$$

By defining an inner voltage vector, that contains information on flux and speed,

$$\underline{u}_S = -\frac{R_R}{1 + \sigma_R} \underline{i}_{mS} + j\omega L_S \left( \frac{\underline{i}_{mS}}{1 + \sigma_S} - \sigma \underline{i}_S \right), \quad (12.69)$$

Eqs.(12.67, 12.66) assume the form,

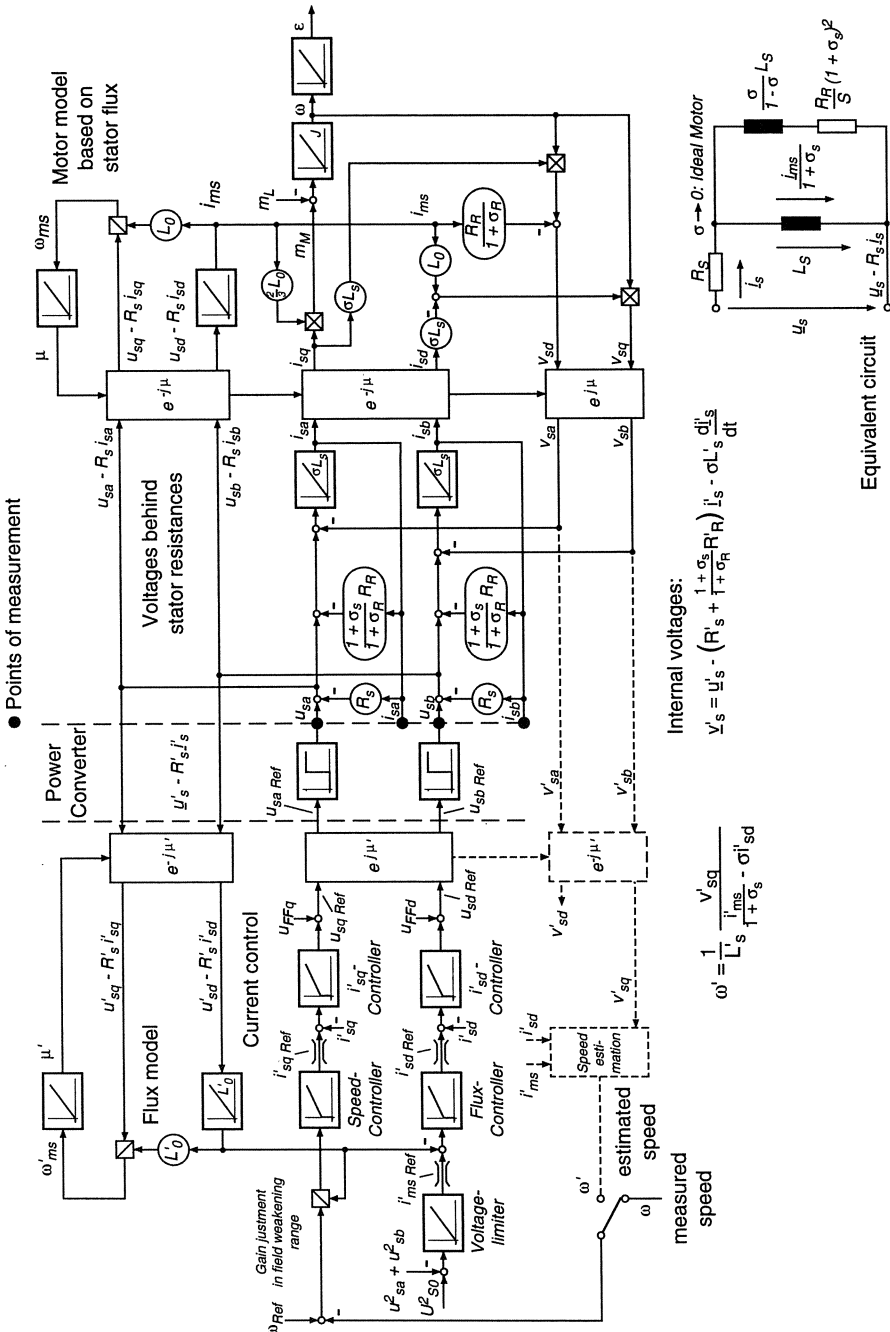


Fig. 12.39. Dynamic model of an AC motor in stator- flux coordinates and example of a control scheme without a mechanical sensor

$$\underline{u}_S = \underline{u}_S - (R_S + \frac{1 + \sigma_S}{1 + \sigma_R} R_R) \underline{i}_S - \sigma L_S \frac{di_S}{dt}. \quad (12.70)$$

Finally, when substituting the rotor current in Eq.(10.40) by  $i_{mS}$ , the expression for the motor torque becomes

$$m_M(t) = \frac{2}{3} L_0 \text{Im}[\underline{i}_S \underline{i}_{mS}^*] = \frac{2}{3} L_0 \text{Im}[i_{mS} i_{Sq}]. \quad (12.71)$$

These equations still represent the original model of the induction motor, Eqs. (10.38 - 10.41), written in terms of stator based currents and voltages; they are graphically shown at the right hand side of Fig. 12.39 with the measurable terminal quantities  $\underline{u}_S$  and  $\underline{i}_S$  in stator- and the motor dynamics in stator flux-coordinates.

### 12.5.2 A possible Principle of “Encoderless Control”

Proceeding in Fig. 12.39 from the motor terminals to the left, a voltage source inverter is assumed, feeding the motor with two orthogonal AC source voltages  $u_{Sa}$  and  $u_{Sb}$ , which in turn are controlled by command signals  $u_{SaRef}$  and  $u_{SbRef}$ ; the inverter is simplified by its effective delay. If the reference voltages, already available as digital signals in the control computer, can be substituted for the terminal voltages, a difficult measuring problem is avoided, because the voltages produced by a voltage source inverter have a large bandwidth, calling for costly A/D converters; another option worth trying is the reconstruction of the terminal voltages from the DC link voltage and switching signals.

The part at the left of the diagram represents an example of an “encoderless control”; its inputs are the measured electrical signals indicated by the orthogonal set  $u_{Sa}, u_{Sb}, i_{Sa}, i_{Sb}$  of AC quantities. Integration of the “voltages behind the stator resistances”,  $u_{Sa} - R_S i_{Sa}$  and  $u_{Sb} - R_S i_{Sb}$  produces the stator flux; transformation of Eq. (12.66) into field coordinates results in

$$L_0 \left( \frac{di_{mS}}{dt} + j i_{mS} \frac{d\mu}{dt} \right) = (\underline{u}_S - R_S \underline{i}_S) e^{-j\mu} = (u_{Sd} - R_S i_{Sd}) + j(u_{Sq} - R_S i_{Sq}), \quad (12.72)$$

where

$$\frac{d\mu}{dt} = \omega_{mS} \quad (12.73)$$

is the instantaneous angular velocity of the stator flux vector. Hence, the equations of the stator flux model are

$$L_0 \frac{di_{mS}}{dt} = u_{Sd} - R_S i_{Sd}, \quad (12.74)$$

$$L_0 \frac{d\mu}{dt} = \frac{u_{Sq} - R_S i_{Sq}}{i_{mS}}. \quad (12.75)$$

Deriving the stator flux from terminal voltages and currents is difficult because open integrations are subject to sensing errors and integrator drift at low stator frequency; on the other hand, if the operation is performed inside a feedback loop, as is the case when being carried out in field coordinates, the effects of integrator drift are reduced to normal offsets, common in analogue signal processing. The result of the flux modelling are estimates of the magnetising current vector expressed by  $i'_{ms}$ ,  $\mu'$ , and  $\omega'_{ms}$ . Clearly when measuring stator voltages and currents, the flux model does not require a speed signal; this makes the scheme fit the needs of "encoderless" control.

The flux model shown in the upper left hand part of Fig. 12.39 may be interpreted as the inverse of the corresponding part of the motor dynamics, creating a copy of the stator flux; its function resembles that of a phase locked loop (PLL). The signal processing may be done with an analogue/digital sensing circuit, where the trigonometric functions are represented digitally in a ROM, to be multiplied in D/A converters with analogue voltage signals [J10, J11].

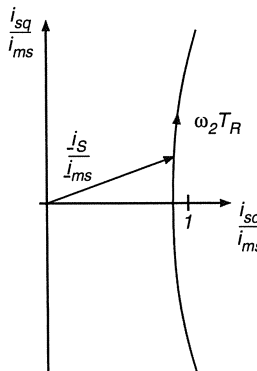


**Fig. 12.40.** Stator flux orientated current components as a function of rotor frequency.

Once estimates of the magnitude and orientation of stator flux are established, it is easy to compute with a microcomputer the remaining quantities needed for a two- channel field orientated control structure. This is seen in the lower left hand portion of Fig. 12.39, where a voltage limiter generates the flux reference  $i'_{msRef}$  which serves as a command value for a flux controller producing  $i'_{sdRef}$ ; similarly, the output of the speed controller is the reference for the quadrature current,  $i'_{sqRef}$ . The stator current control in field coordinates corresponds to that shown in Fig. 12.27. Clearly, if the voltages  $v'_S(t)$  containing relevant information on the rotor can be derived from the terminal quantities, there is a good chance of obtaining estimates of the motor speed  $\omega'$  and the rotor resistance  $R'_R$ . Reconstruction of  $v'_S$  with the help of Eq. (12.70) involves a differentiation of the stator currents which can again be implemented in analogue form. When transforming Eq.(12.69) into field coordinates

$$v_S e^{-j\mu} = v_{Sd} + j v_{Sq} = \frac{-R_R i_{mS}}{1 + \sigma_R} + \omega \sigma L_S i_{Sq} + j \omega L_S \left( \frac{i_{mS}}{1 + \sigma_S} - \sigma i_{Sd} \right), \quad (12.76)$$

it is seen that, assuming reliable estimates of the field orientated currents, the speed can be estimated on the basis of  $v'_{Sq}$ , whereas a change of the rotor resistance might be detected from  $v'_{Sd}$ . This is indicated at the lower end of the control part in Fig.12.39.

On the other hand, should a mechanical sensor be available for speed control, the structure in Fig. 12.39 becomes a normal field orientated control scheme, based on stator- instead of rotor-flux, where  $\omega'$  is replaced by the measured speed  $\omega$ . The flux acquisition is unaffected, still being based on measured voltages and currents. Also, the outer layers of control are the same, whether the control is rotor flux- or stator flux orientated; they could be extended to include a position control loop.

The advantages of stator flux coordinates are that the rotor resistance enters the flux model only indirectly, that the stator temperature causing changes of the stator resistance can be easily measured and that the effect of saturation is already contained in the voltages. On the other hand, the stator flux model is more sensitive at low frequency to detuned parameters such as  $R_S$  compared with the rotor flux model shown in Fig. 12.16 b; also, measurements of the terminal voltages, the accuracy of which is quite critical at low speed, are needed as input and the magnitude of the magnetising current is produced by an integration with speed dependent nonlinear feedback instead of a linear lag term.

It is of interest to note that the current components  $i_{Sd}, i_{Sq}$  defined in stator flux coordinates are not completely decoupled, as was the case with rotor flux coordinates; there is a slight coupling effect similar to armature reaction with a DC motor. This becomes apparent when transforming Eq.(12.67) into field coordinates; in steady state, i.e. with constant values of  $i_{mS}, i_{Sd}, i_{Sq}, \omega, \omega_{mS} = \omega_1$ , and  $\omega_2 = \omega_{mS} - \omega$  we find

$$i_{Sd} = \frac{i_{mS}}{1 + \sigma_S} + \omega_2 \sigma T_R i_{Sq}, \quad (12.77)$$

$$i_{Sq} = \omega_2 T_R \left( \frac{i_{mS}}{1 + \sigma_S} - \sigma i_{Sd} \right). \quad (12.78)$$

Solving for  $i_{Sd}, i_{Sq}$  results in

$$i_{Sd} = \frac{1 + \sigma (\omega_2 T_R)^2}{1 + (\omega_2 \sigma T_R)^2} \frac{i_{mS}}{1 + \sigma_S}, \quad (12.79)$$

$$i_{Sq} = \frac{(1 - \sigma) \omega_2 T_R}{1 + (\omega_2 \sigma T_R)^2} \frac{i_{mS}}{1 + \sigma_S}, \quad (12.80)$$

where  $\omega_2 T_R$  is a measure of torque, as found in Eq.(12.3).The two functions are combined in Fig.12.40; clearly, if the stator flux is to be maintained at constant level,  $i_{Sd}$  must increase with the load. This could be achieved with a flux controller.

### 12.5.3 Simulation and Experimental Results

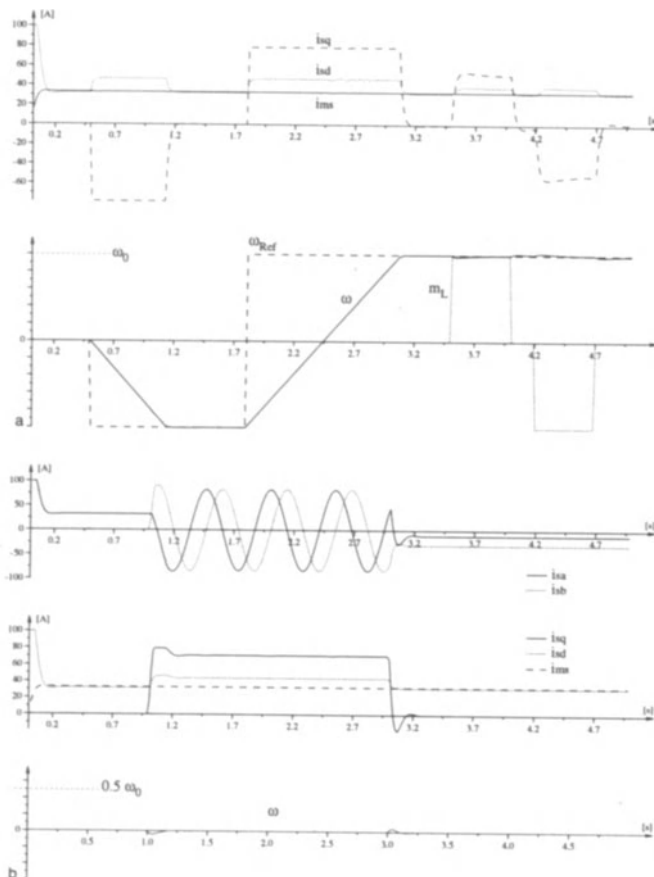


**Fig. 12.41.** Simulation results of the stator flux orientated induction motor control scheme shown in Fig.12.39, using **measured** speed feedback.a) Starting, reversing and loading transients; b) loading transients at zero speed.

Some simulation results with the control scheme in Fig.12.39 and based on parameters of a 22 kW motor are seen in Figs.12.41 and 12.42; they show starting and reversing as well as loading transients at zero speed reference. In Fig 12.41 the 'measured' speed  $\omega$  and in Fig.12.42 the 'estimated' speed  $\omega'$  is used as feedback signal. Naturally, there is little difference as long as the motor parameters are accurately known but, as mentioned before, the flux model is sensitive to detuned parameters at low speed.

Some experimental results with an "encoderless" induction motor drive have been obtained with a 1.5 kW standard motor, fed by a commercial IGBT inverter switched at 8.8 kHz and a control scheme similar to the one shown in Fig.

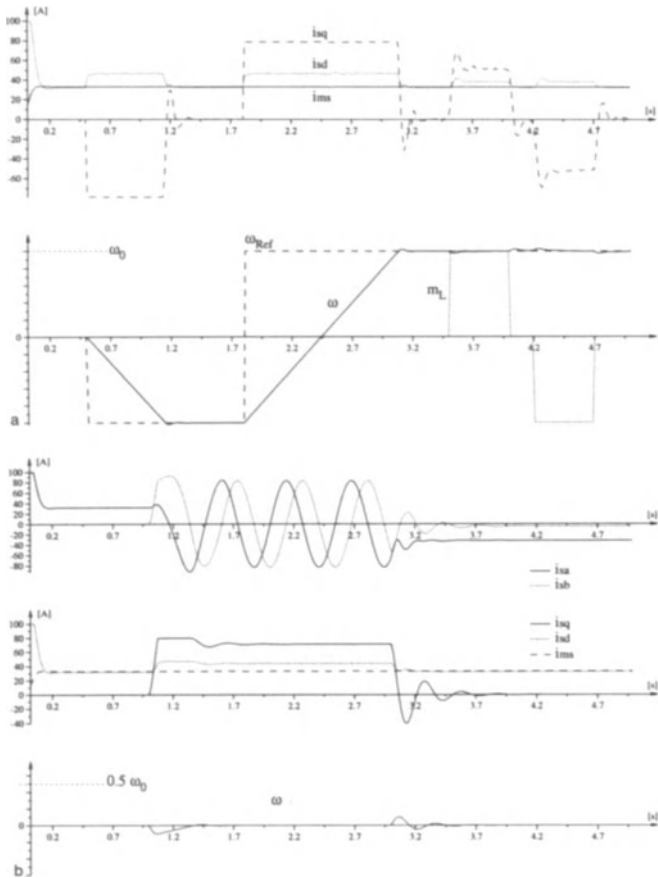


**Fig. 12.42.** Simulation results of the stator flux orientated induction motor control scheme shown in Fig. 12.39, using estimated speed feedback. **a)** Starting, reversing and loading transients; **b)** loading transients at zero speed.

12.39 [J11]. Transients following step changes of the speed reference are seen in Fig. 12.43, with the measured speed also plotted for comparison. Fig. 12.44 shows the transients following step changes of the load torque corresponding to  $\pm 0.4$  of rated torque at the very low speed of  $0.03\omega_o$ , indicating remarkably good performance under these difficult test conditions.

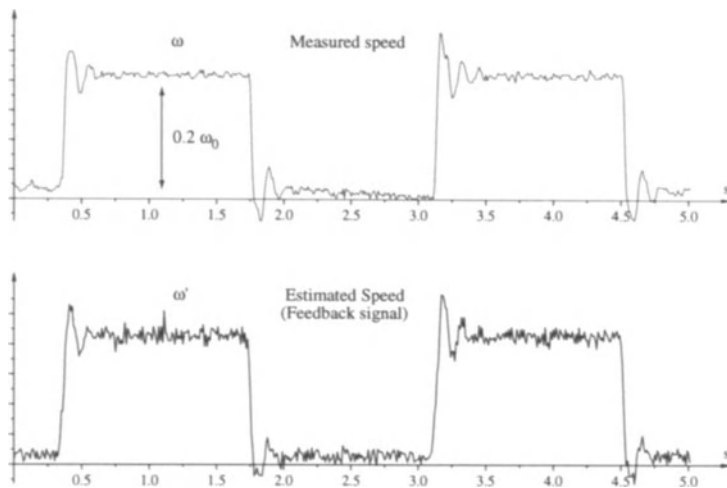


**Fig. 12.43.** Experimental results of a stator flux orientated induction motor control scheme similar to Fig.12.39, using **estimated** speed feedback, transients following step changes of speed reference.

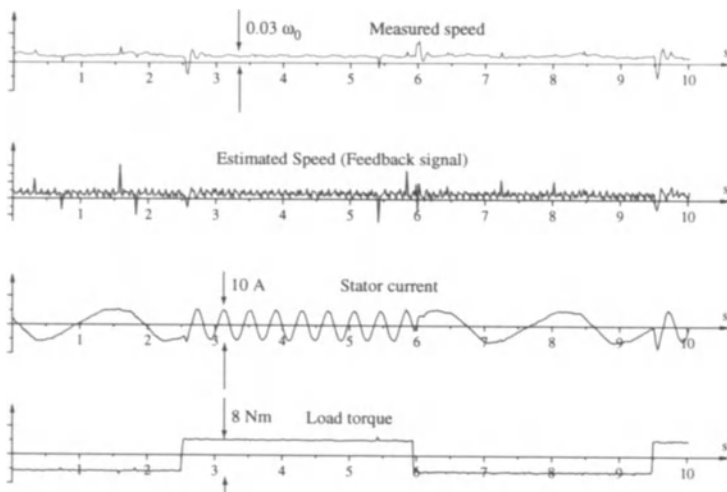


**Fig. 12.44.** Experimental results of a stator flux orientated induction motor control scheme similar to Fig.12.39, using **estimated** speed feedback, transients following step changes of load torque at very low speed.

## 12.6 Rotor Flux Orientated Control of an Induction Motor Without a Mechanical Sensor, Using a Combined Flux Model

From the preceding section it became apparent that employing stator voltages as inputs to a "voltage model" based on the stator voltage equation, Eq.(10.38), has weaknesses in the low speed range because the terminal voltages decrease with speed until they are eventually dominated by the voltage drops across the temperature dependent stator resistors and have little bearing on the magnetic fields in the motor. Also, use of stator flux coordinates creates additional coupling terms between the stator current components in field coordinates and the stator flux (Eqs. 12.79, 12.80). With the "current model" based on the rotor voltage equation, Eq.(10.39), and with rotor flux orientation (Fig. 12.16b), these coupling terms are not present and zero speed is within the validity range of the model; on the other hand, a speed signal is needed, which is undesirable and should now be eliminated. Hence one could consider a combined solution, where the two flux models in rotor flux coordinates are computed simultaneously and a speed-dependent selection of their results is made, such that the control signals from the current model are preferred at low speed and those from the voltage model at higher speed.

The "voltage model" is obtained by converting Eq.(12.51) into rotor field coordinates and splitting it in real and imaginary parts (for the real part this was already done in Eq.(12.52)). This results in

$$e_{Sd} = (1 - \sigma) L_S \frac{di_{mR}}{dt} = u_{Sd} - R_S i_{Sd} - \sigma L_S \frac{di_{Sd}}{dt} + \omega_{mR} \sigma L_S i_{Sq}, \quad (12.81)$$

and

$$e_{Sq} = (1 - \sigma) L_S i_{mR} \omega_{mR} = u_{Sq} - R_S i_{Sq} - \sigma L_S \frac{di_{Sq}}{dt} - \omega_{mR} \sigma L_S i_{Sd}, \quad (12.82)$$

where

$$e_S(t) e^{-j\varrho} = e_{Sd} + j e_{Sq} \quad (12.83)$$

are again the "voltages behind the transient stator impedance". Eqs.(12.81,12.82) constitute the "voltage model" in rotor flux coordinates.

The "current model" was defined by Eqs.(12.29, 12.30) as

$$T_R \frac{di_{mR}}{dt} + i_{mR} = i_{Sd}, \quad (12.84)$$

$$\frac{d\varrho}{dt} = \omega_{mR} = \omega + \frac{i_{Sq}}{T_R i_{mR}} = \omega + \omega_2, \quad (12.85)$$

where the measured speed  $\omega$  will now have to be substituted by a suitable estimate  $\omega'$  obtained by the combined evaluation algorithm.

Clearly when both models are operating simultaneously on the measured currents and voltages, they are bound to produce for the field orientated quantities somewhat different results, indicated in the following by an additional

subscript S and R. The control will employ a weighted mean of these values, depending on the estimated speed.

An example of how the combined flux estimation could be implemented is shown in Fig. 12.45 In order to avoid a differentiation of the current signals in the voltage model, an observer-like structure is chosen, where the signals  $e'_{SdS}$ ,  $e'_{SqS}$  are obtained implicitly by matching the predicted and measured current signals  $i'_{SS}$  and  $i_S$ . This results in a lag effect that has to be duplicated in the current model for obtaining consistent results.

The combined flux estimation vector containing  $i'_{mR}$ ,  $\omega'_{mR}$ ,  $i'_{Sd}$  and  $i'_{Sq}$ , which serves as a basis for the control of the drive may be defined as the weighted mean of the voltage and current model estimates. For the example of the flux vector angular velocity this is given by

$$\omega'_{mR} = f(\omega') \omega'_{mRR} + (1 - f(\omega')) \omega'_{mRS} \quad (12.86)$$

where  $0 \leq f(\omega') \leq 1$  is a speed dependent weighting function; corresponding definitions are used for all the estimates derived by the flux models. With a suitably shaped weighting function  $f(\omega')$  as shown in Fig.12.45 the control is purely "current model based" at zero speed and converges to "voltage model based" operation at higher speeds, where the terminal voltages are of sufficient magnitude and the uncertainty of the resistive voltage drop becomes negligible. The estimated speed signal  $\omega'$  to be used in the weighting function  $f(\omega')$  as well as for the encoderless speed control may be obtained by combining Eqs.(12.82, 12.85)

$$\omega' = \frac{1}{(1 - \sigma) L_S i_{mR}} (e_{Sq} - \frac{R_R i_{Sq}}{(1 + \sigma_R)^2}), \quad (12.87)$$

as is indicated in Fig.12.45.

If the flux model is implemented in stator coordinates, processing variable frequency AC quantities, the speed dependent transition of the estimates from the current-based to the voltage-based section could also be done dynamically by taking advantage of the frequency response of the observer; again, at low speed the results of the current model would dominate whereas the signals obtained from the voltages can be considered to be coming from a more reliable source at higher speed [J4].

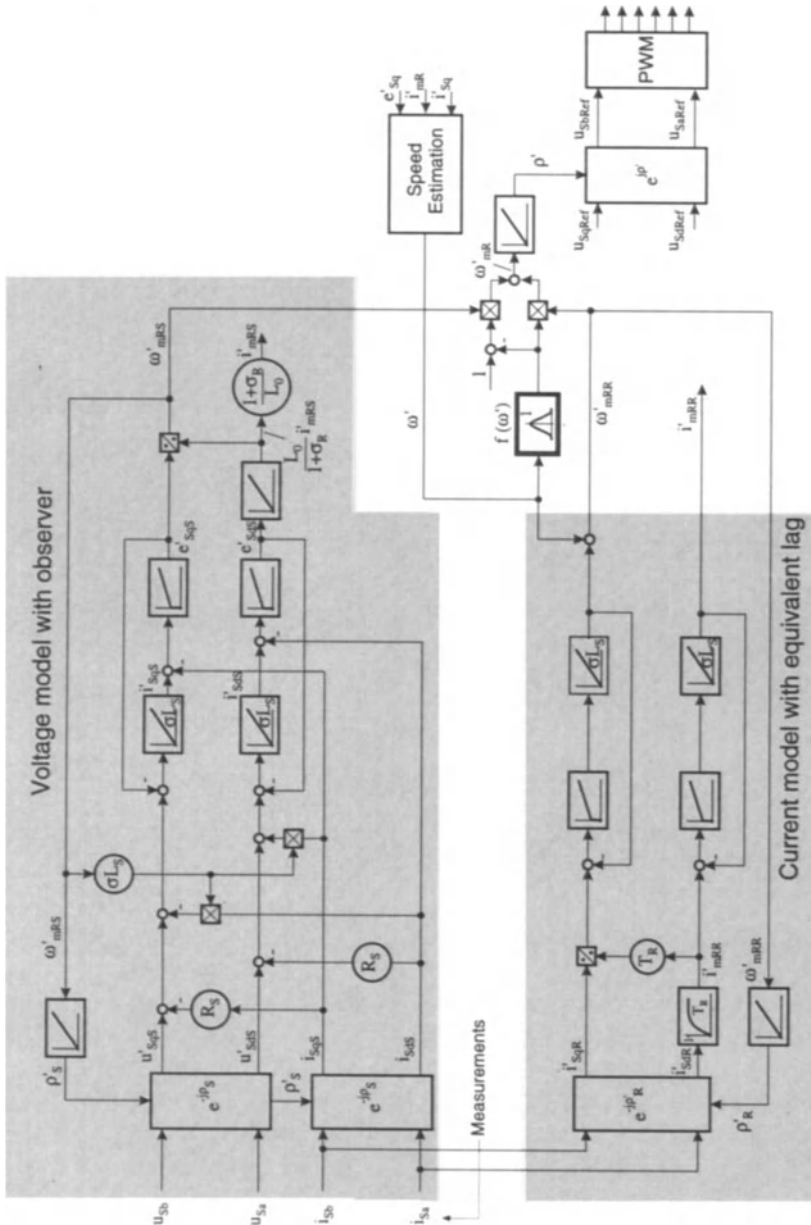


Fig. 12.45. Combined voltage/current model for rotor flux estimation

# 13. Induction Motor Drive with Restricted Speed Range

Some mechanical loads, such as fans or centrifugal pumps, exhibit a strong dependence of the load torque on speed, so that a limited speed control range suffices for achieving the desired control effect. The same is true for rotating converters employing a flywheel (Sect. 7.4); since the kinetic energy of the rotating masses varies with the square of the speed, there is little incentive in varying the speed by more than, say, 20 or 25%. A similar situation exists if an electrical island grid with a somewhat fluctuating frequency, for example a railway grid, is to be supplied from the public constant frequency system through a rotating converter. For applications of this kind a wound rotor induction motor drive presents an interesting solution; if the stator is connected to the constant frequency grid and the rotor is fed with slip frequency by a static converter, its power is determined by the desired speed range  $\Delta\omega$  only, and can be kept relatively small. The slip power may still be substantial with large machines, calling for an efficient control scheme.

Beginning at about the turn of the century, a variety of drive circuits has been developed that made use of additional machines such as rotary frequency changers; with the progress of power electronics new solutions have become possible here too, one of which will be discussed in Sect. 13.1. The simplified mathematical model of the symmetrical induction machine derived in Chap. 10 can be used for this purpose with minor modifications.

## 13.1 Doubly-fed Induction Machine with Constant Stator Frequency and Field-orientated Rotor Current Control

When direct current is supplied to the slippings of a wound rotor induction motor, the stator of which is connected to the constant frequency line, the motor assumes the characteristics of a synchronous machine; constant torque can only be produced if the rotor is in synchronism with the stator field. The machine can then deliver reactive power, but at the same time all the limitations of the line-fed synchronous machine become apparent, which includes the problems of starting, synchronisation as well as oscillatory transients and pull-out torque; this is still true, if instead of the direct current excitation, a constant frequency

alternating current excitation is applied to the rotor winding; only the speed of the motor must change until the stator and rotor ampereturns waves are again moving in synchronism. It is for this reason that doubly-fed machines operated at constant rotor frequency are not particularly attractive.

The situation is different, however, if the AC excitation of the rotor is made dependent on the line voltage vector and the angular position of the rotor. The machine then loses its synchronous characteristics entirely and can operate at variable speed and reactive line current; the speed transients can be well damped [A10, A11, A25, D26, L11, L23, L36, W10]. The basic circuit depicted in Fig. 13.1 a shows a wound rotor motor, the stator of which is connected to the symmetrical three phase supply with constant rated line voltage  $U_{S0}$  and frequency  $\omega_0$ ; the rotor is fed with impressed three phase currents of variable amplitude, frequency and phase. The power supply in the rotor-circuit could either be a current controlled cycloconverter or a DC-link converter (Chap. 11). Thus the hatched operating range of the speed-torque plane in Fig. 13.1 b becomes accessible. The voltage rating and frequency of the converter is directly dependent on the desired speed range.

The impressed rotor currents must be derived on the basis of the rotor position and the vector of the line voltages; speed and reactive power control with current limit can then be superimposed. It would also be possible to choose a motor with a two phase rotor winding instead of the usual three phases; the mode of operation would be the same, except for the harmonics on the line side caused by the switching of the converter. For the following considerations a three-phase rotor with  $N_R = N_S$  is assumed.

The mathematical model of the symmetrical AC machine, Eqs. (10.38-10.41), which was derived with various simplifying assumptions can be employed here also; it only needs to be adapted to the new constraints. The rotor is now fed by a converter, Eq. (10.39),

$$R_R \underline{i}_R + L_R \frac{d\underline{i}_R}{dt} + L_0 \frac{d}{dt} (\underline{i}_S e^{-j\varphi}) = \underline{u}_R(t), \quad (13.1)$$

where

$$\underline{u}_R(t) = u_{R1} + u_{R2} e^{j\gamma} + u_{R3} e^{j2\gamma} \quad (13.2)$$

is the vector of the rotor voltages supplied by the converter to the sliprings of the machine. When again assuming that the converter is equipped with fast responding current control loops in each phase, the rotor currents  $\underline{i}_R(t)$  are in effect produced by current sources; hence the rotor voltage equation (13.1) has no significance with regard to the dynamics of the drive as long as the converter is able to impress the rotor currents, i.e. possesses adequate ceiling voltage and control bandwidth. This results in considerable simplification of the dynamic structure of the drive.

The situation is in fact quite similar to the case of the stator-fed induction motor; an added simplification is that now both, stator and rotor currents, can be readily measured. Hence it is appropriate to follow again the field orientated approach.

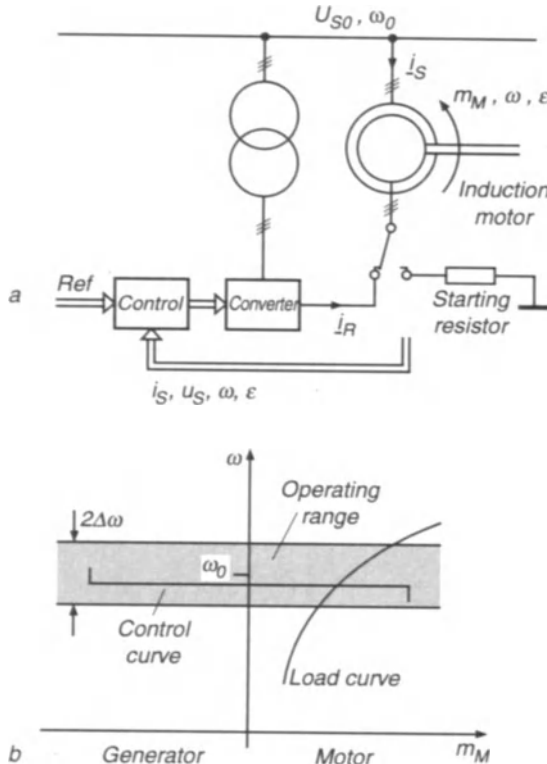


**Fig. 13.1.** Wound rotor induction motor with variable frequency rotor supply  
a) Circuit; b) Operating range

As in Sec. 12.2 the stator voltage equation (10.38) is written in the form

$$R_S \underline{i}_S + L_0 \frac{d}{dt} [(1 + \sigma_S) \underline{i}_S + \underline{i}_R e^{j\epsilon}] = \underline{u}_S, \quad (13.3)$$

where according to Eq. (12.65)

$$\underline{i}_{mS}(t) = (1 + \sigma_S) \underline{i}_S + \underline{i}_R e^{j\epsilon} = i_{mS}(t) e^{j\mu(t)} \quad (13.4)$$

is an extended magnetising current vector responsible for the stator flux including stator leakage. Should the symmetrical three phase supply to which the stator is connected, exhibit a noticeable internal impedance,  $R_G + j\omega_0 L_G$ , for instance caused by a transformer or a section of the power line, it can be included in the effective stator transient impedance

$$R_S + j\omega_0 \sigma_S L_0 \equiv R_{S0} + R_G + j\omega_0 (\sigma_{S0} L_0 + L_G), \quad (13.5)$$

where  $R_{S0} + j\omega_0 \sigma_{S0} L_0$  is the transient impedance of the machine proper. By eliminating the stator current  $\underline{i}_S$  from Eqs. (13.3, 13.4), we find

$$T_S \frac{di_{mS}}{dt} + i_{mS} = \frac{1 + \sigma_S}{R_S} \underline{u}_S + i_R e^{j\epsilon}, \quad (13.6)$$

where  $T_S = L_S/R_S$  is the main time constant of the stator circuit. The expression for the electrical torque is, Eq. (10.40),

$$m_M = \frac{2}{3} L_0 \operatorname{Im} [\underline{i}_S (i_R e^{j\epsilon})^*] = \frac{2}{3} \frac{L_0}{1 + \sigma_S} \operatorname{Im} [i_{mS} (i_R e^{j\epsilon})^*]. \quad (13.7)$$

When introducing the rotor current vector in stator coordinates

$$\underline{i}_R e^{j\epsilon} = i_R(t) e^{j(\xi+\epsilon)}, \quad (13.8)$$

the torque equation becomes

$$m_M = -\frac{2}{3} (1 - \sigma) L_R i_{mS} i_R \sin(\xi + \epsilon - \mu) = -\frac{2}{3} (1 - \sigma) L_R i_{mS} i_{Rq}. \quad (13.9)$$

The position of the rotor current vector in field coordinates,

$$\delta = \xi + \epsilon - \mu, \quad (13.10)$$

corresponds to the load angle. The angular relations of the various vectors are shown in Fig. 13.2. The instantaneous angular velocities are

$$\frac{d\xi}{dt} = \omega_2, \quad \frac{d\epsilon}{dt} = \omega, \quad \frac{d\mu}{dt} = \omega_{mS}. \quad (13.11)$$

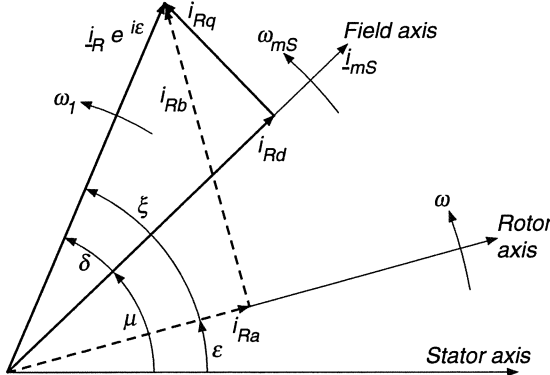


**Fig. 13.2.** Angular relationships of current vectors for doubly fed induction machine

The real and imaginary parts of

$$\begin{aligned} i_R e^{j(\xi+\epsilon-\mu)} &= i_R e^{j\delta} = i_R \cos \delta + j i_R \sin \delta \\ &= i_{Rd} + j i_{Rq} \end{aligned} \quad (13.12)$$

are defined as  $d - q$ -components of the rotor current vector in a stator flux-orientated reference frame or as direct and quadrature components of the rotor current “in field coordinates”; they are DC signals in steady state.

When assuming a symmetrical three-phase system of sinusoidal line voltages having the constant frequency  $\omega_0$ , the voltage vector rotates on a circular path,

$$\underline{u}_S(t) = \frac{3\sqrt{2}}{2} U_S e^{j\omega_0 t}, \quad (13.13)$$

where  $U_S$  is the RMS-value of the line-to-neutral voltages.

Transforming Eq. (13.6) into field coordinates with the help of Eqs. (13.4, 13.8, 13.11, 13.12, 13.13) and splitting the result into real and imaginary components yields two real differential equations for the magnitude and angle of the magnetising current vector,

$$T_S \frac{di_{mS}}{dt} + i_{mS} = \frac{1 + \sigma_S}{R_S} u_{Sd} + i_{Rd}, \quad (13.14)$$

$$\frac{d\mu}{dt} = \omega_{mS} = \frac{1}{T_S i_{mS}} \left[ \frac{1 + \sigma_S}{R_S} u_{Sq} + i_{Rq} \right], \quad (13.15)$$

where

$$u_{Sd} = \frac{3\sqrt{2}}{2} U_S \cos(\omega_0 t - \mu), \quad (13.16)$$

$$u_{Sq} = \frac{3\sqrt{2}}{2} U_S \sin(\omega_0 t - \mu) \quad (13.17)$$

are the field orientated direct and quadrature components of the line voltages.

The  $d - q$ -components of the rotor currents can be derived from the measured rotor currents  $i_{R1}$ ,  $i_{R2}$ ,  $i_{R3}$  according to Eq. (13.12); the transition is again performed in two steps by first converting  $\underline{i}_R$  to an orthogonal two phase AC system which is subsequently transformed into field coordinates. With an isolated neutral of the rotor winding we have with  $\gamma = 2\pi/3$

$$\begin{aligned} \underline{i}_R(t) &= i_R e^{j\xi} = i_{R1} + i_{R2} e^{j\gamma} + i_{R3} e^{j2\gamma} \\ &= \frac{3}{2} i_{R1} + j \frac{\sqrt{3}}{2} (i_{R2} - i_{R3}) = i_{Ra} + j i_{Rb}, \end{aligned} \quad (13.18)$$

which, upon transformation into field coordinates, becomes

$$\begin{aligned} \underline{i}_R e^{j(\varepsilon-\mu)} &= i_R e^{j(\xi+\varepsilon-\mu)} = i_R e^{j\delta} = [i_{Ra} + j i_{Rb}] [\cos(\varepsilon - \mu) + j \sin(\varepsilon - \mu)] \\ &= i_{Ra} \cos(\varepsilon - \mu) - i_{Rb} \sin(\varepsilon - \mu) \\ &\quad + j [i_{Ra} \sin(\varepsilon - \mu) + i_{Rb} \cos(\varepsilon - \mu)] = i_{Rd} + j i_{Rq}; \end{aligned} \quad (13.19)$$

the angle  $\varepsilon - \mu$  may be interpreted as the rotor position in field coordinates.

The block diagram of the doubly-fed machine is contained in the upper part of Fig. 13.3, showing the interactions described by the preceding equations. One recognises considerable similarity with the block diagram of the induction motor

(Fig. 12.12) with the exception that there is an additional electrical input in the form of the line voltage  $U_S$ . The angle  $\omega_0 t - \mu$  constitutes the advance of the voltage vector  $\underline{u}_S$  against the magnetising vector  $\underline{i}_{mS}$ . Since the stator circuit is connected to a low impedance source, the angle  $\omega_0 t - \mu \approx \frac{\pi}{2}$  is subject to small changes only. As in the case of the stator-fed induction motor the magnitude of the flux can only be altered through a large lag  $T_S$ , whereas the quadrature current  $i_{Rq}$  is available for rapidly controlling torque.

Provided the converter with current control may be approximated by a three phase current source with negligible lag, the idea of control in field coordinates can again be applied. In this case it means that the coordinate transformation  $e^{j(\varepsilon-\mu)}$  taking place within the machine should be cancelled by an external transformation  $e^{-j(\varepsilon-\mu)}$ ; with the subsequent phase split a balanced three phase system of current references is formed. This is seen in the lower left portion of Fig. 13.3. The angle of transformation,  $\varepsilon - \mu$ , is readily available from measurements of rotor position as well as the stator and rotor currents. The transformation from field into rotor coordinates, in effect a modulation, is based on the following algorithm

$$\begin{aligned} i_{R\text{Ref}} &= [i_{R1} + i_{R2} e^{j\gamma} + i_{R3} e^{j2\gamma}]_{\text{Ref}} \\ &= [i_{Ra} + j i_{Rb}]_{\text{Ref}} = [i_{Rd} + j i_{Rq}]_{\text{Ref}} e^{-j(\varepsilon-\mu)}. \end{aligned} \quad (13.20)$$

This results in

$$\begin{aligned} i_{Ra\text{Ref}} &= i_{Rd\text{Ref}} \cos(\varepsilon - \mu) + i_{Rq\text{Ref}} \sin(\varepsilon - \mu), \\ i_{Rb\text{Ref}} &= -i_{Rd\text{Ref}} \sin(\varepsilon - \mu) + i_{Rq\text{Ref}} \cos(\varepsilon - \mu). \end{aligned} \quad (13.21)$$

The equivalent balanced three phase system of current references is

$$\begin{aligned} i_{R1\text{Ref}} &= \frac{2}{3} i_{Ra\text{Ref}}, \\ i_{R2\text{Ref}} &= -\frac{1}{3} i_{Ra\text{Ref}} + \frac{1}{\sqrt{3}} i_{Rb\text{Ref}}, \\ i_{R3\text{Ref}} &= -\frac{1}{3} i_{Ra\text{Ref}} - \frac{1}{\sqrt{3}} i_{Rb\text{Ref}}. \end{aligned} \quad (13.22)$$

Clearly the decoupled control scheme offers direct access to the  $d - q$ -current components. There are various possibilities for the design of the higher level control as can be deduced from a discussion of the steady state characteristics of the drive.

Under the assumption of constant speed and load torque, the rotor angle is  $\varepsilon = \omega t$  and the flux vector rotates in synchronism with the voltage vector,  $\omega_{mS} = \omega_0$ . Analogous to Eq. (13.13) the vector of the stator currents is, neglecting harmonics,

$$\underline{i}_S(t) = \frac{3\sqrt{2}}{2} \underline{I}_S e^{j\omega_0 t}, \quad \underline{I}_S = I_S e^{j\varphi_S}, \quad (13.23)$$

where  $\underline{I}_S$  is a complex phasor. Similarly the rotor current vector in stator coordinates is

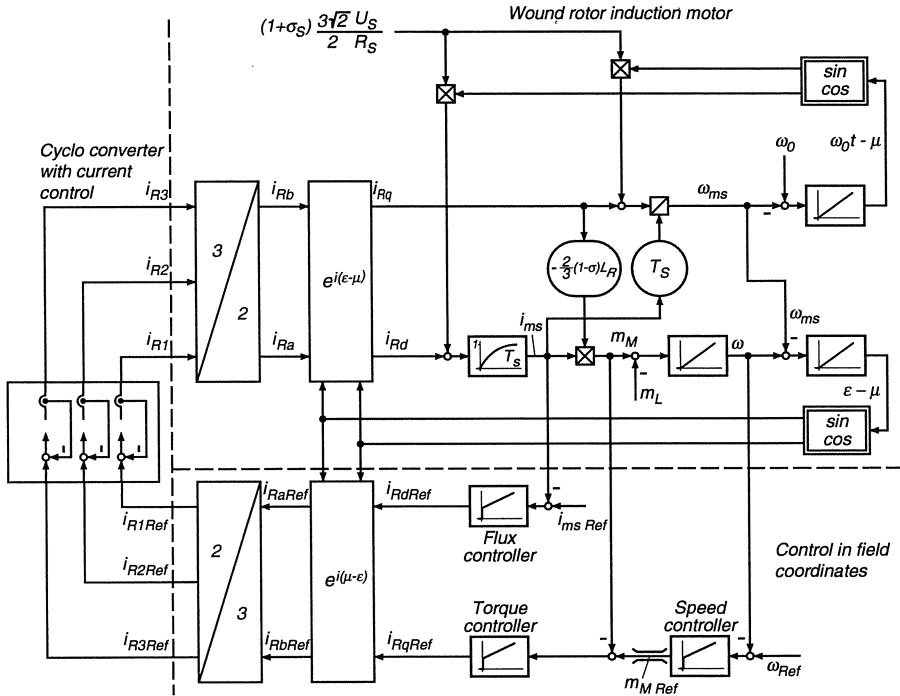


Fig. 13.3. Field orientated control of doubly fed induction machine

$$\underline{i}_R(t) e^{j\epsilon} = \frac{3\sqrt{2}}{2} \underline{I}_R e^{j(\omega_0 + \omega)t} = \frac{3\sqrt{2}}{2} \underline{I}_R e^{j\omega_0 t}, \quad \underline{I}_R = \underline{I}_R e^{j\varphi_R}. \quad (13.24)$$

Inserting these definitions into Eq. (13.3) leads to a steady state phasor equation

$$R_S \underline{I}_S + j\omega_0 L_S \underline{I}_S + j\omega_0 L_0 \underline{I}_R = \underline{U}_{S0}, \quad (13.25)$$

which, with \$L\_S = (1 + \sigma\_S)L\_0\$, is illustrated by the equivalent circuit in Fig. 13.4.

The stator resistance may be neglected with larger machines,

$$R_S \ll \omega_0 L_S,$$

which results in the phasor of the magnetising current being mainly determined by the impressed stator voltage,

$$\underline{I}_{mS} = (1 + \sigma_S) \underline{I}_S + \underline{I}_R \approx \frac{\underline{U}_{S0}}{j\omega_0 L_0}. \quad (13.26)$$

The no-load stator current (\$I\_R = 0\$) is

$$\underline{I}_{S0} \approx \frac{\underline{U}_{S0}}{j\omega_0 L_S}. \quad (13.27)$$

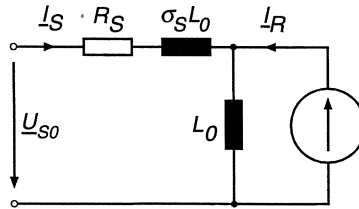


**Fig. 13.4.** Steady state equivalent circuit of doubly- fed induction machine with impressed rotor currents

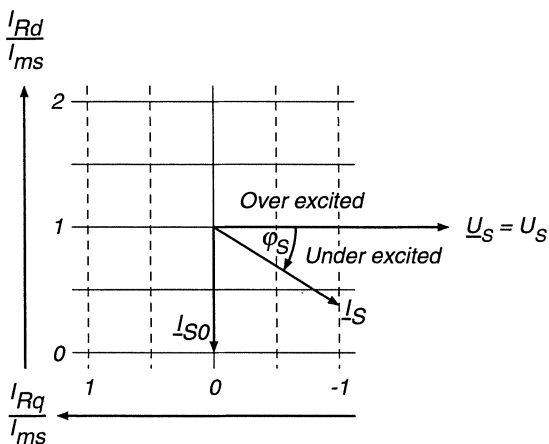


**Fig. 13.5.** Orthogonal control of stator current

Hence Eq. (13.25) may be written in the form

$$\begin{aligned} \underline{I}_S &\approx \underline{I}_{S0} \left[ 1 - \frac{\underline{I}_R}{\underline{I}_{mS}} \right] = \underline{I}_{S0} \left[ 1 - \frac{\underline{I}_R}{\underline{I}_{mS}} e^{j(\xi + \epsilon - \mu)} \right] \\ &= \underline{I}_{S0} \left[ 1 - \frac{\underline{I}_R}{\underline{I}_{mS}} e^{j\delta} \right] = \underline{I}_{S0} \left[ 1 - \frac{\underline{I}_{Rd}}{\underline{I}_{mS}} - j \frac{\underline{I}_{Rq}}{\underline{I}_{mS}} \right]. \end{aligned} \quad (13.28)$$

This indicates that the decoupled control of the rotor current in  $d - q$ -components corresponds directly to orthogonal control of the stator current in the direction of reactive and active current as is shown by the orthogonal grid in Fig. 13.5. Note that this operation in all four quadrants of the current plane is not limited to constant speed but applies to the whole speed-torque area (Fig. 13.1b) accessible with the voltage, current and frequency of the converter. Depending on the operating condition of the drive, power is flowing from the rotor via the converter to the line or vice versa as shown in Fig. 13.6.

When assessing the reactive power balance, the reactive power drawn from the line by the converter must also be taken into account. If a cycloconverter

is used, its lagging reactive input current may be substantial; it can impair the ability of the drive to operate with overall leading power factor. Measures for reducing the lagging reactive line current of the converter such as the reduction of its supply voltage with a transformer when operating the drive at low slip are frequently taken.

Starting the drive is accomplished with the help of resistors, as seen in Fig. 13.1a; as soon as the drive has reached the operating speed range the converter is switched in.

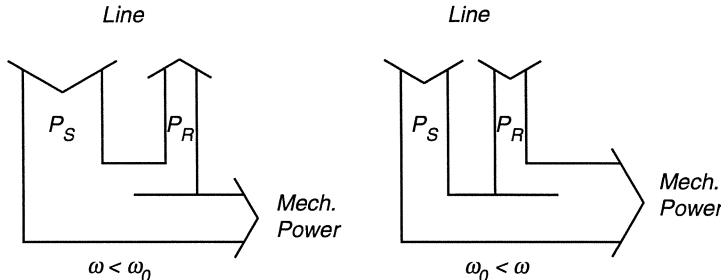


**Fig. 13.6.** Power flow of doubly fed induction motor drive below and above synchronism

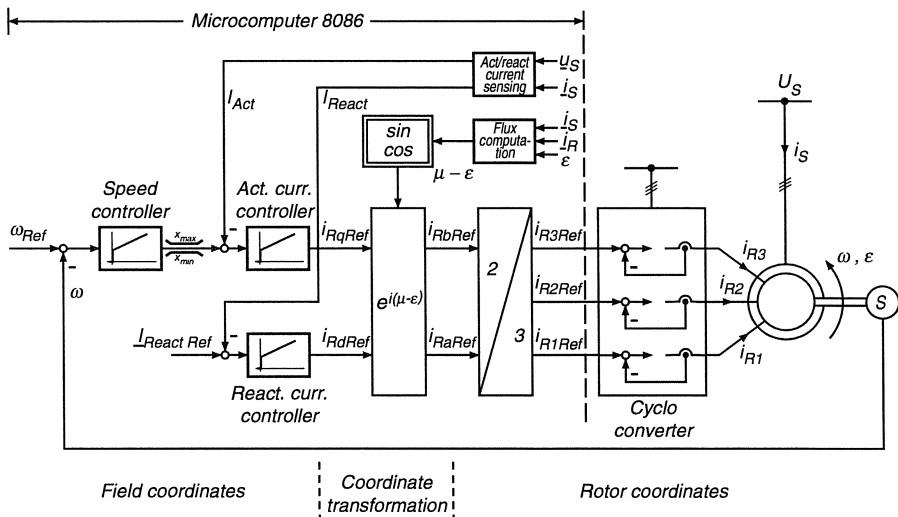


**Fig. 13.7.** Control scheme of doubly fed induction motor drive with microcomputer

The orthogonal grid in Fig. 13.5 gives a clear indication of how the higher level control should be arranged. As the stator flux ( $i_{mS}$ ) is essentially prescribed by the line voltage  $U_S$ , the  $d$ -component of the rotor current could be used

to maintain the reactive stator current at a fixed value or possibly at a value dependent on voltage (reactive power bias). On the other hand, the  $q$ -component is the ideal input for active current or torque control to which the speed control can be superimposed. All reference quantities should be limited in order to avoid undesirable operating conditions and to protect the equipment. The control section in the lower part of Fig. 13.3 represents only one of several possibilities; it yields speed torque curves with torque limit as indicated in Fig. 13.1b.

Figure 13.7 depicts the control scheme of an experimental 22 kW drive with microprocessor control [A10]. The rotor winding is supplied from a 6-pulse cycloconverter with analogue current control; the converter was chosen to have adequate power rating up to 7.5 Hz corresponding to 15% slip. In order to improve the steady state accuracy of the current control loops, feed-forward voltage signals were added in order to counteract the slip-proportional induced voltages in the rotor windings.

As was mentioned before, the angle  $\mu$  of the magnetising current (stator flux) can either be computed from measurements of the currents, Eq.(13.4), or from stator voltages and currents; in combination with a measurement of the rotor position  $\varepsilon$  this provides the information for the modulation in order to produce the reference signals for the rotor currents.

The field-orientated control structure makes this drive suitable for high dynamic performance, even though this may not be necessary with some of the applications mentioned; still, the decoupled orthogonal control is an attractive feature because it renders the control transparent and very flexible.

Figure 13.8 shows the beneficial effect of voltage feed-forward on the performance of a current loop in steady-state. The cycloconverter is operating at a frequency of 6.7 Hz corresponding to a speed of 1700 1/min of the 4-pole machine. The choice of the feed-forward scheme is based on the rotor voltage Eq. (13.1) which, after introducing the magnetising current, reads with  $L_R/R_R = T_R$

$$\sigma T_R \frac{di_R}{dt} + i_R = \frac{1}{R_R} u_R - (1 - \sigma) T_R \frac{d}{dt}(i_{mS} e^{-j\varepsilon}). \quad (13.29)$$

The last term may be expanded in the form

$$e_R = (1 - \sigma) L_R \frac{d}{dt}(i_{mS} e^{-j\varepsilon}) \quad (13.30)$$

$$= (1 - \sigma) L_R \frac{d}{dt}(i_{mS} e^{j(\mu-\varepsilon)}) \quad (13.31)$$

$$= (1 - \sigma) L_R \left[ \frac{di_{mS}}{dt} + j(\omega_{mS} - \omega) i_{mS} \right] e^{j(\mu-\varepsilon)}; \quad (13.32)$$

with  $i_{mS} \approx \text{const.}$ , this represents the slip-induced voltage acting as a load disturbance for the current controller; its effect is compensated by feed-forward. The necessary signals are generated in the microprocessor (Fig. 14.16).

The measured step response of the control loop for active stator power (with the speed control disabled) is seen in Fig. 13.9; it exhibits good dynamic performance and little cross coupling with the reactive power control loop. The

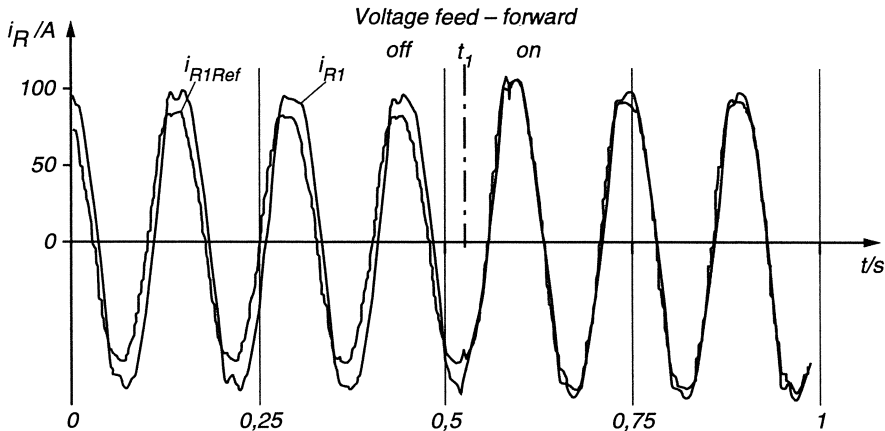


**Fig. 13.8.** Effect of voltage feed-forward on current control with a cycloconverter

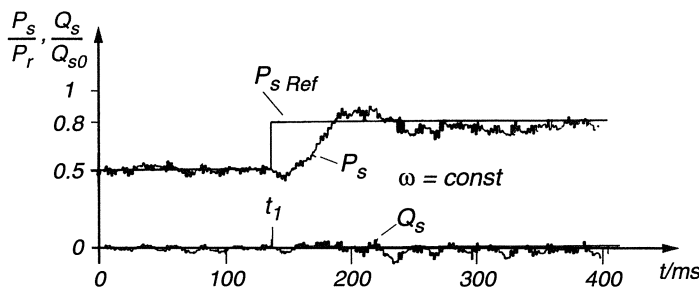


**Fig. 13.9.** Decoupled control of active/reactive power with a cycloconverter

ripple on the recorded traces is caused by harmonics of the cycloconverter and quantisation effects.

When employing a DC link PWM-converter instead of a cycloconverter for supplying the rotor-winding, the performance of the drive can be further improved in view of the higher switching frequency and the reduced harmonic interactions on the line- and motor-side. The reactive power drawn by the converter from the line can also be greatly reduced. Fig. 13.10 depicts the total line current, comprising the stator as well as the converter input currents, when a symmetrical voltage source converter with GTO thyristors is used, as shown in Fig. 11.13. By designing a decoupled orthogonal control structure also for the line side converter, based on the voltage vector, the active and reactive parts of the total line current can be controlled; this provides complete freedom with regard to the line-side characteristics of the drive, which may also be employed

for power factor correction, apart from high dynamic performance drive control [A25].

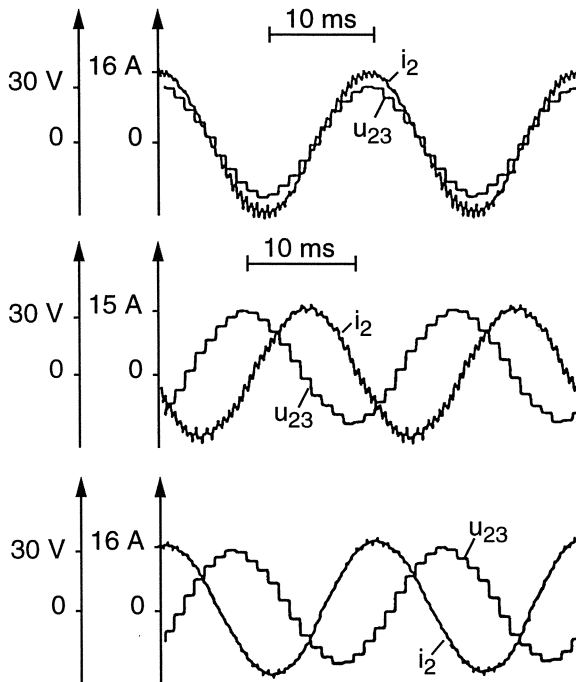


**Fig. 13.10.** Waveforms of total line-side current of a 22 kW doubly-fed drive with symmetrical GTO voltage source converter at different reactive power setpoints. Line current a) in phase, b) lagging, c) leading

Even though this type of drive shows very interesting characteristics, the amount of hardware for the rotor side converter is considerable which is likely to limit its use to higher power and special drives, where the added flexibility provided by two-axes control is important. One prominent area of application is that of generators in large wind power stations operating on the constant frequency grid; the variable speed operation effectively uses the high-inertia wind rotor as a flywheel during gusts. This helps to smooth the power fluctuations and reduces the peak rating of the generator as well as stresses on mechanical components such as shaft and gears. Another example are constant frequency ship- board generators, driven by the main Diesel engine at variable speed, so called shaft generators.

When operating the doubly- fed machine as a generator, it is preferable to omit the rotor current controllers and instead use the machine- side inverter for impressing rotor voltages, in order not to inhibit any transient currents from the stator side from freely flowing in the rotor winding. This is shown

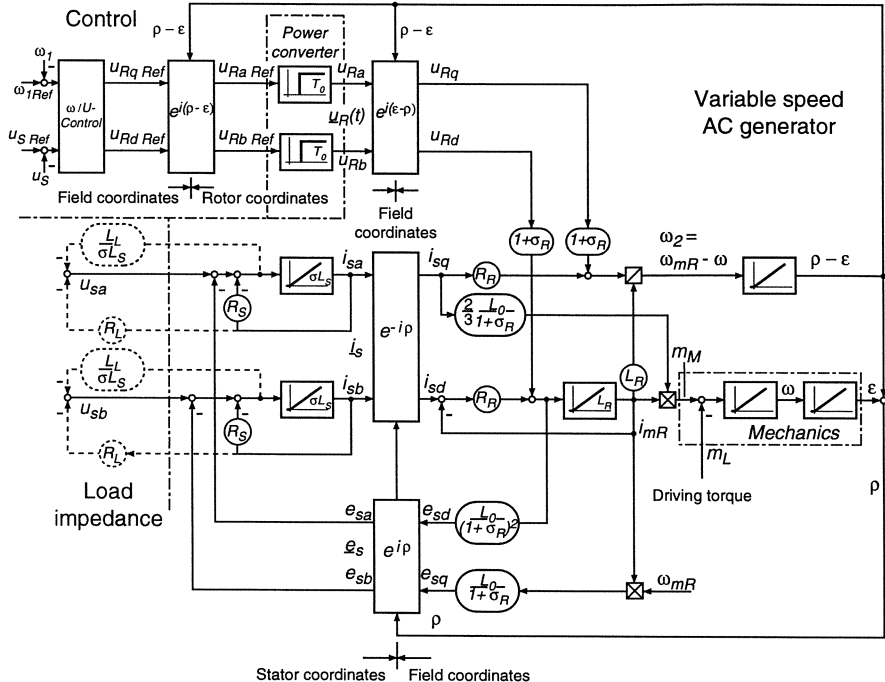


**Fig. 13.11.** Block diagram of a variable speed AC generator with impressed rotor voltages feeding an island grid at constant frequency

in the block diagram in Fig. 13. 11, where the converter is drawn in rotor coordinates; the stator- fed AC grid is represented by a load impedance  $R_L$ ,  $L_L$  in stator- and the electromagnetic interactions in rotor flux- coordinates. The structure of the diagram is similar to that shown in Fig. 12. 36. A two- axes control is indicated for the stator voltage and stator frequency; with the help of two separate PI- controllers, the simulated results in Fig. 13.12 are obtained, showing the transients after a step change of the voltage reference and when the mechanical speed follows a ramp change; when rotor passes through the synchronous speed the sequence of the rotor voltages is inverted.

Future high power applications for this type of control are found in pumped storage hydro power stations for changing the speed of the turbine/pump when it operates with varying head, thus improving the hydraulic efficiency. Also, changing the speed of the motor- generator- set by small amounts allows to activate kinetic energy and thus offers the option of contributing to the dynamic stability of the power grid [H38, H57, T3].

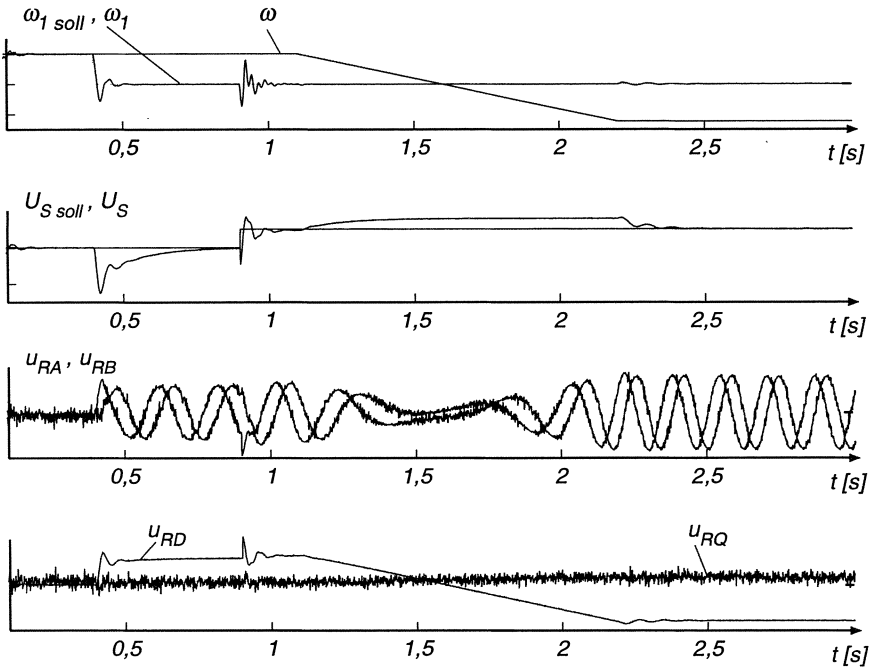


**Fig. 13.12.** Simulation results of a variable speed AC generator with impressed rotor voltages. Transients following a step change of the voltage reference and a ramp change of speed

### 13.2 Wound Rotor Induction Motor with Slip-Power Recovery

The doubly fed machine described in the preceding section can operate as a motor or generator in a speed band above or below synchronism drawing, in principle, leading or lagging stator current from the line. Depending on the operating condition power flows from the converter to the rotor or in the reverse direction. This high degree of flexibility results in a relatively costly converter; simplifications are possible, however, when the specifications are relaxed. For example, when rectifying the three phase rotor currents with diodes and feeding a DC link, the power flow becomes unidirectional. This is so because both voltage and current at the DC side of the rectifier are restricted to positive values; on the AC side the rectifier looks like a nonlinear, purely resistive network. The purpose of this scheme may therefore be to recover the slip power that would otherwise be lost in external rotor resistors; it can either be converted to mechanical power in a DC motor coupled to the shaft of the induction motor (Krämer-drive) or fed back to the AC line with the help of a line-commutated or other type of inverter (static Scherbius-drive) as is explained in Fig. 13.13 a.

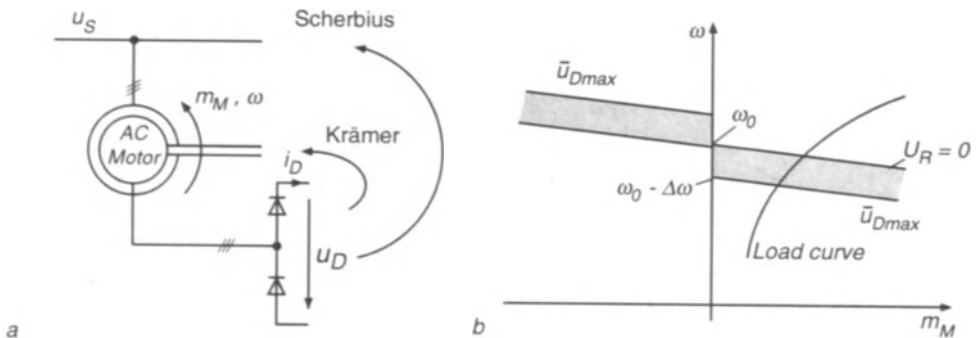


**Fig. 13.13.** Wound rotor motor with slip power recovery scheme.

a) Circuit; b) Operating range

Again, slip power recovery is of particular interest at higher power rating such as needed for rotating converters with flywheel storage in rolling mill drives (Sect. 7.4) or for boiler feed pumps extending into the 20 MW-range. While the Krämer-drive requiring an additional DC machine is no longer of interest, the Scherbius-drive with the associated solid state equipment is still used today.

In view of the diode rectifiers in the rotor circuit the operating range is now restricted to areas that would be available with external rotor resistors, i.e. motor operation below and regeneration above the torque-speed curve that is valid for short circuited rotor,  $U_R = 0$ , as shown in Fig. 13.13 b. Also, since the rotor currents cannot be impressed at will, there is always lagging reactive power at the stator terminals, just as on a wound rotor motor with secondary resistors. This excludes the possibility of controlling the stator voltage as with the scheme in Fig. 13.1 a. Speed control is achieved by changing the back voltage  $u_D$  in the DC link. If  $u_D$  is increased, the speed must drop in order that the rectified rotor voltage can drive a current through the DC link; without current in the rotor windings the rotor produces no torque. Closed loop control is usual with this type of drive in order to have fast access to torque and speed and to protect the equipment against overload.

Analytical modelling of the drive is made complicated by the rectifier-generated harmonics in the rotor windings which also cause distortion of the stator currents. The subsequent discussion is only an approximation, a more detailed analysis would have to be based on digital simulation.

The circuit of the Scherbius-drive and the usual control scheme employing an inner current and an outer speed loop is shown in Fig. 13.14. The starting resistor serves to bring the motor up to the specified speed range, where the rotor voltage has decreased sufficiently to allow switching in the converter. The DC link contains a smoothing choke, in order to obtain continuous current flow over most of the load range, and a line-commutated inverter designed to feed the slip power back to the grid.

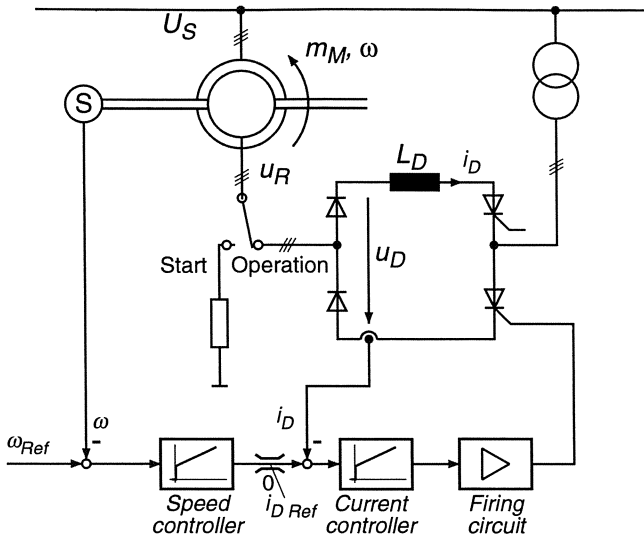


**Fig. 13.14.** Control scheme of static Scherbius-drive

A step-down transformer serves to match the supply voltage to the voltage in the DC link, which is quite low in the usual speed range; the transformer helps to reduce the reactive current at the line side of the inverter which is caused by delayed firing around  $\alpha \approx \frac{\pi}{2}$ . Often the transformer ratio is changed in several steps in order to have optimal conditions over a wider speed range.

The rotor current and, hence, the current in the intermediate circuit are roughly proportional to torque; the inner current control loop, seen in Fig. 13.14, provides therefore a good substitute for torque control and torque limit, while the speed controller is superimposed, generating the necessary current reference. Further control functions may be added if the need arises; for example approximately constant line power could be specified for a flywheel drive and pulsating load, resulting in a fluctuating speed level.

The steady state torque speed curves of the static Scherbius-drive are indicated in Fig. 13.15 for  $\omega_{Ref} = \text{const}$ . As long as the direct current is below the current limit, the speed is kept constant by the PI-controller; with increased load the speed controller eventually saturates causing the speed torque curve to bend down until the maximum voltage of the inverter is reached. Further drop in speed must be avoided since it will inevitably lead to a commutation failure of the inverter as explained in Fig. 8.17.

A simplified block diagram of the controlled drive is drawn in Fig. 13.16 with the control loops arranged according to Fig. 13.14; the normalising quantities  $U_{R0}, m_0, i_{D0}$  etc. are suitably chosen.

The inverter with the mean direct voltage  $\bar{u}_D$  is represented by a control delay as described in Fig. 8.31;  $\bar{u}_D$  is the back voltage opposing the rectified

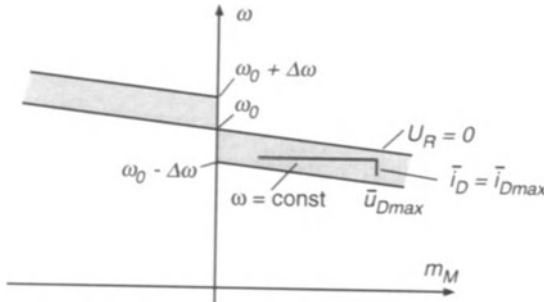


Fig. 13.15. Speed-torque curves of controlled Scherbius-drive

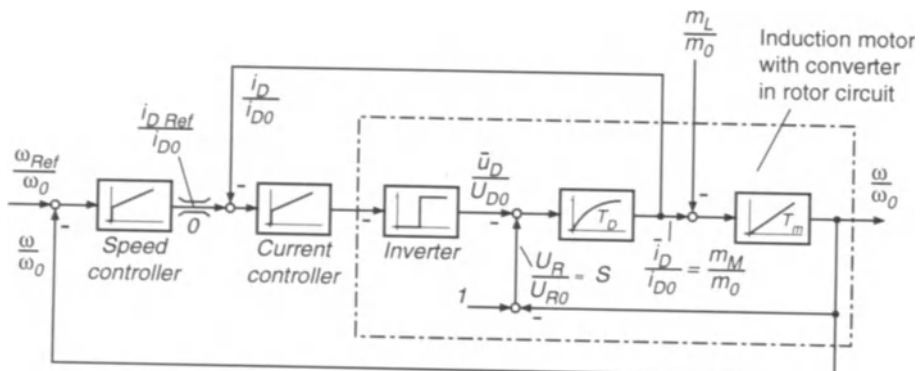


Fig. 13.16. Simplified block diagram of Scherbius-drive

rotor voltage, with the difference driving the current through the DC link and the rotor windings.  $T_D$  is the filter time constant which is mainly determined by the smoothing reactor. Clearly, the whole structure strongly resembles that of a controlled DC drive; therefore similar transients should be expected.

As mentioned before, the details are of considerable complexity, in particular the current waveforms in the rotor and stator at different speed and load. This may be explained by simulated results and measurements conducted on a 22 kW experimental Scherbius-drive [A10].

The measured waveforms of the stator and rotor currents at two operating points in the generating (above synchronous speed) region are shown in Fig. 13.17; the direct link current is the same in both cases,  $i_D = 50$  A. The speed-dependent distortion of the stator currents is clearly noticeable.

A recorded step response of the inner current control loop is depicted in Fig. 13.18 showing the good dynamic characteristics of the electronic torque control. The effect of a changing link current between 0 and 50 A on the stator and rotor currents at constant speed (1725 1/min) is seen in Fig. 13.19.

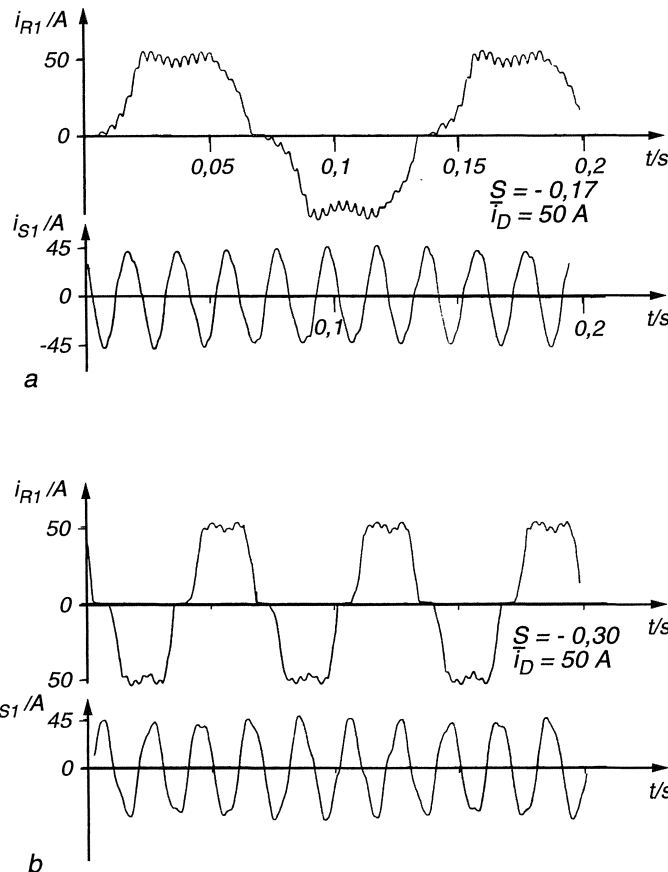


**Fig. 13.17.** Stator and rotor currents of Scherbius-drive in steady state operation above synchronous speed. **a)**  $S = -0.17$ ; **b)**  $S = -0.30$

As an example of the results obtainable through digital simulation, Fig. 13.20 shows some computed curves of voltages and currents as well as electrical torque. Clearly, the deviations from sinusoidal waveforms are substantial; of particular interest are the long commutation intervals of the uncontrolled rectifier, caused by the small slip-proportional driving voltage and the relatively large rotor leakage reactance. On the other hand, this tends to smooth the currents and thus reduces the higher frequency harmonics.

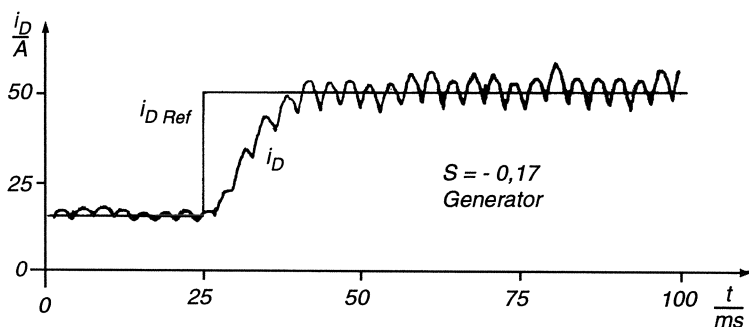


Fig. 13.18. Step response of link current control loop

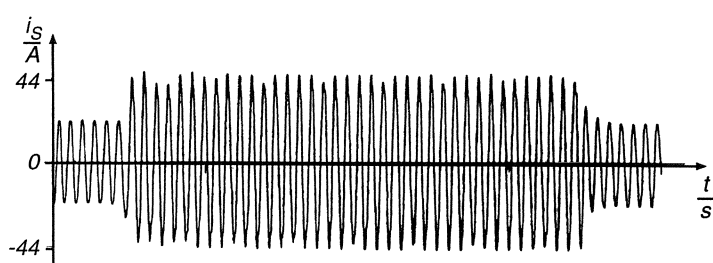
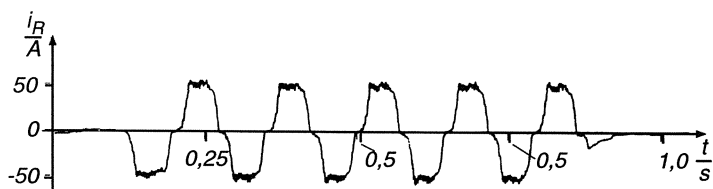


Fig. 13.19. Stator and rotor currents during step change of link current reference

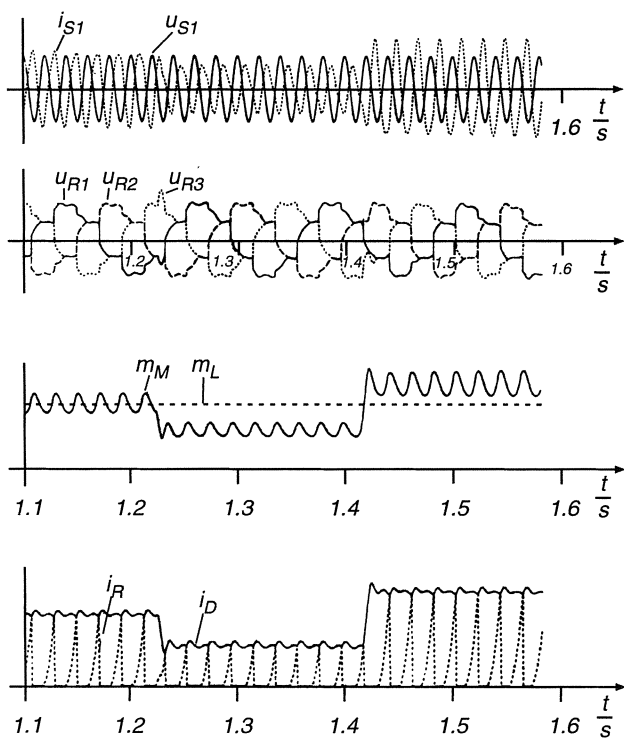


Fig. 13.20. Simulation results

## 14. Variable Frequency Synchronous Motor Drives

The speed of a synchronous motor with constant rotor excitation is determined by the stator frequency and the number of poles. As long as an efficient, variable frequency power supply was not available this meant constant speed operation at fixed frequency. There are drive applications, where constant speed is desired or where the reactive power that can be generated with line-connected synchronous motors is an important feature. These are, apart from electric clocks, mainly high power drives, such as for compressors in the chemical industry. Another field of application exists in pumped storage power plants, where the synchronous generators are used as motors in periods of low demand for electrical power to drive pumps, feeding water into elevated reservoirs for later use during hours of peak demand. The type of motor is, of course, not a free choice in this instance but the synchronous machine is very well suited for this duty; it is, in fact, the only one that could be used at a power level of, possibly, several hundred MW. Problems with large synchronous motors operating on a constant frequency supply may be caused by the inherent oscillatory response and the required start-up procedure. Asynchronous starting at full or reduced line voltage with the help of the damper winding and the short circuited field winding as well as special starting motors are common practice; more recently, large synchronous machines are also started with variable frequency supplied from static inverters. This can be extended into a variable speed drive with many interesting characteristics.

Historically, the synchronous motor fed with variable frequency from a DC link converter with thyratrons represented the first attempt of assigning the task of the commutator in a DC machine to external static equipment [A12, W22]. The thyratrons, gas filled discharge tubes with heated cathodes, that were available in those days, were of course hardly suitable for converter duty. Thereafter, the converter-fed synchronous motor has not received much attention but with the solid state converters available today this has changed rapidly.

There are three main areas of application for adjustable speed synchronous motor drives; they are also shown in the synopsis in Table 11.1.

- Large, low speed reversing drives, such as needed for gear-less rolling mills or mine hoists, with stringent requirements for fast dynamic response. In the past, these were mainly DC drives but they can now be built as AC synchronous motors supplied by cycloconverters, thereby eliminating all

the design- and operating-restrictions inherent in DC machines [J1, L5, N4, R17, S3, S4, S56, S58, S66].

- Large, high speed drives far into the tens of MW range, where the induced source voltages and, as a consequence, the capability of the synchronous machine of supplying reactive current, permits the use of simple DC link converters with natural or load commutation [G22, H5, N13].

Since a synchronous motor does not have to be magnetised through the inverter, as is the case with induction motors, a larger airgap is no disadvantage and is desirable for mechanical reasons. The slip-rings for supplying the rotating field winding with direct current can be omitted if an AC exciter with rotating rectifiers is employed as is common on large turbo-generators.

- A third field of application are low power servo drives (usually < 10 kW) of high dynamic performance with permanent magnet excitation and transistor inverter supplies. Their main advantage, when compared with induction motors, is the almost complete elimination of rotor losses; on the other hand, field weakening is more difficult [G29, L42, L45, P14]. There are also prototype motors of much larger power rating with permanent magnet excitation as listed in Table 11. 1.

Apart from these major applications for synchronous motors there are other synchronous machine designs such as reluctance machines which can also be incorporated into controlled drives [D9, L12, L16, P9].

With today's possibilities for signal processing, controlled drives with synchronous machines are offering real alternatives to the DC drives that are still in wide use in the areas mentioned above, except for the high speed, high power applications, for which DC drives could not be built.

The analysis and design of a control system for an electric drive calls for a dynamic model of the motor; with a synchronous machine this may be of considerable complexity if details are to be taken into account, but this is not the purpose of this more general discussion. Substantial simplification may be achieved without much loss of information, by restricting ourselves to machines with cylindrical rotors, i.e. neglecting saliency of poles and excluding the switched reluctance motor, because then the mathematical model of a symmetrical three phase machine described in Sect. 10.1 remains applicable.

This is demonstrated in Table 10.1 showing how the general model of AC motors can be adapted to the various constraints. Larger synchronous motors usually have a symmetrical damper winding in order to reduce the effects of harmonics and negative sequence current components produced by the power converter; a damper winding also tends to lower the transient reactance of the machine and thus facilitates commutation. For simplicity, the single axis field winding of a synchronous machines may be incorporated into the symmetrical damper winding by inserting an ideal DC voltage source  $u_F$  having no internal impedance into a common rotor winding, as seen in Table 10.1. This simplification is adequate for designing the control, it would be far too inaccurate for the design of the machine.

Smaller motors, such as synchronous servo motors with permanent magnet excitation, usually do not possess damper windings but there is a slight electrical damping effect due to the eddy currents in the magnets; of course, all the mechanical damping of the drive can now be achieved by control.

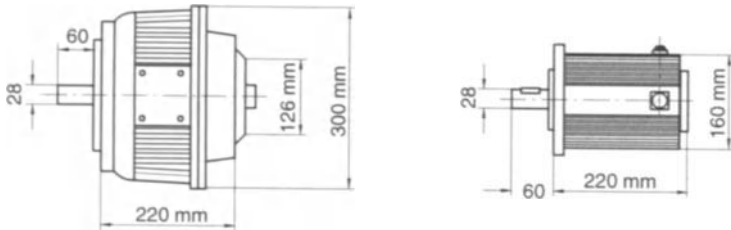
Since the control of permanent magnet excited machines is simpler than that of machines with field and damper windings, this case will be treated first.

## 14.1 Control of Synchronous Motors with PM Excitation

Permanently excited synchronous motors are an attractive solution for servo drives in the kW-range. There are various designs, depending on the type of magnetic material used; best results are obtained with “rare earth” magnetic materials such as Samarium-Cobalt or Neodymium-Iron-Boron, which combine high flux density (beyond 1 T) with very large coercive force (up to 7000 A/cm). This makes it practical to magnetise the pole pieces separately rather than have to magnetise the complete assembly in place, as is necessary for instance with Alnico-magnets. Rare-earth magnets require also much less space and, with proper design, there is no danger of accidental demagnetisation through short circuit currents. Unfortunately magnets of this type are still quite expensive.

Synchronous motors with rare earth permanent magnets have higher power density than comparable DC motors because the limiting effects of the mechanical commutator are absent; the power density exceeds also that of induction motors because there is no need for rotor currents producing torque. A comparison is seen in Fig. 14.1, showing the outline of an axial field DC disk motor, until a few years ago the ultimate in dynamic performance, and a synchronous AC servo motor with rare earth magnet excitation. The AC motor is not only more powerful having lower mass and inertia, it exhibits also a much larger impulse torque  $m_{\max} \Delta t = 900$  Nms as compared to 5.5 Nms of the disk motor; this is important for quickly accelerating an inertia load through a given speed range  $\Delta\omega$ . The reason for this large difference is the thermal capacity of the AC winding which is embedded in slots, as compared to the open conductors of the printed armature winding in a DC disk motor. Due to their high power density and, consequently, the smaller size, permanent magnet synchronous motors have in recent years evolved as the preferred solution for positioning drives on machine tools and robots, where the motors are to be integrated into the mechanical load.

As an example, Figure 14.2 shows the cross section of an 1.2 kW, 4 pole synchronous motor (continuous rating) with a hollow steel rotor to which Sm-Co-Magnets assembled from standard size bars are attached; this also reduces the quadrature field. The whole rotor assembly may be bandaged after the hollow parts have been filled with light-weight nonconducting material. The stator is skewed in order to reduce torque ripple caused by the stator slots [L45, P14].



DC-PM disk motor		AC-PM synchronous motor
4.5 kW, 3000 min <sup>-1</sup> , 14.3 Nm	Cont. Rating	6.7 kW, 4000 min <sup>-1</sup> , 16 Nm
114 Nm for 50 ms or 1 % duty cycle	Max. Torque	90 Nm for 10 s or 15 % duty cycle
5.7 Nms	Torque Impulse	900 Nms
4300 min <sup>-1</sup>	Max. Speed	4500 min <sup>-1</sup>
35 kg	Mass	16 kg
74 kg cm <sup>2</sup>	Inertia	45 kg cm <sup>2</sup>

Fig. 14.1. Comparison of DC and AC servo motors

Rare earth permanent magnets can be considered as ampereturns sources; since they combine relatively high electrical resistivity and unity permeability for external magnetic fields, they may be viewed as part of the air gap. Hence the motor is characterised by a constant wide air gap resulting in a relatively small synchronous reactance which minimises armature reaction.

In order to adapt the mathematical model of the symmetrical 2 pole three phase machine derived in Sect. 10.1 to this constraint, the rotor circuit is assumed to be fed from two current sources (Fig. 14.3). According to Eq. (10.8) this produces an impressed rotor current vector

$$\underline{i}_R(t) = I_F - \frac{I_F}{2} e^{j\gamma} - \frac{I_F}{2} e^{j2\gamma} = \frac{3}{2} I_F, \quad \xi = 0, \quad (14.1)$$

which is rigidly fixed to the rotor and produces an ampereturns distribution moving synchronously with the rotor. The same result would be obtained with an induction motor having a supraconducting rotor winding, i.e. inserting  $T_R \rightarrow \infty$  into Eq. (12.27).

By further assuming that the stator currents of the servo motor are supplied by a current-controlled switched transistor inverter of the type shown in Fig. 11.3, having adequate ceiling voltage and high clock frequency, the stator windings can also be considered as being fed by current sources following the commands from a set of reference values. More realistically, the response of the current control loops may be approximated by equivalent lags,

$$T_e \frac{di_{S\nu}}{dt} + i_{S\nu} = i_{S\nu\text{Ref}} \quad \nu = 1, 2, 3 \quad (14.2)$$

with  $\sum_1^3 i_{S\nu} = 0$ , where in practice  $T_e$  may be in the order of 1 ms or less. Figure 14.4 shows the step response of a stator current control loop for the servo motor in Fig. 14.2, measured in standstill. In steady state condition the currents are approximately sinusoidal.

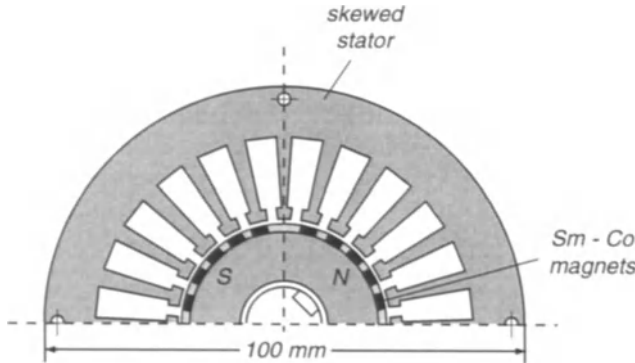


**Fig. 14.2.** Cross section of 4 pole synchronous servo motor with rare-earth permanent magnets

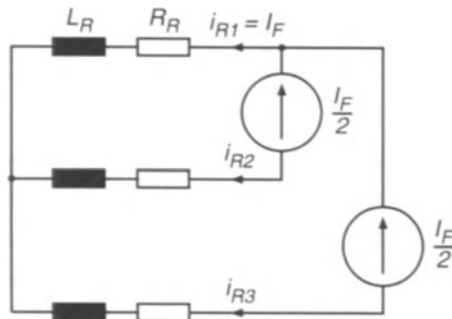


**Fig. 14.3.** Equivalent rotor circuit of synchronous motor with permanent magnet excitation

The stator voltage Eq. (10.38), while being of no consequence for the drive dynamics when the currents are impressed, is important for the inverter design. With Eq. (14.1) and the angular rotational speed  $\omega = d\varepsilon/dt$  we have

$$R_S \dot{i}_S + L_S \frac{di_S}{dt} + j \omega \frac{3}{2} \Phi_F e^{j\varepsilon} = \underline{u}_S(t) , \quad (14.3)$$

with  $\Phi_F = L_0 I_F$ .

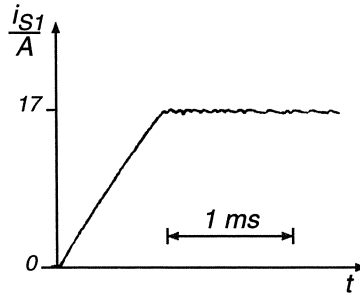


**Fig. 14.4.** Step response of stator current control loop, employing a transistor inverter with high switching frequency

The expression for the electric torque is

$$m_M(t) = \frac{2}{3} L_0 \operatorname{Im} [\underline{i}_S (\underline{i}_R e^{j\epsilon})^*] = \Phi_F \operatorname{Im} [\underline{i}_S e^{-j\epsilon}] = \Phi_F i_{Sq} \quad (14.4)$$

where  $\underline{i}_S e^{-j\epsilon}$  is the stator current vector in a coordinate frame given by the rotor position. Since  $\epsilon$  is easy to measure, this is the preferred orientation here; it corresponds to the  $d - q$  or Park-Transformation commonly used with synchronous machines.

The mathematical model of the synchronous motor is contained in the right hand section of Fig. 14.5. The principle of controlling the motor is similar to the field orientated control of an induction motor except that now the rotor position serves as the angle of reference; hence there is no need for a flux model. The drive should of course be operated in such a way as to make best use of the motor and inverter.

The appropriate mode of control may be deduced from a phasor diagram, describing the voltage equation (14.3) in steady state. With  $\omega_1 = \omega = \text{const.}$ ,  $\epsilon = \omega t$ , the stator current and voltage vectors are

$$\underline{i}_S(t) = \frac{3\sqrt{2}}{2} \underline{I}_S e^{j\omega t}, \quad \underline{u}_S(t) = \frac{3\sqrt{2}}{2} \underline{U}_S e^{j\omega t}. \quad (14.5)$$

After simplification, Eq. (14.3) assumes the form

$$(R_S + j\omega L_S) \underline{I}_S + j E = \underline{U}_S, \quad (14.6)$$

where

$$E = \frac{1}{\sqrt{2}} \omega \Phi_F \quad (14.7)$$

is the RMS-value of the source voltage induced in the stator winding by the permanent magnets (Fig. 14.6 a).

The expression

$$\underline{i}_S(t) e^{-j\omega t} = \frac{3\sqrt{2}}{2} \underline{I}_S = \frac{3\sqrt{2}}{2} \underline{I}_S e^{j\delta} = \frac{3\sqrt{2}}{2} (I_{Sa} + j I_{Sq}) \quad (14.8)$$

represents the stator current in rotor coordinates, with  $\delta$  being the current load angle;  $\delta = 0$  is the no-load position. The phasor diagram is drawn in Fig. 14.6 b for  $\delta = \frac{\pi}{2}$  which is the optimal mode of operation, where the motor produces maximum torque for a given stator current. With a synchronous motor operating on the constant frequency line, it would correspond to the static stability limit, but this is of no consequence here as the motor is self-controlled, similar to a DC machine where the commutator is fixed to the rotor.

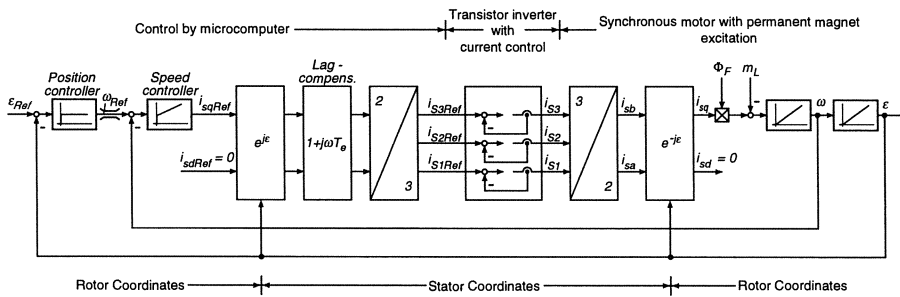


**Fig. 14.5.** Control of synchronous motor with permanent magnet excitation

Clearly,  $\delta = \pm\frac{\pi}{2}$ ,  $I_{Sd} = 0$  is the best choice as long as the inverter can supply the necessary voltage, i.e. below base speed. Direct field weakening is not feasible with a permanently excited machine but a similar effect can be achieved by advancing the current vector beyond  $\delta = \frac{\pi}{2}$ , i.e. introducing a current component in the negative  $d$ -axis. This is indicated in Fig. 14.6 b in dashed lines showing a decrease of the terminal voltage  $U_{S1}$ . As a consequence  $I_{Sq}$  may have to be reduced in order not to exceed the limit for the total current

$$I_S = \sqrt{I_{Sd}^2 + I_{Sq}^2} < I_{S\max}; \quad (14.9)$$

this leads to a corresponding reduction of torque, which is a characteristic for operation at reduced field.

The optimal control procedure is thus as follows: Operation with  $I_{Sd} = 0$ ,  $|I_{Sq}| < I_{S\max}$  up to the voltage limit, which is reached at the base speed; a further increase in speed can then be achieved by shifting the current into the unstable region,  $|\delta| > \frac{\pi}{2}$ , while maintaining constant voltage. In view of the large effective air gap with rare-earth permanent magnets, this method of "field weakening by armature reaction" calls for a large stator current in the direct axis and, hence, is a much less efficient procedure than would be possible with a synchronous machine having a DC field winding. However, as a short time measure it may be acceptable. As seen in Fig. 14.6 c the need for field weakening is likely to occur mainly in the motoring quadrants but, in principle, it is applicable to braking operation as well.

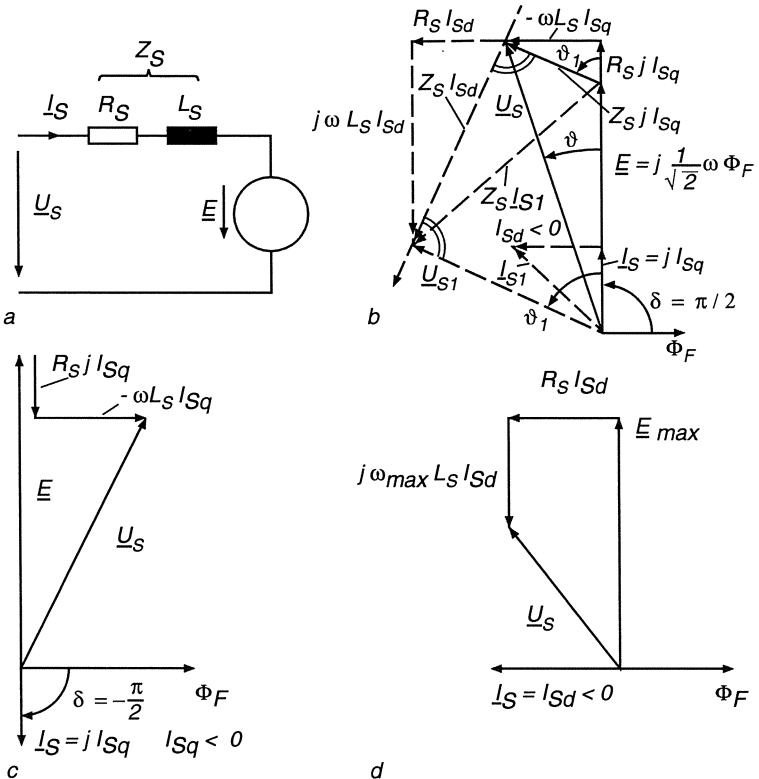


**Fig. 14.6.** Phasor diagrams of synchronous motor with permanent magnet excitation  
a) Equivalent circuit diagram, b) Phasor diagram showing effect of field weakening, c) Phasor diagram during regeneration, d) Phasor diagram at maximum no-load speed.

A possible solution to the control problem is sketched in the lower part of Fig. 14.7, where field weakening is initiated by an auxiliary control loop with the purpose of limiting the magnitude of the stator voltage.

The degree of field weakening that may be achieved by armature reaction can be estimated from the phasor diagram (Fig. 14.6 b). By initially assuming a purely quadrature current, the voltage components are

$$\begin{aligned} U_S \cos \vartheta &= E + R_S I_{Sq}, \\ U_S \sin \vartheta &= \omega L_S I_{Sq}. \end{aligned} \quad (14.10)$$

The voltage angle  $\vartheta$  depends on speed and load,

$$\vartheta = \arctan \frac{\omega L_S I_{Sq}}{E + R_S I_{Sq}}. \quad (14.11)$$

By now adding a direct component,  $I_{Sd} < 0$ , while maintaining  $I_{Sq}$  and hence torque, the voltage phasor  $\underline{U}_S$  moves along the dashed straight line in the indicated direction. The minimum value of the voltage is reached when the phasor  $\underline{U}_S$  is orthogonal to this line, hence

$$U_{S1} = U_S \cos(\vartheta_1 - \vartheta) \quad (14.12)$$

where

$$\vartheta_1 = \arctan \frac{\omega L_S}{R_S}. \quad (14.13)$$

There is no point in advancing the voltage angle beyond  $\vartheta_1$ , as the stator voltage then begins to rise again.

The additional direct component  $I_{Sd}$ , which appears as a reactive current component at the motor terminals, causes an increase of the stator current  $I_S$ ; the current  $I_{S1}$  for the condition of minimum stator voltage is found from the related triangles

$$I_{S1} = \sqrt{\frac{E^2 + U_{S1}^2 - 2E U_{S1} \cos \vartheta_1}{E^2 + U_S^2 - 2E U_S \cos \vartheta}} I_{Sq}. \quad (14.14)$$

Since the stator current is limited by the inverter, this calls for a corresponding reduction of the maximum quadrature current.

The following parameters, taken from the 1.2 kW servo motor (Fig. 14.2), are used as an example of what can be expected with this method [L45]. At the base speed (2000 1/min) and at rated torque (5.7 Nm), the relative voltage across the stator impedance is

$$\frac{\omega L_S I_{Sq}}{E} = 0.139, \quad \frac{R_S I_{Sq}}{E} = 0.066,$$

which results in  $U_S/E = 1.075$  and  $\vartheta = 7.5^\circ$ .

By adding a negative  $I_{Sd}$ -component and adjusting it for minimum stator voltage, the voltage angle becomes

$$\vartheta_1 = \arctan \frac{\omega L_S}{R_S} = 64.5^\circ$$

and the stator voltage is reduced to

$$\frac{U_{S1}}{E} = \frac{U_S}{E} \cos(\vartheta_1 - \vartheta) = 0.584.$$

At the same time, however, the stator current rises to, Eq. (14.14),

$$\frac{I_{S1}}{I_{Sq}} \approx 6.0.$$

The torque and speed in this assumed operating condition remain unchanged, but the copper losses are of course greatly increased. Hence the effective stator

impedance is reduced by a factor  $(U_{S1}/I_{S1})/(U_S/I_{Sq}) = 0.091$ , which permits access to suitably defined operating points in the high speed-low torque region as long as the voltage and current limits of the inverter are not exceeded. In view of the reduced efficiency this procedure is of course restricted to short transients at light load which is in direct analogy to common practice with DC or induction motor AC drives.

As a limiting case the situation depicted in Fig. 14.6 d may be considered, where the stator ampereturns are opposing the rotor excitation. This would result in the maximum speed obtainable by controlled armature reaction at zero torque,  $I_S = I_{Sd} < 0$ .

From the voltage equation

$$U_S^2 = (E_{\max} + \omega_{\max} L_S I_{Sd})^2 + (R_S I_{Sd})^2, \quad (14.15)$$

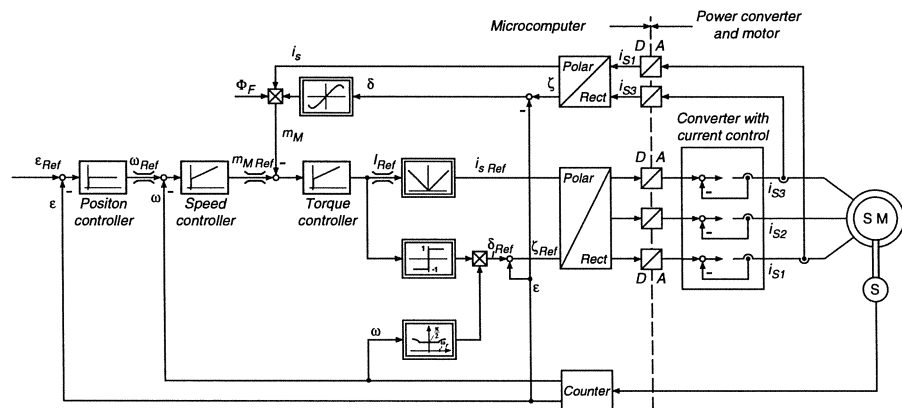
the maximum no-load speed at rated current, referred to base speed, is with  $E_{\max}/E = \omega_{\max}/\omega$

$$\frac{\omega_{\max}}{\omega_0} = \frac{\sqrt{(U_S)^2 - (R_S I_{Sd})^2}}{E + (\omega L_S I_{Sd})} \quad (14.16)$$

with the numbers listed above this results in

$$\omega_{\max}/\omega_0 = 1.25.$$

Of course, much higher speeds may be obtained by temporarily increasing the stator current. With the particular servo motor described, the no load speed at five times rated current is 8000 1/min.



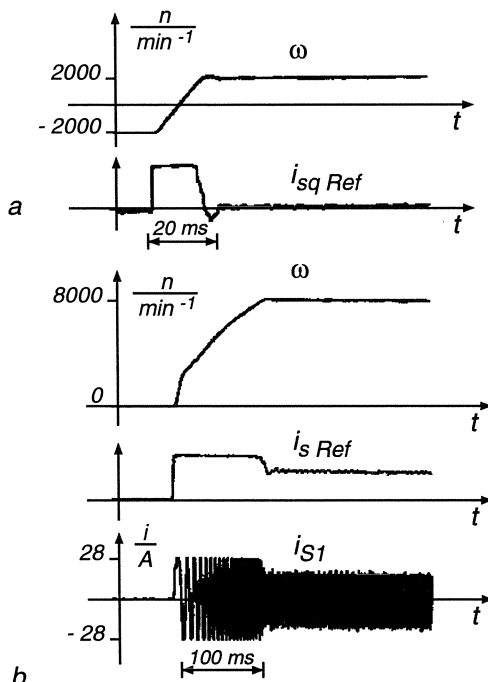
**Fig. 14.7.** Synchronous motor servo drive with microprocessor control in polar coordinates

Figure 14.5 contains a block diagram of the control scheme in rectangular coordinates but the rotor orientated control can of course be presented in polar coordinates as well. This is shown in Fig. 14.7, where a microcomputer performs

all the control functions up to position control; operation at reduced field is achieved with the help of a suitably defined function  $\delta_{Ref} = f(\omega)$ .

The transformations from stator to rotor coordinates and vice versa now call for a simple modulo  $2\pi$  addition of  $\varepsilon$ . All the inner control functions are executed in 0.6 ms-intervals which is adequate for stator frequencies of up to about 200 Hz but a further extension of the frequency range could be achieved with the help of special processors.

Transients that have been recorded with the 1.2 kW permanently excited synchronous motor at six times rated current are displayed in Figs. 14.8 and 14.9. The control is performed by a microcomputer with a control structure similar to the one shown in Fig. 14.7; however, special adaptive software features have been added to the speed- or position-control function in order to combine fast response with aperiodic damping [L45].



**Fig. 14.8.** Speed transients of microcomputer-controlled synchronous motor servo drive at no-load

The response of the drive is by no means limited by the motor or the type of control but only by the maximum current which the inverter can supply. Given sufficient stator current, the motors have very high short time overload capacity which is important for servo drives designed for intermittent duty, Fig. 14.1.

The control circuits in Figs. 14.5 and 14.7 contain current control loops in stator coordinates, producing approximately impressed stator currents. Their

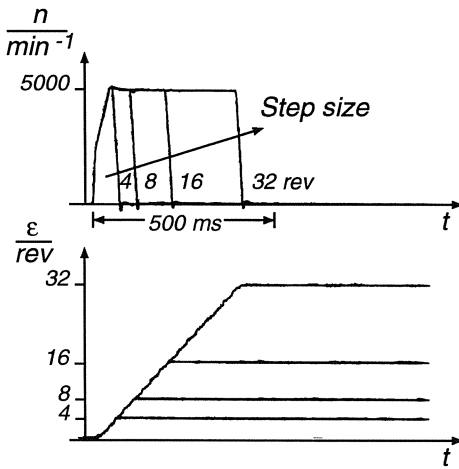


**Fig. 14.9.** Step response of time-optimal position control with synchronous motor servo drive at no-load

references are sinusoidal in steady state which calls for careful tuning of the current controllers with regard to undesirable phase shifts. An alternative and usually preferable arrangement is shown in its basic form in Fig. 14.10, where the currents are controlled in moving rotor coordinates; this has the advantage that the controllers for  $i_{Sd}$ ,  $i_{Sq}$  are processing DC signals in steady state.

This control circuit can also be extended for limited field weakening as before, possibly also including a torque control loop. Signals for voltage feed forward are normally added at the output of the current controllers, as shown before, in order to counteract the effects of the induced motor voltages.

## 14.2 Cycloconverter-fed Synchronous Motors with Field and Damper Windings

Another range of adjustable speed synchronous motor drives employs machines of conventional design having in the rotor a symmetrical damper winding and a single axis field winding which is fed with direct current through slip rings or from an AC exciter with rotating rectifiers. The stator can be supplied by a cycloconverter with line commutation which makes this scheme particularly attractive for high power drives at low speed, as long as the frequency range of the cycloconverter suffices; also, the large number of thyristor branches is less objectionable at high power where parallel thyristors might otherwise be needed. The basic circuit of this type of drive is shown in Fig. 14.11.

Typical applications are large gearless drives, where DC machines have dominated in the past, for example drives for reversing rolling mills, mine hoists, ore mills and rotary cement kilns; at lower power, elevators or direct wheel drives on

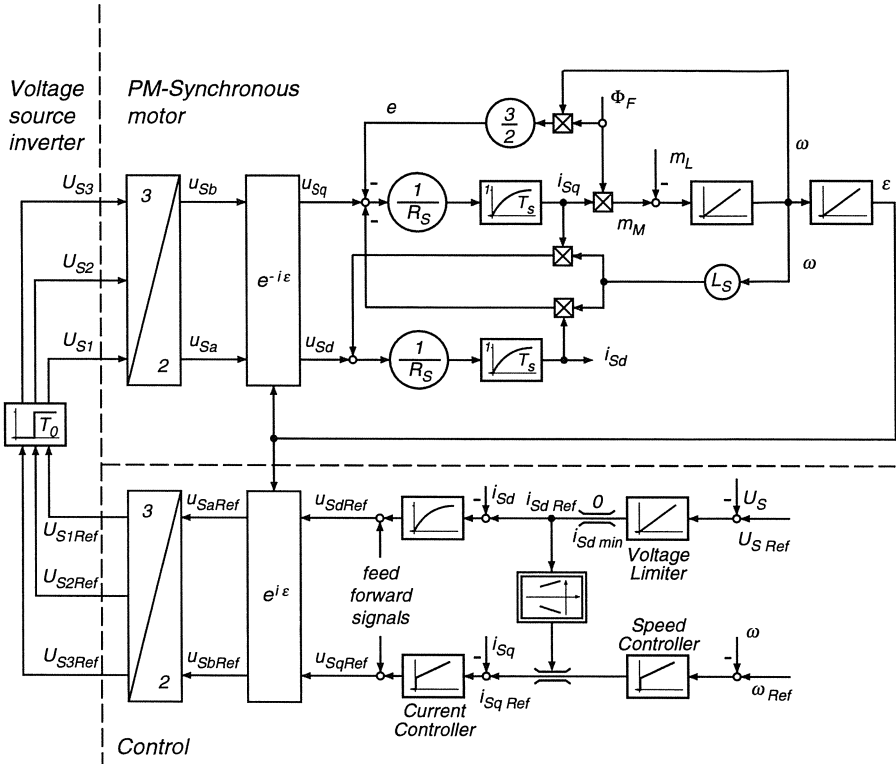


Fig. 14.10. PM-Synchronous motor drive with voltage source inverter and current control in rotor coordinates

excavators in open-cast mines are further possible applications. The drive permits 4-quadrant operation with smooth transitions including standstill; hence it is perfectly suited for speed as well as position control requiring rapid response. The torque harmonics due to the cycloconverter are small and of relatively high frequency.

Large, low speed motors are normally, but not exclusively, built with salient poles; they include damper windings, not needed here for start-up or for damping oscillations as this can be achieved by converter control, but for reducing unavoidable harmonics and negative sequence components caused by the cycloconverter. In addition the damper windings can speed up commutations by reducing the motor transient reactance.

Clearly a detailed analysis of the drive requires an extended machine model that could not be dealt with manually or by intuition. For qualitative purposes, however, the model derived in Sect. 10.1 remains still useful as seen in Table 10.1c. We therefore assume that the motor containing a non-salient rotor and a symmetrical three phase rotor winding has a field power supply consisting of

an ideal source of direct voltage  $u_F$  according to Fig. 14.11. Since this variable voltage source exhibits no internal impedance, the damping effect of the rotor winding is not impeded; at the same time the symmetrical rotor winding serves for DC excitation [L38].

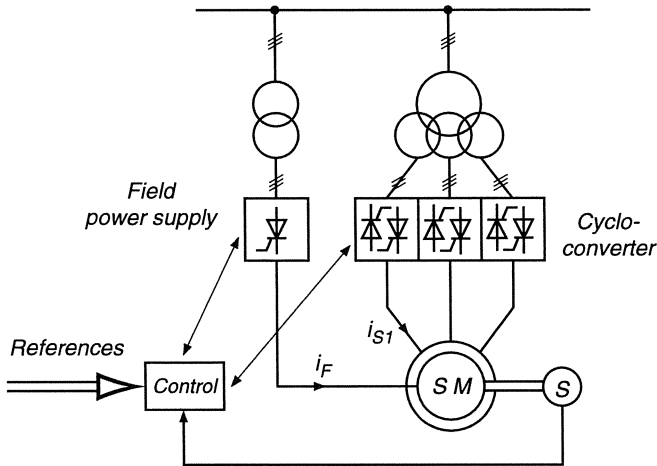


Fig. 14.11. Variable frequency synchronous motor drive with cycloconverter

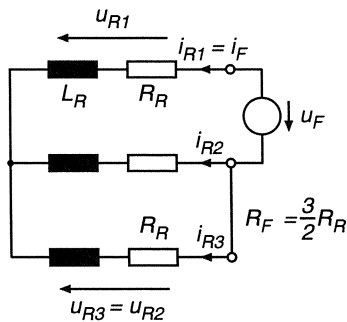


Fig. 14.12. Symmetrical rotor winding with DC excitation from a voltage source

This simplified model cannot, of course, describe all the details nor does it offer the freedom of design with separate and concentrated rotor windings but it serves the present purpose of designing a control strategy and clarifies the main features of this type of drive.

In order to adapt the mathematical model derived in Sect. 10.1 to this constraint, we again define with  $\gamma = 2\pi/3$  a vector of externally applied rotor voltages

$$\underline{u}_R(t) = u_{R1} + u_{R2} e^{j\gamma} + u_{R3} e^{j2\gamma} = u_{R1} - \frac{1}{2}(u_{R2} + u_{R3}) + j \frac{\sqrt{3}}{2}(u_{R2} - u_{R3}). \quad (14.17)$$

Because of the short circuit between phase 2 and 3,

$$u_{R2} = u_{R3},$$

hence

$$\underline{u}_R(t) = u_{R1} - u_{R2} = u_F(t). \quad (14.18)$$

Thus the voltage vector is real, being identical with the applied field voltage, Fig. 14.12.

The rotor currents have mean values, to which transient terms  $i'_R$  are superimposed. Considering the isolated neutral of the winding, we find

$$\begin{aligned} \underline{i}_R(t) &= (I_F + i'_{R1}) + \left(-\frac{I_F}{2} + i'_{R2}\right) e^{j\gamma} + \left(-\frac{I_F}{2} + i'_{R3}\right) e^{j2\gamma} \\ &= \frac{3}{2}(I_F + i'_{R1}) + j \frac{\sqrt{3}}{2}(i'_{R2} - i'_{R3}). \end{aligned} \quad (14.19)$$

Hence the mean of the rotor current vector is also real,

$$\underline{i}_{R0} = \frac{3}{2}I_F = \frac{3}{2}\frac{U_F}{\frac{3}{2}R_R} = \frac{u_F}{R_R}, \quad (14.20)$$

but under dynamic conditions the vector is deflected by induced current components.

Best results of the drive control may be expected if the stator currents are again current-sourced by the cycloconverter with the help of fast current control loops, as was shown in Sect. 13.1. This leaves the rotor voltage equation and the mechanical equations for modelling the drive dynamics, Eqs.(10.38- 10.41),

$$R_R \dot{\underline{i}}_R + L_R \frac{d\underline{i}_R}{dt} + L_0 \frac{d}{dt}(\underline{i}_S e^{-j\varepsilon}) = u_F, \quad (14.21)$$

$$J \frac{d\omega}{dt} = \frac{2}{3}L_0 \operatorname{Im}[\underline{i}_S (\underline{i}_R e^{j\varepsilon})^*] - m_L, \quad (14.22)$$

$$\frac{d\varepsilon}{dt} = \omega. \quad (14.23)$$

The design of a control scheme in field coordinates calls for the selection of a suitable frame of reference. In the case of the synchronous motor with permanent magnets (Sect. 14.1) the rotor position  $\varepsilon$  was the natural choice since this was the orientation of the magnets producing the ampereturns; however, the situation is different here, where the induced rotor currents can shift the ampereturns-wave with respect to the rotor (Fig. 14.8). It is therefore appropriate to employ a flux vector as with the induction motor. A suitable choice is the rotor flux, defined by Eq. 12.21,

$$\underline{i}_{mR} = \underline{i}_S + (1 + \sigma_R) \underline{i}_R e^{j\varepsilon} = i_{mR} e^{j\varrho}; \quad (14.24)$$

this makes sense because the rotor circuit in Fig. 14.12 has all the features of an induction machine; the only difference is that in steady state the magnetising current vector  $\underline{i}_{mR}$  is in synchronism with the rotor,  $\varrho - \varepsilon = \text{const.}$ , whereas it was moving with slip frequency across the rotor of the induction motor (Fig. 12.11).

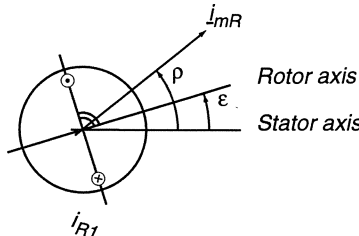


**Fig. 14.13.** Definition of coordinate system

By eliminating  $i_R$  from Eqs. (14.21, 14.24) we find

$$T_R \frac{di_{mR}}{dt} + (1 - j\omega T_R) \underline{i}_{mR} = \underline{i}_S + (1 + \sigma_R) \frac{u_F}{R_R} e^{j\varepsilon}, \quad (14.25)$$

which can be expanded into two real differential equations

$$T_R \frac{di_{mR}}{dt} + i_{mR} = i_{Sd} + (1 + \sigma_R) \frac{u_F}{R_R} \cos(\varrho - \varepsilon), \quad (14.26)$$

$$\frac{d}{dt} (\varrho - \varepsilon) = \omega_{mR} - \omega = \frac{1}{i_{mR} T_R} \left[ i_{Sq} - (1 + \sigma_R) \frac{u_F}{R_R} \sin(\varrho - \varepsilon) \right], \quad (14.27)$$

where

$$\underline{i}_S e^{-j\varrho} = i_S e^{j(\zeta - \varrho)} = i_{Sd} + j i_{Sq} \quad (14.28)$$

is again the stator current vector in rotor flux coordinates.

Since the vector  $\underline{i}_{mR}$  moves synchronously with the rotor in steady state, the right hand side of Eq. (14.27) vanishes,

$$i_{Sq}|_{t \rightarrow \infty} = (1 + \sigma_R) \frac{u_F}{R_R} \sin(\varrho - \varepsilon)|_{t \rightarrow \infty}. \quad (14.29)$$

The equation (12.26) for the driving torque remains unchanged,

$$m_M = \frac{2}{3} L_0 \operatorname{Im} [\underline{i}_S (i_R e^{j\varepsilon})^*] = \frac{2}{3} (1 - \sigma) L_S i_{mR} i_{Sq} = k i_{mR} i_{Sq}. \quad (14.30)$$

These equations describing the synchronous machine in field coordinates are graphically represented by the block diagram in the upper part of Fig. 14.14, containing once more the transformations from the stator- or rotor- orientated coordinate system into field coordinates. The diagram corresponds to that of the

induction motor with the exception of the field voltage  $u_F$  which, after transformation into flux-orientated  $d - q$ -components, is added as an additional input signal at the appropriate points. In practice  $u_F$  may be supplied by a separate two-quadrant converter with closed loop voltage control, thus underlining the characteristics of a low impedance voltage source. It would of course be possible also to substitute a control loop for the field current in order to eliminate the effect of changing field winding resistance due to temperature. The drive would then respond faster in the field weakening range, but the damping effect by transient currents induced in the low impedance field circuit would be reduced; also the model of the machine would have to be modified.

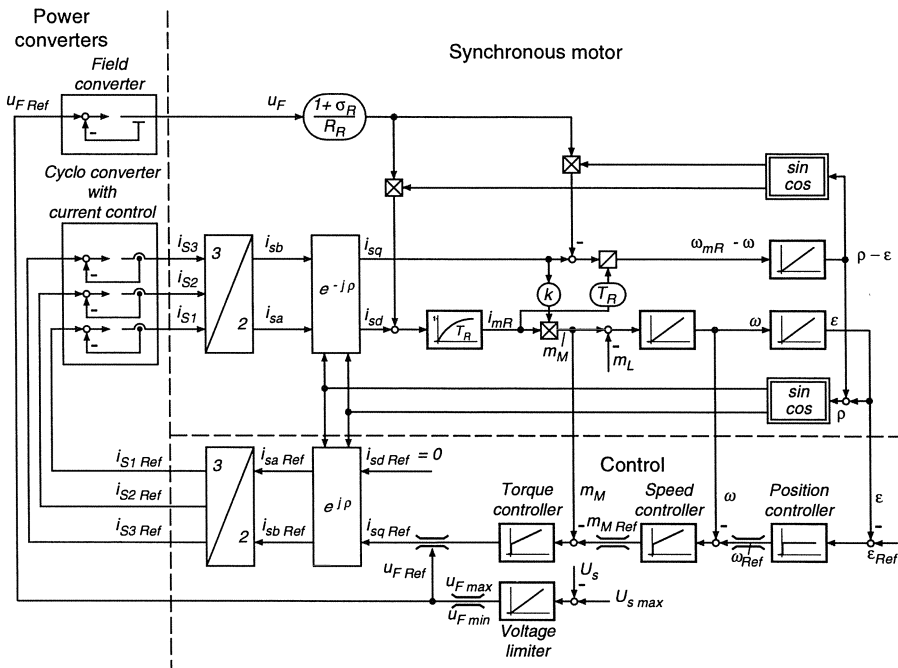


Fig. 14.14. Control of synchronous motor in field-coordinates

In contrast to Fig. 14.6 there is no need to apply stator current in the  $d$ -axis, since field weakening is now more effectively achieved by reducing the field voltage rather than increasing the stator current. Again, the need for field weakening becomes manifest when the magnitude of the stator voltage approaches its limit. Alternatively, field weakening could be accomplished by an  $i_{mR}$ -control loop, the reference of which is generated as a nonlinear function of speed,  $i_{mR Ref}(\omega)$ .

The flux angle  $\varphi$  required for modulation and for computation of  $i_{mR}$ ,  $i_{sq}$  and  $m_M$  is derived from a flux model, which can be processed on line by a microcomputer. As in case of the induction machine, the flux model may be defined in stator or in field coordinates (Fig. 12.16 a,b). Computational advan-

tages are gained by following the second approach, i.e. referring to Eqs. (14.26, 14.27), which describe the magnitude of the flux vector and its position relative to the rotor. This is represented by the block diagram in Fig. 14.15 which is a replica of the motor model in Fig. 14.14. Clearly, with  $u_F = 0$ , the flux model of the induction machine, Fig. 12.16 b, results. The angle  $\varrho - \varepsilon$  is approximately constant in steady state.

The accuracy with which the stator currents are tracking the current references may again be considerably improved, if voltage feed-forward is employed; its purpose is to cancel the voltage  $e_S$  behind the transient reactance which is induced in the stator windings by the magnetising current, i.e. the main flux.

The stator voltage was derived in Eq. (12.45)

$$\underline{u}_S(t) = R_S \underline{i}_S + \sigma L_S \frac{d\underline{i}_S}{dt} + (1 - \sigma) L_S \frac{d\underline{i}_{mR}}{dt}, \quad (14.31)$$

which in steady state, with

$$\omega_{mR} = \omega_1 = \omega = \text{const}, \quad i_{mR} = \text{const}, \quad i_S = \text{const}$$

assumes the form

$$\underline{u}_S(t) = (R_S + j\omega\sigma L_S) \underline{i}_S + \underline{e}_S(t), \quad (14.32)$$

where

$$\underline{e}_S(t) = j\omega(1 - \sigma) L_S \underline{i}_{mR} \quad (14.33)$$

is the inner voltage mentioned before.

If the control functions are performed by a microcomputer, the sinusoidal three phase components of  $\underline{e}_S$  can be easily computed and fed into the current loops behind the current controllers as is shown in Fig. 14.16. The same technique was described in Chap. 13.

If the current controllers are of the analogue form, being part of the power converters, the scheme in Fig. 14.16 a would require a second D/A converter which can be omitted by mixing the signals within the microcomputer, as shown in Fig. 14.16 b.

Of course, perfect cancellation of  $\underline{e}_S$  cannot be achieved by any of these schemes since the nonlinear control dynamics of the converter separate the point of compensation from the actual point of entry of the disturbance. Still, a considerable improvement results as was shown in Fig. 13.8. The residual lag of the current loops may be further reduced by inserting lead-lag filters at the reference inputs of the current controllers; this is also indicated in Fig. 14.16.

An alternative approach would again be controlling the currents in field coordinates so that the current controllers are processing DC signals in steady state.

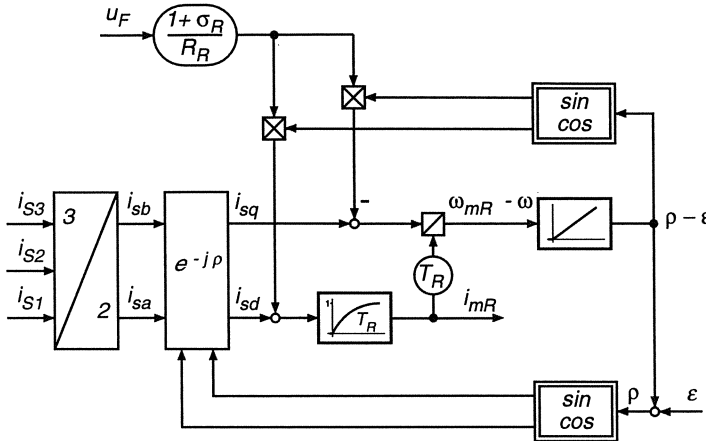


Fig. 14.15. Dynamic model for computing rotor flux of synchronous machine

### 14.3 Synchronous Motor with Load-commutated Inverter (LCI)

The variable frequency synchronous motor drive with cycloconverter supply discussed in the preceding paragraph is suitable for large drives with high dynamic performance. Since the cycloconverter is line-commutated, only converter-grade thyristors are needed, although in a large quantity. A limitation is caused by the narrow frequency range effectively covered by a cycloconverter; with a 50 Hz supply and 6-pulse circuits it extends to about  $f_1 = 20 \dots 25$  Hz. This is sufficient for a rolling mill motor having a base speed of 60 1/min and a maximum speed of 120 1/min; it could be realised with up to 20 poles at practically any power rating [S3, S66].

However, when higher speed is required, for example 4500 1/min on a large turbo-compressor for a pipe line or a blast furnace, a maximum stator frequency of 75 Hz would be needed even with a 2-pole motor, so a cycloconverter could provide no solution; neither could a DC drive have been built for this duty.

The simplest way of eliminating the restrictions imposed by the line frequency is a two-stage conversion, inserting a DC link for decoupling of the line- and the machine-side converters. Figure 11.14 showed such a circuit containing only 12 thyristors; the machine-side converter can now be simplified even further because the stator winding of the synchronous machine contains a voltage source  $e_S$  in series with a transient impedance, Eq. (14.32). Hence the machine-side inverter can be commutated by the load without resorting to forced commutation as was necessary with the induction motor; in other words the synchronous machine should be operated in the overexcited region so that it can absorb the reactive current produced by the phase-controlled machine-side converter. The basic circuit is depicted in Fig. 14.17.

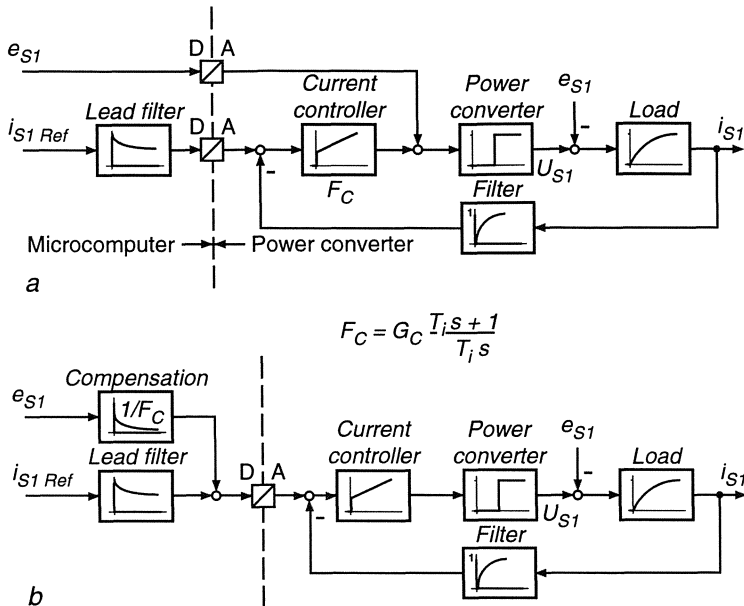
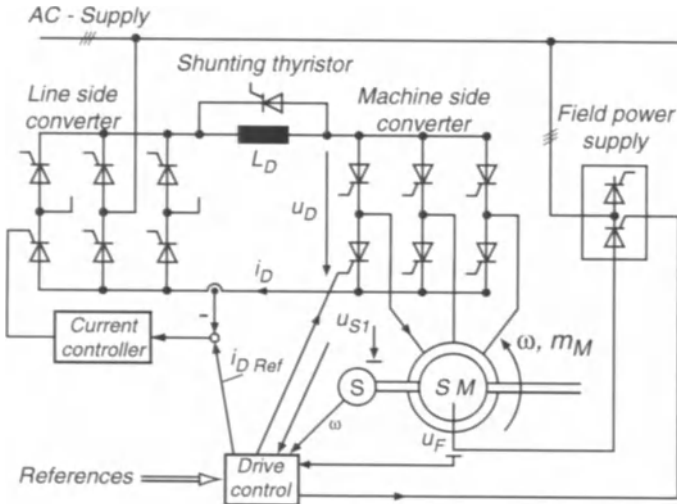


Fig. 14.16. Voltage feed-forward in current control loop

The remaining problem is then the commutation at start-up, where the induced voltage is insufficient, but this can be solved by intermittently blanking the current with the help of the line-side converter. This produces torque pulsations, but there are many applications where constant torque in the very low speed range, say below 10% of rated speed, is not necessary; examples are the turbo-compressors mentioned before or gas-turbine sets which are started with the synchronous generator acting as motor, the starting of pumped storage sets etc.

Apart from the very low speed range, where the current  $i_D$  must be made intermittent in order to allow commutation of the machine-side converter, the drive can operate smoothly in all four quadrants of the torque-speed plane. This is shown in Fig. 14.18. During regeneration the voltage  $\bar{u}_D$  is reversed by delayed firing of the line-side converter while the direction of rotation is determined by the sequence of the firing pulses for the machine-side converter. The voltage  $\bar{u}_D$  rises with speed up to the limit given by the converter, a further increase of speed is then achieved by reducing the field current, i.e. by field weakening as with a DC drive. The line interactions of this type of drive are also similar to those of a converter-fed reversible DC drive (Chap. 8).

The basic mode of operation of the machine-side converter corresponds to that of Fig. 11.16, except that the firing of thyristors cannot be initiated at arbitrary instants; it needs to be synchronised with the source voltage  $e_S$  which is performing the commutation. Outside the commutation intervals the stator



**Fig. 14.17.** Converter with DC link for supplying a synchronous machine

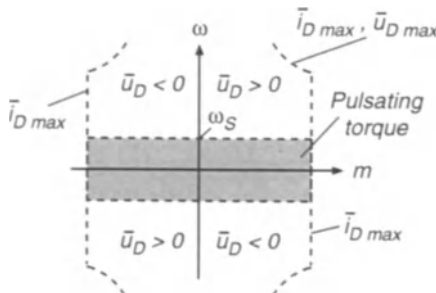


**Fig. 14.18.** Operating range of synchronous motor drive with direct current link

current, flowing through two phases of the motor, is current-sourced by the DC link; its magnitude is maintained by closed loop control via the line-side converter.

The stator current has approximately the same waveform consisting of  $120^\circ$  blocks as shown in Fig. 11.15; one stator phase carries no current. The distorted waveform of the currents, which also produces torque pulsations, and the need for low impedance commutating paths make it desirable to provide continuous damper windings which assist the formation of a smoothly moving rotational flux wave, as was shown in Fig. 12.35. The combination of

- current sources in the stator (except during commutation, where two terminals are shorted through the converter), and
- low impedance rotor circuit

indicates that a detailed analysis of the system is complex and could only be handled by digital simulation [M12]; however, as an approximation the same mathematical model of the machine can be employed as in the preceding section, Eqs. (14.21–14.23). The flux vector, Eq. (14.24), the induced voltage, Eq. (14.33) and the computational model for the rotor flux, (Fig. 14.15), also remain valid.

In spite of this similarity of the plant structure the field orientated control schemes drawn in Figs. 12.31 and 14.14 are not directly applicable; this is so because the stator currents cannot be determined at will, as was possible with the current source inverter employing forced commutation or the cycloconverter with line commutation and current control. Instead, the firing of the machine-side inverter must now be so timed as to

- permit safe commutation,
- result in minimum link current for a given torque; the line-side converter would otherwise operate at an unnecessarily low power factor.

These are overriding conditions which can best be fulfilled by operating the machine-side converter at the limits of the control range, i.e.

- zero firing delay ( $\alpha = 0$ ) when regenerating and
- maximum firing delay ( $\alpha_{max}$ ) in the motoring region.

The firing delay  $\alpha$  is defined with respect to the voltage behind the transient impedance.

The two modes of operation are sketched in Fig. 14.19. Clearly the commutation period and the fact that the commutation must be completed before  $\tau = \pi$ , prevent operation with purely quadrature current. The situation is particularly critical in motor operation with the machine-side converter serving as an inverter because the extinction angle  $\gamma$ , explained in Fig. 8.17, should be small in order not to reduce the torque unnecessarily but on the other hand it must be of sufficient magnitude to allow safe recovery of the outgoing thyristor. If the extinction angle becomes too small, a commutation failure may be the consequence; while it would not constitute a major disturbance, with the link reactor preventing excessive rise of the current, it would still cause a severe torque transient until the current control loop has restored the link current and the inverter returns to its regular firing sequence.

Another problem is the synchronisation of the machine side converter; timing of the firing circuit with respect to the terminal voltages of the machine would be unsatisfactory since these voltages are highly distorted and not in phase with the nearly sinusoidal induced voltages  $e_S$ .

There are two possibilities for detecting  $e_S$  which are the driving voltages of the commutating circuits. One is based on Eq. (14.31),

$$\underline{e}_S(t) = (1 - \sigma) L_S \frac{d\underline{i}_{mR}}{dt} = \underline{u}_S(t) - R_S \underline{i}_S - \sigma L_S \frac{d\underline{i}_S}{dt} \quad (14.34)$$

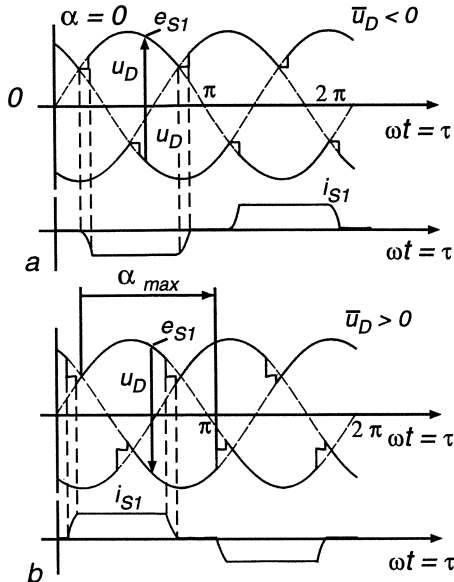


**Fig. 14.19.** Current and voltage waveforms of machine-side converter with natural commutation. **a)** regenerating, **b)** motoring

which could be evaluated with analogue circuitry or by a microcomputer. A second option is to use the flux model in Fig. 14.15, where two orthogonal stator currents  $i_{Sa}$ ,  $i_{Sb}$ , the angular rotor position  $\varepsilon$  and the field voltage  $u_F$  represent the input signals; this method would definitely require a microcomputer for executing the various nonlinear operations. The first of the two approaches seems to be more straight forward and less sensitive to uncertain parameters of the motor.

If the reconstruction of the induced motor voltages  $e_S$  is of sufficient accuracy, a closed loop control for the extinction angle could also be envisaged, as is common practice on high voltage DC transmissions (HVDC). However, the draw-back even of sophisticated nonlinear extinction angle control schemes is that they cannot entirely exclude commutation failures because there may always be late disturbances that are not taken into account when the firing instant is determined. The problem with every extinction margin control is that only hindsight can tell with certainty, whether the previously calculated firing angle was adequate.

A major difference between the firing control schemes for the line- and the machine-side converter is that the latter has to function with both directions of sequence and over a wide frequency range; this is a strong incentive to employ digital methods, where a variable clock frequency may be used to change the slope of saw-tooth signals etc.

The commutation itself is quite frequency independent, as long as the resistance of the commutation circuit can be neglected, because the driving voltages increase with speed and the time available for commutation is reduced inversely with speed, resulting in an approximately constant commutation angle  $\tau_c$ .

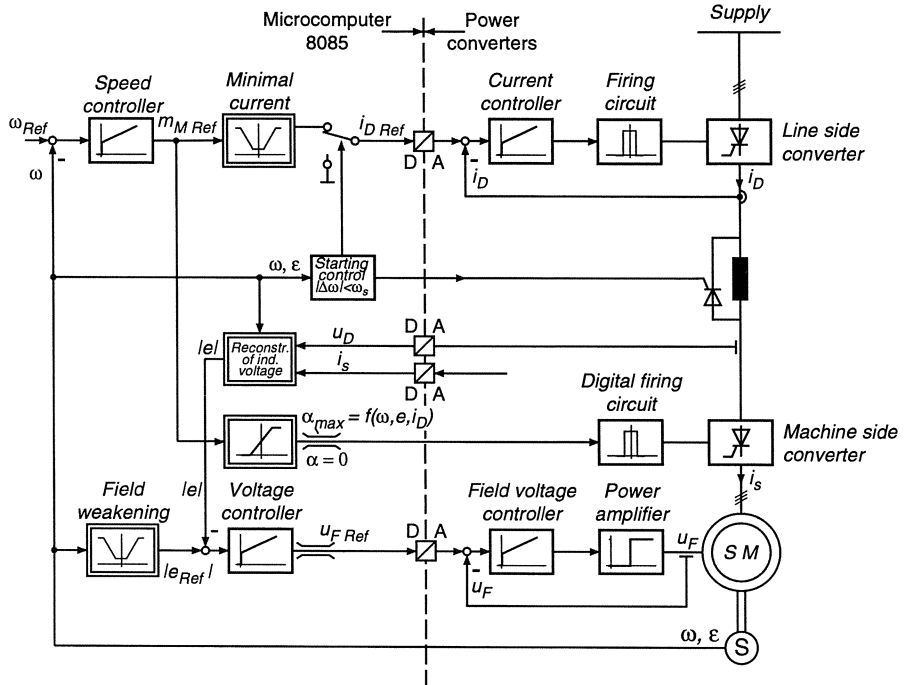


Fig. 14.20. Microcomputer based speed control of synchronous motor drive with DC link converter

At very low speed, however, this is no longer true because the resistances consume an increasing portion of the available voltage-time area; the minimal speed, where natural commutation ceases to function is usually below 10% of rated speed. Operation in this speed range is still possible when reverting to intermittent link current; this is achieved by commanding zero link current, to which the current controller responds by temporarily shifting the firing pulses of the line-side converter to the commutation limit, i.e. applying maximum negative voltage to the DC-link. As soon as the current in the stator windings has decayed to zero and the recovery time for the thyristors has elapsed, the next thyristor-pair of the machine-side converter is made conducting and the link current can be restored.

The delay necessary for reducing and restoring the link current can be considerably shortened if a shunt thyristor in parallel with the link inductor is fired at the same time, when the current reference is blanked [L1]; this short-circuits the link inductor allowing the current to circulate freely without affecting the

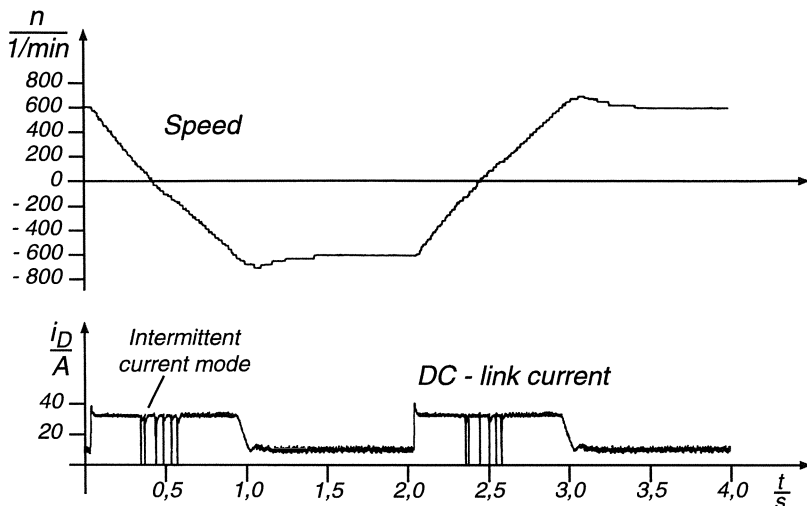


Fig. 14.21. Reversing transient of synchronous motor drive at half rated speed

commutation. As soon as the machine-side inverter is switched to the new conducting state and the line-side converter is reactivated, the shunting thyristor is quickly blocked by the voltages in the intermediate loop. This allows a substantial reduction of the blanking time intervals in the low speed region and reduces the effects of pulsating torque.

It was mentioned above in connection with Fig. 14.19 that the machine converter, operating with natural commutation, invariably causes a certain amount of current in the  $d$ -axis, i.e. unintentional load dependent armature reaction. This must be offset by a corresponding change of field current. One possibility is to control the magnitude of the induced motor voltages  $e_S$  to a reference value which rises with speed; by limiting the voltage reference above base speed, field weakening is initiated.

A control scheme incorporating these features is shown in Fig. 14.20 [R11, R12, R13]. The power circuit contains four converters of different type and size

- Line converter,
- Machine converter,
- Shunting thyristor,
- Field power supply,

for which the microcomputer is producing coordinated control commands. They are the reference values for the link current and field voltage as well as signals for the digital firing circuit of the machine-side converter and the shunting thyristor.

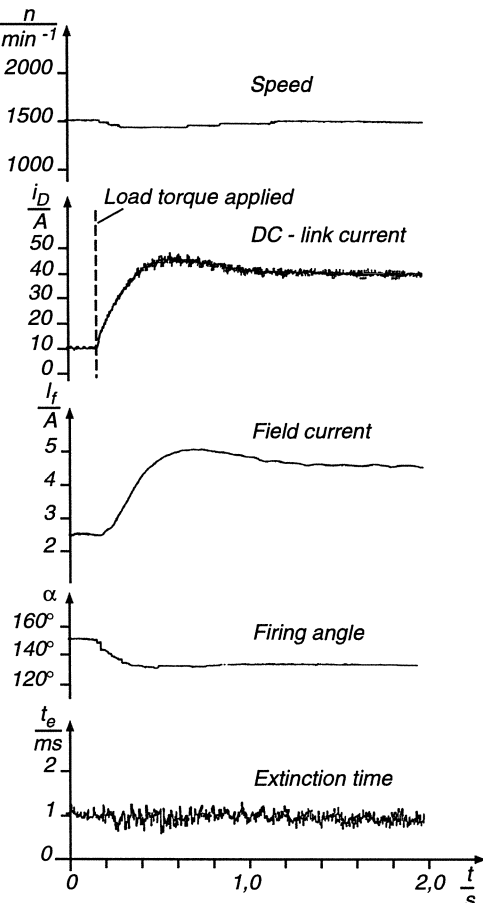
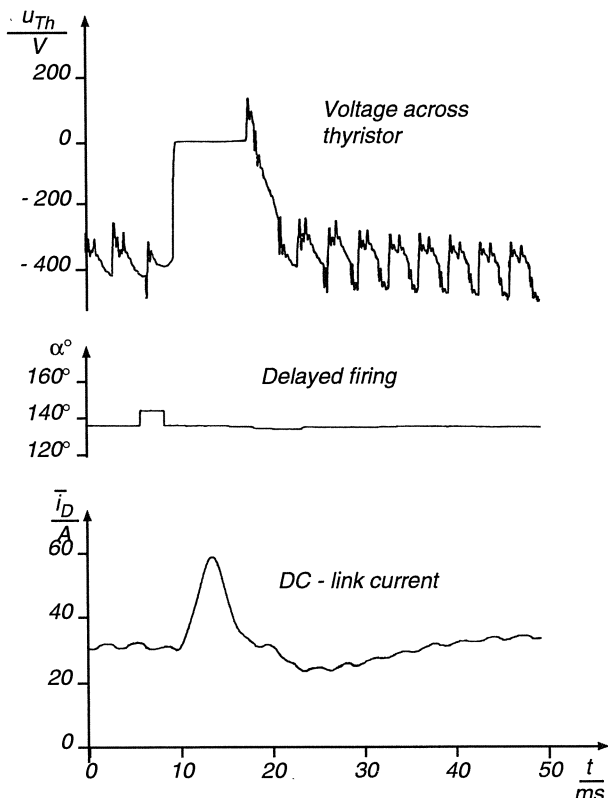


Fig. 14.22. Loading transient of synchronous motor drive

The function generator prescribing the link current reference has the purpose of assuring continuous current flow; in the minimal current mode control is effected through the firing angle of the machine-side converter which quickly assumes its upper or lower limit  $\alpha = 0$  or  $\alpha = \alpha_{max}$  as the link current reference begins to respond to increased torque demand. The inverter limit angle  $\alpha_{max}$  must be continuously adjusted in order to achieve minimal but safe extinction time; it can be determined either by open loop computation based on current, voltage and speed or by closed loop control, possibly with feed forward compensation from the current. The control loop for the field voltage  $u_F$  is included in Fig. 14.20 which corresponds to the low impedance rotor model in Fig. 14.12. Also, a control loop for the field voltage responds more favourably to transient currents induced in the field winding due to armature reaction, when load is suddenly applied. A control loop for the field current  $i_F$  would tend to temporarily reduce

the field voltage at a time, when it should be increased. On the other hand, a control loop for the field current would eliminate the effect of changing field winding resistance and improve the dynamic response in the field weakening region.



**Fig. 14.23.** Intentional commutation failure of machine-side converter

An important feature is the starting control algorithm that becomes effective in the very low speed range by temporarily blanking the current and firing the shunt thyristor. The firing sequence for the machine-side converter can be based on a signal representing the angular flux position  $\varrho$  (Fig. 14.15) or on rotor position  $\varepsilon$ , if a voltage model is used, Eq. (14.34), which is inaccurate at very low speed. Blanking the link current via the line-side converter is a convenient way of quickly altering the mode of operation, such as torque reversal at low speed which otherwise could take too long.

A 20 kW synchronous motor drive with microcomputer control has been designed in the laboratory and tested [R11- 13]. Figure 14.21 shows a recorded reversing transient at half rated speed with the inertia of the drive increased by a dynamometer at no load. The blanking of the current at low speed as

well as the upper and lower current limits are clearly seen. The oscillogram demonstrates that the dynamic response is slower than could be expected with a field orientated type of control. However, there are many applications where fast response is not a primary concern.

More details are seen in Fig. 14.22 where load torque is applied; the rise of the field current is caused by the control loop for the induced motor voltages  $e_s$ , thus neutralising the effects of armature reaction. The trace of the extinction time indicates the good performance of this rather critical control function.

Finally, Fig. 14.23 shows the effect of a deliberately triggered commutation failure which causes a rapid rise of the link current. However, the current controller is able to quickly restore the link current so that the machine-side inverter can resume firing in the regular pattern.

## 15. Some Applications of Controlled Drives

The preceding chapters were dealing mainly with the different types of electrical drives and their control; applications were only mentioned as they affected the operation of the machine and the associated equipment. Also, the specifications for a mechanical power supply are normally not met by just one type of electrical drive and the variety of applications can be bewildering. In this chapter the problems of applying controlled electrical drives will be explained in more detail. For this we begin with a 4-quadrant drive, be it DC or AC, the basic structure of which is contained within the dashed lines of Fig. 15.1. The moving masses are at first assumed to be rigidly coupled, represented by a lumped inertia. The inner loop which comprises the power converter and part of the electrical machine assures fast torque control; with an integrating controller it exhibits unity gain and serves for linearisation. Once the torque loop with the equivalent lag  $T_e$  is closed, there is little difference between a DC and an AC drive. By limiting the torque reference, protection of the power converter and the mechanical load is achieved. Torque control is mandatory on high performance drives, except for the smallest power ratings, because it serves as the controlling input to the mechanical system. Whenever load torque must be counteracted or the speed is to be changed, it is only possible by acting on the torque reference; hence the response of the torque control loop limits the control bandwidth of the complete drive. In view of the practical difficulties of measuring mechanical torque over a wide frequency range it is most desirable to have an electrical substitute available as feedback signal; since torque control is usually embedded in higher level controls offering a corrective input, steady state precision of the torque signal is not of primary importance as long as the dynamic behaviour of the real motor torque is properly reflected.

Sometimes it is possible to obtain an estimate of the load torque  $\hat{m}_L$ , derived from a dynamic load model, and use this signal for feed-forward at the reference input of the torque controller; this is called inverse load modelling. Clearly, this would give the ultimate in dynamic response that cannot be further improved unless an actuator with faster access, i.e. wider control bandwidth is chosen.

For the following the closed torque loop is considered to be part of the drive equipment. For safety reasons — because its internal functions may be involved and subject to critical adjustment — it is normally not at the disposition of the user.

## 15.1 Speed Controlled Drives

By superimposing a speed control loop to the torque controller a very frequently encountered drive control scheme results; its steady state characteristics were drawn in Fig. 2.5, where the torque limit may correspond to twice rated torque. If the speed reference  $\omega_{\text{Ref}}$  is manually set, it is normally specified on larger drives that speed changes should take place with less than maximum torque; on the other hand the control should respond as quickly as possible to load changes. These at first sight contradictory demands can be met by making the speed loop as fast as is practical and including a rate-of-change limiter at the reference input, but outside the control loop. This is seen in Fig. 7.11, also showing transients of the speed reference following a step change of the speed set-point. The rate-of-change limiter may be interpreted as a simple dynamic model having a desirable and safe response, no matter how quickly an impatient or careless operator may be changing the speed setpoint. Similar provisions are of course also necessary if the setpoint is generated automatically; for example on programmed rolling mill or machine tool drives where the various controlled motions have to be coordinated in order to achieve the desired end result, for instance an accurate spatial trajectory of a robot hand.

Sometimes, when the mechanical part of the plant is of large physical dimension, it is desirable to share the load between several motors. Figure 15.2 shows an example of a multiple motor drive on rotary printing presses, where eight or more individual printing stations may be mechanically coupled by a long drive shaft. In order to avoid the transmission of large fluctuating torques through the shaft which would result in undesirable torsional motions, each section is driven by a motor that is supposed to carry most of the sectional load with only small synchronising torques being exchanged through the drive shaft; the load in the different sections and, correspondingly, the motor sizes may be different. Similar problems arise with multiple motor drives on paper machines of earlier design having a mechanical drive shaft and on trains or rapid transit vehicles with multiple drives.

Since the motors in Fig. 15.2 are semi-rigidly coupled, only one speed controller is needed for which the feedback signal is taken from a suitably placed tachometer. (Each motor is usually equipped with a speed sensor because the drive system may be frequently rearranged by opening and closing the clutches.) Sharing of the total torque is achieved by torque controllers assigned to each drive which receive their share of torque reference from the common speed controller; a simplified block diagram of this control scheme is drawn in Fig. 15.2 b.

If the motors of a multiple drive system are not rigidly connected, a different situation exists, where each motor needs its own speed controller. This problem arises for instance on large paper machines without mechanical drive shaft extending over a length of 100 m and containing 30 or more individual drive motors; similar structures are found in continuous hot strip rolling mills and many production processes in the fibre and textile industry.

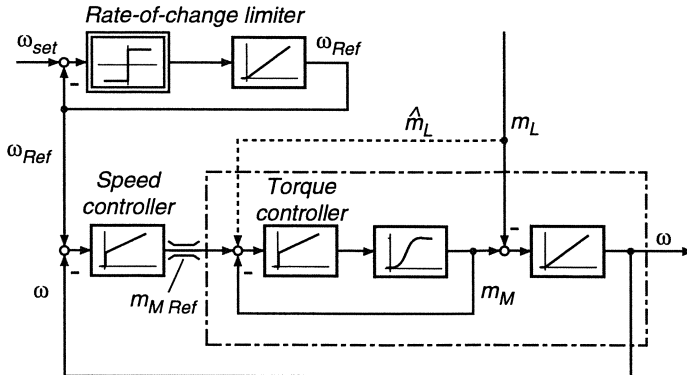


**Fig. 15.1.** Speed control loop with rate-of-change-limiter and load feed- forward

A characteristic of such drives is that the individual sections are only lightly coupled through a strip of red-hot steel or a continuous web of thin material that cannot sustain any appreciable forces; on the other hand, the material must be kept sufficiently taut in order to avoid creases or folds. Figure 15.3 shows a schematic representation of a continuous process with a multiple drive system. The velocity of the material is usually increasing as it proceeds through the different stations; this is obvious with the continuous rolling mill, where the metal sheet, by passing through each pair of rolls, becomes thinner and longer; but it also applies to the paper machine, even though the required increase in speed may only be a fraction of one percent in each section. The speed of each motor must therefore be maintained in precise relative synchronism with the preceding and subsequent sections (omitting constant or slowly varying scale factors such as gear ratios or roll diameters). The speed ratios must be accurately maintained independent of the speed level that may be changing during the process and with the type of production [K24].

It is appropriate for this type of drive system to derive the speed references in a serial form, so that the ratios of successive reference speeds,

$$\alpha_n = \left. \frac{\omega_n}{\omega_{n+1}} \right|_{\text{Ref}},$$

remains fixed even though the speed ratio may have been changed in another section of the drive. This control principle, called "progressive draw" is indicated in Fig. 15.3 b; a change of the overall velocity reference  $v_{\text{Ref}}$  or of a preceding ratio simultaneously affects all subsequent drives in the desired way.

If all the speed references  $\omega_n \text{ Ref}$  were derived in parallel from the common velocity reference  $v_{\text{Ref}}$ , the change of one speed ratio would require all subsequent settings to be changed as well; this scheme which has its merits in other applications is sketched in Fig. 15.3 c. The idea of achieving "progressive draw" by deriving the speed reference  $\omega_n \text{ Ref}$  from the measured speed  $\omega_{n+1}$  of the preceding drive can be discounted because after a few repetitions this procedure

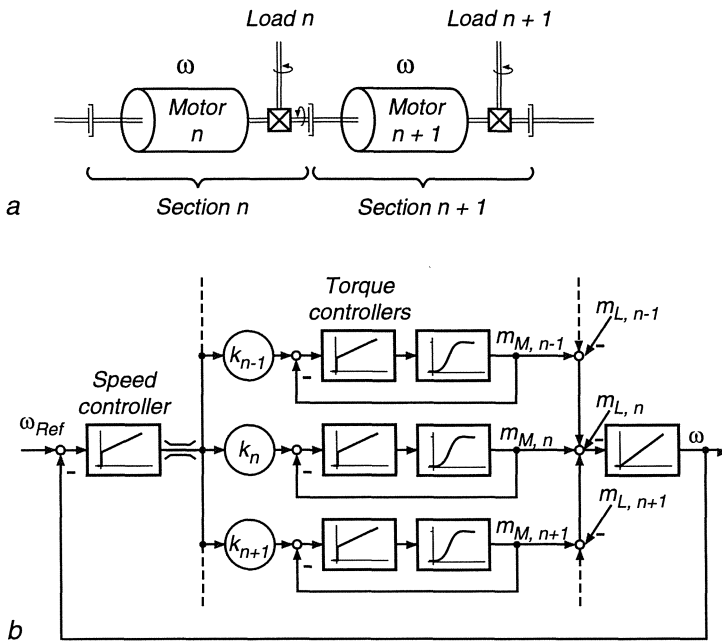


**Fig. 15.2.** Multiple motor drive with mechanical drive shaft.

a) Mechanical system; b) Block diagram

would result in poorly damped and even unstable transients, similar to a queue of motor cars where the attention of each driver is rigidly fixed on the rear of the vehicle in front.

Processing of the reference variables is usually done with analogue means including operational amplifiers or precision potentiometers but digital methods are becoming more widely used; the main reasons are

- Better accuracy,
- Possibility of storing reference data and
- Processing measurements.

The improved accuracy of digital methods is due to the fact that speeds can be measured to high resolution by counting angular increments and that very precise reference frequencies are readily available from crystal oscillators ( $\Delta f/f_0 < 10^{-6}$ ); also digital controllers exhibit no drift effects. An example of a digital speed control is described in Sect. 15.3. Typically, the specified error of speed ratios on a large paper machine may be  $< 10^{-4}/\text{day}$ , which would be very difficult to achieve with analogue methods.

It was mentioned in Chap. 2 that the assumption of a lumped inertia may not apply to some drives where the mechanical construction results in appreciable elasticity. This could be due to a long drive shaft or gears separating the

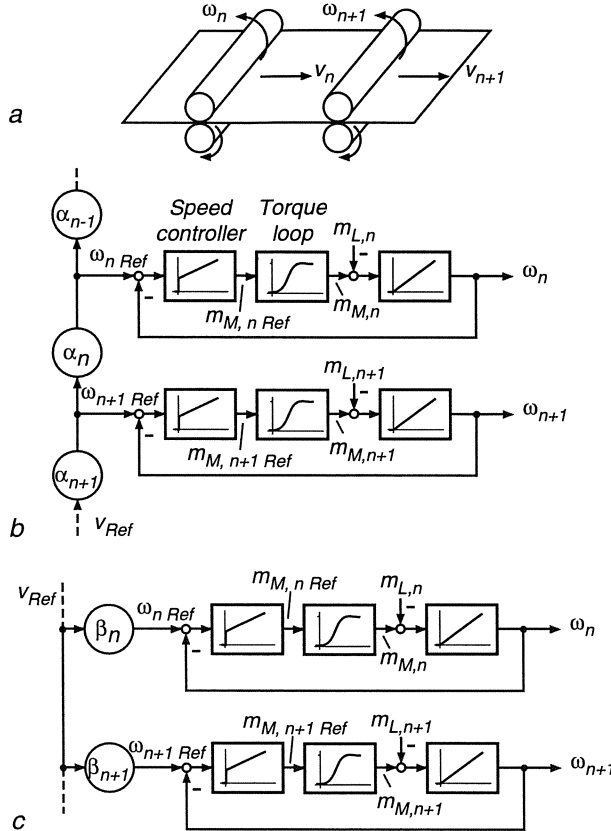


**Fig. 15.3.** Sectional drive system for continuous production process.  
 a) Mechanical system;  
 b) Block diagram with serial reference chain;  
 c) Block diagram with parallel reference structure

motor from the load; the same is true for cranes or hoists where the elasticity of the rope is not negligible [J13, R2]. Another example are robots, where elasticity is the consequence of a lightweight construction. A model of this type of drive is depicted in Fig. 15.4 together with a simplified linear block diagram.  $K$  is the torsional spring constant of the flexible transmission; its inertia as well as its inherent damping are neglected.  $\varepsilon_1 - \varepsilon_2$  is the torsional displacement of the shaft. The load torque may again consist of various components including lift torque and friction: it is represented here by a variable independent torque  $m_L$ . In practice part of the load torque would be speed-dependent and, hence, could exert a damping effect.

The inner torque control loop of the motor, which in the case of a DC drive would be the armature current loop, is represented by an equivalent lag having

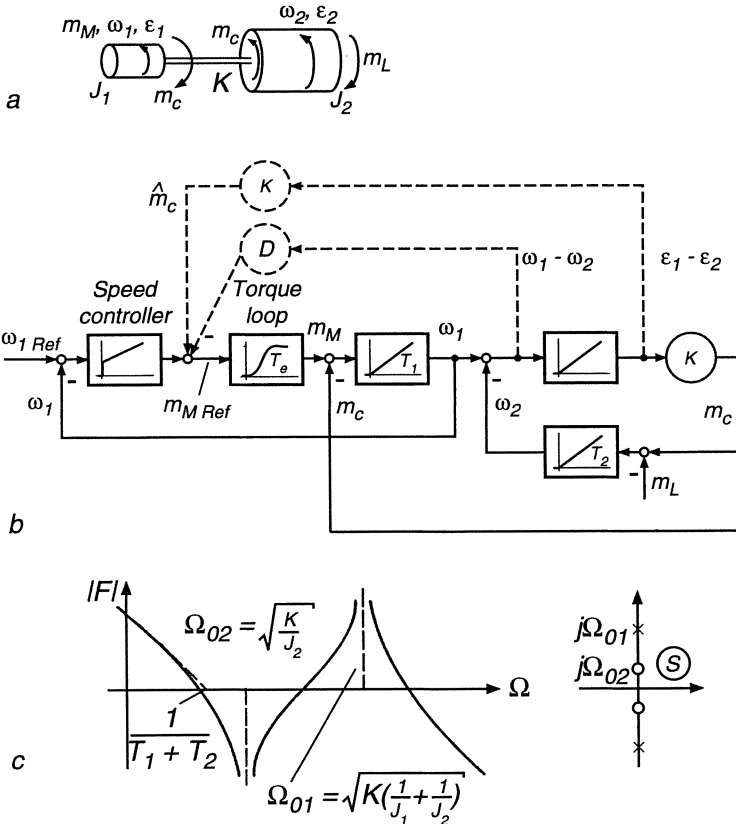


**Fig. 15.4.** Two-mass drive system with torsional elasticity.

a) Mechanical scheme; b) Block diagram; c) Bode diagram

unity gain and time constant  $T_e$ ; the control loop must be sufficiently fast to effectively control this type of plant. The reason is again that corrective action can only be applied at the reference side of the torque controller, i.e. through the torque control loop. The oscillatory mechanical part of the plant contains two inner loops around two integrators each. The open loop transfer function between torque and motor speed is,

$$F_1(s) = \frac{L(\omega_1/\omega_0)}{L(m_M/m_0)} = \frac{1}{(T_1 + T_2)s} \frac{(s/\Omega_{02})^2 + 1}{(s/\Omega_{01})^2 + 1}, \quad (15.1)$$

where

$$T_1 = \frac{J_1 \omega_0}{m_0}, \quad T_2 = \frac{J_2 \omega_0}{m_0}, \quad \Omega_{01} = \sqrt{K \left( \frac{1}{J_1} + \frac{1}{J_2} \right)}, \quad \Omega_{02} = \sqrt{\frac{K}{J_2}}. \quad (15.2)$$

It contains imaginary pairs of poles and zeros which make this a very difficult plant to control; the Bode-diagram is sketched in Fig. 15.4 c.

When attempting to control the motor speed  $\omega_1$ , which is the usual practice because the speed sensor is normally attached to the free end of the motor shaft, it is discovered that a reasonably damped speed loop with a PI-controller can only be achieved if the condition

$$\frac{J_1}{J_2} = \frac{T_1}{T_2} \gg 1$$

holds, i.e. if poles and zeros are close together and nearly cancelling. This is seen in Fig. 15.5, where step responses of the speed control loop are shown for different cases following changes of the speed reference  $\omega_{1\text{ Ref}}$  and the load torque  $m_L$ . The transients were recorded on a DC drive, with the resonant load being simulated by another controlled DC drive. The parameters of the PI-controller were in each case so chosen as to obtain optimal results [B53].

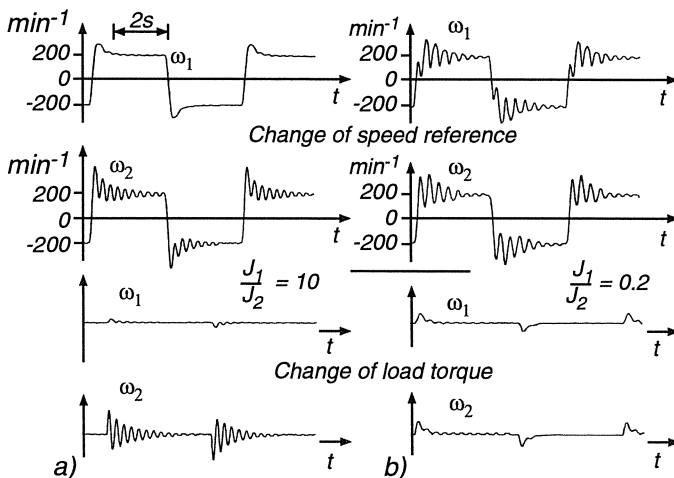


**Fig. 15.5.** Transients of speed control loop with two-mass system, recorded with a 40 kW DC drive. **a)**  $J_1 = 10 J_2$ ; **b)**  $J_1 = 0.2 J_2$

It is realised that, even if the motor speed follows the reference speed in a swift and well damped transient, the load speed, being coupled to the motor speed through the transfer function

$$F_2(s) = \frac{L(\omega_2/\omega_0)}{L(\omega_1/\omega_0)} = \frac{1}{(s/\Omega_{02})^2 + 1} \quad (15.3)$$

remains outside the control loop and exhibits practically undamped oscillations. Obviously, this calls for a different approach for controlling this plant. When assuming for a moment that in an ideal case both speeds  $\omega_1$ ,  $\omega_2$  as well as

the torsional displacement  $\varepsilon_1 - \varepsilon_2$  of the shaft are measurable, then a very effective scheme for decoupling the mechanical plant could be devised, which is indicated by the dashed signal paths in Fig. 15.4 b: By feeding back to the torque controller a signal which is proportional to differential speed, damping can be achieved because the two masses are kept aligned, thus removing the cause for subsequent oscillations. Also, when adding an estimate of the coupling torque  $m_c$  to the torque reference, the actual loading on the motor is in effect compensated by feed-forward and one of the two internal feed-back paths is opened [T23]. Again, a precondition for the success of these measures is that the torque loop is responding sufficiently fast,  $T_e \ll T_1, T_2$ . The effectiveness of  $\Delta\omega$ -feedback for the speed control of the two mass system is apparent from the transients in Fig. 15.6.

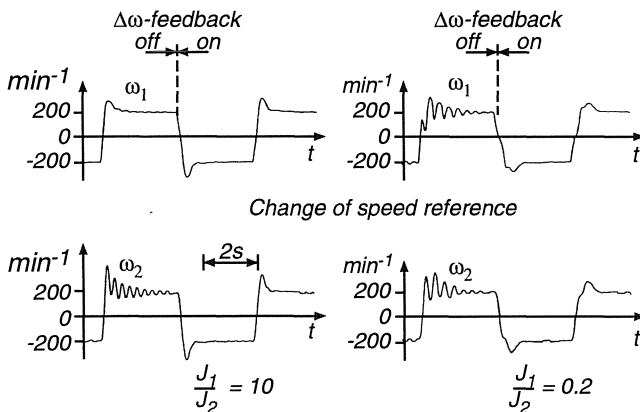


**Fig. 15.6.** Effect of auxiliary  $\Delta\omega$ -feedback on speed control of a two-mass system, recorded with a 40 kW DC drive

Unfortunately, feedback signals for speed and position of the load inertia,  $\omega_2$  and  $\varepsilon_2$ , are usually not available. There may be practical reasons, for example that the load is driven through a gear and rotates at a very low speed so that mounting a speed sensor would be difficult and expensive. Similar problems exist if the motion of the load inertia is translational, for instance on an elevator or mine hoist.

In such a situation one could attempt to derive the necessary information from a dynamic model, called an observer [W15, W16], which is shown in simplified form in Fig. 15.7. The observer is a mathematical model of the plant that is evaluated in real time in parallel with the actual transients of the plant. Establishing this model requires the structure and the parameters of the plant to be known fairly accurately, which is usually no great problem with mechanical systems. The model is driven by the measurable inputs of the plant, in this case the torque reference; the remaining inputs, particularly the load and frictional torques, are unknown and have to be estimated. Keeping the model in line with

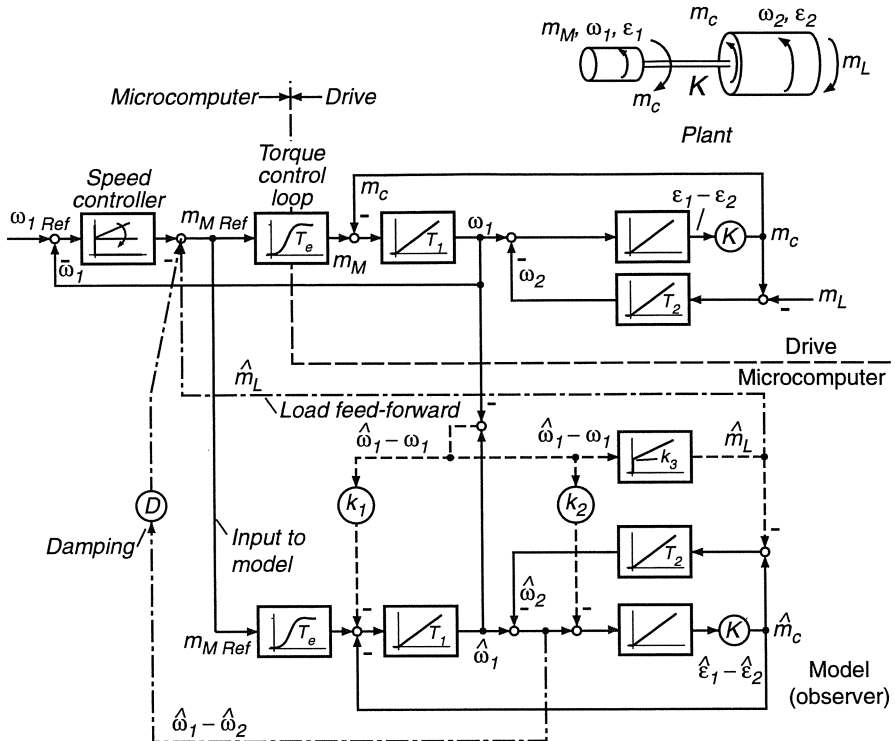
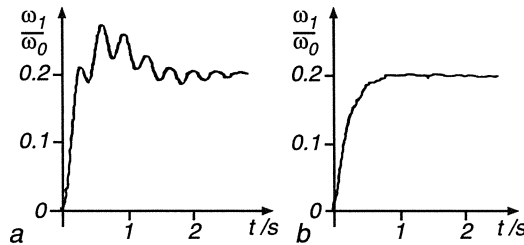


Fig. 15.7. Speed control of a two-mass drive system with auxiliary feedback signals derived from an observer

the actual plant is achieved by comparing a measurable output variable from the plant, for example the motor speed  $\omega_1$ , with its estimated counterpart  $\hat{\omega}_1$  and correcting the model by additional inputs so that the error vanishes. If the model parameters are accurately representing the plant, it can be assumed that the remaining estimated variables in the model are also tracking the real variables, i.e. that the model serves as an accurate observer. Clearly, designing an observer calls for a detailed analysis of the system to be modelled [L66].

Realisation of observers for complex applications has only become practical since distributed digital signal processing is possible with microelectronic components; neither analogue techniques nor a main-frame process computer could provide an economic solution for this problem.

The structure of the observer seen in Fig. 15.7 gives an idea of how the correction of the model can be achieved; each of the integrators in the model is influenced by the error  $\hat{\omega}_1 - \omega_1$  in order to obtain maximum flexibility in selecting the eigenvalues of the observer by suitable choice of the gain factors  $k_i$ . This is so because the observer represents itself a feedback system, the dynamic properties of which are the subject of separate analysis.



**Fig. 15.8.** Step response of speed control of a two-mass system, recorded with a 1 kW DC drive.

a) PI-speed controller; b) P-speed controller and observer

The estimate of the load torque,  $\hat{m}_L$ , is generated by integrating the speed error  $\hat{\omega}_1 - \omega_1$ ; this permits the use of a proportional instead of a proportional plus integral (PI) speed controller thus reducing the speed overshoot following a change of the reference without sacrificing steady state accuracy. Results for a 1 kW DC drive with microcomputer control are shown in Fig. 15.8 [W12]. The step response of the speed control loop with an optimally adjusted PI-speed controller for  $J_1 = 5J_2$  and a resonant frequency  $f_{01} = 5$  Hz is shown in Fig. 15.8 a. As seen in Fig. 15.8 b, it is possible to improve this rather unsatisfactory transient considerably by applying feed-forward and damping signals from the observer; the oscillations are now all but eliminated. The algorithms for the speed controller and the observer have been implemented in a single board 8086-microcomputer. The sampling period for the complete algorithm was 2 ms, the storage requirement < 1 k byte of Read Only Memory.

The characteristics of the plant and its parameter must be known in order that the computed variables derived from the observer are trustworthy. While the dynamic structure of mechanical systems is usually known from the geometry, the distribution of masses with their linkages etc. may not be known accurately or may change under varying operating conditions. Examples are mine hoists, where the winding rope at different lengths acts like a variable spring, or robots with changing geometry, positioning a mass by a rotary movement at a varying radius. If the parameter changes are known or can be derived from other sources of information, it is of course possible to include them in the model, forming a time varying observer; this is easy if the observer is implemented in a microcomputer.

However, when the variations of plant parameters are unknown or even the structure of the plant is uncertain, the problem of estimating internal variables becomes much more complex because it involves the identification of the plant as well as the adaptation of the observer and the controllers. This task has also come now within reach of the microcomputer but it would require a more detailed presentation than is possible in the present context [B55, M14, W12].

## 15.2 Linear Position Control

In many applications of electrical drives it is specified that the shaft of the motor or the load should be controlled to a constant or variable reference angle or that a machine part, for instance the tool support of a milling machine, should follow a prescribed trajectory; this rotational or translational control may be part of a multi-dimensional motion. It is exemplified by a robot containing six or more position-controlled drives in order to be able to place the tool in any position of the workspace and point it in any direction. Position-controlled electrical servo drives at lower power rating ( $< 10 \text{ kW}$ ) are of particular importance for use as feed drives on machine tools or robots, but this is by no means the sole area of application. Servo drives are found wherever mechanical motion is required for controlling technical equipment in industry or transportation, be it the positioning of servo-actuated valves in chemical plants and power stations or the deflection of control surfaces on an aircraft. On the other hand, position control is also found on higher power drives, such as elevators, mine-hoists or automatic commuter trains.

Depending on the application there are of course different requirements with regard to accuracy or dynamic response; some are discussed in the following sections. At the same time they demonstrate again the immense variability of electrical drives.

Let us assume at first that the position reference and the feedback signal representing the measured position are continuous or sampled variables and that a linear position control scheme is desired. Specifications of this type apply for example to elevator drives, servo drives for radar or satellite antennae or to feed drives on machine tools for contour milling. If the reference input is a mechanical signal, such as the position of a pick-up sensing the contour of a mechanical model to be duplicated by the machine tool in a different scale, the control system is also called a position follower, but in most cases the position reference and the feedback signals are represented electrically.

It is further assumed for the subsequent arguments that the rotation of the motor shaft is converted by a suitable gear into the translational motion of a machine part having the velocity  $v$  and the position  $x$ . Transmission errors such as nonlinearity of the lead screw or ambiguity due to backlash can be reduced either by employing a precise spindle or by using a direct position measurement instead of a rotary sensor attached to the motor shaft. Position sensors are available in great variety, operating on different principles and covering a wide range of accuracy; in some cases a simple potentiometer may suffice, while digital encoders or high resolution incremental sensors may be required in others; ultimate precision can be provided, if necessary, by optical methods employing laser interferometry. With increasing accuracy, the cost and complexity rise steeply.

The principle of cascaded control was explained in Fig. 7.5, showing a system of several superimposed control loops for torque, speed and position. An acceleration control loop which has the purpose of eliminating the effect of load

torque, is occasionally added as an option, usually on the basis of an approximate feedback signal derived from the speed measurement. Acceleration control is no substitute for the torque control loop, however, because it cannot prevent static overload, for instance in case of mechanical blocking of the drive.

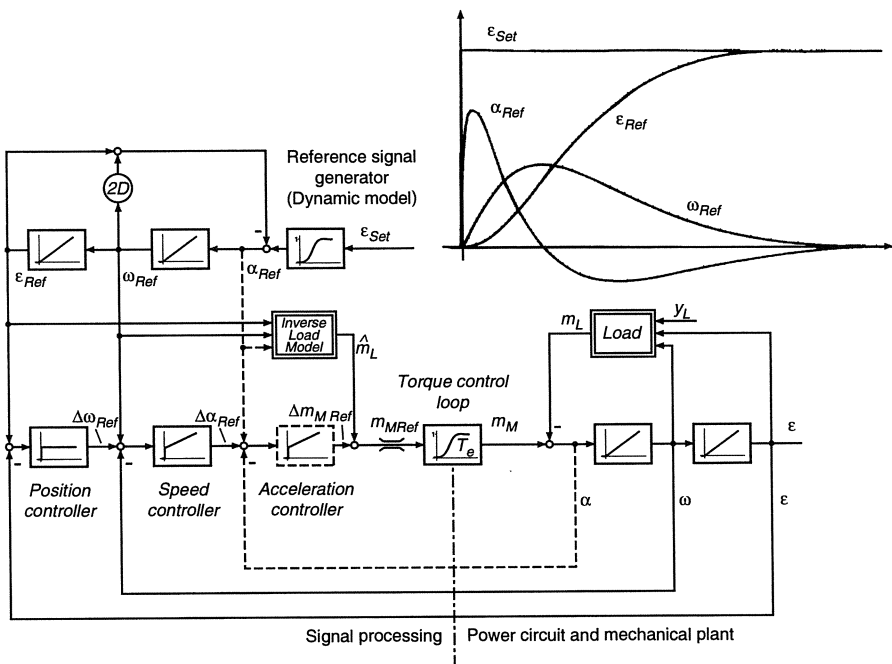
The advantages of nested control loops have been described before; they are

- Transparent structure, employing all measurable state variables
- Step-by-step design, beginning with the innermost loop, thereby solving the stability problem in several smaller steps,
- Use of standard controllers, P, PI, PID etc.
- The effects of nonlinearities, for instance in the power actuator, are delimited by the next loop, resulting in a quasi-linear, unity gain response,
- Disturbances acting on the plant are quickly removed by the appropriate inner loops,
- Intermediate variables can be limited through the pertinent reference variables,
- Commissioning is greatly simplified by closing one control loop after the other, beginning with the innermost loop,
- Opening of outer loops permits simple procedures for diagnostic and field tests.

There is only one at first sight serious drawback of the cascade control structure as seen in Fig. 7.5, that is caused by the fact that the response to the reference input becomes progressively slower as more loops are added; it can be shown that under simplifying assumptions the closed loop equivalent time constant increases by a factor of at least two for each additional loop [K20, 35]; hence the response to reference inputs of a multiple loop control system may be slower than the response of a corresponding single loop system – provided, of course, that a stable single loop control can be devised. As a result, the position control scheme in Fig. 7.5 may exhibit an unacceptable dynamic error when the reference position is time-varying.

Fortunately, this disadvantage can be completely removed by employing feed-forward to the inner loops, as shown in Fig. 15.9, where a signal generator produces reference variables that otherwise would have to be generated by controllers responding to dynamic errors in the outer loops. The feed-forward signals must, of course, be coordinated for compatibility, otherwise there could be contradictory demands with the result of possibly saturating individual controllers.

On multiple-axis drives such as used on continuous milling machines, where the tool should accurately follow a given spatial contour, the set of reference signals  $(x, v, a)_{\text{Ref}}$  is usually computed off-line for all axes and stored in a memory in order to be fed in parallel to the various drive controllers.



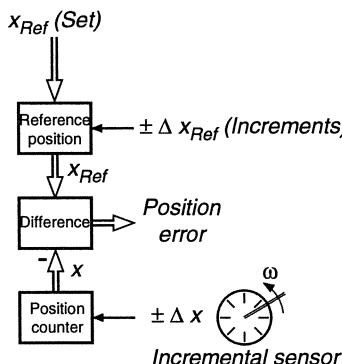
**Fig. 15.9.** Multiple-loop position control with feed-forward from a dynamic model of the reference trajectory and the load

Figure 15.9 describes another solution where the reference variables for each axis are generated by a dynamic model representing the desired response of the drive; the effect of this scheme is that temporary saturation of controllers is avoided which would occur if unrealistic (for instance discontinuous), reference functions were applied; by employing a suitably chosen reference model the dynamic behaviour of the control system becomes reproducible and dependable because all the controllers operate in their linear high-gain mode and keep the respective errors small. Naturally provision must be made for unexpected disturbances such as load torque or line voltage fluctuations which means that the torque control loop must have sufficient margin for absorbing the additional load, should it occur.

The existence of a dynamic model can also be very useful in other applications; for example, controlling a high-speed elevator swiftly and still agreeably for the passengers requires that certain limits of acceleration  $a(t)$  and jerk  $da/dt$  should not be exceeded; this can be achieved by a dynamic model producing a set of smooth reference variables. Since the feed-forward signals improve the precision of the trajectory, it also becomes possible to accurately predict the stopping distance from any initial condition  $(x, v, a)_0$ ; this is important in order to be able to decide instantly whether a call from one of the forward floors

or a late stopping demand by one of the passengers can still be answered or whether the caller has to wait for the next opportunity, since speed reversal between scheduled stops is ruled out. Also, position overshoot is often not allowed, on an elevator because the passengers would dislike it, and on a machine tool because it could leave marks on the work piece.

The ultimate in dynamic performance is achieved by feeding an estimate of the load torque  $\hat{m}_L$  directly to the input of the torque control loop, thus relieving the speed controller from generating the main part of the torque reference, as is indicated in Fig. 15.9. The torque estimate must be based on a model of the load and the reference trajectory, definitely not on measured values of acceleration, speed and position; otherwise there would be the danger of instability due to unavoidable inaccuracies and computational delays. Since forming an estimate of the load torque for a given trajectory of motion effectively involves the inversion of the equation of motion, this is also called "feed forward by inverse load model" [F24, L37]. With multiple axes robots the inverse load model may be of considerable complexity; a simple example was shown in Fig. 2.4.



**Fig. 15.10.** Digital position control

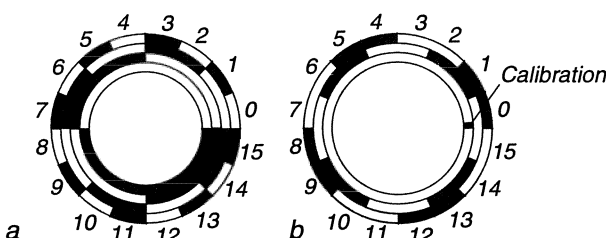


**Fig. 15.11.** Absolute and incremental position sensors

When controlling the movement of a machine tool to high precision, for example with a maximum position error of  $10^{-5}$  m out of a total travel distance of 1 m, it is necessary to employ digital signal processing not only for the position reference but also for the feedback signal and the error detection (Fig. 15.10). This is the only way to avoid drift effects which would occur with analogue signal processing; only a digital controller is capable of determining with certainty minute differences between two large numbers, for example 25,000 and 24,999. Because a digital speed controller does not exhibit drift, and position is the true integral of speed, the position controller can be of the proportional type; there is no need for an integrating channel for achieving a high steady state accuracy.

Naturally, this calls for comparable precision in the measurement as well; fortunately, digital sensors for rotary and translational motion combining high accuracy and resolution are readily available. An encoder (Fig. 15.11 a) produces an absolute measurement of the distance from a fixed position, for example by supplying  $n$  bit of a dual word covering the range of  $0 \leq x \leq (2^n - 1)\Delta$ , where  $\Delta$  is the resolution. It is preferable to employ codes where only one bit changes at any one time, in order to exclude ambiguity (Gray code); a similar effect is achieved by a synchronising signal from the channel with the highest resolution.

Another somewhat simpler sensor is of the incremental type (Fig. 15.11 b), which generates a forward or reverse pulse for every increment of travel; by counting these pulses, the actual position is obtained, provided the counter has been initially set by a separate calibrating pulse or some other calibrating position measurement. The incremental type of sensor which normally functions on a magnetic or optical basis, is sometimes considered unsatisfactory because pulses might be lost, causing a corresponding undetected position error until the calibrating position is passed again. However, with todays sensors, using a LED light source and the associated integrated circuitry, incremental sensors can be regarded as very reliable components; if desired, battery-buffering of the counter could be provided.

The function of an incremental sensor for angle measurements is explained with the help of Fig. 15.12. There are two optical or magnetic measuring channels producing out-of-phase signals, approximating  $x_a = \hat{x} \sin N\varepsilon$  and  $x_b = \hat{x} \cos N\varepsilon$ , where  $\varepsilon$  is the angle to be measured and  $N$  is the number of periods per revolution of the sensor shaft; a typical value is  $N = 2^{12}$ . By clipping these signals, two orthogonal square wave functions sign  $x_a$  and sign  $x_b$  are created. Whenever one of these functions is changing sign, an incremental motion of  $\Delta\varepsilon = \pm 2\pi/4N$  is registered, with the direction derived from the direction of the change and the value of the other signal. With  $N = 2^{12}$ , this corresponds to an angular resolution of  $2^{-14}$  of one revolution of the sensor shaft or about 1/16 000.

By analogue interpolation, also shown in Fig. 15.12, this resolution can be greatly improved [S41]. While the signals  $x_a$  and  $x_b$  may not be exactly sinusoidal and the amplitude  $\hat{x}$  may depend on the speed of rotation  $\omega = d\varepsilon/dt$ , by forming the ratio  $x_a/x_b$  and computing  $\arctan x_a/x_b$ , several lower bits of angular position measurement are generated, increasing the total resolution to

18-20 bit, or 250 000 to 1 Mio increments per revolution. While the dependability of the additional bits may be somewhat in doubt, the extension serves as a most welcome increase of the measurement bandwidth when detecting slow rotational speeds. A similar principle of analogue interpolation could also be applied to the absolute position sensor shown in Fig. 15.11.

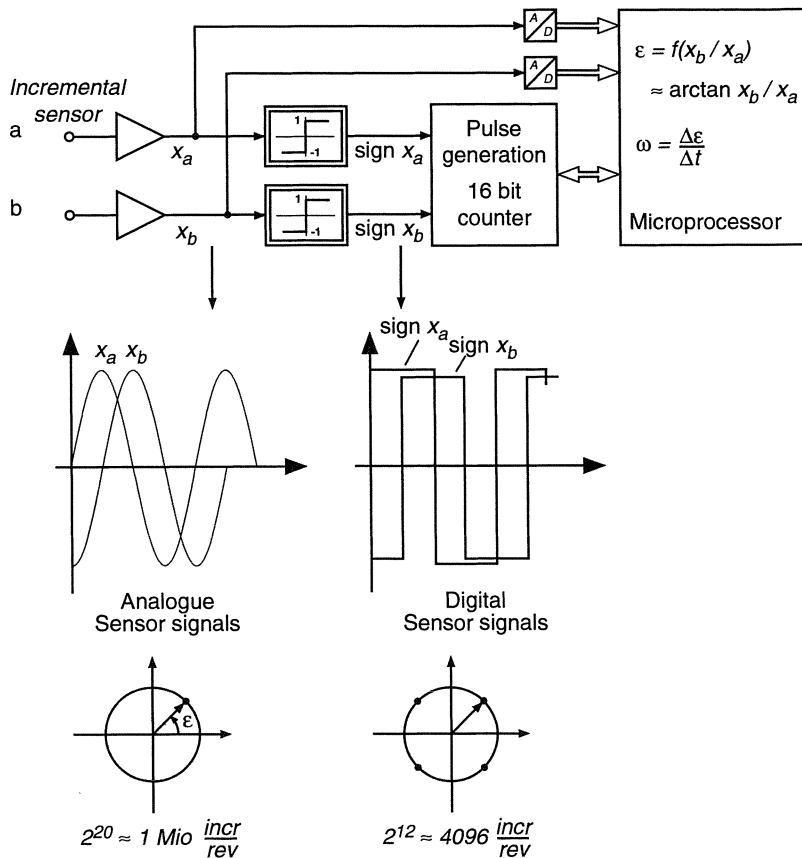


**Fig. 15.12.** Enlarging the resolution of an incremental encoder by analogue interpolation

With both types of position sensors it is also possible to realise a simple digital velocity measurement. By sampling in short and precise time intervals  $T$  the position signal available at the output of the encoder or the counter and subtracting subsequent readings, the average velocity in the last sampling interval is obtained.

$$v(\nu + 1) = \frac{1}{T} [x(\nu + 1) - x(\nu)]; \quad (15.4)$$

similarly, an acceleration signal can be detected from subsequent velocity measurements,

$$a(\nu + 1) = \frac{1}{T} [v(\nu + 1) - v(\nu)] = \frac{1}{T^2} [x(\nu + 1) - 2x(\nu) + x(\nu - 1)]. \quad (15.5)$$

With a given sampling interval  $T$  the resolution of a digital speed measurement is reduced at low speed because fewer angular increments are being accumulated in each period  $T$ ; the limit is reached when only a few counts are providing a very coarse representation of speed with questionable value. This then calls for either increasing the resolution of the sensor (e.g. by analogue interpolation) or enlarging the sampling period. This could be done by going to a multiple  $mT$  or converting from a frequency-based measurement, as described, to a time-based measurement, where the interval between successive angular pulses are counted with a stable high frequency reference and the result is inverted for obtaining a speed signal. With a microcomputer, both sensing schemes may be used in parallel, selecting whichever value is offering the better resolution. In any case two measurement channels are needed in order to detect the direction of motion.

In the past, when digital signal processing equipment was bulky and expensive, it was used only when it was absolutely necessary to achieve the required accuracy, i.e. in the outer position control loop. However, with todays micro-electronic hardware this situation is changing rapidly. All the control functions in Fig. 15.9, including the field orientated control of an induction motor and the dynamic model, can now be incorporated as a modular algorithm in a micro-computer requiring a simple printed card. The sampling time which at present may be about 1 ms is considerably reduced with new processors so that DC servo motors are rapidly superseded by digitally controlled and very compact AC servo motors. This is a remarkable development only made possible by the joint advances of microelectronics and power electronics.

It was mentioned before that backlash in gears and couplings may cause problems with position controlled drives because the contact between two adjoining parts of the drive is temporarily lost when the transmitted force is reversed; as a consequence the surfaces formerly exerting opposite forces are moving apart, until contact is again made at the other side of the gear tooth. Clearly this discontinuity of the transmitted force is in conflict with the desire for smooth and precise position control.

Backlash can be avoided by employing high quality mechanical components, but wear cannot be excluded. A mechanical solution would be the use of spring loaded gears with split wheels which maintain a bilateral contact force irrespective of the sign of the transmitted load force. Another scheme requiring only standard gears is to split the drive into several units and to preload the gears electrically; this is of particular interest if the type of load makes a distribution of the driving force desirable anyway. An example could be the azimuth motion of a large satellite antenna, i.e. the rotation around the vertical axis; antennae of this type require very accurate positioning, for example with a final tolerance of less than  $1/100^\circ$ . This corresponds to a resolution of the full circle to one part in 36,000 which definitely calls for direct measurement by a digital sensor mounted at the pivot bearing of the main construction. The two or more servo

motors could be arranged at symmetrical points around the circumference and exert torque through pinion drives to the central gear. A simplified schematic is drawn in Fig. 15.13 assuming two motors, where the main structure of the antenna and the two drive motors are lumped into three separate rigid bodies. The pinion gears, forming the interfaces between motors and load, may exhibit backlash and elasticity.

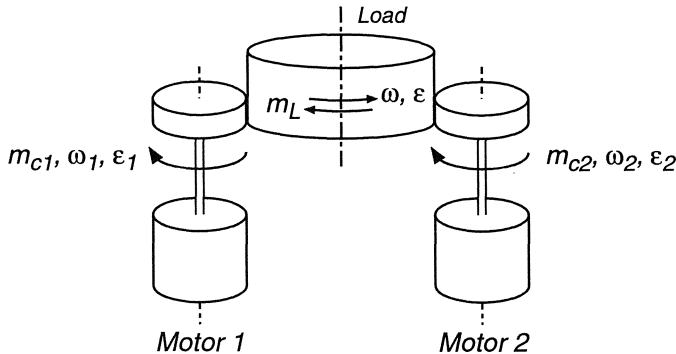


**Fig. 15.13.** Position drive with two servo motors and electrically preloaded gears for excluding backlash

By assuming symmetry between the two motors, neglecting all frictional torques and referring all angles, angular velocities, inertias and torques to the central axis, the block diagram in the right hand side of Fig. 15.14 results, describing the mechanics of the drive.

The torque control loops are again replaced by equivalent lags having unity gain. In addition to inherent damping effects not shown in Fig. 15.14, such as speed dependent frictional torques, active damping will definitely be needed with this complicated mechanical structure. Two kinds of oscillations are likely to require counter measures

- oscillations of the two drive motors in phase opposition while the central mass remains at rest,
- oscillations of the two motors in phase against the central mass.

Provided the torque control loops respond sufficiently fast, both oscillations can be damped by adding suitable signals to the torque references,

$$\begin{aligned}\Delta m_{M1\text{ Ref}} &= - D_1(\omega_1 - \omega_2) - D_2(\omega_1 + \omega_2 - 2\omega), \\ \Delta m_{M2\text{ Ref}} &= D_1(\omega_1 - \omega_2) - D_2(\omega_1 + \omega_2 - 2\omega).\end{aligned}\quad (15.6)$$

The signals for the motor speeds  $\omega_1, \omega_2$  can be derived from sensors attached to the motor shafts. It is noted that the steady state characteristics of the drive system are not altered by these auxiliary feedback loops because the signals vanish in steady state under symmetrical conditions [T24].

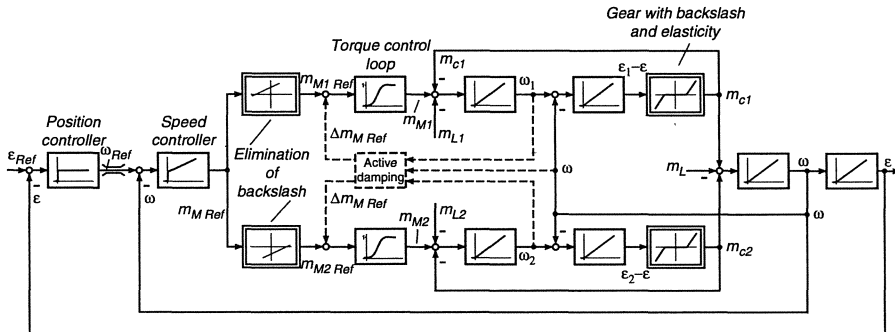


**Fig. 15.14.** Simplified block diagram of three-mass twin drive with preloaded gears for excluding backlash

The backlash assumed in both gear trains can be made ineffective by adding opposite offset signals to the torque references; this results in preloading the gears in the low torque region, where backlash would be most troublesome. As the required load torque  $m_M Ref$  increases, the motor that initially opposed the motion, eventually reverses its torque and comes to the help of the other motor until there is nearly equal load sharing at full torque. Figure 15.15 shows another pair of nonlinear functions that would be advantageous for the preloading of gears because they cause the motors to produce equal torque at full load while maintaining constant overall gain in the speed control loop. Again these nonlinear functions would be cumbersome to realise with analogue circuitry but they present no problems when microcomputers are employed for the control.

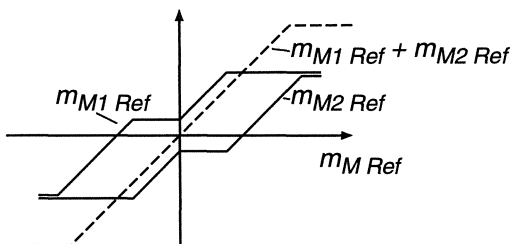


**Fig. 15.15.** Torque functions for electrically preloading gear train of twin-drive

Another example of a dual axis position controlled drive is shown in Fig. 15.16 a. It could be part of a machine tool or a robot with a mechanical structure in cylindrical coordinates  $r, \epsilon, z$ , where each motion is activated by a separate position controlled drive having an inner torque control loop with the equivalent lag  $T_e$ . This is a simplification of the example discussed in Chap. 2. For the particular application it could be necessary to generate the reference trajectory in  $x, y, z$ -coordinates, while only machine orientated  $r, \epsilon, z$ -measurements are available. Clearly the motion in the  $z$ -direction is decoupled

if it is orientated vertically, thus excluding gravitational effects, but a transformation between  $(r, \epsilon)$  and  $(x, y)$  is needed. This can be achieved by transforming the  $x, y$ -reference data into polar coordinates or inversely by converting the  $r, \epsilon$ -feedback signals into cartesian coordinates; the first possibility is chosen for the microcomputer based control scheme in Fig. 15.16 b because all the inner control functions are then performed in the actual drive coordinates.  $(x, y, z)_{Ref}$  would again be produced by a suitable reference generator.

Dynamic coupling effects between the  $r, \epsilon$  motions caused by centrifugal and Coriolis-forces can be approximately compensated by introducing suitable corrective terms to the torque references, as was mentioned before; the effectiveness of this method of compensation, called inverse load modelling, depends of course on a fast response of the inner control loops.

With the present state of microelectronics all the control functions seen in Fig. 15.16 b could be executed with 1 kHz sampling frequency, which would be quite adequate in most cases.

### 15.3 Linear Position Control with Moving Target Point

In Sect. 15.1 it was mentioned that there are cases, for example with paper mills, where the speed of each drive section must be controlled with high precision in relative synchronism to the speed of a neighbouring section. This task can also be considered as a position control problem, where the reference changes in steady state at a fixed rate. As an example the digital speed control scheme in Fig. 15.17 which had been developed prior to the advent of microelectronics may be briefly discussed.

It is based on a conventional analogue speed control loop using, for example, a DC tachometer as speed sensor. Due to unavoidable drift of the analogue components there is a normal control error, usually below  $10^{-2}$  of rated speed, which could, of course, be reduced by one or two orders of magnitude, but only with considerable effort, such as thermal stabilisation of the critical components, and at high cost.

The idea of the scheme in Fig. 15.17 is to add a digital corrective loop for compensating the steady state error of the analogue speed control; rapid response is not important since a well-tuned analogue speed control leaves little to be desired in this respect.

The digital controller compares the pulse train  $f_2$  from an incremental sensor, where each pulse corresponds to an angular increment  $\Delta\epsilon$ , with a reference pulse train  $f_1$  derived from a high accuracy frequency source. A reversible counter registers the forward and reverse pulses, none of which must be lost; the content of the counter is then a measure of the angular error of the drive with respect to the fictitious reference angle. With the help of a digital-to-analogue converter it is transformed into a small corrective signal  $\Delta\omega_1$  for the analogue

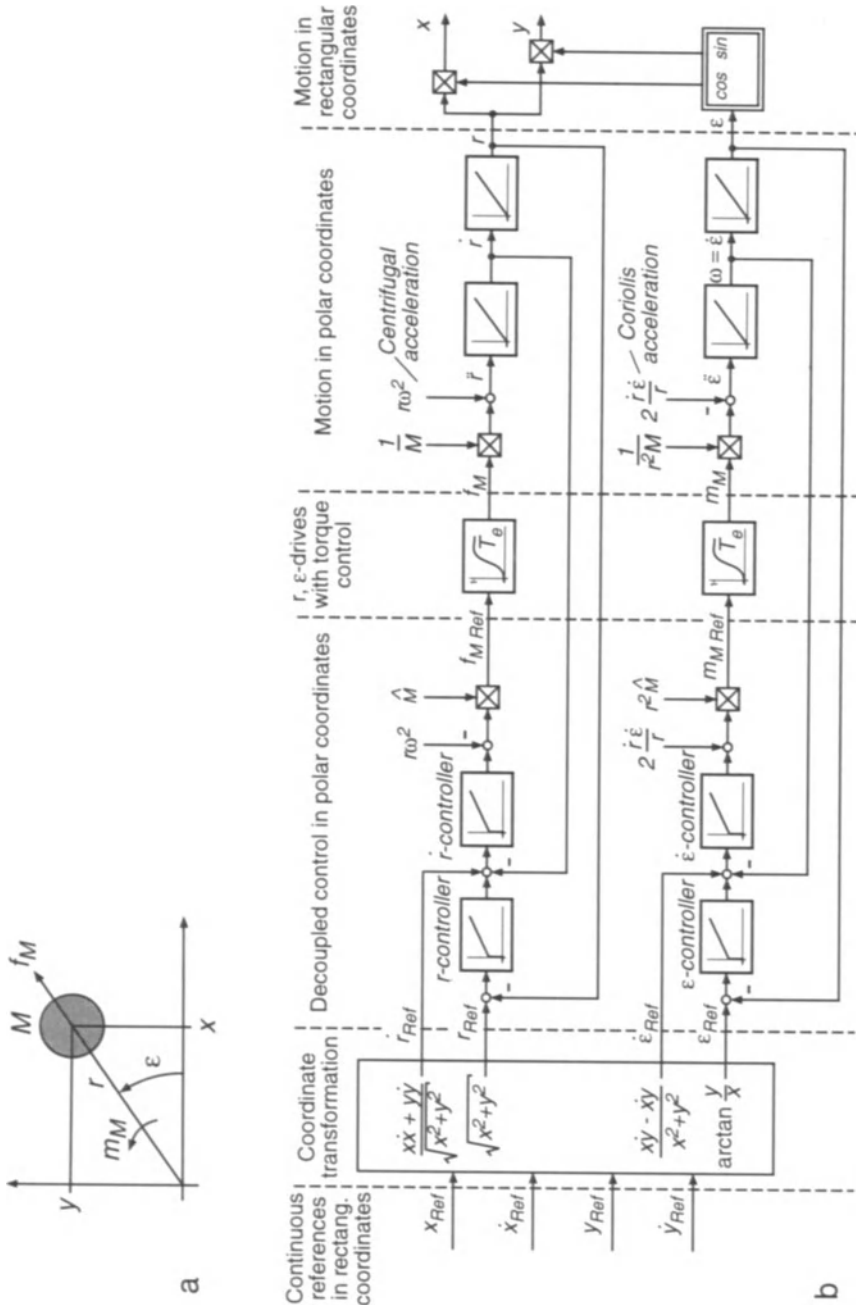


**Fig. 15.16.** Dual axis position control in polar coordinates with reference signals supplied in cartesian coordinates.

a) Mechanical model; b) Block diagram

speed loop. Thus the digital channel may be understood as an integral speed controller without drift or as a proportional position controller [J19, L27].

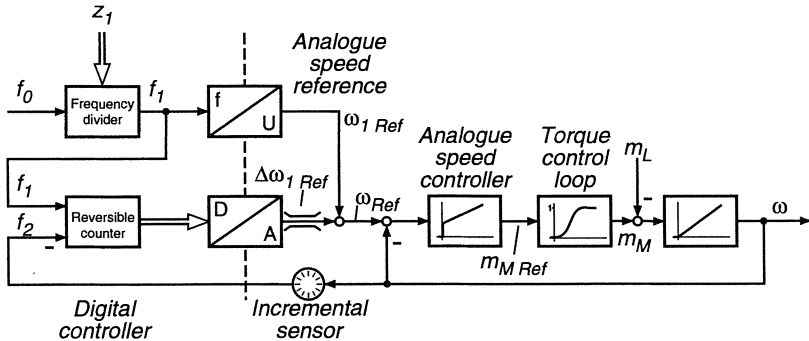


Fig. 15.17. Quasi-continuous digital speed control

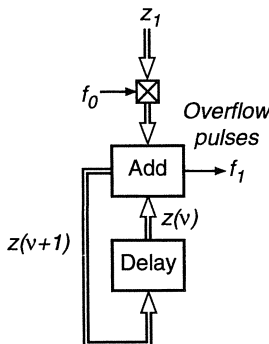


Fig. 15.18. Programmable frequency divider

In order to generate a finely adjustable reference frequency  $f_1$  having the same steady state accuracy as the fixed clock frequency  $f_0$  derived from a Quartz oscillator, the programmable frequency divider shown in Fig. 15.18 might be used. It contains an arithmetic unit for executing a recursive addition according to

$$z(\nu + 1) = [z(\nu) + z_1] \bmod z_{\max}, \quad (15.7)$$

where  $z_{\max}$  is the capacity of the register while  $z_1 < z_{\max}$  corresponds to the desired reference frequency  $f_1$ , which is established by the overflow pulses. The addition is synchronised by the clock frequency  $f_0$ . The mean balance of the continued addition is

$$f_1 z_{\max} = f_0 z_1$$

resulting in a pulse train, the mean frequency of which is adjustable in fine steps but still has the same precision as the constant clock frequency  $f_0$ ,

$$f_1 = \frac{z_1}{z_{\max}} f_0 . \quad (15.8)$$

The overflow pulses are not quite equidistant but by operating the frequency divider at a sufficiently high clock frequency, this inherent phase modulation has no effect on the speed of the motor [L28].

Similar methods are used in the process industry for in-line blending, where the flow rates of liquids to be mixed in prescribed ratios are measured by turbine wheel flow meters whose speed is transmitted and processed in the form of pulse series [R8].

Adjustable reference frequencies may also be formed with the help of a phase-locked loop, having a scaler with capacity  $z_1$  in the feedback path; this produces a multiple frequency  $f = z_1 f_0$  of the constant clock frequency  $f_0$  which may then be reduced by a scaler with capacity  $z_{\max}$ .

In various production lines where continuous strips or webs of material are processed in subsequent stations it is often specified that the processing should be decoupled in order to prevent tension in the material. For this purpose a limited storage of material is accumulated in the form of a loop between the stations which, by taking up the difference of incoming and outgoing material, represents a measure of the synchronism between the two adjoining drives. Naturally, one should attempt to maintain the loop at approximately constant mean length in order to have adequate reserves in case of temporary speed fluctuations of the two drives.

The problem is explained in Fig. 15.19 a showing the principle of a magnetic tape drive as used on computers. The incoming tape is fed from a reel and pressed against the drive rolls  $A_1, A'_1$  in order to be transported with high acceleration and velocity past the read-write head  $S$ ; subsequently the tape is rewound on another reel driven by a separate motor. By keeping the tape between the reels taut, the maximum acceleration would be severely limited by the winding motors loaded with the inertia of the reels; also, excessive force in the tape could not be excluded. In order to avoid these problems, loops are formed on both sides of the drive rolls which are kept orderly under moderate forces by mechanical or pneumatic means. This greatly reduces the effective inertia and the applied forces, when the tape is accelerated. The more slowly accelerating reel drives must of course possess sufficient maximum speed for preventing the storage loops from reaching their upper or lower limit.

Only the left half of the tape drive in Fig. 15.19 a is considered in the following, with the tape velocity  $v_1$  at the read-write head  $S$  assumed to be an independent (impressed) variable. The speed  $v_2$  of the feed rolls should be so controlled as to maintain the length  $x_2$  of the storage loop at a prescribed value. Because of

$$\frac{dx_2}{dt} = \frac{1}{2} (v_2 - v_1) \quad (15.9)$$

the block diagram in Fig. 15.19 b results, where the storage represents an integrator with two inputs cancelling in steady state. Normally the feeding reel is controlled such as to maintain constant force of the unwinding tape.

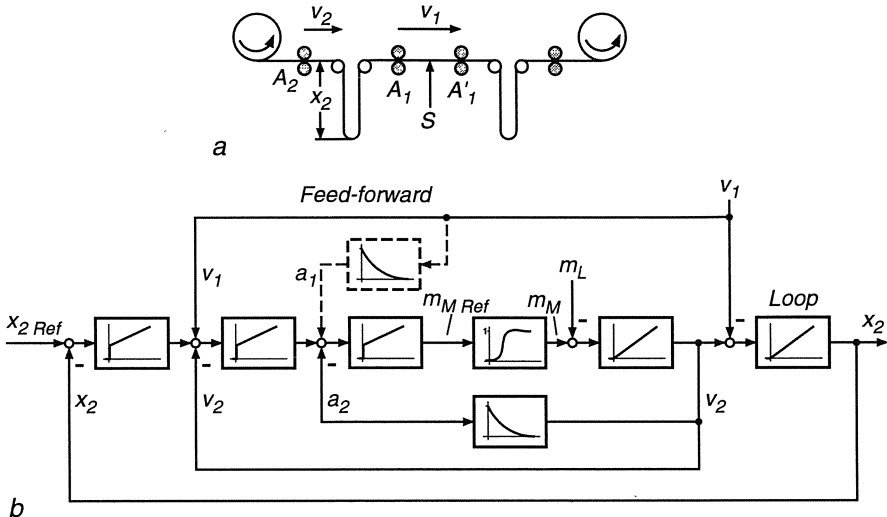


**Fig. 15.19.** Feed drive for magnetic tape.

a) Schematic; b) Block diagram

The quality of the control can be further improved by introducing to the speed controller of the feed rolls  $A_2$  a feed-forward signal from the velocity  $v_1$ , which acts as a disturbance. In view of the quickly changing operating conditions it could even be appropriate to provide acceleration feed-forward in order to reduce the necessary length of the storage loop.

It is noted that the inertia of the reel drive depends on whether the spool is full or nearly empty; also, most magnetic tape drives are reversible, i.e. they can operate in either direction.

On multi-stand continuous rolling mills the storage loops between successive stands, which are necessary to trim the coordinated speed control described in Sect. 15.1, have a different geometry, as shown in Fig. 15.20; an electrically or hydraulically powered looper roll pushes the material with a force  $f_L$  upwards and thereby keeps the strip taut. Due to the geometry of the loop there is a nonlinearity between the deflection  $x$  and the length of the loop,  $l = \sqrt{b^2 + x^2}$  leading to a nonlinear differential equation

$$\frac{2b}{v_0} \frac{x}{l} \frac{d(x/b)}{dt} = \frac{v_2}{v_0} - \frac{v_1}{v_0}, \quad (15.10)$$

where  $v_0$  could be the rated velocity; the integrating time constant

$$T_i = \frac{2b}{v_0} \frac{x}{l} \quad (15.11)$$

depends on the ratio  $x/l$ , i.e. the shape of the loop.  $x/l = 1$  corresponds to the special case in Fig. 15.19 a. Operating the loop at small values of  $x/l$  becomes increasingly difficult because the integrating time constant is reduced;

this calls for fast response of the looper and the adjoining main mill drive used for controlling the loop.

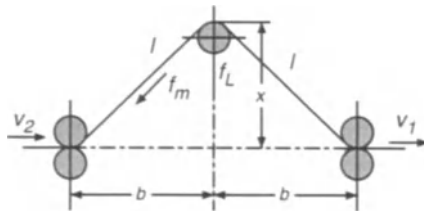


**Fig. 15.20.** Geometry of loop in a continuous rolling mill

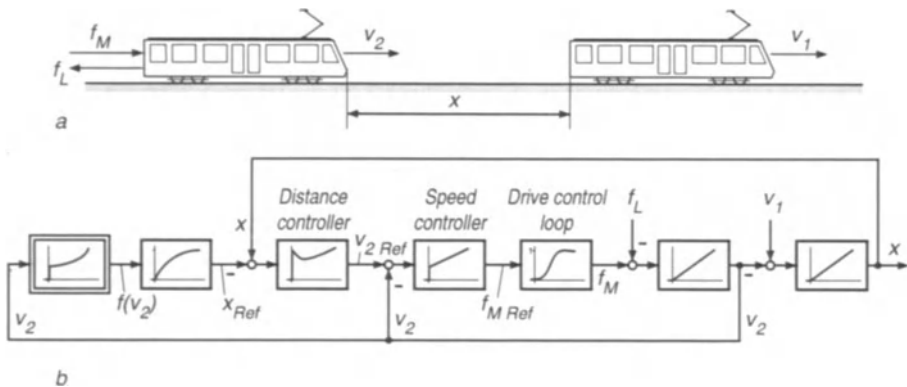


**Fig. 15.21.** Distance control of tracked vehicles.  
a) Schematic; b) Block diagram

The force  $f_m$  exerted on the material is also a function of the loop geometry; in relation to the vertical force  $f_L$  exerted by the looper roll, it is

$$\frac{f_m}{f_L} = \frac{1}{2} \frac{l}{x}, \quad (15.12)$$

also indicating a critical range at small values of  $x/l$ , where the gain becomes very large.

A similar problem as with loop control arises with automated tracked vehicles developed in recent years for urban transportation (Fig. 15.21 a). The distance  $x$  of each vehicle to the leading vehicle must be controlled to a speed-dependent safe value  $x_{\text{Ref}}$  by applying driving or braking force  $f_M \geq 0$ . The distance can be measured, for example, by radar or by sensing equipment installed in the guideway.

When again regarding the velocity of the forward vehicle as an independent disturbance, the control system for the distance between the vehicles could have

the form shown in Fig. 15.21 b. It represents a cascaded scheme containing inner loops for the driving force and velocity. The desired distance  $x_{\text{Ref}}$  to the leading vehicle is generated as a delayed nonlinear function of velocity, for example a parabola approximating the safe braking distance.

A computed transient of the distance control scheme is shown in Fig. 15.22; it may be caused by a sudden constant deceleration of the leading vehicle; a PID-controller and a linear function  $x_{\text{Ref}}(v_2)$  were assumed for the example. Transients of this sort and their dangers are well known to the motorist. It is, of course, possible to alleviate the task of maintaining a safe distance by taking advantage of advance signals, such as feed-forward from the retardation of the leading vehicle or the rate of distance change, as is common practice in road traffic by use of braking lights or warning signs.

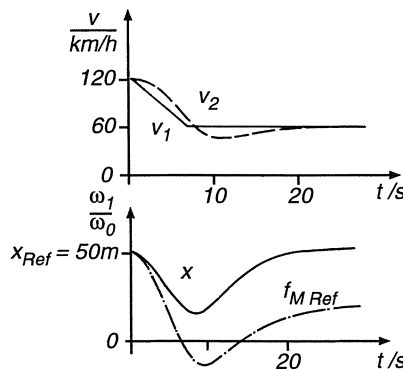


**Fig. 15.22.** Braking transients of distance control scheme

## 15.4 Time-optimal Position Control with Fixed Target Point

Some applications of drives call for the discontinuous motion of a machine part from one steady state position to another. Examples are boring machines where the tool must be positioned for the next drilling operation or reversing rolling mills where the upper roll is lowered by a screw-down drive as soon as the slab of material has left the roll gap. Since the load is disengaged during the travel, there is no specified trajectory  $x(t)$ ; the only requirement is that the drive should follow the discontinuous position reference in minimum time – given the power rating of the drive – and without overshooting the target position.

Under the assumption that

- the response time of the torque control loop can be neglected,

- the jerk, i.e. the derivative of acceleration, need not be restricted (which would be necessary if a transportation system with on-board passengers or a weakly damped mechanical structure were involved),
- the frictional torques are omitted,

the drive with the associated mechanical linkages can be approximated by a double integrator having the acceleration  $a(t)$  as input and the position  $x(t)$  as output; this is shown in Fig. 15.9.

The well known time-optimal solution that could be derived with the calculus of variations, consists of two intervals of maximum acceleration/deceleration and possibly an intermediate interval with constant maximum velocity. This is shown in Fig. 15.23 for two different step changes of the reference position [35, 41]. Velocity and position are plotted versus time as well as in state space which, because  $x$  and  $v$  are the only state variables, reduces to a state plane. Beginning at  $t = 0$  in steady state condition,  $v(0) = x(0) = 0$ , a new position reference is commanded,  $x_{\text{Ref}} = x_{01}$ , calling for a new target state at  $v(t_e) = 0$ ,  $x(t_e) = x_{01}$  with  $t_e \rightarrow \min$ . The time optimal transient consists of maximum initial acceleration, operation at maximum speed and controlled deceleration to the prescribed target point; the maximum values of acceleration and deceleration are assumed equal in Fig. 15.23. If the amplitude of the position step is reduced,  $x_{02} < x_{01}$ , the maximum velocity may not be reached; the acceleration is then immediately followed by deceleration with the switch-over taking place at half the distance travelled.

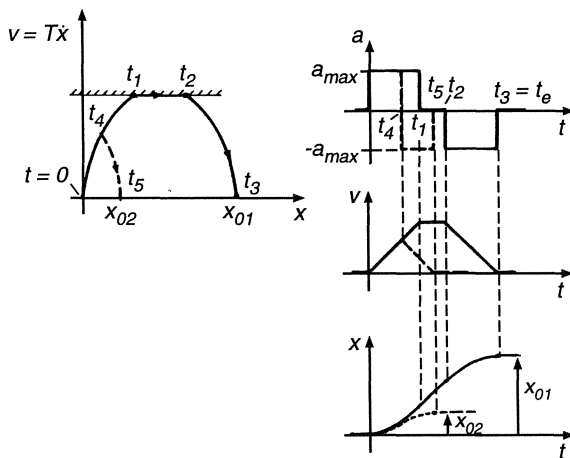


**Fig. 15.23.** Idealised time-optimal positioning transient with limited acceleration.  
a) State plane; b) Response vs. time

In the state plane, the intervals of constant acceleration or deceleration are characterised by parabolae marked with time, the interval at constant velocity appears as a straight line parallel to the  $x$ -axis.

The multi-loop position control scheme in Fig. 15.24 has characteristics that closely approach the idealised behaviour shown in Fig. 15.23 [A20]. The nonlinear position controller is often realised digitally in order to achieve reproducible accuracy at high resolution, for example 0.1 mm with a maximum distance of 1 m on a screw-down positioning drive. The scheme differs from the linear one in Fig. 15.9 by the nonlinear function in the position controller,

$$v_{\text{Ref}} = \sqrt{2 a_{\max} |e|} \text{ sign } e, \quad (15.13)$$

which generates the velocity reference as a function of the remaining position error  $e$ ; its purpose is to guide the drive with constant maximum deceleration into the target point. The mode of operation, after a step change of the position reference has occurred, is as follows: When  $x_{\text{Ref}}$  changes by a value exceeding twice the maximum braking distance, the velocity reference  $v_{\text{Ref}}$  initially assumes its maximum value  $v_{\max}$  causing the velocity controller to become saturated and the drive to start at maximum acceleration. When the velocity reaches the reference value, the velocity controller reverts to linear operation and maintains maximum velocity. As the position error is gradually reduced,  $v_{\text{Ref}}(e)$  follows the parabolic function, resulting in constant deceleration until the target position is reached. The drive may then be disconnected by disabling the power supply and arrested with a mechanical brake. This is necessary because of instability due to the infinite gain of the position controller at  $e \approx 0$ . In case the position reference changes by less than twice the maximum braking distance, the drive will switch from acceleration to deceleration before the maximum velocity is attained.

The torque control loop in Fig. 15.24 serves only for protection in case of overload; the maximum current should be adequate to produce maximum acceleration at full load torque.

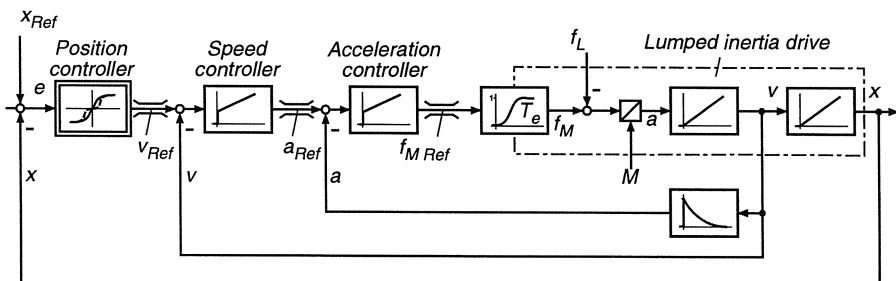
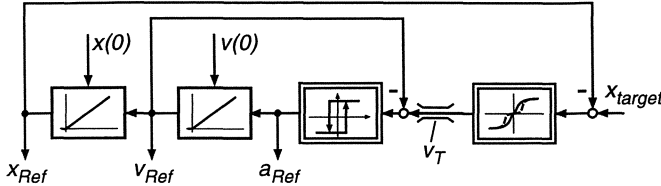


Fig. 15.24. Time-optimal position control scheme

Another possibility for realising minimum time position control is shown in Fig. 15.25, where the linear reference signal generator of Fig. 15.9 has been modified to generate the feed-forward signals required for time-optimal transients. The advantage of this arrangement is that the control system itself remains



**Fig. 15.25.** Dynamic reference model for minimal-time position control

linear and optimally tuned; the choice, whether the transients should be linear or time-optimal only affects the reference model.

This scheme is particularly convenient if the control is realised in a microcomputer. As a further variation, the nonlinear function in Fig. 15.25 is modified around zero (in dashed lines) in order to prevent overshoot and to achieve a stable control mode at the target position. The advantages of both control strategies are then combined: For large position error, the drive performs nearly time-optimally while it assumes linear characteristics once the position error has entered a narrow range around steady state condition. The same may be applied to the position controller in Fig. 15.24.

It has been mentioned that the second order approximation is only applicable as long as the residual lag of the torque control loop can be neglected. Thus the application of this control scheme is restricted to converter supplied DC or AC drives having an effective lag of the torque loop of a few ms. A time-optimal transient of an AC servo drive was shown in Fig. 14.9; some simulated transients, assuming different initial conditions, are plotted in Fig. 15.26.

Controlled deceleration profiles are also used on other drives such as elevators or automatic trains, where at any time a fictitious braking curve  $v(x, t)$  must be known, along which the vehicle could be decelerated or brought to standstill with maximum specified deceleration. By continuously comparing this projected velocity profile with possible forward speed restrictions, it can be determined, when braking should begin in order to meet the next restriction. Figure 15.27 depicts the situation, where an automatic train with its projected velocity profile enters a restricted speed zone.

Whenever passengers on board vehicles are involved, it is usually specified that the accelerating forces must change gradually in order not to create discomfort or anxiety (as every passenger who is standing in a bus knows); a similar problem exists, when complex mechanical structures such as satellite aerials or robots are to be moved, because abruptly changing accelerating or decelerating forces would create unnecessary oscillations. This calls for smooth but swift positioning, still using all the available drive power. Some idealised time-optimal positioning transients with limited rate-of-change of acceleration (jerk) are drawn in Fig. 15.28 beginning with large change of position reference (a) which is gradually reduced (b-e); (b) and (d) are limiting cases separating different modes of operation. Clearly, the condition that  $da/dt$  should be finite

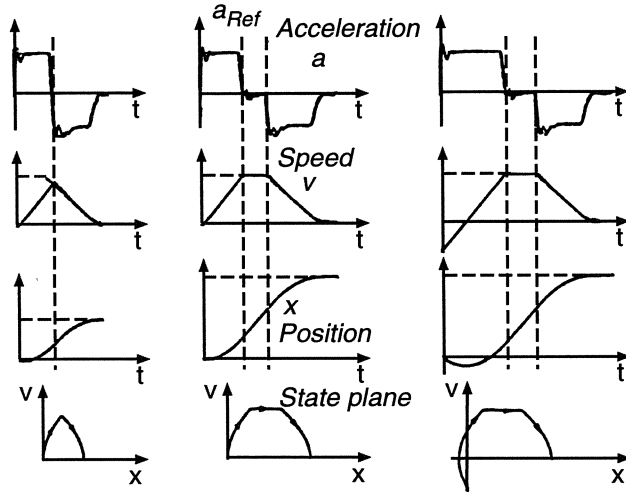


**Fig. 15.26.** Minimal-time positioning transients with different initial conditions

amounts to the definition of acceleration  $a(t)$  as another continuous state variable; hence, the state vector  $[a(t), v(t), x(t)]$  could be represented as a continuous trajectory in a three-dimensional space.

As this is difficult to visualise, some characteristic curves are plotted in Fig. 15.29 in the  $x, v$ -plane, showing how the controlled deceleration phase of the transient could be implemented; the starting phase is no particular problem because it follows the simple strategy of applying maximum  $da/dt$  until the peak values of acceleration and, possibly, velocity have been reached.

Figure 15.30 shows yet another modification of the dynamic model to be used for generating the reference functions  $[a(t), v(t), x(t)]_{\text{Ref}}$  for time-optimal positioning. The acceleration reference is now the output of a third integrator, making it a continuous state variable of the dynamic model. The reference variables are again to be used as inputs for an optimally tuned linear multi-loop position control scheme as seen in Fig. 15.9. The nonlinear function

$$a_T(t) = f(e, v, a) \quad (15.14)$$

is so chosen as to generate in each interval a target acceleration  $a_T$  which the acceleration reference then assumes with constant slope.

Clearly, the main advantage of control with the help of a dynamic reference model is that the computation of the complex set of reference functions can be performed on an idealised arithmetic basis that is not affected by the approximations required when tuning the real drive control system.

As is indicated in Fig. 15.30 it is, of course, necessary to bring the initial conditions of the model in line with the plant; this would best be done in standstill, i.e. with  $v(0) = a(0) = 0$ .

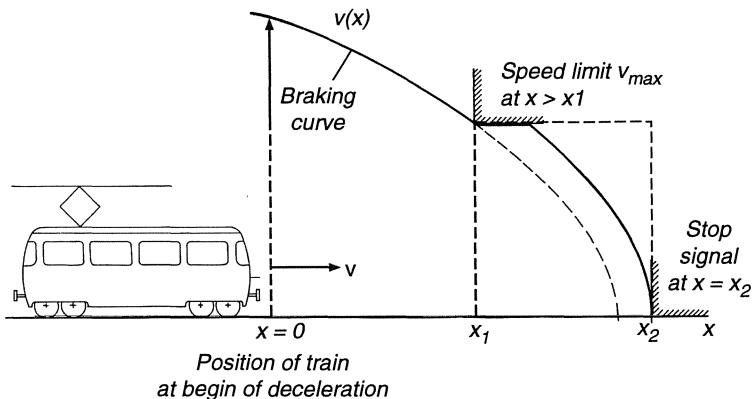


**Fig. 15.27.** Controlled deceleration of automatic train

## 15.5 Time-optimal Position Control with Moving Target Point

In some applications the task of positioning in minimum time is made more complicated by the fact that the target itself is moving. This could assume the form of a rendez-vous-problem, where the drive is required not only to reach the target in minimum time but also to assume the same final velocity as the target. The minimum time requirement could be due to the condition that the initial state of the drive should be subject to least restrictions for reaching the rendez-vous position in time.

Diverging examples for this type of problem are the control of a robot having the task of gently picking up an object from a moving conveyer or of a flying shear that is to cut a strip of metal, emerging from a rolling mill at full speed, into various custom-length sections. Similar problems exist also with rotary printing presses, when a new supply roll of paper must be attached to the end of the outgoing roll while the press is running. The situation vaguely resembles a relay race, where the new runner must start in time for accepting the token from his predecessor in the specified space, or a merger at full speed at the ramp to a motorway, where the entering vehicle is joining a line of cars already moving on the motorway.

The basic layout of a rotating shear is sketched in Fig. 15.31. The strip- or rod-shaped material coming from the last stand of a rolling mill moves with velocity  $v_1$  through the shear, which consists of two mechanically coupled drums bearing opposite cutting tools. Initially the shear may be at rest; at a predetermined time  $t_1$  it is accelerated, so that the tools separate the material at a prescribed point. The blades and the material should move in approximate synchronism during the separation, but a slightly higher velocity of the tools could also be specified for separating the material. Following the cut, the shear

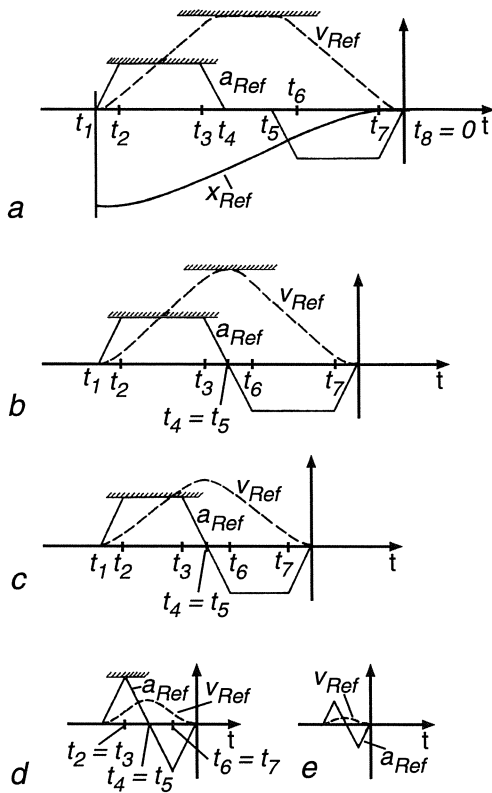


Fig. 15.28. Idealised time-optimal positioning transients with limited jerk

is decelerated and usually set at rest at a selected waiting position. It is noted that the accelerating and decelerating phase must be completed in less than two revolutions of the shear which calls for high dynamic performance of the drive; with DC machines this condition was sometimes met by using tandem motors in order to reduce the effective inertia. There is no limiting specification on the jerk in this application, except the finite rise time of the motor torque.

Beside this discontinuous mode of operation there is also a continuous mode, when the shear, because of lack of time, keeps rotating at pulsating speed without coming to a standstill. The reason may be increased velocity of the material or the need for shorter length cuts of material.

An idealised accelerating, cutting and subsequent positioning cycle is shown in Fig. 15.32 with the variables plotted vs. time and in the state plane; the circular motion of the shear is represented by the circumferential path of the blades. Time and position are defined relative to the cut, i.e. the acceleration phase takes place in the negative range of time and position; the material velocity is assumed to remain constant after the start of the shear,  $v_1 = \text{const}$ . The shear

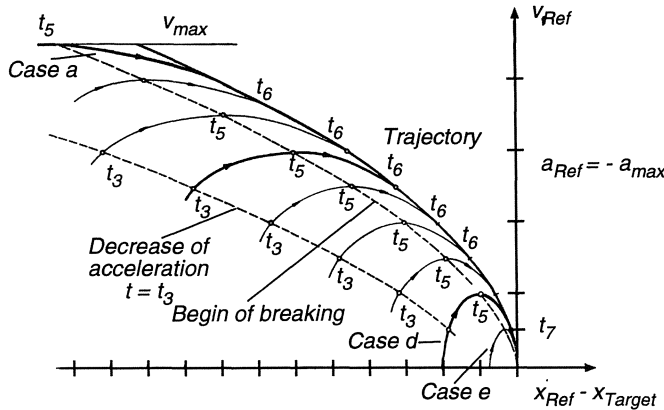


Fig. 15.29. Switching curves and trajectories in state-plane

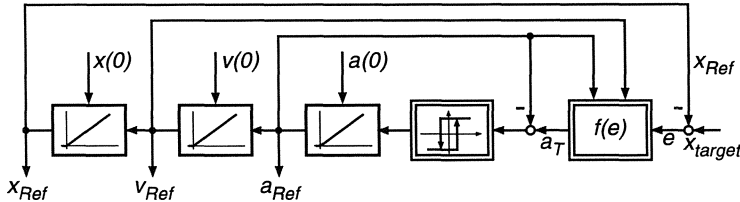


Fig. 15.30. Dynamic model for minimum time, limited jerk, positioning transients

begins to accelerate with  $a = a_{\max}$  at  $t = t_1$ ; at  $t_2$  it reaches cutting speed and then continues in synchronism with the material until the cut occurs at  $t = 0$ . The interval  $t_2 < t < 0$  serves for correction of velocity and position in order to eliminate errors caused by tolerances and the finite response time of the speed loop.

Because of the assumed constant velocity of the material the position  $x_1(t)$  of the target point changes linearly with time, while the shear position  $x_2(t)$  follows in the interval  $t_1 < t < t_2$  a parabolic function. During the acceleration phase

$$t_a = t_2 - t_1 = \frac{v_1}{a_{\max}} \quad (15.15)$$

the target point moves by

$$x_1(t_2) - x_1(t_1) = v_1 t_a = \frac{v_1^2}{a_{\max}} . \quad (15.16)$$

The shear velocity rises linearly with time

$$v_2(t) = (t - t_1) a_{\max} = v_1 \frac{t - t_1}{t_2 - t_1} , \quad t_1 \leq t \leq t_2 , \quad (15.17)$$

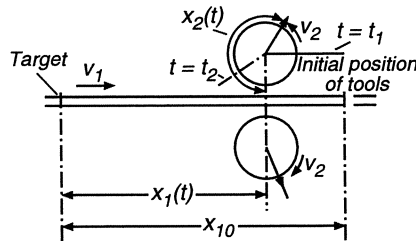


Fig. 15.31. Principle of a flying shear

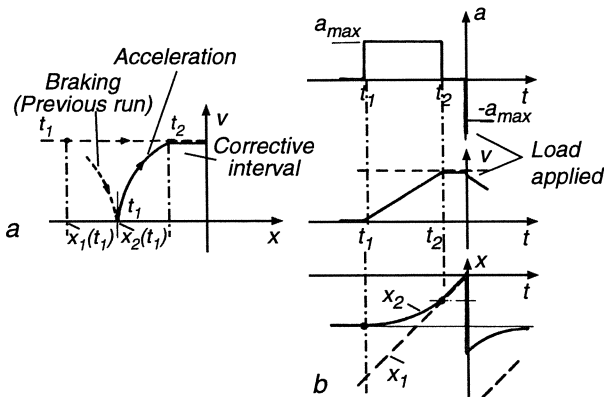


Fig. 15.32. Discontinuous motion of flying shear

which results in a necessary travel for acceleration

$$x_2(t_2) - x_2(t_1) = \frac{1}{2} a_{\max} (t_2 - t_1)^2 = \frac{1}{2} \frac{v_1^2}{a_{\max}} ; \quad (15.18)$$

this is half the distance covered by the target point during the same interval. The remaining corrective interval is travelled in approximate synchronism,

$$x_1(t_2) = x_2(t_2) = v_1 t_2 < 0 . \quad (15.19)$$

While it would be possible to determine the instant when the shear should start at maximum acceleration by a time-based criterion, it seems more appropriate to use a closed loop control scheme for velocity and position which remains in operation during the complete cycle until the shear comes to rest again; this has the advantage that tolerances such as a slightly varying target velocity can be compensated during the final part of the approach [B13, K53, L35].

The control of the shear drive is facilitated by the use of a suitable dynamic model in combination with a high performance multiloop position control scheme such as known from Fig. 15.9. The dynamic model in Fig. 15.33 is of

the type shown in Fig. 15.25 producing the reference signals for minimal time positioning transients; the only difference is a feed-forward signal of the target velocity  $v_1$ , for example coming from measuring rolls. There are two modes of operation, intermittent and continuous motion:

- In reset of the intermittent mode the feed-forward signal is removed and the position reference corresponds to the starting position  $x_{20}$  which is a function of target velocity

$$x_{20} = -\frac{v_1^2}{2 a_{\max}} + v_1 t_2 . \quad (15.20)$$

This condition (Reset and Wait) is maintained until time  $t_1$  when the target position counter reaches the starting position count

$$x_1(t_1) = -\frac{v_1^2}{a_{\max}} + v_1 t_2 . \quad (15.21)$$

- The position reference input for the model is now derived from the target position counter which is counted towards zero by angular increments taken from the measurements rolls; at the same time  $t_1$  the velocity feed-forward signal is added. As a consequence, the drive starts with maximum acceleration.
- As soon as the target position counter reaches zero and the cut occurs, the model is again put into reset while the desired length  $x_{10}$  of the next section is inserted into the target position counter as an initial condition for the next run.

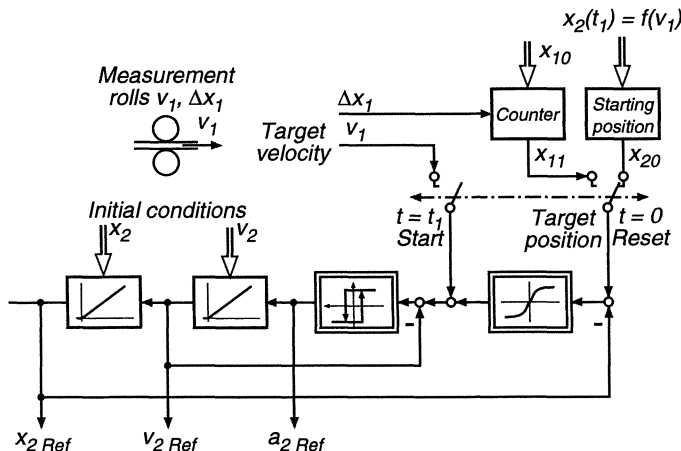


Fig. 15.33. Dynamic model for control of flying shear

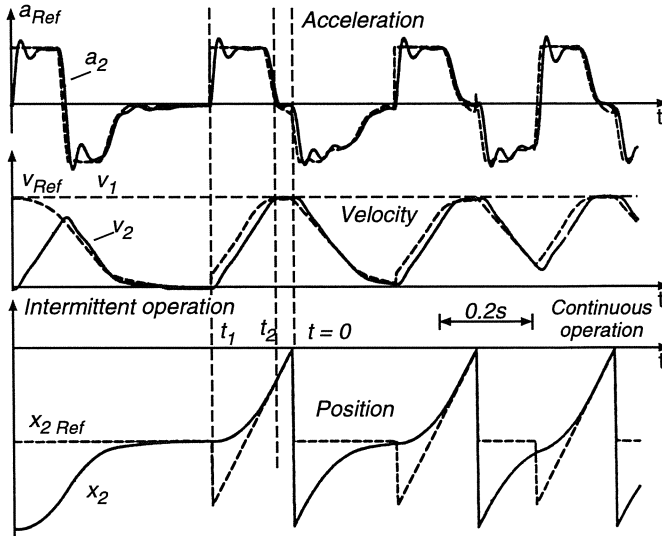
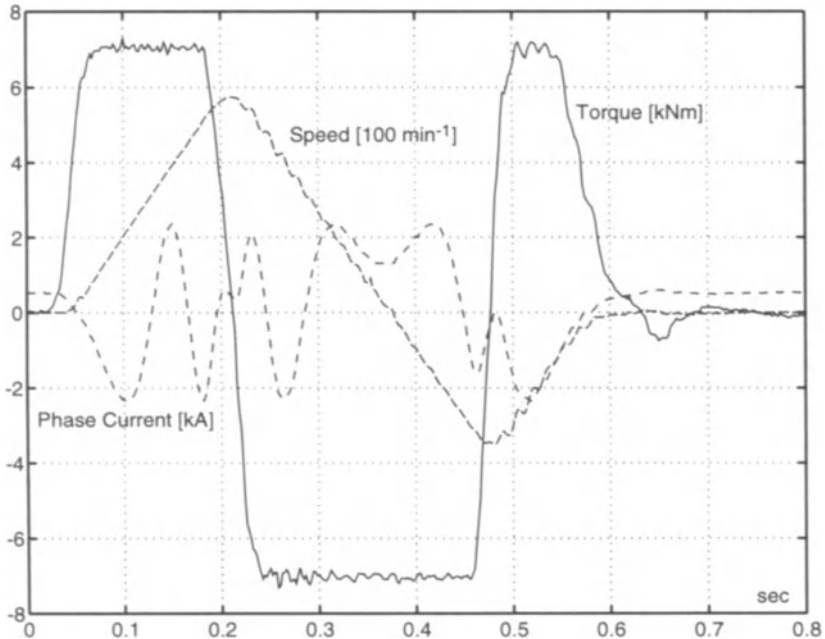


Fig. 15.34. Simulated transients of time-optimal shear drive

It can be shown that the model in Fig. 15.33 produces time-optimal positioning transients as long as the physical restrictions imposed by the drive are not exceeded. Some simulated transients of the drive, i.e. without model, are depicted in Fig. 15.34 where the operating conditions are changed by reducing the desired length of the sections which results in a transition from discontinuous to continuous mode. The transients show that the control scheme can in principle meet these difficult specifications; it is of course important to select a drive that is able to follow rapidly the reference functions.

Also on intermittent drives of this kind, calling for ample overload capacity and fastest possible response, controlled AC motors are now successfully superseding DC motors; their reduced inertia is an added advantage. An example is seen in Fig. 15.35 showing recorded transients of a flying shear drive during an acceleration and repositioning cycle. The 500 kW induction motor is supplied from a 800 kVA GTO voltage source inverter and has a control structure as shown in Fig. 12.28 [K58].

The accuracy of the material lengths which may be expected from this type of drive control depends of course on many factors such as accuracy and response of the drive control loops, accuracy and resolution of the measurements from the moving material as well as the length of time  $t_2$  available for correction during the final approach. Typically, some cm tolerance could be expected, when cutting material of 10 m length. The task of controlling a flying shear is quite complex; on the other hand, the gain in productivity is substantial, when comparing it with a shear that can cut only when the material is at rest.



**Fig. 15.35.** Measured transients during the cutting cycle of a flying shear drive with a 500 kW induction motor having voltage source GTO- inverter supply and field orientated control

The next step towards fully automatic operation is on-line minimisation of scrap by computing an optimal combination of different custom lengths sections that can be produced from a given size ingot. All these control functions, the flying shear control with a dynamic reference model as well as the optimisation can be executed today by a single board microcomputer.

# Bibliography

## Books (referred to by number, e.g. [1])

- [1] Bedford, B.D., Hoft, R.G., Principles of inverter circuits. Wiley, New York 1964
- [2] Bird, B.M., King, K.G., An introduction to power electronics. Wiley, New York 1983
- [3] Bödefeld, Th., Sequenz, H., Elektrische Maschinen. 8th Edition, Springer, Berlin-Heidelberg-New York 1971
- [4] Bose, B.K., Power electronics and AC drives, Prentice Hall, Englewood Cliffs, N.J. 1986
- [5] Böhler, H., Einführung in die Theorie geregelter Gleichstromantriebe. Birkhäuser, Basel-Stuttgart 1962
- [6] Böhler, H., Einführung in die Theorie geregelter Drehstromantriebe, Vol. 1 Grundlagen, Vol. 2 Anwendungen. Birkhäuser, Basel-Stuttgart 1977
- [7] Buxbaum, A., Schierauf, K., Berechnung von Regelkreisen der Antriebstechnik. Elterna, Berlin 1974
- [8] Concordia, C., Synchronous machines - Theory and performance. Wiley, New York 1951
- [9] Davis, R.M., Power diode and thyristor circuits. Peter Peregrinus, 1971
- [10] De, G., Electrical drives and their controls. Acad. Books Ltd, Bombay-New Delhi 1970
- [11] Dewan, S.B., Straughen, A., Power semiconductor circuits. Wiley, New York 1975
- [12] Eckhardt, H., Grundzüge elektrischer Maschinen. Teubner, Stuttgart 1981
- [13] Ernst, D., Ströle, D., Industrieelektronik. Springer, Berlin 1973
- [14] Finney, D., The power thyristor and its applications. Mc Graw Hill, New York 1980
- [15] Fröhr, F., Ortenburger, F., Technische Regelstreckenglieder bei Gleichstromantrieben. Siemens AG, Berlin-München 1971
- [16] Groß , H., Stute, G., Elektrische Vorschubantriebe für Werkzeugmaschinen. Siemens AG, Berlin-München 1981
- [17] Gyugyi, L., Pelley, B.R, Static power frequency changers. Wiley, New York 1976
- [18] Habinger, E., Die Technik der elektrischen Antriebe. VEB Technik, Berlin 1979
- [19] Hamming, R.W., Numerical methods for scientists and engineers. Mc Graw Hill, New York 1962
- [20] Heumann, K., Grundlagen der Leistungselektronik, 2nd Ed. Teubner, Stuttgart 1978

- [21] Heumann, K., Stumpe, A.C., Thyristoren. Teubner, Stuttgart 1969
- [22] Hofmann, A., Stocker, K., Thyristor-Handbuch, 4th Ed. Siemens AG, Berlin-München 1976
- [23] Hoft, R.G., Semiconductor power electronics. Van Nostrand Reinhold 1986
- [24] Jötten, R., Leistungselektronik I. Vieweg, Braunschweig 1977
- [25] Jordan, H., Weis, M., Asynchronmaschinen, Vieweg, Braunschweig 1969
- [26] Kessler, C. (Ed.), Digitale Signalverarbeitung in der Regelungstechnik. VDE-Buchreihe Bd. 8, VDE, Berlin 1962
- [27] Kleinrath, H., Stromrichtergespeiste Drehfeldmaschinen. Springer, Wien 1980
- [28] Kovacz, K.P., Racz, J., Transiente Vorgänge in Wechselstrommaschinen. Ung. Akad. d. Wiss., Budapest 1959
- [29] Kümmel, F., Elektrische Antriebstechnik. Springer, Berlin-Heidelberg-New York 1971
- [30] Kusko, A., Solid state DC motor drives. MIT Press, Cambridge 1969
- [31] Laible, Th., Die Theorie der Synchronmaschine im nichtstationären Betrieb. Springer, Berlin 1952
- [32] Langhoff, J., Raatz, E., Geregelte Gleichstromantriebe in der Praxis der Stromrichter- und Regelungstechnik. Elitera, Berlin 1977
- [33] Lappe, R., Thyristorstromrichter für Antriebsregelungen. VEB-Technik, Berlin 1970
- [34] Leonhard, A., Elektrische Antriebe, 2nd Ed. Enke, Stuttgart 1959
- [35] Leonhard, W., Einführung in die Regelungstechnik, 6th Ed. Vieweg, Braunschweig 1991
- [36] Leonhard, W., Regelung in der elektrischen Antriebstechnik. Teubner, Stuttgart 1974
- [37] Leonhard, W. (Ed.), Control in power electronics and electrical drives. 1. IFAC Symp., Düsseldorf 1974, VDI/VDE, 1974
- [38] Leonhard, W. (Ed.), Control in power electronics and electrical drives. 2. IFAC Symp., Düsseldorf 1977, Pergamon Press, Oxford 1977
- [39] Leonhard, W. (Ed.), Microelectronics in power electronics and electrical drives. ETG-Fachberichte Vol. 11, VDE, Berlin 1982
- [40] Leonhard, W. Digitale Signalverarbeitung in der Mess- und Regelungstechnik. 2nd Ed. Teubner, Stuttgart, 1990
- [41] Lerner, A.J., Schnelligkeitsoptimale Regelungen. (Translated from Russian), Oldenbourg, München 1963
- [42] Lyon, W.V., Transient analysis of alternating- current machinery. MIT Press and J. Wiley & Sons, New York 1954
- [43] Marti, K., Winograd, O., Stromrichter. Oldenbourg, München 1933
- [44] Mazda, F.F., Thyristor control. Wiley, New York 1973
- [45] Meyer, M., Selbstgeführte Thyristor-Stromrichter, 3.-Ed. Siemens AG, Berlin-München 1974
- [46] Möltgen, G., Netzgeführte Stromrichter mit Thyristoren, 3rd Ed. Siemens AG, Berlin – München 1974
- [47] Möltgen, G., Line commutated thyristor converters. Siemens and Pitman, London 1972
- [48] Mohan, N., Undeland,T.M., Robbins, W.P., Power electronics, Converters, applications and design, J. Wiley, New York 1989

- [49] Mohr, O. (Ed.), Steuerungen und Regelungen elektrischer Antriebe. VDE-Buchreihe Bd. 4, VDE, Berlin 1959
- [50] Murphy, J.M.D., Thyristor control of AC motors. Pergamon Press, Oxford 1973
- [51] Murphy, J.M.D., Turnbull, F.G., Power electronic control of AC motors. Pergamon Press, Oxford 1988
- [52] Orttensburger, F., Das regelungstechnische Verhalten der Gleichstrommaschine. Siemens AG, Berlin-München 1972
- [53] Pearman, R.A., Power electronics: Solid state motor control. Prentice Hall, 1980
- [54] Pelly, B.R., Thyristor phase-controlled converters and cycloconverters. Wiley, New York 1971
- [55] Pfaff, G., Regelung elektrischer Antriebe. Oldenbourg, München 1971
- [56] Pfaff, G., Meier, Ch., Regelung elektrischer Antriebe II, (Geregelte Gleichstromantriebe). Oldenbourg, München 1982
- [57] Puchstein, A.F., Lloyd, T.C., Conrad, A.G., Alternating current machines. Wiley, New York 1954
- [58] Say, M G., Alternating current machines, 5th Ed. Pitman, London 1983
- [59] Say, M.G., Taylor, E.O., Direct current machines, Halsted Press 1980
- [60] Schönfeld, R., Digitale Regelung elektrischer Antriebe. Hüthig, Heidelberg 1990
- [61] Seefried, E., Müller, G., Frequenzgesteuerte Drehstrom- Asynchronantriebe. Verlag Technik, München 1992
- [62] Sen, P.C., Thyristor DC-drives. Wiley, New York 1981
- [63] Sen, P.C., Principles of electrical machines and power electronics. Wiley, New York 1989
- [64] Simon, W., Die numerische Steuerung von Werkzeugmaschinen. Hanser, München 1971
- [65] Slemmon, G.R., Straughen, A., Electric machines. Addison Wesley, 1980
- [66] Späth, H., Steuerverfahren für Drehstrommaschinen. Springer, Berlin-Heidelberg-New York-Tokyo 1983
- [67] Steimel, K., Jötten, R., (Eds.), Energietechnik und geregelte elektrische Antriebe. VDE-Buchreihe Vol. 11, VDE, Berlin 1966
- [68] Steven, R.E., Electrical machines and power electronics. Van Nostrand Reinhold, 1983
- [69] Taegen, P., Einführung in die Theorie der Elektrischen Maschinen I, II. Vieweg, Braunschweig 1971
- [70] Tschilkin, M.G., Elektromotorische Antriebe. (Translated from Russian), VEB-Technik, 1957
- [71] Uhlmann, E., Power transmission by Direct Current. Springer, Berlin-Heidelberg-New York 1975
- [72] Vas, P., Vector control of AC machines. Clarendon Press, 1990
- [73] VEM-Handbuch – Leistungselektronik. VEB-Technik, Berlin 1979
- [74] VEM-Handbuch – Die Technik der elektrischen Antriebe. VEB-Technik, Berlin 1979
- [75] Vogel, J., Elektrische Antriebstechnik. 5th Ed. Hüthig, Heidelberg, 1991
- [76] Wasserrab, Th., Schaltungslehre der Stromrichtertechnik. Springer, Berlin-Göttingen-Heidelberg 1962
- [77] Watzinger, H., Stromrichter-Gleichstromantriebe. Hüthig, Heidelberg 1980
- [78] Weber, W., Adaptive Regelsysteme. Oldenbourg, München 1971

- [79] Weh, H., Elektrische Netzwerke und Maschinen in Matrizen-Darstellung. Teubner, Stuttgart 1968
- [80] Wood, P., Switching power converters, Van Nostrand Reinhold 1981
- [81] Yamamura, S., AC motors for high performance applications, analysis and control. Marcel Dekker, New York 1986
- [82] Zadeh, L.A., Desoer, C.A., Linear system theory. McGraw Hill, New York 1963

**Papers, Surveys, Dissertations** (referred to by initial and number, e.g. [A1])

- [A1] Abbondanti, A., Method of flux control in induction motors driven by variable frequency, variable voltage supplies. Int. Semiconductor Power Converter Conf. Rec. 1977, pg. 177
- [A2] Abbondanti, A., Brennen, M.B., Variable speed induction motor drives use electronic slip calculation based on motor voltages and currents. IEEE Trans. Ind. Appl. 1975, pg. 483
- [A3] Abraham, L., Transient characteristics and limits of a squirrel-cage motor fed from a frequency-converter with DC current link. 2. IFAC Symp., Control in Power Electronics and Electrical Drives, Düsseldorf 1977, pg. 475
- [A4] Abraham, L., Heumann, K., Koppelmann, F., Wechselrichter zur Drehzahlsteuerung von Käfigläufermotoren. AEG Mitteilungen 1964, pg. 89
- [A5] Abraham, L., Koppelmann, F., Käfigläufermotoren mit hoher Drehzahldynamik. AEG Mitteilungen 1965, pg. 118
- [A6] Ahrens, D., Günther, H., Elektrische und mechanische Einflußgrößen bei Lageregelkreisen. AEG Mitteilungen 1976, pg. 249
- [A7] Ahrens, D., Raatz, E., Regelungstechnische Untersuchungen von Antrieben mit Kupplungs- oder Getriebelose. AEG Mitteilungen 1973, pg. 210
- [A8] Ainsworth, J.D., Harmonics instability between controlled static convertors and AC-networks. Proc. IEE 1967, pg. 949
- [A9] Akagi, H., Nabae, A., A new control scheme for compensating the torque transfer function of a self-controlled synchronous motor. IEEE Trans. Ind. Appl. 1984, pg. 795
- [A10] Albrecht, P., Die geregelte doppeltgespeiste Asynchronmaschine als drehzahlvariabler Generator am Netz. Diss. TU Braunschweig 1984
- [A11] Albrecht, P., Vollstedt, W., Microcomputer control of a variable speed doubly-fed induction generator operating on the fixed frequency grid. Microelectronics in Power Electronics and Electrical Drives, Darmstadt 1982, ETG-Fachberichte 11, pg. 363
- [A12] Alexanderson, E.F.W., Mittag, A.H., The thyratron motor. AIEE Trans. 1934, pg. 1517
- [A13] Ambrozic, V., Klaassen, H., A modified method for the determination of the rotor time constant of an induction motor in a cold state. Proc. 8th EDPE, Pula, 1994, pg. 66
- [A14] Amler, G., Ein neues Steuer- und Regelverfahren für einen Stromzwischenkreis-Umrichter mit abschaltbaren Leistungshalbleitern. Diss. TU Braunschweig, 1991
- [A15] Amler, G., A new control method for current source inverters with self-extinction devices, combining low distortion of voltage and current with fast dynamic response. Proc. EPE 91, Firenze, pg. 3- 211

- [A16] Andresen, E. C., Pfeiffer, R., Werth, L., Fundamentals for the design of high speed induction motor drives with transistor inverter supply. Proc. EPE 89, Aachen, pg. 823
- [A17] Andresen, E. C., Gediga, S., Schwartz, H. J., A continuous PWM- square wave transition method for voltage vector control of induction motors. Proc. EPE 91, Firenze, pg. 2- 156
- [A18] Andresen, E. C., Haun, A., Influence of the pulse width modulation control method on the performance of frequency inverter induction motor drives. Europ. Trans. on Electr. Power Engng. 1993, pg.151
- [A19] Andria, G., Salvatore, L., Signal processing for determining flux and torque of induction motors. Proc. IEE-Power Electronics and Variable Speed Drives, London 1988, pg. 296
- [A20] Anke, K., Ertel, K., Sinn, G., Digitale Wegregelung. Siemens Zeitschrift 1960, pg. 664
- [A21] Anke, K., Kessler, G., Müller, H., Digitale Drehzahlregelung. Siemens Zeitschrift 1960, pg. 660
- [A22] Antic, D., Klaassens, J.B., Deleroi, W., An integrated boost- buck and matrix converter topology for low speed drives. Proc. EPE 93, Brighton, pg. 5- 21
- [A23] Appt, D., Baisch, R., Brömer, G., Wegmessung und Wegregelung an numerisch gesteuerten Werkzeugmaschinen. Siemens-Zeitschrift 1974, Beiheft Steuerung und Antriebe zur Automatisierung der Werkzeugmaschine, pg. 12
- [A24] Appun, P., Control of rotating and linear induction motors for vehicle drives. 2. IFAC Symp., Control in Power Electronics and Electrical Drives, Düsseldorf 1977, pg. 809
- [A25] Arsudis, D., Doppeltgespeister Drehstromgenerator mit Spannungzwischenkreis- Umrichter im Rotorkreis für Windkraftanlagen. Diss. TU Braunschweig 1989
- [A26] Arsudis, D., Vollstedt, W., Sensorlose Regelung einer doppeltgespeisten Asynchronmaschine mit geringen Netzrückwirkungen. Archiv für Elektrotechnik, 1991, pg. 89
- [A27] Atkinson, D.J., Acarnley, P.P., Finch, J.W., Parameter identification techniques for induction motor drives. Proc. EPE 89 Aachen, pg. 307
- [A28] Atkinson, D.J., Acarnley, P.P., Finch, J.W., Method for the estimation of rotor resistance in induction motors. Proc. EPE 91, Firenze, pg. 3- 338
- [A29] Atkinson, D.J., Acarnley, P.P., Finch, J.W., Observers for induction motor state and parameter estimation. IEEE Trans. Ind. Appl. 1991, pg. 1119
- [B1] Bachmann, G., Engel, D., Geregelte Gleichstrom-Hauptantriebe bis 400 kW für Werkzeugmaschinen. Siemens Energietechnik 1981, pg. 269
- [B2] Bader, W., Theorie der Schaltungen für die Widerstandsbremse von selbsterregten Gleichstrom-Reihenschlußmotoren bei elektrischen Fahrzeugen. Wiss. Veröff. Siemens Konzern 1930, pg. 209
- [B3] Balestrino, A., De Maria, G., Sciavicco, L., Adaptive control design in servosystems. 3. IFAC Symp. Control in Power Electronics and Electrical Drives, Lausanne 1983, pg. 125
- [B4] Bassi, E., Benzi, F., Scattolini, R., Design of a digital adaptive controller for electrical drives in industrial applications. IEEE Trans. Ind. Electr. 1992, pg. 120

- [B5] Bassi, E., Benzi, F.P., Bolognani, S., Buja, G.S., A field orientation scheme for current- fed induction motor drives based on the torque angle closed- loop control. IEEE Trans. Ind. Appl. 1992, pg.1038
- [B6] Bauer, F., Heinle, G., Eliminating the harmonics from measured current values in PWM drives. Proc. EPE 91, Firenze, pg. 3- 343
- [B7] Bayer, K.H., Waldmann, H., Weibelzahl, M. Die TRANSVEKTOR-Regelung für den feldorientierten Betrieb einer Synchronmaschine. Siemens Zeitschrift 1971, pg. 765
- [B8] Bayer, K.-H., Blaschke, F., Stability problems with the control of induction machines using the method of field orientation. 2. IFAC Symp., Control in Power Electronics and Electrical Drives, Düsseldorf 1977, pg. 483
- [B9] Becker, H., Dynamisch hochwertige Drehzahlregelung einer umrichtergespeisten Asynchronmaschine. Regelungstechnische Praxis 1973, pg. 217
- [B10] Becker, H., ROBOT CONTROL, eine Mikroprozessorsteuerung für Industrieroboter. Siemens Energietechnik 1980, pg. 137
- [B11] Bellini, A., Figalli, G., Tosti, F., Linearised model of induction motor drives via nonlinear feedback decoupling. Proc. EPE 91, Firenze, pg. 3- 36
- [B12] Belmans, R.J.M., Verdyck, D., Geysen, W., Findlay, R.D., Electro- mechanical analysis of the audible noise of an inverter- fed squirrel- cage induction motor. IEEE Trans. Ind. Appl. 1991, pg. 539
- [B13] Bender, K., Pandit, M., Weber, W., Verlustoptimale Regelung von rotierenden Scheren. Regelungstechnik 1970, pg. 540; 1971.,pg. 8
- [B14] Bender, K., Beschleunigungsgeregelte Antriebe in optimalen Regelkreisen. Regelungstechnik 1972, pg. 423
- [B15] Ben Ammar, F. Pietrzak- David, M., de Fornel, B., Mirzaian, A., Field- oriented control of high- power induction motor drives by Kalman filter observation. Proc. EPE 91, Firenze, pg. 2- 182
- [B16] Ben Ammar, F. Pietrzak- David, M., de Fornel, B., Mirzaian, A., Power range extension of an induction motor speed drive by using a three- level GTO inverter with space vector modulation. Proc. EPE 93, Brighton, pg. 5- 219
- [B17] Ben Brahim, L., Kawamura, A., Digital current regulation of field- oriented controlled induction motor based on predictive flux observer. IEEE Trans. Ind. Appl. 1991, pg. 956
- [B18] Ben Brahim, L., Kawamura, A., A fully digitised field- oriented controlled induction motor drive using only current sensors. IEEE Trans. Ind. Electr. 1992, pg. 241
- [B19] Bergin, T. J., Cholewka, J., The direct load angle control of a CSI drive. Proc. IEE-Power Electronics and Variable Speed Drives, London 1988, pg. 305
- [B20] Best, J., Mutschler, P., Methods of microcomputer-based SCR-DC-motor drive control. Microelectronics in Power Electronics and Electrical Drives, Darmstadt 1982, ETG-Fachberichte 11, pg. 265
- [B21] Bichler, U., Synchronmaschinen mit aktiver Dämpfung. Diss. TU Braunschweig 1985
- [B22] Bilewski, M., Fratta, A., Giordano, L., Vagati, A., Villata, F., Control of high- performance interior permanent magnet synchronous drives. IEEE Trans. Ind. Appl. 1993, pg. 328
- [B23] Blaabjerg, F., Pedersen, J.K., Digital implemented random modulation strategies for AC and switched reluctance drives. Proc. IECON 93, Maui, pg. 676

- [B24] Blaschke, F., Ripperger, H., Steinkönig, H., Regelung umrichtergespeister Asynchronmaschinen mit eingeprägtem Ständerstrom. Siemens Zeitschrift 1968, pg. 773
- [B25] Blaschke, F., Hütter, G., Scheider, U., Zwischenkreisumrichter zur Speisung von Asynchronmaschinen für Motor- und Generatorbetrieb. ETZ-A, 1968, pg. 108
- [B26] Blaschke, F., Das Prinzip der Feldorientierung, die Grundlage für die TRANSVEKTOR-Regelung von Asynchronmaschinen. Siemens Zeitschrift 1971, pg. 757
- [B27] Blaschke, F., The principle of field orientation as applied to the new TRANSVEKTOR closed loop control system for rotating field machines. Siemens Review 1972, pg. 217 .
- [B28] Blaschke, F., Das Verfahren der Feldorientierung zur Regelung der Asynchronmaschine. Siemens Forschungs- und Entwicklungsberichte 1972, pg. 184
- [B29] Blaschke, F., Das Verfahren der Feldorientierung zur Regelung der Drehfeldmaschine. Diss. TU Braunschweig 1973
- [B30] Blaschke, F., Böhm, K., Verfahren der Flüßerfassung bei der Regelung stromrichtergespeister Asynchronmaschinen. 1. IFAC-Symp., Control in Power Electronics and Electrical Drives, Düsseldorf 1974, Vol. 1, pg. 635
- [B31] Blaschke, F., Ströle, D., Transformationen zur Entflechtung elektrischer Antriebsregelstrecken. Regelungstechnik 1973, pg. 105
- [B32] Bodson, M., Chiasson, J., Novotnak, R., A systematic approach to selecting flux references for torque maximization in induction motors. IEEE Trans. Control Syst. Techn. 1995, pg. 388
- [B33] Bodson, M., Chiasson, J., Novotnak, R., Nonlinear speed observer for high-performance induction motor control. IEEE Trans. Ind. Electr. 1995, pg. 337
- [B34] Böcker, J., Janning, J., Discrete-time flux observer for PWM inverter fed induction motors. Proc. EPE 91, Firenze, pg. 2- 171
- [B35] Böhm, E., Führung und Regelung von Antennenantrieben für Satelliten-Bodenstationen. Siemens Zeitschrift 1974, pg. 828
- [B36] Böhm, K., Wesselak, F., Drehzahlregelbare Drehstromantriebe mit Umrichter-speisung. Siemens Zeitschrift 1971, pg. 753
- [B37] Boehringer, A., Knöll, H., Transistorschalter im Bereich hoher Leistungen und Frequenzen. ETZ 1979, pg. 664
- [B38] Boehringer, A., Stute, G., Ruppmann, C., Vogt, G., Würslin, R., Entwicklung eines drehzahlgesteuerten Asynchronmaschinenantriebs für Werkzeugmaschinen. Zeitschrift für industrielle Fertigung 1979, pg. 463
- [B39] Böning, B., Leonhard, W., Propulsion control of a track-powered linear synchronous motor for a magnetically levitated vehicle on the basis of power measurements in the inverter station. Proc. Int. Conf. on Electrical Machines, Brus sel 1978, paper L 5/ 1
- [B40] Boidin, M., de Fornel, B., Reboulet, C., Commande en couple sans capteur mécanique d'une machine asynchrone d'induction. Conumel 83, Toulouse pg. IV-43
- [B41] Borojevic, D., Robust nonlinear control algorithm for fast positioning in servo drives. Proc. EPE 89, Aachen, pg. 1375
- [B42] Bose, B.K., Adjustable speed AC drives – a technology status review. Proc. IEEE 1982, pg. 116

- [B43] Bose, B.K.(Ed.), Microcomputer control of power electronics and drives. IEEE, New York 1987
- [B44] Bose, B.K., Power electronics and motion control– Technology status and recent trends. IEEE Trans. Ind. Appl. 1993, pg. 902
- [B45] Bowes, S.R., Bird, B.M., Novel approach to the analysis and synthesis of modulation processes in power converters. Proc. IEE 1975, pg. 507
- [B46] Bowes, S.R., Midoun, A., Microprocessor implementation of new optimal PWM switching strategies. Proc. IEE 1988, Pt. B. pg. 269
- [B47] Bowes, S.R., New regular- sampled harmonic elimination PWM techniques for drives and static power converters. Proc. EPE 91, Firenze, pg. 3- 241
- [B48] Bowes, S.R., Advanced regular- sampled PWM control techniques for drives and static power converters. Proc. IECON 93, Maui, pg. 662
- [B49] Bowler, P., Carter, R.C., Jones, D.M., The development and performance of a digital subharmonic modulator for AC drives. Proc. IEE-Power Electronics and Variable Speed Drives, London 1988, pg. 403
- [B50] Braga, G., Farini, A., Fuga, F., Manigrasso, R., Synchronous drive for motorised wheels without gearbox for light rails system and electric cars. Proc. EPE 91, Firenze, pg. 4- 78
- [B51] Brandstetter, P., Cermak, T., Chlebis, P., Kozina, J., Stefanik, M., Microcomputer system control in field coordinates of synchronous machine. Proc. EPE 91, Firenze, pg. 4- 560
- [B52] Bressani, M., Odorico, A., Sica, M., High- speed, large- power induction motors for direct coupling to variable- speed gas compressors. Proc. EPE 93, Brighton, pg. 5- 366
- [B53] Brickwedde, A., Microprocessor-based adaptive control for electrical drives. 3. IFAC Symp. Control in Power Electronics and Electrical Drives, Lausanne 1983, pg. 119
- [B54] Brickwedde, A., Head, D., Graham, H., Microprocessor controlled 50 kVA PWM inverter drive. IEEE Ind. Appl. Ann. Meet. 1981, pg. 666
- [B55] Brickwedde, A., Selbsteinstellender, on- line adaptiver Regler auf Mikrorechnerbasis für elektrische Antriebe. Diss. TU Braunschweig 1985
- [B56] Brown, G.M., Szabados, B., Belmans, R.J.M., High power cycloconverter drive for double- fed induction motors. Proc. EPE 91, Firenze, pg. 2- 282
- [B57] Brunsbach, B.J., Henneberger, G., Klepsch, Th., Position controlled permanent excited synchronous motor without mechanical sensors. Proc. EPE 93, Brighton, pg. 6- 38
- [B58] Bühler, E., Eine zeitoptimale Thyristor-Stromregelung unter Einsatz eines Mikroprozessors. Regelungstechnik 1978, pg. 37
- [B59] Bühler, H., Investigation of a rectifier regulating circuit as a sampled data system. 4. IFAC-Congress, Warsaw 1969
- [B60] Bühler, H., Umrichtergespeiste Antriebe mit Asynchronmaschinen. Neue Technik 1974, pg. 121
- [B61] Bünte, A., Grotstollen, H., Parameter identification of an inverter- fed induction motor at standstill with a correlation method. Proc. EPE 93, Brighton, pg. 5- 97
- [B62] Buja, G.S., Indri, G.B., Optimal pulse width modulation for feeding AC motors. IEEE Trans. Ind. Appl. 1977, pg. 38

- [B63] Buja, G.S., Fiorini, P., Microcomputer control of PWM inverters. IEEE Trans. Ind. Electr. 1982, pg. 212
- [B64] Buja, G.S., Menis, R., Valla, M.I., Disturbance torque estimation in a sensorless DC drive. Proc. IECON 93, Maui, pg. 977
- [B65] Busse, A., Holtz, J., A digital space vector modulator for the control of a three-phase power converter. Microelectronics in Power Electronics and Electrical Drives, Darmstadt 1982 ETG-Fachberichte 11, pg. 189
- [B66] Buxbaum, A., Regelung von Stromrichterantrieben bei lückendem und nichtlückendem Ankerstrom. AEG Mitteilungen 1969, pg. 348
- [B67] Buxbaum, A. Aufbau und Funktionsweise des adaptiven Ankerstromreglers. AEG Mitteilungen 1971, pg. 371
- [B68] Buxbaum, A., Einsatz von adaptiven Reglern bei geregelten Stromrichter-Stellgliedern. VDE-Aussprachetag Freiburg 1973, pg. 99
- [B69] Bystron, K., Strom- und Spannungsverhältnisse beim Drehstrom-Drehstrom-Umrichter mit Gleichspannungs-Zwischenkreis. ETZ-A, 1966, pg. 264
- [B70] Bystron, K., Meissen, W., Drehzahlsteuerung von Drehstrommotoren über Zwischenkreisumrichter. Siemens Zeitschrift 1965, pg. 254
- [C1] Cambronne, J.P., Semail, B., Rombaut, C., Vector control of a PWM current source inverter- fed induction motor. Proc. EPE 91, Firenze, pg. 2- 177
- [C2] Capolino, G.A., Du, B., Extended Kalman observer for induction machine rotor currents. Proc. EPE 91, Firenze, pg. 3- 672
- [C3] Cardoletti, L., Jufer, M., Sensorless position detection using the supply voltage for a programmable current drive for synchronous motors. Proc. EPE 91, Firenze, pg. 4- 123
- [C4] Case, M.J., Kulentic, P.K., A microprocessor controller for the cycloconverter. Microelectronics in Power Electronics and Electrical Drives, Darmstadt 1982, ETG-Fachberichte 11, pg. 171
- [C5] Case, M. J., Van Wyk, Trantputer based induction motor flux- control method. Proc. EPE 91, Firenze, pg. 2- 192
- [C6] Chauprade, R., Abbondanti, A., Variable speed drives: Modern concepts and approaches. Int. Semiconductor Power Conv. Conf. 1982, Ind. Appl., pg. 20
- [C7] Chen, H.H., Microprocessor control of a three-pulse cycloconverter. Proc. IECI 1977, pg. 226
- [C8] Chiasson, J., Dynamic feedback linearization of the induction motor. IEEE Trans. Aut. Contr. 1993, pg. 1588
- [C9] Chiasson, J., Nonlinear controllers for induction motors. IEEE Trans. Aut. Contr. 1995
- [C10] Chiba, A., Fukao, T., A closed loop operation of super high speed reluctance motor for quick torque response. IEEE Trans. Ind. Electr. 1992, pg. 600
- [C11] Chollet, G., Commande par microprocesseur d'un commutateur de courant pour moteur asynchrone de traction. Conumel 83, Toulouse pg. IV-1
- [C12] Claussen, U., Adaptive zeitoptimale Lageregelung eines linearen Stellantriebes mit synchronem Linearmotor. Diss. TU Braunschweig 1979
- [C13] Claussen, U., Fromme, G., Motorregelung mit Mikrorechner. Regelungstechnische Praxis 1978, pg. 355
- [C14] Claussen, U., Leonhard, W., Microprocessor-controlled linear synchronous motor as positioning drive. Proc. Int. Conf. on Electrical Machines, Brussel 1978, L 5/2

- [C15] Colak, I., Garvey, S., Wright, M.T., Mixed- frequency testing of induction machines using inverters. Proc. EPE 93, Brighton, pg. 5- 317
- [C16] Collings, T.D., Wilson, W.J., A fast response current controller for microprocessor based SCR- DC motor drives. IEEE Trans. Ind. Appl. 1991, pg. 921
- [C17] Conrath, C., Commande à microprocesseur d'une machine asynchrone autopilotée. Application à un système de levage. Conumel 83, Toulouse, pg. IV-7
- [C18] Cordeschi, G., Parasiliti, F., A variable structure approach for speed control of field- oriented induction motor. Proc. EPE 91, Firenze, pg. 2- 222
- [C19] Cornell E.P., Lipo, T.A., Modelling and design of controlled current induction motor drive systems. IEEE Trans. Ind. Appl. 1977, pg. 321
- [D1] Da Costa Branco, P.J., Stephan, R.M., A simple adaptive scheme for indirect field orientation of an induction motor. Proc. EPE 91, Firenze, pg. 2- 208
- [D2] Dakhouche, K., Roye, D., Digital vector control of induction machine using a PWM inverter. Proc. EPE 91, Firenze, pg. 2- 227
- [D3] Dallago, E., Sassone, G., Study and application of a digital speed control in a DC brushless drive. Europ. Trans. on Electr. Power Engng. 1991, pg. 169
- [D4] Dallhammer, R., Gotthardt, K.-J., The operation of microcomputers in railways with the example of the H-Bahn. Microelectronics in Power Electronics and Electrical Drives, Darmstadt 1982, ETG-Fachberichte 11, pg. 409
- [D5] Dannhauer, D., Prüfstand für Werkzeugmaschinenantriebe mit einer permanenterregten Synchronmaschine als Belastungseinheit. Diss. TU Braunschweig 1993
- [D6] Daum, D., Unterdrückung von Oberschwingungen durch Pulsbreitensteuerung. ETZ-A, 1972, pg. 528
- [D7] Daum, D., Digitale Steuereinrichtung für Stromrichteranlagen. ETZ-A, 1973, pg. 299
- [D8] Daum, D., Untersuchung eines Einphasenstromrichters mit nahezu sinusförmigem Netzstrom und gut geglätteten Gleichgrößen. Diss. Univ. Bochum 1974
- [D9] Davis, R.M., Melling, J., Quantitative comparison of commutation circuits for bridge inverters. Proc. IEE 1977, pg. 237
- [D10] Davis, R.M., A variable speed drive that took a century and a half to develop. Electrical Times, 1983
- [D11] De Carli, A., Marola, G., Optimal pulse-width modulation for three-phase voltage supply. Microelectronics in Power Electronics and Electrical Drives, Darmstadt 1982, ETG-Fachberichte 11, pg. 197
- [D12] De Carli, A., Steady state behaviour of converter fed systems. 3. IFAC Symp. Control in Power Electronics and Electrical Drives. Lausanne, 1983, Survey
- [D13] De Carli, A., Qualification of drives for motion control. Proc. EPE 91, Firenze, pg. 2- 589
- [D14] De Doncker, R.W.A.A., Synthesis and digital implementation of adaptive field orientation controllers for induction machines with air gap flux control and deep bar compensation. Diss. Kath. U. Leuven, 1986
- [D15] De Doncker, R.W.A.A., Field- oriented controllers with rotor deep bar compensation circuits. IEEE Trans. Ind. Appl. 1992, pg. 1062
- [D16] de Fornel, B., Bach, J.L., Pietrzak-David, M., Control law of an AC variable speed drive without mechanical sensors. Microelectronics in Power Electronics and Electrical Drives Darmstadt 1982, ETG-Fachberichte 11, pg. 329

- [D17] de Jager, W.A.G., Tubbing, G.H., A vector oriented control strategy for a 4-quadrant line side converter. Proc. EPE 93, Brighton, pg. 5- 213
- [D18] Deleroi, W., Winterling, M.W., Commutation analysis of synchronous machine drives. Proc. EPE 91, Firenze, pg. 4- 572
- [D19] Depenbrock, M., Einphasenstromrichter mit sinusförmigem Netzstrom und gut geglätteten Gleichgrößen. ETZ-A, 1973, pg. 466
- [D20] Depenbrock, M.; Einphasenstromrichter mit optimiertem Leistungsfaktor. ETZ-A, 1974, pg. 360
- [D21] Depenbrock, M., Direkte Selbstregelung (DSR) für hochdynamische Drehfeldantriebe mit Umrichterspeisung, ETZ- Archiv 1985, pg. 211
- [D22] Depenbrock, M., Direct self control (DSC) of inverter- fed induction machine. IEEE Trans. Power Electr. 1988, pg.420
- [D23] Depping, F., Voits, M., Automatic selection of control algorithms for an electrical drive with microcomputer-based speed control. 3. IFAC Symp. Control in Power Electronics and Electrical Drives, Lausanne 1983, pg. 507
- [D24] Dessaint, L.A., Saad, M., Hebert, B., Al- Haddad, K., An adaptive controller for a direct- drive scara robot. IEEE Trans. Ind. Electr. 1992, pg. 105
- [D25] Dietrich, D., Naunin, D., Closed loop speed control of an induction motor by microcomputers. Microelectronics in Power Electronics and Electrical Drives, Darmstadt 1982, ETG-Fachberichte 11, pg. 335
- [D26] Dirr, R., Neuffer, I., Schlüter, W., Waldmann, H., Neuartige elektronische Regeleinrichtungen für doppeltgespeiste Asynchronmotoren großer Leistung. Siemens Zeitschrift 1971, pg. 362
- [D27] Dobrovski, I.A., Beiträge zum Entwurf und zur Dimensionierung von Thyristorgleichstrom-Umrichtern. Diss. TU Braunschweig 1976
- [D28] Dote, Y., Stabilization of controlled current induction motor drive system via new nonlinear state observer. IEEE Trans. Ind. El. Contr. Instr. 1980, pg. 77
- [D29] Dote, Y., Anbo, K., Combined parameter and state estimation of controlled current induction motor drive system via stochastic nonlinear filtering techniques. IEEE Ind. Appl. Ann. Conf. Rec. 1979, pg. 838
- [D30] Dote, Y., Manabe, T., Murakami, S., Microprocessor-based force control for manipulator using variable structure with sliding mode. 3. IFAC Symp. Control in Power Electronics and Electrical Drives, Lausanne 1983, pg. 145
- [D31] Du, T., Brdys, M.A., Taufiq, J.A., Analytical parameter sensitivity expressions for a field oriented induction motor drive. Proc. EPE 91, Firenze, pg. 3- 623
- [D32] Dunford, W.G., Dewan, S.G., The design of a control circuit for a two-quadrant chopper based on the motorola 6800 microprocessor. IEEE Trans. Ind. Appl. 1980, pg. 495
- [E1] Eckhardt, H., Berechnung des quasistationären Betriebs einer pulswechselrichtergespeisten Synchronmaschine kleiner Leistung. ETZ-Archiv 1982, pg. 321
- [E2] Eder, E., Die Ungleichförmigkeit der von einem dekadischen Frequenzteiler erzeugten Pulsfrequenzen. Regelungstechnik 1976, pg. 53
- [E3] Eibel, J., Jötten, R., Control of a 3-level switching inverter, feeding a three-phase machine, by a microprocessor. Microelectronics in Power Electronics and Electrical Drives, Darmstadt 1982, ETG-Fachberichte 11, pg. 217
- [E4] Eisenack, H., Hofmeister, H., Digitale Nachbildung von elektrischen Netzwerken mit Dioden und Thyristoren. AfE 1972, pg. 32

- [E5] Elger, H., Weiß , M., Untersynchrone Stromrichterkaskade als drehzahlregelbarer Antrieb für Kesselspeisepumpen. Siemens Zeitschrift 1968, pg. 308
- [E6] Endo, T., Tajima, F., Okuda, H., Iizuka, K., Kawaguchi, Y., Uzuhashi, H., Okada, Y., Microcomputer-controlled brushless motor without a shaft-mounted position sensor. Int. Power Electr. Conf., Tokyo 1983, pg. 938
- [E7] Engelhardt, W., Schlingenheber und deren Antriebe an Fertigstraßen von Breitbandwalzwerken. Siemens Zeitschrift 1973, Beiheft Antriebstechnik und Prozeßautomatisierung in Hütten- und Walzwerken, pg. 89
- [E8] Enjeti, P.N., Ziogas, P.D., Lindsay, J.F., A current source PWM inverter with instantaneous current control capability. IEEE Trans. Ind. Appl. 1991, pg. 582
- [E9] Enjeti, P.N., Ziogas, P.D., Lindsay, J.F., Rashid, M.H., A new current control scheme for AC motor drives. IEEE Trans. Ind. Appl. 1992, pg. 842
- [E10] Ernst- Cathor, J., Drehzahlvariable Windenergieanlage mit Gleichstromzwischenkreis- Umrichter und optimum- suchendem Regler. Diss TU Braunschweig 1986
- [E11] Ertugrul, N., Acarnley, P.P., French, C.D., Real- time estimation of rotor position in PM motors during transient operation. Proc. EPE 93, Brighton, pg. 5- 311
- [E12] Eschenauer, H., Henning, G., Tröndle, H.-P., Digitale Simulation des dynamischen Verhaltens und der Antriebsregelung von Großantennen. Siemens Zeitschrift 1974, pg 833
- [E13] Espelage, P.M., Chiera, J.A., Turnbull, F.G., A wide range static inverter suitable for AC induction motor drives. IEEE Trans. Ind. Gen. Appl. 1969, pg. 438
- [E14] Ettlinger, G., Leitgeb, W., Popfinger, H., Simotron-Antriebe mittlerer Leistung. Siemens Zeitschrift 1971, pg. 186
- [F1] Fadel, M., de Fornel, B., Control laws of a synchronous machine fed by a PWM voltage source inverter. Proc. EPE 89, Aachen, pg. 859
- [F2] Farrer, W., Miskin, J.D., Quasi-sine-wave fully regenerative inverter. Proc. IEE 1973, pg. 969
- [F3] Favre, J.-P., Microprocessor-based speed control of a SCR-DC-motor. Microelectronics in Power Electronics and Electrical Drives, Darmstadt 1982, ETG-Fachberichte 11, pg.257
- [F4] Fedor, P., Fedak, V., Bober, P., Timko, J., Field- oriented induction motor drive with indirect rotor flux sensing. Proc. EPE 91, Firenze, pg. 2- 214
- [F5] Ferranti, M., Ferraris, L., Laner, E., Villata, F., Induction motor drives for traction application. Proc. EPE 93, Brighton, pg. 5- 282
- [F6] Ferraris, P., Fratta, A., Vagati, A., Villata, F., About the vector control of induction motors for special applications without speed sensor. Proc. Evolution and modern Aspects of Induction machines, 1986, Torino, pg. 444
- [F7] Fetz, J., Horstmann, D., Comparison of different field oriented control methods for an induction motor fed by a PWM controlled inverter. Proc. EPE 89, Aachen, pg. 1079
- [F8] Fieger, K., Über die Anwendung der Abtasttheorie auf nichtlineare Regelkreise mit nichtstetigen Stellgliedern. Diss. TU Braunschweig 1967
- [F9] Fieger, K.: Zum dynamischen Verhalten thyristorgespeister Gleichstrom-Regelantriebe. ETZ-A, 1969, pg. 311

- [F10] Fieger, K., Middel, J., Vereinfachte Behandlung linearer Abtastregelkreise. Regelungstechnik 1967, pg. 445
- [F11] Finlayson, P.T., Washburn, D.C., Cycloconverter controlled synchronous machine for load compensation on AC power systems. IEEE Trans. Ind. Appl. 1974, pg. 806
- [F12] Fischer, J., Digitale Fahrkurvenrechner für Positionieranlagen. AEG Mitteilungen 1976, pg. 269
- [F13] Fischer, R., Geissing, H., Halbleiterstromrichter in kreisstromfreier Gegenparallelschaltung für Umkehrantriebe. Siemens Zeitschrift 1964, pg. 240
- [F14] Flöte, R., Velte, H., Die thyristorgespeiste Fördermaschine in Feldumkehrschatzung. AEG Mitteilungen 1972, pg. 254
- [F15] Flöter, W., Ripperger, H., Die TRANSVEKTOR-Regelung für den feldorientierten Betrieb einer Asynchronmaschine. Siemens Zeitschrift 1971, pg. 761
- [F16] Flügel, W., Drehzahlregelung der spannungsumrichtergespeisten Asynchronmaschine im Grund- und Feldschwächbereich. ETZ-Archiv 1982, pg. 143
- [F17] Foerst, R.: Der Löschwinkelregelkreis einer Hochspannungs-Gleichstrom-Übertragung mit symmetrischer Drehspannung. Diss. TH Darmstadt 1967
- [F18] Fossard, A.J., Clique, M., A general model for switched DC-DC converters including filters. 2. IFAC-Symp. Control in Power Electronics and Electrical Drives, Düsseldorf 1977, pg. 117
- [F19] Frankl, G., Control modes for a variable speed drive with a converter- fed synchronous machine. Proc. EPE 91, Firenze, pg. 4- 592
- [F20] Fratta, A., Vagati, A., Villata, F., Vector control of induction motors without shaft transducers. Proc. IEEE- PESC 88, Kyoto, pg.839
- [F21] Fratta, A., Grassi, R., Vagati, A., High performance spindle drives adopting IPM synchronous machines; theoretical goals and a practical solution. Proc. EPE 91, Firenze, pg. 3- 476
- [F22] Fratta, A., Vagati, A., Villata, F., Extending the voltage saturated performance of DC brushless drive. Proc. EPE 91, Firenze, pg. 4- 134
- [F23] Fratta, A., Vagati, A., Villata, F., On the evolution of AC machines for spindle drive applications. IEEE Trans. Ind. Appl. 1992. pg. 1081
- [F24] Freund, E., Hoyer, H., Das Prinzip nichtlinearer Systemtentkopplung mit der Anwendung auf Industrieroboter. Regelungstechnik 1980 pg. 80
- [F25] Frick, A., von Westerholt, E., de Fornel, B., Nonlinear control of induction motors via input- output decoupling. Europ. Trans. on Electr. Power Engng. 1994, pg. 261
- [F26] Fritzsche, W., Genaue und schnelle Regelungen von Drehzahlen durch digitale Methoden. AEG Mitteilungen 1960, pg. 419
- [F27] Fujimaki, T., Ohniwa, K., Miyashita, O., Simulation of the chopper controlled DC series motor. 2. IFAC-Symp. Control in Power Electronics and Electrical Drives, Düsseldorf 1977, pg. 609
- [F28] Fujita, K., Sado, K., Instantaneous speed detection with parameter identification for AC servo systems. IEEE Trans. Ind. Appl. 1992. pg. 864
- [F29] Fukunda, S., Itoh, Y., Nii, A., A microprocessor-controlled speed regulator for commutator-less motor drives. Int. Power Electr. Conference, Tokyo 1983, pg. 938

- [F30] Furuhashi, T., Sangwongwanich, S., Okuma, S., A position- and velocity- sensorless control for brushless DC motors using an adaptive sliding mode observer. IEEE Trans. Ind. Electr. 1992, pg. 89
- [G1] Gabriel, R., Leonhard, W., Nordby, C., Microprocessor control of induction motors employing field coordinates. 2. Int. Conf. on Electrical Variable Speed Drives, IEE London 1979, pg. 146
- [G2] Gabriel, R., Leonhard, W., Nordby, C., Regelung der stromrichtergespeistenen Drehstrom-Asynchronmaschine mit einem Mikrorechner. Regelungstechnik 1979, pg. 379
- [G3] Gabriel, R., Leonhard, W., Nordby, C., Field orientated control of a standard AC motor using microprocessors. IEEE Trans. Ind. Appl. 1980, pg. 186
- [G4] Gabriel, R., Leonhard, W., Nordby, C., Microprocessor control of the converter-fed induction motor. Process Automation 1980, pg. 35
- [G5] Gabriel, R., Feldorientierte Regelung einer Asynchronmaschine mit einem Mikrorechner. Diss. TU Braunschweig 1982
- [G6] Gabriel, R., Leonhard, W., Microprocessor control of induction motor. Int. Semiconductor Power Converter Conf. 1982, pg. 385
- [G7] Garces, L.J., Ein Verfahren zur Parameteranpassung bei der Drehzahlregelung der umrichtergespeistenen Käfigläufermaschine. Diss. TH Darmstadt 1978
- [G8] Garces, L.J., Parameter adaption for the speed controlled static AC drive with squirrel cage induction motor. IEEE Trans. Ind. Appl. 1980, pg. 173
- [G9] Garcia- Cerrada, A., Taufiq, J.A., Convergence of rotor flux estimation in field oriented control. Proc. IEE-Power Electronics and Variable Speed Drives, London 1988, pg. 291
- [G10] Garcia, G.O., Stephan, R.M., Watanabe, E.H. Comparing the indirect field-oriented control with a scalar method. Proc. IECON 91, Kobe, pg. 475
- [G11] Gastli, A., Matsui, N., Stator flux controlled V/f PWM inverter with identification of IM parameters. IEEE Trans. Ind. Electr. 1992, pg. 334
- [G12] Gekeler, M., Jötten, R., Control device for a pulsed 3-level inverter feeding a three-phase machine implemented by EPROMS and MSI digital circuitry. Microelectronics in Power Electronics and Electrical Drives, Darmstadt 1982, ETG-Fachberichte 11, pg. 207
- [G13] Gelman, V., High performance current source inverter drive. Int. Semiconductor Power Conv. Conf. 1982, pg. 266
- [G14] Gelot, N.S., Alsina, P.J., A discrete model of induction motors for real- time control applications. IEEE Trans. Ind. Electr. 1993, pg. 317
- [G15] Georgiou, G., Le Piouffe, B., Nonlinear speed control of a synchronous servomotor with robustness. Proc. EPE 91, Firenze, pg. 3- 42
- [G16] Gerecke, E., New methods of power control with thyristors. Survey, 3. IFAC Congress London 1966
- [G17] Geschke, B., Haspelanlage einer Warmband-Kontistraße. Siemens Zeitschrift 1973, Beiheft Antriebstechnik und Prozeßautomatisierung in Hütten- und Walzwerken, pg. 97
- [G18] Geyer, W., Regelungstechnische Probleme bei der Regelung eines Gleichstrommotors bei gleichzeitigem Eingriff in Anker- und Feldstromkreis. In Energieelektronik und geregelte elektrische Antriebe VDE-Buchreihe, Vol. 11 1962, pg. 472
- [G19] Geyer, W., Ströle, D., Entwicklungstendenzen bei geregelten elektrischen Antrieben. Siemens Zeitschrift 1965, pg. 490

- [G20] Geyer, W., Waller, S., Direktführung numerisch gesteuerter Werkzeugmaschinen mit einem Fertigungsleitrechner. Siemens Zeitschrift 1970, Beiheft Numerische Steuerungen, pg. 11
- [G21] Gewecke, J., Untersynchrone Drehstrom-Bremsschaltungen für Hebezeuge. Siemens Zeitschrift 1929, pg. 9
- [G22] Götz, G., Grumbrecht, P., Umrichtergespeiste Synchronmaschinen. AEG Mitteilungen 1973, pg. 141
- [G23] Gosbell, V.J., Dalton, P.M., Current control of induction motors at low speed. IEEE Trans. Ind. Appl. 1992. pg. 482
- [G24] Grieve, D.W., Cross, D M., Recent developments in the design and application of large, high performance cycloconverter drive systems. Proc. IEE-Power Electronics and Variable Speed Drives, London 1988, pg. 309
- [G25] Grötzbach, M., Analyse von Gleichstromstellerschaltungen im lückenden und nichtlückenden Betrieb. ETZ-Archiv, 1979, pg. 29
- [G26] Groß , H., Riedel, H., Angepaßte Vorschubantriebe für Werkzeugmaschinen. Siemens Zeitschrift 1976, pg. 30
- [G27] Grotstollen, H., Zusammenhänge und Kennwerte bei der Bemessung beschleunigungsoptimaler Antriebe. ETZ-A, 1974, pg. 663
- [G28] Grotstollen, H., Comparison of speed controlled DC drives with and without subordinate current control. 2. IFAC Symp., Control in Power Electronics and Electrical Drives, Dusseldorf 1977, pg. 583
- [G29] Grotstollen, H., Pfaff, G., Bürstenloser Drehstrom-Servoantrieb mit Erregung durch Dauermagnete. ETZ 1979, pg. 1382
- [G30] Gruber, M., Möller-Nehring, P., Digitaler Geschwindigkeitsregler auf Mikroprozessorbasis im System MODULPAC C. Siemens Energietechnik 1979, pg. 117
- [G31] Güthlein, H., Die neue elektrische Lokomotive 120 der Deutschen Bundesbahn in Drehstrom-Antriebstechnik. Elektrische Bahnen, 1979
- [G32] Gumaste, V., Slement, G.R., Steady state analysis of a permanent magnet synchronous motor drive with voltage-fed inverter. IEEE Ind. Appl. Ann. Meet. Conf. Rec. 1980, pg. 618
- [G33] Gutt, H.J., Wanderfeldmotoren im Vergleich zu Drehfeldmaschinen herkömmlicher Bauart. ETZ-A, 1971, pg. 342
- [G34] Gutt, H.J., Scholl, F.D., Investigations on a new electrical drive concept for the vertical axis of a selective compliance arm robot. Proc. IEE- Power Electronics and Variable Speed Drives, London 1988, pg. 257
- [G35] Gutzwiller, R., Methode der digitalen Simulation von Stromrichterschaltungen am Beispiel des Gleichstromstellers. ETZ-A, 1978, pg. 8
- [H1] Habetler, T.G., A space vector- based rectifier regulator for AC/DC/AC converters. Proc. EPE 91, Firenze, pg. 2- 101
- [H2] Habetler, T.G., Divan, D.M., Control strategies for direct torque control using discrete pulse modulation. IEEE Trans. Ind. Appl. 1991, pg. 893
- [H3] Habetler, T.G., Profumo, F., Pastorelli, M., Tolbert, L.M., Direct torque control of induction machines using space vector modulation. IEEE Trans. Ind. Appl. 1992, pg. 1045
- [H4] Haböck, A., Speisung von Synchronmaschinen über Umrichter mit eingeprägtem Strom im Zwischenkreis. VDE Fachtagung Elektronik 1969, pg. 163

- [H5] Haböck, A., Köllensperger, D., Stand und Entwicklung des Stromrichtermotors. Siemens Zeitschrift 1971, pg. 177
- [H6] Hackstein, D., Time optimal 3-dimensional trajectory control. 3. IFAC Symp. Control in Power Electronics and Electrical Drives, Lausanne 1983, pg. 553
- [H7] Härer, H., Horn, U., Investigation of a doubly- fed induction generator using a simple cycloconverter. Proc. EPE 91, Firenze, pg. 2- 254
- [H8] Halász, S., Optimal control of voltage source inverters supplying induction motors. 2. IFAC Symp., Control in Power Electronics and Electrical Drives, Düsseldorf 1977, pg. 379
- [H9] Hannakam, L., Übergangsverhalten des Drehstrom-Schleifringläufermotors. Regelungstechnik 1959, pg. 393, 421
- [H10] Hannakam, L., Digitales Universalprogramm für Schaltvorgänge an Drehstrom-Asynchronmaschinen. ETZ-A, 1961, pg. 493
- [H11] Hapiot, J.C., Pietrzak-David, M., Bach, J.L., Regulation de vitesse d'une machine asynchrone alimentée en courant sans capteur de vitesse. Conumel 83, Toulouse, pg. IV-12
- [H12] Harashima, F., Yanase, T., State space analysis of AC motors fed by thyristor inverters. 1. IFAC Symp., Control in Power Electronics and Electrical Drives, Düsseldorf 1974, vol. 1, pg. 149
- [H13] Harashima, F., Naitoh, H., Dynamic performance of converter-fed synchronous motors. 2. IFAC-Symp. Control in Power Electronics and Electrical Drives, Düsseldorf 1977, pg. 369
- [H14] Harashima, F., Hayashi, H., Dynamic performance of current source inverter-fed induction motors. IEEE Ind. Appl. Ann. Meet. Conf. Rec. 1978, pg. 904
- [H15] Harashima, F., Naitoh, H., Haneyoshi, T., Dynamic performance of a self controlled synchronous motor fed by current source inverters. IEEE Trans. Ind. Appl. 1979, pg. 36
- [H16] Harley, R.G., Wishart, M.T., Diana, G., Teaching field oriented control of VSI and CSI fed asynchronous and permanent magnet synchronous machines using a programmable high speed controller. Proc. EPE 91, Firenze, pg. 2- 556
- [H17] Harms, K., Beiträge zur Regelung der Drehstrom-Asynchronmaschine unter Berücksichtigung veränderlicher Maschinenparameter. Diss. TU Braunschweig 1988
- [H18] Hars, W., Siebenphasiger Synchronmotor mit Pulswechselrichter in hochintegrierter Bauweise. ETG Fachberichte Nr. 22, 1988, VDE Verlag Berlin, Offenbach
- [H19] Hasse, K., Zur Dynamik drehzahlgeregelter Antriebe mit stromrichtertergespeisten Asynchron-Kurzschlußläufermaschinen. Diss. TH Darmstadt 1969
- [H20] Hasse, K., Drehzahlregelverfahren für schnelle Umrichterantriebe mit stromrichtertergespeisten Asynchron-Kurzschlußläufermotoren. Regelungstechnik 1972, pg. 60
- [H21] Hattori, M., Ishikawa, T., Taniguchi, M., Ohnishi, T., Kurata, Y., Kamiyama, K., Imagawa, K., Takahashi, J., Sukegawa, T., Saito, K.: An experience with cycloconverter- fed IM drives for a modern tandem cold mill. Proc. EPE 91, Firenze, pg. 2- 260
- [H22] Heinemann, G., Comparison of several control schemes for AC induction motors under steady state and dynamic conditions. Proc. EPE 89, Aachen, pg. 843
- [H23] Heinemann, G., Selbsteinstellende, feldorientierte Regelung für einen asynchronen Drehstromantrieb. Diss. TU Braunschweig 1992

- [H24] Heinemann, G., Leonhard, W., Self-tuning field-orientated control of an induction motor drive. *Intl. Power Electr. Conf.* 90, Tokyo, pg. 465
- [H25] Heinle, G., The structure of optimised pulse pattern. *Proc. EPE 93*, Brighton, pg. 5- 378
- [H26] Heinze, K., Tappeiner, H., Weibelzahl, M., Pulswechselrichter zur Drehzahlsteuerung von Asynchronmaschinen. *Siemens Zeitschrift* 1971, pg. 154
- [H27] Heintze, K., Wagner, R., Elektronische Gleichstromsteller zur Geschwindigkeitssteuerung von aus Fahrleitung gespeisten Gleichstrom-Triebfahrzeugen. *ETZ-A*, 1966, pg. 165
- [H28] Hengsberger, A., Putz, U., Vettler, L., Thyristor-Stromrichter für Bahnmotoren. *AEG Mitteilungen* 1964, pg. 435
- [H29] Henneberger, G., Dynamic behaviour and current control methods of brushless DC motors. *Proc. EPE 89*, Aachen, pg. 1531
- [H30] Henneberger, G., Brunsbach, B. J., Klepsch, Th., Field oriented control of synchronous and asynchronous drives without mechanical sensors using a Kalman-filter. *Proc. EPE 91*, Firenze, pg. 3- 664
- [H31] Henneberger, G., Lutter, T., Brushless DC-motor with digital state controller. *Proc. EPE 91*, Firenze, pg. 4- 104
- [H32] Hertlein, K., Entwicklungstendenzen bei Banddickenregelungen für Kaltwalzwerke. *AEG Mitteilungen* 1979, pg. 38
- [H33] Heumann, K., Jordan, K.G., Das Verhalten des Käfigläufermotors bei veränderlicher Speisefrequenz und Stromregelung. *AEG Mitteilungen* 1964, pg. 107
- [H34] Hill, W.A., Ho, E.Y.Y., Neuzil, I.J., Dynamic behavior of cycloconverter systems. *IEEE Trans. Ind. Appl.* 1991, pg. 750
- [H35] Hillenbrand, F., A method for determining the speed and rotor flux of the asynchronous machine by measuring the terminal quantities only. *3. IFAC Symp. Control in Power Electronics and Electrical Drives Lausanne* 1983, pg. 55
- [H36] Hofer, K., Digital speed control by adaptive computation of firing angle using microprocessors. *Microelectronics in Power Electronics and Electrical Drives*, Darmstadt 1982, *ETG-Fachberichte* 11, pg. 295
- [H37] Hoffmann, A H., Brushless synchronous motors for large industrial drives. *IEEE Trans. Ind. Gen. Appl.* 1969, pg. 158
- [H38] Hoffmann, E., Schäufele, R., Einsatz einer regelbaren Speicherpumpe in der Netzregelung, *Elektrizitätswirtschaft*, Heft 25, 1993
- [H39] Hofmann, W., A suboptimal predictive current controller for VSI-PWM inverters. *Proc. EPE 91*, Firenze, pg. 3- 316
- [H40] Hofstetter, M., Umrichter mit quasiresonant gepulstem Gleichspannungszwischenkreis für ein Drehstromantriebssystem. *Archiv für Elektrotechnik*, 1993, pg. 309
- [H41] Hoft, R.G., Casteel, J.B., Power electronic circuit analysis techniques, survey. *2. IFAC Symp., Control in Power Electronics and Electrical Drives*, Düsseldorf 1977, pg. 987
- [H42] Hoft, R.G., Singh, D., Microcomputer-controlled single phase cycloconverter. *IEEE Trans. Ind. Electr. and Contr. Instr.* 1977, pg. 226
- [H43] Holl, E., Neumann, G., Piepenbreier, B., Tölle, H.-J., Water-cooled inverter for synchronous and asynchronous electric vehicle drives. *Proc. EPE 93*, Brighton, pg. 5- 289

- [H44] Holliday, D., Green, T.C., Williams, B.W., On- line parameter measurement of induction machines. Proc. IECON 93, Maui, pg. 992
- [H45] Holtz, J., Ein neues Zündsteuerverfahren für Stromrichter am schwachen Netz. ETZ-A, 1970, pg. 345
- [H46] Holtz, J., Kraftkomponenten und deren betriebliche Steuerung beim eisenlosen Synchronlinearmotor. ETZ-A, 1975, pg. 396
- [H47] Holtz, J., Schwellenberg, U., A new fast-response current control scheme for line controlled converters. Int. Semiconductor Power Converter Conf. 1982, pg. 175
- [H48] Holtz, J., Stadtfeld, S., A predictive controller for the stator current vector of AC-machines fed from a switched voltage source. Int. Power Electric Conference, Tokyo 1983, pg. 1665
- [H49] Holtz, J., Bube, E., Field- oriented asynchronous pulse- width modulation for high- performance AC machine drives operating at low switching frequency. IEEE Trans. Ind. Appl. 1991, pg. 574
- [H50] Holtz, J., Thimm, T., Identification of the machine parameters in a vector-controlled induction motor drive. IEEE Trans. Ind. Appl. 1991, pg. 1111
- [H51] Holtz, J., Pulsewidth modulation— a survey. IEEE Trans. Ind. Electr. 1992, pg. 410
- [H52] Holtz, J., Beyer, B., Optimal synchronous pulse width modulation with a trajectory- tracking scheme for high dynamic performance. IEEE Trans. Ind. Appl. 1993, pg. 1098
- [H53] Holtz, J., Speed estimation and sensorless control of AC drives. Proc. IECON 93, Maui, pg. 649
- [H54] Holtz, J., Beyer, B., Optimal pulsewidth modulation for AC servos and low- cost industrial drives. IEEE Trans. Ind. Appl. 1994, pg. 1039
- [H55] Holtz, J., Beyer, B., The trajectory tracking approach— a new method for minimum distortion PWM in dynamic high- power drives. IEEE Trans. Ind. Appl. 1994, pg. 1048
- [H56] Hombu, M., Ueda, S., Ueda, A., A current source inverter with sinusoidal inputs and outputs. IEEE Trans. Ind. Appl. 1987, pg. 247
- [H57] Hombu, M., Futami, M., Miyazaki, S., Kubota, Y., Bando, A., Azusawa, N., Harmonics analysis on a slip-power recovery system fed by a DC link GTO converter. Proc. EPE 95, Sevilla, pg. 3- 239
- [H58] Hori, Y., Umeno, T., Uchida, T., Konno, Y., An instantaneous speed observer for high performance control of DC servomotor using DSP and low resolution shaft encoder. Proc. EPE 91, Firenze, pg. 3- 647
- [H59] Hosono, I., Katsuki, K., Yano, M., Static converter starting of large synchronous motors. IEEE Ind. Appl. Ann. Meet. Conf. Rec. 1976, pg. 536
- [H60] Huang, H., Davat, B., Lajoie- Mazenc, M., Study of control strategies and regulation in cycloconverter- fed synchronous machines. Proc. EPE 89, Aachen, pg. 871
- [H61] Huang, L., Tadokoro, Y., Matsuse, K., Deadbeat flux level control of direct- field- oriented high-horsepower induction motor using adaptive rotor flux observer. IEEE Trans. Ind. Appl. 1994, pg. 954
- [H62] Hugel, J., Die Berechnung von Stromrichter-Regelkreisen. AfE 1970, pg. 224

- [H63] Hussels, P., Mehne, M., Hentschel, F., Synthesis of cycloconverter and current source inverter—Presentation of a new control strategy. Proc. EPE 93, Brighton, pg. 5- 33
- [I1] Inaba, H., Hirasawa, K., Ando, T., Hombu, M., Nakazato, M., Development of a high- speed elevator controlled by current source inverter system with sinusoidal input and output. IEEE Trans. Ind. Appl. 1992, pg. 893
- [I2] Irisa, T., Takata, S., Ueda, R., Sonoda, T., Mochizuki, T., A novel approach on parameter self- tuning method in AC servo systems. 3. IFAC Symp. Control in Power Electronics and Electrical Drives, Lausanne 1983, pg. 41
- [I3] Iwakane, I., Inokuchi, H., Kai, T., Hirai, J., AC servo motor drive for precise positioning control. Int. Power Electr. Conf. Tokyo 1983, pg. 1453
- [I4] Iwasaki, M., Matsui, N., Robust speed control of IM with torque feedforward control. IEEE Trans. Ind. Electr. 1993, pg. 553
- [I5] Iwens, R.P., Lee, F.C., Triner, J.E., Discrete time domain modelling and analysis of DC-DC converters with continuous and discontinuous inductor current. 2. IFAC Symp., Control in Power Electronics and Electrical Drives, Düsseldorf 1977, pg. 87
- [J1] Jacovides, L.J., Matuoka, M.F., Shimer, D.W., A cycloconverter synchronous motor drive for traction applications. IEEE Ind. Appl. Ann. Meet. Conf. Rec. 1980, pg. 549
- [J2] Jakubowicz, A., Nougaret, M., Perret, R., Simplified model and closed loop control of a commutatorless DC motor. IEEE Ind. Appl. Ann. Meet. Conf. Rec. 1979, pg. 857
- [J3] Jansen, P.L., Lorenz, R.D., Novotny, D.W., Observer- based direct field orientation: Analysis and comparison of alternative methods. IEEE Trans. Ind. Appl. 1994, pg. 945
- [J4] Jansen, P.L., Thompson, C.O., Lorenz, R.D., High-quality torque control at zero and very high speed operation. IEEE IAS Magazine, 1995, No.4, pg. 7
- [J5] Jayne, M.G., Bowes, S.R., Bird, B.M., Developments in sinusoidal PWM-inverters. 2. IFAC Symp., Control in Power Electronics and Electrical Drives, Düsseldorf 1977, pg. 145
- [J6] Jenni, F., Zwicky, R., Speed and flux control of a pulse width modulated current source inverter drive. Proc. IEE-Power Electronics and Variable Speed Drives, London 1988, pg. 374
- [J7] Jentsch, W., Mathematisches Modell der Asynchronmaschine für die digitale Simulation des dynamischen Verhaltens. Simposio sulle macchine elettriche ed i convertitori statici di frequenza, Napoli 1971
- [J8] Jezernik, K., Cuk, B., Harnik, J., Variable structure field oriented control of an induction motor drive. Proc. EPE 91, Firenze, pg. 2- 161
- [J9] Ji, J.K., Lee, D.C., Sul, S.K., LQG based speed controller for torsional vibration suppression in two mass motor drive system. Proc. IECON 93, Maui, pg. 1157
- [J10] Jönsson, R., Method and apparatus for controlling an AC induction motor by indirect measurement of the airgap voltage, PCT Patent Application No. PCT/SE 91/00086, International filing date 8.2.91. European Patent 0515469, Issued 1994. US- Patent 5 294 876, Issued 1994
- [J11] Jönsson, R., Leonhard, W., Control of an induction motor without a mechanical sensor, based on the principle of "natural field orientation" (NFO). Proc. IPED Yokohama, 1995, pg. 303

- [J12] Jötten, R., French patent 1.331.612, 1961
- [J13] Jötten, R, Regelungstechnische Probleme bei elastischer Verbindung zwischen Motor und Arbeitsmaschine. In Energietechnik und geregelte elektrische Antriebe, VDE- Buchreihe, Vol. 11, 1962, pg. 446
- [J14] Jötten, R., Die Berechnung einfacher und mehrfach integrierender Regelkreise der Antriebstechnik. AEG Mitteilungen 1962, pg. 219
- [J15] Jötten, R., Signalverarbeitung für die Regelung umrichtergespeister Drehfeldmaschinen. 1. IFAC Symp., Control in Power Electronics and Electrical Drives, Düsseldorf 1974, vol. 1, pg. 681
- [J16] Jötten, R., Mäder, G., Control methods for good dynamic performance induction motor drives based on current and voltage as measured quantities. Int. Semiconductor Power Converter Conf. 1982, pg. 397
- [J17] Jötten, R, Zimmermann, P., Sub- and super-synchronous cascade with current source inverter. 3. IFAC-Symp. Control in Power Electronics and Electrical Drives, Lausanne 1983, pg. 337
- [J18] Jötten, R., Kehl, C., A fast space- vector control for a three- level voltage source inverter. Proc. EPE 91, Firenze, pg. 2- 70
- [J19] Jones, C.I., van Nice, R., Frequenzgeber und -teiler mit veränderlicher Frequenz. German Patent 1.100.084, 1958
- [J20] Jones, R., Wymeersch, W., Lataire, Ph., Vector controlled drives in a steel processing application. EPE 93, Brighton, pg. 5- 508
- [K1] Kaczmarek, B., Mayeur, X., Legros, W., Capieaux, Ph., Commande optimisée par microprocesseurs d'une machine synchrone autopilotée. Conumel 83, Toulouse, pg. IV-19
- [K2] Kamiyama, K., Azusawa, N., Miyahara, Y., Ohmae, T., Kivisawa, T., Microprocessorcontrolled fast response speed regulator for thyristorised reversible regenerative DC-motor drives. IEEE Ind. Electr. and Control Instr. Ann. Meet. Rec. 1978, pg. 216
- [K3] Kamiyama, K., Nagasaki, H., Saito, K., Matsuka, S., Shiraishi, H., Ohmae, T., Microprocessor-based high-speed internal controllers for industrial drives. Microelectronics in Power Electronics and Electrical Drives, Darmstadt 1982, ETG-Fachberichte 11
- [K4] Kanzaki, T., Yanagida, K., Yasouka, I., Inverter control system for driving induction-motors in rapid transit cars using high-powered GTO thyristors. Int. Semiconductor Power Converter Conf. 1982, pg. 145
- [K5] Kao, Y.T., Liu, C.H., Analysis and design of microprocessor- based vector-controlled induction motor drives. IEEE Trans. Ind. Electr. 1992, pg. 46
- [K6] Kappius, F., Zur Drehzahlsteuerung von Drehstrom-Kurzschlußläufertmotoren mit einer gleichstromgespeisten Stromrichteranordnung in sechspulsiger Mittelpunktschaltung. Diss. TH Braunschweig 1965
- [K7] Kastner, G., Pfaff, G., Sack, L., Design and performance of an acceleration drive with permanent magnets. IEEE Trans. Ind. Appl. 1991, pg . 908
- [K8] Kawamura, A., Yokoyama, T., Comparison of five control methods for digital feedback controlled PWM inverters. Proc. EPE 91, Firenze, pg. 2- 35
- [K9] Kazmierkowski, M.P., Köpke, H.-J., Comparison of dynamic behaviour of frequency converter fed induction machine drives. 3. IFAC Symp. Control in Power Electronics and Electrical Drives Lausanne 1983, pg. 313

- [K10] Kazerani, M., Ooi, B.T., Direct AC/AC matrix converter based on three- phase voltage- source converter modules. Proc. IECON 93, Maui, pg.812
- [K11] Kazmierkowski, M.P., Kasprowicz, A., Improved torque and flux vector control of PWM inverter- fed induction motor drive. Proc. EPE 93, Brighton, pg.5- 115
- [K12] Kazuno, H., A wide range speed control of an induction motor with static Scherbius and Kramer systems. J. Electr. Engg. Japan 1969, pg. 10
- [K13] Kempkes, J., Sattler, Ph.K., Comparison of true running at different concepts of controlling brushless DC motors. Proc. EPE 93, Brighton, pg.5- 15
- [K14] Kennel, R., Schröder, D., Predictive control strategy for converters. 3. IFAC Symp. Control in Power Electronics and Electrical Drives, Lausanne 1983, pg. 415
- [K15] Kerkman, R.J., Rowan, T.M., Leggate, D., Indirect field- oriented control of an induction motor in the field- weakening region. IEEE Trans. Ind. Appl. 1992, pg. 850
- [K16] Kerkman, R.J., Leggate, D., Seibel, B.J., Rowan, T.M., An overmodulation strategy for PWM voltage inverters. Proc. IECON 93, Maui, pg. 1215
- [K17] Kessler, C., Über die Vorausberechnung optimal abgestimmter Regelkreise. Regelungstechnik 1954: pg. 274, 1955: pg. 11, 40
- [K18] Kessler, C., Das symmetrische Optimum. Regelungstechnik 1958, pg. 395, 432
- [K19] Kessler, C., Meinhardt, W., Neuffer, I., Rube, G., Die Gleichstrom- Fördemaschine mit Siemens-TRANSIDYN-Regelung. Siemens Zeitschrift 1958, pg. 555
- [K20] Kessler, C., Ein Beitrag zur Theorie mehrschleifiger Regelungen. Regelungstechnik 1960, pg. 261
- [K21] Kessler, G., Das zeitliche Verhalten einer kontinuierlichen elastischen Bahn zwischen aufeinander folgenden Walzenpaaren. Regelungstechnik 1960: pg. 436, 1961: pg. 154
- [K22] Kessler, G., Digitale Regelung der Relation zweier Drehzahlen. ETZ-A, 1961, pg. 574
- [K23] Kessler, G., Digitale Regelung der Drehzahl und der Relation zweier Drehzahlen. In Digitale Signalverarbeitung in der Regelungstechnik, VDE- Buchreihe, Vol. 8, 1962, pg. 152
- [K24] Kessler, G., Electrical drive systems for paper-, rubber- and plastics-industries, survey. IFAC Conference, Brussels 1976
- [K25] Khambadkone, A., Holtz, J., Low switching frequency high power inverter drive based on field oriented pulselwidth modulation. Proc. EPE 91, Firenze, pg. 4- 672
- [K26] Khanniche, M.S., Belaroussi, M., Sethuraman, S.K., An algorithm for generating optimised PWM for real time micro control applications. Proc. IEE-Power Electronics and Variable Speed Drives, London 1988, pg. 386
- [K27] Kiel, E., Schumacher, W., Ehrenberg, J., Letas, H. H., Schrader- Hausmann, U., High performance digital control of uninterruptible power supply (UPS) using an application specific integrated circuit (ASIC). Proc. EPE 91, Firenze, pg. 3- 174
- [K28] Kiel, E., Schumacher, W., Gabriel, R., PWM Gate- array for AC drives. Proc. EPE 87, Grenoble, pg. 653

- [K29] Kiel, E., Schumacher, Vecon; A high- performance single- chip- servovontroller for AC drives. IPEC 95 Yokohama, 1995, pg. 1289
- [K30] Kiel, E., Anwendungsspezifische Schaltkreise in der Drehstrom- Antriebstechnik. Diss. TU Braunschweig, 1994
- [K31] Kielgas, H., Nill, R., Converter propulsion systems with three phase induction motors for electrical traction. Int. Semiconductor Power Converter Conf. Rec. 1977, pg. 304
- [K32] Kim, G.S., Ha, I.J., Ko, M.S., Control of induction motors for both high dynamic performance and high power efficiency. IEEE Trans. Ind. Electr. 1992, pg. 323
- [K33] Kim, J.M.S., Dewan, S.B., closed loop voltage regulation of dual converters with circulating- current mode, used in four- quadrant DC magnet power supplies. IEEE Trans. Ind. Appl. 1991, pg . 1026
- [K34] Kim, Y.R., Sul, S.K., Park, M.H., Speed sensorless vector control of induction motor using extended Kalman filter. IEEE Trans. Ind. Appl. 1994, pg. 1225
- [K35] Kinniment, D.J., Acarnley, P.P., Jack, A.G., An integrated circuit controller for brushless DC drives. Proc. EPE 91, Firenze, pg. 4- 111
- [K36] Kinniment, D.J., Kappos, E., Acarnley, P.P., Experience of the use of ASIC methods in a motor control application. Proc. EPE 93, Brighton, pg. 458
- [K37] Klaes, N.R., Identifikationsverfahren für die betriebspunktabh"-angigen Parameter einer wechselrichtergespeisten Induktionsmaschine. Diss. Univ. Bochum, 1992
- [K38] Klaes, N.R., On- line tuning of the rotor resistance in an inverter- fed induction machine with direct- self- control. Europ. Trans. on Electr. Power Engng. 1994, pg. 5
- [K39] Klaassen, H., Selbsteinstellende, feldorientierte Regelung einer Asynchronmaschine und geberlose Drehzahlregelung, Diss. TU Braunschweig, 1996
- [K40] Klautscheck, H., Das Verhalten der Induktionsmaschine bei Speisung über Strom-Zwischenkreisumrichter. ETZ 1974, pg. 283
- [K41] Klautscheck, H., Asynchronmaschinenantriebe mit Strom-Zwischenkreisumrichtern. Siemens Zeitschrift 1976, pg. 23
- [K42] Klein, G., Stebel, H., Steuerung und Regelung von Hochlaufscheren und -sägen. BBC Nachrichten 1964, pg. 200
- [K43] Kleinsorge, N., Putz, U., Stemmler, H., Large adjustable speed AC drives. Proc. EPE 87, Grenoble, pg. 491
- [K44] Kliman, G.B., Plunkett, A.B., Development of a modulation strategy for a PWM inverter drive. IEEE Trans. Ind. Appl. 1979, pg. 72
- [K45] Klug, R.- D., Effects and correction of switching dead times in 3- phase PWM inverter drives. Proc. EPE 89, Aachen, pg. 1261
- [K46] Koch, W.H., Thyristor controlled pulsating field reluctance motor system. Electric Machines and Electromechanics 1977, pg. 201
- [K47] Köllensperger, D., Die Synchronmaschine als selbstgesteuerter Stromrichtermotor. Siemens Zeitschrift 1967, pg. 830
- [K48] Körber, J., Teich, W., Lokomotiven mit Drehstromantriebstechnik zur IVA 79, Beispiele eines breiten Anwendungsgebietes. Elektrische Bahnen 1979, pg. 151
- [K49] Kolar, J.W., Ertl, H., Zach, F.C., Influence of the modulation method on the conduction and switching losses of a PWM converter system. IEEE Trans. Ind. Appl. 1991, pg. 1063

- [K50] Konhäuser, W., Naunin, D., Digital control of a subsynchronous converter cascade by microcomputers. Microelectronics in Power Electronics and Electrical Drives, Darmstadt 1982, ETG-Fachberichte 11, pg. 369
- [K51] Konishi, T., Kamiyama, K., Miyahara, Y., Ohmae, T., Sugimoto, N., An application technology of microprocessor to adjustable speed motor drives. IEEE Ind. Appl., Ann. Meet. Conf. Rec. 1978, pg. 669
- [K52] Konishi, T., Kamiyama, K., Ohmae, T., A performance analysis of microprocessor-based control systems applied to adjustable speed motor drives. IEEE Trans. Ind. Appl. 1980, pg. 378
- [K53] Koopmann, K., Meersmann, H., Restendloses Aufteilen von Walzgut durch rotierende Scheren. Siemens Zeitschrift 1964, pg. 218
- [K54] Korb, F., Die Gefäßfolgesteuerung, ein Mittel zur Verminderung der Blindleistung von Stromrichteranlagen. ETZ-A, 1958, pg. 273
- [K55] Korb, F., Drehzahlgeregelter Positionierantrieb. BBC Nachrichten 1968, pg. 102
- [K56] Koseki, T., Morizane, T., Ohsaki, H., Masada, E., Novel linear induction drive: control scheme and converters. Proc. EPE 91, Firenze, pg. 1- 481
- [K57] Koyama, M., Yano, M., Two degrees of freedom speed controller using reference system model for motor drives. Proc. EPE 91, Firenze, pg. 3- 60
- [K58] Kranenburg, R., Klaassen, H., Torri, G., Gatti, E., High performance induction machine drive for a flying shear, Proc. EPE 95, Sevilla, pg. 3- 481
- [K59] Krause, J., Zur Regelgüte von Thyristorstromrichter-Umkehrantrieben. Messen, Steuern, Regeln 1969, pg. 430
- [K60] Krause, P.C., Method of multiple reference frames applied to the analysis of symmetrical machinery. IEEE-PAS, 1968, pg. 218
- [K61] Krishnan, K., Ramaswami, B., A thyristorised four-quadrant DC motor drive. 1. IFAC Symp. Control in Power Electronics and Electrical Drives, Düsseldorf 1974, vol. 2, pg. 113
- [K62] Krishnan, R., Stefanovic, V.R., Control principles in current source induction motor drives. IEEE Ind. Appl. Ann. Meet. Conf. Rec. 1980, pg. 605
- [K63] Krishnan, R., Control and operation of PM synchronous motor drives in the field- weakening region. Proc. IECON 93, Maui, pg. 745
- [K64] Krzeminski, Z., Speed and rotor resistance estimation in observer system of induction motor. Proc. EPE 91, Firenze, pg. 3- 538
- [K65] Kubo, K., Watanabae, M., Ohmae, I., Kamiyama, K., A software-based speed regulator for motor drives. Int. Power Electr. Conf., Tokyo 1983, pg. 1500
- [K66] Kubota, H., Matsuse, K., Disturbance torque estimation for field oriented induction motor drives without rotational transducers. Proc. IECON 92, San Diago, pg. 336
- [K67] Kubota, H., Speed sensorless field- oriented control of induction motor with rotor resistance adaptation. IEEE Trans. Ind. Appl. 1994, pg. 1219
- [K68] Kübler, E., Der Stromrichtermotor. ETZ-A, 1958, pg. 15
- [K69] Kühnert, S., Antriebe mit untersynchroner Stromrichterkaskade für Kessel- speisepumpen. BBC Nachrichten 1975, pg. 588
- [K70] Kulski, Z.H., Method of the air- gap electromagnetic torque identification for a current- fed AC drive system. Europ. Trans. on Electr. Power Engng. 1994, pg. 287

- [K71] Kumar, P.P., Parimelalagan, R., Ramaswami, B., A microprocessor- based DC drive control scheme using predictive synchronization. IEEE Trans. Ind. Electr. 1993, pg.445
- [K72] Kume, T., Iwakane, T., Sawa, T., Yoshida, T., Nagai, I., A wide constant power range vector- controlled AC motor drive using winding changeover technique. IEEE Trans. Ind. Appl. 1991, pg. 934
- [K73] Kume, T., Sonoda, S., Ryu, H., Watanabe, E., A novel PWM technique to decrease lower harmonics. Proc. EPE 91, Firenze, pg. 3- 223
- [K74] Kume, T., Sawa, T., Yoshida, T., Sawamura, M., Sakamoto, M., A high speed vector controlled spindle motor drive with closed transition between with and without encoder control. IEEE Trans. Ind. Appl. 1992, pg. 421
- [K75] Kunz, U., Eine digitale zeitoptimale Lageregelung. Diss. TH Darmstadt 1971
- [K76] Kurz, R., Hochgenaue Drehzahlregelung mit Hilfe des Phase locked-loop. Elektricte 1978, pg. 658
- [K77] Kusko, A., Application of microprocessors to AC and DC electric motor drive systems. IEEE Ind. Appl. Ann. Meet. Conf. Rec. 1977, pg. 1079
- [L1] Labahn, D., Untersuchungen an einem Stromrichtermotor in sechs- und zwölfpulsiger Schaltung. Diss. TU Braunschweig, 1961
- [L2] Läuger, A., The commutatorless DC motor with three-phase current excitation. 2. IFAC Symp., Control in Power Electronics and Electrical Drives, Düsseldorf 1977, pg. 619
- [L3] Lagasse, J., Prajoux, R, Behaviour of control systems including controlled converters, especially rectifiers: A review of existing theories, survey. 1. IFAC Symp., Control in Power Electronics and Electrical Drives, Düsseldorf 1974, pg. 1
- [L4] Laithwaite, E.R., Kuznetsov, S.B., Development of an induction machine commutated thyristor inverter for traction drives. IEEE Ind. Appl. Ann. Meet. Conf. Rec. 1980, pg. 580
- [L5] Langer, J., Umrichterspeisung von Synchronmotoren fur Rohrmühlen. BBC Mitteilungen 1970, pg. 112
- [L6] Langweiler, F., Richter, M., Flußverfassung in Asynchronmaschinen. Siemens Zeitschrift 1971, pg. 768
- [L7] Lataire, P., Induction motor drives with power transistor inverters. IEEE Ind. Appl. Ann. Meet. Conf. Rec. 1978, pg. 763
- [L8] Lataire, Ph., Maggetto, G., Modern teaching on variable speed induction motor drives. Proc. EPE 89, Aachen, pg. 1445
- [L9] Lataire, Ph., Van Muylem, H., Maggetto, G., Experiments for teaching on current- source inverter- fed induction motors with indirect flux control. Proc. EPE 91, Firenze, pg. 3- 612
- [L10] Latzel, W., Berechnung der Laststörung von drehzahlgeregelten Gleichstromantrieben mit geschachteltem Stromregelkreis. Regelungstechnik 1965, pg. 375
- [L11] Lauffer, H., Die Drehstrommaschine mit polradwinkelabhängig eingeprägten Läuferströmen AfE 1968, pg. 289
- [L12] Lawrenson, P.J., Ray, W.F., Davis, RM., Stephenson, J.M., Fulton, N.N., Blake, R.J., Controlled-speed switched-reluctance motors: present status and future potential. Drives/Motors/Controls 82, Leeds

- [L13] Lecocq, D., Lataire, Ph., Study of a variable speed, double fed induction motor drive system with both stator- and rotor- voltages controllable. Proc. EPE 91, Firenze, pg. 2- 337
- [L14] Lee, D.C., Sul, S.K., Park, M.H., High performance current regulator for a field- oriented controlled induction motor drive. IEEE Trans. Ind. Appl. 1994, pg. 1247
- [L15] Le-Huy, H., Perret, R., Roye, D., Microprocessor control of a current fed synchronous motor drive. IEEE Ind. Appl. Ann. Meet. Conf. Rec. 1979, pg. 873
- [L16] Leitgeb, W., Zur Bemessung drehzahlveränderlicher Antriebe konstanter Leistung mit stromrichtergespeisten Drehfeldmaschinen. ETZ 1973, pg. 584
- [L17] Leimgruber, J., Stationary and dynamic behaviour of a speed controlled synchronous motor with  $\cos \delta$  or commutation limit line control. 2. IFAC Symp., Control in Power Electronics and Electrical Drives, Düsseldorf 1977, pg. 463
- [L18] Leonard, H.W., A new system of electric propulsion. Trans. AIEE 1892, pg. 566
- [L19] Leonard, H.W., Volts v. Ohms – Speed regulation of electric motors. Trans. AIEE 1896, pg. 377
- [L20] Leonhard, A., Kennlinien von Gleichstrommotoren. Elektrotechnik und Maschinenbau 1942, pg. 261
- [L21] Leonhard, A., Anlassen von Asynchronmotoren über KUSA-Widerstand. Elektrotechnik und Maschinenbau 1943, pg. 122
- [L22] Leonhard, A., Die Asynchronmaschine bei Laständerungen. Elektrotechnik und Maschinenbau 1965, pg. 3
- [L23] Leonhard, A., Die Drehstrommaschine mit eingeprägten Sekundärströmen. ETZ-A, 1968, pg. 97
- [L24] Leonhard, R., Schröder, D., New precalculating current control strategy for DC drives. Proc. EPE 87, Grenoble, pg. 659
- [L25] Leonhard, W., Elements of reactor controlled reversible induction motor drives. AIEE Trans. 1959, Pt II, pg. 106
- [L26] Leonhard, W., Digitale Regelung und Programmregelung in Digitale Signalverarbeitung in der Regelungstechnik. VDE-Buchreihe, Vol. 8, 1962, pg. 101
- [L27] Leonhard, W., Müller, H., Ein stetig wirkender digitaler Drehzahlregler. ETZ-A, 1962, pg. 381
- [L28] Leonhard, W., Zählende Rechenschaltungen für Regelaufgaben. AfE 1964, pg. 215
- [L29] Leonhard, W., Regelkreise mit symmetrischer Übertragungsfunktion. Regelungstechnik 1965, pg. 4
- [L30] Leonhard, W., Dynamic behaviour of a nonlinear sampled-data control loop using pulse width controlled thyristors as power amplifiers. 3. IFAC Congress, London 1965, Paper 34 C.
- [L31] Leonhard, W., Regelkreis mit gesteuertem Stromrichter als nichtlineares Abtastproblem. ETZ 1965, pg. 513
- [L32] Leonhard, W., Regelprobleme bei der stromrichtergespeisten Drehstrom-Asynchronmaschine. VDE-Fachberichte 1968, pg. 50
- [L33] Leonhard, W., Cascade control, a versatile structural principle for technical and cybernetical control systems. Control and Instruments Systems 1970, pg. 28
- [L34] Leonhard, W., Optimale Zielsteuerung eines kräftefrei beweglichen Massenpunktes. AfE 1970, pg. 65

- [L35] Leonhard, W., Zeitoptimale Scherenregelung. AfE 1976, pg. 61
- [L36] Leonhard, W., Field orientated control of a variable speed alternator connected to the constant frequency line. IEEE Conf., Control in Power Systems, College Station 1979
- [L37] Leonhard, W., Elektrische Regelantriebe für den Maschinenbau. VDI-Zeitschrift 1981, pg. 419
- [L38] Leonhard, W., Microcomputer Control of High Dynamic Performance ac-Drives – A Survey, Automatica 1986, pg. 1
- [L39] Leonhard, W., Adjustable speed AC drives. Proc. IEEE 1988, pg. 455
- [L40] Leonhard, W., 30 years space vectors, 20 years field orientation, 10 years digital signal processing with controlled AC drives. EPE- Journal 1991, pg. 13, pg. 89
- [L41] Le Pioufle, B., Louis, J.P., Influence of the dynamics of the mechanical speed of a synchronous servomotor on its torque regulation. Proc. EPE 91, Firenze, pg. 3- 412
- [L42] Lessmeier, R., Schumacher, W., Leonhard, W., Microprocessor- controlled AC servo drives with synchronous or induction motors: Which is preferable? IEEE Trans. Ind. Appl. 1986, pg. 812
- [L43] Lessmeier, R., Digitale Signalverarbeitung für mehrachsige Antriebssysteme mit Drehstrom- Stellmotoren. Diss. TU Braunschweig 1989
- [L44] Letas, H.H., Leonhard, W., Dual axis servo drive in cylindrical coordinates using permanent magnet synchronous motors with microprocessor control. Conumel 83, Toulouse 1983, pg. II-23
- [L45] Letas, H.-H., Mikrorechner- geregelter Synchron- Stellantrieb. Diss. TU Braunschweig 1985
- [L46] Levi, E., Vuckovic, V., Effects of main flux saturation on behavior of a stator and airgap flux oriented induction machine. Proc. EPE 91, Firenze, pg. 3- 618
- [L47] Levi, E., Adaptive decoupling circuit for universal field oriented controller operating in the airgap flux frame. Proc. EPE 93, Brighton, pg. 5- 57
- [L48] Li, Y.D., de Fornel, B., Pietrzak- David, M., New approach for flux control of PWM fed induction motor drive. Proc. IEE-Power Electronics and Variable Speed Drives, London 1988, pg. 301
- [L49] Liao, F., Sheng, J., Lipo, T.A., A new energy recovery scheme, for doubly fed, adjustable- speed induction motor drives. IEEE Trans. Ind. Appl. 1991, pg. 728
- [L50] Lienau, W., Commutation modes of a current source inverter. 2. IFAC Symp., Control in Power Electronics and Electrical Drives, Düsseldorf 1977, pg. 219
- [L51] Lienau, W., Müller-Hellmann, A., Skudelny, H.Ch., Power converters for feeding asynchronous traction motors of single phase AC vehicles. Int. Semiconductor Power Converter Conf. Rec. 1977, pg. 295
- [L52] Lin, A.K., Koepsel, W.W., A microprocessor speed control system. IEEE Trans. Ind. Electr. and Control Instrumentation 1977, pg. 241
- [L53] Lin, F.J., Liaw, C.M., Control of indirect field- oriented induction motor drives considering the effects of dead- time and parameter variations. IEEE Trans. Ind. Electr. 1993, pg.486
- [L54] Lipo, T.A., Krause, P.C., Stability analysis of a rectifier inverter induction motor drive. IEEE Trans. Power Appl. Syst. 1969, pg. 55
- [L55] Lipo, T.A., State variable steady state analysis of a controlled current induction motor drive. IEEE Trans. Ind. Appl. 1975, pg. 704

- [L56] Lipo, T.A., Analysis and control of torque pulsations in current-fed induction motor drives. Proc. Power Electronics Specialists Conf. 1978
- [L57] Liu, S., Stiebler, M., A continuous discrete time state estimator for a synchronous motor fed by a PWM voltage source inverter. Proc. EPE 89, Aachen, pg. 865
- [L58] Lockwood, M., Fox, A.M., A novel high power transistor inverter. Proc. Int. Power Electronics Conference, Tokyo 1983, pg. 637
- [L59] Löser, F., Sattler, Ph.K., Optimizing of the efficiency by the control of inverter-fed induction machines especially regarding saturation and heat effects. 3. IFAC Symp. Control in Power Electronics and Electrical Drives, Lausanne 1983, pg. 25
- [L60] Lorenz, R.D., Van Patten, K.W., High resolution velocity estimation for all-digital, AC servo drives. IEEE Trans. Ind. Appl. 1991, pg. 701
- [L61] Lorenz, R.D., Yang, S.M., Efficiency- optimised flux trajectories for closed-cycle operation of field- orientation induction machine drives. IEEE Trans. Ind. Appl. 1992, pg. 574
- [L62] Loron, L., Stator parameters influence on the field- oriented control tuning. Proc. EPE 93, Brighton, pg. 5- 79
- [L63] Louis, J.P., Nonlinear and linearised models for control systems including static converters. 3. IFAC Symp. Control in Power Electronics and Electrical Drives, Lausanne 1983, pg. 9
- [L64] Low, T.S., Lee, T.H., Chang, K.T., A nonlinear speed observer for permanent-magnet synchronous motors. IEEE Trans. Ind. Electr. 1993, pg.307
- [L65] Ludwig, E., German Patent 1.072.704, 1960
- [L66] Luenberger, D.G., Observing the state of a linear system. IEEE Trans. Mil. Electr. 1964, pg. 74
- [M1] Maag, R.B., Characteristics and application of current source slip regulated AC induction motor drives. IEEE Ind. Gen. Appl. Ann. Meet. Conf. Rec. 1971, pg. 44
- [M2] Maeda, A., Huai Chin, T., Tanaka, H., Koga, T., Ohtani, T., Today's AC drive for industrial application in Japan. Proc. EPE 91, Firenze, pg. 2- 618
- [M3] Magyar, P., The dynamic behaviour of the current control loop of a microcomputer-controlled DC drive in discontinuous current mode operation. Microelectronics in Power Electronics and Electrical Drives, Darmstadt 1982, ETG-Fachberichte 11, pg. 183
- [M4] Magyar, P., Schnieder, E., Vollstedt, W., Digitale Regelung und Steuerung einer stromrichtergetriebenen Gleichstrommaschine mit Mikrorechner. Regelungstechnik 1982, pg. 378
- [M5] Maikath, R., Putz, U., Saupe, R., An all digital control for the LCI feeding a synchronous machine. EPE 91, Firenze, pg. 4- 586
- [M6] Malesani, L., Tenti, P., Gaio, E., Piovan, R., Improved current control technique of VSI PWM inverters with constant modulation frequency and extended voltage range. IEEE Trans. Ind. Appl. 1991, pg. 365
- [M7] Malesani, L., Tomasin, P., PWM current control techniques of voltage source inverters- a survey. Proc. IECON 93, Maui, pg. 670
- [M8] Mathys, S., Microprocessor-based multimode synchronous pulse width modulation. Microelectronics in Power Electronics and Electrical Drives, Darmstadt 1982, ETG-Fachberichte 11, pg. 237

- [M9] Matsui, N., Sensorless operation of brushless DC motor. Proc. IECON 93, Maui, pg. 739
- [M10] Mauch, K., Ito, M.R., A multi-microprocessor AC drive controller. IEEE Ind. Appl. Ann. Meet. Conf. Rec., 1980, pg. 634
- [M11] Maurer, F., Vergleich verschiedener Zündsteuerverfahren für netzgeführte Stromrichter. ETZ-A, 1974, pg. 50
- [M12] Maurer, F., Stromrichtergespeiste Synchronmaschine als Vierquadrant-Regelantrieb. Diss. TU Braunschweig 1975
- [M13] McLaren, S.G., Direct digital control of thyristors. 1. IFAC Symp., Control in Power Electronics and Electrical Drives, Düsseldorf 1974, Vol. 2, pg. 147
- [M14] Meiners, U., Beiträge zur adaptiven Regelung elektrischer Antriebe. Diss. TU Braunschweig, 1996
- [M15] Mertens, A., Harmonic distortion in three- phase inverters controlled by synchronous sigma- delta- modulation. Europ. Trans. on Electr. Power Engng. 1992, pg. 351
- [M16] Mestha, L.K., Evans, P. D., Optimisation of losses in PWM inverters. Proc. IEE-Power Electronics and Variable Speed Drives, London 1988, pg. 394
- [M17] Meyer, D., Vergleich klassischer und moderner Regelverfahren am Beispiel einer Schachtförderanlage. Diss. TU Braunschweig 1995
- [M18] Meyer, H.G., Static frequency changers for starting synchronous machines. BBC Review 1964, pg. 526
- [M20] Meyer, M., Möltgen, G., Wesselak, F., Der Quecksilberdampf-Stromrichter als Stellglied in Regelkreisen. Siemens Zeitschrift 1960, pg. 592
- [M21] Meyer, M., über die untersynchrone Stromrichterkaskade. ETZ 1961, pg. 589
- [M22] Meyer, S., Sondermann, E., Mehrmotorenantrieb für Rotationsdruckmaschinen. Siemens Zeitschrift 1977, pg. 387
- [M23] Miki, I., Nakao, O., Nishiyama, S., A new simplified current control method for field- oriented induction motor drives. IEEE Trans. Ind. Appl. 1991, pg. 1081
- [M24] Miyashita, I., Ohmori, Y., Improvement of robustness on speed sensorless vector control of induction motor. Proc. EPE 91, Firenze, pg. 4- 660
- [M25] Miyashita, I., Ohmori, Y., A new speed observer for an induction motor using the speed estimation technique. Proc. EPE 93, Brighton, pg. 349
- [M26] Mittenzwei, K., Probst, E., Thyristorgespeiste Fördermaschinen. BBC Nachrichten 1976, pg. 153
- [M26] Möltgen, G., Neuffer, I., Stand der Technik der Antriebe mit netzgeführten Stromrichtern. In Energieelektronik und geregelte elektrische Antriebe, VDE-Buchreihe Vol. 11, 1960, pg. 239
- [M27] Möltgen, G., Salzmann, Th., Power factor and current harmonics with cyclo-converters fed by a three-phase supply. 2. IFAC Symp., Control in Power Electronics and Electrical Drives, Düsseldorf 1977, pg. 181
- [M28] Moghbelli, H., Adams, G.E., Hoft, R.G., Performance of a 10 HP switched reluctance motor and comparison with induction motors. IEEE Trans. Ind. Appl. 1991, pg. 531
- [M29] Moerschell, J., Signal processor based field oriented vector control for an induction motor drive. Proc. EPE 91, Firenze, pg. 2- 145
- [M30] Moerschell, J., Tursini, M., A new vector control scheme for inverter- fed permanent magnet synchronous motor using DSP. Proc. EPE 91, Firenze, pg. 4- 683

- [M31] Mok, H.S., Kim, J.S., Kim, R.Y., Park, M.H., Sul, S.K., A stator flux orientation speed control of induction motor without speed sensor. Proc. EPE 91, Firenze, pg. 4- 678
- [M32] Mokrytzki, B., Pulse width modulated inverters for AC motor drives. IEEE Trans. Ind. Gen. Appl. 1967, pg. 493
- [M33] Mokrytzki, B., The controlled slip static inverter drive, IEEE Trans. Ind. Appl. 1968, pg. 312
- [M34] Moreira, J.C., Lipo, T.A., Blasko, V., Simple efficiency maximiser for an adjustable frequency induction motor drive. IEEE Trans. Ind. Appl. 1991, pg. 940
- [M35] Moreira, J.C., Lipo, T.A., Modeling of saturated AC machines including air gap flux harmonic components. IEEE Trans. Ind. Appl. 1992, pg. 343
- [M36] Moreira, J.C., Hung, K.T., Lipo, T.A., Lorenz, R.D., A simple and robust adaptive controller for detuning correction in field- oriented induction machines. IEEE Trans. Ind. Appl. 1992, pg. 1359
- [M37] Moschetti, A., Microprocessor-based PWM-system for inverter-fed squirrel-cage motor traction drives. Microelectronics in Power Electronics and Electrical Drives, Darmstadt 1982, ETG-Fachberichte 11, pg. 425
- [M38] Moynihan, J., Kavanagh, R.C., Egan, M.G., Murphy, J.M.D., Indirect phase current detection for field oriented control of a permanent magnet synchronous motor drive. Proc. EPE 91, Firenze, pg. 3- 641
- [M31] Mozdzer, A., Bose, B.K., Three phase AC power control using power transistors, IEEE Trans. Ind. Gen. Appl. 1976, pg. 499
- [M40] Mühlöcker, H., Elektrische Ausrüstung einer großen Windkraftanlage. Siemens-Energietechnik 1979, S. 443
- [M41] Murakami, T., Yu, F., Ohnishi, K., Torque sensorless control in multidegree-of- freedom manipulator. IEEE Trans. Ind. Electr. 1993, pg. 259
- [M42] Murphy, J.M.D., Hoft, R.G., Howard, L.S., Controlled slip operation of an induction motor with optimum waveforms. 2. Int. Conf. on Electr. Variable Speed Drives, IEE London 1979, pg. 157
- [M43] Murphy, J.M.D., Egan, M.D., An analysis of induction motor performance with optimum PWM waveforms. Proc. Int. Conf. Electrical Machines, 1980, pg. 642
- [M44] Mutoh, N., Sakai, K., Ueda, A., Tomita, H., Nandoh, K., Stabilizing methods at high frequencies for an induction motor driven by a PWM inverter. Proc. EPE 91, Firenze, pg. 2- 352
- [M45] Mutschler, P., Schulze, H., Control of current source inverter by single board computer for squirrel-cage motor drive of urban transport system. Microelectronics in Power Electronics and Electrical Drives, Darmstadt 1982, pg. 417
- [N1] Nabae, A., Otsuka, K., Uchino, H., Kurosawa, R., An approach to flux control of induction motors operated with variable frequency power supply. IEEE Trans. Ind. Appl. 1980, pg. 342
- [N2] Nabae, A., Agaki, H., Osanai, T., Unity power factor commutator-less motors based on a new commutation principle. Int. Semiconductor Power Converter Conf. 1982, pg. 342
- [N3] Nagase, H., Matsuda, Y., Ohnishi, K., Ninomiya, H., Koike, T., High Performance Induction Motor Drive System using a PWM Inverter. IEEE-IAS-1983 Annual Meeting, 1983

- [N4] Nakano, T., Oksawa, H., Endoh, K., A high performance cycloconverter-fed synchronous machine drive system. Int. Semiconductor Power Converter Conf. 1982, pg. 334
- [N5] Nashiki, M., Dote, Y., High performance current-controlled PWM transistor inverter-fed brushless servomotor. Int. Semiconductor Power Converter Conf. 1982, pg. 349
- [N6] Naunin, D., Ein Beitrag zum dynamischen Verhalten der frequenzgesteuerten Asynchronmaschine. Diss. TU Berlin 1968
- [N7] Naunin, D., The calculation of the dynamic behaviour of electric machines by spacephasors. Electric Machines and Electromechanics, 1979, pg. 33
- [N8] Neft, C.L., Schauder, C.D., Theory and design of a 30 HP matrix converter. IEEE Trans. Ind. Appl. 1992, pg. 546
- [N9] Neuffer, I., Stromrichterantriebe mit Momentumkehr. Siemens Zeitschrift 1965, pg. 1079
- [N10] Nielsen,P.E., Thomsen, E.Chr., Nielse, M.T., Digital Voltage vector control with adaptive parameter tuning. Proc. EPE 89, Aachen, pg. 313
- [N11] Nielsen,P.E., Mueller, K., Vammen, S., Speed and position AC servo drive based on current vector control. Proc. EPE 91, Firenze, pg. 3- 635
- [N12] Nilsen, R., Modeling, identification and control of an induction machine. Diss. NTH Trondheim, 1987
- [N13] Nitschke, H.J., Der bürstenlose Motor, ein neuer universeller drehzahlregelbarer Drehstromantrieb. AEG Mitteilungen 1973, pg. 73
- [N14] Nobuyuki, K., Kamatani, M., Watanabe, H., Current source inverter drive – Speed sensor- less vector controlled induction motor. Proc. IECON 93, Maui, pg. 983
- [N15] Nonaka, S., Neba Y., A PWM GTO current source converter- inverter system with sinusoidal inputs and outputs. IEEE Trans. Ind. Appl. 1989, pg. 76
- [N16] Nonaka, S., Neba Y., Quick regulation of sinusoidal output current in PWM converter- inverter system. IEEE Trans. Ind. Appl. 1991, pg. 1055
- [N17] Nonaka, S., Yamasaki, K., Hirohata, S., PWM current source converter- inverter system for railways application. Proc. EPE 91, Firenze, pg. 4- 72
- [N18] Nonaka, S., Kawaguchi, T., A new variable speed AC generator system using a brushless self- excited type synchronous machine. IEEE Trans. Ind. Appl. 1992, pg. 490
- [N19] Nonaka, S., Neba Y., Current regulated PWM- CSI induction motor drive system without a speed sensor. IEEE Trans. Ind. Appl. 1994, pg. 116
- [N20] Nuß , U., Huck, S., Systemdynamischer Zusammenhang zwischen Strommodell, Spannungsmodell und Beobachter bei der Asynchronmaschine. etz- Archiv, 1990, pg. 227
- [N21] Nystrom, A., Hylander, J., Thorberg, K., Harmonic currents and torque pulsations with pulse width modulation methods in AC motor drives. Proc. IEE- Power Electronics and Variable Speed Drives, London 1988, pg. 378
- [O1] Ogasawara, S., Akagi H., Nabae, A., The generalised theory of indirect vector control for AC machines. IEEE Trans. Ind. Appl. 1988, pg. 470
- [O2] Ogasawara, S., Akagi H., An approach to position sensorless drive for brushless DC motors. IEEE Trans. Ind. Appl. 1991, pg. 928

- [O3] Ogino, Y., Murakami, Y., Ohishi, K., Nakaoka, M., High performance ultra-low speed control of inverter- fed linear induction motor using vector control scheme. Proc. EPE 93, Brighton, pg. 5- 464
- [O4] Ohm, H.J., Oppermann, K., Raatz, E., Steuerung einer durchlaufenden Säge mit einem Kleinrechner. AEG Mitteilungen 1976, pg. 266
- [O5] Ohmae, T., Matsuda, T., Suzuki, T., Azuwada, N., Kamiyama, K., Konishi, T., A microprocessor-controlled fast-response speed regulator with dual mode current loop for DCM drives. IEEE Trans. Ind. Appl. 1980, pg. 388
- [O6] Ohtani, T., Takada, N., Tanaka, K., Vector control of induction motor without shaft encoder. IEEE Trans. Ind. Appl. 1992, pg. 157
- [O7] Oldenkamp, J.L., Peak, S.C., Selection and design of an inverter driven induction motor for a traction drive system. GE-Report 83 CRD 191, 1983
- [O8]. Orlik, B., Zum Betriebsverhalten mikrorechner- geregelter und pulswechselrichter- gespeister Synchronmaschinen mit Permanenterregung. Diss. TU Braunschweig 1987
- [O9] Orlik, B., Economical inverter- fed AC drives with fully digital control by means of an 8 bit microcontroller. Proc. EPE Firenze 91, pg. 4- 578
- [O10] Orlik, B., Feldorientierte sensorlose Drehzahlzegelung von Drehstrom- Asynchronmaschinen, Proc. Drives 94, Sindelfingen, 1994, pg. 541
- [O11] Oumamar, A., Louis, J.P., El-Hefnawy, A., Design of an optimal, autoadaptive current loop for DC motor. Realization with a hybrid device including a microprocessor. 2. IFAC Symp., Control in Power Electronics and Electrical Drives, Düsseldorf 1977, pg. 593
- [P1] Pachter, M., Speed control of a field controlled d.c. traction motor. Automatica 1981, pg. 627
- [P2] Pagano, E., Perfetto, A., A comparison between operating conditions of inverter-fed asynchronous motors. 2. IFAC Symp., Control in Power Electronics and Electrical Drives, Düsseldorf 1977, pg. 399
- [P3] Paice, D.A., Induction motor speed control by stator voltage control. IEEE Trans. Power Appl. Syst. 1968, pg. 585
- [P4] Parasuram, M.K., Ramaswami, B., Analysis and design of a current-fed inverter. 2. IFAC Symp., Control in Power Electronics and Electrical Drives, Düsseldorf 1977, pg. 235
- [P5] Patel, H.S., Hoft, R.G., Generalised techniques of harmonic elimination and voltage control in thyristor inverters. IEEE Trans. Ind. Appl., Part I, Harmonic elimination 1973, pg. 310; Part II, Voltage control techniques 1974, pg. 666
- [P6] Pedersen, J.K., Blaabjerg, F., Jensen, J.W., Thogersen, P., An ideal PWM- VSI inverter with feedforward and feedback compensation. Proc. EPE 93, Brighton, pg. 5- 501
- [P7] Peng, F.Z., Fukao, T., Robust speed identification for speed- sensorless vector control of induction motors. IEEE Trans. Ind. Appl. 1994, pg. 1234
- [P8] Perin, A.J., da Cunha, A.A., de Oliveira, M.A., Variable optimal PWM for voltage source rectifiers and current source inverters. Proc. EPE 89, Aachen, pg. 1279
- [P9] Peterson, B., Valis, J., Oscillations in inverter fed induction motor drives. Proc. EPE Firenze 91, pg. 2- 369
- [P10] Peterson, B., Induction machine speed estimation; observations on observers. Diss. TH Lund, 1996

- [P11] Pfaff, G., Zur Dynamik des Asynchronmotors bei Drehzahlsteuerung mit veränderlicher Speisefrequenz. ETZ-A 1964, pg. 719
- [P12] Pfaff, G., Time-response analysis of inverter-fed induction motors with controlled stator current. 2. IFAC Symp., Control in Power Electronics and Electrical Drives, Düsseldorf 1977, pg. 493
- [P13] Pfaff, G., Scheurer, H.G., Parameterunempfindliche Regelung von Gleichstrommotoren im Feldschwächebereich. ETZ-A, 1969, pg. 400
- [P14] Pfaff, G., Weschta, A., Wick, A., Design and experimental results of a brushless AC servo motor. IEEE Ind. Appl. Ann. Meet. Conf. Rec. 1982, pg. 692
- [P15] Pfaff, G., Wick, A., Direkte Stromregelung bei Drehstromantrieben mit Pulswechselrichter. Regelungstechn. Praxis 1983, pg. 472
- [P16] Pfaff, G., Segerer, H., Resistance corrected and time discrete calculation of rotor flux in induction motors. Proc. EPE Aachen 89, pg. 499
- [P17] Pfitscher, G.H., A microprocessor control scheme for naturally commutated thyristor converter with variable frequency supply. 3. IFAC Symp. Control in Power Electronics and Electrical Drives, Lausanne 1983, pg. 431
- [P18] Phillips, K.P., Current source converter for AC motor drives. IEEE Trans. Ind. Appl. 1972, pg. 679
- [P19] Pienaar, A.I., A contribution to the solution of instability problems in supply commutated power electronic converter-fed systems. Diss. Randse Africaanse Universiteit Johannesburg 1980
- [P20] Pietrzak- David, M., de Fornel, B., Universal PWM inverter fed asynchronous drive with a dynamic flux control. Proc. EPE 89, Aachen, pg. 1329
- [P21] Plaetrick, H., Digitale Lageregelungen. AEG Mitteilungen 1976, pg. 291
- [P22] Plunkett, A.B., Direct flux and torque regulation in a PWM inverter-induction motor drive. IEEE Trans. Ind. Appl. 1977, pg. 139
- [P23] Plunkett, A.B., A current-controlled PWM transistor inverter drive. IEEE Ind. Appl. Ann. Meet. Conf. Rec. 1979, pg. 785
- [P24] Plunkett, A.B., Lipo, T.A., New methods of induction motor torque regulation. IEEE Trans. Ind. Appl. 1976, pg. 47
- [P25] Plunkett, A.B., Turnbull, F.G., Load commutated inverter synchronous motor drive without a shaft position sensor. IEEE Trans. Ind. Appl. 1979, pg. 63
- [P26] Pohl, K., Rumold, G., Digitaler Regler in TTL-Technik für genaue Drehzahl- und Drehzahlverhältnisregelung. Siemens Zeitschrift 1972, pg. 335
- [P27] Pollmann, A., Gabriel, R., Zündsteuerung eines Pulswechselrichters mit Mikrorechner. Regelungstechnische Praxis 1980, pg. 145
- [P28] Pollmann, A., A digital pulse-width modulator employing advanced modulation techniques. IEEE Trans. Ind. Appl. 1983, pg. 409
- [P29] Pollmann, A., Comparison of PWM techniques. Microelectronics in Power Electronics and Electrical Drives, Darmstadt 1982, ETG-Fachberichte, pg. 231
- [P30] Pollmann, A., Ein Beitrag zur digitalen Pulsbreitenmodulation bei wechselrichtergespeisten Asynchronmotoren. Diss. TU Braunschweig, 1984
- [P31] Pollmann, A., Tosetto, A., Brea, P., Microprocessor based control system for rolling mills. Proc. EPE Firenze 91, pg. 1- 64
- [P32] Prajoux, R., Jalade, J., Marpinard, J.C., Mazankine, J., A modelling method for the behaviour of converters operating in control loops. 2. IFAC Symp., Control in Power Electronics and Electrical Drives, Düsseldorf 1977, pg. 67

- [P33] Preuß , H.-P., Störungsunterdrückung durch Zustandsregelung. Regelungstechnik 1980, pg. 227, 266
- [P34] Probst, U., Comparison of disturbance suppression strategies for servo- drives. Proc. EPE 93, Brighton, pg. 5- 442
- [P35] Probst, E., Antriebstechnik in Konti-Walzwerken. BBC Nachrichten 1977, pg. 485
- [P36] Profumo, F., Pastorelli, M., Ferraris, P., De Doncker, R.W., Comparison of Universal Field Oriented (UFO) controller in different reference frames. Proc. EPE Firenze 91, pg. 4- 689
- [P37] Putz, U., Thyristor industrial drives. Int. Semiconductor Power Converter Conf. Rec. 1977, pg. 340
- [Q1] Quang, Ng.Ph., Schnelle Drehmomenteinprägung in Drehstromstellantrieben. Diss. TU Dresden, 1991
- [Q02] Quang, Ng.Ph., Schönfeld, R., Dynamische Stromregelung zur Drehmomenteinprägung in Drehstromantrieben mit Pulswechselrichter. Archiv für Elektrotechnik, 1993, pg. 317
- [R1] Raatz, E., Der Einsatz von adaptiven Drehzahlreglern in der Antriebstechnik. AEG Mitteilungen 1970, pg. 375
- [R2] Raatz, E., Der Einfluß von elastischen Übertragungselementen auf die Dynamik geregelter Antriebe. AEG Mitteilungen 1973, pg. 205
- [R3] Raducanu, D.C., Hochdynamisches Positionsregelsystem Axumerik. BBC Nachrichten 1977, pg. 301
- [R4] Rapp, H., Examination of transient phenomena in induction machines, caused by an incorrectly adjusted rotor time constant in a field- orientated control scheme. Europ. Trans. on Electr. Power Engng. 1993, pg. 397
- [R5] Ray, W.F., Al- Bahadly, I.H., Sensorless methods for determining the rotor position of switched reluctance motors. Proc. EPE 93, Brighton, pg. 6- 7
- [R6] Rebhan, M., Modulare Echtzeitsimulation in der elektrischen Energietechnik. Proc. EPE Firenze 91, pg. 1- 74
- [R7] Retif, J.M., Allard, B., Jorda, X., Perez, A., Use of ASIC's in PWM techniques for power converters. Proc. IECON 93, Maui, pg. 683
- [R8] Ribbeck, G., Gudakowski, M., Digitale Mischungsregelung System BLENDOMAT. AEG Mitteilungen 1963, pg. 217
- [R9] Ribickis, L.S., Ivbuls, U.V., Greivulis, J.P., Petrov, S.S., Static Krämer drive with specially designed voltage inverter. Proc. EPE Firenze 91, pg. 2- 301
- [R10] Richardson, J. Bezanov, G., A PWM 3- phase on- line controller for AC drives. Proc. EPE Firenze 91, pg. 3- 299
- [R11] Richter, W., Microprocessor-controlled inverter-fed synchronous motor drive. IEE Conf. on Variable Speed Drives, London 1979, pg. 161
- [R12] Richter, W., Einsatz eines Mikrorechners zur Regelung eines Stromrichtermotors bei Betrieb mit maximalem Leistungsfaktor. Diss. TU Braunschweig 1981
- [R13] Richter, W., Microprocessor control of the inverter-fed synchronous motor. Process Automation 1981, pg. 100
- [R14] Riedo, P.-J., Cascade digital control by state variable feedback method applied to DC-motor. Microelectronics in Power Electronics and Electrical Drives, Darmstadt 1982 ETG-Fachberichte 11, pg. 249

- [R15] Riedo, P.-J., Cascade control by state variable feedback method applied to a synchronous motor. 3. IFAC Symp. Control in Power Electronics and Electrical Drives, Lausanne 1983, pg. 111
- [R16] Riefenstahl, U., Einsatz von Mikrorechnern zur Steuerung und Regelung elektrischer Antriebssysteme. Elektric 1978, pg. 245
- [R17] Riehlein, D., Getriebeloser Antrieb für eine Zementmahlanlage. Siemens Zeitschrift 1971, pg. 189
- [R18] Robyns, B., Buyse, H., Labrique, F., Comparison of the sensitivity of the flux control to parameter uncertainties in two induction actuator indirect field oriented control schemes. Proc. EPE 93, Brighton, pg. 5- 402
- [R19] Rosa, J., Utilization and rating of machine commutated inverter synchronous motor drives. IEEE Trans. Ind. Appl. 1979, pg. 155
- [R20] Rowan, T.M., Kerkman, R.J., Leggate, D., A simple on- line adaptation for indirect field orientation of an induction machine. IEEE Trans. Ind. Appl. 1991, pg. 720
- [R21] Ruff, M., Grotstollen, H., Identification of the saturated mutual inductance of an asynchronous motor at standstill by recursive least squares algorithm. Proc. EPE 93, Brighton, pg. 5- 103
- [S1] Salama, S., Lennon, S., Overshoot and limit cycle free current control method for PWM inverters. Proc. EPE Firenze 91, pg. 3- 247
- [S2] Salvatore, L., Stasi, S., Tarchoni, L., A new EKF- based algorithm for flux estimation in induction machines. IEEE Trans. Ind. Electr. 1993, pg. 496
- [S3] Salzmann, Th., Wokusch, H., Direktumrichterantrieb für große Leistungen und hohe dynamische Anforderungen. Siemens Energietechnik 1980, pg. 409
- [S4] Salzmann, Th., Kratz, G., Däubler, Chr., High power drive system with advanced power circuitry and improved digital control. IEEE Trans. Ind. Appl. 1993, pg. 168
- [S5] Santisteban, J.A., Stephan, R.M., Comparative study of vector control methods for induction machines. Proc. EPE 93, Brighton, pg. 5- 390
- [S6] Sato, N., A study of commutatorless motor. Electr. Engin. in Japan 1964, pg. 42
- [S7] Sato, N., A brushless DC motor with armature induced voltage commutation. IEEE Trans. Ind. Gen. Appl. 1971, pg. 1485
- [S8] Sato, N., Semenov, V.V., Adjustable speed drive with a brushless DC motor. IEEE Trans. Ind. Gen. Appl. 1971, pg. 539
- [S9] Sato, N., Ishida, M., Sawaki, N., Some characteristics of induction motor driven by current source inverter. Int. Semiconductor Power Converter Conf. Rec. 1977, pg. 477
- [S10] Sattler, P.K., Balsliemke, G., Experimental and theoretical investigations concerning the design of induction machines with high power density with respect to the inverter supply and speed regulation. 2. IFAC Symp., Control in Power Electronics and Electrical Drives, Düsseldorf 1977, pg. 387
- [S11] Sattler, Ph.K., Stärker, K., Estimation of speed and pole position of an inverter fed permanent excited synchronous machine. Proc. EPE 89, Aachen, pg. 1207
- [S12] Sawaki, N., Sato, N., Steady-state and stability analysis of induction motor driven by current source inverter. IEEE Trans. Ind. Gen. Appl. 1977, pg. 244

- [S13] Schäfer, U., Brandenburg, G., Compensation of Coulomb friction in industrial elastic two- mass systems through model reference adaptive control. Proc. EPE 89, Aachen, pg. 1409
- [S14] Schauder, C., Adaptive speed identification for vector control of induction motors without rotational transducers. IEEE Trans. Ind. Appl. 1992, pg. 1054
- [S15] Schierling, H., Self- commissioning, a novel feature of inverter- fed motor drives. Proc. IEE-Power Electronics and Variable Speed Drives, London 1988, pg. 287
- [S16] Schlabach, L.A., Analysis of discontinuous current in a 12- pulse thyristor DC motor drive. IEEE Trans. Ind. Appl. 1991, pg. 1048
- [S17] Schnieder, E., Control of DC-drives by microprocessors. 2. IFAC Symp., Control in Power Electronics and Electrical Drives, Düsseldorf 1977, pg. 603
- [S18] Schnieder, E., Digitale Nachbildung stromrichtergespeister Maschinen unter besonderer Berücksichtigung der wechselrichtergespeisten reihenschlußerregten Reluktanzmaschine. Diss. TU Braunschweig 1978
- [S19] Schnieder, E., Modelling and simulation of numerically controlled thyristor-fed- drives. Proc. CONUMEL 80, p. III/12-23
- [S20] Schönfeld, R., Einfluß der Getriebelose auf Stabilität und Genauigkeit von Lageregelkreisen. Messen, Steuern, Regeln 1965, pg. 40
- [S21] Schönfeld, R., Krug, H., Näherungsverfahren zur dynamischen Beschreibung der Stromrichterstellglieder. Messen, Steuern, Regeln 1972, pg. 246
- [S22] Schönfeld, R., Das dynamische Verhalten des Stromrichterstellgliedes im Lückbereich. Messen, Steuern, Regeln 1977, pg. 79
- [S23] Schönfeld, R., Entwicklungstendenzen der elektrischen Antriebstechnik. Elektric 1981, pg. 451
- [S24] Schönfeld, R., Franke, M., Hasan, H., Müller, F., Intelligent drives in systems with decentralised intelligence. Proc. EPE 93, Brighton, pg. 5- 489
- [S25] Schönung, A., Stemmler, H., Geregelter Drehstrom-Umkehrantrieb mit gesteuertem Umrichter nach dem Unterschwingungsverfahren. BBC Nachrichten 1964, pg. 555
- [S26] Schönung, A., Stemmler, H., Static frequency changers with subharmonic control in conjunction with reversible variable speed drives. BBC Review 1964, pg. 555
- [S27] Schräder, A., Eine neue Schaltung zur Kreisstromregelung in Stromrichteranlagen. ETZ-A, 1969, pg. 331
- [S28] Schröder, D., Untersuchung der dynamischen Eigenschaften von Stromrichterstellgliedern mit natürlicher Kommutierung. Diss. TH Darmstadt 1969
- [S29] Schröder, D., Die dynamischen Eigenschaften von Stromrichterstellgliedern mit natürlicher Kommutierung. ETZ-A, 1970, pg. 242
- [S30] Schröder, D., Grenzen der Regel�ynamik von Regelkreisen mit Stromrichterstellgliedern. Regelungstechnik 1973, pg. 322
- [S31] Schröder, D., Einsatz adaptiver Regelverfahren bei Regelkreisen mit Stromrichterstellgliedern. VDE-Aussprachetag Freiburg 1973, pg. 81
- [S32] Schröder, D., Selbstgeführter Stromrichter mit Phasenfolgelöschung und eingeprägtem Strom. ETZ-A, 1975, pg. 520
- [S33] Schroedl, M., Sensorless control of permanent magnet synchronous machines at arbitrary operating points using a modified "inform" flux model. Europ. Trans. on Electr. Power Engng. 1993, pg. 277

- [S34] Schroedl, M., Hennerbichler, D., Wolbank, T.M., Induction motor drive for electric vehicles without speed and position sensors. Proc. EPE 93, Brighton, pg. 5- 271
- [S35] Schütting, L., Skudelny, H.-Ch., A control method for permanent magnet synchronous motors with trapezoidal electromotive force. Proc. EPE 91, Firenze, pg. 4- 117
- [S36] Schütze, T., Strönisch, V., Low floor trams with IGBT- 3- level inverter. Proc. EPE 93, Brighton, pg. 6- 92
- [S37] Schumacher, W., Microprocessor controlled AC servo drive. Microelectronics in Power Electronics and Electrical Drives, Darmstadt 1982, ETG-Fachberichte, pg. 311
- [S38] Schumacher, W., Leonhard, W., Transistor-fed AC-servo drive with microprocessor control. Int. Power Electronic Conf. Rec., Tokyo 1983, pg. 1465
- [S39] Schumacher, W., Letas, H.-H., Leonhard, W., Microprocessor-controlled AC-servo-drives with synchronous and asynchronous motors. Proc. IEE Conf. on Power Electronics and Variable-Speed-Drives, London 1984, pg. 233
- [S40] Schumacher, W., Mikrorechner-geregelter Asynchron- Stellantrieb. Diss. TU Braunschweig 1985
- [S41] Schumacher, W., Rojek, P., Letas, H.H., Hochauflösende Lage- und Drehzahlerfassung optischer Geber für schnelle Stellantriebe. Elektronik, 1985, pg.65
- [S42] Seefried, E., Stromregelung im Lückbereich von Stromrichter-Gleichstromantrieben. Elektric 1976, pg. 308
- [S43] Sepe, R.B., Lang, J.H., Real- time observer based (adaptive) control of a permanent- magnet synchronous motor without mechanical sensors. IEEE Trans. Ind. Appl. 1992, pg. 1345
- [S44] Serrano- Iribarnegaray, L., The modern space- phasor theory. Part I: Its coherent formulation and its advantages for transient analysis of converter- fed AC machines. Europ. Trans. on Electr. Power Engng. 1993, pg. 171. Part II: Comparison with the generalised machine theory and the space vector theory. Europ. Trans. on Electr. Power Engng. 1993, pg. 213
- [S45] Shepherd, W., On the analysis of three-phase induction motor with voltage control by thyristor switching. IEEE Trans. Ind. Gen. Appl. 1968, pg. 304
- [S46] Shepherd, W., Stanway, J., Slip power recovery in an induction motor by the use of a thyristor inverter. IEEE Trans. Ind. Appl. 1969, pg. 74
- [S47] Simons, S., Robuste kartesische Bahnregelung eines sensorgeführten Industrieroboters mit digital geregelten Drehstromantrieben. Diss. TU Braunschweig 1995
- [S48] Singh, D., Hoft, R.G., Microcomputer-controlled single-phase cycloconverter. Proc. IECI 1978, pg. 233
- [S49] Skudelny, H.-Ch., Stromrichterschaltungen für Wechselstrom-Triebfahrzeuge. ETZ-A 1966, pg. 249
- [S50] Sobottka, U., Einfluß der Temperatur auf das Betriebsverhalten der drehzahlgeregelten Asynchronmaschine. Siemens Zeitschrift 1969, pg. 760
- [S51] Soran, I. F., Kisch, D. O., Improved scheme for speed control of an asynchronous machine by field oriented method. Proc. EPE 91, Firenze, pg. 2- 218
- [S52] Speth, W., Selbstanpassende Regelsysteme in der Antriebstechnik. Diss. TU Braunschweig 1971

- [S53] Springmeier, F., Steinke, J.K., Field- weakening with the direct self control (DSC) as a control scheme for high power GTO inverters. Proc. EPE 91, Firenze, pg. 4- 666
- [S54] Steimer, P.K., Redundant, fault- tolerant control system for a 13 MW high speed drive. Proc. IEE-Power Electronics and Variable Speed Drives, London 1988, pg. 343
- [S55] Steinke, J.K., Switching frequency optimal PWM control of a three- level inverter. Proc. EPE 89, Aachen, pg. 1267
- [S56] Stemmler, H., Speisung einer langsam laufenden Synchronmaschine mit einem direkten Umrichter. VDE-Fachtagung Elektronik 1969, pg. 177
- [S57] Stemmler, H., Ein- und mehrpulsige Unterschwingungswechselrichter, Steuerverfahren, Strom- und Spannungsverhältnisse. 1. IFAC Symp., Control in Power Electronics and Electrical Drives, Düsseldorf 1974, vol. 1, pg. 457
- [S58] Stemmler, H., Wirk- und Blindleistungsregelung von Netzkupplungsumformern 50 Hz-16 2/3 Hz mit Umrichterkaskade. BBC-Mitteilungen 1978, pg. 614
- [S59] Stemmler, H., Guggenbach, P., Configurations of high power voltage source inverter drives. Proc. EPE 93, Brighton, pg. 5- 7
- [S60] Stemmler, H., Power electronics in electric traction applications. Proc. IECON 93, Maui, pg. 707
- [S61] Stepina, J., Fundamental equations of the space vector analysis of electrical machines. Acta Technica CSAV 13, 1968, pg. 184
- [S62] Stephan, R.M. Field oriented and field acceleration control for induction motors: is there a difference? Proc. IECON 91, Kobe, pg. 567
- [S63] Stoschek, J., 5 MVA-Umrichter für einen Linearmotorantrieb. BBC Nachrichten 1975, pg. 192
- [S64] Ströle, D., Vogel, H., TRANSIDYN-Regelungen für Walzwerk'antriebe. Regelungstechnik 1960, pg. 194
- [S65] Ströle, D., Adaptivsysteme der elektrischen Antriebstechnik. ETZ-A, 1967, pg. 182
- [S66] Sugi, K., Naito, Y., Kurosawa, R., Kano, Y., Katayama, S., Yoshida, T., A microcomputer based high capacity cycloconverter drive for main rolling mill. Int. Power Electr. Conf., Tokyo 1983, pg. 744
- [S67] Sukegawa, T., Kamiyama, K., Mizuno, K., Matsui, T., Okuyama, T., Fully digital, vector- controlled PWM VSI- fed AC drives with an inverter dead-time compensation strategy. IEEE Trans. Ind. Appl. 1991, pg. 552
- [S68] Sukegawa, T., Kamiyama, K., Takahashi, J., Imiki, T., Matsutake, M., A multiple PWM GTO line- side converter for unity power factor and reduced harmonics. IEEE Trans. Ind. Appl. 1992, pg. 1302
- [S69] Sumner, M., Asher, G.M., Pena, R., The experimental investigation of rotor time constant identification for vector controlled induction motor drives during transient operating condition. Proc. EPE 93, Brighton, pg. 5- 51
- [S70] Syrbe, M., Vermischte Regelkreise, eine Möglichkeit zur Vereinfachung von Regelaufgaben. Tagung Heidelberg 1956, Oldenbourg 1957, pg. 78
- [T1] Tadakuma, S., Ehara, M., Historical and predicted trends of industrial AC drives. Proc. IECON 93, Maui, pg. 655
- [T2] Tadros, Y., Junge, G., Salama, S., Design aspects of high power PWM inverter with IGBT. Proc. EPE 91, Firenze, pg. 2- 83

- [T3] Taguchi, T., Aida, K., Mukai, K., Yanagisawa, T., Kanai, T., Variable speed pumped storage system fed by large- scale cycloconverter. Proc. EPE 91, Firenze, pg. 2- 237
- [T4] Tajima, H., Hori, Y., Speed sensor- less field- orientation control of the induction machine. IEEE Trans. Ind. Appl. 1993, pg. 175
- [T5] Takahashi, I., Noguchi, T., A new quick- response and high efficiency control strategy of an induction motor. IEEE- Trans. Ind. Appl. 1986, pg.820
- [T6] Takahashi, I., Kanmachi, Ultra- widw speed control with a quick torque response AC servo by a DSP. Proc. EPE 91. Firenze, pg. 3- 572
- [T7] Tamura, Y., Tanaka, S., Tadakuma, S., Control method and upper limit of output frequency in circulating current type cycloconverter. Int. Semiconductor Power Converter Conf. 1982, pg. 313
- [T8] Taniguchi, K., Tomiyama, Y., Iwatani, T., Irie, H., Acoustic noise reduced PWM converter and inverter using BJT's and IGBT's. Proc. EPE 91. Firenze, pg. 3- 252
- [T9] Taufiq, J.A., Evaluating the step response of a traction VSI drive. IEE-Power Electronics and Variable Speed Drives, London 1988, pg. 340
- [T10] Tez, E.S., MOTONIC- Chip set: High performance intelligent controller for industrial variable speed AC drives. Proc. IEE-Power Electronics and Variable Speed Drives, London 1988, pg. 382
- [T11] Theocharis, J., Petridis, V., Harmonic insertion in PWM inverter drive schemes. Europ. Trans. on Electr. Power Engng. 1992, pg 143
- [T12] Theuerkauf, H., Digitale Nachbildung drehzahlgeregelter Drehstrom-Antriebe mit Stromrichterspeisung. 1. IFAC Symp., Control in Power Electronics and Electrical Drives, Düsseldorf 1974, vol. 1, pg. 709
- [T13] Theuerkauf, H., Zur digitalen Nachbildung von Antriebsschaltungen mit umrichtergespeisten Asynchronmaschinen. Diss. TU Braunschweig 1975
- [T14] Timmer, R.A., PWM frequency inverters in the metal industry. Proc. EPE 91. Firenze, pg. 1- 48
- [T15] Timpe, W., Cycloconverter drives for rolling mills. IEEE Trans. Ind. Appl. 1982, pg. 400
- [T16] Thomas, J.L., Boidin, M., An internal model control structure in field oriented controlled VSI induction motors. Proc. EPE 91. Firenze, pg. 2- 202
- [T17] Török, V., Valis, J., High accuracy and fast response digital speed measurement for control of industrial motor drives. 2. IFAC Symp., Control in Power Electronics and Electrical Drives, Düsseldorf 1977, pg. 721
- [T18] Török, V., Near optimum on-line modulation of PWM inverters. 3. IFAC Symp. Control in Power Electronics and Electrical Drives, Lausanne 1983, pg. 247
- [T19] Török, V., Loreth, K., The world's simplest motor for variable speed control? The Cyrano motor, a PM- biased SR- motor of high torque density. Proc. EPE 93, Brighton, pg. 6- 44
- [T20] Tondos, M.S., Minimizing electromechanical oscillations in the drives with resilient couplings by means of state and disturbance observers. Proc. EPE 93, Brighton, pg. 5- 360
- [T21] Tonnes, M., Rasmussen, H., Robust self tuning of AC servo drive. Proc. EPE 91. Firenze, pg. 3- 49

- [T22] Tripathi, A., Sen, P.C., Comparative Analysis of fixed and sinusoidal band hysteresis current controllers for voltage source inverters. IEEE Trans. Ind. Electr. 1992, pg. 63
- [T23] Tröndle, H.-P., Regelung elastisch gekoppelter Vielmassensysteme. Siemens Forschungs- und Entwicklungs-Berichte 1975, pg. 45
- [T24] Tröndle, H.-P., Regelung einer Spiegelantenne. Siemens Forschungs- und Entwicklungs- Berichte 1975, pg. 75
- [T25] Trzynadlowski, A.M., Kirlin, R.L., Legowski, S., Space vector PWM technique with minimum switching losses and a variable pulse rate. Proc. IECON 93, Maui, pg. 689
- [T26] Tso, S.K., Ho, P.T., Dedicated microprocessor scheme for thyristor phase control of multiphase converters. Proc. IEE 1981, pg. 128
- [T27] Tsuji, T., Sakakibara, J., Naka, S., CSI drive induction motor by vector approximation. IEEE Trans. Ind. Appl. 1991, pg. 715
- [T28] Turnbull, F.G., Selected harmonic reduction in static DC-AC inverters. IEEE Trans. Comm. Electr. 1964, pg. 374
- [U1] Uchijima, T., Takigawa, M., Saijo, T., Speed control over a wide operating range of brushless DC motor applying optimal feedback control. Proc. EPE 91. Firenze, pg. 3- 54  
inverters. IEEE Trans. Comm. Electr. 1964, pg. 374
- [U2] Urbanke, C., Microcomputer control systems for rapid transit vehicles with AC-drives. Microelectronics in Power Electronics and Electrical Drives, Darmstadt 1982, ETG-Fachberichte 11, pg. 401
- [U3] Utkin, V.I., Variable structure systems with sliding mode. IEEE Trans. Autom. Contr. 1977, pg. 212
- [V1] van der Broeck, H., Analysis of harmonics in voltage fed inverter drives caused by PWM schemes with discontinuous switching operation. Proc. EPE 91. Firenze, pg. 3- 261
- [V2] van der Broeck, H., Analysis of the voltage harmonics of PWM voltage fed inverters using high switching frequencies and different modulation functions. Europ. Trans. on Electr. Power Engng. 1992, pg. 341
- [V3] van der Broeck, H., Gerling, D., Bolte, E., Switched reluctance drive and PWM induction motor drive compared for low cost applications. Proc. EPE 93, Brighton, pg. 6- 71
- [V4] Vas, P., Alaküla, M., Hallenius, K.E., Brown, J.E., Field- oriented control of saturated AC machines. Proc. IEE-Power Electronics and Variable Speed Drives, London 1988, pg. 283
- [V5] Völker, C.F., German patent 906 951, 1944
- [V6] Vollstedt, W., Magyar, P., Adaptive control of DC drives by microcomputer. Microelectronics in Power Electronics and Electrical Drives, Darmstadt 1982, ETG-Fachberichte 11, pg. 289
- [V7] von Raumer, T., Dion, J.M., Dugard, L., Thomas, J.L., Applied nonlinear control of an induction motor using digital signal processing. IEEE Trans. Contr. Syst. Techn. 1994, pg.
- [V8] Voss, U., Gleichstromstellertechnik in Nahverkehrsfahrzeugen. Elektrische Bahnen 1977, pg. 162

- [V9] Vukosavic, S.L., Stojic, M.R., On- line tuning of the rotor time constant for vector- controlled induction motor in position control applications. IEEE Trans. Ind. Electr. 1993, pg. 130
- [W1] Wagner, R., Elektronischer Gleichstromsteller für die Geschwindigkeitsteuerung elektrischer Triebfahrzeuge. Siemens Zeitschrift 1964, pg. 14
- [W2] Wagner, R., Beitrag zur Theorie des direkten Gleichstrom-Gleichstrom-Umrichters. Diss. TU Braunschweig 1968
- [W3] Wagner, R., Thyristorteknik für Gleichstrombahnen. Siemens Zeitschrift 1974, pg. 780
- [W4] Waidmann, M., Drehstromantrieb für Gleichstrombahnen. Siemens Zeitschrift 1976, pg. 493
- [W5] Walczyna, A.M., Koczara, W., Simulation study of current- controlled doubly-fed induction machine. Proc. EPE 89, Aachen, pg. 876
- [W6] Walczyna, A.M., Comparison of dynamics of doubly- fed induction machine controlled in field- and rotor- oriented axes. Proc. EPE 91. Firenze, pg. 2- 231
- [W7] Waldmann, H., Koordinatentransformationen bei der Mehrgrößenregelung von Wechsel- und Drehstromsystemen. Diss. TU Braunschweig 1977
- [W8] Walker, L.H., Espelage, P.M., A high performance controlled-current inverter drive. IEEE Trans. Ind. Appl. 1980, pg. 193
- [W9] Wang, Y., Grotstollen, H., Control strategies for the discontinuous current mode of AC drives with PWM inverters. Proc. EPE 91. Firenze, pg. 3- 217
- [W10] Warnecke, O., Einsatz einer doppeltgespeisten Asynchronmaschine in der großen Windenergieanlage Growian. Siemens Energietechnik 1983, pg. 364
- [W11] Waschatz, U., Adaptive control of electrical drives. Microelectronics in Power Electronics and Electrical Drives, Darmstadt 1982, ETG-Fachberichte 11, pg. 135
- [W12] Waschatz, U., Adaptive Regelung elektrischer Antriebe mit Hilfe von Mikrorechnern. Diss. TU Braunschweig 1984
- [W13] Weber, W., Ein systematisches Verfahren zum Entwurf linearer und adaptiver Regelungssysteme. ETZ-A, 1967, pg. 138
- [W14] Weibull, H., Magnusson, T., Valis, J., Standstill testing of properties of induction motors for inverter control. Proc. EPE 91. Firenze, pg. 2- 363
- [W15] Weihrich, G., Drehzahlregelung von Gleichstromantrieben unter Verwendung eines Zustands- und Störgröß enbeobachters. Regelungstechnik 1978, pg. 349, 392
- [W16] Weihrich, G., Wohld, D., Adaptive speed control of DC drives using adaptive observers. Siemens Forschungs- und Entwicklungs-Berichte 1980, pg. 283
- [W17] Weiss, H.W., Adjustable speed AC drive systems for pump and compressor applications. IEEE Trans. Ind. Appl. 1975, pg. 162
- [W18] Weninger, R., Einfluß der Maschinenparameter auf Zusatzverluste, Momentoberschwingungen und Kommutierung bei der Umrichterspeisung von Asynchronmaschinen. AfE 1981, pg. 19
- [W19] Wheatley, C.T., Drives. Proc. EPE 93, Brighton, pg. 1- 33
- [W20] Wheeler, P.W., Grant, D.A., A low loss matrix converter for AC variable speed drives. Proc. EPE 93, Brighton, pg. pg. 5- 27
- [W21] Wilharm, H., Fick, H., Einsatz eines Beobachters zur genauen Bestimmung von Torsionsschwingungen. VDI-Berichte 1978, pg. 69

- [W22] Willis, G.H., A study of the thyratron commutator motor. Gen. Electric Review 1933
- [W23] Willner, L., Falk, M., Beitrag zur Regelung mechanischer Schwingungen beim Haspeln von Band. Regelungstechnik 1977, pg. 101
- [W24] Wishart, M.T., Harley, R.G., Diana, G., The application of field oriented control to the brushless DC machine. Proc. EPE 91. Firenze, pg. 3- 629
- [W25] Wollenberg, G., Schwarz, W., Anwendungen von Mikroprozessoren in numerischen Steuerungen fur Werkzeugmaschinen. Elektric 1980, pg. 452
- [W26] Wolters, P., Auslegung stetiger Vorschubantriebe für Werkzeugmaschinen. Regelungstechnik 1978, pg. 363
- [W27] Wu, B., Slemmon, G.S., Dewan, B.D., PWM- CSI induction motor drive with phase angle control. IEEE Trans. Ind. Appl. 1991, pg. 970
- [W28] Wu, R., Slemmon, G.S., A permanent magnet motor drive without a shaft sensor. Trans. Ind. Appl. 1991, pg. 1005
- [W29] Wu, B., Dewan, S.B., Slemmon, G.R., PWM- CSI inverter for induction motor drives. IEEE Trans. Ind. Appl. 1992, pg. 64
- [W30] Würslin, R., Pulsumrichtergespeister Asynchronmaschinenantrieb mit hoher Taktfrequenz und sehr großem Feldschwächbereich. Diss. Univ. Stuttgart, 1984
- [W31] Wyk van, J.D., Holtz, H.R., A simple and reliable four quadrant variable frequency AC drive for industrial application up to 50 kW. 2. IEE Int. Conf. Electr. Variable Speed Drives, IEE London 1979, pg. 34
- [W32] Wyss, W., Gierse, H., Dupré- Latour, B., AC servo drives. Proc. EPE 89, Aachen, pg. 1061
- [X1] Xue, Y., Xu, X., Habetsler, T.G., Divan, D.M., A stator flux- oriented voltage source variable- speed drive based on DC link measurement. IEEE Trans. Ind. Appl. 1991, pg. 962
- [X2] Xu, X., Novotny, D.W., Implementation of direct stator flux orientation control on a versatile DSP system. IEEE Trans. Ind. Appl. 1991, pg. 694
- [X3] Xu, X., Novotny, D.W., Bus utilization of discrete CRPWM inverters for field-oriented drives. IEEE Trans. Ind. Appl. 1991, pg. 1128
- [X4] Xu, X., Novotny, D.W., Selection of the flux reference for induction machine drives in the field weakening region. IEEE Trans. Ind. Appl. 1992, pg. 1353
- [Y1] Yang, G., Chin, T.-H., Adaptive speed identification scheme for a vector controlled speed sensor less inverter induction motor drive. IEEE Trans. Ind. Appl. 1993, pg. 820
- [Y2] Yeomans, K.A., The controlled retardation of Ward Leonard drives. Proc. IEE, 1962, pg. 559
- [Y3] Yeomans, K.A., Ward Leonard drives, 75 years of development. Electronics & Power, 1968 pg. 144
- [Z1] Zach, F.C., Thiel, F.A., Pulse width modulated inverters for efficiency optimal control of AC-drives-Switching angles and efficiency/loss profiles. 3. IFAC Symp. Control in Power Electronics and Electrical Drives, Lausanne 1983, pg. 231
- [Z1] Zägelein, W., Drehzahlregelung des Asynchronmotors unter Verwendung eines Beobachters mit geringer Parameterempfindlichkeit. Diss. Univ. Erlangen-Nürnberg, 1984

- [Z2] Zai, L.C., De Marco, Chr.L., Lipo, T.A., An extended Kalman filter approach to rotor time constant measurement in PWM induction motor drives. IEEE Trans. Ind. Appl. 1992, pg. 96
- [Z3] Zeitz, M., Nichtlineare Beobachter. Regelungstechnik 1979, pg. 241
- [Z4] Zimmermann, P., Super-synchronous static converter cascade. 2. IFAC Symp., Control in Power Electronics and Electrical Drives, Düsseldorf 1977, pg. 559
- [Z5] Zubek, J., Abbondanti, A., Nordby, C., Pulsewidth modulated inverter motor drives with improved modulation. IEEE Trans. Ind. Appl. 1975, pg. 695
- [Z6] Zürneck, H., Ein drehzahlgeregelter spannungsgesteuerter Stromrichter-Asynchronmotor. Diss. TH Darmstadt 1965

# Index

- acceleration, 6  
acceleration signal, 350  
acquisition of signals, 246  
active power, 102  
actuating variable, 62, 77  
actuator, 127, 135  
adaptive current control, 132, 140  
airgap, 53, 69, 156  
alternating current, 100, 154  
ampereturns, 49, 157  
ampereturns source, 310  
ampereturns-wave, 267  
analogue interpolation, 349  
angular acceleration, 6  
angular frequency, 168  
angular momentum, 6  
angular position, 76  
angular velocity, 6, 242  
antiparallel thyristors, 139  
arc-back, 96  
armature, 49  
armature and field control, 54  
armature circuit, 79  
armature control, 55, 60, 77  
armature current, 49, 60, 62, 75  
armature flux, 49  
armature power supply, 56  
armature reaction, 49, 57  
armature reversal, 136  
armature time constant, 79  
armature voltage, 55, 62, 77, 87  
armature winding, 49  
asynchronous motor, 155  
auxiliary thyristor, 147, 216  
back voltage, 140  
backlash, 351  
balanced three phase voltages, 193  
base speed, 77  
bipolar transistor, 144, 208  
block diagram, 15, 54, 61, 78, 80, 81, 132, 149, 186, 191, 192  
blocking voltage, 98  
Bode-diagram, 84, 341  
cascade control, 79, 80, 86  
catenary, 135, 145  
ceiling voltage, 88, 93, 250, 252  
characteristic equation, 189  
chopper circuit, 150  
circle diagram, 172  
circulating current, 140, 226  
clock frequency, 212, 264  
clutch, 177  
coiler, 58  
combined armature and field control, 58  
combined flux model, 285  
commutating capacitor, 215  
commutating coil, 50  
commutating pole, 50  
commutation, 50, 100, 118  
commutation failure, 55, 114, 139, 147, 333  
commutation interval, 110, 113  
commutator, 49, 155  
compensating winding, 50  
complex roots, 235  
conjugate complex, 84  
continuous, 140  
continuous current, 100, 108, 115  
continuous rolling mill, 337, 359  
continuous web, 357  
control amplifier, 80  
control of active/reactive power, 297  
control of DC Drives, 135  
control of synchronous motor, 321

- controlled oscillator, 236
- controlled rectifier, 96
- controller, 77
- controller wind-up, 135
- converter, 105
- converter-machine combinations, 207
- coordinate system, 182, 188
- coordinate transformation, 292
- correlation, 260
- Coulomb friction, 22
- coupling torque, 342
- cross-over frequency, 83, 130
- current control, 79, 82, 130, 131, 262, 288
- current distribution, 165, 166
- current locus, 178
- current model, 283
- current phasor, 169
- current reference, 85
- current rise, 113
- current sensor, 139
- current source, 249
- current source converter, 221, 266, 270
- current vector, 159, 160, 240
- cycloconverter, 288, 319
- cylindrical coordinates, 353
- damper winding, 167, 309, 318
- damping, 83
- damping ratio, 64, 84, 130
- DC disk motor, 309
- DC-link, 206, 221
- DC/DC converter, 146, 148
- decoupling, 246, 250
- delay, 264
- delayed firing, 103
- delta – connection, 164
- demagnetisation, 309
- detuned flux model, 258, 262
- Diesel engine, 90
- difference equation, 128
- differential equation, 27, 52, 185
- digital control, 338, 349, 354
- digital signal processing, 351
- digitalisation, 252
- diode, 95, 97
- direct component, 291, 315
- discontinuous, 140
- discontinuous current, 108, 109
- disturbance, 61, 88, 129
- doubly fed induction machine, 290
- doubly-fed machine, 168
- doubly-fed machine, 287
- dual converter, 138
- duty cycle, 146
- dynamic control error, 86
- dynamic coupling, 354
- dynamic performance, 257
- eddy current rotor, 181
- efficiency, 176
- eigenvalues, 62, 187
- electric car, 61
- electric torque, 50
- electron tube, 95
- electronic switch, 95
- encoder, 345, 349
- encoderless control, 277
- end-effect, 157
- energy conversion, 75
- energy storage, 170
- energy, kinetic, 10, 90
- energy, potential, 11
- equivalent circuit, 52, 169, 176, 232
- equivalent lag, 83, 352
- excitation, 51
- extinction margin control, 329
- feed-forward, 346
- feedback control, 75
- feedback variable, 79
- field control, 56
- field coordinates, 243, 263, 291, 322
- field effect transistor, 144, 209
- field orientated control, 264, 269, 279
- field orientation, 252
- field parameter, 61
- field reversal, 59
- field voltage, 88
- field weakening, 56, 68, 69, 87, 245, 264, 314
- field weakening , 62
- field winding, 49
- filter, 103
- firing, 98
- firing angle, 104, 108, 115, 132
- firing circuit, 139

- firing pulse, 101
- flux density, 162
- flux linkage, 161
- flux model, 248, 258, 261, 273
- flux reversal, 137
- flux signals, 247
- flux vector, 162, 184
- flux wave, 188, 247
- flying shear, 365
- flywheel, 32, 91, 301
- force commutation, 215
- forced commutation, 101, 135, 144, 220
- forced cooling, 45
- forward blocking, 96
- four quadrant drive, 59
- four-quadrant operation, 136
- frequency divider, 356
- friction, 22
- function generator, 105, 232, 264
- fundamental component, 100, 126, 220
- gain, 78
- gas-turbine set, 326
- gate current, 96, 98
- Gate-Turn-Off thyristors, 144
- gear, 9
- geometrical progression, 48
- gravitational force, 22
- gravity, 7
- GTO current source converter, 224
- GTO-thyristors, 99
- half-controlled converter circuit, 126
- Hall sensors, 247
- harmonics, 103, 124, 135
- heat flow, 42
- high dynamic performance, 79
- household appliance, 67
- identification, 259
- IGBT, 145
- IGBT- inverter, 208
- Ilgner-set, 91
- impedance, 75, 79
- impressed currents, 233, 288
- impressed voltage, 182
- incremental sensor, 254, 349
- induced armature voltage, 75, 79
- induced voltage, 51, 59, 70, 88
- inductances, 161
- induction machine, 167
- induction motor, 155
- inertia, 7, 79
- inrush current, 181, 191
- instability, 25
- insulated gate bipolar transistor, 144
- integer arithmetic, 257
- integration, 27
- intermittent current, 136
- intermittent operation, 152
- intermittent torque, 326
- interphase transformer, 124
- inverse load modelling, 335, 348
- inverse transformation, 244
- inverter, 113, 117
- iron losses, 49
- isolated neutral, 157, 164, 182, 192
- jerk, 363
- junction temperature, 98
- Kirchhoffs law, 110
- Krämer-drive, 301
- lag element, 63
- laminated, 49, 88, 156
- latching threshold, 97
- lead term, 130
- lead-lag term, 81
- leakage current, 95, 97
- leakage factor, 170, 172
- leakage impedance, 103
- line commutated converter, 100, 115, 125, 135, 225
- line impedance, 111, 119
- line voltage, 100
- line-side converter, 220, 333
- line-to-line voltages, 116, 193
- line-to-neutral voltage, 116, 163, 182
- load angle, 258
- load commutation, 308
- load disturbance, 75, 85, 130
- load feed-forward, 337
- load surge, 61, 86
- load torque, 53, 72, 79
- load transient, 64
- locus of current vector, 269
- looper roll, 358

- lumped inertia, 16, 166, 335
- machine-side converter, 222, 325
- magnetic amplifier, 76
- magnetic circuit, 69
- magnetic field, 157
- magnetic leakage, 160
- magnetic saturation, 53
- magnetisation curve, 53, 68
- magnetising current, 171, 234, 264, 269, 278, 289
- magnetomotive force, 157
- mathematical model, 166, 263
- mathematical model of AC machine, 288
- mathematical model of synchronous motor, 312
- Mc Murray circuit, 215
- mean delay, 131
- mechanical model, 229
- mechanical power, 95
- mechanical time constant, 58, 63, 185
- mercury arc converter, 76
- mercury arc valve, 96
- microprocessor, 140, 252
- mine hoist, 90, 318
- modulation, 245
- moment of inertia, 6
- momentum, 5
- MOSFET, 144
- motor parameter, 260
- moving coordinates, 182
- multi loop, 79
- multi-loop control, 362
- multi-phase circuit, 103
- multi-pole machine, 157
- multiple commutation, 122
- multiple motor drive, 336
- multivariable, 62
- nameplate, 184
- natural commutation, 144
- negative sequence, 192
- nested control loop, 80
- nested control loops, 346
- neutral zone, 50
- Newton's law, 5
- no-load speed, 56
- nominal operating point, 68
- nonlinear feedback, 85
- numerical integration, 38
- numerical overflow, 257
- observer, 257, 284, 342
- On-Off controller, 209
- On-Off-controller, 150
- open loop flux control, 233
- open loop transfer function, 85
- operational amplifier, 82, 85
- orthogonal control, 294
- overflow pulses, 357
- overload capacity, 178
- overshoot, 85
- Park-transformation, 312
- peak torque, 174, 185
- permanent magnet excitation, 51, 309
- permeability, 156
- phasor, 168
- phasor diagram, 101, 192, 313
- PI-controller, 81, 88, 130, 132
- PID-controller, 82, 130, 256
- polar coordinates, 266
- position control, 79, 309, 354
- position-control, 345
- positive sequence, 192
- power actuator, 95
- power density, 309
- power factor, 103, 126, 172, 178, 328
- power gain, 103
- power tool, 67
- predictive control, 140
- preloaded gear, 352
- progressive draw, 337
- protective interval, 214
- pseudo-random binary sequence, 260
- pull-out slip, 170, 172
- pulse-width modulation, 147, 209, 268
- pumped storage set, 326
- quadrature axis, 49, 188, 244
- quantisation, 253
- radius of gyration, 8
- railway grid, 287
- rare earth permanent magnets, 309
- rate-of-change limiter, 85, 336
- rated operating point, 171
- reactive current, 101, 135

- reactive power, 111, 125
- recovery time, 98
- rectangular coordinates, 316
- rectifier, 95, 117
- reduced reactive power, 125
- reference, 76, 130
- reference frame, 183
- reference generator, 80, 346
- reference model, 363
- refiring, 114
- regeneration, 77
- regenerative brake, 67
- relative synchronism, 337
- rendez-vous-problem, 365
- residual delay, 78
- resolution, 254, 350
- resonant circuit, 147, 215
- response, 103
- restricted speed range, 287
- reverse current, 98
- reverse voltage, 98
- reversing contactor, 137
- reversing transient, 265
- rigid coupling, 79
- ring counter, 267
- ripple current, 109, 209
- rise time, 265, 269
- rolling mill, 58, 90
- root locus, 63, 188
- rotating converter, 90, 95
- rotating exciter, 92
- rotating generator, 76
- rotating mass, 95
- rotor coordinates, 313
- rotor current vector, 290, 321
- rotor flux, 240
- rotor flux coordinates, 322
- rotor orientation, 312
- rotor position, 242
- rotor resistance, 259
- rotor resistance adaptation, 261
- rotor resistor, 168
- run-out test, 12
- sampled data control, 104, 150, 255
- sampling frequency, 253, 265
- sampling time, 351
- saturation, 70, 73, 259
- saturation-dependent flux model, 260
- saw-tooth function, 121
- Scherbius-drive, 302
- screw-down drive, 360
- sectional drive, 337
- self-excitation, 72
- self-locking gear, 136
- self-tuning, 261
- semiconductor switch, 96
- sensing coil, 248
- separately excited DC machine, 49, 51, 60, 89
- series field winding, 67, 68
- series wound commutator motor, 155
- series wound DC motor, 72
- servo drive, 62, 135, 152, 308, 310
- shaft generator, 298
- shunting diode, 125, 146
- signal processing, 246, 252
- signal processor, 265, 272
- simulation, 129
- single phase converter, 102
- single-phase electric brake, 198
- six pulse bridge-converter, 138
- six pulse circuit, 115
- six pulse converter, 86, 121, 129
- slip, 35, 172, 195
- slip frequency, 169
- slip power recovery, 301
- slot harmonics, 247
- smoothing reactor, 109, 120, 131
- snubber, 98, 216
- solid state, 77
- spatial distribution, 159, 160
- spatial trajectory, 76
- speed control, 336
- speed controller, 79, 85, 88
- speed error, 88
- speed sensor, 274, 341
- squirrel cage rotor, 167
- stability, 25, 82
- stalled torque, 58
- standstill, 55
- star-connection, 156
- starting of induction motor, 178
- starting winding, 180
- state plane, 361
- state space, 361

- static converter, 93, 95  
 stator ampereturns-wave, 238  
 stator current vector, 266  
 stator flux coordinates, 275  
 stator flux vector, 277  
 stator resistance, 249, 275  
 stator voltage equation, 209  
 steady state, 54, 64, 104, 169, 194  
 steady state machine model, 230  
 step response, 62, 85  
 storage loop, 358  
 switched converters, 77  
 switching devices, 95  
 switching frequency, 262  
 switching pattern, 218  
 switching state, 266  
 symmetrical components, 192  
 symmetrical GTO converter, 271  
 symmetrical induction motor, 181, 186, 187  
 symmetrical optimum, 83, 130, 131  
 symmetrical switching sequence, 213  
 synchronous machine, 167  
 synchronous motor drive, 307  
 tachometer generator, 77  
 terminal voltage, 223  
 terminal voltages, 249  
 thermal capacity, 98  
 thermal transient, 44  
 thermal transients, 41  
 three-phase converter, 115  
 three-phase supply, 168  
 thyratron, 95, 307  
 thyristor, 95–97, 100, 103  
 thyristor module, 138  
 torque, 6, 169, 184  
 torque control, 79, 150  
 torque limit, 76  
 torque-speed curves, 55, 231  
 torque-speed plane, 56, 77, 143  
 tracked vehicles, 359  
 traction drive, 67, 125  
 transducer, 81  
 transfer function, 63, 80, 81, 132, 257,  
     340  
 transformation, 186, 241, 317  
 transient, 61, 85, 131, 189  
 transient impedance, 262, 271  
 triplen harmonics, 217  
 turn-off, 98  
 twin drive, 353  
 twin motor, 90  
 two pulse circuit, 115  
 two pulse converter, 132  
 two quadrant operation, 103  
 two-phase oscillator, 235  
 two-mass system, 341  
 types of AC machines, 167  
 unidirectional torque, 135  
 universal motor, 67  
 unsymmetrical starting circuit, 200  
 unsymmetrical supply voltages, 194  
 vectorial PWM, 210, 265  
 vehicle drive, 71  
 voltage feed-forward, 296  
 voltage gain, 132  
 voltage limiter, 278  
 voltage model, 283  
 voltage source inverter, 208, 262  
 voltage vector, 168, 184  
 voltage-time-area, 112, 123  
 waiting interval, 128  
 Ward Leonard, 76, 82, 89  
 waveform, 157  
 zero current interval, 140  
 zero sequence, 192  
 zero vector, 211

# Springer Verlag and the environment

We at the Springer-Verlag firmly believe that an international science publisher has a special obligation to the environment, and our corporate policies consistently reflect this conviction. We also expect our business partners – paper mills, printers, packaging manufacturers, etc. – to commit themselves to using environmentally friendly materials and production processes. The paper in this book is made from low- or no-chlorine pulp and is acid free, in conformance with international standards for paper permanency.



Springer